Oxidative Medicine and Cellular Longevity

Strategies for Modulating Oxidative Stress under Diverse Physiological and Pathological Conditions

Lead Guest Editor: Karolina Szewczyk-Golec
Guest Editors: Jolanta Czuczejko, Przemko Tylzanowski, and Joanna Lecka

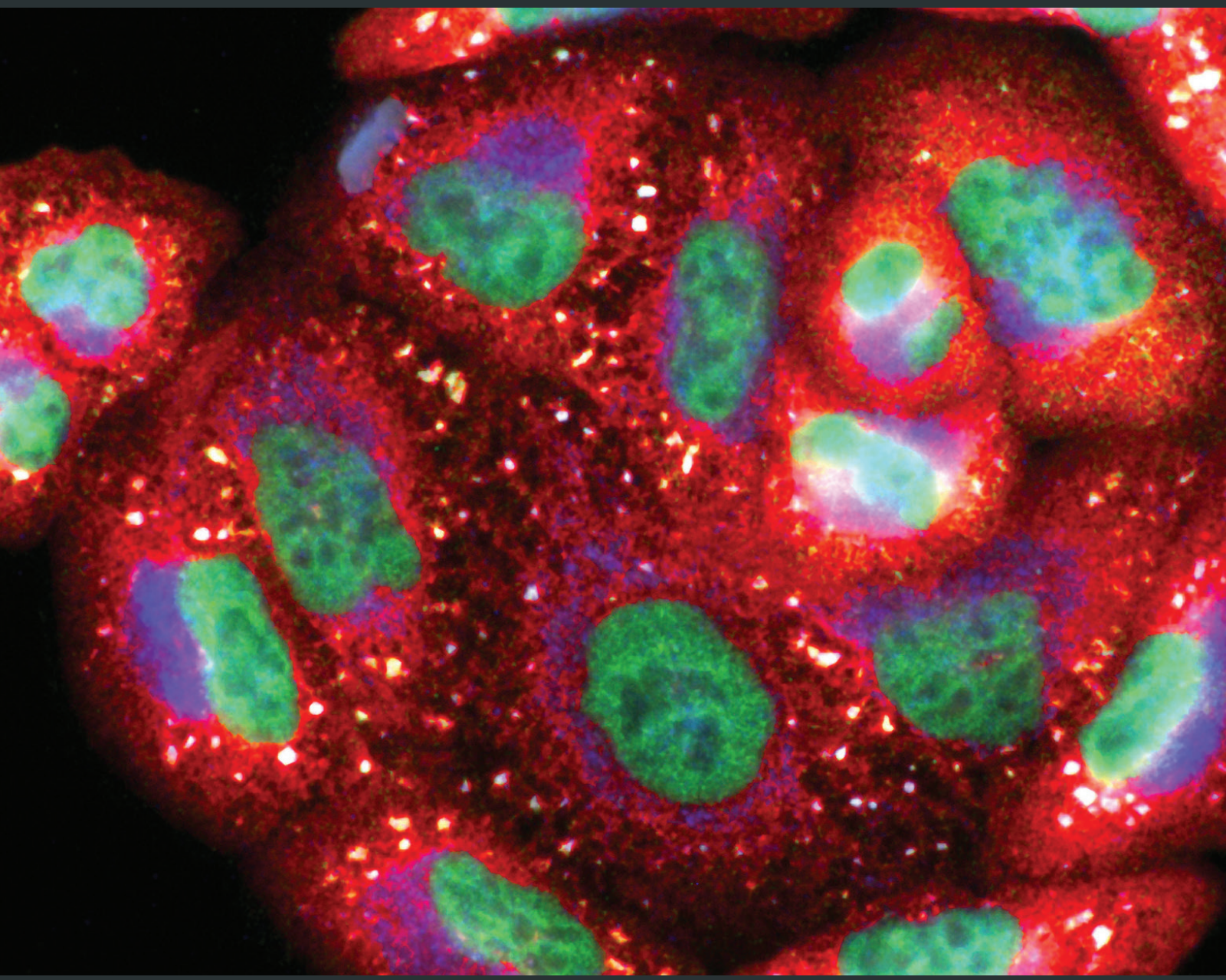

Strategies for Modulating Oxidative Stress under Diverse Physiological and Pathological Conditions

Oxidative Medicine and Cellular Longevity

Strategies for Modulating Oxidative Stress under Diverse Physiological and Pathological Conditions

Lead Guest Editor: Karolina Szewczyk-Golec
Guest Editors: Jolanta Czuczejko, Przemko Tylzanowski, and Joanna Lecka

Editorial Board

Contents

Hindawi
Oxidative Medicine and Cellular Longevity
Volume 2018, Article ID 3987941, 5 pages
https://doi.org/10.1155/2018/3987941

Editorial

Strategies for Modulating Oxidative Stress under Diverse Physiological and Pathological Conditions

Karolina Szewczyk-Golec,[1] **Jolanta Czuczejko**,[2] **Przemko Tylzanowski**,[3,4] **and Joanna Lecka**[5]

[1]*Department of Medical Biology and Biochemistry, L. Rydygier Collegium Medicum in Bydgoszcz, Nicolaus Copernicus University in Torun, Bydgoszcz, Poland*
[2]*Department of Nuclear Medicine, Oncology Centre Prof. Franciszek Łukaszczyk Memorial, Bydgoszcz, Poland*
[3]*Laboratory for Developmental and Stem Cell Biology, Skeletal Biology and Engineering Research Center, Department of Development and Regeneration, KU Leuven, Leuven, Belgium*
[4]*Department of Biochemistry and Molecular Biology, Medical University of Lublin, Lublin, Poland*
[5]*Eau Terre Environnement Research Centre, Institut National de la Recherche Scientifique (INRS-ETE), Université du Québec, Québec, Canada*

Correspondence should be addressed to Karolina Szewczyk-Golec; karosz@cm.umk.pl

Received 1 November 2018; Accepted 1 November 2018; Published 30 December 2018

Numerous physiological and pathological conditions are related to the augmentation of oxidative stress. The weakened antioxidant defense and the increased production of reactive oxygen and nitrogen species are thought to be involved in the etiology of cardiovascular, neurodegenerative, and immune diseases as well as cancer, diabetes mellitus, obesity, aging, and others. Obesity, chronic diseases, and age-related disorders such as dementia and Parkinson's disease belong to the major healthcare problems worldwide. Many studies have been conducted to understand the role of oxidative stress in the pathogenesis of chronic diseases. However, the mechanisms and molecular effects of strategies modifying oxidative stress on these conditions are still not well recognized. These strategies include different procedures, such as antioxidant substance supplementation, physical activity, exercise, or therapeutic hypo- and hyperthermia. The expanding of the knowledge in the field of therapies regulating pro/antioxidant balance in the organism seems to be crucial for world healthcare. It is very important to understand how these strategies influence antioxidant processes and protect cells and organs against the deleterious action of reactive oxygen and nitrogen species. Therefore, this special issue focuses on the following aims: (i) to identify new therapies modifying pro/antioxidant balance in health and disease progression and (ii) to understand the biochemical and molecular mechanisms involved in the therapeutic strategies that may decrease oxidative stress and in consequence may influence the inflammatory state.

The selection of original research and review articles in this special issue covers a wide range of topics, including new antioxidant strategies used in diabetes mellitus, arthritis, and nervous system injury as well as in cardiovascular, renal, and oral cavity diseases, oxidative stress in semen with the correlation to male fertility, new biomarkers of aging, and age-related frailty. Additionally, topics of metabolic surgery, exercise, and cryotherapy as the procedures improving pro/antioxidant balance in health and disease are addressed. Moreover, the effect of regular training on the exercise-induced oxidative stress is also discussed.

In the original research article, A. Ahangarpour et al. considered the role of oxidative stress in the pathogenesis of type 2 diabetes mellitus. They observed increased lipid peroxidation, measured as malondialdehyde (MDA) level, and decreased catalase (CAT) activity in the pancreas of diabetic mice, as well as decreased superoxide dismutase (SOD) activity in skeletal myotube cell lines. They also evaluated the antioxidant and antidiabetic effect of plant-derived antioxidant—myricitrin—in the *in vivo* (mice) and *in vitro* (skeletal

myotube cell line) studies. Authors observed that the administration of solid lipid nanoparticles (SLNs) of myricitrin enhanced antioxidant capacity and reduced lipid peroxidation in the pancreas and this effect is stronger *in vitro*. Moreover, they discovered that SLN myricitrin administration in diabetic mice protects the muscle and pancreatic tissue from weight loss and damage. In conclusion, the authors claimed that SLN myricitrin shows not only antioxidant but also antidiabetic effect through the improvement of hyperglycemia, hyperinsulinemia, and β-cell function index.

The association between increased oxidative stress and type 2 diabetes mellitus (T2D) is also the subject of O. Lushchak et al.'s review. They report that, in patients with T2D, abnormal reactive oxygen species (ROS) concentrations may damage lipid, protein, and nucleic acid molecules, including disturbances in the patterns of gene expression and signal transduction, and also may influence on telomere attrition in pancreatic beta-cells and adipocytes. An increase in ROS levels can then result in the increase of advanced glycation end product (AGE) formation and impair antioxidant defense. The authors emphasized that modulating the processes of ROS, AGE formation, and telomere attrition by innovative technology of metallic nanoparticles (NPs) could provide a promising way for preventing the progression of T2D. Metallic NPs, including cerium oxide, iron oxide, cobalt oxide, copper oxide, manganese dioxide, vanadium pentoxide, gold, silver, and platinum, are known as "nanoantioxidants" and may imitate SOD, CAT, and oxidase and peroxidase activities. O. Lushchak et al. underlined that, due to their properties, NPs have a great clinical potential.

The implication of ROS in diabetic retinopathy (DR) pathogenesis in hyperglycemic conditions is the subject of M.-Y. Wu et al.'s review. According to the authors, excessive glucose oxidation and accumulation of ROS in the retina may lead to local inflammation and endothelial cell death. Endothelial cell death may result in the inflammatory state and microvascular dysfunction in the retina, which further causes blindness. They specified five metabolic pathways, namely, the pathway of sorbitol-aldose reductase, hexosamine, angiotensin II, AGE synthesis, and protein kinase C (PKC), which can be overactivated in hyperglycemic conditions and then become the source of ROS. The authors emphasized that increased oxidative stress damaged the structure and function of the mitochondria leading to the disturbances in levels and activities of mitochondrial SOD, CAT, glutathione peroxidase (GPx), MDA, uncoupling proteins, aldose reductase, AGEs, nitrotyrosine, and 8-hydroxyguanosine. They mentioned decreases in MnSOD expression in DR patients with retinal neuron apoptosis. M.-Y. Wu et al. emphasized that the pathogenesis of DR is complex and has not been completely elucidated; nevertheless, the observation that neurovascular dysfunction may be the result of ROS overproduction is a very interesting issue.

In the research article, Y. Zhang et al. investigated the role of nicotinamide adenine dinucleotide phosphate (NADPH) oxidases (NOXs) in calpain activity, endoplasmic stress (ER), autophagy, and apoptosis during metabolic stress in human cell line ARPE-19, which has functional and structural characteristics similar to retinal pigment epithelial (RPE) cells. Located in the retina, RPE cells are highly metabolically active and play a vital role in maintaining normal visual function. They are vulnerable to oxidative stress and their ROS-induced damage is considered to be involved in the pathogenesis of various ocular diseases. The authors found that Earle's balanced salt solution (EBSS), used as an inducer of cell metabolic stress, resulted in an increase in NOX2, NOX4, p22phox protein, and NOX5 compared to NOX1 in the ARPE-19 cells. Moreover, they also observed reduced ER and autophagy, decreased ROS generation, and alleviated cell apoptosis after suppression of NOXs. The silencing of NOX4, NOX5, and p22phox, but not NOX1, results in the decrease of cell damage. The effect of taurine administration on the cell response to EBSS stress is also investigated. It is demonstrated that taurine attenuated ER, autophagy, and apoptosis in the ARPE-19 cells via the suppression of NOX-derived ROS-mediated calpain induction pathway.

A. B. Sá-Nakanishi et al. studied the actions of fatty acid-derived cyclopentanone—methyl jasmonate (MeJA)—on systemic inflammation and oxidative status in rats with adjuvant-induced arthritis. Authors observed intensified inflammation and increased oxidative stress in arthritic rats. Oxidative stress is demonstrated by increased plasma levels of protein carbonyl groups and higher levels of ROS, lipoperoxides, and carbonyl groups in the arthritic liver. Deficiency in CAT and a very low reduced/oxidized glutathione ratio (GSH/GSSG) are observed in the arthritic liver. Authors claim that impaired ROS scavenging system and the increased production of ROS in arthritic rats are the result of proinflammatory cytokine action. They showed that MeJA administration decreases inflammatory processes, reduces ROS level in the liver, and restores GSH/GSSG ratio but stimulated mitochondrial ROS production in the arthritic rats. The authors prove that this stimulation does not increase hepatic oxidative stress because the effect of MeJA as a ROS scavenger predominates its actions as a stimulator of ROS production.

In turn, X. Li et al. investigated the neuroprotective effect and mechanisms of propofol (anesthetic drug) action in hippocampal neurons expose to ischemia-reperfusion (IR) injury. The results show that treatment of propofol significantly suppresses the apoptosis of hypoxia-reoxygenated hippocampal neurons via the reduction of intracellular calcium overload. The authors hypothesized that propofol may regulate the activation of phosphokinases and phosphatases and thus it would exert neuroprotective effect in IR injury by activating a transcriptional coactivator—Yes-associated protein (YAP). In the study, it is proved that propofol could dephosphorylate YAP, resulting in its activation. This finding supports the therapeutic role of propofol against IR injury in the nervous system.

The aim of C. Tomas-Sanchez et al.'s study is to evaluate the efficacy of prophylactic zinc and therapeutic selenium supplementation against transient hypoxic-ischemic event in cerebral hypoxia-ischemia rat model. The authors reported interesting information about zinc and selenium action against hypoxic-ischemic injury. They claimed that zinc causes a decrease in interleukin-1 (IL-1) and interleukin

23 (IL-23) expression, as well as in oxidative stress intensity (measured as the Cu-Zn-SOD activity), and an increase in chemokine and growth factor levels. In turn, the selenium treatment decreases oxidative stress via both the mechanism of inhibition of inducible nitric oxide synthase (iNOS) and cyclooxygenase-2 (COX-2) expression and via the action of selenoproteins, namely, GPx and thioredoxin reductase, that catalyze peroxide reduction. For this reason, C. Tomas-Sanchez et al. administrated zinc (0.2 mg/kg of body weight daily, i.p.) for 14 days before and after a 10 min common carotid artery occlusion (CCAO) and sodium selenite (6 μg/kg of body weight daily, i.p.) after CCAO for 7 days. The authors found that prophylactic administration of zinc decreases nitrosative/oxidative stress and increases GPx and SOD expression and activity, as well as nitric oxide synthase (eNOS) expression in the temporoparietal cerebral cortex of the examined rats. The therapeutic administration of selenium maintains the effect of zinc up to the late phase of hypoxia-ischemia. Additionally, long-term memory is improved. The results show that the prophylactic zinc and therapeutic selenium administration induces effective neuroprotection in the early and late phases after CCAO.

The cardiovascular disease issue is addressed by J. Zhang et al. who investigated the mechanisms of the potential protective role of exogenous hydrogen sulphide (H_2S), a gasotransmitter with a variety of cardiovascular protective effects, against myocardial hypertrophy. They found that NaHS significantly reduces the cardiac index of isoproterenol- (ISO-) induced mice, decreases the cross-sectional area of cardiomyocytes, and inhibits the expressions of atrial natriuretic peptide (ANP) and brain natriuretic peptide (BNP) mRNAs. The activities of total antioxidant capacity (T-AOC) and SOD in the myocardium are increased, whereas the level of MDA is decreased and superoxide anion production was attenuated. The expression of optic atrophy 1 (OPA1), a protein important for proper mitochondrial function, is upregulated, while dynamin-related protein 1 (DRP1) expression is downregulated. However, all the above protective effects are unavailable in ISO-induced sirtuin 3 (SIRT3) knockout mice. In summary, exogenous H_2S supplementation results in the inhibition of ISO-induced cardiac hypertrophy depending on SIRT3, which might be associated with oxidative stress. The authors highlighted that SIRT3 may be a novel therapeutic target for the protective effect of H_2S against myocardial hypertrophy.

B. Qin et al. investigated the effect of losartan on the prevention and treatment of hyperoxaluria nephrolithiasis. They hypothesized that the overproduction of ROS is associated with renal tubular cell injury in states of high levels of oxalate and calcium oxalate (CaOx) crystals. ROS are involved in the formation of CaOx stones by regulating multiple signaling pathways, including nuclear factor kappa-light-chain-enhancer of activated B cells (NF-κB) and mitogen-activated protein kinase. Authors claimed that NADPH oxidase and angiotensin II (Ang II) are responsible for the production of excessive ROS amounts in hyperoxaluric conditions. They observed that serum Ang II concentration is increased in hyperoxaluric rats. Moreover, the activity of NADPH oxidase is increased, and ROS production and lipid peroxidation levels were enhanced. The authors noticed that losartan reduces renal crystallization via inhibiting NADPH oxidase and decrease of oxidative stress. Hence, losartan may be a potential preventive and therapeutic candidate for hyperoxaluria nephrolithiasis.

Renoprotective effect of platelet-rich plasma (PRP) is the subject of N. Salem et al.'s research. Taking into account that PRP is considered as the source of growth factors that may induce tissue repair, the authors aim to find its application against cisplatin- (CP-) evoked nephrotoxicity in male rats. They found that treatment with PRP reduces creatinine and blood urea nitrogen (BUN), intercellular adhesion molecule-1 (ICAM-1), kidney injury molecule-1 (KIM-1), caspase-3, transforming growth factor (TGF-β1) levels, and N-acetyl glucosaminidase (NAG) activity but increases epidermal growth factor (EGF) concentration. Moreover, histopathological investigation reveals the restoration of normal renal tissue architecture after the PRP treatment. The results suggest that PRP may be considered as a promising agent to improve the therapeutic index of cisplatin.

Next, biological activities and potential oral applications of N-acetylcysteine (NAC) is the subject of Y. Pei et al.'s review. The oral cavity is a source of oxidative stress and inflammation induced by environmental insults. Additionally, some dental materials (including resin) have the potential to induce oxidative stress, DNA damage, and inflammatory reactions. Taking into account the therapeutic effects of NAC over a wide range of disorders, its anti-inflammatory, antimicrobial, and anticarcinogenic properties, as well as its acting as a direct antioxidant and a GSH precursor, NAC is considered as a therapeutic agent in oral health care. The authors emphasized antioxidant properties of NAC, pointing that the compound reacts rapidly with hydroxyl radical ($^{\cdot}OH$), nitrogen dioxide ($^{\cdot}NO_2$), and carbon trioxide ion ($CO_3^{\cdot-}$) and detoxifies ROS produce by leukocytes. Y. Pei et al. state that NAC exerts protective effect against resin monomer-related cytotoxicity due to its antioxidant properties and because it reacts directly with the methacrylic group of resin monomers, reducing the availability of free dental resin monomers. The authors underlined that clinical efficacy of NAC needs further investigations that should especially consider NAC application in dental, implantable, and intracanal materials, the use of NAC alone or with other drugs to treat oral lichen planus. Also, the clinical effectiveness of NAC for the treatment of wound healing and the clinical application of NAC as an anticancer adjuvant for oral cancer treatment should be taken under the account.

In their research, D. Chyra-Jach et al. evaluated the parameters of inflammatory processes (interleukin 12 (IL-12), interleukin 8 (IL-8), monocyte chemoattractant protein-1 (MCP-1), and macrophage inflammatory protein-1β (MIP-1β)), oxidative stress (MDA), and antioxidant defense (albumin, uric acid (UA), total SOD, Cu-Zn-SOD, Mn-SOD, and GPx activities) in patients with abnormalities in spermogram. The level of MDA is significantly higher in seminal plasma and significantly lower in spermatozoa lysate in males with spermogram abnormalities. According to the authors, the levels of MDA, MCP-1, and IL-8 in seminal

plasma negatively correlate with sperm motility. Moreover, D. Chyra-Jach et al. showed a decrease in total SOD and Mn-SOD activities but an increase in the activity of spermatozoa lysate Cu-Zn-SOD and an increase in the activity of GPx from seminal plasma in males with spermogram abnormalities. The authors found positive correlation between SOD activity in spermatozoa lysate and sperm volume, sperm cell count, rapid progressive motility after 1 hour, and motile spermatozoa after 24 hours. Their results show the protective role of SOD against oxidative stress in semen. As the authors explained, Mn-SOD may protect the mitochondria against prolonged oxidative stress, which may lead to mitochondrial DNA (mtDNA) damage, mitochondria disruption, ATP pool depletion, and sperm motility impairment. Additionally, seminal plasma and spermatozoa contain nonenzymatic ROS scavengers, such as UA and albumin. The levels of UA and albumin in seminal plasma are significantly higher in males with spermogram abnormalities in the presented research. The authors concluded that abnormalities in spermogram may be related to the decrease in activity of Mn-SOD in spermatozoa and increase in levels of chemokines in seminal plasma.

Relationships between standard semen parameters, markers of oxidative stress, and antioxidant defense functions were also the subject of M. Dobrakowski et al.'s study. Their observations suggested higher activity of enzymatic antioxidant defense (SOD, CAT, and glucose 6-phosphate dehydrogenase (G6PD)) in the group of males with excellent sperm quality (EX) than in the group with mediocre (ME) semen quality. According to the authors, higher sperm motility in EX is associated with intensive metabolism and in a consequence with more intense ROS production than in ME. Comparable ROS levels in both groups indicated that the antioxidant defense system in EX was more effective. Moreover, the authors demonstrated that the levels of cytokines do not differ between the examined groups suggesting that the semen of fertile males is rather homogenous with respect to immune system parameters.

Next, I. Rusanova et al. evaluated microRNAs (miRNAs) as possible biomarkers of age and frailty and their correlation with oxidative and inflammatory level in human blood. The authors analyzed three inflammation-related miRNAs (miR-21, miR-146a, and miR-223), one miRNA related with the control of melatonin synthesis (miR-483), plasma cytokines (IL-6, IL-8, IL-10, and TNFα), plasma advanced oxidation protein products (AOPPs), and lipid oxidation products (LPOs) in three groups of patients: healthy (control), aged robust, and aged fragile (with sarcopenia). The aged fragile subjects have higher miR-21, miR-223, miR-483, all cytokines, TNFα/IL-10, AOPP, and LPO levels than controls. Increased miR-223, miR-483, all cytokines, AOPP, and LPO levels are observed in aged robust group. Positive correlations between miR-21 and AOPP and between miR-483 and IL-8 are detected. Furthermore, the authors positively correlated the expression of miR-21 and the TNFα/IL-10 ratio with the presence of frailty. Their findings confirm that chronic inflammation and oxidative stress accompanied aging and age-related frailty. I. Rusanova et al. underlined that miR-21and TNFα/IL-10 ratio may be considered as possible biomarkers for aged-related frailty and that the evaluation of stable miRNAs in the blood gives new possibility in systemic biomarker research.

The influence of exercise training on water-pipe smoke (WPS) exposure-induced increase of airway resistance, lung inflammation, oxidative stress, and DNA damage was a subject of A. Nemmar et al.'s research. This project was carried out on mice exposed to WPS in the period of two months. The authors observed that WPS induces a significant increase in tumor necrosis factor α (TNFα), interleukin 6 (IL-6), and 8-isoprostane levels in lung homogenates, stimulates the expression of NF-κB, and nonsignificantly influences the expression of nuclear factor 2 (Nrf2). Exercise training significantly reduces the effect of WPS on inflammatory and oxidative stress markers, averts DNA damage, inhibits the effect of NF-κB overactivation, and activates the Nrf2 signaling pathway. The authors emphasized that the protective impact of regular exercise training could be explained by its anti-inflammatory and antioxidant effects.

B. Skrzep-Poloczek et al. examined the influence of duodenal-jejunal omega switch surgery (DJOS) in combination with high-fat (HF) or control (CD) diet on the antioxidant status in the soleus muscle of rats. The authors emphasized that both obesity and chronic use of fat diet are related to enhance oxidative stress, which in turn causes many unfavorable health problems. Among these consequences, altered lipid and glucose metabolism in skeletal muscle may be observed. Under obesogenic conditions, including high-fat diet, the ability of the muscle tissue to oxidize the fat content was strongly reduced and could lead to an increased level of ROS. Surgical treatment of obesity may be considered as a metabolic surgery because it causes not only a reduction in body weight but also influences different metabolic pathways. Thus, in the Skrzep-Poloczek et al. experiment, after eight weeks of HF or CD diet, rats were subjected to DJOS or control (SHAM) surgery. After surgery, half of DJOS/SHAM rats had a changed diet, and half had the same type of food. The authors observed significantly lower CAT and GPx activities in the rat soleus muscle after DJOS, regardless of the type of diet. In turn, the activities of CAT, SOD, glutathione reductase (GR), Cu-Zn-SOD, and GPx are altered in the CD/HF or HF/CD group. After DJOS, the lowest muscle concentration of MDA is observed in the CD/CD group and the highest in the CD/HF group. It was shown in this study that DJOS surgery significantly decreases antioxidant systems in the soleus muscles of rats. CD/HF and HF/CD dietary patterns lead to an increase in antioxidant activity, while remaining on unchanged diet (CD or HF) is associated with reduced oxidative stress. The authors concluded that metabolic surgery together with mixed dietary patterns could be used as a strategy to modulate oxidative stress under pathological conditions.

In their study, A. Stanek et al. aimed to estimate the impact of whole body cryotherapy (WBC) performed in a closed cryochamber on oxidative stress in patients with ankylosing spondylitis (AS). WBC is a method of physical medicine, used in the treatment of rheumatic and inflammatory diseases and muscle spasticity. In the experiment, the effect of ten WBC procedures lasting 3 minutes a day with

a subsequent 60-minute session kinesiotherapy on oxidative stress in male AS patients was investigated. The WBC group was compared to the kinesiotherapy (KT) group. To assess the disease activity, the Bath Ankylosing Spondylitis Diseases Activity Index (BASDAI) and Bath Ankylosing Spondylitis Functional Index (BASFI) were calculated. The antioxidant enzymatic and nonenzymatic status, lipid peroxidation products, total oxidative status (TOS), and oxidative stress index (OSI) were measured one day before the beginning and one day after the completion of the research program. According to the authors, WBC procedures performed in a closed cryochamber with subsequent kinesiotherapy significantly decrease oxidative stress as well as BASDAI and BASFI indexes in AS patients during the active phase of the disease.

Finally, Y. Spanidis et al. evaluated the effects of the training background on free radical generation and adaptations after eccentric exercise. In the experiment, trained and untrained volunteers performed eccentric exercise. Biomarkers of oxidative damage and the antioxidant profile of the participants were measured in plasma and erythrocyte lysate at baseline and 24, 48, and 72 hours after the conducted exercise. The authors found more severe oxidative damage, weaker antioxidant status, and weaker radical scavenging activity in the untrained group compared to the trained participants. Their research showed that trained individuals are less susceptible to oxidative damage, suggesting that generalized nutritional recommendations regarding recovery after exercise should be avoided. The authors emphasized that individualized nutritional approach could help to fine-tune the recovery process and consequently improve health status and performance after eccentric exercise.

Overall, the work reported in this special issue highlights the significance of different strategies modulating oxidative stress in diverse physiological and pathological conditions. Moreover, the attention is focused on our understanding regarding the molecular mechanisms of antioxidant action of some interesting procedures, including the use of specific substances, exercise training, cryotherapy, or metabolic surgery. New insight into the effect of regular training on pro/antioxidant balance is also provided.

Conflicts of Interest

The authors declare that there is no conflict of interest regarding the publication of this article.

Karolina Szewczyk-Golec
Jolanta Czuczejko
Przemko Tylzanowski
Joanna Lecka

Hindawi
Oxidative Medicine and Cellular Longevity
Volume 2018, Article ID 9396089, 17 pages
https://doi.org/10.1155/2018/9396089

Research Article

Exogenous Hydrogen Sulfide Supplement Attenuates Isoproterenol-Induced Myocardial Hypertrophy in a Sirtuin 3-Dependent Manner

Jingyao Zhang,[1] Jin Yu,[1,2] Yun Chen,[1] Lulu Liu,[1] Mengting Xu,[1] Linlin Sun,[1] Huiqin Luo,[1] Yuqin Wang,[1] and Guoliang Meng[1]

[1]*Department of Pharmacology, School of Pharmacy, Nantong University, Key Laboratory of Inflammation and Molecular Drug Target of Jiangsu Province, Nantong, 226001 Jiangsu, China*
[2]*Department of Pharmacology, Yancheng City No. 1 People's Hospital, Yancheng, 224001 Jiangsu, China*

Correspondence should be addressed to Guoliang Meng; mengguoliang@ntu.edu.cn

Received 16 April 2018; Accepted 11 October 2018; Published 17 December 2018

Academic Editor: Przemko Tylzanowski

Hydrogen sulfide (H_2S) is a gasotransmitter with a variety of cardiovascular protective effects. Sirtuin 3 (SIRT3) is closely related to mitochondrial function and oxidative stress. We found that NaHS increased SIRT3 expression in the preventive effect on isoproterenol- (ISO-) induced myocardial hypertrophy. We further investigated whether exogenous H_2S supplement improved ISO-induced myocardial hypertrophy in a SIRT3-dependent manner. 10-week-old male 129S1/SvImJ (WT) mice and SIRT3 knockout (KO) mice were intraperitoneally injected with NaHS (50 μmol/kg/d) for two weeks and then intraperitoneally injected with ISO (60 mg/kg/d) for another two weeks. In WT mice, NaHS significantly reduced the cardiac index of ISO-induced mice, decreased the cross-sectional area of cardiomyocytes, and inhibited the expressions of atrial natriuretic peptide (ANP) and brain natriuretic peptide (BNP) mRNA. The activity of total antioxidant capacity (T-AOC) and superoxide dismutase (SOD) in the myocardium was increased, but the level of malondialdehyde (MDA) was decreased. The fluorescence intensity of dihydroethidium staining for superoxide anion was attenuated. Optic atrophy 1 (OPA1) expression was upregulated, while dynamin-related protein 1 (DRP1) expression was downregulated. ERK, but not P38 and JNK, phosphorylation was downregulated. However, all above protective effects were unavailable in ISO-induced SIRT3 KO mice. Our present study suggested that exogenous H_2S supplement inhibited ISO-induced cardiac hypertrophy depending on SIRT3, which might be associated with antioxidant stress.

1. Introduction

Myocardial hypertrophy is a compensatory process with increased cardiac mass and myocardial contractility under a long-term pressure overload, which is beneficial to maintaining normal blood circulation [1]. However, there is no adequate coronary artery blood to meet the needs of the heart because hypertrophic myocardium requires more oxygen. It is easy to result in myocardial ischemia, myocardial contractility impairment, and eventually heart failure if the heart suffers from persistent pathological hypertrophy [2]. Multilevel and complex factors, such as oxidative stress, energy metabolism disorder, hemodynamic factors, neurohumoral factors, cardiovascular autocrine/paracrine factors, insulin resistance, microRNAs, and genetics, are involved in the progress of myocardial hypertrophy [3–9]. Until now, the exact molecular mechanism for myocardial hypertrophy is still incompletely clarified. It is important to find novel compounds to delay or reverse myocardial hypertrophy.

In the traditional concept, hydrogen sulfide (H_2S) is a gas with highly toxic, which damages physiological functions [10]. A small amount of high concentration of H_2S might achieve a fatal effect in a short time after inhalation [11]. But with the deepening understanding of H_2S in recent years, it has revealed that H_2S has important physiological functions in the nervous system, the immune system, the

digestive system, and so on [12–17]. H_2S widely exists in many mammals and is widely concerned as the third gasotransmitter followed by nitric oxide and carbon monoxide [18]. H_2S is mainly produced by three enzymes: cystathionine γ-lyase (CSE), cystathionine β-synthase (CBS), and 3-mercaptopyruvate sulfurtransferase (MPST) [19].

Our previous studies found that H_2S decreased blood pressure in spontaneously hypertensive rats (SHR) [20] and transverse aortic constricted mice [21], inhibited myocardial fibrosis in SHR [22], improved vascular endothelial function [23], and prevented diabetic atherosclerosis [24]. It suggested that H_2S played an important role in cardiovascular system. However, the mechanisms of H_2S on cardiac hypertrophy were not completely clear. Glucose-6-phosphate dehydrogenase [25], miR-133a upregulation [26], nuclear factor E2-related factor 2 (Nrf2) activation [27], and specific protein 1 S-sulfhydration [20] were previously thought to be the principal reasons for the protective effect of H_2S on myocardial hypertrophy. These studies suggested that the detailed mechanisms for the effects of H_2S on myocardial hypertrophy in different models were not completely consistent. Therefore, it is vital to explore the specific mechanism of H_2S for delaying or reversing myocardial hypertrophy.

Sirtuin 3 (SIRT3) is a histone deacetylase which was encoded by the SIRT3 gene and localized in the mitochondria [28]. It is found that SIRT3 deficiency promoted cardiac fibrosis and left ventricular dilatation, which might even deteriorate to decompensated cardiac dysfunction in the aging mice [29]. In the rodent model of heart failure, SIRT3 expression and activity were decreased. Levels of mitochondrial protein lysine acetylation were increased, which might promote oxidative stress [30]. Impaired SIRT3 blocked fatty acid oxidation, glucose oxidation, tricarboxylic acid cycle, and oxidative phosphorylation, which might be a potential mechanism for contraction dysfunction and adaptation impairment [31–33]. Contrarily, SIRT3 protected the heart from reactive oxygen species- (ROS-) induced oxidative damage. Different pharmacological approaches to increase SIRT3 expression or to enhance SIRT3 activity were a potent strategy to attenuate myocardial hypertrophy and other cardiovascular diseases [34–38]. Our previous research also found that H_2S increased SIRT3 promoter activity and SIRT3 expression in angiotensin II-induced cardiomyocyte hypertrophy [21]. However, the detailed information about the potential role of SIRT3 on myocardial hypertrophy by H_2S *in vivo* was not known well.

As well as we know, dynamin-related protein 1 (DRP1) is a mitochondrial fission-associated protein, while optic atrophy 1 (OPA1) is a mitochondrial fusion-associated protein [39–42]. The balance of DRP1 and OPA1 plays an important role in maintaining mitochondrial structure and function. However, whether H_2S regulated DRP1 and OPA1 in the protective effect against myocardial hypertrophy was unknown.

The aims of the present study were to examine whether exogenous H_2S supplement attenuated isoproterenol- (ISO-) induced myocardial hypertrophy in SIRT3 knockout (KO) mice. It is beneficial to elucidate the possible role of SIRT3 in this protective effect of H_2S.

2. Materials and Methods

2.1. Treatment of Animals. Male C57BL/6, 129S1/SvImJ (WT), and SIRT3 knockout (KO) mice at 10 weeks of age were randomly administrated with NaHS (50 μmol/kg/d; Sigma-Aldrich, St. Louis, MO, USA) or normal saline (NS) once daily. After 2 weeks, the mice were given isoproterenol (ISO, 60 mg/kg; Sigma-Aldrich, St. Louis, MO, USA) by intraperitoneal injection to induce myocardial hypertrophy followed by NaHS or NS administration once daily for another 2 weeks [43].

Animal experiments were performed in accordance with the NIH guidelines for Care and Use of Laboratory Animals. The study was approved by the Committee on Animal Care of Nantong University (approval no. NTU-ERLAUA-20160115).

2.2. Measurement of Blood Pressure. After 2-week administration of ISO, systolic blood pressure (SBP), diastolic blood pressure (DBP), and mean arterial pressure (MAP) were detected from left carotid artery before sacrifice.

2.3. Echocardiography. After treatment, mice were anesthetized with isoflurane (1.5%). Echocardiography was used to detect the heart configuration through parasternal long axis view using a small animal color ultrasonic diagnostic apparatus (Visual Sonic Vevo 2100) with 30 MHz probe. Images were obtained by M-mode echocardiography. Thickness of inter ventricular septum (IVS) and left ventricular posterior wall (LVPW) was recorded. The average ejection fraction (EF) and left ventricular fraction shortening (FS) in 10 cycles were calculated.

2.4. Measure of H_2S Concentration in the Plasma and H_2S Production in the Myocardium. H_2S specific microelectrodes (World Precision Instruments) connected to the free radical analyzer (TBR4100, World Precision Instruments) were used to measure the concentration of H_2S in the plasma [23]. The sensor was depolarized before the experiment and then was calibrated with different concentration of Na_2S (0.5, 1, 2, 4, and 8 μmol/L). The current increased after the plasma was added. According to the enhanced current and Na_2S concentration, the standard curve was drawn, and the concentration of H_2S in plasma was calculated.

Myocardial homogenate was prepared with potassium phosphate buffer (1/10, myocardial tissue weigh/buffer volume). After centrifugation, H_2S production in the myocardium was measured as previously described, which represented the activity of H_2S synthase enzymes [23]. CSE, CBS, and MPST mRNA expressions were measured by quantitative real-time PCR.

2.5. Measurement of Cardiac Index. After echocardiography, the hearts were collected. The heart weight (HW) and left ventricular weight (LVW) were measured. The heart mass index (HMI) and left ventricular mass index (LVMI) were normalized by body weight (BW). HMI was represented as the ratio of HW to BW. LVMI was represented as the ratio of LVW to HW. The tibia length (TL) from the tibial plateau to medial malleolus of the right hindlimb was measured. The

ratio of LVW to TL was calculated, which was proportional to heart mass.

2.6. Wheat Germ Agglutinin (WGA) Staining. Heart tissue sections were reconstituted with different concentrations of ethanol (100%, 95%, 85%, 75%, and 50% for 1 min, respectively), then were washed in distilled water for 1 min. Tissue sections were washed with 0.1 M PBS on a shaker 3 times for 5 min. After drying, the sections were put in a dark box and were incubated with working solution containing WGA-FITC (100 μg/mL; Sigma-Aldrich, St. Louis, MO, USA) and $CaCl_2$ (1 mM) for 60 min. After washing carefully for 3 times with PBS, tissue sections were photographed with a fluorescence microscope. Cardiomyocyte areas were quantified by morphometric analysis.

2.7. Quantitative Real-Time PCR. The total RNA of myocardium was extracted by Trizol separation reagent according to the reagent instructions. RNA sample was subjected to reverse transcription with the following procedure: 37°C 15 min, 85°C 5 s, and 4°C forever. The cDNAs were amplified with SYBR Green Fast qPCR mix (Takara, Otsu, Shiga, Japan) using ABI StepOne PCR System (ABI, Carlsbad, CA, USA). 18S was serviced as the house-keep gene. The average cycle threshold (CT) values from triplicate experiments were normalized to 18S, and the group of WT + NS was served as control samples. Relative mRNA expressions were calculated as the fold of control samples. The structures of all primers used are listed in Table 1.

2.8. Measurement of Superoxide Formation in Myocardium. Superoxide production in myocardium was measured with the fluorescent probe dihydroethidium (DHE). After incubation with DHE (Beyotime, Shanghai, China; 2 μM) in Krebs' 4-(2-hydroxyethyl)-1-piperazineethanesulfonic acid (HEPES) buffer (NaCl 99 mM, KCl 4.7 mM, $MgSO_4$ 1.2 mM, KH_2PO_4 1.0 mM, $CaCl_2$ 1.9 mM, $NaHCO_3$ 25 mM, glucose 11.1 mM, Na HEPES 20 mM; pH 7.4) at 37°C for 30 min, myocardial sections (5 μm) were examined with fluorescence microscope (Nikon, Tokyo, Japan) with excitation and emission wavelengths at 480 nm and 610 nm, respectively.

Myocardial malondialdehyde (MDA) level in myocardium was measured with thiobarbituric acid method (Beyotime, Shanghai, China) and was represented as nmol/mg protein. Myocardial total antioxidant capacity (T-AOC) was assessed with 2,2′azino-bis(3-ethylbenzthi-azoline-6-sulfonic acid, ABTS) method (Beyotime, Shanghai, China) and was represented as μmol/mg protein. The myocardial activity of total superoxide dismutase (SOD), Cu-Zn/SOD, and Mn-SOD was evaluated with 2-(4-Iodophenyl)-3-(4-nitrophenyl)-5-(2,4-disulfophenyl)-2H-tetrazolium (WST-1) method (Beyotime, Shanghai, China) and was represented as U/mg protein. The detailed experimental procedure was performed according to the information of the kits.

2.9. Western Blot Analysis. Mitochondria in the myocardium were collected with a Tissue Mitochondria Isolation Kit (Beyotime, Shanghai, China). Total proteins or mitochondrial proteins extracted from myocardium lysates were separated by SDS-polyacrylamide gel electrophoresis and transferred to a PVDF membrane (Millipore, Billerica, MA, USA). After blocking in TBST with 5% nonfat milk for 2 h, protein blots were incubated overnight with anti-OPA1 (1 : 1000; Santa Cruz Biotechnology, Santa Cruz, CA, USA), anti-DRP1, anti-extracellular-regulated protein kinase (ERK), phosphor-ERK, P38, phosphor-P38, c-Jun N-terminal kinase (JNK), phosphor-JNK (1 : 1000, Cell Signaling Technology, Danvers, MA, USA), anti-voltage-dependent anion-selective channel proteins 1 (VDAC1, 1 : 1000; Santa Cruz Biotechnology, Santa Cruz, CA, USA), and anti-GAPDH (1 : 5000, Sigma-Aldrich, St. Louis, MO, USA) at 4°C followed by horseradish peroxidase- (HRP-) conjugated secondary antibody at room temperature for 2 h. Enhanced chemiluminescence (ECL, Thermo Fisher Scientific Inc., Rockford, IL, USA) was added to visualize the protein bands.

2.10. Immunofluorescence. Frozen sections of myocardium were incubated with anti-OPA1 (1 : 50; Santa Cruz Biotechnology, Santa Cruz, CA, USA) and anti-DRP1 (1 : 50; Cell Signaling Technology, Danvers, MA, USA) antibodies overnight at 4°C followed by Alexa Fluor 488- or Cy3-conjugated IgG (1 : 500; Beyotime, Shanghai, China) at 37°C for 1 h. The nuclei were counterstained with DAPI for several seconds. Tissue sections were photographed with a fluorescence microscope.

2.11. Statistical Analysis. All data were expressed as mean ± standard error of the mean (SEM) and were analyzed by 1-way ANOVA followed by Bonferroni post hoc test as appropriate (Stata13.0 software, Stata Corp, College Station, TX, USA). Values of $P < 0.05$ were considered as statistically significant.

3. Result

3.1. NaHS Inhibited Myocardial Hypertrophy and Increased SIRT3 Expression in the Mice after ISO Administration. ISO administration increased ANP and BNP mRNA expressions, and these hypertrophic indicators were significantly inhibited by NaHS (Figures 1(a)–1(b)).

We then assessed the involvement of SIRT1-SIRT7 in the protective effect of NaHS on ISO-induced myocardial hypertrophy. The mRNA expression of SIRT1 and SIRT3 was reduced in the myocardium after ISO administration, while that of SIRT2 and SIRT4-SIRT7 kept unchanged. The expression of SIRT3 mRNA, but not SIRT1, was restored by NaHS, suggesting that SIRT3, but not SIRT1, was involved in the preventive effect of NaHS on ISO-induced hypertrophy (Figure 1(c)). Further experiments confirmed that NaHS increased SIRT3 protein expression in ISO-administrated mice (Figure 1(d)).

3.2. NaHS Did Not Change Blood Pressure in Both WT Mice and SIRT3 KO Mice after ISO Administration. As well as we know, blood pressure is one of the important factors to affect cardiac hypertrophy [44]. In the present study, invasive blood pressure including SBP, DBP, and MAP showed no significant difference in different groups (Figures 2(a)–2(c)).

Table 1: Sequences of primers for mice.

Gene	Sense primer	Antisense primer
SIRT1	5′-CGGCTACCGAGGTCCATATAC-3′	5′-CAGCTCAGGTGGAGGAATTGT-3′
SIRT2	5′-GAGCCGGACCGATTCAGAC-3′	5′-AGACGCTCCTTTTGGGAACC-3′
SIRT3	5′-GGATTCGGATGGCGCTTGA-3′	5′-CACCTGTAACACTCCCGGAC-3′
SIRT4	5′-GAGCATTCTTACTAGGGATTCCA-3′	5′-AACGGCTAAACAGTCGGGTT-3′
SIRT5	5′-GCCACCGACAGATTCAGGTT-3′	5′-CCACAGGGCGGTTAAGAAGT-3′
SIRT6	5′-CCAAATCGTCAGGTCAGGGA-3′	5′-CAGAGTGGGGTACAGGGATG-3′
SIRT7	5′-CTAAGCGAAGCGGAGCCTAC-3′	5′-GTGGAGCCCATCACAGTTCT-3′
ANP	5′-GAGAAGATGCCGGTAGAAGA-3′	5′-AAGCACTGCCGTCTCTCAGA-3′
BNP	5′-CTGCTGGAGCTGATAAGAGA-3′	5′-TGCCCAAAGCAGCTTGAGAT-3′
CSE	5′-GCTTGGAAAAAGCAGTGGCT-3′	5′-TCGTAATGGTGGCAGCAAGA-3′
CBS	5′-AGCTGGAACCTGCTCCTTTT-3′	5′-GTTGGCTCTTGAGTCCCCTC-3′
MPST	5′-TGGTATCTGCTACCCAACGC-3′	5′-CAGAGCTCGGAAAAGTTGCG-3′
18S	5′-AGTCCCTGCCCTTTGTACACA-3′	5′-CGATCCGAGGGCCTCACTA-3′

3.3. NaHS Enhanced Plasma H_2S Level and Myocardial H_2S Production in Both WT Mice and SIRT3 KO Mice after ISO Administration. H_2S concentration in plasma and H_2S production in myocardium was decreased in ISO-administrated mice, which was restored by *NaHS* in both WT mice and SIRT3 KO mice (Figures 3(a)–3(b)). ISO also reduced CSE mRNA expression, which was rescued by NaHS in all the mice (Figure 3(c)). There was no significant difference in the expression of CBS and MPST mRNA in different groups (Figures 3(d)–3(e)).

3.4. NaHS Improved Cardiac Configuration in WT Mice but Not in SIRT3 KO Mice after ISO Administration. In order to assess the effect of H_2S on cardiac hypertrophy in mice, echocardiography was used to detect the cardiac configuration. It was found that after two weeks of ISO administration, the thickness of IVS and LVPW significantly increased, which was reduced by NaHS in WT mice. However, NaHS failed to decrease IVS and LVPW thickness in SIRT3 KO mice (Figures 4(a)–4(c)). There was no statistical difference between EF and FS in each group (Figures 4(d)–4(e)).

3.5. NaHS Decreased Cardiac Indexes in WT Mice but Not in SIRT3 KO Mice after ISO Administration. After echocardiography, the cardiac index was measured. ISO administration increased HW, HMI, LVMI, and LVW/TL, which was attenuated by NaHS in WT mice. However, the inhibitory effect on cardiac index by NaHS was unavailable in SIRT3 KO mice (Figures 5(a)–5(d)).

3.6. NaHS Attenuated Myocardial Hypertrophy in WT Mice but Not in SIRT3 KO Mice after ISO Administration. WGA staining was used to measure the cross-sectional areas of cardiomyocytes. It was found that cell areas were increased after 2-week ISO administration. NaHS reduced the areas of cardiomyocytes in WT mice but not in SIRT3 KO mice (Figures 6(a)–6(b)). NaHS also alleviated two hypertrophic genes ANP and BNP expressions in WT mice but not in SIRT3 KO mice (Figure 6(c)).

3.7. NaHS Suppressed Oxidative Stress in WT Mice but Not in SIRT3 KO Mice after ISO Administration. After ISO administration, myocardial DHE fluorescence and level of MDA were elevated, suggesting more superoxide production and severe oxidative stress. After NaHS pretreatment, above two parameters for oxidative stress were reduced significantly in WT mice but not in SIRT3 KO mice (Figures 7(a)–7(b)). ISO also impaired myocardial T-AOC and total SOD activity (especially Mn-SOD but not Cu-Zn/SOD), which was restored by NaHS in WT mice but not in SIRT3 KO mice (Figures 7(c)–7(d)).

3.8. NaHS Alleviated Myocardial ERK Phosphorylation in WT Mice but Not in SIRT3 KO Mice after ISO Administration. Mitogen-activated protein kinases (MAPKs) family (including ERK1/2, P38, and JNK) is one of the most important downstream signal pathways of oxidative stress [45]. The present study found that phosphorylation of ERK, but not P38 or JNK, was enhanced in the myocardium of mice after ISO administration, while NaHS diminished myocardial ERK phosphorylation in WT mice but not in SIRT3 KO mice after ISO administration (Figures 8(a)–8(c)).

3.9. NaHS Enhanced OPA1 Expression but Attenuated DRP1 Formation in WT Mice but Not in SIRT3 KO Mice after ISO Administration. OPA1 is a vital protein to maintain mitochondrial fusion, while DRP1 is important to regulate mitochondrial fission [46]. Immunofluorescence and western blot were used to detect the expression of the above two proteins. We found that OPA1 fluorescent intensity and protein expression were impaired, but DRP1 formation was increased in hypertrophic myocardium after ISO

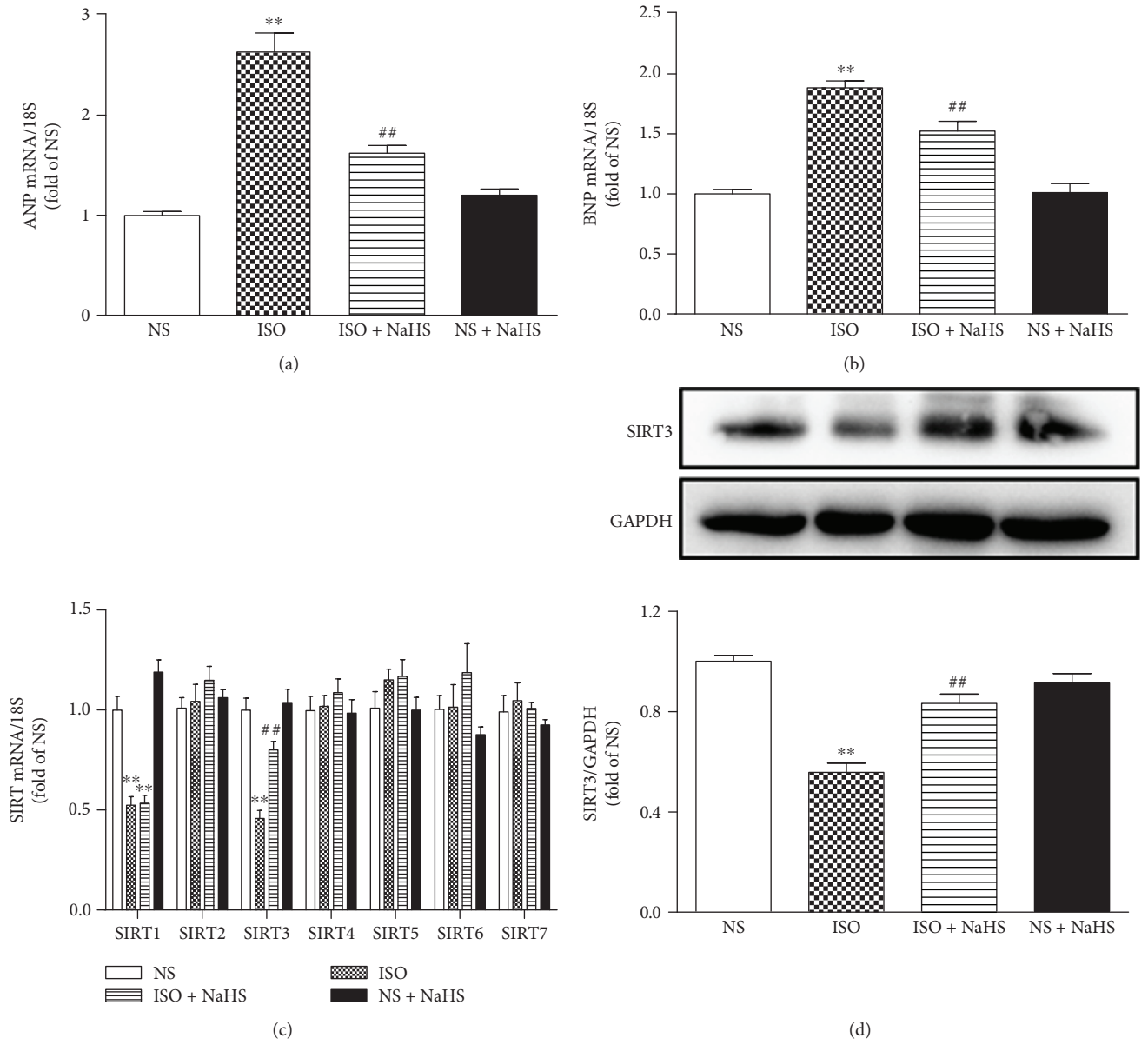

Figure 1: Effect of NaHS on myocardial hypertrophy and SIRT3 expression in the mice after ISO administration. Male C57BL/6 mice at 10 weeks of age were administrated with NaHS (50 μmol/kg/d) or normal saline (NS) once daily. After 2 weeks, the mice were given isoproterenol (ISO, 60 mg/kg) by intraperitoneal injection followed by NaHS or NS administration once daily for another 2 weeks. (a–b) ANP and BNP mRNA expressions were quantified by real-time PCR. 18S was serviced as a house-keep gene. (c) Quantification of SIR2 family (SIRT1-SIRT7) mRNA expression was assessed by real-time PCR. 18S was serviced as a house-keep gene. (d) The expression of SIRT3 protein in the myocardium of mice was measured by western blot. GAPDH was serviced as a loading control. Plots represent the mean ± SEM; $n = 6$. Statistical significance: $^{**}P < 0.01$ compared with NS; $^{\#\#}P < 0.01$ compared with ISO.

administration. Moreover, NaHS enhanced OPA1 expression but attenuated DRP1 formation in WT mice but not in SIRT3 KO mice after ISO administration (Figures 9(a)–9(d)).

4. Discussion

Hypertension, as the key risk factor of cardiovascular disease, is the main cause of death in patients suffering from cardiovascular disease worldwide [47]. Studies have indicated that H_2S played an important role in hypertension. General knockout of CSE, as the main enzyme for H_2S production in cardiovascular system, resulted in lower H_2S content in serum, heart, aorta, and other tissues and impaired vascular diastolic function and higher blood pressure. Exogenous NaHS dosage dependently reduced blood pressure in CSE knockout mice [48]. H_2S supplementation attenuated hypertension in different hypertensive animal models [17]. Previous studies have found that H_2S donor GYY4137 prevented NG-nitro-L-arginine methyl ester- (L-NAME-) induced hypertension. The administration of GYY4137 significantly decreased blood pressure in SHR, and there was a gradual recovery without sudden rebound if GYY4137 was stopped

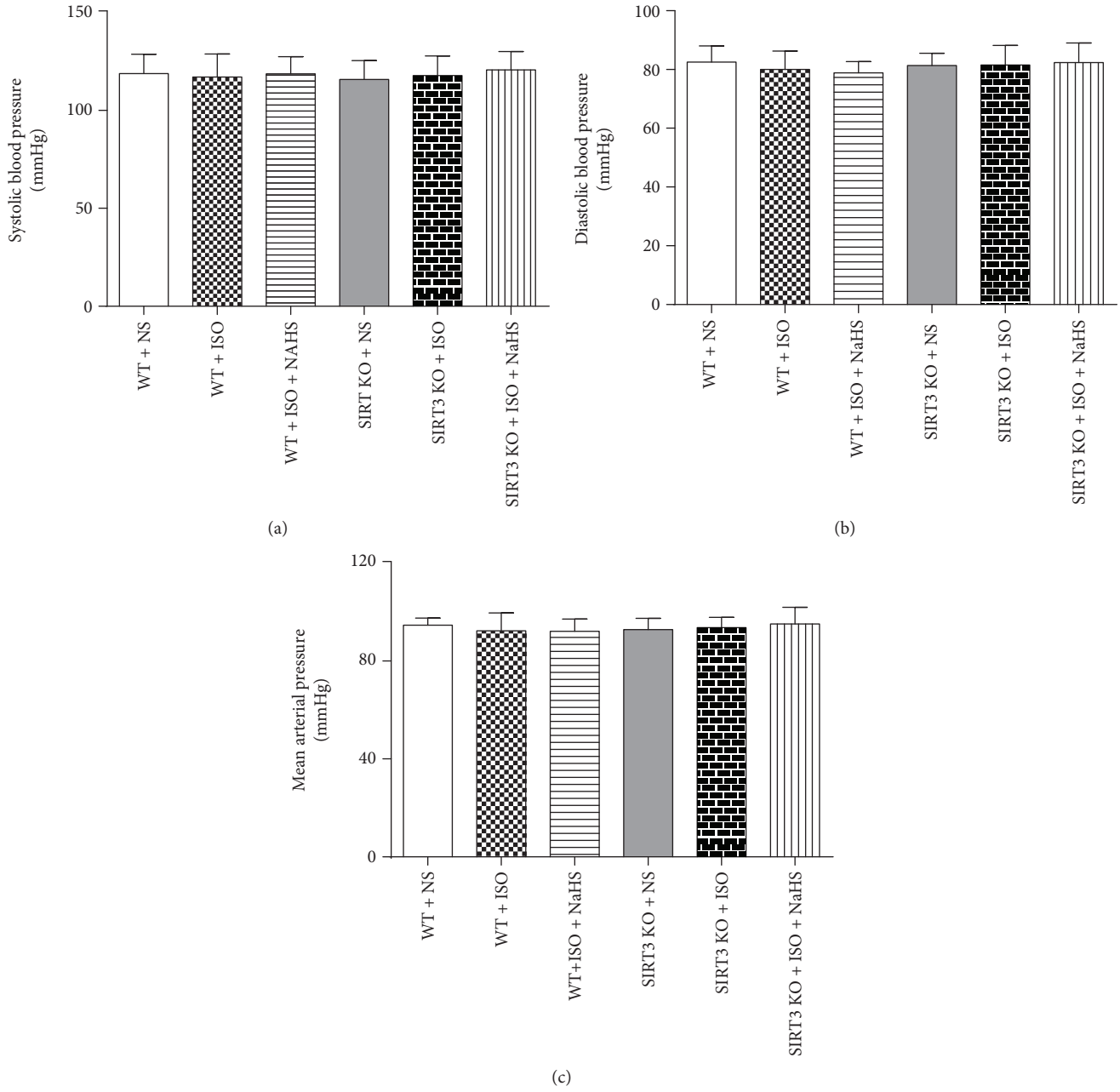

Figure 2: Effect of NaHS on blood pressure in WT mice and SIRT3 KO mice after ISO administration. Male 129S1/SvImJ (WT) and SIRT3 knockout (KO) mice at 10 weeks of age were administrated with NaHS (50 μmol/kg/d) or normal saline (NS) once daily. After 2 weeks, the mice were given isoproterenol (ISO, 60 mg/kg) by intraperitoneal injection followed by NaHS or NS administration once daily for another 2 weeks. (a–c) Invasive arterial blood pressures, including systolic blood pressure (SBP), diastolic blood pressures (DBP), and mean arterial pressure (MAP), were measured from left carotid artery. Plots represent the mean ± SEM; $n = 6$.

[49]. GYY4137 also reduced blood pressure in angiotensin II-induced hypertensive mice [50] and in SHR [20]. In normotensive animals, $Na_2S{\cdot}9H_2O$ saline solution at doses of 100 mg/kg and 300 mg/kg, but not of 30 mg/kg, induced a significant reduction on blood pressure in Wistar Kyoto rats. The administration of Na_2S in doses of 0.1–0.5 mg/kg with intravenous injection significantly decreased MAP in the anesthetized Sprague-Dawley rat [51]. In our present study, the reduction on SIRT1 after ISO administration could not be restored by NaHS, suggesting that SIRT1 is not involved in the protective effect by H_2S on ISO-induced myocardial hypertrophy. NaHS pretreatment only enhanced SIRT3 mRNA levels in the presence of ISO stimulation. Therefore, we focused on SIRT3 in subsequent experiments. Moreover, NaHS (50 μmol/kg/d) supplement restored endogenous H_2S level, but NaHS did not influence blood pressure in both WT mice and SIRT3 KO mice with normotension. It suggested that the different effects of NaHS on ISO-induced myocardial hypertrophy between WT mice and SIRT3 KO mice were not due to blood pressure or endogenous H_2S level.

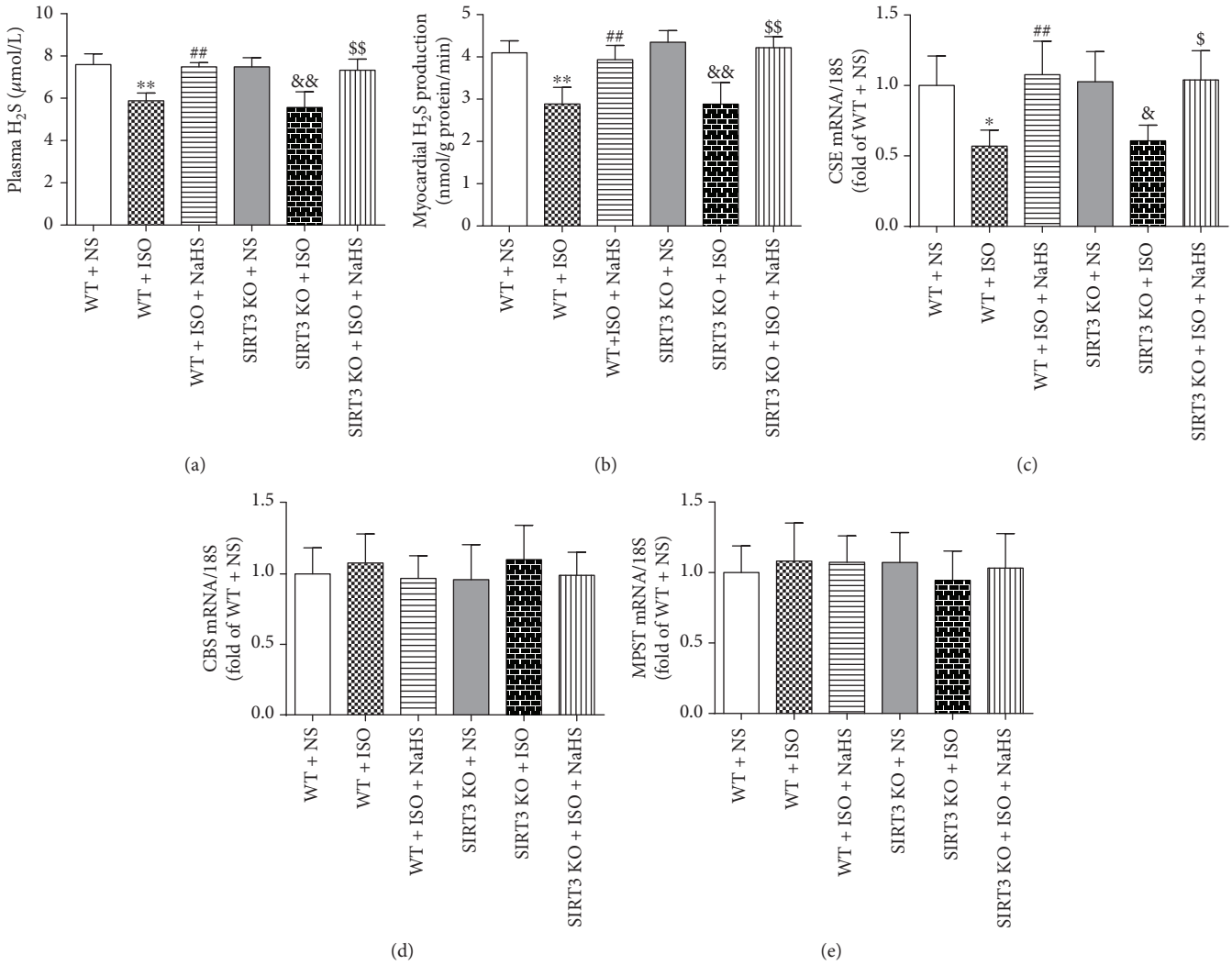

Figure 3: Effect of NaHS on plasma H_2S level and myocardial H_2S production in WT mice and SIRT3 KO mice after ISO administration. Male 129S1/SvImJ (WT) and SIRT3 knockout (KO) mice at 10 weeks of age were administrated with NaHS (50 μmol/kg/d) or normal saline (NS) once daily. After 2 weeks, the mice were given isoproterenol (ISO, 60 mg/kg) by intraperitoneal injection followed by NaHS or NS administration once daily for another 2 weeks. (a–b) Plasma H_2S level and myocardial H_2S production were measured with H_2S specific microelectrodes connected to the free radical analyzer. (c–e) CSE, CBS, and MPST mRNA expressions were measured by quantitative real-time PCR. 18S was serviced as a house-keep gene. Plots represent the mean ± SEM; $n = 6$. Statistical significance: $^{*}P < 0.05$, $^{**}P < 0.01$ compared with WT + NS; $^{\#\#}P < 0.01$ compared with WT + ISO; $^{\&}P < 0.05$, $^{\&\&}P < 0.01$ compared with SIRT3 KO + NS; $^{\$}P < 0.05$, $^{\$\$}P < 0.01$ compared with SIRT3 KO + ISO.

During hypertension, cardiomyocyte structure, function, and genetic phenotype are subjected into adaptive changes to result in myocardial hypertrophy gradually [52–54]. But there is controversy on the inhibitory effect of H_2S against cardiac hypertrophy. Some studies have confirmed that NaHS inhibited abdominal aortic constriction-induced cardiac hypertrophy [55]. NaHS alleviated myocardial hypertrophy via angiotensin type 1 receptor in 2-kidney 1-clip rats [56]. NaHS administration prior to transverse aortic constriction in mice or angiotensin II exposure in cardiomyocyte protected against hypertrophy via a PI3K/Akt-dependent Nrf2 pathway activation [57]. NaHS also inhibited high-salt diet-induced myocardial hypertrophy in rats [58]. However, it was also found that NaHS treatment for 3 months did not reduce the left ventricular weight index and other important indicators of cardiac hypertrophy [59]. The divergent effects of H_2S on cardiac hypertrophy might be due to the model types or degrees of myocardial hypertrophy, the pharmacokinetic characteristics of H_2S donor, or the times of H_2S administration. In our present study, cardiac configuration, cardiac index, cardiomyocyte areas, and hypertrophic genes expression suggested that NaHS effectively attenuated myocardial hypertrophy in WT mice but not in SIRT3 KO mice. Associated with the similar effect on blood pressure and H_2S concentration in all the mice, SIRT3 might be the critical factor on the protective effects against myocardial hypertrophy by H_2S.

H_2S has a potential ability of antioxidative stress in different tissues. Previous study found NaHS inhibited the levels of MDA and 4-hydroxy-2-trans-nonenal (4-HNE)

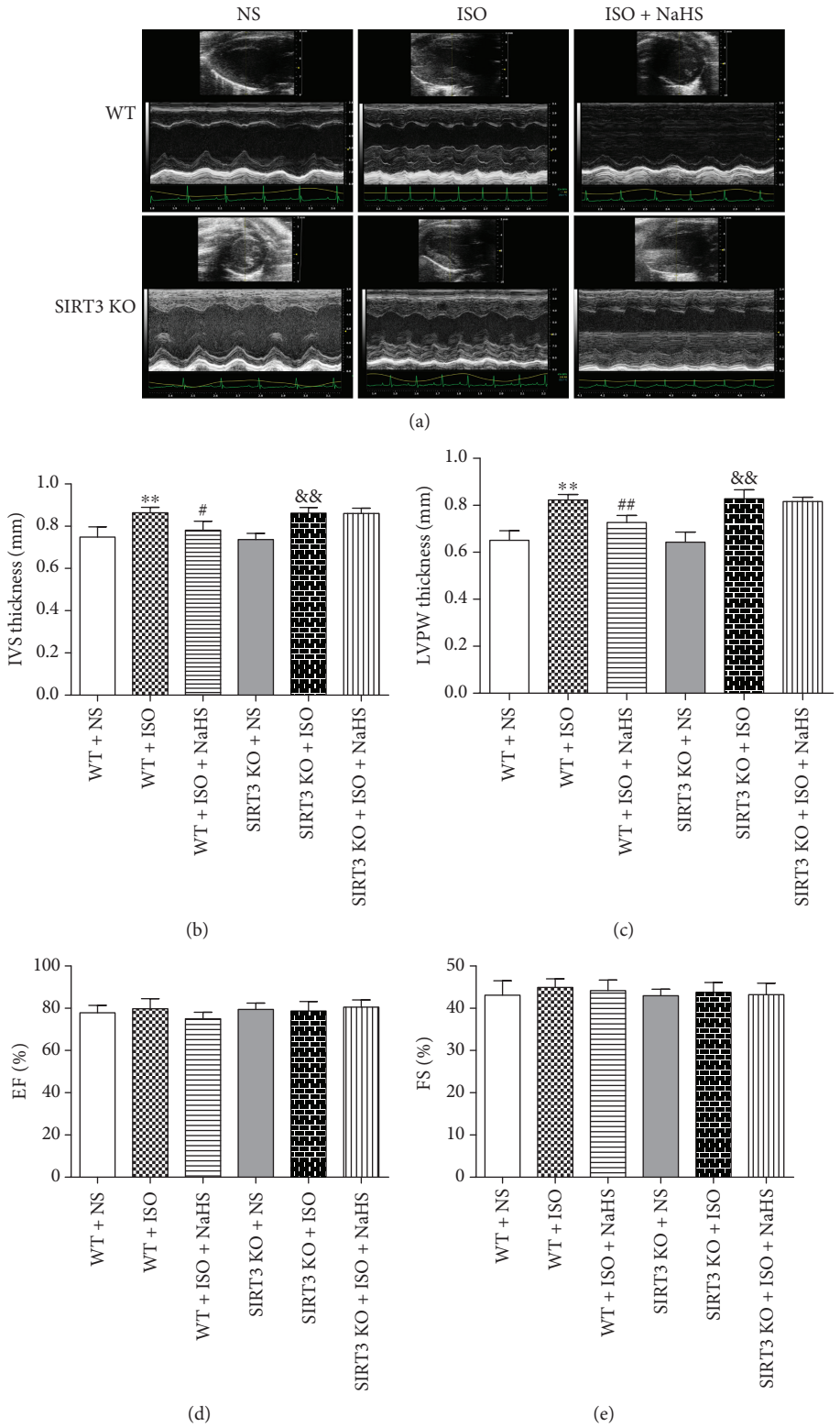

Figure 4: Effect of NaHS on cardiac configuration and function in WT mice and SIRT3 KO mice after ISO administration. Male 129S1/SvImJ (WT) and SIRT3 knockout (KO) mice at 10 weeks of age were administrated with NaHS (50 μmol/kg/d) or normal saline (NS) once daily. After 2 weeks, the mice were given isoproterenol (ISO, 60 mg/kg) by intraperitoneal injection followed by NaHS or NS administration once daily for another 2 weeks. (a) Representative 2-D M-mode echocardiograms of the heart by echocardiography. (b–c) IVS and LVPW thickness were quantified by echocardiography. (d–e) EF and FS were quantified by echocardiography. Plots represent the mean ± SEM; $n = 6$. Statistical significance: $^{**}P < 0.01$ compared with WT + NS; $^{\#}P < 0.05$, $^{\#\#}P < 0.01$ compared with WT + ISO; $^{\&\&}P < 0.01$ compared with SIRT3 KO + NS.

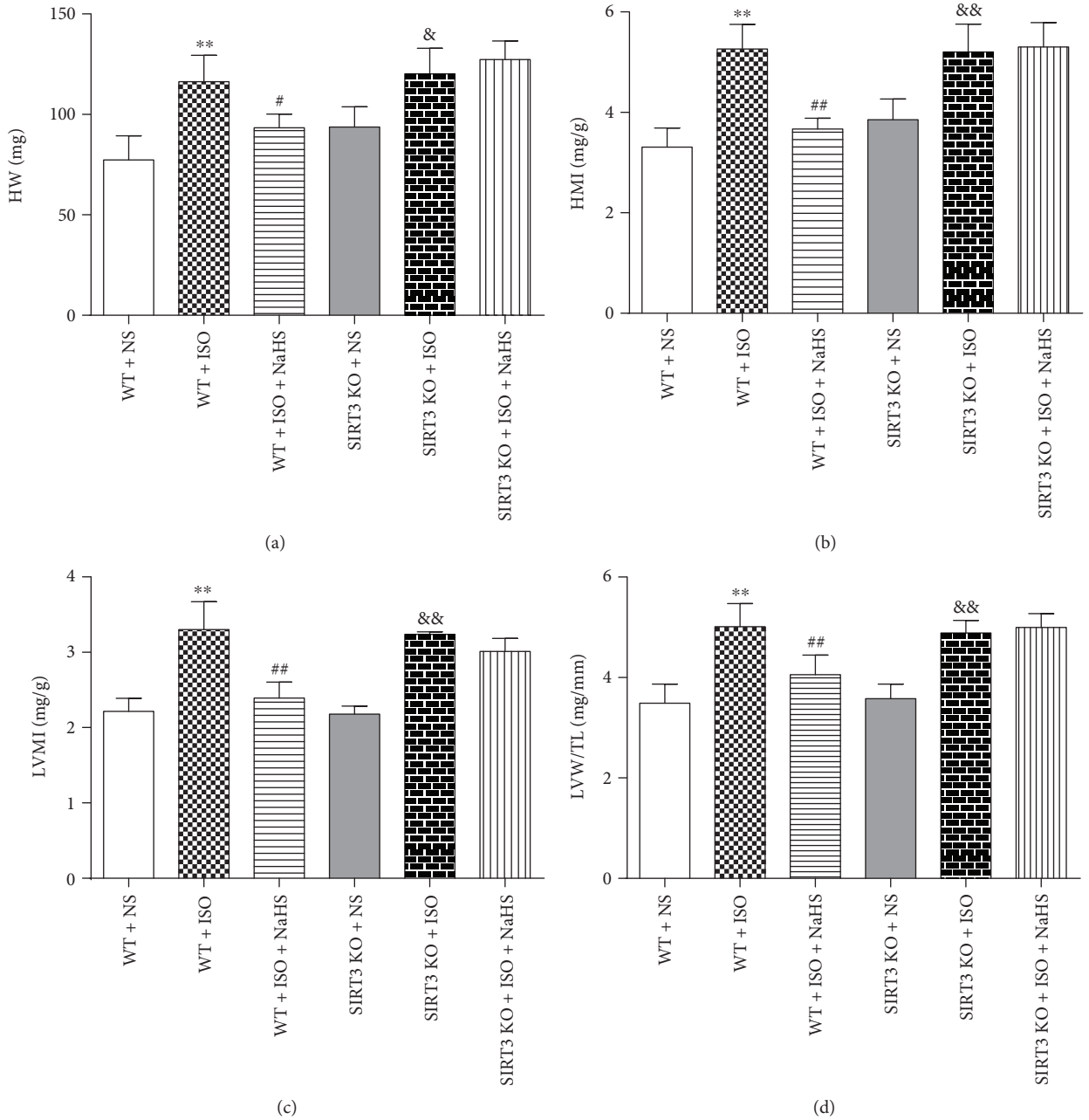

Figure 5: Effect of NaHS on cardiac indexes in WT mice and SIRT3 KO mice after ISO administration. Male 129S1/SvImJ (WT) and SIRT3 knockout (KO) mice at 10 weeks of age were administrated with NaHS (50 μmol/kg/d) or normal saline (NS) once daily. After 2 weeks, the mice were given isoproterenol (ISO, 60 mg/kg) by intraperitoneal injection followed by NaHS or NS administration once daily for another 2 weeks. (a) The heart was collected, and the heart weight (HW) was measured. (b–c) The heart mass index (HMI) and left ventricular mass index (LVMI) were normalized by body weight (BW). (d) The tibia length (TL) was measured, and the ratio of LVW to TL (LVW/TL) were calculated. Plots represent the mean ± SEM; $n = 6$. Statistical significance: $^{**}P < 0.01$ compared with WT + NS; $^{\#}P < 0.05$, $^{\#\#}P < 0.01$ compared with WT + ISO; $^{\&}P < 0.05$, $^{\&\&}P < 0.01$ compared with SIRT3 KO + NS.

in hippocampus of chronic unpredictable mild stress-induced rats [60]. Our latest research demonstrated that H_2S inhibited the generation of superoxide anion in artery of streptozotocin-administrated $LDLr^{-/-}$ mice and in high glucose and oxidized LDL-stimulated primary peritoneal macrophages, which indicated that H_2S suppressed oxidative stress in diabetes-accelerated atherosclerosis [24]. H_2S reduced the accumulation of intracellular ROS in alcoholic fatty liver [61], ameliorated oxidative injury in hypoxia/reoxygenation-treated aging cardiomyocytes [62], inhibited renal oxidative stress to alleviate high-salt diet-induced renal injury [63], and lightened smoke inhalation-induced oxidative stress and lung injury [64]. More importantly, H_2S exerts cardioprotective effect through antioxidant effects. H_2S reduced the ROS generation and accumulation in myocardium after myocardial ischemia reperfusion

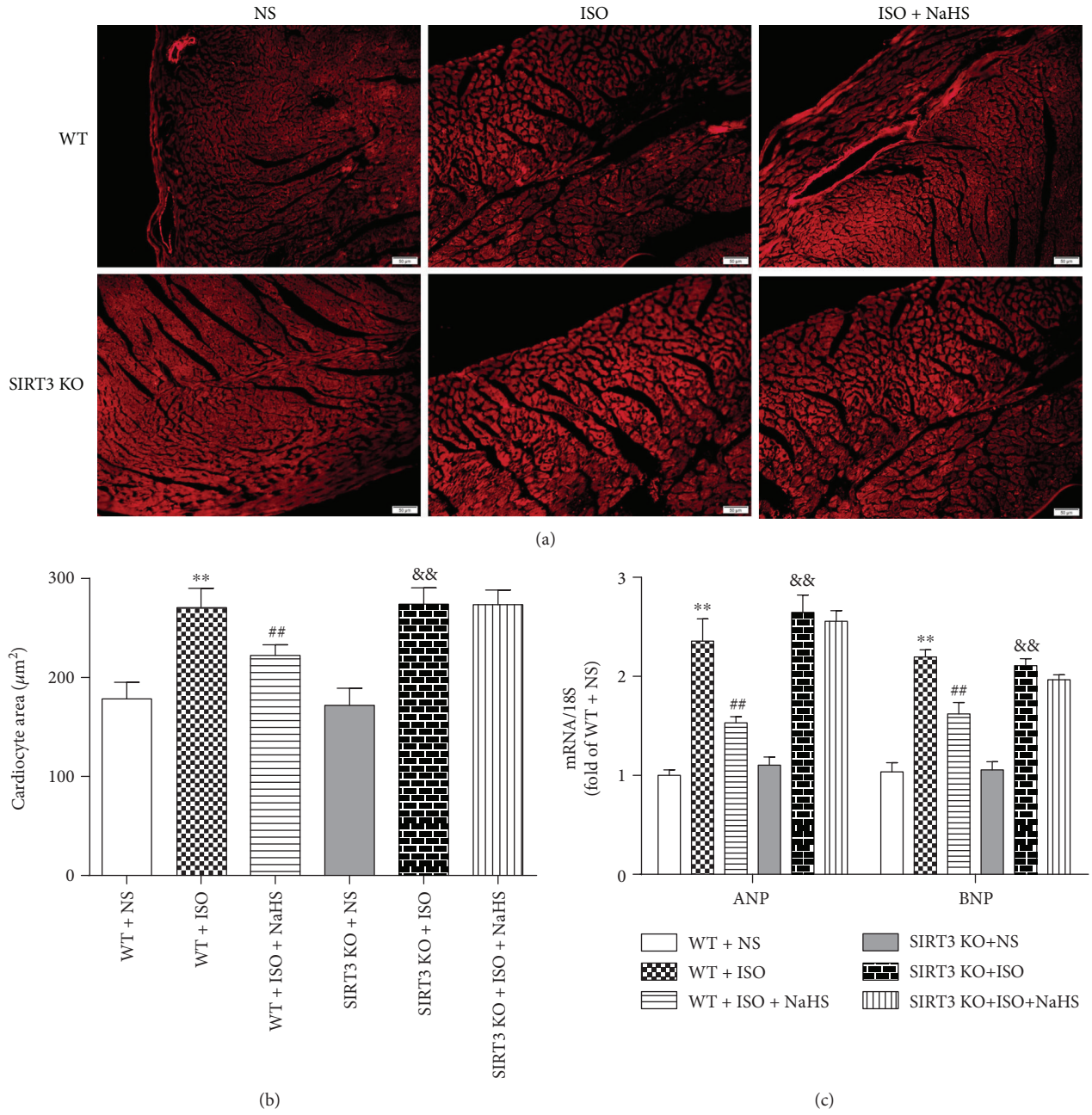

FIGURE 6: Effect of NaHS on myocardial hypertrophy in WT mice and SIRT3 KO mice after ISO administration. Male 129S1/SvImJ (WT) and SIRT3 knockout (KO) mice at 10 weeks of age were administrated with NaHS (50 μmol/kg/d) or normal saline (NS) once daily. After 2 weeks, the mice were given isoproterenol (ISO, 60 mg/kg) by intraperitoneal injection followed by NaHS or NS administration once daily for another 2 weeks. (a) The myocardium of mice was stained with WGA and was photographed with a fluorescence microscope. Bar = 50 μm. (b) Cardiomyocyte area was quantified by morphometric analysis. (c) ANP and BNP mRNA expressions were quantified by real-time PCR. 18S was serviced as a house-keep gene. Plots represent the mean ± SEM; $n = 6$. Statistical significance: $^{**}P < 0.01$ compared with WT + NS; $^{\#\#}P < 0.01$ compared with WT + ISO; $^{\&\&}P < 0.01$ compared with SIRT3 KO + NS.

[65]. Na_2S protected against oxygen-free radical induced myocardial cell death [66]. Our present study confirmed that NaHS decreased MDA levels in serum, attenuated superoxide anion production, and restored T-AOC and SOD activity in the heart of the WT mice after ISO administration, which verified the antioxidative ability of NaHS in myocardium hypertrophy.

Until now, the effect of H_2S on MAPK signaling pathway, which is one of the most important downstream signal pathways of oxidative stress, has not been completely consistent under different conditions. In smooth muscle cells, exogenous H_2S or overexpression of CSE activated ERK and p38 pathway [67]. H_2S increased ERK and P38 activity to induce apoptosis in human arterial smooth muscle cells, which

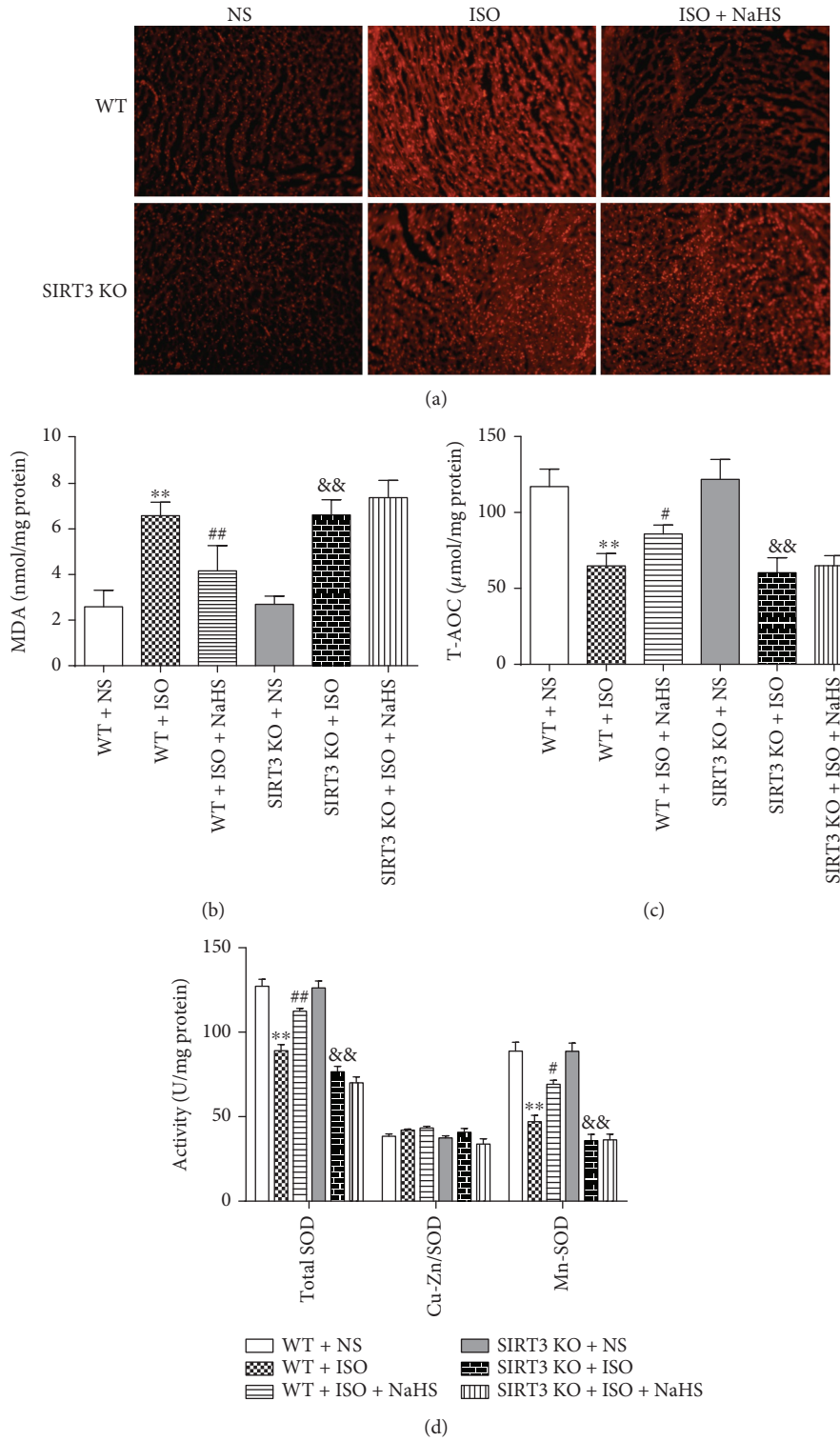

Figure 7: Effect of NaHS on oxidative stress in WT mice and SIRT3 KO mice after ISO administration. Male 129S1/SvImJ (WT) and SIRT3 knockout (KO) mice at 10 weeks of age were administrated with NaHS (50 μmol/kg/d) or normal saline (NS) once daily. After 2 weeks, the mice were given isoproterenol (ISO, 60 mg/kg) by intraperitoneal injection followed by NaHS or NS administration once daily for another 2 weeks. (a) The myocardium of mice was stained with DHE and was photographed with a fluorescence microscope. (b) MDA level in the myocardium was measured. (c) T-AOC of the myocardium was assessed. (d) SOD, Cu-Zn/SOD, and Mn-SOD activity of myocardium were evaluated. Plots represent the mean ± SEM; $n = 6$. Statistical significance: $^{**}P < 0.01$ compared with WT + NS; $^{\#}P < 0.05$, $^{\#\#}P < 0.01$ compared with WT + ISO; $^{\&\&}P < 0.01$ compared with SIRT3 KO + NS.

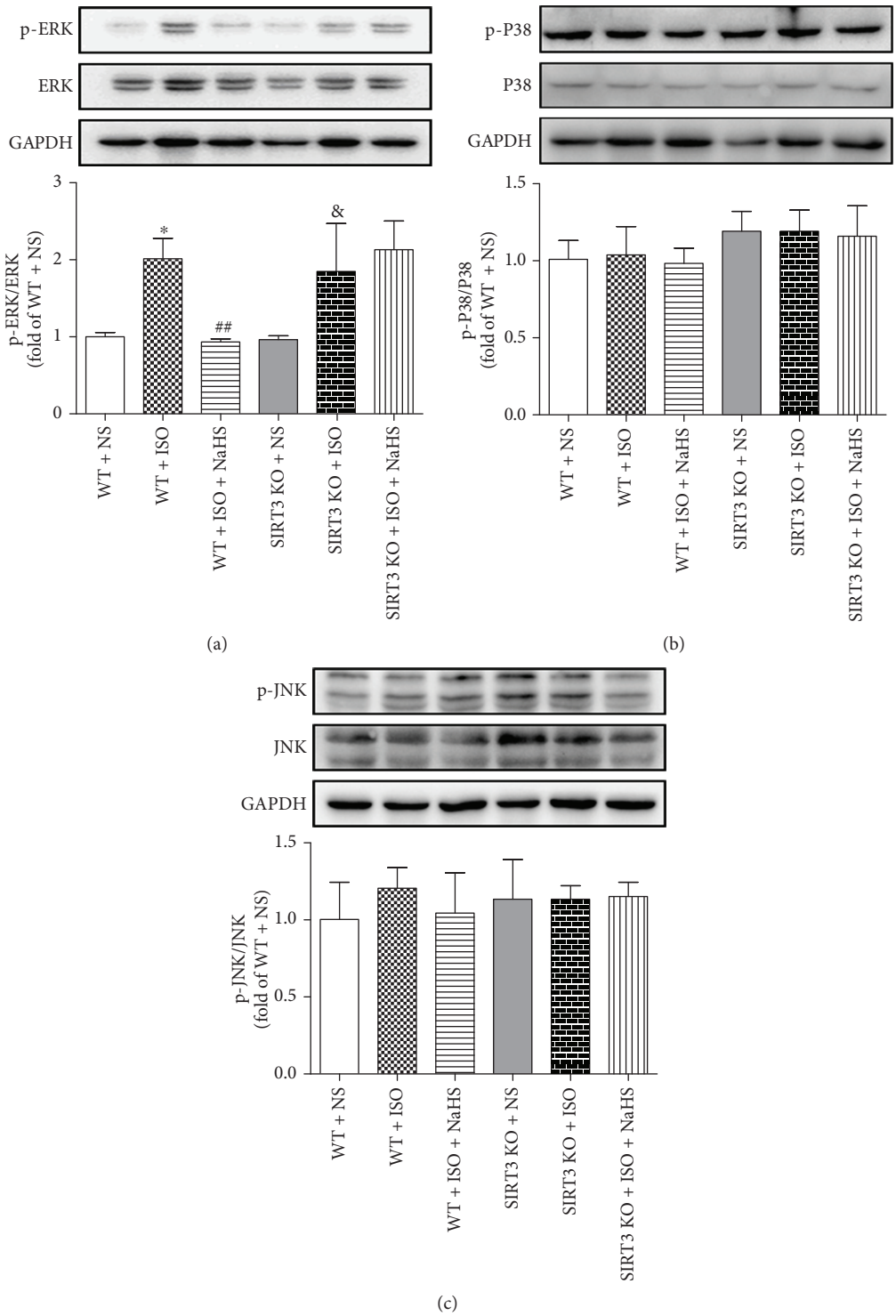

Figure 8: Effect of NaHS on MAPK expression and phosphorylation in WT mice and SIRT3 KO mice after ISO administration. Male 129S1/SvImJ (WT) and SIRT3 knockout (KO) mice at 10 weeks of age were administrated with NaHS (50 μmol/kg/d) or normal saline (NS) once daily. After 2 weeks, the mice were given isoproterenol (ISO, 60 mg/kg) by intraperitoneal injection followed by NaHS or NS administration once daily for another 2 weeks. (a–c) MAPK expression and phosphorylation in the myocardium of mice were measured by western blot. GAPDH was serviced as a loading control. Plots represent the mean ± SEM; $n = 6$. Statistical significance: $^{*}P < 0.05$ compared with WT + NS; $^{\#\#}P < 0.01$ compared with WT + ISO; $^{\&}P < 0.05$ compared with SIRT3 KO + NS.

was abolished by ERK inhibitors but not P38 inhibitors [68]. But ERK1/2 and P38 were considered as promoters of cardiac hypertrophy [69, 70]. NaHS concentration-dependent downregulated ERK expression and inhibited the proliferation of smooth muscle cells, but not in serum-free culture cells [71]. Na_2S preadministration 7 days before

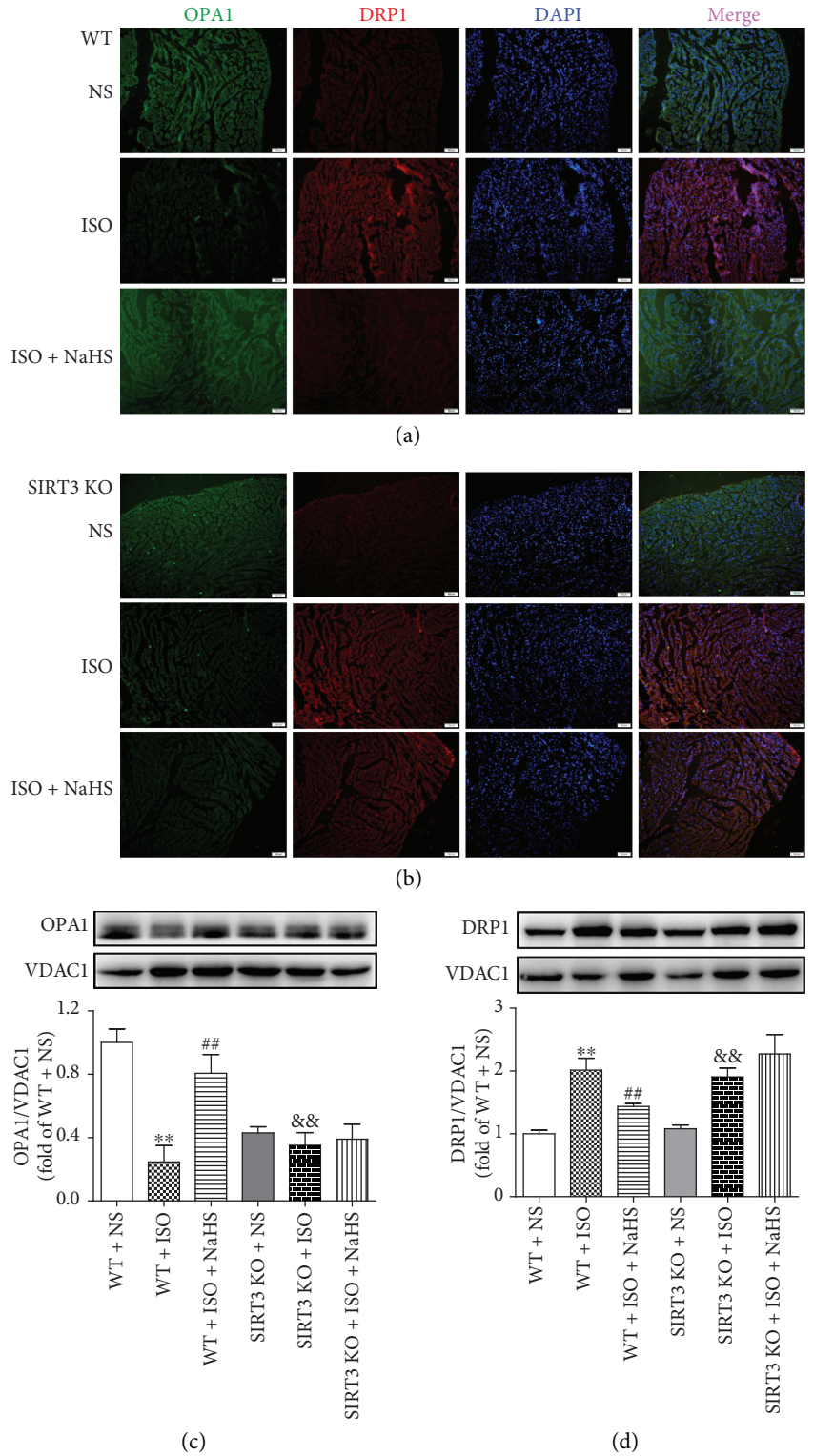

Figure 9: Effect of NaHS on OPA1 and DRP1 in WT mice and SIRT3 KO mice after ISO administration. Male 129S1/SvImJ (WT) and SIRT3 knockout (KO) mice at 10 weeks of age were administrated with NaHS (50 μmol/kg/d) or normal saline (NS) once daily. After 2 weeks, the mice were given isoproterenol (ISO, 60 mg/kg) by intraperitoneal injection followed by NaHS or NS administration once daily for another 2 weeks. (a–b) The myocardium of mice was stained with OPA1 and DRP1 followed by Alexa Fluor 488- or Cy3-conjugated IgG, respectively. Tissue sections were photographed with a fluorescence microscope. The nuclei were counterstained with DAPI (blue). Bar = 100 μm. (c–d) The expression of OPA1 and DRP1 in mitochondrial proteins from the myocardium of mice was measured by western blot. VDAC1 was serviced as a loading control. Plots represent the mean ± SEM; $n = 6$. Statistical significance: $^{**}P < 0.01$ compared with WT + NS; $^{\#\#}P < 0.01$ compared with WT + ISO; $^{\&\&}P < 0.01$ compared with SIRT3 KO + NS.

ischemia reperfusion significantly enhanced the phosphorylation of ERK to protect the heart from ischemia reperfusion injury in diabetic mice [72]. Exogenous H_2S protected H9C2 cardiac cells against high glucose-induced injury and attenuated doxorubicin-induced cardiotoxicity by inhibiting the activities of the P38 or ERK1/2 pathway [73, 74]. H_2S also alleviated doxorubicin-induced cardiomyopathy through suppressing JNK activation in the hearts [75]. Moreover, H_2S failed to decrease the phosphorylation of JNK, but it was still able to attenuate the phosphorylation of P38 and ERK in H_2O_2-stimulated endothelial cells [23]. Our study discovered that exogenous NaHS administration significantly decreased the phosphorylation of ERK in hypertrophic myocardium, which was unavailable in SIRT3 deficiency mice. In other words, although H_2S plays diverse roles on MAPK signal pathway with different status, H_2S-attenuated myocardial hypertrophy is, in part, mediated through blocking the ERK pathway via a SIRT3-dependent manner.

However, the detailed mechanism of the antioxidative ability of H_2S remains unknown until now. It was interesting to find that the above protective effects on myocardial hypertrophy were abolished in the SIRT3 KO mice in the present study. Our previous study also found that H_2S protected endothelial cells against oxidative stress in a SIRT3-dependent manner [23]. SIRT3 regulates the deacetylation of mitochondrial proteins, and the mitochondrial proteins were highly acetylated in the SIRT3 deficiency mice, which alleviated protein activity and disordered the ATP formation, suppressed the Krebs cycle, inhibited the electron transport chain transmission, and eventually aggravated the tissue damage and resulted in oxidative stress [76]. SIRT3 is vital for attenuating myocardial ischemia reperfusion injury [77, 78], maintaining vascular biology, and suppressing atherogenesis [79]. In contrast, SIRT3 overexpression in mice hearts protected against myocardial hypertrophy and fibrosis [80, 81]. These data indicated that SIRT3 was important in both physiology and oxidative stress-associated pathological situations [82]. Our study confirmed that NaHS attenuated myocardial hypertrophy in the WT mice, which might be related to the preventive effect on mitochondrial function and oxidative stress [83]. However, NaHS failed to attenuate IVS and LVPW thickness, cardiac indexes, cardiomyocyte area, hypertrophic gene expression, oxidative stress, and ERK phosphorylation in the SIRT3 KO mice, which might be related to the increased acetylated proteins after SIRT3 was deficient.

OPA1 regulates mitochondrial structure, respiratory regulation efficiency, respiratory chain component, and protein complex. It plays an important role in the maintenance of mitochondrial integrity and mitochondrial fusion [84, 85]. Previous studies found that the OPA1 was acetylated at lysine 926 and lysine 931 residues in SIRT3-deficient cells by mass spectrometry, so as to regulate mitochondrial dynamics during stress [86]. DRP1 is a member of the super family of protein in GTPases and is crucial for the fission of mitochondria and peroxidase in mammalian cells. It is considered to be the novel target for cardiovascular diseases [87–89]. We found that NaHS failed to enhance OPA1 expression and reduce DRP1 formation in ISO-administrated SIRT3 KO mice, which may be one of the reasons that NaHS failed to improve oxidative stress and myocardial hypertrophy after ISO administration in SIRT3 KO mice.

In conclusion, the study suggested that exogenous H_2S supplement inhibited ISO-induced cardiac hypertrophy depending on SIRT3, and the possible mechanisms might be associated with antioxidant stress. It highlighted a novel therapeutic target, SIRT3, for the protective effect of H_2S against myocardial hypertrophy.

Data Availability

The data used to support the findings of this study are available from the corresponding author upon request.

Conflicts of Interest

The authors declare that there is no conflict of interests regarding the publication of this paper.

Authors' Contributions

Jingyao Zhang, Jin Yu, and Yun Chen contributed equally to this study.

Acknowledgments

This work was supported by grants from the National Natural Science Foundation of China (81770279, 31500649), a major project of the Natural Science Research of Jiangsu Higher Education Institutions of China (18KJA310005), the project of the "Six Talent Peaks Project in Jiangsu Province" (2018-WSN-062), a project funded by the China Postdoctoral Science Foundation (2017M610342), Postgraduate Research & Practice Innovation Program of Jiangsu Province (1701050A), a research and innovation project of the Graduate Students in Jiangsu Province (KYCX18_2401, KYLX16_0979) and Nantong University (YKC16055), grants from the Natural Science Foundation of Nantong City (MS12015015, MS12015101), and the Nantong University Cooperative Innovation Program of Small Molecular Compound R&D (NTU2016-1).

References

[1] M. A. Peterzan, C. A. Lygate, S. Neubauer, and O. J. Rider, "Metabolic remodeling in hypertrophied and failing myocardium: a review," *American Journal of Physiology-Heart and Circulatory Physiology*, vol. 313, no. 3, pp. H597–H616, 2017.

[2] T. Stanton and F. G. Dunn, "Hypertension, left ventricular hypertrophy, and myocardial ischemia," *The Medical Clinics of North America*, vol. 101, no. 1, pp. 29–41, 2017.

[3] A. M. Rababa'h, A. N. Guillory, R. Mustafa, and T. Hijjawi, "Oxidative stress and cardiac remodeling: an updated edge," *Current Cardiology Reviews*, vol. 14, no. 1, pp. 53–59, 2018.

[4] L. Zhao, D. Wu, M. Sang, Y. Xu, Z. Liu, and Q. Wu, "Stachydrine ameliorates isoproterenol-induced cardiac hypertrophy and fibrosis by suppressing inflammation and oxidative stress through inhibiting NF-κB and JAK/STAT signaling pathways

in rats," *International Immunopharmacology*, vol. 48, pp. 102–109, 2017.

[5] J. Lu, Y. Shen, L. J. Liu, H. Y. Qian, and C. L. Zhu, "Combining epinephrine and esmolol attenuates excessive autophagy and mitophagy in rat cardiomyocytes after cardiac arrest," *Journal of Cardiovascular Pharmacology*, vol. 66, no. 5, pp. 449–456, 2015.

[6] R. J. Liao, L. J. Tong, C. Huang et al., "Rescue of cardiac failing and remodelling by inhibition of protein phosphatase 1γ is associated with suppression of the alternative splicing factor-mediated splicing of Ca^{2+}/calmodulin-dependent protein kinase δ," *Clinical and Experimental Pharmacology*, vol. 41, no. 12, pp. 976–985, 2014.

[7] X. L. Xu, Q. Y. Zhu, C. Zhao et al., "The effect of 2,3,4′,5-tetrahydroxystilbene-2-O-β-D-glucoside on pressure overload-induced cardiac remodeling in rats and its possible mechanism," *Planta Medica*, vol. 80, no. 2-3, pp. 130–138, 2014.

[8] C. Chen, M. Ponnusamy, C. Liu, J. Gao, K. Wang, and P. Li, "MicroRNA as a therapeutic target in cardiac remodeling," *Biomed Research International*, vol. 2017, Article ID 1278436, 25 pages, 2017.

[9] S. Liu, Y. Ji, J. Yao et al., "Knockout of the prostaglandin E2receptor subtype 3 promotes eccentric cardiac hypertrophy and fibrosis in mice," *Journal of Cardiovascular Pharmacology and Therapeutics*, vol. 22, no. 1, pp. 71–82, 2016.

[10] G. Meng, S. Zhao, L. Xie, Y. Han, and Y. Ji, "Protein S-sulfhydration by hydrogen sulfide in cardiovascular system," *British Journal of Pharmacology*, vol. 175, no. 8, pp. 1146–1156, 2018.

[11] S. J. Chan and P. T. H. Wong, "Reprint of: hydrogen sulfide in stroke: protective or deleterious?," *Neurochemistry International*, vol. 107, pp. 78–87, 2017.

[12] J. Pichette and J. Gagnon, "Implications of hydrogen sulfide in glucose regulation: How H_2S can alter glucose homeostasis through metabolic hormones," *Oxidative Medicine and Cellular Longevity*, vol. 2016, Article ID 3285074, 5 pages, 2016.

[13] S. Panthi, H. J. Chung, J. Jung, and N. Y. Jeong, "Physiological importance of hydrogen sulfide: emerging potent neuroprotector and neuromodulator," *Oxidative Medicine and Cellular Longevity*, vol. 2016, Article ID 9049782, 11 pages, 2016.

[14] Z. Z. Xie, Y. Liu, and J. S. Bian, "Hydrogen sulfide and cellular redox homeostasis," *Oxidative Medicine and Cellular Longevity*, vol. 2016, Article ID 6043038, 12 pages, 2016.

[15] Y. Shen, Z. Shen, S. Luo, W. Guo, and Y. Z. Zhu, "The cardioprotective effects of hydrogen sulfide in heart diseases: from molecular mechanisms to therapeutic potential," *Oxidative Medicine and Cellular Longevity*, vol. 2015, Article ID 925167, 13 pages, 2015.

[16] S. Zhang, C. Pan, F. Zhou et al., "Hydrogen sulfide as a potential therapeutic target in fibrosis," *Oxidative Medicine and Cellular Longevity*, vol. 2015, Article ID 593407, 12 pages, 2015.

[17] G. Meng, Y. Ma, L. Xie, A. Ferro, and Y. Ji, "Emerging role of hydrogen sulfide in hypertension and related cardiovascular diseases," *British Journal of Pharmacology*, vol. 172, no. 23, pp. 5501–5511, 2015.

[18] S. R. Lee, B. Nilius, and J. Han, "Gaseous signaling molecules in cardiovascular function: from mechanisms to clinical translation," *Reviews of Physiology Biochemistry and Pharmacology*, vol. 174, pp. 81–156, 2018.

[19] Y. Xu, H. P. du, J. Li et al., "Statins upregulate cystathionine γ-lyase transcription and H_2S generation via activating Akt signaling in macrophage," *Pharmacological Research*, vol. 87, pp. 18–25, 2014.

[20] G. Meng, Y. Xiao, Y. Ma et al., "Hydrogen sulfide regulates Krüppel-like factor 5 transcription activity via specificity protein 1 S-sulfhydration at Cys664 to prevent myocardial hypertrophy," *Journal of the American Heart Association*, vol. 5, no. 9, article e004160, 2016.

[21] G. Meng, J. Liu, S. Liu et al., "Hydrogen sulfide pretreatment improves mitochondrial function in myocardial hypertrophy via a SIRT3-dependent manner," *British Journal of Pharmacology*, vol. 175, no. 8, pp. 1126–1145, 2018.

[22] G. Meng, J. Zhu, Y. Xiao et al., "Hydrogen sulfide donor GYY4137 protects against myocardial fibrosis," *Oxidative Medicine and Cellular Longevity*, vol. 2015, Article ID 691070, 14 pages, 2015.

[23] L. Xie, H. Feng, S. Li et al., "SIRT3 mediates the antioxidant effect of hydrogen sulfide in endothelial cells," *Antioxidants & Redox Signaling*, vol. 24, no. 6, pp. 329–343, 2016.

[24] L. Xie, Y. Gu, M. Wen et al., "Hydrogen sulfide induces keap1 S-sulfhydration and suppresses diabetes-accelerated atherosclerosis via NRF2 activation," *Diabetes*, vol. 65, no. 10, pp. 3171–3184, 2016.

[25] A. Chhabra, S. Mishra, G. Kumar et al., "Glucose-6-phosphate dehydrogenase is critical for suppression of cardiac hypertrophy by H_2S," *Cell Death Discovery*, vol. 4, no. 1, 6 pages, 2018.

[26] V. Kesherwani, S. S. Nandi, S. K. Sharawat, H. R. Shahshahan, and P. K. Mishra, "Hydrogen sulfide mitigates homocysteine-mediated pathological remodeling by inducing miR-133a in cardiomyocytes," *Molecular and Cellular Biochemistry*, vol. 404, no. 1-2, pp. 241–250, 2015.

[27] X. Zhou, L. Zhao, J. Mao, J. Huang, and J. Chen, "Antioxidant effects of hydrogen sulfide on left ventricular remodeling in smoking rats are mediated via PI3K/Akt-dependent activation of Nrf2," *Toxicological Sciences*, vol. 144, no. 1, pp. 197–203, 2015.

[28] X. Tang, X. F. Chen, H. Z. Chen, and D. P. Liu, "Mitochondrial sirtuins in cardiometabolic diseases," *Clinical Science*, vol. 131, no. 16, pp. 2063–2078, 2017.

[29] B. Martín-Fernández and R. Gredilla, "Mitochondria and oxidative stress in heart aging," *Age*, vol. 38, no. 4, pp. 225–238, 2016.

[30] J. M. Grillon, K. R. Johnson, K. Kotlo, and R. S. Danziger, "Non-histone lysine acetylated proteins in heart failure," *Biochimica et Biophysica Acta (BBA) - Molecular Basis of Disease*, vol. 1822, no. 4, pp. 607–614, 2012.

[31] S. S. Bharathi, Y. Zhang, A. W. Mohsen et al., "Sirtuin 3 (SIRT3) protein regulates long-chain acyl-CoA dehydrogenase by deacetylating conserved lysines near the active site," *The Journal of Biological Chemistry*, vol. 288, no. 47, pp. 33837–33847, 2013.

[32] C. Koentges, C. Bode, and H. Bugger, "SIRT3 in cardiac physiology and disease," *Frontiers in Cardiovascular Medicine*, vol. 3, 2016.

[33] S. Matsushima and J. Sadoshima, "The role of sirtuins in cardiac disease," *American Journal of Physiology-Heart and Circulatory Physiology*, vol. 309, no. 9, pp. H1375–H1389, 2015.

[34] V. B. Pillai, S. Samant, N. R. Sundaresan et al., "Honokiol blocks and reverses cardiac hypertrophy in mice by activating

mitochondrial Sirt3," *Nature Communications*, vol. 6, no. 1, p. 6656, 2015.

[35] T. Chen, J. Li, J. Liu et al., "Activation of SIRT3 by resveratrol ameliorates cardiac fibrosis and improves cardiac function via the TGF-β/Smad3 pathway," *American Journal of Physiology-Heart and Circulatory Physiology*, vol. 308, no. 5, pp. H424–H434, 2015.

[36] C. F. Lee, J. D. Chavez, L. Garcia-Menendez et al., "Normalization of NAD^+ redox balance as a therapy for heart failure," *Circulation*, vol. 134, no. 12, pp. 883–894, 2016.

[37] T. Yamamoto, J. Byun, P. Zhai, Y. Ikeda, S. Oka, and J. Sadoshima, "Nicotinamide mononucleotide, an intermediate of NAD^+ synthesis, protects the heart from ischemia and reperfusion," *PLoS One*, vol. 9, no. 6, article e98972, 2014.

[38] J. Liu, T. Wang, X. Wang et al., "Development of novel β-carboline-based hydroxamate derivatives as HDAC inhibitors with DNA damage and apoptosis inducing abilities," *MedChemComm*, vol. 8, no. 6, pp. 1213–1219, 2017.

[39] Y. Xu, Y. Wang, G. Wang et al., "YiQiFuMai powder injection protects against ischemic stroke via inhibiting neuronal apoptosis and PKCδ/Drp1-mediated excessive mitochondrial fission," *Oxidative Medicine and Cellular Longevity*, vol. 2017, Article ID 1832093, 17 pages, 2017.

[40] X. Ren, L. Chen, J. Xie et al., "Resveratrol ameliorates mitochondrial elongation via Drp1/Parkin/PINK1 signaling in senescent-like cardiomyocytes," *Oxidative Medicine and Cellular Longevity*, vol. 2017, Article ID 4175353, 20 pages, 2017.

[41] B. Wu, J. Li, H. Ni et al., "TLR4 activation promotes the progression of experimental autoimmune myocarditis to dilated cardiomyopathy by inducing mitochondrial dynamic imbalance," *Oxidative Medicine and Cellular Longevity*, vol. 2018, Article ID 3181278, 15 pages, 2018.

[42] C. Busquets-Cortés, X. Capó, M. Martorell, J. A. Tur, A. Sureda, and A. Pons, "Training enhances immune cells mitochondrial biosynthesis, fission, fusion, and their antioxidant capabilities synergistically with dietary docosahexaenoic supplementation," *Oxidative Medicine and Cellular Longevity*, vol. 2016, Article ID 8950384, 10 pages, 2016.

[43] Y. H. Yang, H. L. Fang, M. Zhao et al., "Specific α7 nicotinic acetylcholine receptor agonist ameliorates isoproterenol-induced cardiac remodelling in mice through TGF-β1/Smad3 pathway," *Clinical and Experimental Pharmacology and Physiology*, vol. 44, no. 12, pp. 1192–1200, 2017.

[44] P. Wang, L. Luo, Q. Shen et al., "Rosuvastatin improves myocardial hypertrophy after hemodynamic pressure overload via regulating the crosstalk of Nrf2/ARE and TGF-β/smads pathways in rat heart," *European Journal of Pharmacology*, vol. 820, pp. 173–182, 2018.

[45] C. Wang, X. Nie, Y. Zhang et al., "Reactive oxygen species mediate nitric oxide production through ERK/JNK MAPK signaling in HAPI microglia after PFOS exposure," *Toxicology and Applied Pharmacology*, vol. 288, no. 2, pp. 143–151, 2015.

[46] X.-D. Yang, Q. Shi, J. Sun et al., "Aberrant alterations of mitochondrial factors Drp1 and Opa1 in the brains of scrapie experiment rodents," *Journal of Molecular Neuroscience*, vol. 61, no. 3, pp. 368–378, 2017.

[47] V. S. S. Gonçalves, K. R. C. Andrade, K. M. B. Carvalho, M. T. Silva, M. G. Pereira, and T. F. Galvao, "Accuracy of self-reported hypertension: a systematic review and meta-analysis," *Journal of Hypertension*, vol. 36, no. 5, pp. 970–978, 2018.

[48] G. Yang, L. Wu, B. Jiang et al., "H_2S as a physiologic vasorelaxant: hypertension in mice with deletion of cystathionine gamma-lyase," *Science*, vol. 322, no. 5901, pp. 587–590, 2008.

[49] L. Li, M. Whiteman, Y. Y. Guan et al., "Characterization of a novel, water-soluble hydrogen sulfide-releasing molecule (GYY4137): new insights into the biology of hydrogen sulfide," *Circulation*, vol. 117, no. 18, pp. 2351–2360, 2008.

[50] G. J. Weber, S. B. Pushpakumar, and U. Sen, "Hydrogen sulfide alleviates hypertensive kidney dysfunction through an epigenetic mechanism," *American Journal of Physiology-Heart and Circulatory Physiology*, vol. 312, no. 5, pp. H874–H885, 2017.

[51] K. W. Swan, B. M. Song, A. L. Chen et al., "Analysis of decreases in systemic arterial pressure and heart rate in response to the hydrogen sulfide donor sodium sulfide," *American Journal of Physiology-Heart and Circulatory Physiology*, vol. 313, no. 4, pp. H732–H743, 2017.

[52] C. Cuspidi, C. Sala, M. L. Muiesan, N. de Luca, G. Schillaci, and Working Group on Heart, Hypertension of the Italian Society of Hypertension., "Right ventricular hypertrophy in systemic hypertension: an updated review of clinical studies," *Journal of Hypertension*, vol. 31, no. 5, pp. 858–865, 2013.

[53] C. Cuspidi, M. Rescaldani, C. Sala, and G. Grassi, "Left-ventricular hypertrophy and obesity: a systematic review and meta-analysis of echocardiographic studies," *Journal of Hypertension*, vol. 32, no. 1, pp. 16–25, 2014.

[54] T. Oka, H. Akazawa, A. T. Naito, and I. Komuro, "Angiogenesis and cardiac hypertrophy: maintenance of cardiac function and causative roles in heart failure," *Circulation Research*, vol. 114, no. 3, pp. 565–571, 2014.

[55] J. Huang, D. Wang, J. Zheng, X. Huang, and H. Jin, "Hydrogen sulfide attenuates cardiac hypertrophy and fibrosis induced by abdominal aortic coarctation in rats," *Molecular Medicine Reports*, vol. 5, no. 4, pp. 923–928, 2012.

[56] S. Y. Liu, X. C. Duan, S. Jin et al., "Hydrogen sulfide improves myocardial remodeling via downregulated angiotensin II/AT1R pathway in renovascular hypertensive rats," *American Journal of Hypertension*, vol. 30, no. 1, pp. 67–74, 2017.

[57] M. Shao, C. Zhuo, R. Jiang et al., "Protective effect of hydrogen sulphide against myocardial hypertrophy in mice," *Oncotarget*, vol. 8, no. 14, pp. 22344–22352, 2017.

[58] P. Huang, Z. Shen, W. Yu et al., "Hydrogen sulfide inhibits high-salt diet-induced myocardial oxidative stress and myocardial hypertrophy in Dahl rats," *Frontiers in Pharmacology*, vol. 8, p. 128, 2017.

[59] Y. X. Shi, Y. Chen, Y. Z. Zhu et al., "Chronic sodium hydrosulfide treatment decreases medial thickening of intramyocardial coronary arterioles, interstitial fibrosis, and ROS production in spontaneously hypertensive rats," *American Journal of Physiology-Heart and Circulatory Physiology*, vol. 293, no. 4, pp. H2093–H2100, 2007.

[60] M. Hu, W. Zou, C. Y. Wang et al., "Hydrogen sulfide protects against chronic unpredictable mild stress-induced oxidative stress in hippocampus by upregulation of BDNF-TrKB pathway," *Oxidative Medicine and Cellular Longevity*, vol. 2016, Article ID 2153745, 10 pages, 2016.

[61] L. Y. Chen, Q. Chen, X. J. Zhu et al., "Diallyl trisulfide protects against ethanol-induced oxidative stress and apoptosis via a hydrogen sulfide-mediated mechanism," *International Immunopharmacology*, vol. 36, pp. 23–30, 2016.

[62] L. Li, M. Li, Y. Li et al., "Exogenous H_2S contributes to recovery of ischemic post-conditioning-induced cardioprotection by decrease of ROS level via down-regulation of NF-κB and JAK2-STAT3 pathways in the aging cardiomyocytes," *Cell&-Bioscience*, vol. 6, no. 1, p. 26, 2016.

[63] P. Huang, Z. Shen, J. Liu et al., "Hydrogen sulfide inhibits high-salt diet-induced renal oxidative stress and kidney injury in dahl rats," *Oxidative Medicine and Cellular Longevity*, vol. 2016, Article ID 2807490, 15 pages, 2016.

[64] Z. H. I.-H. A. I. Han, Y. Jiang, Y. Y. Duan, X. Y. Wang, Y. Huang, and T. Z. Fang, "Protective effects of hydrogen sulfide inhalation on oxidative stress in rats with cotton smoke inhalation-induced lung injury," *Experimental and Therapeutic Medicine*, vol. 10, no. 1, pp. 164–168, 2015.

[65] E. Dongó, I. Hornyák, Z. Benkő, and L. Kiss, "The cardioprotective potential of hydrogen sulfide in myocardial ischemia/reperfusion injury (review)," *Acta Physiologica Hungarica*, vol. 98, no. 4, pp. 369–381, 2011.

[66] G. Szabó, G. Veres, T. Radovits et al., "Cardioprotective effects of hydrogen sulfide," *Nitric Oxide: Biology and Chemistry*, vol. 25, no. 2, pp. 201–210, 2011.

[67] P. Wang, J. X. Zhang, J. P. Gong, L. F. Li, P. L. Jin, and C. M. Ding, "Effects of hydrogen sulfide on pulmonary surfactant in rats with acute lung injury induced by lipopolysccharide," *Chinese Journal of Applied Physiology*, vol. 27, no. 4, pp. 485–489, 2011.

[68] G. Yang, X. Sun, and R. Wang, "Hydrogen sulfide-induced apoptosis of human aorta smooth muscle cells via the activation of mitogen-activated protein kinases and caspase-3," *FASEB Journal*, vol. 18, no. 14, pp. 1782–1784, 2004.

[69] P. Arabacilar and M. Marber, "The case for inhibiting p38 mitogen-activated protein kinase in heart failure," *Frontiers in Pharmacology*, vol. 6, 2015.

[70] M. Mutlak and I. Kehat, "Extracellular signal-regulated kinases 1/2 as regulators of cardiac hypertrophy," *Frontiers in Pharmacology*, vol. 6, 2015.

[71] J. Du, Y. Hui, Y. Cheung et al., "The possible role of hydrogen sulfide as a smooth muscle cell proliferation inhibitor in rat cultured cells," *Heart and Vessels*, vol. 19, no. 2, pp. 75–80, 2004.

[72] B. F. Peake, C. K. Nicholson, J. P. Lambert et al., "Hydrogen sulfide preconditions the db/db diabetic mouse heart against ischemia-reperfusion injury by activating Nrf2 signaling in an Erk-dependent manner," *American Journal of Physiology-Heart and Circulatory Physiology*, vol. 304, no. 9, pp. H1215–H1224, 2013.

[73] R. Guo, J. Lin, W. Xu et al., "Hydrogen sulfide attenuates doxorubicin-induced cardiotoxicity by inhibition of the p38 MAPK pathway in H9c2 cells," *International Journal of Molecular Medicine*, vol. 31, no. 3, pp. 644–650, 2013.

[74] W. Xu, W. Wu, J. Chen et al., "Exogenous hydrogen sulfide protects H9c2 cardiac cells against high glucose-induced injury by inhibiting the activities of the p38 MAPK and ERK1/2 pathways," *International Journal of Molecular Medicine*, vol. 32, no. 4, pp. 917–925, 2013.

[75] H. Zhang, A. Zhang, C. Guo et al., "S-diclofenac protects against doxorubicin-induced cardiomyopathy in mice via ameliorating cardiac gap junction remodeling," *PLoS One*, vol. 6, no. 10, article e26441, 2011.

[76] N. Treviño-Saldaña and G. García-Rivas, "Regulation of sirtuin-mediated protein deacetylation by cardioprotective phytochemicals," *Oxidative Medicine and Cellular Longevity*, vol. 2017, Article ID 1750306, 16 pages, 2017.

[77] G. A. Porter, W. R. Urciuoli, P. S. Brookes, and S. M. Nadtochiy, "SIRT3 deficiency exacerbates ischemia-reperfusion injury: implication for aged hearts," *American Journal of Physiology-Heart and Circulatory Physiology*, vol. 306, no. 12, pp. H1602–H1609, 2014.

[78] X. He, H. Zeng, and J. X. Chen, "Ablation of SIRT3 causes coronary microvascular dysfunction and impairs cardiac recovery post myocardial ischemia," *International Journal of Cardiology*, vol. 215, pp. 349–357, 2016.

[79] B. Sosnowska, M. Mazidi, P. Penson, A. Gluba-Brzózka, J. Rysz, and M. Banach, "The sirtuin family members SIRT1, SIRT3 and SIRT6: their role in vascular biology and atherogenesis," *Atherosclerosis*, vol. 265, pp. 275–282, 2017.

[80] N. R. Sundaresan, M. Gupta, G. Kim, S. B. Rajamohan, A. Isbatan, and M. P. Gupta, "Sirt3 blocks the cardiac hypertrophic response by augmenting Foxo3a-dependent antioxidant defense mechanisms in mice," *The Journal of Clinical Investigation*, vol. 119, no. 9, pp. 2758–2771, 2009.

[81] Y. Chen, H. Q. Luo, L. L. Sun et al., "Dihydromyricetin attenuates myocardial hypertrophy induced by transverse aortic constriction via oxidative stress inhibition and SIRT3 pathway enhancement," *International Journal of Molecular Sciences*, vol. 19, no. 9, article E2592, 2018.

[82] C. K. Singh, G. Chhabra, M. A. Ndiaye, L. M. Garcia-Peterson, N. J. Mack, and N. Ahmad, "The role of sirtuins in antioxidant and redox signaling," *Antioxidants&Redox Signaling*, vol. 28, no. 8, pp. 643–661, 2018.

[83] H. D. T. F. Facundo, R. E. Brainard, F. R. . L. Caldas, and A. M. B. Lucas, "Mitochondria and cardiac hypertrophy," *Advances in Experimental Medicine and Biology*, vol. 982, pp. 203–226, 2017.

[84] S. Cogliati, C. Frezza, M. E. Soriano et al., "Mitochondrial cristae shape determines respiratory chain supercomplexes assembly and respiratory efficiency," *Cell*, vol. 155, no. 1, pp. 160–171, 2013.

[85] K. Tsushima, H. Bugger, A. R. Wende et al., "Mitochondrial reactive oxygen species in lipotoxic hearts induce post-translational modifications of akap121, DRP1, and OPA1 that promote mitochondrial fission," *Circulation Research*, vol. 122, no. 1, pp. 58–73, 2018.

[86] S. A. Samant, H. J. Zhang, Z. Hong et al., "SIRT3 deacetylates and activates OPA1 to regulate mitochondrial dynamics during stress," *Molecular and Cellular Biology*, vol. 34, no. 5, pp. 807–819, 2014.

[87] W. W. Sharp, "Dynamin-related protein 1 as a therapeutic target in cardiac arrest," *Journal of Molecular Medicine*, vol. 93, no. 3, pp. 243–252, 2015.

[88] S. C. J. Helle, Q. Feng, M. J. Aebersold et al., "Mechanical force induces mitochondrial fission," *Elife*, vol. 6, article e30292, 2017.

[89] K. Atkins, A. Dasgupta, K. H. Chen, J. Mewburn, and S. L. Archer, "The role of Drp1 adaptor proteins MiD49 and MiD51 in mitochondrial fission: implications for human disease," *Clinical Science*, vol. 130, no. 21, pp. 1861–1874, 2016.

Hindawi
Oxidative Medicine and Cellular Longevity
Volume 2018, Article ID 9416432, 17 pages
https://doi.org/10.1155/2018/9416432

Research Article

Prophylactic Zinc and Therapeutic Selenium Administration Increases the Antioxidant Enzyme Activity in the Rat Temporoparietal Cortex and Improves Memory after a Transient Hypoxia-Ischemia

Constantino Tomas-Sanchez,[1] Victor-Manuel Blanco-Alvarez,[1] Daniel Martinez-Fong,[2] Juan-Antonio Gonzalez-Barrios,[3] Alejandro Gonzalez-Vazquez,[1] Ana-Karina Aguilar-Peralta,[1] Maricela Torres-Soto,[1] Guadalupe Soto-Rodriguez,[4] Ilhuicamina Daniel Limón,[1] Eduardo Brambila,[1] Lourdes Millán-Pérez-Peña,[5] Jorge Cebada,[4] Carlos E. Orozco-Barrios,[2] and Bertha Alicia Leon-Chavez[1]

[1]*Facultad de Ciencias Químicas, Benemérita Universidad Autónoma de Puebla, 14 sur y Av. San Claudio, 72570 Puebla, PUE, Mexico*
[2]*Departamento de Fisiología, Biofísica y Neurociencias, Centro de Investigación y de Estudios Avanzados del Instituto Politécnico Nacional, Apartado Postal 14-740, 07000 Mexico City, Mexico*
[3]*Laboratorio de Medicina Genómica, Hospital Regional 1° de Octubre, ISSSTE, Avenida Instituto Politécnico Nacional No. 1669, 07760 Mexico City, Mexico*
[4]*Facultad de Medicina, Benémerita Universidad Autónoma de Puebla, 13 sur 2702, Los Volcanes, 72420 Puebla, PUE, Mexico*
[5]*Centro de Química, ICUAP, Benémerita Universidad Autónoma de Puebla, 14 sur y Av. San Claudio, 72570 Puebla, PUE, Mexico*

Correspondence should be addressed to Bertha Alicia Leon-Chavez; alileonch@gmail.com

Received 16 April 2018; Accepted 31 July 2018; Published 6 September 2018

Academic Editor: Karolina Szewczyk-Golec

In the cerebral hypoxia-ischemia rat model, the prophylactic administration of zinc can cause either cytotoxicity or preconditioning effect, whereas the therapeutic administration of selenium decreases the ischemic damage. Herein, we aimed to explore whether supplementation of low doses of prophylactic zinc and therapeutic selenium could protect from a transient hypoxic-ischemic event. We administrated zinc (0.2 mg/kg of body weight; ip) daily for 14 days before a 10 min common carotid artery occlusion (CCAO). After CCAO, we administrated sodium selenite (6 μg/kg of body weight; ip) daily for 7 days. In the temporoparietal cerebral cortex, we determined nitrites by the Griess method and lipid peroxidation by the Gerard-Monnier assay. qPCR was used to measure mRNA of nitric oxide synthases, antioxidant enzymes, chemokines, and their receptors. We measured the enzymatic activity of SOD and GPx and protein levels of chemokines and their receptors by ELISA. We evaluated long-term memory using the Morris-Water maze test. Our results showed that prophylactic administration of zinc caused a preconditioning effect, decreasing nitrosative/oxidative stress and increasing GPx and SOD expression and activity, as well as eNOS expression. The therapeutic administration of selenium maintained this preconditioning effect up to the late phase of hypoxia-ischemia. Ccl2, Ccr2, Cxcl12, and Cxcr4 were upregulated, and long-term memory was improved. Pyknotic cells were decreased suggesting prevention of neuronal cell death. Our results show that the prophylactic zinc and therapeutic selenium administration induces effective neuroprotection in the early and late phases after CCAO.

1. Introduction

Zinc plays a dual role in the cerebral hypoxia-ischemia depending on its concentration in the cerebral stroke area; this concentration is known to be determined by zinc serum levels [1]. Accordingly, low serum levels of zinc have long been considered as a risk factor for stroke [2]. In contrast, the input of low concentration of zinc chloride ($ZnCl_2$) or zinc protoporphyrin (ZnPP) reduces the size of postischemic brain damage [3]. Several mechanisms can be accounted for the latter effect. For instance, the decrease in interleukin-1 (IL-1) and IL-23 expression [4], increase in chemokine and growth factor levels [5], and decrease in oxidative stress are because of the antioxidant activity of Cu and Zn superoxide dismutase (SOD1 and 3) [6]. However, excessive accumulation of zinc can also cause neuronal degeneration in the hippocampus and cerebral cortex [7]. Therefore, hypothermia by preventing the accumulation of zinc decreases the cell death [8–10], the degeneration of hippocampal neurons, and the loss of memory after hypoxia-ischemia [11]. The mechanism underpinning the hypothermia effect is the reduction of zinc transport from the presynaptic neurons into the postsynaptic neurons during experimental global ischemia.

Selenium has been shown to preserve mitochondrial function, stimulate mitochondrial biogenesis, and reduce infarct volume after focal cerebral ischemia [12]. Selenium treatment in a rat ischemia model decreases oxidative stress [13]. Furthermore, the oral administration of selenium improves learning and memory in an Alzheimer's disease rat model [14]. Administration of sodium selenite together with melatonin 30 min before medial cerebral artery occlusion (MCAO) and for 3 days postreperfusion decreases oxidative stress [15]. A mechanism for the antioxidant effect of selenium is the inhibition of inducible nitric oxide synthases (iNOS) and COX-2 expression through the inactivation of p38 MAPK and NF-κB [16]. Another mechanism is the incorporation of selenium into selenoproteins such as glutathione peroxidase and thioredoxin reductase, thus making the removal of peroxides more efficient [17].

Our group has reported opposite effects of zinc administration in the 10 min common carotid artery occlusion (CCAO) rat model, where CCAO causes cell death by apoptosis and necrosis without producing an ischemic core [11, 18]. The subacute administration of zinc (2.5 mg/kg) before CCAO exerts a neuroprotective effect by increasing the expression of CCL2/CCR2, FGF2, and IGF-1 in the temporoparietal rat cortex [5]. In contrast, chronic zinc administration at a low dose (0.5 mg/kg body weight) before CCAO decreases CCL2/CCR2, CCL3/CCR1, CCL4/CCR8, and CXCL13/CXCR5 and increases CXCL12/CXCR4, but does not prevent cell death in the late phase [19]. The antioxidant effect of selenium has been used to exert neuroprotection alone [12] or in combination with other antioxidants such as melatonin [15], *Ginkgo biloba* [13], and alpha-tocopherol [20]. Therefore, we propose that the combination of the prophylactic effect of zinc with the therapeutic effect of selenium can maintain the neuroprotection on neuroinflammation and neurodegeneration induced by transient CCAO.

To test that hypothesis, we administered zinc (0.2 mg/kg body weight; ip) for 14 days before CCAO, followed by sodium selenite (6 μg/kg body weight; ip) administration for 7 days after CCAO. We determined nitrosative-oxidative stress (nitrites, lipid peroxidation, NOSs, and antioxidant enzymes), markers of neuroinflammation (chemokines and their receptors) and cell death, over time after CCAO. We also measured neuronal plasticity using the Morris-Water maze test. Because the temporoparietal cortex resulted to be more affected than the hippocampus, we only reported the findings in the temporoparietal cortex. Our results demonstrate that the combined treatment of zinc with selenium extends the effective neuroprotection against CCAO-induced hypoxia-ischemia.

2. Materials and Methods

2.1. Experimental Animals. Male Wistar rats (body weight 190 to 240 g) were obtained from the vivarium of CINVESTAV and maintained in suitable rooms with controlled conditions of temperature ($22 \pm 3^{\circ}$C) and light-dark cycles (12 h–12 h; light onset at 07 : 00). Five rats per cage (acrylic; 34 cm × 44 cm × 20 cm) were housed. Food (Laboratory Autoclavable Rodent Diet 5010, 130 ppm of zinc, and 0.47 ppm of selenium) and drinking water were provided ad libitum. All procedures were by the current Mexican legislation, NOM-062-ZOO-1999 (SAGARPA), which in turn is based on the Guide for the Care and Use of Laboratory Animals, NRC. The Institutional Animal Care and Use Committee approved the experimental procedures with the protocol number 09-102. All efforts were made to minimize animal suffering.

2.2. Zinc and Selenium Administration. Zinc was administered as $ZnCl_2$ (0.2 mg/kg of body weight in water for injection, ip; Sigma-Aldrich; Saint Louis, MO, USA) every day for 14 days (chronic zinc administration). Sodium selenite (6 μg/kg of body weight in the water for injection, ip Sigma-Aldrich; Saint Louis, MO, USA) administration started 24 h after the last dose of Zn and continued every day for 7 days. Rats were grouped as follows: (1) control, healthy rats without treatment and surgery, (2) zinc, chronic zinc administration, (3) Zn + Se, chronic zinc administration followed by a single selenium administration on day 15, (4) CCAO, common carotid artery occlusion for 10 min, (5) Zn + CCAO, chronic zinc administration before CCAO, and (6) Zn + CCAO + Se, chronic zinc administration before CCAO followed by selenium administration for 7 days. The rats of groups (1), (2), and (3) were euthanized on day 15 to dissect out their brains. The brains of groups (4), (5), and (6) were obtained at different times (3, 6, 24, and 168 h) after reperfusion. All the variables studied were measured in the temporoparietal cortex, and all rat groups were age-matched.

2.3. Common Carotid Artery Occlusion (CCAO). The asepsis procedures were performed in the surgical instruments and surgical area. The animals were anesthetized with a mixture of ketamine (70 mg/kg) and xylazine (6 mg/kg) at a dose of 200 μL/100 g of body weight, ip. A 0.5 cm-long midline

skin incision was made in the neck area, and the left common carotid artery was carefully dissected. Then, the artery was occluded for 10 min with a clamp (Bulldog Clamps, INS6000119; Kent Scientific Corporation; Torrington, CT, USA). Upon completion of the occlusion, the reperfusion of the artery was visually verified, and the incision was sutured with a 3-0 silk thread (Atramat; Ciudad de Mexico, Mexico). The animals were kept in an individual cage under a 100-Watt, yellow light source until their complete recovery. The animals were euthanized and beheaded in the corresponding time postreperfusion using ketamine (70 mg/kg) and xylazine (6 mg/kg) at a dose of 200 μL/100 g of body weight. The ipsilateral temporoparietal cortex from the different groups was obtained for the biochemical, cellular, and molecular assays.

2.4. Nitrites. The temporoparietal cortex ($n = 5$ rats in each group) was mechanically homogenized in phosphate-buffered saline solution (PBS), pH 7.4, and centrifuged at 12,500 rpm for 30 min at 4°C by using a Z 216 MK microcentrifuge (HERMLE Labortechnik; Wehingen, Germany). The production of NO was assessed through the accumulation of nitrites (NO_2^-) in the supernatants as described elsewhere [21]. Briefly, the nitrite concentration in 100 μL of the supernatant was measured by using a colorimetric reaction generated by the addition of 100 μL of Griess reagent, composed of equal volumes of 0.1% N-(1-naphthyl)ethylenediamine dihydrochloride and 1.32% sulfanilamide in 60% acetic acid. The absorbance of the samples was determined at 540 nm with a SmartSpec 3000 spectrophotometer (Bio-Rad; Hercules, CA, USA) and interpolated by using a standard curve of $NaNO_2$ (1 to 10 μM) to calculate the nitrite concentration.

2.5. Lipid Peroxidation. Malondialdehyde (MDA) and 4-hydroxyalkenals (4-HAD) were measured in the same supernatant where the nitrites were measured ($n = 5$ rats in each group), following the procedure described elsewhere [22]. The colorimetric reaction was made using 200 μL of the supernatant after the subsequent addition of 650 μL of 10.3 mM N-methyl-2phenyl-indole (Sigma-Aldrich; Saint Louis, MO, USA) diluted in a mixture of acetonitrile : methanol (3 : 1) and 150 μL of methanesulfonic acid (Sigma-Aldrich; Saint Louis, MO, USA). The reaction mixture was vortexed and incubated at 45°C for 1 h and afterward centrifuged at 3000 rpm for 10 min. The absorbance in the supernatant was read at 586 nm with a SmartSpec 3000 spectrophotometer (Bio-Rad; Hercules, CA, USA). The absorbance values were compared to a standard curve in the concentration range of 0.5 to 5 μM of 1,1,3,3-tetramethoxypropane (10 mM stock) to calculate the content of malondialdehyde + 4-hydroxyalkenal (MDA + 4-HAD) in the samples.

2.6. Glutathione Peroxidase Activity. GPx activity was measured using the Glutathione Peroxidase Assay Kit (ab102530; Abcam; Cambridge, UK) following the manufacturer's instructions. A sample of 50 mg of the temporoparietal cortex was washed with cold PBS and homogenized in 200 μL cold assay buffer with a mechanic homogenizer on ice for 15 passes and centrifuged at 10000g for 15 min at 4°C. The supernatants were collected into a fresh corresponding tube and samples of 50 μL were distributed in the respective wells of ELISA microplates (Costar, Corning Incorporated; NY, USA). Then, 40 μL of the fresh reaction mix was added to the well, mixed, and incubated at room temperature for 15 min. Then, 10 μL of cumene hydroperoxide solution was added to each well, mixed, and read at 340 nm on a plate reader (Bio-Rad; Hercules, California, USA). Then, the plates were incubated in the dark at 25°C for 5 min and read again at 340 nm. The activity of GSH-Px in nmol/mL was calculated according to the manufacturer's instructions.

2.7. Superoxide Dismutase Activity. SOD activity was measured using the Superoxide Dismutase Activity Colorimetric Assay kit (ab65354, Abcam; Cambridge, UK) following the manufacturer's instructions. A temporoparietal cortex sample of 50 mg from each rat group was washed in cold PBS and homogenized with a mechanic homogenizer on ice for 15 passes in cold 0.1 M Tris/HCl, pH 7.4 (containing 0.5% Triton X-100, 5 mM β-ME, and 0.1 mg/mL PMSF). Then, the homogenates were centrifuged for 5 min at 4°C at 14000g. The supernatants were collected into a fresh corresponding tube, and samples of 20 μL were distributed in the respective wells of ELISA microplates (Costar, Corning Incorporated; NY, USA). Then, 200 μL of WST working solution was added into each well followed by the addition of 20 μL of Enzyme Working Solution. The plates were mixed and incubated for 20 min at 37°C before reading using a microplate reader (Bio-Rad; Hercules, California, USA) at 450 nm. The OD of each sample was normalized with untreated control (group 1).

2.8. Enzyme-Linked Immunosorbent Assay (ELISA). CCL2/CCR2, CXCL12/CXCR4, and CXCL13/CXCR5 levels were measured by ELISA in homogenates of the temporoparietal cortex ($n = 5$ for each group). Protein content was determined using the Sedmak and Grossberg method [23]. Aliquots containing 5 μg of total protein were placed into wells of ELISA plates. Subsequently, 100 μL of 0.1 M carbonate buffer was added into each well and the plates were incubated at 4°C for 18 h. To block nonspecific binding sites, 200 μL of 0.5% bovine serum albumin (IgG free) was added into each well at room temperature. After 30 min incubation, the wells were washed thrice with PBS-Tween 20 (0.1%) solution. The primary antibodies were rabbit monoclonal antibodies to CCL2 (Bio-Rad/AbD Serotec Cat. number AAR31, RRID:AB_2071792, 1 : 500 dilution), and the following antibodies were obtained from Abcam (Abcam; Cambridge, UK), CCR2 (Abcam Cat. number ab21667, RRID:AB_446468, 1 : 500 dilution), CXCL12 (Abcam Cat. number ab25118, RRID:AB_448630, 1 : 500 dilution), CXCL13 (Abcam Cat. number ab112521, RRID:AB_10863283, 1 : 500 dilution), CXCR4 (Abcam Cat. number ab2074, RRID:AB_302814, 1 : 500 dilution), and CXCR5 (Abcam Cat. number ab10405, RRID:AB_2089665, 1 : 500 dilution). The primary antibodies were added to each well and incubated for 2 h at room temperature. After three washes with PBS-Tween 20

Table 1: List of chemokines and receptors assessed in qPCR: TaqMan probe used was obtained from Thermo Fisher Scientific Inc.

Gene	Gene name	Assay
Ccl2	Chemokine (C-C motif) ligand 2	Rn00580555_m1
Ccr2	Chemokine (C-C motif) receptor 2	Rn01637698_s1
Cxcl12	Chemokine (C-X-C motif) ligand 12	Rn00573260_m1
Cxcr4	Chemokine (C-C motif) receptor 4	Rn00573522_s1
Cxcl13	Chemokine (C-X-C motif) ligand 13	Rn01450028_m1
Cxcr5	Chemokine (C-C motif) receptor 5	Rn02132880_s1
Nos1	Nitric oxide synthase 1, neuronal	Rn00583793_m1
Nos2	Nitric oxide synthase 2, inducible	Rn00561646_m1
Nos3	Nitric oxide synthase 3, endothelial	Rn02132634_s1
Sod1	Superoxide dismutase 1, cytosolic	Rn006566938_m1
Sod2	Superoxide dismutase 2, mitochondrial	Rn00690588_g1
Sod3	Superoxide dismutase 3, extracellular	Rn00563570_m1
Gpx4	Glutathione peroxidase 4	Rn00820188_g1

(0.1%), a horseradish-peroxidase-conjugated goat anti-rabbit or mouse IgG (1 : 1000 dilution; Dako North America Inc; Carpinteria, CA, USA) was added into the wells and incubated for 2 h at room temperature. The antibody-antigen complex was revealed by addition of 100 μL of 2,2′-azinobis(3-ethylbenzthiazoline-6-sulfonic acid) (ABTS) containing 0.3% H_2O_2 into each well. After 15 min, optical density (OD) was determined using a Benchmark multiple reader at 415 nm (Bio-Rad; Hercules, CA, USA). All samples were processed under the same experimental conditions and time.

2.9. Retrotranscription. Total RNA was isolated from 100 mg of temporoparietal cortex using 1 mL of TRIzol (Invitrogen Corporation; Carlsbad, CA, USA) and then RNA-treated with RNase-free DNase I and quantified using a NanoDrop Spectrophotometer (Thermo Scientific NanoDrop Technologies; Wilmington, DE, USA). cDNA was obtained from 5 μg of total RNA using 1 μL of SuperScript III reverse transcriptase kit (Catalog 18080093, Invitrogen; Carlsbad, CA, USA),1 μL of Oligo dT 50 μM, 1 μL of dNTP mix 10 mM, and water grade molecular biology to 13 μL. Retrotranscription conditions were denaturation at 70°C for 10 min, hybridization at 42°C for 5 min, synthesis of cDNA at 55°C for 50 min and then 70°C for 15 min, and removal of RNA at 37°C for 20 min. Finally, 1 μL of RNase H (Invitrogen; Carlsbad, CA, USA) was added and samples were incubated at 37°C for 20 min.

2.10. qPCR. Fresh cDNA was used to amplify each gene using TaqMan probes (Table 1) obtained from Thermo Fisher (Thermo Fisher Scientific; Waltham, MA, USA). The amplification reactions contained 0.25 μL of the respective TaqMan probe, 2.5 μL of Master Mix (TaqMan Universal Master Mix; Life Technologies; Carlsbad, CA, USA), and 2.25 μL of cDNA in a final volume of 5 μL. The conditions for qPCR were 10 min for denaturation at 95°C, followed by 45 cycles of amplification of 15 s at 95°C and 1 min at 60°C. Rat β-actin was used as internal control and for normalization. The amplification assays were made using a 7900HT Fast Real-Time PCR System (Applied Biosystems; Foster City, CA, USA). The $2^{-\Delta\Delta Ct}$ analyses were used to calculate the relative transcript levels expressed as fold change for gene expression.

2.11. Spatial Reference Learning and Memory. The Morris water maze was used to measure the spatial reference memory. The measurements were conducted in a round tank, 150 cm in diameter and 80 cm deep, filled with water, and divided into four imaginary quadrants. Water was maintained at a temperature of 23 ± 2°C. Several distal visual cues were placed on both walls of the Morris water maze and the room in which it had been installed. This evaluation consisted of five test days of four consecutive trials per day. During the trial, each animal was placed in the tank facing the wall and allowed to swim freely to an escape platform (40 cm in height and 15 cm in diameter), which was submerged by 2 cm under the water surface and conserved to the center of the southeast (SE) quadrant of the tank. If the animals did not find the platform during a period of 60 s in the first trial of each test day, they were gently guided to it, allowed to remain on the platform for 30 s, and then removed from the tank. This procedure was used to ensure that the animals retained the visual-spatial information of the maze online during the execution of the swimming task [24]. Long-term memory was evaluated in the absence of the platform on day 7 after learning. The latency to reach the platform and the number of times that rats pass by the platform location were measured.

2.12. Histopathological Study. The animals were anesthetized with ketamine (70 mg/kg) and xylazine (6 mg/kg) at a dose of 200 μL/100 g of body weight, ip, and intracardially perfused with 200 mL of PBS followed by 100 mL of 4% paraformaldehyde. The brains were obtained and kept in 4% paraformaldehyde at 4°C for 24 h. The brains were embedded in paraffin using a Histokinette (Leica Microsystems; Wetzlar, Germany). The steps of the tissue processing were consecutive dehydration in different ethanol concentrations (80% for 1 h, 96% for 3 h, and 100% for 3), clearance in pure xylol for 2 h, and inclusion in paraffin at 56°C for 2 h. The tissues were placed in blocks using metallic cassettes. The histological sections of 3 μm were made in a rotary microtome-type Minot (Leica RM2135; Wetzlar, Germany) and placed on slides recovered with poly-L-lysine and finally fixed with heat at 60°C for 30 min. The slices were deparaffinized in an oven at 60°C and placed in xylene 2 times for 15 min. The hydration of slices was made by two consecutive passages in decreasing concentration of ethanol (100%, 96%, and 80%) and finally in tap water for 5 min. Hematoxylin staining was performed for 5 min or less until sections look blue. After washing with tap water, the differentiation was carried out with 1% acid alcohol (1% HCl in 70% alcohol) for 1 dip. The slices were washed in running tap water and dipped again in an alkaline solution (i.e., a saturated solution of lithium carbonate) followed by a tap water washing. The staining in 1% eosin Y was done for 10 minutes. The slices were

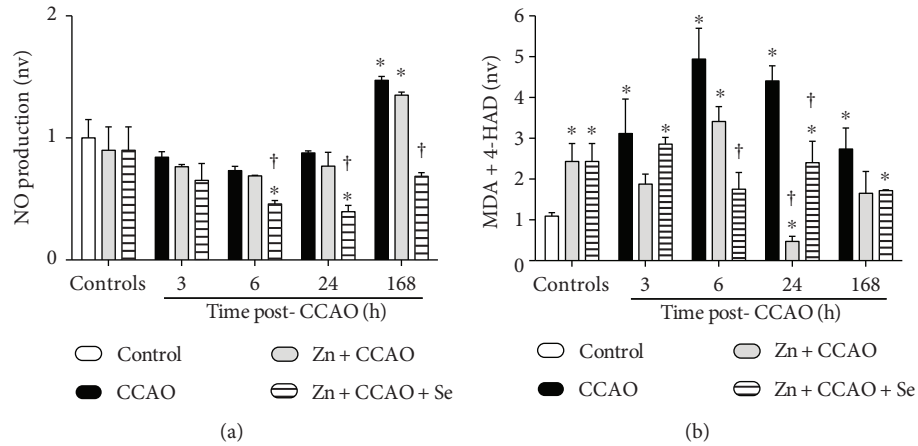

Figure 1: The combined treatment with zinc and selenium decreases the CCAO-induced nitrosative-oxidative stress in the temporoparietal cortex. (a) Nitrosative stress and (b) lipid peroxidation. CCAO: common carotid artery occlusion for 10 min; Zn + CCAO: chronic zinc administration before CCAO; Zn + CCAO + Se: chronic zinc administration before CCAO followed by selenium administration. The values were normalized against the control untreated group; nv: normalized values. Each value represents mean ± SEM of 5 independent experiments made in triplicate. $^{*}P < 0.05$, one-way ANOVA with post hoc Dunnett's test when compared to the control untreated group. $^{\dagger}P < 0.05$, Student's t-test when compared with the respective CCAO group.

washed again with tap water for 1 min. The dehydration of slices was made by ten consecutive dippings in increasing concentration of alcohols (80%, 96%, and 100%) and clearing with xylene. Finally, the slices were mounted on glass slides using Entellan (Merck KGaA; Darmstadt, Germany) and protected with coverslips. The slides were then examined with a light microscope equipped with 10x objective (Leica Microsystems; Wetzlar, Germany). The count of pyknotic cells in 20 fields of 4 brains in layer 5 of the temporoparietal cortex was made using ImageJ software (RRID:SCR_003070, National Institutes of Health).

2.13. Experimental Design and Statistical Analysis. All values were expressed as mean ± SEM from 5 independent experiments including the controls. The values of each variable studied were normalized concerning group 1 (untreated control), except the qPCR values that were expressed as a fold change ($2^{-\Delta\Delta Ct}$). One-way ANOVA and Dunnett's post hoc test were used to compare all groups with the untreated control group. Student's t-test was used to compare the treated groups concerning the CCAO group. All statistical analyses were performed using the GraphPad Prism 6 software. The results of learning memory were analyzed with Kruskal-Wallis one-way analysis of variance for comparison of multiple groups, and the Mann-Whitney U test was used for the statistical analysis of two groups. P values <0.05 were considered statistically significant. All statistical analyses were performed using data analysis software (GraphPad Prism, RRID:SCR_0158070).

3. Results

CCAO increased NO production at 168 h (43 ± 2%, $P = 0.0001$) postreperfusion in the temporoparietal cortex when compared with the untreated control (Figure 1(a)). The Zn + CCAO group did not prevent the CCAO-induced increase at 168 h in nitrite levels (35 ± 2%, $P = 0.0001$) when compared with the untreated control (Figure 1(a)). In contrast, the combined treatment with zinc and selenium (Zn + CCAO + Se) completely normalized the nitrite levels when compared with the CCAO group (Figure 1(a)), suggesting a reduction of nitrosative stress. In addition, this combined treatment reduced nitrite levels at 6 h (27 ± 4%, $P = 0.0036$), 24 h (54 ± 6%, $P = 0.0009$), and 168 h (53 ± 2% $P = 0.0004$) after CCAO, when compared to the respective CCAO group (Figure 1(a)).

CCAO also increased lipid peroxidation in the temporoparietal cortex from 3 h (211 ± 84%, $P = 0.0405$), with a maximum peak at 6 h (340 ± 37%, $P = 0.0010$) postreperfusion (Figure 1(b)). The zinc group caused a preconditioning effect, generating an increase in MDA + 4-HAD levels (123 ± 30%, $P = 0.0130$) when compared with the untreated control (Figure 1(b)). The Zn + CCAO group decreased the CCAO-induced increase in lipid peroxidation (89 ± 2%, $P = 0.0492$) only at 24 h, whereas the combined treatment Zn + CCAO + Se decreased lipid peroxidation levels as early as 6 h after CCAO until the end of the study as compared with the respective CCAO group (Figure 1(b)). The reduction in MDA + 4-HAD levels in the Zn + CCAO + Se group at 6 h was 64 ± 8% ($P = 0.0260$), at 24 h was 44 ± 12% ($P = 0.0362$), and at 168 h was 37 ± 1% ($P = 0.0285$).

We evaluated the transcription and expression of NOSs to determine their participation in the NO production in the temporoparietal cortex (Figure 2). CCAO increased mRNA levels for *Nos1* (Figure 2(a)) and *Nos3* (Figure 2(e)), but not for *Nos2* (Figure 2(c)). The increase was statistically significant at 3 h (3.89 ± 0.72, $P = 0.0157$) for *Nos1* and 6.43 ± 3.05, $P = 0.0358$, for *Nos3* at 168 h (3.3 ± 0.4, $P = 0.0499$ for *Nos1* and 7.7 ± 1.1 for *Nos3*, $P = 0.0147$) after CCAO (Figures 2(a) and 2(e), resp.). An upregulation of *Nos1* (3.4 ± 0.69 fold change, $P = 0.0497$) and *Nos3* (12.1 ± 1.25 fold change, $P = 0.0289$) mRNAs was induced by the Zn + Se group; the latter administration also upregulated Nos2 mRNA (6.82 ± 0.1 fold change, $P = 0.0001$) (Figure 2(c)).

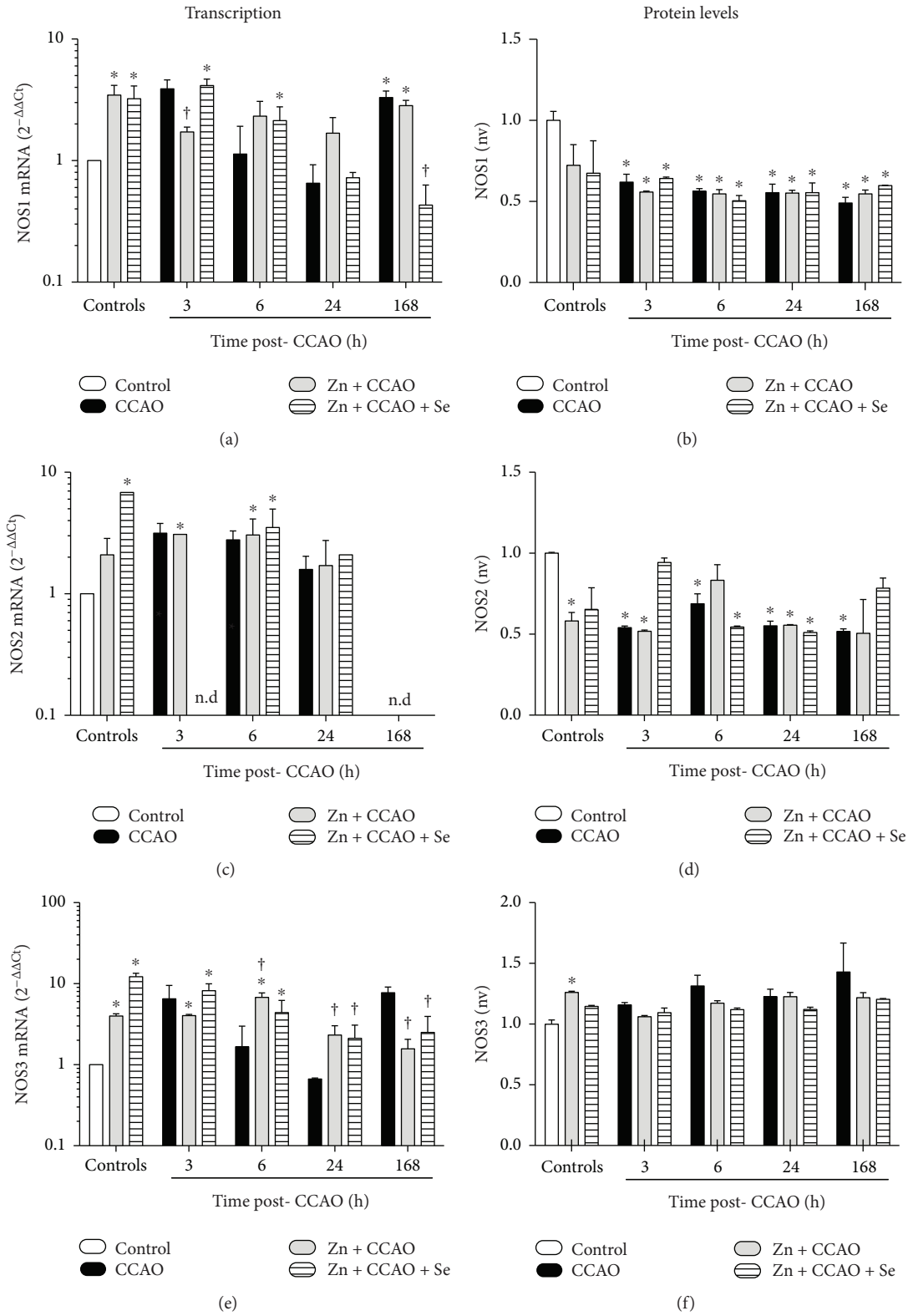

Figure 2: Effect of the combined treatment with zinc and selenium on nitric oxide synthase transcription and translation in the temporoparietal cortex of ischemic rats. (a), (c), and (e) mRNA levels; (b), (d), and (f) protein levels. CCAO: common carotid artery occlusion for 10 min; Zn + CCAO: chronic zinc administration before CCAO: Zn + CCAO + Se: chronic zinc administration before CCAO followed by selenium administration. The values were normalized against the control group. nv: normalized values. Each value represents mean ± SEM of 5 independent experiments made in triplicate. $^{*}P < 0.05$, one-way ANOVA with post hoc Dunnett's test when compared to the control untreated group; $^{\dagger}P < 0.05$, Student's t-test when compared with the respective CCAO group.

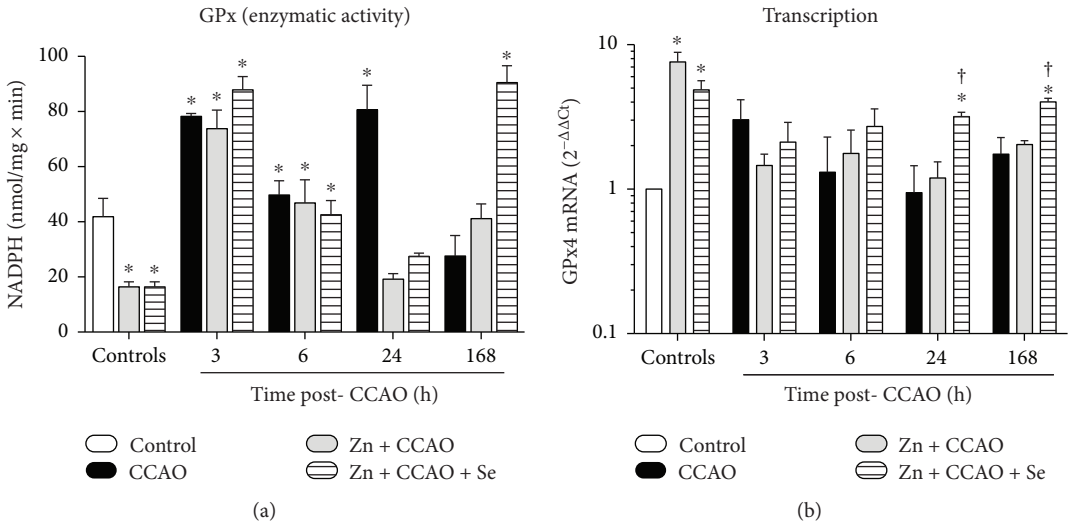

Figure 3: The combined treatment with zinc and selenium increased the enzymatic activity and transcription of glutathione peroxidase in the late phase of hypoxia-ischemia in the rat. (a) Enzymatic activity of GPx and (b) mRNA levels of GPx4. CCAO: common carotid artery occlusion for 10 min; Zn + CCAO: chronic zinc administration before CCAO; Zn + CCAO + Se: chronic zinc administration before CCAO followed by selenium administration. The values were normalized against the control group. Each value represents mean ± SEM of 5 independent experiments made in triplicate. $^{*}P < 0.05$, one-way ANOVA with post hoc Dunnett's test when compared to the control untreated group; $^{\dagger}P < 0.05$, Student's t-test when compared with the respective CCAO group.

Zn + CCAO only prevented the CCAO-induced increase in *Nos1* mRNA at 3 h after CCAO and in *Nos3* mRNA at 168 after CCAO (Figure 2(a) and Figure 2(e)). The combined treatment Zn + CCAO + Se prevented the CCAO-induced increase in *Nos1* and Nos3 mRNAs only at 168 h after CCAO (Figures 2(a) and 2(e)). It is interesting to note that *Nos2* mRNA was not detected in the Zn + CCAO + Se group at 3 h and 168 h after CCAO (Figure 2(c)). A similar effect occurred in the CCAO group and Zn + CCAO group at 168 h after CCAO (Figure 2(c)).

Concerning NOSs protein expression, the CCAO do not modify NOS3 (Figure 2(f)). NOS1 (Figure 2(b)) and NOS2 (Figure 2(d)) in the temporoparietal cortex decreased their expression over time in all groups when compared with the untreated controls, and there was no statistical difference among the groups. The average of decrease was 43% ($P < 0.004$) for NOS1 and 44% ($P < 0.005$) for NOS2.

CCAO increases GPx activity in the temporoparietal cortex at 3 h (86 ± 2%, $P = 0.0132$) and at 24 h postreperfusion (92 ± 11%, $P = 0.0100$) when compared with the untreated controls (Figure 3(a)). The Zn + Se group significantly decreased at the same levels (60 ± 4%, $P = 0.0311$) for GPx activity (Figure 3(a)). A significant decrease in GPx activity was observed at 24 h postreperfusion (Figure 3(a)) in the Zn + CCAO (76 ± 3%, $P = 0.0027$) and Zn + CCAO + Se groups (65 ± 2%, $P = 0.0043$). At 168 h postreperfusion, only the Zn + CCAO + Se group increased by 227 ± 22% for GPx ($P = 0.0028$) activity when compared with the respective CCAO group (Figure 3(a)), showing an antioxidant effect in the late phase.

In the absence of CCAO, *Gpx4* mRNA was upregulated with zinc administration (7.6 ± 1.25, $P = 0.0008$) and Zn + Se administration (4.8 ± 0.7, $P = 0.0190$) when compared with the untreated controls (Figure 3(b)). CCAO did not affect the basal levels of *Gpx4* mRNA (Figure 3(b)). The combined treatment Zn + CCAO + Se increased *Gpx4* mRNA at 24 h (3.35 ± 0.25, $P = 0.0459$) and at 168 h (2.3 ± 0.13, $P = 0.0485$) postreperfusion (Figure 3(c)) as compared with the CCAO group (Figure 3(b)).

SOD activity in the temporoparietal cortex was increased at 258 ± 12% ($P = 0.0021$) by the zinc or Zn + Se group when compared with untreated controls (Figure 4(a)). CCAO decreases SOD activity (65 ± 11%, $P = 0.0486$) at 168 h when compared with the untreated controls (Figure 4(a)). At this time, only Zn + CCAO increased SOD activity (78 ± 20%, $P = 0.0457$) when compared with the respective CCAO group (Figure 4(a)).

The zinc or Zn + Se group is differentially regulated in the *Sod* isoforms. The zinc group did not affect *Sod1* transcript levels (Figure 4(b)), whereas it upregulated *Sod2* (3.0 ± 0.69, $P = 0.0453$) and Sod3 (2.9 ± 0.76, $P = 0.0280$) transcripts when compared with the untreated controls (Figures 4(c) and 4(d)). The increases in mRNA levels were 2.78 ± 0.23-fold ($P = 0.0030$) for *Sod1*, 2.8 ± 0.2-fold ($P = 0.0395$) for *Sod2*, and 2.4 ± 0.3-fold ($P = 0.0383$) for *Sod3*. CCAO did not affect *Sod1* transcripts. Whereas CCAO upregulated *Sod2* (2.9 ± 0.46, $P = 0.0422$) at 3 h (Figure 4(c)) and *Sod3* at 3 h (2.8 ± 0.28, $P = 0.0038$) and 168 h (2.5 ± 0.39, $P = 0.0065$), CCAO did not modify when compared with the untreated controls (Figure 4(d)). None of the treatments modified *Sod1* transcripts in the times studied when compared with the respective CCAO group (Figure 4(b)). Zn + CCAO + Se only upregulated *Sod2* (5.3 ± 1.3, $P = 0.0051$) and *Sod3* (6.13 ± 0.9, $P = 0.0290$) at 24 h postreperfusion when compared to the respective CCAO group (Figures 4(c) and 4(d)).

Chemokine transcription levels in the temporoparietal cortex are shown in Figure 5. CCAO did not affect transcription of *Ccl2* and its receptor *Ccr2* in the time studied

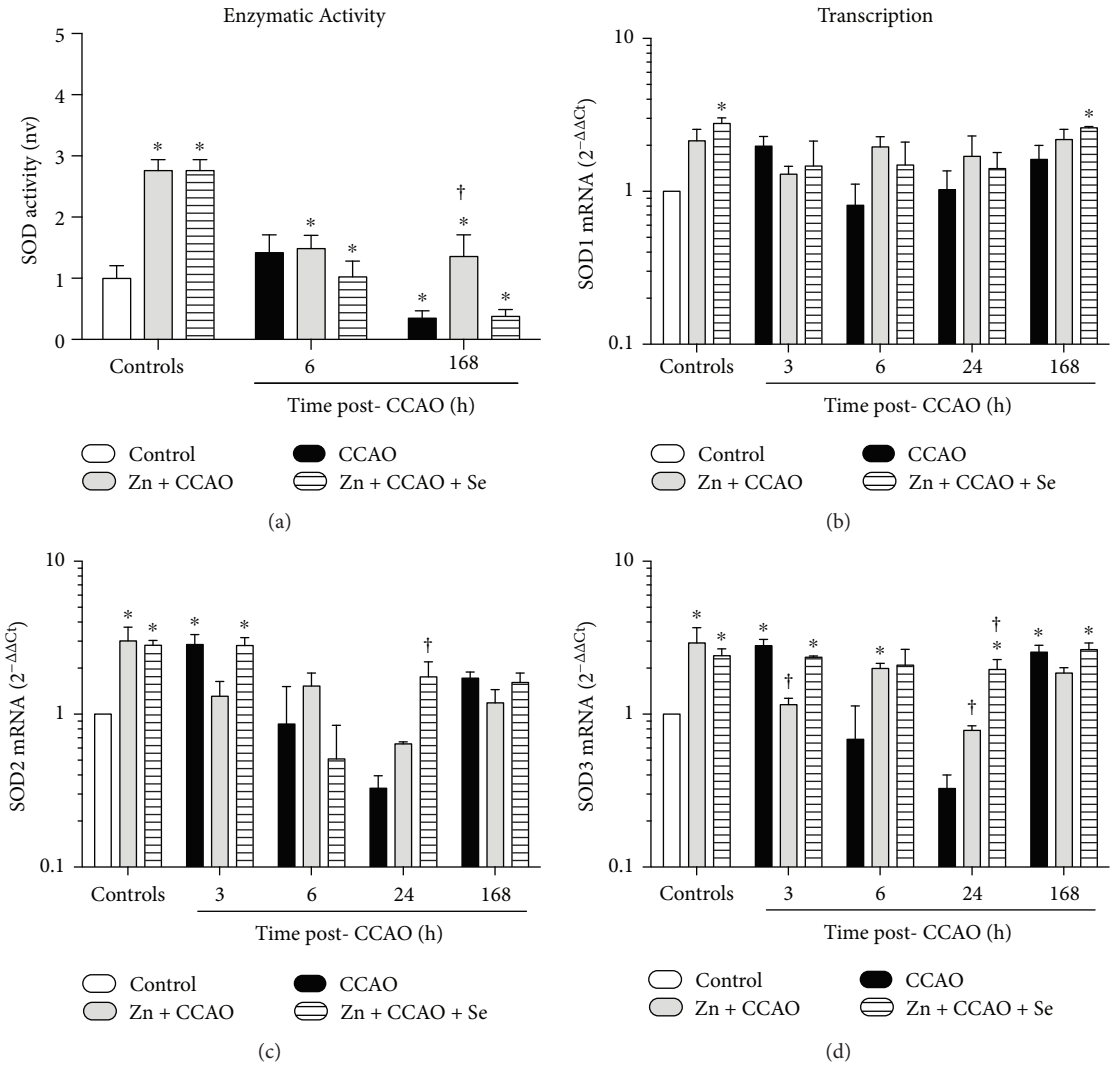

Figure 4: Differential effect of the combined treatment with zinc and selenium on the enzymatic activity and transcription of superoxide dismutase in the rat hypoxia-ischemia model. (a) Enzymatic activity of SOD, (b) mRNA levels of Sod1, (c) mRNA levels of Sod2, and (d) mRNA levels of Sod3. CCAO: common carotid artery occlusion for 10 min; Zn + CCAO: chronic zinc administration before CCAO; Zn + CCAO + Se: chronic zinc administration before CCAO followed by selenium administration. The values were normalized against the control group. Each value represents mean ± SEM of 5 independent experiments made in triplicate. $^{*}P < 0.05$, one-way ANOVA with post hoc Dunnett's test when compared to the control untreated group; $^{\dagger}P < 0.05$, Student's t-test when compared with the CCAO group.

(Figures 5(a) and 5(b)). As compared with the control group, CCAO upregulated the following chemokines and their receptors: *Cxcl12* at 3 h (3 ± 0.7, $P = 0.0426$; Figure 5(c)), its receptor *Cxcr4* at 3 h (2.7 ± 0.61, $P = 0.0475$; Figure 5(d)) and 6 h post-CCAO (3.9 ± 0.9, $P = 0.0354$; Figure 5(d)), and *Cxcl13* at 3 h (3.84 ± 0.0204, $P = 0.01$; Figure 5(e)) and its receptor *Cxcr5* at 3 h (16.6 ± 2.2, $P = 0.0005$; Figure 5(f)) and at 6 h (8.0 ± 2.3, $P = 0.0316$; Figure 5(f)).

Zinc caused an upregulation only of *Cxcr4* (5.5 ± 0.9, $P = 0.0354$; Figure 5(d)), *Cxcl13* (3.5 ± 0.8, $P = 0.0218$; Figure 5(e)), and *Cxcr5* (8.3 ± 1.4, $P = 0.0261$; Figure 5(f)), whereas Zn + Se upregulated *Ccr2* (3.19 ± 0.77, $P = 0.0164$, Figure 5(b)), *Cxcl12* (11.2 ± 1.56, $P = 0.0001$; Figure 5(c)), *Cxcr4* (8.8 ± 1.8, $P = 0.0006$, Figure 5(d)), *Cxcl13* (3.6 ± 0.13, $P = 0.0268$; Figure 5(e)), and *Cxcr5* (9.1 ± 1,6, $P = 0.0085$; Figure 5(f)).

As compared with CCAO effect, Zn + CCAO upregulated the following chemokines and their receptors: *Ccl2* at 168 h (2.4 ± 0.2, $P = 0.0307$; Figure 5(a)), *Cxcl12* at 6 h (3.8 ± 0.69, $P = 0.0376$; Figure 5(c)), and *Cxcr4* at 24 h (4.4 ± 0.2, $P = 0.0001$; Figure 5(d)). Upregulation and downregulation were observed in *Cxcl13* at 3 h (0.38 ± 0.12, $P = 0.0321$) and at 6 h (3.49 ± 0.44, $P = 0.0428$; Figure 5(e)) and in *Cxcr5* at 3 h (0.23 ± 0.07, $P = 0.0075$) and at 168 h (2.3 ± 0.55, $P = 0.0473$; Figure 5(f)).

As compared with the CCAO group, Zn + CCAO + Se caused an upregulation of *Ccl2* at 168 h (3.7 ± 0.69, $P = 0.0226$; Figure 5(a)) and *Cxcl12* at 3 h (2.5 ± 0.43, $P = 0.0367$) and 6 h (4 ± 1, $P = 0.0314$, Figure 5(c)). *Cxcr4* was upregulated since 24 h (5.5 ± 1.1, $P = 0.0162$) to 168 h (2.65 ± 0.49, $P = 0.0413$; Figure 5(d)) post-CCAO. *Cxcl13* was upregulated at 24 h (5.9 ± 1.6, $P = 0.0357$; Figure 5(e)), and

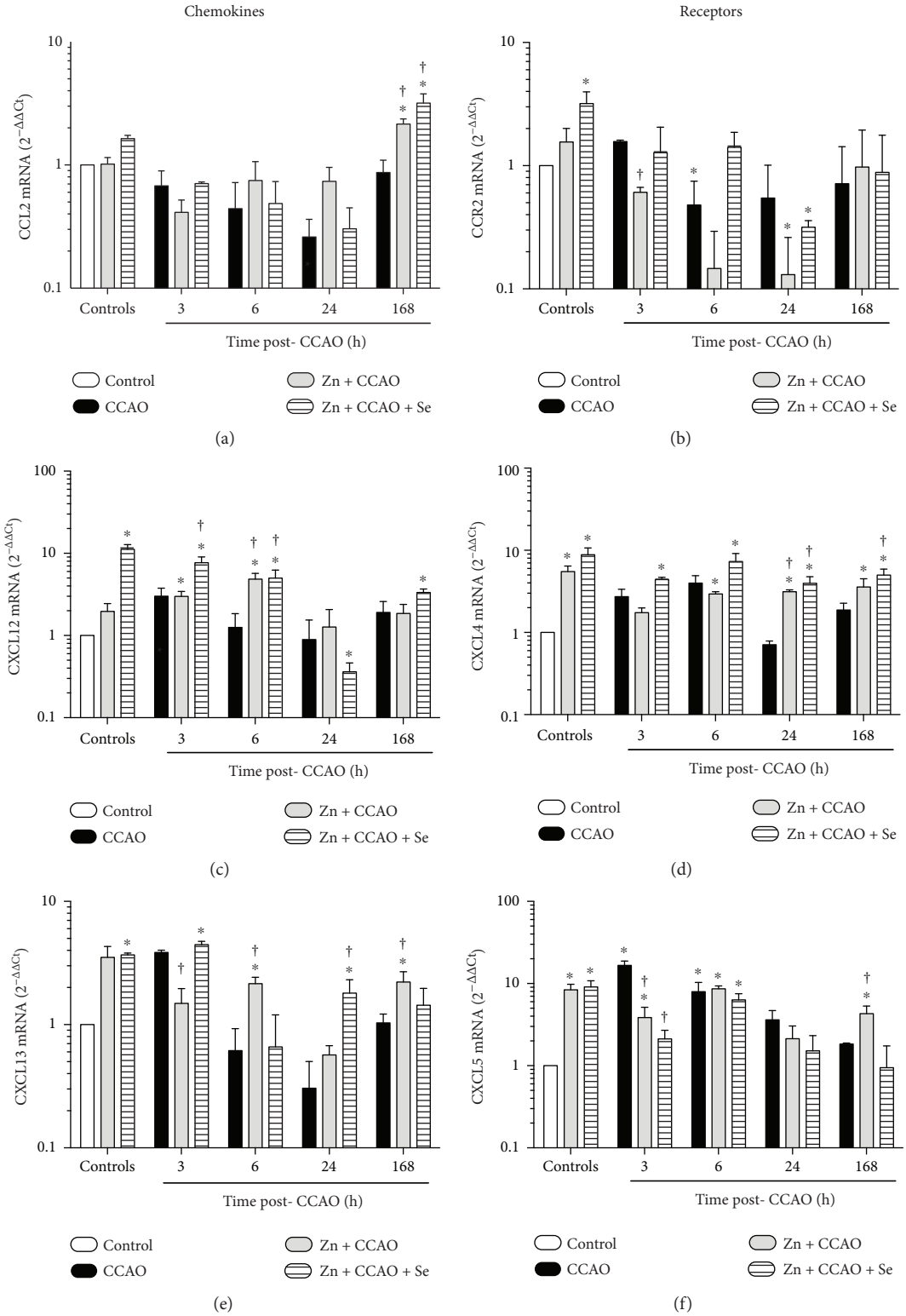

Figure 5: Differential effect of the combined treatment with zinc and selenium on chemokine and receptor transcription in the rat hypoxia-ischemia model. (a), (c), and (e) Chemokines levels; (b), (d), (f) receptors of the respective chemokines. CCAO: common carotid artery occlusion for 10 min; Zn + CCAO: chronic zinc administration before CCAO; Zn + CCAO + Se: chronic zinc administration before CCAO followed by selenium administration. The values were normalized against the control group. Each value represents mean ± SEM of 5 independent experiments made in triplicate. $^{*}P < 0.05$, one-way ANOVA with post hoc Dunnett's test when compared to the control untreated group; $^{\dagger}P < 0.05$, Student's t-test when compared with the respective CCAO group.

Cxcr5 was downregulated at 3 h (0.12 ± 0.03, $P = 0.0031$; Figure 5(f)).

Protein levels of CCR2 were increased by CCAO at 24 h ($17 \pm 6\%$, $P = 0.0457$; Figure 6(b)) in the temporoparietal cortex. CXCL12 levels were increased by Zn + CCAO at 24 h ($24 \pm 4\%$, $P = 0.0114$; Figure 6(c)) or Zn + CCAO + Se at 24 h ($32 \pm 6\%$, $P = 0.0026$; Figure 6(c)), whereas CXCL13 levels were increased by Zn + CCAO + Se ($16 \pm 1\%$, $P = 0.0425$; Figure 6(e)) at 168 h post-CCAO.

The histopathology studies showed the presence of pyknotic cells at 168 h after CCAO (Figure 7(b)) as compared with the control group (Figure 7(a)). Zinc (Figure 7(c)) or Zn + Se (Figure 7(e)) did not modify the histological morphology as compared with the untreated control. On the contrary, CCAO caused a significant increase in the number of pyknotic cells (indicative of apoptosis) by $1460 \pm 188\%$ ($P = 0.0001$) at 168 h postreperfusion as compared with the untreated control (Figures 7(b) and 7(h)). Zn + CCAO reduced the number of pyknotic cells by $80\% \pm 3\%$ ($P = 0.001$) at 168 h, as compared with the CCAO group (Figures 7(d) and 7(h)), but there was a statistical difference as compared with the untreated control group (Figure 7(g)). Zn + CCAO + Se significantly decreased the number of pyknotic cells by $90 \pm 2\%$ ($P = 0.0001$) as compared with CCAO (Figure 7(f) and 7(h)) and reached the basal values of the untreated control (Figure 7(g)).

The functional recovery from CCAO was assessed through the learning and memory test using the Morris water maze. There was not any statistical difference in information acquisition among the groups (Figure 8(a)). In memory evaluation, 7 days after the training, CCAO increased the escape latency by $53.9 \pm 17\%$ ($P = 0.0238$; Figure 8(b)) and decreased the crossing by the platform location by $37 \pm 10\%$ ($P = 0.0272$; Figure 8(c)) as compared with the controls. On the contrary, Zn + CCAO or Zn + CCAO + Se significantly decreased the latency time to remember the localization of the escape platform by $44 \pm 11\%$ ($P = 0.0197$) and $56 \pm 7\%$ ($P = 0.0046$), respectively, as compared with CCAO, suggesting improvement of consolidation of information. Only the Zn + CCAO + Se group showed a crossing by the platform location ($65 \pm 14\%$ $P = 0.0348$) higher than CCAO, thus confirming that this treatment favors the neuronal functionality and exerts effective neuroprotection against hypoxia-ischemia.

4. Discussion

Our results show that the combined prophylactic of zinc and therapeutic of selenium administration had better effective protection against a transient hypoxic-ischemic event in the temporoparietal cortex, unlike other strategies we have tested such as the prophylactic administration of Se alone or combined with Zn (data not shown). This neuroprotection can be mainly explained by the increase in transcription and enzymatic activity of GPx and SOD, which prevented lipid peroxidation, and the significant decrease in neuronal cell death that is shown by the improvement of long-term memory.

Several studies have shown that chronic prophylactic administration of zinc shows a preconditioning effect [25–27]. This preconditioning effect can be explained by the induction of antioxidant enzymes, chemokines, and DNA methylases through zinc finger proteins [28–30]. Selenium has also been involved in the epigenetic regulation at least of antioxidant enzymes and DNA methylases [31]. Accordingly, our results show that the administration of those elements caused an upregulation of N*os3*, *Gpx4*, and *Sod* and the chemokines *Ccl2*, *Cxcl12*/*Cxcr4*, and *Cxcl13*/*Cxcr5*; the translation of NOS3; and the increase in the enzymatic activity of GPx and SOD. However, the protein levels of these chemokines and their receptors were not modified by zinc or selenium administration in the period studied. Therefore, the major contributor to the preconditioning effect in the transient hypoxia-ischemia model was the antioxidant effect and the preservation of NO bioavailability through NOS3 expression. As reported in a similar hypoxia-ischemia model, NOS3 is essential in the preservation and maintenance of microcirculation, inhibiting platelet aggregation, leukocyte adhesion, and migration and decreasing the inflammatory response [32]. The increased expression of NOS3 induced by zinc might be associated with the zinc finger protein ZFP580 [33]. Also, zinc stabilizes the dimerization of NOS3, which can prevent the production of superoxide anion and promote the increase in nitric oxide (NO) in the early phase of the hypoxia-ischemia process [34, 35]. Interestingly, selenium enhanced NOS3 expression similarly to only zinc administration at the early phase of CCAO, thus recovering the endothelial function as shown in an endothelial dysfunction model [36].

Our results showed that the prophylactic chronic zinc administration in the transient hypoxia-ischemia model increased the enzymatic activity of SOD and the levels of the transcripts of *sod1*, *sod2*, and *sod3*. These enzymes are known to play a major role in protecting from intracellular, extracellular, and mitochondrial oxidative stress, as reported in the cerebral cortex and hippocampus [37–39]. A mechanism that accounts for the increase in SOD1 and SOD3 activity is their stabilization by zinc [40]. Also, the antioxidant effect of zinc might be due to the induction of metallothioneins, which are involved in the homeostasis of zinc and ROS [41]. Our results also show that the therapeutic administration of selenium maintains the level of enzymatic activity and transcription of SOD2 in the early phase, SOD1 in the late phase, and SOD3 in the complete period of the study post-CCAO. These three enzymes could have provided an effect of resistance/tolerance to ischemia in the early and late phases of cerebral hypoxia-ischemia, as reported in transgenic mice [42–45]. Furthermore, the effects of SOD on preventing the disruption of the blood-brain barrier [46], decreasing karyorrhexis, and attenuating the activation of NF-κB [47] might also explain the neuroprotection induced by the combined treatment with zinc and selenium. Results in *sod1* [48], *sod2*, and *sod3* knockout models [37, 49, 50] also confirmed the neuroprotective effect of SOD. Accordingly, the deficiency of SOD enzymatic activity in the late phase of ischemia has been associated with increases in the size of the infarction, the release

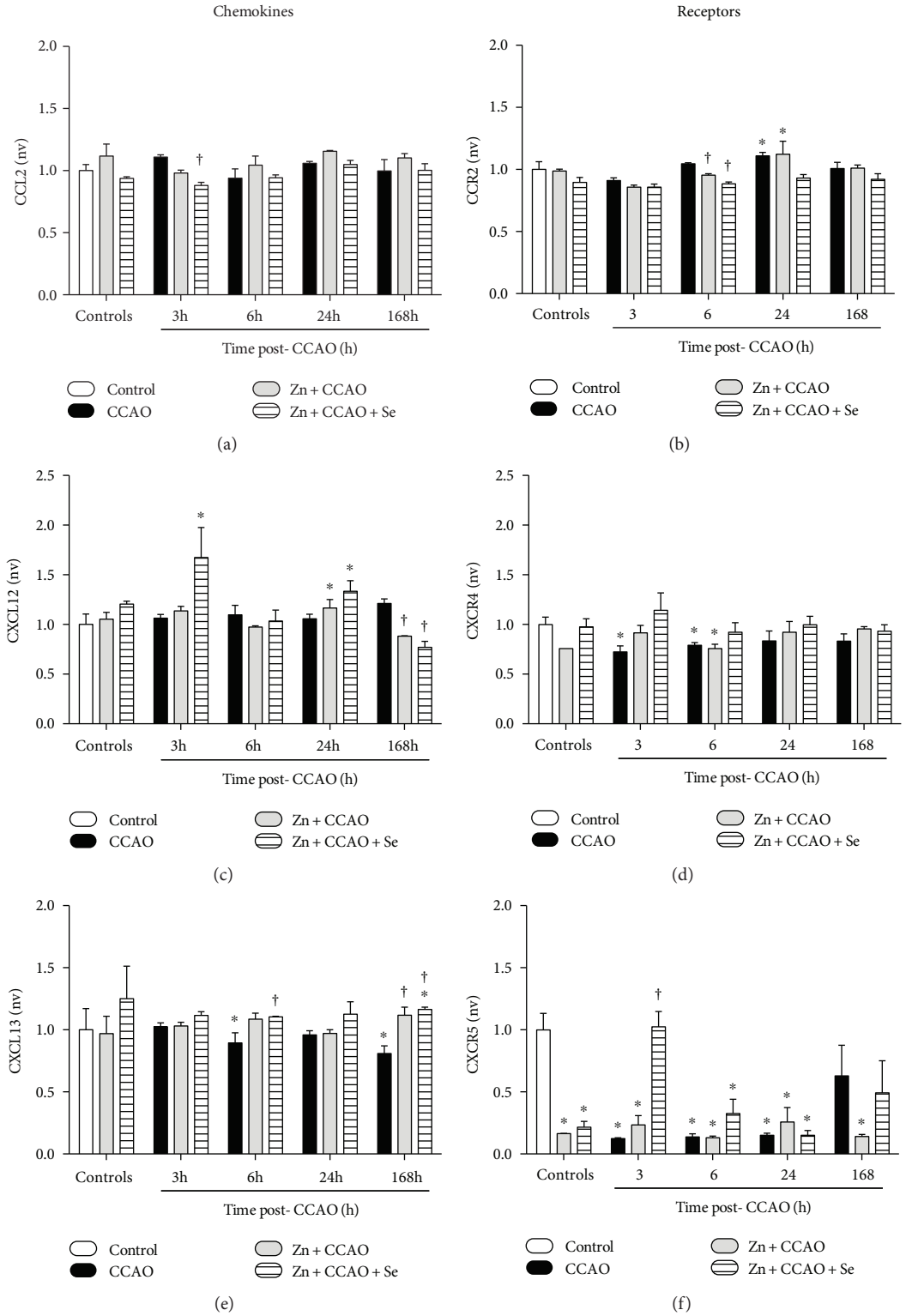

Figure 6: The administration of the combined treatment with zinc and selenium modifies the protein levels of chemokines and receptors in the rat hypoxia-ischemia model. (a), (c), and (e) Chemokine levels, and (b), (d), (f) receptors of the respective chemokines. CCAO: common carotid artery occlusion for 10 min; Zn + CCAO: chronic zinc administration before CCAO. Zn + CCAO + Se: chronic zinc administration before CCAO followed by selenium administration. The values were normalized against the control group. nv: normalized values. Each value represents mean ± SEM of 5 independent experiments made in triplicate. $^{*}P < 0.05$, one-way ANOVA with post hoc Dunnett's test when compared with the untreated control group; $^{\dagger}P < 0.05$, Student's t-test when compared with the respective CCAO group.

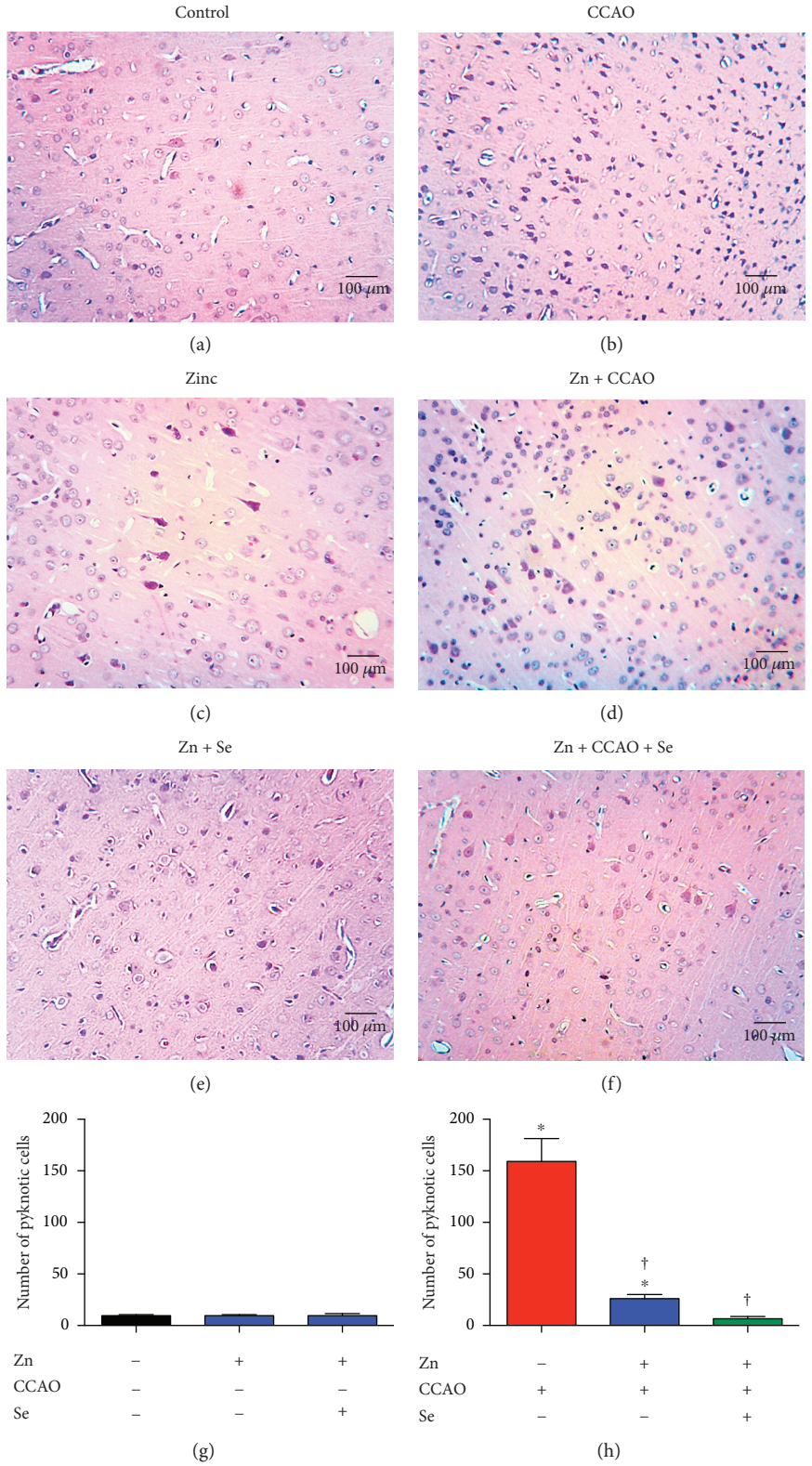

Figure 7: The administration of the combined treatment with zinc and selenium decreases the number of pyknotic cells in the temporoparietal cortex of hypoxia-ischemic rats. Representative micrographs with hematoxylin-eosin staining. The headings indicate the different experimental conditions. (g) Counting of pyknotic cells in the control groups treated with zinc or zinc + Se. (h) Counting of pyknotic cells in the groups with CCAO and treated with zinc (zinc) or the combined treatment with zinc (zinc + CCAO) and selenium (zinc + CCAO + Se). Each value represents mean ± SEM of 5 independent experiments made in triplicate. $^{*}P < 0.05$, one-way ANOVA with post hoc Dunnett's test when compared with the untreated control group; $^{\dagger}P < 0.05$, Student's t-test when compared with the CCAO group.

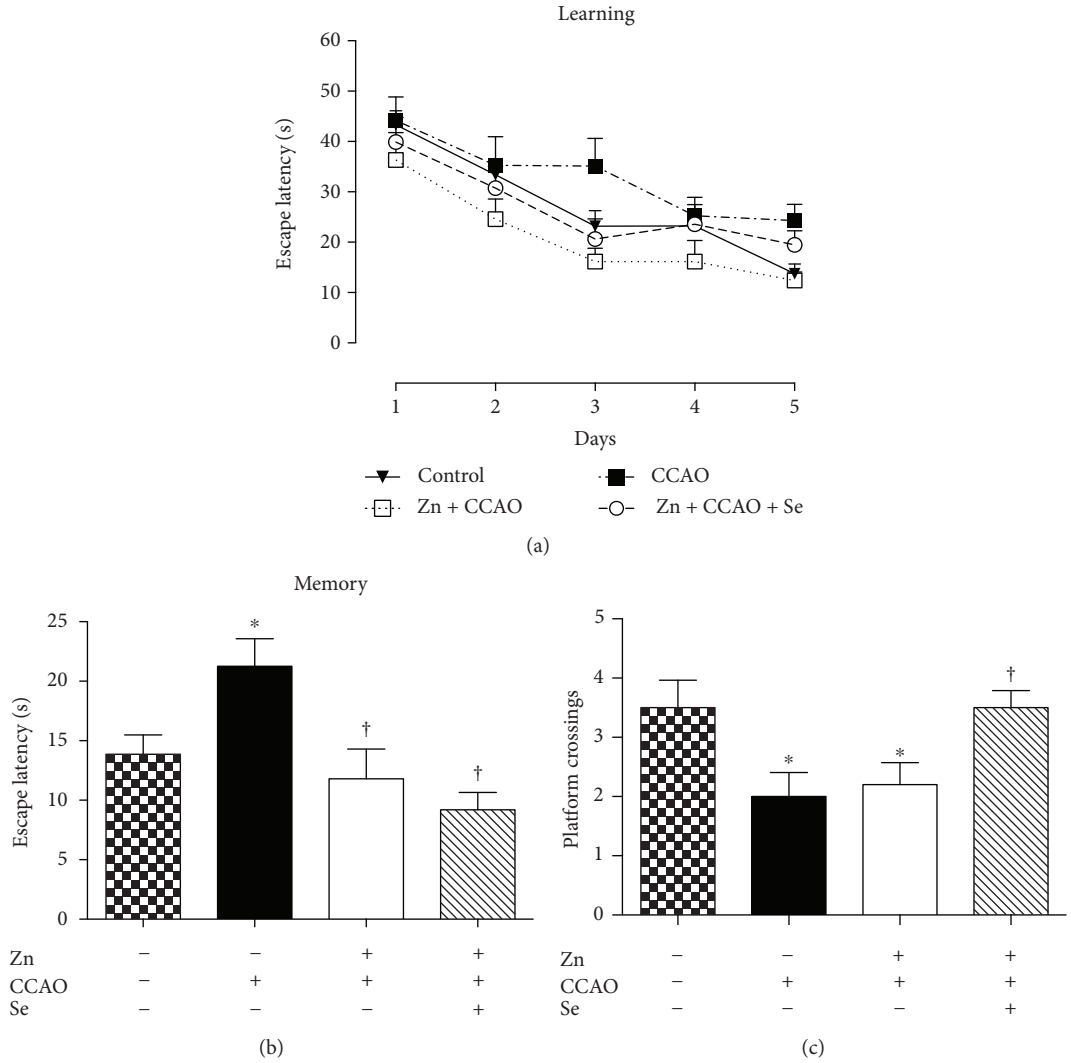

Figure 8: The administration of the combined treatment with zinc and selenium improves information consolidation in the hypoxia-ischemia model in rats. Control = untreated rats; Zn = zinc; CCAO = common carotid artery occlusion; Zn + CCAO = chronic zinc administration before CCAO; Zn + CCAO + Se = chronic zinc administration before CCAO followed by selenium (Se) administration. Each value represents mean ± SEM of 5 independent experiments made in triplicate. $^{*}P < 0.05$, one-way Kruskal-Wallis analysis of variance with post hoc Dunnett's test when compared with the untreated control group; $^{\dagger}P < 0.05$, Mann-Whitney U test when compared with the CCAO group.

of cytochrome c, and the production of mitochondrial superoxide radicals [51]. Of the three SOD isoforms, SOD2 is thought to be the primary contributor to the protective effect in both transient and permanent occlusion [52, 53]. Our results support this proposal.

We found that the combined treatment with zinc and selenium also causes upregulation of *Gpx4* in the early and late phases of CCAO. This result suggests that GPx4 also contributes to the neuroprotective effect of zinc and selenium, removing peroxides from cell membranes and macromolecules such as lipids, proteins, and DNA [54, 55]. Another mechanism of neuroprotection by GPx4 is to prevent apoptosis, counteracting the activity of lipoxygenase (LOX) [56] and promoting survival and proliferation [57]. In agreement with the antiapoptotic effect, *Gpx* knockout mice develop an increased volume of myocardial infarction in a hypoxia-ischemia event [58]. Furthermore, selenium can inhibit TRPM2 and TRPV1 receptors (activated by increasing H_2O_2), thus preventing the entry of calcium into the cell that is known to detonate oxidative stress and inflammation [59].

Our results show that CCAO upregulated the mRNA for *Cxcl12*/*Cxcr4* and *Cxcl13*/*Cxcr5* without modifying their protein levels, although it decreased CXCL13 protein levels. In contrast with our transient CCAO model for 10 min, the permanent occlusion of the middle cerebral artery (MCAO) increases CCL2, CXCL2, and CXCL13 levels after 2 days, gradually decreasing after 7 days of MCAO [60, 61]. Therefore, the transient effect of hypoxia-ischemia might be insufficient to alter the protein levels of chemokines and receptors in the time points we have studied. Moreover, the lack of the effect in protein levels can be explained by posttranscriptional regulation of miRNAs [62, 63] or a posttranslational regulation at the level of

degradation after receptor-ligand desensitization [64]. In this latter case, those chemokines could have exerted their function before their degradation. Then, the upregulated *Ccl2*/*Ccr2* by the combined zinc and selenium administration in the late phase of hypoxia-ischemia might be neuroprotective because they are known to decrease cell death and improve memory [65]. Furthermore, CCL2 also stimulates the migration of neuronal precursor cells to the damaged area [66]. We have previously reported that high levels of CCL2 by a subacute prophylactic administration of zinc are associated with a preconditioning process [5]. However, the combined treatment with zinc and selenium did not maintain the preconditioning effect of zinc but exerted the therapeutic effect of selenium in the late phase. This effect is reflected by a decrease in cell death and recovery of long-term memory.

CXCL12 and CXCL13 have been associated with a deleterious role during cerebral ischemia [67] attracting lymphocytes [68]. Nevertheless, CXCL12 and CXL13 can also attract neuronal precursor cells mainly through interaction with CXCR4 or CXCR5, respectively [69–72]. CXCL12 and CXCL13 promote the migration of neuroblasts from the subventricular zone in neonatal mice [73], although the main promoter of neuroblast migration is CXCL12 [74]. In this study, we found that the combined treatment with zinc and selenium upregulated *Cxcl12* and *Cxcl13* and increased CXCL13 protein levels. Therefore, these chemokines can be associated with the neuroprotective effect of the combined treatment with zinc and selenium.

The effect of selenium on memory consolidation has been shown in other models different from hypoxia-ischemia like Alzheimer's disease [75]. The facilitation of learning and improvement of cognitive development have been associated to the neuroprotective effect of zinc, which decreases free radicals produced by cerebral ischemia [76]. Our group showed similar results in the preconditioning effect of subacute zinc administration in the CCAO rat model [5]. However, the prophylactic chronic zinc administration (0.2 mg/kg of body weight/days) exerted a partial effect because there was no memory consolidation as reported previously with a higher dose of zinc [19]. In contrast, the therapeutic administration of selenium improved the long-term memory consolidation, which is consistent with the significant decrease in neuronal cell death induced by cerebral ischemia in the temporoparietal cortex.

In summary, the combination of the chronic prophylactic zinc administration with the therapeutic selenium administration exerts effective neuroprotection against transient hypoxia-ischemia. In this effect, GPx and SOD seem to be the key players in reducing oxidative stress and cell death, suggesting possible participation in neuroregeneration. The perspective of this work consists of challenging the present therapeutic strategy with a longer time of common carotid artery occlusion as it happens in humans.

Data Availability

The data used to support the findings of this study are included within the article.

Conflicts of Interest

The authors declare no competing financial interest, personal or other relationships with other people or organizations within five years of beginning the submitted work.

Acknowledgments

Constantino Tomas-Sanchez, Victor Manuel Blanco-Alvarez, Alejandro Gonzalez-Vazquez, and Ana Karina Aguilar-Peralta are recipients of scholarships from CONACYT. This work was supported by VIEP (Grant NAT/2017).

References

[1] N. Tonder, F. F. Johansen, C. J. Frederickson, J. Zimmer, and N. H. Diemer, "Possible role of zinc in the selective degeneration of dentate hilar neurons after cerebral ischemia in the adult rat," *Neuroscience Letters*, vol. 109, no. 3, pp. 247–252, 1990.

[2] A. Bhatt, M. U. Farooq, S. Enduri et al., "Clinical significance of serum zinc levels in cerebral ischemia," *Stroke Research and Treatment*, vol. 2010, Article ID 245715, 4 pages, 2010.

[3] Y. Yamasaki, T. Suzuki, H. Yamaya, N. Matsuura, H. Onodera, and K. Kogure, "Possible involvement of interleukin-1 in ischemic brain edema formation," *Neuroscience Letters*, vol. 142, no. 1, pp. 45–47, 1992.

[4] T. Doi, H. Hara, M. Kajita, T. Kamiya, and T. Adachi, "Zinc regulates expression of IL-23 p19 mRNA via activation of eIF2α/ATF4 axis in HAPI cells," *Biometals*, vol. 28, no. 5, pp. 891–902, 2015.

[5] V. M. Blanco-Alvarez, G. Soto-Rodriguez, J. A. Gonzalez-Barrios et al., "Prophylactic subacute administration of zinc increases CCL2, CCR2, FGF2, and IGF-1 expression and prevents the long-term memory loss in a rat model of cerebral hypoxia-ischemia," *Neural Plasticity*, vol. 2015, Article ID 375391, 15 pages, 2015.

[6] F. Lopez, J. Hernandez-Palazon, R. Lopez, E. Alarcon, and J. F. Martinez-Lage, "Activity of copper-zinc superoxide dismutase in a global ischemic brain lesion model without arterial hypotension," *Neurocirugía*, vol. 15, no. 2, pp. 151–158, 2004.

[7] D. R. Morris and C. W. Levenson, "Zinc in traumatic brain injury: from neuroprotection to neurotoxicity," *Current Opinion in Clinical Nutrition and Metabolic Care*, vol. 16, no. 6, pp. 708–711, 2013.

[8] F. F. Johansen, N. Tonder, M. Berg, J. Zimmer, and N. H. Diemer, "Hypothermia protects somatostatinergic neurons in rat dentate hilus from zinc accumulation and cell death after cerebral ischemia," *Molecular and Chemical Neuropathology*, vol. 18, no. 1-2, pp. 161–172, 1993.

[9] D. Tsuchiya, S. Hong, S. W. Suh, T. Kayama, S. S. Panter, and P. R. Weinstein, "Mild hypothermia reduces zinc translocation, neuronal cell death, and mortality after transient global ischemia in mice," *Journal of Cerebral Blood Flow & Metabolism*, vol. 22, no. 10, pp. 1231–1238, 2002.

[10] K. Matsushita, K. Kitagawa, T. Matsuyama et al., "Effect of systemic zinc administration on delayed neuronal death in the gerbil hippocampus," *Brain Research*, vol. 743, no. 1-2, pp. 362–365, 1996.

[11] V. M. Blanco-Alvarez, P. Lopez-Moreno, G. Soto-Rodriguez et al., "Subacute zinc administration and L-NAME caused an increase of NO, zinc, lipoperoxidation, and caspase-3 during

a cerebral hypoxia-ischemia process in the rat," *Oxidative Medicine and Cellular Longevity*, vol. 2013, Article ID 240560, 10 pages, 2013.

[12] S. L. Mehta, S. Kumari, N. Mendelev, and P. A. Li, "Selenium preserves mitochondrial function, stimulates mitochondrial biogenesis, and reduces infarct volume after focal cerebral ischemia," *BMC Neuroscience*, vol. 13, no. 1, p. 79, 2012.

[13] G. Erbil, S. Ozbal, U. Sonmez et al., "Neuroprotective effects of selenium and ginkgo biloba extract (EGb761) against ischemia and reperfusion injury in rat brain," *Neurosciences*, vol. 13, no. 3, pp. 233–238, 2008.

[14] B. V. Lakshmi, M. Sudhakar, and K. S. Prakash, "Protective effect of selenium against aluminum chloride-induced Alzheimer's disease: behavioral and biochemical alterations in rats," *Biological Trace Element Research*, vol. 165, no. 1, pp. 67–74, 2015.

[15] A. Ahmad, M. M. Khan, T. Ishrat et al., "Synergistic effect of selenium and melatonin on neuroprotection in cerebral ischemia in rats," *Biological Trace Element Research*, vol. 139, no. 1, pp. 81–96, 2011.

[16] S. H. Kim, V. J. Johnson, T. Y. Shin, and R. P. Sharma, "Selenium attenuates lipopolysaccharide-induced oxidative stress responses through modulation of p38 MAPK and NF-κB signaling pathways," *Experimental Biology and Medicine*, vol. 229, no. 2, pp. 203–213, 2004.

[17] N. D. Solovyev, "Importance of selenium and selenoprotein for brain function: from antioxidant protection to neuronal signalling," *Journal of Inorganic Biochemistry*, vol. 153, pp. 1–12, 2015.

[18] P. Aguilar-Alonso, D. Martinez-Fong, N. G. Pazos-Salazar et al., "The increase in zinc levels and upregulation of zinc transporters are mediated by nitric oxide in the cerebral cortex after transient ischemia in the rat," *Brain Research*, vol. 1200, pp. 89–98, 2008.

[19] C. Tomas-Sanchez, V. M. Blanco-Alvarez, J. A. Gonzalez-Barrios et al., "Prophylactic chronic zinc administration increases neuroinflammation in a hypoxia-ischemia model," *Journal of Immunology Research*, vol. 2016, Article ID 4039837, 15 pages, 2016.

[20] T. G. Dzhandzhgava and R. R. Shakarishvili, "Effect of alpha-tocopherol and selenium on the activity of antioxidant enzymes and level of lipid peroxidation products in erythrocytes of patients with cerebral ischemia," *Voprosy Meditsinskoĭ Khimii*, vol. 37, no. 5, pp. 79–82, 1991.

[21] J. A. Gonzalez-Barrios, B. Escalante, J. Valdes, B. A. Leon-Chavez, and D. Martinez-Fong, "Nitric oxide and nitric oxide synthases in the fetal cerebral cortex of rats following transient uteroplacental ischemia," *Brain Research*, vol. 945, no. 1, pp. 114–122, 2002.

[22] D. Gerard-Monnier, I. Erdelmeier, K. Regnard, N. Moze-Henry, J. C. Yadan, and J. Chaudiere, "Reactions of 1-methyl-2-phenylindole with malondialdehyde and 4-hydroxyalkenals. Analytical applications to a colorimetric assay of lipid peroxidation," *Chemical Research in Toxicology*, vol. 11, no. 10, pp. 1176–1183, 1998.

[23] J. J. Sedmak and S. E. Grossberg, "A rapid, sensitive, and versatile assay for protein using Coomassie brilliant blue G250," *Analytical Biochemistry*, vol. 79, no. 1-2, pp. 544–552, 1977.

[24] R. Morris, "Developments of a water-maze procedure for studying spatial learning in the rat," *Journal of Neuroscience Methods*, vol. 11, no. 1, pp. 47–60, 1984.

[25] J. M. Gidday, "Cerebral preconditioning and ischaemic tolerance," *Nature Reviews. Neuroscience*, vol. 7, no. 6, pp. 437–448, 2006.

[26] J. M. Lee, J. M. Lee, K. R. Kim, H. Im, and Y. H. Kim, "Zinc preconditioning protects against neuronal apoptosis through the mitogen-activated protein kinase-mediated induction of heat shock protein 70," *Biochemical and Biophysical Research Communications*, vol. 459, no. 2, pp. 220–226, 2015.

[27] S. K. Kansal, U. Jyoti, S. Sharma, A. Kaura, R. Deshmukh, and S. Goyal, "Effect of zinc supplements in the attenuated cardioprotective effect of ischemic preconditioning in hyperlipidemic rat heart," *Naunyn-Schmiedeberg's Archives of Pharmacology*, vol. 388, no. 6, pp. 635–641, 2015.

[28] V. Narayan, K. C. Ravindra, C. Liao, N. Kaushal, B. A. Carlson, and K. S. Prabhu, "Epigenetic regulation of inflammatory gene expression in macrophages by selenium," *The Journal of Nutritional Biochemistry*, vol. 26, no. 2, pp. 138–145, 2015.

[29] Y. D. Hu, W. Pang, C. C. He et al., "The cognitive impairment induced by zinc deficiency in rats aged 0 ~ 2 months related to BDNF DNA methylation changes in the hippocampus," *Nutritional Neuroscience*, vol. 20, no. 9, pp. 519–525, 2017.

[30] B. Speckmann, S. Schulz, F. Hiller et al., "Selenium increases hepatic DNA methylation and modulates one-carbon metabolism in the liver of mice," *The Journal of Nutritional Biochemistry*, vol. 48, pp. 112–119, 2017.

[31] E. Jablonska and E. Reszka, "Selenium and epigenetics in cancer: focus on DNA methylation," *Advances in Cancer Research*, vol. 136, pp. 193–234, 2017.

[32] R. Greco, C. Demartini, A. M. Zanaboni, F. Blandini, D. Amantea, and C. Tassorelli, "Endothelial nitric oxide synthase inhibition triggers inflammatory responses in the brain of male rats exposed to ischemia-reperfusion injury," *Journal of Neuroscience Research*, vol. 96, no. 1, pp. 151–159, 2017.

[33] S. Wei, J. Huang, Y. Li et al., "Novel zinc finger transcription factor ZFP580 promotes differentiation of bone marrow-derived endothelial progenitor cells into endothelial cells via eNOS/NO pathway," *Journal of Molecular and Cellular Cardiology*, vol. 87, pp. 17–26, 2015.

[34] M. H. Zou, C. Shi, and R. A. Cohen, "Oxidation of the zinc-thiolate complex and uncoupling of endothelial nitric oxide synthase by peroxynitrite," *The Journal of Clinical Investigation*, vol. 109, no. 6, pp. 817–826, 2002.

[35] A. V. Santhanam, L. V. d'Uscio, L. A. Smith, and Z. S. Katusic, "Uncoupling of eNOS causes superoxide anion production and impairs NO signaling in the cerebral microvessels of hph-1 mice," *Journal of Neurochemistry*, vol. 122, no. 6, pp. 1211–1218, 2012.

[36] H. Ren, J. Mu, J. Ma et al., "Selenium inhibits homocysteine-induced endothelial dysfunction and apoptosis via activation of AKT," *Cellular Physiology and Biochemistry*, vol. 38, no. 3, pp. 871–882, 2016.

[37] G. W. Kim, T. Kondo, N. Noshita, and P. H. Chan, "Manganese superoxide dismutase deficiency exacerbates cerebral infarction after focal cerebral ischemia/reperfusion in mice: implications for the production and role of superoxide radicals," *Stroke*, vol. 33, no. 3, pp. 809–815, 2002.

[38] T. Matsui, A. Ohta, and H. Takagi, "Morphological studies on Mn-SOD, NOS and calcium binding proteins in the rat hippocampus," *Osaka City Medical Journal*, vol. 42, no. 1, pp. 1–13, 1996.

[39] F. Yang, B. Li, X. Dong, W. Cui, and P. Luo, "The beneficial effects of zinc on diabetes-induced kidney damage in murine rodent model of type 1 diabetes mellitus," *Journal of Trace Elements in Medicine and Biology*, vol. 42, pp. 1–10, 2017.

[40] S. Nedd, R. L. Redler, E. A. Proctor, N. V. Dokholyan, and A. N. Alexandrova, "Cu, Zn-superoxide dismutase without Zn is folded but catalytically inactive," *Journal of Molecular Biology*, vol. 426, no. 24, pp. 4112–24, 2014.

[41] M. S. Farias, P. Budni, C. M. Ribeiro et al., "Antioxidant supplementation attenuates oxidative stress in chronic hepatitis C patients," *Gastroenterología y Hepatología*, vol. 35, no. 6, pp. 386–394, 2012.

[42] H. Sheng, R. D. Bart, T. D. Oury, R. D. Pearlstein, J. D. Crapo, and D. S. Warner, "Mice overexpressing extracellular superoxide dismutase have increased resistance to focal cerebral ischemia," *Neuroscience*, vol. 88, no. 1, pp. 185–191, 1999.

[43] H. Sheng, M. Kudo, G. B. Mackensen, R. D. Pearlstein, J. D. Crapo, and D. S. Warner, "Mice overexpressing extracellular superoxide dismutase have increased resistance to global cerebral ischemia," *Experimental Neurology*, vol. 163, no. 2, pp. 392–398, 2000.

[44] K. Sampei, A. S. Mandir, Y. Asano et al., "Stroke outcome in double-mutant antioxidant transgenic mice," *Stroke*, vol. 31, no. 11, pp. 2685–2691, 2000.

[45] J. W. Francis, J. Ren, L. Warren, R. H. Brown Jr., and S. P. Finklestein, "Postischemic infusion of Cu/Zn superoxide dismutase or SOD:Tet 451 reduces cerebral infarction following focal ischemia/reperfusion in rats," *Experimental Neurology*, vol. 146, no. 2, pp. 435–443, 1997.

[46] G. W. Kim, A. Lewen, J. Copin, B. D. Watson, and P. H. Chan, "The cytosolic antioxidant, copper/zinc superoxide dismutase, attenuates blood–brain barrier disruption and oxidative cellular injury after photothrombotic cortical ischemia in mice," *Neuroscience*, vol. 105, no. 4, pp. 1007–1018, 2001.

[47] C. Y. Huang, M. Fujimura, N. Noshita, Y. Y. Chang, and P. H. Chan, "SOD1 down-regulates NF-κB and c-Myc expression in mice after transient focal cerebral ischemia," *Journal of Cerebral Blood Flow & Metabolism*, vol. 21, no. 2, pp. 163–173, 2001.

[48] T. Kondo, A. G. Reaume, T. T. Huang et al., "Reduction of CuZn-superoxide dismutase activity exacerbates neuronal cell injury and edema formation after transient focal cerebral ischemia," *The Journal of Neuroscience*, vol. 17, no. 11, pp. 4180–4189, 1997.

[49] H. Sheng, T. C. Brady, R. D. Pearlstein, J. D. Crapo, and D. S. Warner, "Extracellular superoxide dismutase deficiency worsens outcome from focal cerebral ischemia in the mouse," *Neuroscience Letters*, vol. 267, no. 1, pp. 13–16, 1999.

[50] M. Fujimura, Y. Morita-Fujimura, M. Kawase et al., "Manganese superoxide dismutase mediates the early release of mitochondrial cytochrome C and subsequent DNA fragmentation after permanent focal cerebral ischemia in mice," *The Journal of Neuroscience*, vol. 19, no. 9, pp. 3414–3422, 1999.

[51] H. J. Bidmon, K. Kato, A. Schleicher, O. W. Witte, and K. Zilles, "Transient increase of manganese-superoxide dismutase in remote brain areas after focal photothrombotic cortical lesion," *Stroke*, vol. 29, no. 1, pp. 203–211, 1998.

[52] P. H. Chan, H. Kamii, G. Yang et al., "Brain infarction is not reduced in SOD-1 transgenic mice after a permanent focal cerebral ischemia," *Neuroreport*, vol. 5, no. 3, pp. 293–296, 1993.

[53] K. Murakami, T. Kondo, M. Kawase et al., "Mitochondrial susceptibility to oxidative stress exacerbates cerebral infarction that follows permanent focal cerebral ischemia in mutant mice with manganese superoxide dismutase deficiency," *The Journal of Neuroscience*, vol. 18, no. 1, pp. 205–213, 1998.

[54] J. P. Thomas, P. G. Geiger, M. Maiorino, F. Ursini, and A. W. Girotti, "Enzymatic reduction of phospholipid and cholesterol hydroperoxides in artificial bilayers and lipoproteins," *Biochimica et Biophysica Acta*, vol. 1045, no. 3, pp. 252–260, 1990.

[55] N. Ishibashi, O. Prokopenko, M. Weisbrot-Lefkowitz, K. R. Reuhl, and O. Mirochnitchenko, "Glutathione peroxidase inhibits cell death and glial activation following experimental stroke," *Brain Research. Molecular Brain Research*, vol. 109, no. 1-2, pp. 34–44, 2002.

[56] A. Seiler, M. Schneider, H. Forster et al., "Glutathione peroxidase 4 senses and translates oxidative stress into 12/15-lipoxygenase dependent- and AIF-mediated cell death," *Cell Metabolism*, vol. 8, no. 3, pp. 237–248, 2008.

[57] A. M. Mannes, A. Seiler, V. Bosello, M. Maiorino, and M. Conrad, "Cysteine mutant of mammalian GPx4 rescues cell death induced by disruption of the wild-type selenoenzyme," *The FASEB Journal*, vol. 25, no. 7, pp. 2135–2144, 2011.

[58] P. J. Crack, J. M. Taylor, N. J. Flentjar et al., "Increased infarct size and exacerbated apoptosis in the glutathione peroxidase-1 (Gpx-1) knockout mouse brain in response to ischemia/reperfusion injury," *Journal of Neurochemistry*, vol. 78, no. 6, pp. 1389–1399, 2001.

[59] H. Balaban, M. Naziroglu, K. Demirci, and I. S. Ovey, "The protective role of selenium on scopolamine-induced memory impairment, oxidative stress, and apoptosis in aged rats: the involvement of TRPM2 and TRPV1 channels," *Molecular Neurobiology*, vol. 54, no. 4, pp. 2852–2868, 2016.

[60] N. G. Gourmala, M. Buttini, S. Limonta, A. Sauter, and H. W. Boddeke, "Differential and time-dependent expression of monocyte chemoattractant protein-1 mRNA by astrocytes and macrophages in rat brain: effects of ischemia and peripheral lipopolysaccharide administration," *Journal of Neuroimmunology*, vol. 74, no. 1-2, pp. 35–44, 1997.

[61] X. Che, W. Ye, L. Panga, D. C. Wu, and G. Y. Yang, "Monocyte chemoattractant protein-1 expressed in neurons and astrocytes during focal ischemia in mice," *Brain Research*, vol. 902, no. 2, pp. 171–177, 2001.

[62] L. S. Arabanian, F. A. Fierro, F. Stolzel et al., "MicroRNA-23a mediates post-transcriptional regulation of CXCL12 in bone marrow stromal cells," *Haematologica*, vol. 99, no. 6, pp. 997–1005, 2014.

[63] J. Chen, R. Ning, A. Zacharek et al., "MiR-126 contributes to human umbilical cord blood cell-induced neurorestorative effects after stroke in type-2 diabetic mice," *Stem Cells*, vol. 34, no. 1, pp. 102–113, 2016.

[64] L. D. Bennett, J. M. Fox, and N. Signoret, "Mechanisms regulating chemokine receptor activity," *Immunology*, vol. 134, no. 3, pp. 246–256, 2011.

[65] Y. Kumai, H. Ooboshi, J. Takada et al., "Anti—monocyte chemoattractant protein-1 gene therapy protects against focal brain ischemia in hypertensive rats," *Journal of Cerebral Blood Flow & Metabolism*, vol. 24, no. 12, pp. 1359–1368, 2004.

[66] D. Widera, W. Holtkamp, F. Entschladen et al., "MCP-1 induces migration of adult neural stem cells," *European Journal of Cell Biology*, vol. 83, no. 8, pp. 381–387, 2004.

[67] P. Liu, J. W. Xiang, and S. X. Jin, "Serum CXCL12 levels are associated with stroke severity and lesion volumes in stroke patients," *Neurological Research*, vol. 37, no. 10, pp. 853–858, 2015.

[68] M. C. Kowarik, S. Cepok, J. Sellner et al., "CXCL13 is the major determinant for B cell recruitment to the CSF during neuroinflammation," *Journal of Neuroinflammation*, vol. 9, no. 1, p. 93, 2012.

[69] N. Weiss, C. Deboux, N. Chaverot et al., "IL8 and CXCL13 are potent chemokines for the recruitment of human neural precursor cells across brain endothelial cells," *Journal of Neuroimmunology*, vol. 223, no. 1-2, pp. 131–134, 2010.

[70] F. Del Grosso, S. Coco, P. Scaruffi et al., "Role of CXCL13-CXCR5 crosstalk between malignant neuroblastoma cells and Schwannian stromal cells in neuroblastic tumors," *Molecular Cancer Research*, vol. 9, no. 7, pp. 815–823, 2011.

[71] A. Guyon, "CXCL12 chemokine and its receptors as major players in the interactions between immune and nervous systems," *Frontiers in Cellular Neuroscience*, vol. 8, p. 65, 2014.

[72] A. M. Robin, Z. G. Zhang, L. Wang et al., "Stromal cell-derived factor 1α mediates neural progenitor cell motility after focal cerebral ischemia," *Journal of Cerebral Blood Flow & Metabolism*, vol. 26, no. 1, pp. 125–134, 2006.

[73] J. T. Miller, J. H. Bartley, H. J. Wimborne et al., "The neuroblast and angioblast chemotaxic factor SDF-1 (CXCL12) expression is briefly up regulated by reactive astrocytes in brain following neonatal hypoxic-ischemic injury," *BMC Neuroscience*, vol. 6, no. 1, p. 63, 2005.

[74] P. Thored, A. Arvidsson, E. Cacci et al., "Persistent production of neurons from adult brain stem cells during recovery after stroke," *Stem Cells*, vol. 24, no. 3, pp. 739–747, 2006.

[75] T. Ishrat, K. Parveen, M. M. Khan et al., "Selenium prevents cognitive decline and oxidative damage in rat model of streptozotocin-induced experimental dementia of Alzheimer's type," *Brain Research*, vol. 1281, pp. 117–127, 2009.

[76] A. Piechal, K. Blecharz-Klin, J. Pyrzanowska, and E. Widy-Tyszkiewicz, "Maternal zinc supplementation improves spatial memory in rat pups," *Biological Trace Element Research*, vol. 147, no. 1–3, pp. 299–308, 2012.

Hindawi
Oxidative Medicine and Cellular Longevity
Volume 2018, Article ID 3420187, 12 pages
https://doi.org/10.1155/2018/3420187

Review Article

The Oxidative Stress and Mitochondrial Dysfunction during the Pathogenesis of Diabetic Retinopathy

Meng-Yu Wu,[1,2] **Giou-Teng Yiang**,[1,2] **Tzu-Ting Lai**,[3] **and Chia-Jung Li**[4,5]

[1]*Department of Emergency Medicine, Taipei Tzu Chi Hospital, Buddhist Tzu Chi Medical Foundation, New Taipei 231, Taiwan*
[2]*Department of Emergency Medicine, School of Medicine, Tzu Chi University, Hualien 970, Taiwan*
[3]*Department of Ophthalmology, Taipei Tzu Chi Hospital, Buddhist Tzu Chi Medical Foundation, New Taipei 231, Taiwan*
[4]*Research Assistant Center, Show Chwan Memorial Hospital, Changhua 500, Taiwan*
[5]*Department of Medical Research, Chang Bing Show Chwan Memorial Hospital, Changhua 505, Taiwan*

Correspondence should be addressed to Tzu-Ting Lai; bestmind0402@gmail.com and Chia-Jung Li; nigel6761@gmail.com

Received 1 March 2018; Revised 27 June 2018; Accepted 14 August 2018; Published 5 September 2018

Academic Editor: Joanna Lecka

Diabetic retinopathy is one of the most serious microvascular complications induced by hyperglycemia *via* five major pathways, including polyol, hexosamine, protein kinase C, and angiotensin II pathways and the accumulation of advanced glycation end products. The hyperglycemia-induced overproduction of reactive oxygen species (ROS) induces local inflammation, mitochondrial dysfunction, microvascular dysfunction, and cell apoptosis. The accumulation of ROS, local inflammation, and cell death are tightly linked and considerably affect all phases of diabetic retinopathy pathogenesis. Furthermore, microvascular dysfunction induces ischemia and local inflammation, leading to neovascularization, macular edema, and neurodysfunction, ultimately leading to long-term blindness. Therefore, it is crucial to understand and elucidate the detailed mechanisms underlying the development of diabetic retinopathy. In this review, we summarized the existing knowledge about the pathogenesis and current strategies for the treatment of diabetic retinopathy, and we believe this systematization will help and support further research in this area.

1. Introduction

Diabetes mellitus (DM) is a metabolic disease characterized by hyperglycemia, due to the defects in insulin secretion and impaired insulin resistance. Diabetes, the long-term high blood sugar condition, leads to the damaging of various tissues, especially the eyes, kidneys, heart, and blood vessels, and it may aggravate other functional disorders. Diabetic retinopathy (DR) represents one of the most serious microvascular complications, in which the main pathological changes include retinal inflammation, increased vascular permeability, and abnormal angiogenesis on the surface of the retina. Previously, five classic pathways were shown to be implicated in the development of diabetic complications: polyol pathway activation, induction of the hexosamine pathway, activation of angiotensin II pathways, increase in the advanced glycosylation end product (AGE) levels in response to the activation of the cell-dependent receptors, and the activation of protein kinase C (PKC) due to the high glucose-induced peroxide overexpression [1]. Mitochondrial damage and oxidative stress are important factors affecting the development of DR [2], as they induce the production of reactive oxygen species (ROS) and the apoptosis of endothelial cells and pericytes.

Landmark clinical trials during the 1980s demonstrated that laser photocoagulation can effectively prevent the loss of vision in the patients with proliferative DR or diabetic macular edema (DME) [3, 4]. The progress of the image modalities, especially optical coherence tomography (OCT) and fluorescein angiography (FA), plays an important role in monitoring and diagnosing the disease progression and complications. Furthermore, the introduction of the intraocular administration of anti-vascular endothelial growth factor (VEGF) agents was a revolution in the management of DR, leading to the possibility of reversing the visual outcome [3–5]. Current clinical trials suggest that the anti-VEGF therapy may represent a first-line therapy for proliferative DR treatment [6]. However, although DR has been studied

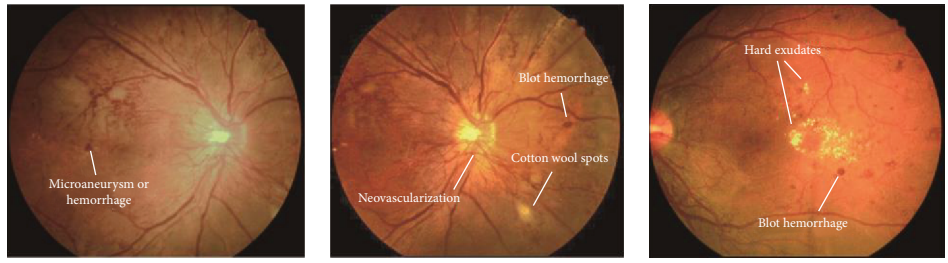

Figure 1: Clinical feature of diabetic retinopathy, including microaneurysm, microhemorrhage, cotton wool spots, neovascularization, and hard exudates.

for a number of years *in vitro* and *in vivo*, the detailed mechanisms underlying DR pathogenesis and progression remain unclear, especially concerning the observed mitochondrial dysfunction and oxidative stress. In this review article, we summarized currently investigated mechanisms and treatments, hoping to provide a stronger foundation for the future development of targeted approaches.

2. Clinical Features of DR

Based on the fundus manifestations during DR progression, different stages of DR can be recognized: mild, moderate, severe nonproliferative, and proliferative DR [7]. In the nonproliferative DR, microaneurysms can be observed, together with some intraretinal hemorrhage and flame-shape hemorrhage, intraretinal microvascular abnormalities (IRMA), and venous caliber changes, while the proliferative DR is characterized by the presence of pathologic neovascularization (Figure 1). Proliferative DR can be further classified according to the location of the new vessels, which can be found either on the optic disc or elsewhere. Neovascularization is usually accompanied by vitreous hemorrhage, traction retinal detachment, iris neovascularization (rubeosis), and angle neovascularization with intraocular pressure elevation (neovascular glaucoma). These lesions can be found years after the diagnosis of type I DM, but they are found at the time of type II DM diagnosis [8]. An important additional category of the DR cases is diabetic macular edema (DME), which represents the most important cause of the vision loss in patients with DR. DME occurs in the DR cases with different severity of disease, even in the mild nonproliferative DR [7]. DME can be categorized into mild cases, located at the posterior pole, but distant from the center of the macula; moderate cases, where the edema is located in the macula but not the center; and severe cases, which involve the center.

3. Mechanisms Underlying the Development and Progression of DR

DR is a multifactorial disease, characterized by hyperglycemia, leukostasis, microvascular damage, microinflammation, increased vascular permeability, vascular occlusion, local ischemia, and general neurodegeneration. Persistent hyperglycemia induces cellular metabolism imbalance, including excessive glucose oxidation, ROS production, local inflammation, and endothelial cell death. The detailed mechanisms underlying the accumulation of oxidative stress remain unclear. Recent studies demonstrated that five major pathways are involved in the pathogenesis of this disease, including polyol and angiotensin II pathways, AGE, PKC, and the hexosamine biosynthesis pathways [9–13]. Oxidative stress activates local inflammation and cell death. Endothelial cells on the retinal capillaries, responsible for the balancing of vascular permeability, are damaged by hyperglycemia, which further leads to fluid leakage and accumulation in the retina due to the breakdown of tight junctions between cells. Endothelial cell apoptosis, necrosis, necroptosis, and mitosis lead to local inflammation and microvascular dysfunction in the retina, which further causes blindness. The generation of ROS, inflammation, and cell death form a vicious cycle, promoting the development of DR. Furthermore, microvascular occlusions and hemorrhage activate ischemic signaling, which is followed by neovascularization through the expressions of VEGF [14, 15]. However, the neovascularized vessels are fragile, and their abnormal structure allows hemorrhaging. Progressive hemorrhage induces an increase in the VEGF expression, chronic inflammation, and retinal neurodegeneration. Neurodegeneration, inflammation, and vascular dysfunction occur in parallel and are closely interconnected (Figure 2).

Although several pathological mechanisms were reported, the details remain unclear. In this review, we focused on the increased oxidative stress, which occurs due to the polyol pathway activation leading to sorbitol accumulation, production of AGEs, activation of the PKC pathway, inflammation, and cell death.

4. Oxidative Stress Roles in the DR Pathogenesis

DR development is a complex pathological process. Although the mechanisms underlying this have not been completely elucidated, oxidative stress was shown to represent a key factor in this process [16]. Clinical and experimental studies demonstrated that hyperglycemia represents the primary factor leading to the pathogenesis of diabetic complications [17]. In the ischemic state, oxidative stress, superoxide dismutase, glutathione, lipid peroxide, and malondialdehyde (MDA) levels were shown to increase, while those of antioxidants decreased, thus inducing the oxidative damage of the retina [17]. *In vitro*, increased superoxide levels were observed in hyperglycemic conditions and shown

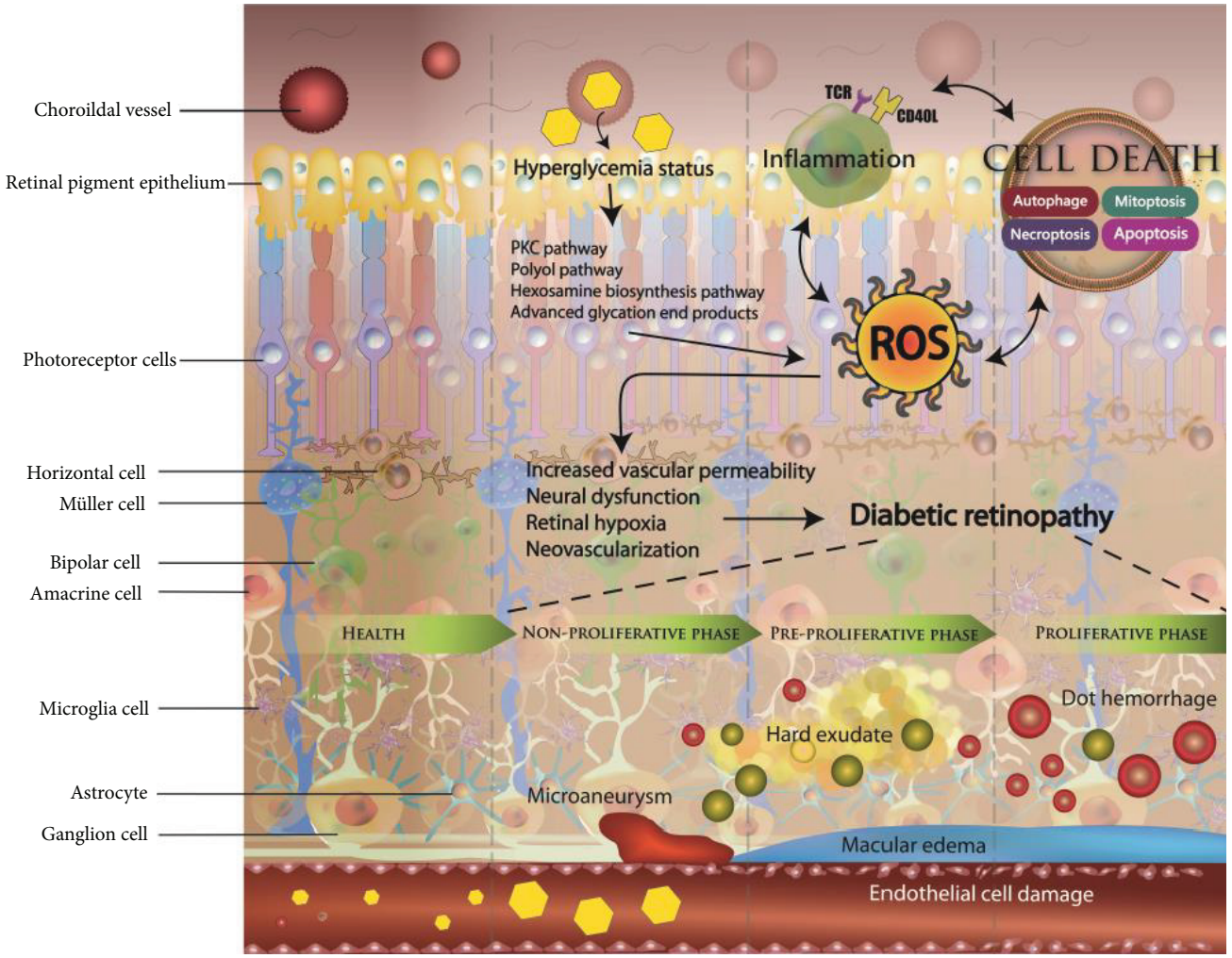

Figure 2: Illustration showing different mechanisms underlying diabetic retinopathy. During hyperglycemia, the excessive production of reactive oxygen species (ROS) via polyol pathway, advanced glycation end product (AGE) pathway, and protein kinase C (PKC) pathway can lead to the development of local inflammation and cell death. This vicious cycle increases vascular permeability, neural dysfunction, retinal hypoxia, and neovascularization. Neurodegeneration, inflammation, and vascular dysfunction operate in parallel and closely, which ultimately leads to the development of diabetic retinopathy.

to be accompanied by an increase in the hydrogen peroxide content in retinal cells [18–20]. Oxidative stress can damage cell membrane integrity as well [21], inducing apoptosis, microvascular damage, and barrier damage and ultimately leading to DR development.

4.1. Polyol Pathway Activation. Polyol pathway activation represents one of the processes observed under the hyperglycemia-induced oxidative stress conditions during DR pathogenesis, and this pathway is known as the sorbitol-aldose reductase pathway as well [22, 23]. Here, glucose is reduced to sorbitol and subsequently oxidized to fructose, with the help of two enzymes: aldose reductase, which converts glucose into sorbitol, and sorbitol dehydrogenase, which oxidize sorbitol into fructose [22]. Aldose reductase and sorbitol dehydrogenase require nicotinamide adenine dinucleotide phosphate (NADPH) and nicotinamide adenine dinucleotide (NAD+) to convert glucose into fructose [24]. Under hyperglycemic conditions, polyol pathway activity increases, which is followed by a decrease in the levels of NADPH that can regenerate an intracellular antioxidant, GSH [22]. The overactivation of the polyol pathway leads to the accumulation of ROS, which induces oxidative stress in cells. Under the physiological conditions, hexokinase returns to the glycolytic pathway by phosphorylating fructose into fructose-6-phosphate. However, high serum glucose levels lead to an imbalance between glycogenesis and the glycolysis pathway, favoring the accumulation of sorbitol. The imbalance in the potential energy reduction process was reported in a study examining mitochondrial dysfunction during DR pathogenesis. An excess of glucose in diabetes is converted to sorbitol by aldose reductase, but sorbitol cannot easily penetrate cellular membrane. One part of sorbitol molecules is catalyzed by the sorbitol dehydrogenase, leading to the oxidation of fructose, which is difficult to process further [25]. Therefore,

sorbitol and fructose accumulate in cells, leading to an increase in osmotic pressure, edema rupture, and membrane permeability damage. Considering the effects of aldose reductase on the retina, the DR pathogenesis is induced by aldose reductase activity together with the changes in the osmotic pressure caused by the accumulation of polyhydric alcohol and the second step of the sorbitol pathway, in which SDH catalyzes the oxidation of sorbitol to fructose [26]. The reduction of NAD+ into NADH, due to hypoxia and redox imbalance, increases intracellular NADH levels, leading to cell edema, structural alterations, metabolic disorders, and microvascular lesion [27].

4.2. Hexosamine Pathway Activation. In the hexosamine pathway, glucose is phosphorylated and converted into fructose-6-phosphate. Glutamine provides an amino group to fructose-6-phosphate, which leads to the formation of glucosamine 6-phosphate by fructose-6-phosphate amidotransferase (GFAT) [28]. Glucosamine 6-phosphate is acetylated and isomerized to N-acetylglucosamine 6-phosphate and finally converted to diphosphate uracil-N-acetylglucosamine (UDP-GlcNAc), which can form proteoglycans, glycolipids, and glycoproteins [29]. Glucosamine can be directly phosphorylated by hexokinase as well, leading to the generation of glucosamine 6-phosphate and conversion to UDP-GlcNAc, a substrate for post-transcriptional modification of intracellular factors [30]. The hexosamine pathway was reported to mediate the toxic effects of ROS in hyperglycemia [28–31]. In the presence of increased glucose levels, a large amount of ROS is generated, which may inhibit glyceraldehyde-3-phosphate dehydrogenase (GAPDH) activity, resulting in the influx of glycolytic products to the hexosamine pathway [10, 32]. Glucosamine produced by the activated hexosamine increases H_2O_2 production, which further results in an increased oxidation, changes in cell endothelium, increased vascular permeability, and angiogenesis. Inhibition of GAPDH induces the AGE pathway activity as well, through the interactions with intracellular methylglyoxal, leading to the increase in retinal oxidative stress [9, 33].

4.3. Activation of the PKC Pathway. The PKC pathway is considered a pathway with the key role in the pathogenesis of DR. Many studies demonstrated that the activation of the PKC pathway can lead to endothelial cell damaging by increasing endothelial permeability, changing NO bioavailability, reducing prostaglandin production, inducing VEGF expression, and inducing the production of thromboxane and endothelin-1 (ET-1) [34–37]. Hyperglycemic status induces the accumulation of ROS and synthesis of diacylglycerol (DAG), leading to the PKC pathway activation. Several PKC isoforms were shown to be activated during DR pathogenesis, such as PKC-α, -β, -δ, and -ε [38, 39]. PKC-β activation was shown to induce the release of NO, ET-1, and VEGF in endothelial cells, leading to an increase in the retinal vascular permeability and decrease in blood flow, causing macular edema. PKC-δ activation induces the formation of ROS and activates the p38 and MAPK pathway, which promotes the expression of SHP-1 and NF-κB, thus inhibiting the expression of platelet-derived growth factor (PDGF) and activating caspase signaling, which ultimately leads to pericyte loss and formation of microaneurysms. *In vitro*, the activity of diabetes-induced oxidative stress was shown to decrease following the administration of the PKC-β-specific inhibitor (LY53331), and the absence of the PKC-β isoform was shown to prevent ROS-mediated diabetic complications [40, 41]. Additionally, LY333531 treatment decreased PKC signaling levels, improving retinal vascular circulation [41, 42]. PKC pathway activation alters NO production through eNOS expression, directly affecting vascular tone and permeability and ultimately promoting endothelial dysfunction.

4.4. AGE Accumulation. Hyperglycemia leads to an increase in the nonenzymatic glycosylation of tissue macromolecules. AGEs are irreversibly cross-linked products, formed from strong glycating dicarbonyl compounds such as methylglyoxal and glyoxal [43]. The receptor for AGE (RAGE) plays an important role in the DR pathogenesis as well [44], as its activation mediates a wide range of biological effects, including ROS level increase, cytokine release, and cell function and death alterations. AGE and RAGE, accumulated in the retinal microvessels, interact directly with intracellular proteins, leading to endothelial dysfunction [45, 46]. Increased AGE accumulation induces pericyte apoptosis in the retina as well, through the activation of NF-κB [47]. In the bovine retinal capillary pericytes, following the treatment with AGE solution, pericyte apoptosis and a decrease in the antioxidant activity were observed [48]. AGEs can promote the release of cytokines and VEGF, affecting vascular endothelial permeability and self-regulation and inducing inflammation.

4.5. Angiotensin II (ANG-II) Induces Retinal Oxidative Damage. ANG-II is the product of renin-angiotensin system (RAS) that is involved in the regulation of the systemic and local blood pressures [49]. ANG-II plays important roles in both atherosclerosis and diabetes pathogeneses [50–52]. During DR pathogenesis, this molecule induces vasoconstriction, inflammation, oxidative stress, cellular dysfunctions, angiogenesis, and fibrosis [53, 54]. Additionally, it can activate NADPH enzyme levels as well, thus increasing the production of ROS and directly damaging endothelial cells [55, 56]. Previously, ANG-II was reported to induce the production of peroxynitrite in vascular endothelial cells and to promote PARP signaling activation, which in turn activates NF-κB and a release of many inflammatory cytokines, leading to the endothelial cell damage [57, 58]. These ANG-II effects can be prevented by the use of NADPH oxidase inhibitors [59, 60].

5. Mitochondrial Dysfunction Roles in the DR Pathogenesis

Mitochondria are the primary source of cellular energy, involved in metabolic processes and respiration [15]. Their main role is adenosine triphosphate (ATP) production, cell metabolism control, and apoptosis regulation [61], and their

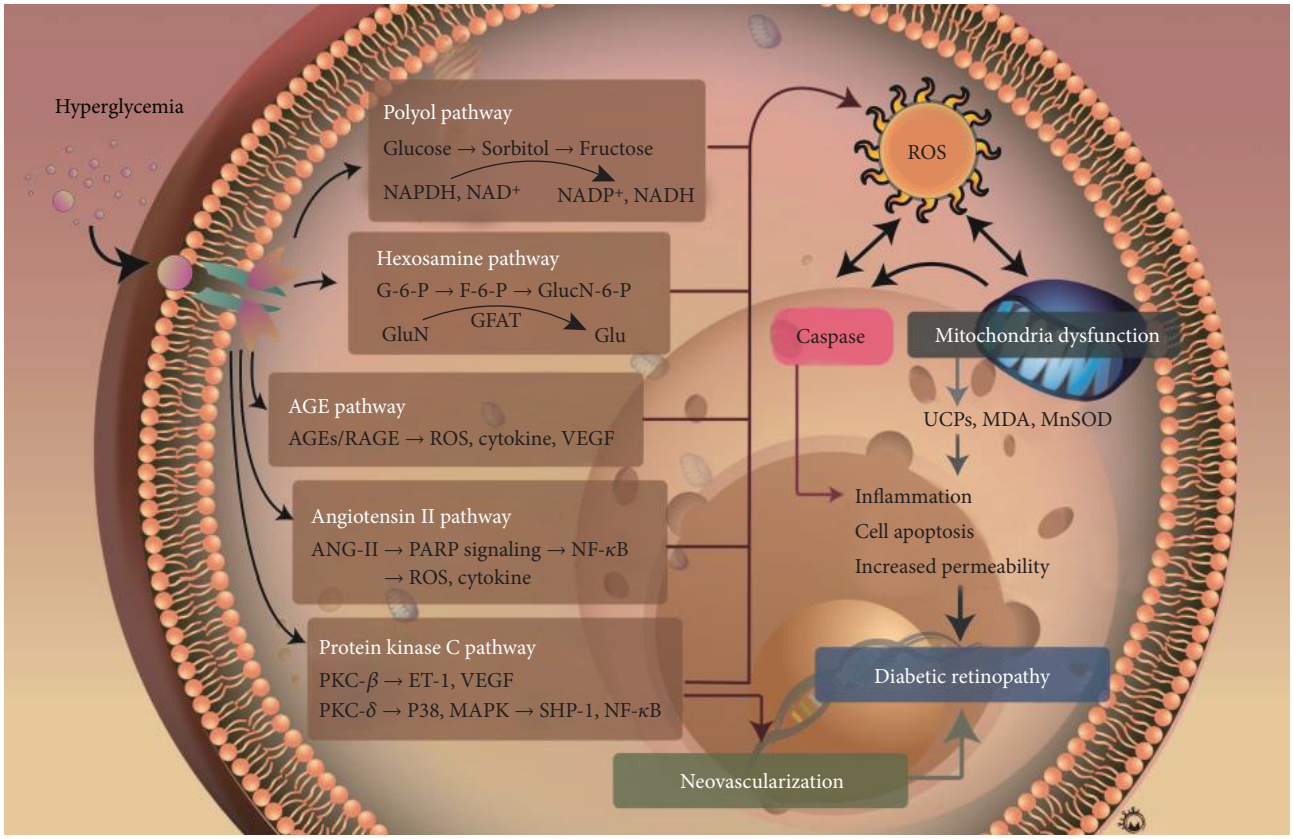

Figure 3: Mechanisms underlying hyperglycemia-induced oxidative stress increase that is involved in diabetic retinopathy pathogenesis.

dysfunction severely affects tissue homeostasis. ROS [62], superoxide dismutase, and hydroxyl radicals are mainly formed in the mitochondria. Under hyperglycemic conditions, ROS is overproduced in the retina, leading to an increase in oxidative processes and the disturbance in the mitochondrial functions, which may lead to the retinal capillary cell apoptosis [63–65]. Oxidative stress increase during hyperglycemia damages the structure and function of mitochondria [63]. The main alterations in the expression levels and activity are associated with these molecules: mitochondrial superoxide dismutase (MnSOD) [66–68], catalase (CAT) [69, 70], MDA [71–73], uncoupling proteins (UCPs) [18, 74, 75], aldose reductase, AGEs, glutathione peroxidase, nitrotyrosine (NT) [15, 76, 77], and 8-hydroxyguanosine (8-OHG and 8-OHdG) [78–80]. The UCPs, MDA, and MnSOD have been investigated the most. UCPs belong to the mitochondrial anion carrier gene family, and the uncoupling refers to the separation of ATP synthesis and mitochondrial respiration, which is achieved through proton leakage [81]. UCP functions include the reduction in the electrochemical gradient by increasing the proton leakage through the mitochondrial inner membrane, thereby reducing ROS production. Previous studies demonstrated that five isoforms of UCPs are expressed in bovine retinal microvascular endothelial cells and pericytes. UCP1, UCP2, and MnSOD were shown to be expressed in high-glucose environment [82]. Retinal neuron apoptosis in DR was observed and shown to be associated with a decrease in *MnSOD* expression [83, 84]. Mitochondrial morphology is altered in these processes as well, and their expansion can be observed in the retina of diabetic rats [20, 85]. Endothelial cells and pericytes gradually lose their original morphological features and become heterogeneous with irregular arrangement, finally leading to retinal cell apoptosis [86]. These processes induce mitochondrial ROS production, endothelial cell and pericyte apoptosis, and, ultimately, DR pathogenesis (Figure 3).

6. Angiogenesis and VEGF Roles during DR Pathogenesis

As early as the 1950s, scholars suggested that the DR development may be associated with retinal ischemia and hypoxia-induced neovascularization, which was first confirmed in 1994 [87, 88]. Two subtypes of VEGF exist, and VEGF2 stimulates the proliferation and migration of endothelial cells to form new blood vessels that may enable ocular microvascular leakage in the proliferative DR (PDR) patients [89]. Recent studies also found that many molecular signaling pathways associated with VEGF in patients with PDR have varying degrees of disruption, resulting in an imbalance of intravitreal angiogenesis [90–92]. The expression of placental growth factor (P1GF) in the vitreous cavity of patients with PDR is significantly increased, which further enhances VEGF signaling [90]. Additionally, the expression of connective tissue growth factor (CTGF)

in the vitreous cavity of patients was shown to be significantly upregulated, and it accelerates the fibrosis process and acts in synergy with VEGF. CTGF plays an important role in the process of fibrogenesis of neovascular membrane and retinal detachment as well [91]. VEGF induces an increased expression of intracellular adhesion molecule-1 (ICAM-1), leading to the stasis and aggregation of white blood cells in the retina, gradually destroying the blood-retinal barrier and causing the damage and death of vascular endothelial cells, which ultimately leads to the formation of capillaries with no perfusion area. With the DR progression, the concentrations of VEGF and ICAM-1 in the vitreous cavity increase as well, and their levels were shown to correlate significantly [93]. VEGF also stimulates the migration of endothelial progenitor cells (EPCs) from the bone marrow to the retina and accelerates the neovascularization by inducing the release of the stem cell factor (SCF) [94, 95]. VEGF may interfere with the balance in the levels of tissue plasminogen activator (t-PA) and plasminogen activator inhibitor (PAI). The overexpression of t-PA and PAI induces extracellular matrix destruction and the degradation of the basement membrane of vascular endothelial cells [96, 97]. Increased VEGF levels may induce the expression of various inflammatory factors, such as transforming growth factor beta-1 (TGF-β1) and interleukin 6 (IL-6) that accelerate PDR progression [98]. Heparan sulfate is an important component of the blood-retinal barrier stroma. Abu et al. [92] demonstrated that heparanase concentrations in the vitreous cavity of the PDR patients are significantly higher compared with those in the controls, suggesting that heparanase accelerates the decomposition of heparan sulfate and the destruction of the blood-retinal barrier, together with inducing VEGF expression and promoting neovascularization. Furthermore, they demonstrated that heparan sulfate expression alterations were more severe in younger patients, which, to some extent, explains why the PDR progression is more difficult to control in younger patients with the anti-VEGF therapy [92, 99, 100].

7. DR Treatment Strategies

Vision loss is the most severe consequence of DR, and it can be managed using different approaches, including intraocular anti-VEGF agents and steroids for the treatment of DME, panretinal laser photocoagulation aimed at proliferative DR treatment, and surgery for vitreous hemorrhage and traction retinal detachment.

7.1. Laser Photocoagulation. Panretinal photocoagulation has been developed since the 1960s and represents a standard treatment for proliferative DR and DME. The principle of laser photocoagulation activity is based on the thermal effects that alleviate retinal ischemia and regulate the hemodynamics of retinal circulation. Improved retinal hypoxia and hemodynamic changes result in the regression of neovascularization and macular edema due to the reduction in the levels of VEGF and other inflammatory factors [101].

The landmark Diabetic Retinopathy Study (DRS) reported the reduction of severe vision loss in the patients with the high-risk proliferative DR and severe nonproliferative DR from 33% to 13% over 5 years following the prompt application of the panretinal photocoagulation [102]. Furthermore, the Early Treatment Diabetic Retinopathy Study (ETDRS) demonstrated that focal laser photocoagulation reduced by 50% the risk of moderate vision loss in patients with the clinically significant DME [102, 103]. Panretinal photocoagulation remains the mainstay of the proliferative DR treatment and should be especially considered for the patients with poor compliance and poor metabolic control, prior to the cataract surgery and severe cataract development, which may limit the applicability of the laser photocoagulation treatment. However, some side effects of this therapy exist, including a moderate decrease in vision, scotoma development, and secondary neovascularization development.

7.2. Treatment with the Intraocular Anti-VEGF Agents. In the 2000s, intraocular injection of anti-VEGF agents was introduced as a new treatment modality for DME, and this approach represents one of the most important approaches recently developed in ophthalmology [104]. Currently, three anti-VEGF treatments are used: ranibizumab (Lucentis, Genentech, South San Francisco, CA, USA), bevacizumab (Avastin, Genentech), and aflibercept (Eylea, Regeneron, Tarrytown, NY, USA).

For the treatment of DME, anti-VEGF currently represents the first-line therapy, which has replaced the focal macular laser treatment. The RESTORE study reported that the ranibizumab monotherapy or ranibizumab in combination with laser treatment demonstrated superior visual acuity gain over standard laser alone in patients with DME [105]. The results showed that the administration of ranibizumab and the deferred laser is superior to that of ranibizumab with prompt laser. For approximately 50% of the eyes treated with intravitreal ranibizumab, no further therapies were required over 5 years. These results suggest that the anti-VEGF treatment lowers the injection frequency with time, while the macular focal laser plays a less important role in the DME treatment [106, 107]. The Ranibizumab for Diabetic Macular Edema (RIDE and RISE) trials examined the effects of monthly ranibizumab injections at 0.3 mg and 0.5 mg, with the 5-year follow-up, and demonstrated that the early and regular application of ranibizumab lowers the risk of proliferative DR development. Furthermore, the use of ranibizumab was observed to prevent retinal nonperfusion [108].

Although multiple intraocular injections are required, the treatment protocol depends on the selected drug, dosage, and retreatment criteria, and different levels of visual improvement can be obtained. In the DRCR.net Protocol T and Cai and Bressler [109, 110] reports, bevacizumab, ranibizumab, and aflibercept were compared, and it was shown that all three drugs can improve vision and are well-tolerated. However, the intravitreal administration of bevacizumab was inferior to that of both aflibercept and ranibizumab. A subgroup analysis demonstrated that aflibercept has a superior effect on the vision improvement with poorer initial baseline BCVA (less than 69 letters) compared with ranibizumab and bevacizumab. The difference in the resulting visual

acuity between aflibercept and ranibizumab was significant in the first year but decreased at 2 years [109, 111]. Additionally, the effects of the anti-VEGF therapy on the high-risk proliferative DR have not been clarified. Recently, the results of the DRCR.net Protocol S were presented, demonstrating that the intravitreal ranibizumab injection is not inferior to the panretinal laser photocoagulation in patients with the increased risk of proliferative DR. At 2 years, mean visual acuity improvement following the application of these two treatment modalities was shown to be similar. Area under the curve (AUC) analysis demonstrated the superiority of ranibizumab to panretinal photocoagulation, with the incidence of vitrectomy lower in the group receiving ranibizumab. Although Protocol S results confirmed only the noninferiority of ranibizumab over panretinal photocoagulation, the cost of consecutive injections was shown to be considerably lower, suggesting that the anti-VEGF therapy may represent a valuable alternative for the treatment of proliferative DR, while the combination of these therapies may be the most practical approach in the clinic [6].

More than 50% of patients with the proliferative DR were shown not to have increased VEGF levels in the vitreous fluid [88], which may explain why some proliferative DR patients are resistant to the anti-VEGF treatment. In this patient subgroup, proinflammatory cytokines most likely play pathological roles, and the application of intravitreal steroids or other cytokine inhibitors may be more plausible treatment options.

7.3. Intraocular Steroid Application. The molecular mechanisms involving inflammatory pathways have been proposed to underlie DME pathogenesis [112, 113]. In addition to the increase in VEGF expression, the secretion of different types of proinflammatory cytokines (TNF-α, IL-6, and IL-1β) represents a common occurrence in patients with the proliferative DR. Corticosteroids suppressing the inflammatory pathways are considered potential DME treatment options. Furthermore, inflammatory cells produce a number of angiogenic growth factors and cytokines, which can promote neovascularization [114]. Corticosteroids downregulate VEGF expression by reducing proinflammatory cytokine levels and regulating the activity of inflammatory cells. However, due to the adverse effects of corticosteroids, such as cataract development, increase in the intraocular pressure, and increased risk of endophthalmitis, and anti-VEGF therapy, they can be administered only to a selected group of patients, such as those with chronic DME.

In a number of trials, the benefits of intravitreal triamcinolone were shown to be inferior to those obtained by using laser treatment alone, during a 3-year follow-up. The DRCR.net also reported that the intravitreal triamcinolone effects lasted for less than 1 year, while the visual acuity outcome was not superior to that of the laser photocoagulation at 2 years [106].

Ozurdex (Allergan, Irvine, California, USA) is a biodegradable implant that slowly releases 0.7 mg of dexamethasone over 6 months. The Macular Edema: Assessment of Implantable Dexamethasone in Diabetes (MEAD) study evaluated the effectiveness of dexamethasone implants in patients with DME. A higher percentage of patients was shown to achieve more than 15-letter improvement over 3 years in comparison with that in the sham group (22.2% vs. 12%, $P < 0.018$) [115]. Iluvien (Alimera Sciences, Alpharetta, GA, USA), another sustained-release intravitreal implant, provides the therapeutic effects up to 36 months by slowly delivering micrograms of fluocinolone acetonide. The Fluocinolone Acetonide in Diabetic Macular Edema study evaluated the effectiveness of the low-dose (0.2 μg per day) and high-dose (0.5 μg per day) fluocinolone implants in patients who received at least one laser therapy, demonstrating the improvement of more than 15 letters in both fluocinolone implant-treated groups, compared with that in the control group. Furthermore, in the subgroup with chronic DME followed up for 3 years, a higher percentage of patients with Iluvien treatment showed a VA improvement of more than 15 letters than that in the control group (28.7% vs. 18.9%) [116].

7.4. Surgery. Vitrectomy is a standard treatment for severe proliferative DR, for patients who do not respond to the panretinal photocoagulation and anti-VEGF therapy or those with persistent vitreous hemorrhage or traction retinal detachment. The DRCR.net Protocol D study investigated the effectiveness of pars plana vitrectomy and membrane peeling in patients with DME and vitreomacular traction, reporting that approximately 40% of patients had improved visual acuity, whereas 22% of patients were shown to have poorer visual acuity outcome, with less than 10-letter gain [117]. Prolonged vitreous hemorrhage and retinal detachment involving macula are common complications of proliferative DR, and these patients should receive surgical treatment. If panretinal photocoagulation has been performed previously, the reabsorption of hemorrhage can be observed, but the surgery is indicated if vitreous hemorrhage persists for longer than 6 months [118, 119]. According to the results of the Diabetic Retinopathy Vitrectomy Study (DRVS), early vitrectomy is strongly suggested, especially in patients with type I diabetes, but no advantages were reported for the patients with type II diabetes [120].

Surgical intervention for the treatment of neovascular glaucoma is indicated in the presence of neovascularization and persistent elevation of intraocular pressure, even after the complete panretinal photocoagulation and anti-VEGF therapy. Glaucoma drainage implants (GDIs) have recently gained popularity for the treatment of neovascular glaucoma (NVG), and their success relies less on the control of intraocular inflammation and bleb failure rate [118, 119].

7.5. New Insights in the Pharmacological Management of DR. Several novel pharmacological therapies are currently developed to target the mechanisms underlying DR development and progression, and these are expected to change our approaches to the DR treatment. The main strategy is preventing the damage to the retinal microvasculature induced by the progression of diabetes. Experimental studies demonstrated that the PKC activity is significantly increased following the increase in blood sugar levels, which

has been implicated in the pathogenesis of microvascular damage. Ruboxistaurin (LY333531), a specific inhibitor of PKC-β1 and -β2, has been shown to prevent microvascular complications and ischemia-associated neovascularization in the animal models of diabetes [40, 121]. Additional trials evaluating the effectiveness and safety of ruboxistaurin are currently being conducted [122–125]. Furthermore, the activity of somatostatin has been linked to the progression of DR, and early studies reported that the octreotide therapy in the patients with nonproliferative DR may decrease the need for the application of laser photocoagulation [126, 127]. However, these effects were not significantly partial in the patients with proliferative DR.

Systemic therapies were shown to reduce the risk of DR progression and to modulate retinal microvasculature via renin-angiotensin system (RAAS) and lipid metabolism. Fenofibrate is the third generation of fibric acid-derivative lipid-regulating drugs, with can prevent the progression of DR through multiple mechanisms, including the well-established lipid-lowering effect, the inhibition of the VEGF pathway, and the maintenance of the normal endothelial structure [128]. The Fenofibrate Intervention and Event Lowering in Diabetes (FIELD) study reported the effects of fenofibrate on the cardiovascular system and the considerable decrease in the need for laser photocoagulation treatment and severe DR progression [129]. Enalapril, an angiotensin-converting enzyme (ACE) inhibitor, was also reported to decrease the neovascularization and progression of the diabetes complications, but it remains unclear whether these beneficial effects are due to the hypotensive activity [130]. However, many drugs are still in the phases I and II of clinical trials, and they may increase the effectiveness of the DR therapy in the future.

8. Conclusions

The pathogenesis of DR is complex and has not been completely elucidated. However, its incidence and severity are high. Current treatment methods are mainly aimed at the treatment of the DMR and advanced-stage proliferative DR. The advantages and disadvantages of the existing single and combined therapies must be evaluated as well. Therefore, the observation that the accumulation of ROS induces neurovascular dysfunction through mitochondrial failure, inflammation, and cell death which are the major mechanisms underlying DR development represents an important conceptual advance in this field.

Conflicts of Interest

The authors declare no conflict of interest.

Authors' Contributions

Meng-Yu Wu and Tzu-Ting Lai contributed equally to this work.

Acknowledgments

This study was funded by grants RD106077 and RD106078 from the Show Chwan Memorial Hospital, Taiwan.

References

[1] M. Brownlee, "Biochemistry and molecular cell biology of diabetic complications," *Nature*, vol. 414, no. 6865, pp. 813–820, 2001.

[2] J. M. Tarr, K. Kaul, M. Chopra, E. M. Kohner, and R. Chibber, "Pathophysiology of diabetic retinopathy," *ISRN Ophthalmology*, vol. 2013, Article ID 343560, 13 pages, 2013.

[3] D. A. Antonetti, R. Klein, and T. W. Gardner, "Diabetic retinopathy," *The New England Journal of Medicine*, vol. 366, no. 13, pp. 1227–1239, 2012.

[4] N. Cheung, P. Mitchell, and T. Y. Wong, "Diabetic retinopathy," *The Lancet*, vol. 376, no. 9735, pp. 124–136, 2010.

[5] R. N. Frank, "Diabetic retinopathy," *The New England Journal of Medicine*, vol. 350, no. 1, pp. 48–58, 2004.

[6] Writing Committee for the Diabetic Retinopathy Clinical Research, J. G. Gross, A. R. Glassman et al., "Panretinal photocoagulation vs intravitreous ranibizumab for proliferative diabetic retinopathy: a randomized clinical trial," *JAMA*, vol. 314, no. 20, pp. 2137–2146, 2015.

[7] C. P. Wilkinson, F. L. Ferris, R. E. Klein 3rd et al., "Proposed international clinical diabetic retinopathy and diabetic macular edema disease severity scales," *Ophthalmology*, vol. 110, no. 9, pp. 1677–1682, 2003.

[8] D. A. Sim, P. A. Keane, R. Rajendram et al., "Patterns of peripheral retinal and central macula ischemia in diabetic retinopathy as evaluated by ultra-widefield fluorescein angiography," *American Journal of Ophthalmology*, vol. 158, no. 1, pp. 144–153.e1, 2014, e141.

[9] P. J. Beisswenger, S. K. Howell, K. Smith, and B. S. Szwergold, "Glyceraldehyde-3-phosphate dehydrogenase activity as an independent modifier of methylglyoxal levels in diabetes," *Biochimica et Biophysica Acta (BBA) - Molecular Basis of Disease*, vol. 1637, no. 1, pp. 98–106, 2003.

[10] X. L. Du, D. Edelstein, L. Rossetti et al., "Hyperglycemia-induced mitochondrial superoxide overproduction activates the hexosamine pathway and induces plasminogen activator inhibitor-1 expression by increasing Sp1 glycosylation," *Proceedings of the National Academy of Sciences of the United States of America*, vol. 97, no. 22, pp. 12222–12226, 2000.

[11] R. L. Engerman, T. S. Kern, and M. E. Larson, "Nerve conduction and aldose reductase inhibition during 5 years of diabetes or galactosaemia in dogs," *Diabetologia*, vol. 37, no. 2, pp. 141–144, 1994.

[12] D. Koya and G. L. King, "Protein kinase C activation and the development of diabetic complications," *Diabetes*, vol. 47, no. 6, pp. 859–866, 1998.

[13] B. Stauble, D. Boscoboinik, A. Tasinato, and A. Azzi, "Modulation of activator protein-1 (AP-1) transcription factor and protein kinase C by hydrogen peroxide and D-alpha-tocopherol in vascular smooth muscle cells," *European Journal of Biochemistry*, vol. 226, no. 2, pp. 393–402, 1994.

[14] R. B. Caldwell, M. Bartoli, M. A. Behzadian et al., "Vascular endothelial growth factor and diabetic retinopathy: role of oxidative stress," *Current Drug Targets*, vol. 6, no. 4, pp. 511–524, 2005.

[15] R. A. Kowluru, "Diabetic retinopathy: mitochondrial dysfunction and retinal capillary cell death," *Antioxidants & Redox Signaling*, vol. 7, no. 11-12, pp. 1581–1587, 2005.

[16] S. A. Madsen-Bouterse, Q. Zhong, G. Mohammad, Y. S. Ho, and R. A. Kowluru, "Oxidative damage of mitochondrial DNA in diabetes and its protection by manganese superoxide dismutase," *Free Radical Research*, vol. 44, no. 3, pp. 313–321, 2010.

[17] W. T. Cade, "Diabetes-related microvascular and macrovascular diseases in the physical therapy setting," *Physical Therapy*, vol. 88, no. 11, pp. 1322–1335, 2008.

[18] Y. Cui, X. Xu, H. Bi et al., "Expression modification of uncoupling proteins and MnSOD in retinal endothelial cells and pericytes induced by high glucose: the role of reactive oxygen species in diabetic retinopathy," *Experimental Eye Research*, vol. 83, no. 4, pp. 807–816, 2006.

[19] Y. Du, C. M. Miller, and T. S. Kern, "Hyperglycemia increases mitochondrial superoxide in retina and retinal cells," *Free Radical Biology & Medicine*, vol. 35, no. 11, pp. 1491–1499, 2003.

[20] R. A. Kowluru and S. N. Abbas, "Diabetes-induced mitochondrial dysfunction in the retina," *Investigative Ophthalmology & Visual Science*, vol. 44, no. 12, pp. 5327–5334, 2003.

[21] D. Bonnefont-Rousselot, "Glucose and reactive oxygen species," *Current Opinion in Clinical Nutrition and Metabolic Care*, vol. 5, no. 5, pp. 561–568, 2002.

[22] M. Lorenzi, "The polyol pathway as a mechanism for diabetic retinopathy: attractive, elusive, and resilient," *Experimental Diabetes Research*, vol. 2007, Article ID 61038, 10 pages, 2007.

[23] C. Altmann and M. Schmidt, "The role of microglia in diabetic retinopathy: inflammation, microvasculature defects and neurodegeneration," *International Journal of Molecular Sciences*, vol. 19, no. 1, p. 110, 2018.

[24] M. Dunlop, "Aldose reductase and the role of the polyol pathway in diabetic nephropathy," *Kidney International Supplement*, vol. 77, pp. S3–12, 2000.

[25] R. E. Schmidt, D. A. Dorsey, L. N. Beaudet et al., "A potent sorbitol dehydrogenase inhibitor exacerbates sympathetic autonomic neuropathy in rats with streptozotocin-induced diabetes," *Experimental Neurology*, vol. 192, no. 2, pp. 407–419, 2005.

[26] F. N. Ferreira, D. Crispim, L. H. Canani, J. L. Gross, and K. G. dos Santos, "Association study of sorbitol dehydrogenase -888G>C polymorphism with type 2 diabetic retinopathy in Caucasian-Brazilians," *Experimental Eye Research*, vol. 115, pp. 140–143, 2013.

[27] E. A. Ellis, D. L. Guberski, B. Hutson, and M. B. Grant, "Time course of NADH oxidase, inducible nitric oxide synthase and peroxynitrite in diabetic retinopathy in the BBZ/WOR rat," *Nitric oxide*, vol. 6, no. 3, pp. 295–304, 2002.

[28] D. R. Jones, W.-J. Keune, K. E. Anderson, L. R. Stephens, P. T. Hawkins, and N. Divecha, "The hexosamine biosynthesis pathway and O-GlcNAcylation maintain insulin-stimulated PI3K-PKB phosphorylation and tumour cell growth after short-term glucose deprivation," *The FEBS Journal*, vol. 281, no. 16, pp. 3591–3608, 2014.

[29] M. G. Buse, "Hexosamines, insulin resistance and the complications of diabetes: current status," *American Journal of Physiology Endocrinology and Metabolism*, vol. 290, no. 1, pp. E1–E8, 2006.

[30] E. D. Schleicher and C. Weigert, "Role of the hexosamine biosynthetic pathway in diabetic nephropathy," *Kidney International Supplement*, vol. 77, pp. S13–S18, 2000.

[31] I. G. Fantus, H. J. Goldberg, C. I. Whiteside, and D. Topic, "The hexosamine biosynthesis pathway," in *The Diabetic Kidney*, Contemporary Diabetes, P. Cortes and C. E. Mogensen, Eds., pp. 117–133, Humana Press, Totowa, NJ, USA, 2006.

[32] X. Du, T. Matsumura, D. Edelstein et al., "Inhibition of GAPDH activity by poly (ADP-ribose) polymerase activates three major pathways of hyperglycemic damage in endothelial cells," *Journal of Clinical Investigation*, vol. 112, no. 7, pp. 1049–1057, 2003.

[33] M. Brownlee, "The pathobiology of diabetic complications: a unifying mechanism," *Diabetes*, vol. 54, no. 6, pp. 1615–1625, 2005.

[34] M. Amadio, C. Bucolo, G. M. Leggio, F. Drago, S. Govoni, and A. Pascale, "The PKCbeta/HuR/VEGF pathway in diabetic retinopathy," *Biochemical Pharmacology*, vol. 80, no. 8, pp. 1230–1237, 2010.

[35] N. Das Evcimen and G. L. King, "The role of protein kinase C activation and the vascular complications of diabetes," *Pharmacological Research*, vol. 55, no. 6, pp. 498–510, 2007.

[36] H. Noh and G. L. King, "The role of protein kinase C activation in diabetic nephropathy," *Kidney International Supplement*, vol. 72, pp. S49–S53, 2007.

[37] H. Ishii, D. Koya, and G. L. King, "Protein kinase C activation and its role in the development of vascular complications in diabetes mellitus," *Journal of molecular medicine*, vol. 76, no. 1, pp. 21–31, 1998.

[38] I. Idris, S. Gray, and R. Donnelly, "Protein kinase C activation: isozyme-specific effects on metabolism and cardiovascular complications in diabetes," *Diabetologia*, vol. 44, no. 6, pp. 659–673, 2001.

[39] T. Inoguchi, R. Battan, E. Handler, J. R. Sportsman, W. Heath, and G. L. King, "Preferential elevation of protein kinase C isoform beta II and diacylglycerol levels in the aorta and heart of diabetic rats: differential reversibility to glycemic control by islet cell transplantation," *Proceedings of the National Academy of Sciences of the United States of America*, vol. 89, no. 22, pp. 11059–11063, 1992.

[40] H. Ishii, M. R. Jirousek, D. Koya et al., "Amelioration of vascular dysfunctions in diabetic rats by an oral PKC beta inhibitor," *Science*, vol. 272, no. 5262, pp. 728–731, 1996.

[41] T. Yokota, R. C. Ma, J. Y. Park et al., "Role of protein kinase C on the expression of platelet-derived growth factor and endothelin-1 in the retina of diabetic rats and cultured retinal capillary pericytes," *Diabetes*, vol. 52, no. 3, pp. 838–845, 2003.

[42] J. Y. Park, S. W. Ha, and G. L. King, "The role of protein kinase C activation in the pathogenesis of diabetic vascular complications," *Peritoneal dialysis international*, vol. 19, Supplement 2, pp. S222–S227, 1999.

[43] M. A. Glomb and V. M. Monnier, "Mechanism of protein modification by glyoxal and glycolaldehyde, reactive intermediates of the Maillard reaction," *The Journal of Biological Chemistry*, vol. 270, no. 17, pp. 10017–10026, 1995.

[44] B. I. Hudson, M. H. Stickland, T. S. Futers, and P. J. Grant, "Effects of novel polymorphisms in the RAGE gene on transcriptional regulation and their association with diabetic retinopathy," *Diabetes*, vol. 50, no. 6, pp. 1505–1511, 2001.

[45] A. W. Stitt, "The role of advanced glycation in the pathogenesis of diabetic retinopathy," *Experimental and Molecular Pathology*, vol. 75, no. 1, pp. 95–108, 2003.

[46] S. Yamagishi and T. Matsui, "Advanced glycation end products (AGEs), oxidative stress and diabetic retinopathy," *Current Pharmaceutical Biotechnology*, vol. 12, no. 3, pp. 362–368, 2011.

[47] M. Katagiri, J. Shoji, N. Inada, S. Kato, S. Kitano, and Y. Uchigata, "Evaluation of vitreous levels of advanced glycation end products and angiogenic factors as biomarkers for severity of diabetic retinopathy," *International Ophthalmology*, vol. 38, no. 2, pp. 607–615, 2017.

[48] M. Yokoi, S. I. Yamagishi, M. Takeuchi et al., "Elevations of AGE and vascular endothelial growth factor with decreased total antioxidant status in the vitreous fluid of diabetic patients with retinopathy," *The British Journal of Ophthalmology*, vol. 89, no. 6, pp. 673–675, 2005.

[49] H. Funatsu and H. Yamashita, "Pathogenesis of diabetic retinopathy and the renin-angiotensin system," *Ophthalmic and Physiological Optics*, vol. 23, no. 6, pp. 495–501, 2003.

[50] K. Y. Chu and P. S. Leung, "Angiotensin II in type 2 diabetes mellitus," *Current Protein & Peptide Science*, vol. 10, no. 1, pp. 75–84, 2009.

[51] A. Ribeiro-Oliveira, A. I. Nogueira, R. M. Pereira, W. W. V. Boas, R. A. S. dos Santos, and A. C. S. e Silva, "The renin–angiotensin system and diabetes: an update," *Vascular Health and Risk Management*, vol. 4, no. 4, pp. 787–803, 2008.

[52] M.-Y. Wu, C.-J. Li, M.-F. Hou, and P.-Y. Chu, "New insights into the role of inflammation in the pathogenesis of atherosclerosis," *International Journal of Molecular Sciences*, vol. 18, no. 10, p. 2034, 2017.

[53] A. K. Sjolie and N. Chaturvedi, "The retinal renin-angiotensin system: implications for therapy in diabetic retinopathy," *Journal of Human Hypertension*, vol. 16, pp. S42–S46, 2002.

[54] B. Williams, "Angiotensin II, VEGF, and diabetic retinopathy," *The Lancet*, vol. 351, no. 9105, pp. 837-838, 1998.

[55] B. L. Seagle, E. M. Gasyna, W. F. Mieler, and J. R. Norris Jr., "Photoprotection of human retinal pigment epithelium cells against blue light-induced apoptosis by melanin free radicals from *Sepia officinalis*," *Proceedings of the National Academy of Sciences of the United States of America*, vol. 103, no. 45, pp. 16644–16648, 2006.

[56] R. A. Kowluru, "Effect of advanced glycation end products on accelerated apoptosis of retinal capillary cells under in vitro conditions," *Life Sciences*, vol. 76, no. 9, pp. 1051–1060, 2005.

[57] E. H. van Dijk, D. E. Duits, M. Versluis et al., "Loss of MAPK pathway activation in post-mitotic retinal cells as mechanism in MEK inhibition-related retinopathy in cancer patients," *Medicine*, vol. 95, no. 18, article e3457, 2016.

[58] Y. Cai, W. Li, H. Tu et al., "Curcumolide reduces diabetic retinal vascular leukostasis and leakage partly via inhibition of the p38MAPK/NF-κB signaling," *Bioorganic & Medicinal Chemistry Letters*, vol. 27, no. 8, pp. 1835–1839, 2017.

[59] T. H. Lai, P. H. Wu, and W. B. Wu, "Involvement of NADPH oxidase and NF-κB activation in CXCL1 induction by vascular endothelial growth factor in human endometrial epithelial cells of patients with adenomyosis," *Journal of Reproductive Immunology*, vol. 118, pp. 61–69, 2016.

[60] G. R. Drummond and C. G. Sobey, "Endothelial NADPH oxidases: which NOX to target in vascular disease?," *Trends in Endocrinology and Metabolism*, vol. 25, no. 9, pp. 452–463, 2014.

[61] I. E. Scheffler, "A century of mitochondrial research: achievements and perspectives," *Mitochondrion*, vol. 1, no. 1, pp. 3–31, 2001.

[62] J. M. Santos, S. Tewari, and R. A. Kowluru, "A compensatory mechanism protects retinal mitochondria from initial insult in diabetic retinopathy," *Free Radical Biology & Medicine*, vol. 53, no. 9, pp. 1729–1737, 2012.

[63] S. A. Madsen-Bouterse, G. Mohammad, M. Kanwar, and R. A. Kowluru, "Role of mitochondrial DNA damage in the development of diabetic retinopathy, and the metabolic memory phenomenon associated with Its progression," *Antioxidants & Redox Signaling*, vol. 13, no. 6, pp. 797–805, 2010.

[64] R. A. Kowluru, "Mitochondria damage in the pathogenesis of diabetic retinopathy and in the metabolic memory associated with its continued progression," *Current Medicinal Chemistry*, vol. 20, no. 26, pp. 3226–3233, 2013.

[65] G. Mohammad and R. A. Kowluru, "Novel role of mitochondrial matrix metalloproteinase-2 in the development of diabetic retinopathy," *Investigative Ophthalmology & Visual Science*, vol. 52, no. 6, pp. 3832–3841, 2011.

[66] S. F. Haghighi, Z. Salehi, M. R. Sabouri, and N. Abbasi, "Polymorphic variant of MnSOD A16V and risk of diabetic retinopathy," *Molekuliarnaia Biologiia*, vol. 49, no. 1, pp. 114–118, 2015.

[67] M. Kanwar, P. S. Chan, T. S. Kern, and R. A. Kowluru, "Oxidative damage in the retinal mitochondria of diabetic mice: possible protection by superoxide dismutase," *Investigative Ophthalmology & Visual Science*, vol. 48, no. 8, pp. 3805–3811, 2007.

[68] R. A. Kowluru, L. Atasi, and Y. S. Ho, "Role of mitochondrial superoxide dismutase in the development of diabetic retinopathy," *Investigative Ophthalmology & Visual Science*, vol. 47, no. 4, pp. 1594–1599, 2006.

[69] T. Bek, "Mitochondrial dysfunction and diabetic retinopathy," *Mitochondrion*, vol. 36, pp. 4–6, 2017.

[70] C. R. Giordano, "Catalase therapy corrects oxidative stress-induced pathophysiology in incipient diabetic retinopathy," *Investigative Ophthalmology & Visual Science*, vol. 56, no. 5, pp. 3095–3102, 2015.

[71] S. Kumari, S. Panda, M. Mangaraj, M. K. Mandal, and P. C. Mahapatra, "Plasma MDA and antioxidant vitamins in diabetic retinopathy," *Indian Journal of Clinical Biochemistry*, vol. 23, no. 2, pp. 158–162, 2008.

[72] M. Kumawat, S. Kharb, V. Singh, N. Singh, S. K. Singh, and M. Nada, "Plasma malondialdehyde (MDA) and antioxidant status in diabetic retinopathy," *Journal of the Indian Medical Association*, vol. 112, no. 1, pp. 29–32, 2014.

[73] A. Turk, I. Nuhoglu, A. Mentese, S. C. Karahan, H. Erdol, and C. Erem, "The relationship between diabetic retinopathy and serum levels of ischemia-modified albumin and malondialdehyde," *Retina*, vol. 31, no. 3, pp. 602–608, 2011.

[74] J. Liu, J. Li, W.-J. Li, and C.-M. Wang, "The role of uncoupling proteins in diabetes mellitus," *Journal of Diabetes Research*, vol. 2013, 7 pages, 2013.

[75] S. Rousset, M.-C. Alves-Guerra, J. Mozo et al., "The biology of mitochondrial uncoupling proteins," *Diabetes*, vol. 53, Supplement 1, pp. S130–S135, 2004.

[76] R. A. Kowluru, M. Kanwar, P. S. Chan, and J. P. Zhang, "Inhibition of retinopathy and retinal metabolic

abnormalities in diabetic rats with AREDS-based micronutrients," *Archives of ophthalmology*, vol. 126, no. 9, pp. 1266–1272, 2008.

[77] X. Zhan, Y. Du, J. S. Crabb, X. Gu, T. S. Kern, and J. W. Crabb, "Targets of tyrosine nitration in diabetic rat retina," *Molecular & cellular proteomics*, vol. 7, no. 5, pp. 864–874, 2008.

[78] Q. Y. Dong, Y. Cui, L. Chen, J. Song, and L. Sun, "Urinary 8-hydroxydeoxyguanosine levels in diabetic retinopathy patients," *European Journal of Ophthalmology*, vol. 18, no. 1, pp. 94–98, 2008.

[79] H. Z. Pan, H. Zhang, D. Chang, H. Li, and H. Sui, "The change of oxidative stress products in diabetes mellitus and diabetic retinopathy," *The British Journal of Ophthalmology*, vol. 92, no. 4, pp. 548–551, 2008.

[80] Y. Wakabayashi, Y. Usui, Y. Shibauchi, H. Uchino, and H. Goto, "Increased levels of 8-hydroxydeoxyguanosine in the vitreous of patients with diabetic retinopathy," *Diabetes Research and Clinical Practice*, vol. 89, no. 3, pp. e59–e61, 2010.

[81] D. Salvemini, Z. Q. Wang, J. L. Zweier et al., "A nonpeptidyl mimic of superoxide dismutase with therapeutic activity in rats," *Science*, vol. 286, no. 5438, pp. 304–306, 1999.

[82] I. Osorio-Paz, S. Uribe-Carvajal, and R. Salceda, "In the early stages of diabetes, rat retinal mitochondria undergo mild uncoupling due to UCP2 activity," *PLoS One*, vol. 10, no. 5, article e0122727, 2015.

[83] X. Li, M. Zhang, and H. Zhou, "The morphological features and mitochondrial oxidative stress mechanism of the retinal neurons apoptosis in early diabetic rats," *Journal of Diabetes Research*, vol. 2014, Article ID 678123, 8 pages, 2014.

[84] B. M. de Souza, L. A. Brondani, A. P. Bouças et al., "Associations between *UCP1 -3826A/G*, *UCP2 -866G/A*, Ala55Val and Ins/Del, and *UCP3* -55C/T polymorphisms and susceptibility to type 2 diabetes mellitus: case-control study and meta-analysis," *PLoS One*, vol. 8, no. 1, article e54259, 2013.

[85] M. Barot, M. R. Gokulgandhi, and A. K. Mitra, "Mitochondrial dysfunction in retinal diseases," *Current Eye Research*, vol. 36, no. 12, pp. 1069–1077, 2011.

[86] C. Li, X. Miao, F. Li et al., "Oxidative stress-related mechanisms and antioxidant therapy in diabetic retinopathy," *Oxidative Medicine and Cellular Longevity*, vol. 2017, Article ID 9702820, 15 pages, 2017.

[87] J. Spranger and A. F. Pfeiffer, "New concepts in pathogenesis and treatment of diabetic retinopathy," *Experimental and Clinical Endocrinology & Diabetes*, vol. 109, Supplement 2, pp. S438–S450, 2001.

[88] L. P. Aiello, R. L. Avery, P. G. Arrigg et al., "Vascular endothelial growth factor in ocular fluid of patients with diabetic retinopathy and other retinal disorders," *The New England Journal of Medicine*, vol. 331, no. 22, pp. 1480–1487, 1994.

[89] M. Shibuya, "Differential roles of vascular endothelial growth factor receptor-1 and receptor-2 in angiogenesis," *Journal of Biochemistry and Molecular Biology*, vol. 39, no. 5, pp. 469–478, 2006.

[90] K. Kovacs, K. V. Marra, G. Yu et al., "Angiogenic and inflammatory vitreous biomarkers associated with increasing levels of retinal ischemia," *Investigative Ophthalmology & Visual Science*, vol. 56, no. 11, pp. 6523–6530, 2015.

[91] I. Klaassen, R. J. van Geest, E. J. Kuiper, C. J. van Noorden, and R. O. Schlingemann, "The role of CTGF in diabetic retinopathy," *Experimental Eye Research*, vol. 133, pp. 37–48, 2015.

[92] A. M. Abu El-Asrar, K. Alam, M. I. Nawaz et al., "Upregulated expression of heparanase in the vitreous of patients with proliferative diabetic retinopathy originates from activated endothelial cells and leukocytes," *Investigative Ophthalmology & Visual Science*, vol. 56, no. 13, pp. 8239–8247, 2015.

[93] A. Jain, S. Saxena, V. K. Khanna, R. K. Shukla, and C. H. Meyer, "Status of serum VEGF and ICAM-1 and its association with external limiting membrane and inner segment-outer segment junction disruption in type 2 diabetes mellitus," *Molecular Vision*, vol. 19, pp. 1760–1768, 2013.

[94] B. Li, E. E. Sharpe, A. B. Maupin et al., "VEGF and PlGF promote adult vasculogenesis by enhancing EPC recruitment and vessel formation at the site of tumor neovascularization," *The FASEB journal*, vol. 20, no. 9, pp. 1495–1497, 2006.

[95] J. Adamiec-Mroczek and J. Oficjalska-Mlynczak, "Assessment of selected adhesion molecule and proinflammatory cytokine levels in the vitreous body of patients with type 2 diabetes—role of the inflammatory-immune process in the pathogenesis of proliferative diabetic retinopathy," *Graefe's Archive for Clinical and Experimental Ophthalmology*, vol. 246, no. 12, pp. 1665–1670, 2008.

[96] S. L. Wu, D. M. Zhan, S. H. Xi, and X. L. He, "Roles of tissue plasminogen activator and Its inhibitor in proliferative diabetic retinopathy," *International journal of ophthalmology*, vol. 7, no. 5, pp. 764–767, 2014.

[97] A. Verma, Z. Shan, B. Lei et al., "ACE2 and Ang-(1-7) confer protection against development of diabetic retinopathy," *Molecular therapy*, vol. 20, no. 1, pp. 28–36, 2012.

[98] S. Rusnak, J. Vrzalova, M. Sobotova, L. Hecova, R. Ricarova, and O. Topolcan, "The measurement of intraocular biomarkers in various stages of proliferative diabetic retinopathy using multiplex xMAP technology," *Journal of Ophthalmology*, vol. 2015, Article ID 424783, 6 pages, 2015.

[99] Y. Ma, Y. Zhang, T. Zhao, and Y. R. Jiang, "Vascular endothelial growth factor in plasma and vitreous fluid of patients with proliferative diabetic retinopathy patients after intravitreal injection of bevacizumab," *American Journal of Ophthalmology*, vol. 153, no. 2, pp. 307–313.e2, 2012, e302.

[100] K. M. Nishiguchi, H. Ushida, D. Tomida, S. Kachi, M. Kondo, and H. Terasaki, "Age-dependent alteration of intraocular soluble heparan sulfate levels and its implications for proliferative diabetic retinopathy," *Molecular Vision*, vol. 19, pp. 1125–1131, 2013.

[101] N. M. Bressler, R. W. Beck, and F. L. Ferris 3rd, "Panretinal photocoagulation for proliferative diabetic retinopathy," *The New England Journal of Medicine*, vol. 365, no. 16, pp. 1520–1526, 2011.

[102] The Diabetic Retinopathy Study Research Group, "Photocoagulation treatment of proliferative diabetic retinopathy: clinical application of Diabetic Retinopathy Study (DRS) findings, DRS report number 8," *Ophthalmology*, vol. 88, no. 7, pp. 583–600, 1981.

[103] Early Treatment Diabetic Retinopathy Study Research Group, "Early photocoagulation for diabetic retinopathy: ETDRS report number 9," *Ophthalmology*, vol. 98, no. 5, pp. 766–785, 1991.

[104] B. Wirostko, T. Y. Wong, and R. Simo, "Vascular endothelial growth factor and diabetic complications," *Progress in Retinal and Eye Research*, vol. 27, no. 6, pp. 608–621, 2008.

[105] P. Mitchell, F. Bandello, U. Schmidt-Erfurth et al., "The RESTORE study: ranibizumab monotherapy or combined with laser versus laser monotherapy for diabetic macular edema," *Ophthalmology*, vol. 118, no. 4, pp. 615–625, 2011.

[106] M. J. Elman, N. M. Bressler, H. Qin et al., "Expanded 2-year follow-up of ranibizumab plus prompt or deferred laser or triamcinolone plus prompt laser for diabetic macular edema," *Ophthalmology*, vol. 118, no. 4, pp. 609–614, 2011.

[107] M. J. Elman, A. Ayala, N. M. Bressler et al., "Intravitreal ranibizumab for diabetic macular edema with prompt versus deferred laser treatment: 5-year randomized trial results," *Ophthalmology*, vol. 122, no. 2, pp. 375–381, 2015.

[108] M. S. Ip, A. Domalpally, J. K. Sun, and J. S. Ehrlich, "Long-term effects of therapy with ranibizumab on diabetic retinopathy severity and baseline risk factors for worsening retinopathy," *Ophthalmology*, vol. 122, no. 2, pp. 367–374, 2015.

[109] The Diabetic Retinopathy Clinical Research Network, "Aflibercept, bevacizumab, or ranibizumab for diabetic macular edema," *The New England Journal of Medicine*, vol. 372, no. 13, pp. 1193–1203, 2015.

[110] S. Cai and N. M. Bressler, "Aflibercept, bevacizumab or ranibizumab for diabetic macular oedema: recent clinically relevant findings from DRCR.net Protocol T," *Current Opinion in Ophthalmology*, vol. 28, no. 6, pp. 636–643, 2017.

[111] J. A. Wells, A. R. Glassman, A. R. Ayala et al., "Aflibercept, bevacizumab, or ranibizumab for diabetic macular edema: two-year results from a comparative effectiveness randomized clinical trial," *Ophthalmology*, vol. 123, no. 6, pp. 1351–1359, 2016.

[112] R. B. Goldberg, "Cytokine and cytokine-like inflammation markers, endothelial dysfunction, and imbalanced coagulation in development of diabetes and its complications," *The Journal of Clinical Endocrinology and Metabolism*, vol. 94, no. 9, pp. 3171–3182, 2009.

[113] O. Simo-Servat, C. Hernandez, and R. Simo, "Usefulness of the vitreous fluid analysis in the translational research of diabetic retinopathy," *Mediators of Inflammation*, vol. 2012, Article ID 872978, 11 pages, 2012.

[114] A. Zijlstra, M. Seandel, T. A. Kupriyanova et al., "Proangiogenic role of neutrophil-like inflammatory heterophils during neovascularization induced by growth factors and human tumor cells," *Blood*, vol. 107, no. 1, pp. 317–327, 2006.

[115] R. P. Danis, S. Sadda, X. Y. Li, H. Cui, Y. Hashad, and S. M. Whitcup, "Anatomical effects of dexamethasone intravitreal implant in diabetic macular oedema: a pooled analysis of 3-year phase III trials," *The British Journal of Ophthalmology*, vol. 100, no. 6, pp. 796–801, 2016.

[116] P. A. Campochiaro, D. M. Brown, A. Pearson et al., "Sustained delivery fluocinolone acetonide vitreous inserts provide benefit for at least 3 years in patients with diabetic macular edema," *Ophthalmology*, vol. 119, no. 10, pp. 2125–2132, 2012.

[117] Diabetic Retinopathy Clinical Research Network Writing Committee on behalf of the DRCR.netlow asterisk, J. A. Haller, H. Qin et al., "Vitrectomy outcomes in eyes with diabetic macular edema and vitreomacular traction," *Ophthalmology*, vol. 117, pp. 1087–1093.e3, 2010.

[118] T. Sharma, A. Fong, T. Y. Lai, V. Lee, S. Das, and D. Lam, "Surgical treatment for diabetic vitreoretinal diseases: a review," *Clinical & Experimental Ophthalmology*, vol. 44, no. 4, pp. 340–354, 2016.

[119] M. H. Berrocal, L. A. Acaba, and A. Acaba, "Surgery for diabetic eye complications," *Current Diabetes Reports*, vol. 16, no. 10, p. 99, 2016.

[120] The diabetic retinopathy vitrectomy study research group, "Early vitrectomy for severe proliferative diabetic retinopathy in eyes with useful vision: results of a randomized trial—diabetic retinopathy vitrectomy study report 3," *Archives of Ophthalmology*, vol. 103, pp. 1644–1652, 1985.

[121] R. P. Danis, D. P. Bingaman, M. Jirousek, and Y. Yang, "Inhibition of intraocular neovascularization caused by retinal ischemia in pigs by PKCbeta inhibition with LY333531," *Investigative Ophthalmology & Visual Science*, vol. 39, no. 1, pp. 171–179, 1998.

[122] "Ruboxistaurin: LY 333531," *Drugs in R & D*, vol. 8, no. 3, pp. 193–199, 2007.

[123] The PKC-DRS Study Group, "The effect of ruboxistaurin on visual loss in patients with moderately severe to very severe nonproliferative diabetic retinopathy. Initial results of the Protein Kinase C β Inhibitor Diabetic Retinopathy Study (PKC-DRS) multicenter randomized clinical trial," *Diabetes*, vol. 54, no. 7, pp. 2188–2197, 2005.

[124] PKC-DRS2 Group, "Effect of ruboxistaurin on visual loss in patients with diabetic retinopathy," *Ophthalmology*, vol. 113, no. 12, pp. 2221–2230, 2006.

[125] G. Javey, S. G. Schwartz, J. Harry, W. Flynn, L. P. Aiello, and M. J. Sheetz, "Ruboxistaurin: review of safety and efficacy in the treatment of diabetic retinopathy," *Clinical Medicine Insights: Therapeutics*, vol. 2, 2010.

[126] M. B. Grant, R. N. Mames, C. Fitzgerald et al., "The efficacy of octreotide in the therapy of severe nonproliferative and early proliferative diabetic retinopathy: a randomized controlled study," *Diabetes Care*, vol. 23, no. 4, pp. 504–509, 2000.

[127] G. E. Krassas, T. Tzotzas, K. Papazisis, K. Pazaitou-Panayiotou, and K. Boboridis, "The efficacy of somatostatin analogues in the treatment of diabetic retinopathy and thyroid eye disease," *Clinical ophthalmology*, vol. 1, no. 3, pp. 209–215, 2007.

[128] S. F. Abcouwer, "Direct effects of PPARα agonists on retinal inflammation and angiogenesis may explain how fenofibrate lowers risk of severe proliferative diabetic retinopathy," *Diabetes*, vol. 62, no. 1, pp. 36–38, 2013.

[129] A. C. Keech, P. Mitchell, P. A. Summanen et al., "Effect of fenofibrate on the need for laser treatment for diabetic retinopathy (FIELD study): a randomised controlled trial," *The Lancet*, vol. 370, no. 9600, pp. 1687–1697, 2007.

[130] C. J. Moravski, D. J. Kelly, M. E. Cooper et al., "Retinal neovascularization is prevented by blockade of the renin-angiotensin system," *Hypertension*, vol. 36, no. 6, pp. 1099–1104, 2000.

Hindawi
Oxidative Medicine and Cellular Longevity
Volume 2018, Article ID 6249536, 8 pages
https://doi.org/10.1155/2018/6249536

Research Article

The Role of Oxidative Stress, Selected Metals, and Parameters of the Immune System in Male Fertility

Michał Dobrakowski,[1] **Zbigniew Kaletka**,[2] **Anna Machoń-Grecka**,[1] **Sławomir Kasperczyk**,[1] **Stanisław Horak**,[3] **Ewa Birkner**,[1] **Jolanta Zalejska-Fiolka**,[1] **and Aleksandra Kasperczyk**[1]

[1]*Dept. of Biochemistry, School of Medicine with the Division of Dentistry, Medical University of Silesia, ul. Jordana 19, 41-808 Zabrze, Poland*
[2]*Department and Clinic of Urology, School of Medicine with the Division of Dentistry in Zabrze, Medical University of Silesia, ul. 3 Maja 13-15, 41-800 Zabrze, Poland*
[3]*I-st Chair and Clin. of Gynecology, Obstetrics and Gynecological Oncology, School of Medicine with the Division of Dentistry, Medical University of Silesia, ul. Batorego 15, 41-902 Bytom, Poland*

Correspondence should be addressed to Anna Machoń-Grecka; anna.machon-grecka@med.sum.edu.pl

Received 17 April 2018; Accepted 14 August 2018; Published 4 September 2018

Academic Editor: Joanna Lecka

The aim of the study was to investigate the associations between standard semen parameters and the parameters reflecting oxidative stress intensity, antioxidant defense functions, levels of selected macro and trace elements, and parameters characterizing immune system function. The study group consisted of 103 fertile males. Based on semen volume, sperm concentration, total sperm count, and percentage of motile sperm at 1 hour postcollection, the individuals were divided into two equal groups—those with excellent (EX) semen quality and those with mediocre (ME) semen quality. The remaining measured parameters characterizing motility and the percentage of normal morphology were higher in the EX group than in the ME group; however, the seminal plasma pH did not differ between the examined groups. The phosphate level was 31% lower in the EX group than in the ME group, whereas there was a tendency toward a 25% lower level of Fe in the EX group than in the ME group ($p = 0.064$). The activities of enzymes involved in antioxidant defense, CuZn-SOD, CAT, and G6PD, were 14%, 63%, and 39%, respectively, higher in the EX group than in the ME group. However, the level of alpha-tocopherol was 32% lower in the EX group than in the ME group. The other measured parameters characterizing antioxidant defense and the parameters of oxidative stress intensity and immune system function were not significantly different. The value of seminal plasma pH is not related to the semen quality of fertile males. Higher fertility potential estimated based on standard semen parameters in fertile males is associated with lower levels of Fe and higher activities of some antioxidant enzymes.

1. Introduction

Infertility is among the most serious medical problems worldwide. Approximately 80 million people worldwide are affected by infertility. Male factor problems account for up to 40–50% of these cases, and there has been a considerable increase in male infertility in recent decades [1–3].

Generally accepted parameters that reflect the functional ability of spermatozoa include sperm count, motility, and sperm morphology. Most men diagnosed with infertility have low sperm numbers in the semen or an adequate number of sperm with reduced sperm motility or/and abnormal morphology. However, men with normal semen tests may also have impaired sperm-fertilizing ability. Conversely, men with poor sperm characteristics may have no problem achieving fertilization. These facts clearly indicate that standard semen parameters are not sufficient to unambiguously determine male fertility status. To introduce more highly reliable tests of male fertility, there is a need to better understand the factors influencing semen quality [1].

A significant part of male factor infertility cases is believed to be due to the damaging effects of oxidative stress. Oxidative stress is an imbalance between reactive oxygen species (ROS) production and the semen's natural antioxidant defenses. The increased levels of ROS may be due to many factors, such as infections, autoimmunity, chronic diseases, high temperatures, electromagnetic radiation, pesticides and pollutants, and lifestyle factors (e.g., advanced age, alcohol consumption, smoking, stress, obesity, and poor diet) [2]. Several studies have documented the interactions between cytokines and ROS. On the one hand, ROS can promote the expression and production of cytokines; on the other hand, some cytokines can modulate prooxidant and antioxidant systems and generation of ROS. In light of this, seminal cytokines via interaction with oxidative stress could be involved in various pathologic conditions related to defective sperm function [4, 5].

Apart from oxidative stress, macro and trace elements, such as calcium (Ca), magnesium (Mg), zinc (Zn), iron (Fe), copper (Cu), and selenium (Se), exhibit significant effects on male fertility [6]. Ca triggers the acrosome reaction and is involved in sperm motility. Mg acts as an intracellular Ca antagonist and plays a role in sperm motility and in spermatogenesis [6, 7]. Zn acts as a cofactor for most enzymatic reactions, including for some involving sperm motility [6, 8]. Fe and Cu also serve as important cofactors participating in oxygenation, reduction processes, and antioxidant metabolism [9]. Whereas Zn and Cu are cofactors of superoxide dismutase (Cu/Zn-SOD) [10], Se is incorporated into glutathione peroxidases (GPxs), a family of antioxidant selenoproteins found in the spermatozoa midpiece [11]. The protective effects of Se are necessary for testicular development, spermatogenesis, and spermatozoa motility [12].

In light of the aforementioned information, the aim of the present study was to investigate the associations between standard semen parameters characterizing semen quality and the parameters reflecting oxidative stress intensity, antioxidant defense function, levels of selected macro and trace elements, and parameters characterizing immune system function.

2. Materials and Methods

2.1. Study Population. The study group consisted of 103 males who had attended the andrology clinic for the diagnosis of infertility. The inclusion criteria were defined as follows: normal semen profile according to the WHO criteria [13] and no history of drug consumption (including antioxidant medications). The exclusion criteria were defined as follows: smoking, alcohol abuse, a history of any chronic disease (e.g., diabetes), coronary artery disease, or a malignant neoplasm.

The study group was divided into two equal groups according to semen quality. Study subjects were classified to the first group (excellent semen quality—EX group) based on the following criteria: (1) semen volume > 2 ml, (2) sperm cell count in 1 ml > 32 mln/ml, (3) total sperm cell count > 80 mln, and (4) motile sperm 1 hour after collection. Study subjects were classified to the second group (mediocre semen quality—ME group) based on the following criteria: semen volume between 1.5 and 2 ml, sperm cell count in 1 ml between 15 and 32 mln/ml, total sperm cell count between 39 and 80 mln, and motile sperm 1 hour after collection.

The experimental setup has been approved by the Bioethics Committee of the Medical University of Silesia in Katowice (KNW/0022/KB1/I/13/09).

2.2. Sample Collection. Semen was collected on the same day in the morning before the first meal. Semen samples (2–6 ml) were collected by masturbation, at home or at laboratory research facilities, after at least 3 days of sexual abstinence (number of days elapsed since last ejaculation was recorded for each volunteer).

2.3. Semen Analysis. We followed the methods of Kasperczyk et al. [14]. All of the semen specimens were analyzed according to WHO standards [13], including the assessment of seminal volume, sperm cell density, total sperm cell count, motility, and supravital eosin staining (for the percentage of live spermatozoa). Sperm morphology was examined after Papanicolaou staining. The semen samples (1.5 ml) after liquefaction were centrifuged at 6000 g for 10 minutes to separate the spermatozoa from the seminal plasma. The seminal plasma was transferred to fresh tubes and stored at −75°C until being required for the biochemical and lead analyses. Additionally, a 10% spermatozoa lysate in bidistilled water was made.

2.4. Determination of Magnesium. We followed the methods of Kasperczyk et al. [14]. The seminal plasma magnesium was determined using a Unicam flame atomic absorption spectrometer. This method involves diluting seminal plasma with a 0.2% solution of cesium chloride (CsCl), followed by determining the magnesium in solution by measuring the absorbance at a wavelength of 285.2 nm. The concentrations are expressed as mg/dl.

2.5. Determination of Calcium. We followed the methods of Kasperczyk et al. [14]. The seminal plasma calcium concentration was determined using a biochemical analyzer method based on a reaction with o-cresolphthalein at pH > 7. The color intensity is directly proportional to the calcium concentration, which was expressed in mg/dl.

2.6. Determination of Iron. We followed the methods of Kasperczyk et al. [14]. The seminal plasma iron concentration was determined photometrically. In this method, ascorbate reduces Fe^{3+} ions to Fe^{2+} ions, which react with ferrozine to form a colored complex. The color intensity is directly proportional to the iron concentration, which is expressed in μg/dl.

2.7. Determination of Zinc. We followed the methods of Kasperczyk et al. [14]. The concentration of seminal plasma zinc was measured by atomic absorption spectrophotometry using Unicam 929 and 939OZ Atomic Absorption Spectrometers with GF90 and GF90Z, respectively, at a wavelength of 213 nm [15]. The data are shown in mg/l.

2.8. Determination of Copper. We followed the methods of Kasperczyk et al. [14]. The concentration of seminal plasma copper was measured by atomic absorption spectrophotometry using Unicam 929 and 939OZ Atomic Absorption Spectrometers with GF90 and GF90Z, respectively, at a wavelength of 324.8 nm [15]. The data are shown in μg/dl.

2.9. Determination of Selenium. We followed the methods of Kasperczyk et al. [14]. The concentration of Se in seminal plasma was determined by a flameless method using Unicam 929 and 939OZ spectrophotometers. The calibration curve was prepared using Nycomed® standards. Certified Nycomed® controls (containing 78.0 and 11.4 μg/dm^3 of Se) were used to perform the internal control. The data are shown in μg/dl.

2.10. Determination of Lead. Concentration of lead in seminal plasma (PbS) was measured using graphite furnace atomic absorption spectrophotometry Unicam 929 and 939OZ Atomic Absorption Spectrometers with GF90 and GF90Z. The concentration of lead in the semen specimens was calculated from a standard curve. Data are shown in μg/dl.

2.11. Determination of Phosphates. Inorganic phosphorus with ammonium molybdate reacts in the presence of sulfuric acid to form a complex: ammonium phosphomolybdate (NH_3) $[PO_4$ $(MoO_3)_{12}]$. The concentration of the complex formed is measured photometrically in an ultraviolet spectrum at a wavelength of 340 nm.

2.12. Determination of Protein. We followed the methods of Kasperczyk et al. [14]. The protein level was measured by means of an A25 biochemistry analyzer (BioSystems S.A., Barcelona, Spain) according to the manufacturer's instructions. The results for protein levels are expressed in g/l.

2.13. Determination of Malondialdehyde (MDA). MDA, a product of lipid peroxidation, was measured fluorometrically as a 2-thiobarbituric acid-reactive substance (TBARS) in seminal plasma according to Ohkawa et al. [16] with modifications according to Kasperczyk et al. [14]. Concentrations are given in μmol/l.

2.14. Determination of Lipofuscin (LPS). The LPS concentration was determined in seminal plasma according to Jain [17]. Values are presented as relative units (relative fluorescence lipid extract, RF), where X corresponds to a fluorescence solution of 0.1 mg/ml quinidine sulfate (Sigma-Aldrich) in 0.1 N sulfuric acid (POCH).

2.15. Determination of Total Oxidation Status (TOS). The total oxidant status was measured in seminal plasma according to Erel [18]. This method was conducted in an automated analyzer (PerkinElmer) calibrated with hydrogen peroxide. Data are shown in μmol/l.

2.16. Determination of Superoxide Dismutase (SOD) Activity. We followed the methods of Kasperczyk et al. [14]. The method of Oyanagui [19] was used to measure the activity of SOD in seminal plasma. The activity of SOD is equal to 1 nitric unit (NU) when it inhibits nitric ion production by 50%. Activities of SOD in seminal plasma were expressed in NU/mg protein.

2.17. Determination of Thiol Groups. The concentration of thiol groups was determined as described by Koster et al. [20] using 5,5′-dithiobis-(2-nitrobenzoic acid) (DTNB), which undergoes reduction by compounds containing the sulfhydryl groups, yielding the yellow anion derivative, 5-thio-2-nitrobenzoate, which absorbs light at a wavelength of 412 nm. This assay was carried out using an automated analyzer (PerkinElmer). The results were expressed as μmol per g of protein (μmol/g protein).

2.18. Determination of Catalase (CAT) Activity. The catalase (CAT) was measured by using the method of Johansson and Borg [21]. Catalase activity was expressed as international units per milligram of protein (U/g protein).

2.19. Determination of Glucose-6-phosphare Dehydrogenase (G6PD) and Glutathione Reductase (GR) Activity. We followed the methods of Kasperczyk et al. [14]. The activities of glucose-6-phosphare dehydrogenase (G6PD) and glutathione reductase (GR) in seminal plasma were measured according to Richterich [22]. G6PD and GR activities were expressed as international units per milligram of protein (U/g protein).

2.20. Determination of Glutathione Peroxidase (GPx) and Glutathione-S-transferase (GST) Activity. We followed the methods of Kasperczyk et al. [14]. The seminal plasma glutathione peroxidase (GPx) activity was measured by the kinetic method of Paglia and Valentine [23]. The GPx activity was expressed as international units per milligram of protein (U/g protein). The activity of seminal plasma glutathione-S-transferase (GST) was measured according to the kinetic method of Habig and Jakoby [24]. The GST activity was expressed as international units per milligram of protein (U/g protein).

2.21. Determination of Total Antioxidant Capacity (TAC). Total antioxidant capacity was measured in serum according to Erel [25]. This assay was conducted in an automated PerkinElmer analyzer calibrated with Trolox. Data were expressed as mmol/l.

2.22. Determination of α-Tocopherol. The concentration of α-tocopherol in seminal plasma was determined by Shearer and Lim [26]. Concentrations were provided as μg/ml.

2.23. Determination of Cytokines. Levels of interleukin 1β (IL-1β), interleukin 2 (IL-2), interleukin 4 (IL-4), interleukin 5 (IL-5), interleukin 6 (IL-6), interleukin 7 (IL-7), interleukin 8 (IL-8), interleukin 10 (IL-10), interleukin 12 (p70), interleukin 13 (IL-13), interleukin 17 (IL-17), granulocyte colony-stimulating factor (G-CSF), granulocyte-macrophage colony-stimulating factor (GM-CSF), interferon gamma (IFN-γ), monocyte chemoattractant protein-1 (MCP-1), macrophage inflammatory protein 1-α (MIP-1α), and tumor necrosis factor α (TNF-α) were detected in seminal plasma using a Bio-Plex 200 System (Bio-Rad

Table 1: Semen parameters in the study population (group ME: mediocre semen morphology and group EX: excellent semen morphology). p value—Student's t-test.

	ME group $n = 52$		EX group $n = 51$		p value	Relative change
	Mean	SD	Mean	SD		
Age	33.9	6.02	32.4	5.64	0.492	−4%
Volume (ml)	3.44	1.44	4.04	1.97	0.038	17%
pH	7.58	0.08	7.55	0.06	0.080	—
Sperm cell count in 1 ml (mln/ml)	73.0	66.6	84.8	50.4	0.011	16%
Total sperm cell count (mln)	229	198	312	173	0.001	36%
Motile sperm cells after 1 hour (%)	54.1	7.80	62.3	9.39	<0.001	15%
Progressively motile sperm cells after 1 hour (%)	22.9	9.1	29.7	9.55	<0.001	30%
Motile spermatozoa after 24 hours (%)	14.7	13.1	23.3	17.1	0.005	58%
Progressively motile spermatozoa after 24 hours (%)	4.60	5.85	8.38	9.20	0.014	82%
Normal morphology (%)	49.4	8.11	54.0	7.22	0.005	9%

$p < 0.05$.

Table 2: Semen parameters in the study population (group ME: mediocre semen morphology and group EX: excellent semen morphology). p value—Student's t-test.

	ME group		EX group		p value	Relative change
	Mean	SD	Mean	SD		
Phosphates concentration (mg/dl)	97.4	67.8	66.7	33.9	0.033	−31%
Magnesium concentration (mg/dl)	6.15	3.37	5.72	4.16	0.272	−7%
Calcium concentration (mg/dl)	30.2	10.25	29.4	11.5	0.605	−3%
Iron concentration (μg/dl)	4.74	3.68	3.55	3.60	*0.064*	−25%
Zinc concentration (mg/l)	123	54.8	134	59.1	0.650	8%
Copper concentration (μg/dl)	34.6	46.3	36.6	45.1	0.351	6%
Selenium concentration (μg/l)	26.0	8.89	28.8	16.67	0.849	10%
Lead concentration in seminal plasma (μg/dl)	0.99	0.49	1.22	0.57	0.116	23%

$p < 0.05$.

Laboratories Inc., Berkeley, California, USA) according to the manufacturer's instruction. The results were expressed as pg/ml.

2.24. Statistical Analysis. A database was created in MS Excel 2007. Statistical analysis was performed using Statistica 10.0 PL software. Data were reported as the mean and standard deviation (SD) for parameters with a normal distribution and median and interquartile range (IQR) for those with a nonnormal distribution. Shapiro-Wilk's test was used to verify normality, and Levene's test was used to verify the homogeneity of variances. Statistical comparisons between groups were made using a t-test, a t-test with a separate variance, or the Mann-Whitney U test (nonparametric test). A value of $p < 0.05$ was considered to be significant.

3. Results

The mean age in the examined groups did not differ significantly. Semen volume, sperm concentration in 1 ml, total sperm count, and the percentage of motile sperm after 1 hour were higher in the EX group than in the ME group due to the division criteria. Other parameters characterizing motility and the percentage of normal sperm morphology were also higher in the EX group. However, seminal plasma pH did not differ between the examined groups (Table 1).

The phosphate level in semen was significantly lower in the EX group than in the ME group by 31%. There was a tendency toward a 25% lower level of Fe in the EX group than in the ME group ($p = 0.064$). However, the concentrations of the other examined metals (Ca, Mg, Zn, Cu, Se, and Pb) in seminal plasma were not significantly different between the examined groups (Table 2).

The activities of enzymes involved in antioxidant defense, CuZn-SOD, CAT, and G6PD, were 14%, 63%, and 39%, respectively, higher in the EX group than in the ME group. There was a tendency toward a 13% higher activity of total SOD in the EX group than in the ME group ($p = 0.059$). However, the level of alpha-tocopherol was significantly lower in the EX group than in the ME group by 32%. Other measured parameters characterizing antioxidant defense and parameters of oxidative stress intensity were not significantly different (Table 3). Similarly, the parameters of immune system function were the same in both groups (Table 4).

Table 3: The levels or activity of malondialdehyde (MDA), lipofuscin, total oxidant status (TOS), superoxide dismutase (SOD), Mn-SOD, CuZn-SOD, thiol groups, catalase (CAT), glutathione reductase (GR), glutathione peroxidase (GPx), glutathione-S-transferase (GST), glucose-6-phosphate dehydrogenase (G6PD), total antioxidant capacity (TAC), and α-tocopherol in the study population (group ME: mediocre semen morphology and group EX: excellent semen morphology). p value—comparison between the ME and EX groups using Student's t-test.

	ME group		EX group		p value	Relative change
	Mean	SD	Mean	SD	Mean	SD
MDA concentration (μmol/l)	2.32	0.81	2.51	1.13	0.474	8%
Lipofuscin concentration (RF)	3.81	1.50	4.02	1.65	0.975	5%
TOS (μmol/l)	11.00	14.23	11.0	13.7	0.697	0%
SOD activity (NU/mg protein)	4.09	1.59	4.62	1.50	*0.059*	13%
Mn-SOD activity (NU/mg protein)	0.83	1.06	0.88	0.93	0.358	6%
CuZn-SOD activity (NU/mg protein)	3.12	1.46	3.55	1.30	0.050	14%
Thiol group concentration (μmol/g protein)	4.73	2.46	5.43	2.70	0.098	15%
CAT activity (U/g protein)	11.9	7.73	19.3	20.6	0.030	63%
GR activity (U/g protein)	1.64	1.58	1.85	2.09	0.668	13%
GPx activity (U/g protein)	3.13	4.71	1.62	2.91	0.273	−48%
GST activity (mU/g protein)	83.3	60.9	84.8	55.1	0.732	2%
G6PD activity (U/g protein)	1.22	1.09	1.70	1.23	0.049	39%
TAC (mmol/l)	1.38	0.27	1.29	0.22	0.199	−7%
α-Tocopherol concentration (μg/ml)	10.60	3.82	7.18	3.78	<0.001	−32%

$p < 0.05$.

Table 4: The levels of interleukin 1β (IL-1β), interleukin 2 (IL-2), interleukin 4 (IL-4), interleukin 5 (IL-5), interleukin 6 (IL-6), interleukin 7 (IL-7), interleukin 8 (IL-8), interleukin 10 (IL-10), interleukin 12 (p70), interleukin 13 (IL-13), interleukin 17 (IL-17), granulocyte colony-stimulating factor (G-CSF), granulocyte-macrophage colony-stimulating factor (GM-CSF), interferon gamma (IFN-γ), monocyte chemoattractant protein-1 (MCP-1), macrophage inflammatory protein 1-α (MIP-1α), and tumor necrosis factor α (TNF-α) in seminal plasma of the examined population. p value comparison between values obtained in the ME group: mediocre semen morphology and EX group: excellent semen morphology using Mann-Whitney U test.

	ME group		EX group		p value
	Median	IQR	Median	IQR	
IL-1β (pg/ml)	1.29	2.60	1.07	2.61	0.450
IL-2 (pg/ml)	0.00	1.01	0.02	3.62	0.284
IL-4 (pg/ml)	0.09	0.02	0.11	0.17	0.494
IL-5 (pg/ml)	22.3	56.6	49.8	118	0.604
IL-6 (pg/ml)	12.0	17.8	7.13	11.6	0.238
IL-7 (pg/ml)	508	444	606	409	0.116
IL-8 (pg/ml)	179	190	146	156	0.752
IL-10 (pg/ml)	1.37	1.12	1.39	2.27	0.770
IL-12 (p70) (pg/ml)	2.32	3.93	2.80	3.53	0.913
IL-13 (pg/ml)	0.35	1.01	0.42	0.46	0.688
IL-17 (pg/ml)	6.50	8.80	8.07	8.79	0.971
G-CSF (pg/ml)	17.9	29.8	16.1	27.4	0.971
GM-CSF (pg/ml)	188	65.88	196	53.2	0.618
IFN-γ (pg/ml)	57.1	71.3	40.8	93.0	0.643
MCP-1 (MCAF) (pg/ml)	1139	1880	903	1038	0.415
MIP-1b (pg/ml)	46.8	34.9	57.6	35.0	0.458
TNF-α (pg/ml)	3.52	2.82	4.76	4.03	0.569

IQR: interquartile range; $p < 0.05$.

4. Discussion

The normal pH of seminal plasma is between 7.2 and 8.0, depending on the length of time since ejaculation. As a result of carbon dioxide loss, the pH tends to increase shortly after ejaculation [27]. In the present study, significantly different values in the motility, sperm volume and count, and the percentage of sperm with normal morphology observed were accompanied with almost equal pH in two study groups due to the study division criteria. This observation is consistent with the results obtained by Banjoko and Adeseolu [27] who examined two groups of males divided based on sperm motility. Banjoko and Adeseolu [27] reported no significant differences in the seminal plasma pH between these groups. These results support the hypothesis that seminal plasma pH does not have an effect on sperm quality except when the pH levels are excessively abnormal. In contrast to pH, the percentage of normal sperm forms is significantly positively associated with the motility parameters due to the impaired motility of the abnormal forms. Consistently, in the aforementioned study by Banjoko and Adeseolu [27], the percentage of abnormal forms was significantly lower in the males with normal motility.

The most important seminal plasma buffers are HCO_3/CO_2, proteins, and low-molecular weight components, such as citrate, pyruvate, and inorganic phosphate [27]. The inorganic phosphate level was significantly lower in the EX group than in the ME group; however, the observed difference in phosphate levels and its contribution to seminal plasma buffering capacity seemed to be too low to influence seminal plasma pH. However, the results of the present study indicate a significant association between the inorganic phosphate level and standard semen parameters. This association probably results from phosphate ion being crucial to the activities of adenyl cyclase, the primary regulator of sperm motility, and prostatic acid phosphatase (PAP), which has been associated with the liquefaction process of semen [27]. Based on the results of the present study and previous studies [27, 28], we speculate that there is an optimal inorganic phosphate level and any deviation in this level may negatively affect semen quality.

Our previous investigations indicate that the levels of essential metals, such as Ca, Mg, and Cu, as well as Pb, a common xenobiotic metal, generally are not associated with standard semen quality parameters in fertile males [29–32]. The levels of the aforementioned metals were not different between the EX and ME groups, confirming the hypothesis that their influence on semen quality in the group of fertile males is limited. Similarly, the levels of Zn and Se were also not different between the examined groups. By contrast, there was a tendency toward a lower level of Fe in the EX group than in the ME group. These results are supported by our previous work on fertile males [33] indicating that higher levels of Fe are associated with decreased sperm motility and elevated TOS values in seminal plasma of fertile males. On one hand, Fe plays a critical role in the synthesis of nucleic acids and proteins, electron transport, cellular respiration, proliferation, and differentiation. All of these processes are intimately related to spermatogenesis and spermatozoa metabolism. On the other hand, as a transition metal, Fe can easily donate an electron during oxidation, becoming a source of ROS. Therefore, both Fe deficiency and overload could be harmful to spermatozoa. Oxidative stress related to Fe overload causes damage to lipids, proteins, and DNA, impairing spermatogenesis and spermatozoa metabolism [9]. The results of the present study indicate that the Fe status plays a significant role not only in the cases of infertility or subfertility but also in the population of fertile males. In light of this association, under physiological conditions, the Fe level in semen seems to be more closely related to fertility potential than the levels of other examined metals.

To counteract the destructive effects of ROS, seminal plasma has an antioxidant defense system [34] that is a source of antioxidant enzymes, such as SOD, CAT, and GPx. SOD converts superoxide anions to hydrogen peroxide which is, in turn, utilized by CAT and GPx. GPx activity is related to the level of reduced glutathione (GSH). GSH is a major thiol antioxidant in the human body that plays a central role in the defense against oxidative stress by being oxidized to glutathione disulfide (GSSG). To restore GSH content, GSSG is reduced by GR, which requires NADPH provided by G6PD. The second GSH-dependent enzyme is GST. The main role of GST is the utilization of xenobiotics [35, 36]. Apart from GSH, seminal plasma is rich in other nonenzymatic antioxidants, such as ascorbate, urate, alpha-tocopherol, and pyruvate [1]. In the present study, the activities of SOD, CAT, and G6PD were higher in the EX group than in the ME group. This observation suggests higher effectiveness of the enzymatic antioxidant defense in the group of males with better sperm quality. Consistently, several authors suggest that lower activities of SOD and CAT may be associated with decreased fertility. Moreover, activities of these enzymes have been shown to correlate positively with sperm quality markers, such as motility, sperm count, and sperm volume [34, 37–39]. However, the associations between the antioxidant defense system parameters and oxidative stress are not conclusive because there are also studies reporting inconsistent results. Therefore, it has been proposed that each studied pathology connected with poor semen quality, such as varicocele or genitourinary infections, may be related to a definite pattern of markers of oxidative stress and nonenzymatic antioxidant compounds [40].

The major source of ROS in seminal plasma is sperm metabolism [41]. Therefore, the higher sperm motility observed in the EX group than that in the ME group should be associated with elevated oxidative stress due to the higher energy demand of motile spermatozoa. Nevertheless, the levels of measured oxidative stress biomarkers, such as MDA, LPS, and TOS, as well as TAC value and the concentration of thiol groups that reflect antioxidative potential, did not differ between the examined groups. This observation also suggests that the EX group possesses a more effective antioxidant defense system. Surprisingly, only the level of alpha-tocopherol, a powerful nonenzymatic antioxidant, was significantly decreased in the EX group compared to the ME group. Studies generally support the beneficial role of this form of vitamin E in maintenance of male fertility

potential [42–44]. Therefore, the results in the present study need to be verified.

Proinflammatory cytokines, such as IL-1β, IL-6, IL-8, IL-12, and TNF-α, are believed to contribute to poor sperm quality by inducing oxidative stress and lipid peroxidation [45]. However, in the present study, levels of cytokines, including the proinflammatory ones, did not differ between the examined groups. This suggests that semen of fertile males is rather homogenous with respect to immune system parameters.

5. Conclusions

The seminal plasma pH is not related to the semen quality of fertile males. Higher fertility potential estimated based on standard semen parameters in fertile males is associated with lower levels of Fe and higher activities of some antioxidant enzymes due to lower oxidative stress intensity.

Data Availability

The data used to support the findings of this study are available from the corresponding author upon request.

Conflicts of Interest

The authors have no conflicts of interest to declare.

Acknowledgments

This work was supported by the Medical University of Silesia (KNW-1-081/N/6/O).

References

[1] B. Macanovic, M. Vucetic, A. Jankovic et al., "Correlation between sperm parameters and protein expression of antioxidative defense enzymes in seminal plasma: a pilot study," *Disease Markers*, vol. 2015, Article ID 436236, 5 pages, 2015.

[2] M. G. Showell, R. Mackenzie-Proctor, J. Brown, A. Yazdani, M. T. Stankiewicz, and R. J. Hart, "Antioxidants for male subfertility," *Cochrane Database of Systematic Reviews*, vol. 12, 2014.

[3] Y. X. Wang, P. Wang, W. Feng et al., "Relationships between seminal plasma metals/metalloids and semen quality, sperm apoptosis and DNA integrity," *Environmental Pollution*, vol. 224, pp. 224–234, 2017.

[4] L. Jiang, T. Zheng, J. Huang et al., "Association of semen cytokines with reactive oxygen species and histone transition abnormalities," *Journal of Assisted Reproduction and Genetics*, vol. 33, no. 9, pp. 1239–1246, 2016.

[5] S. Seshadri, M. Bates, G. Vince, and D. I. L. Jones, "The role of cytokine expression in different subgroups of subfertile men," *American Journal of Reproductive Immunology*, vol. 62, no. 5, pp. 275–282, 2009.

[6] W. Y. Wong, G. Flik, P. M. W. Groenen et al., "The impact of calcium, magnesium, zinc, and copper in blood and seminal plasma on semen parameters in men," *Reproductive Toxicology*, vol. 15, no. 2, pp. 131–136, 2001.

[7] F. R. Abou-Shakra, N. I. Ward, and D. M. Everard, "The role of trace elements in male infertility," *Fertility and Sterility*, vol. 52, no. 2, pp. 307–310, 1989.

[8] B. Eskenazi, S. A. Kidd, A. R. Marks, E. Sloter, G. Block, and A. J. Wyrobek, "Antioxidant intake is associated with semen quality in healthy men," *Human Reproduction*, vol. 20, no. 4, pp. 1006–1012, 2005.

[9] E. Tvrda, R. Peer, S. C. Sikka, and A. Agarwal, "Iron and copper in male reproduction: a double-edged sword," *Journal of Assisted Reproduction and Genetics*, vol. 32, no. 1, pp. 3–16, 2015.

[10] M. Gavella and V. Lipovac, "In vitro effect of zinc on oxidative changes in human semen," *Andrologia*, vol. 30, no. 6, pp. 317–323, 1998.

[11] A. Eroglu, Z. Dogan, E. G. Kanak, G. Atli, and M. Canli, "Effects of heavy metals (Cd, Cu, Cr, Pb, Zn) on fish glutathione metabolism," *Environmental Science and Pollution Research International*, vol. 22, no. 5, pp. 3229–3237, 2015.

[12] O. Akinloye, A. O. Arowojolu, O. B. Shittu, C. A. Adejuwon, and B. Osotimehin, "Selenium status of idiopathic infertile Nigerian males," *Biological Trace Element Research*, vol. 104, no. 1, pp. 9–18, 2005.

[13] WHO, *The Laboratory Manual for the Examination of Human Semen*, Cambridge University Press, 5 edition, 2010.

[14] A. Kasperczyk, M. Dobrakowski, S. Horak, J. Zalejska-Fiolka, and E. Birkner, "The influence of macro and trace elements on sperm quality," *Journal of Trace Elements in Medicine and Biology*, vol. 30, pp. 153–159, 2015.

[15] A. A. Brown and A. Taylor, "Determination of copper and zinc in serum and urine by use of a slotted quartz tube and flame atomic-absorption spectrometry," *Analyst*, vol. 109, no. 11, pp. 1455–1459, 1984.

[16] H. Ohkawa, N. Ohishi, and K. Yagi, "Assay for lipid peroxides in animal tissues by thiobarbituric acid reaction," *Analytical Biochemistry*, vol. 95, no. 2, pp. 351–358, 1979.

[17] S. K. Jain, "In vivo externalization of phosphatidylserine and phosphatidylethanolamine in the membrane bilayer and hypercoagulability by the lipid peroxidation of erythrocytes in rats," *The Journal of Clinical Investigation*, vol. 76, no. 1, pp. 281–286, 1985.

[18] O. Erel, "A new automated colorimetric method for measuring total oxidant status," *Clinical Biochemistry*, vol. 38, no. 12, pp. 1103–1111, 2005.

[19] Y. Oyanagui, "Reevaluation of assay methods and establishment of kit for superoxide dismutase activity," *Analytical Biochemistry*, vol. 142, no. 2, pp. 290–296, 1984.

[20] J. F. Koster, P. Biemond, and A. J. Swaak, "Intracellular and extracellular sulphydryl levels in rheumatoid arthritis," *Annals of the Rheumatic Diseases*, vol. 45, no. 1, pp. 44–46, 1986.

[21] L. H. Johansson and L. A. Håkan Borg, "A spectrophotometric method for determination of catalase activity in small tissue samples," *Analytical Biochemistry*, vol. 174, no. 1, pp. 331–336, 1988.

[22] R. Richterich, *Chemia kliniczna*, PZWL, Warszawa, 1971.

[23] D. E. Paglia and W. N. Valentine, "Studies on the quantitative and qualitative characterization of erythrocyte glutathione peroxidase," *The Journal of Laboratory and Clinical Medicine*, vol. 70, no. 1, pp. 158–169, 1967.

[24] W. H. Habig and W. B. Jakoby, "[51] Assays for differentiation of glutathione S-Transferases," *Methods in Enzymology*, vol. 77, pp. 398–405, 1981.

[25] O. Erel, "A novel automated direct measurement method for total antioxidant capacity using a new generation, more stable ABTS radical cation," *Clinical Biochemistry*, vol. 37, no. 4, pp. 277–285, 2004.

[26] M. J. Shearer and C. K. Lim, *HPLC of Small Molecules-A Practical Approach*, IRL Press, Oxford, 1986.

[27] S. O. Banjoko and F. O. Adeseolu, "Seminal plasma pH, inorganic phosphate, total and ionized calcium concentrations in the assessment of human spermatozoa function," *Journal of Clinical and Diagnostic Research*, vol. 7, no. 11, pp. 2483–2486, 2013.

[28] D. A. Adamopoulos and V. Deliyiannis, "Seminal plasma magnesium, calcium and inorganic phosphate concentration in normozoospermic and subfertile men," *Andrologia*, vol. 15, no. 6, pp. 648–654, 1983.

[29] A. Kasperczyk, M. Dobrakowski, J. Zalejska-Fiolka, S. Horak, and E. Birkner, "Magnesium and selected parameters of the non-enzymatic antioxidant and immune systems and oxidative stress intensity in the seminal plasma of fertile males," *Magnesium Research*, vol. 28, no. 1, pp. 14–22, 2015.

[30] A. Kasperczyk, M. Dobrakowski, Z. P. Czuba, S. Horak, and S. Kasperczyk, "Environmental exposure to lead induces oxidative stress and modulates the function of the antioxidant defense system and the immune system in the semen of males with normal semen profile," *Toxicology and Applied Pharmacology*, vol. 284, no. 3, pp. 339–344, 2015.

[31] A. Kasperczyk, M. Dobrakowski, Z. P. Czuba, L. Kapka-Skrzypczak, and S. Kasperczyk, "Environmental exposure to zinc and copper influences sperm quality in fertile males," *Annals of Agricultural and Environmental Medicine*, vol. 23, no. 1, pp. 138–143, 2016.

[32] A. Kasperczyk, M. Dobrakowski, J. Zalejska-Fiolka, S. Horak, A. Machoń, and E. Birkner, "Rola wapnia w nasieniu ludzkim i jego związek z układem antyoksydacyjnym. [The role of calcium in human sperm in relation to the antioxidant system]. Environmental," *Medicine*, vol. 17, pp. 34–40, 2014.

[33] A. Kasperczyk, M. Dobrakowski, Z. P. Czuba, L. Kapka-Skrzypczak, and S. Kasperczyk, "Influence of iron on sperm motility and selected oxidative stress parameters in fertile males - a pilot study," *Annals of Agricultural and Environmental Medicine*, vol. 23, no. 2, pp. 292–296, 2016.

[34] M. R. Amini, H. Kohram, A. Zare-Shahaneh, M. Zhandi, H. Sharideh, and M. M. Nabi, "The effects of different levels of catalase and superoxide dismutase in modified Beltsville extender on rooster post-thawed sperm quality," *Cryobiology*, vol. 70, no. 3, pp. 226–232, 2015.

[35] T. Mostafa, L. A. Rashed, A. S. Zeidan, and A. Hosni, "Glutathione-S-transferase-oxidative stress relationship in the internal spermatic vein blood of infertile men with varicocele," *Andrologia*, vol. 47, no. 1, pp. 47–51, 2015.

[36] J. F. Griveau, E. Dumont, P. Renard, J. P. Callegari, and D. Le Lannou, "Reactive oxygen species, lipid peroxidation and enzymatic defence systems in human spermatozoa," *Journal of Reproduction and Fertility*, vol. 103, no. 1, pp. 17–26, 1995.

[37] F. Atig, M. Raffa, H. B. Ali, K. Abdelhamid, A. Saad, and M. Ajina, "Altered antioxidant status and increased lipid per-oxidation in seminal plasma of tunisian infertile men," *International Journal of Biological Sciences*, vol. 8, no. 1, pp. 139–149, 2012.

[38] M. Shiva, A. K. Gautam, Y. Verma, V. Shivgotra, H. Doshi, and S. Kumar, "Association between sperm quality, oxidative stress, and seminal antioxidant activity," *Clinical Biochemistry*, vol. 44, no. 4, pp. 319–324, 2011.

[39] I. Zelen, M. Mitrović, A. Jurisic-Skevin, and S. Arsenijević, "Activity of superoxide dismutase and catalase and content of malondialdehyde in seminal plasma of infertile patients," *Medicinski Pregled*, vol. 63, no. 9-10, pp. 624–629, 2010.

[40] L. Micheli, D. Cerretani, G. Collodel et al., "Evaluation of enzymatic and non-enzymatic antioxidants in seminal plasma of men with genitourinary infections, varicocele and idiopathic infertility," *Andrology*, vol. 4, no. 3, pp. 456–464, 2016.

[41] N. Am-in, R. N. Kirkwood, M. Techakumphu, and W. Tantasuparuk, "Lipid profiles of sperm and seminal plasma from boars having normal or low sperm motility," *Theriogenology*, vol. 75, no. 5, pp. 897–903, 2011.

[42] A. Gvozdjáková, J. Kucharská, J. Dubravicky, V. Mojto, and R. B. Singh, "Coenzyme Q10,α-tocopherol, and oxidative stress could be important metabolic biomarkers of male infertility," *Disease Markers*, vol. 2015, Article ID 827941, 6 pages, 2015.

[43] R. M. Santymire, S. R. Lavin, H. Branvold-Faber, J. Kreeger, and P. Marinari, "Effect of dietary vitamin E and prey supplementation on semen quality in male black-footed ferrets (Mustela nigripes)," *Theriogenology*, vol. 84, no. 2, pp. 217–225, 2015.

[44] E. Moretti, C. Castellini, E. Mourvaki et al., "Distribution of α- and δ-tocopherols in seminal plasma and sperm fractions of men with normal and abnormal semen parameters," *Journal of Andrology*, vol. 32, no. 3, pp. 232–239, 2011.

[45] P. Martínez, F. Proverbio, and M. I. Camejo, "Sperm lipid peroxidation and pro-inflammatory cytokines," *Asian Journal of Andrology*, vol. 9, no. 1, pp. 102–107, 2007.

Hindawi
Oxidative Medicine and Cellular Longevity
Volume 2018, Article ID 2056250, 16 pages
https://doi.org/10.1155/2018/2056250

Research Article

Anti-Inflammatory and Antioxidant Actions of Methyl Jasmonate Are Associated with Metabolic Modifications in the Liver of Arthritic Rats

Anacharis B. Sá-Nakanishi,[1] Jamil Soni-Neto,[1] Lucas S. Moreira,[1] Geferson A. Gonçalves,[1] Francielli M. S. Silva,[2] Lívia Bracht,[1] Ciomar A. Bersani-Amado,[2] Rosane M. Peralta,[1] Adelar Bracht,[1] and Jurandir F. Comar[1]

[1]*Department of Biochemistry, State University of Maringa, 87020900 Maringá-PR, Brazil*
[2]*Department of Pharmacology and Therapeutics, State University of Maringa, 87020900 Maringá-PR, Brazil*

Correspondence should be addressed to Jurandir F. Comar; jurandircomar@yahoo.com.br

Received 28 February 2018; Accepted 21 June 2018; Published 23 August 2018

Academic Editor: Jolanta Czuczejko

Methyl jasmonate (MeJA) is a fatty acid-derived cyclopentanone which shares structural similarities with prostaglandins and has been under study as a promising anti-inflammatory agent. This study investigated the actions of MeJA on systemic inflammation and oxidative status in rats with adjuvant-induced arthritis, a model for rheumatoid arthritis. MeJA (75 to 300 $mg \cdot kg^{-1}$) was administrated orally during 18 days after arthritis induction with Freund's adjuvant. Articular and systemic inflammation was greatly increased in arthritic rats, likewise the oxidative stress in plasma and liver. The hepatic glucokinase activity and glycolysis were increased in arthritic rats. MeJA decreased most inflammatory parameters and abolished the increased protein carbonylation in plasma and liver, diminished the increased hepatic ROS content, and restored the hepatic GSH/GSSG ratio in arthritic rats. However, the MeJA treatment decreased the hepatic glucokinase activity and glycolysis and stimulated mitochondrial ROS production in healthy and arthritic rats. Oxygen uptake was increased by MeJA only in livers from treated arthritic rats. This action may bear relation to the increased activity of mitochondrial $NADP^+$-dependent enzymes to provide reducing equivalents for the glutathione cycle. These beneficial effects, however, are associated with a decreased glucose flux through the glycolysis in the liver of arthritic and healthy rats.

1. Introduction

Jasmonates are fatty acid-derived cyclopentanones widely distributed over the plant kingdom where they act as signaling molecules in response to abiotic and biotic stresses [1]. The jasmonate family consists mainly of jasmonic acid, *cis*-jasmonate, and methyl jasmonate (MeJA), which share structural similarities with prostaglandins, especially with those that have anti-inflammatory activities (Figure 1) [2]. For this reason, many studies have been carried out to evaluate their actions on mammal cells. Jasmonates have been reported to have cytotoxic activity against cancer cells without affecting normal cells [1, 2]. The anticancer activity of MeJA, however, showed to be superior to other jasmonates, and therefore, MeJA and its synthetic derivatives have been lately more intensely investigated as promising agents for cancer treatment [2]. MeJA induces apoptosis and inhibits proliferation in murine and human cancer cell lines, including those of breast, colon, prostate, and lymphoma [2]. In addition, MeJA increases the survival period of mice bearing the EL-4 lymphoma and of mice inoculated with multiple myeloma (MM.1S) cells [3, 4].

Mitochondria of cancer cells seem to be the main target of MeJA action, where it stimulates reactive oxygen species (ROS) production, binds to and detaches mitochondria-bound hexokinase, induces cytochrome *c* release, causes

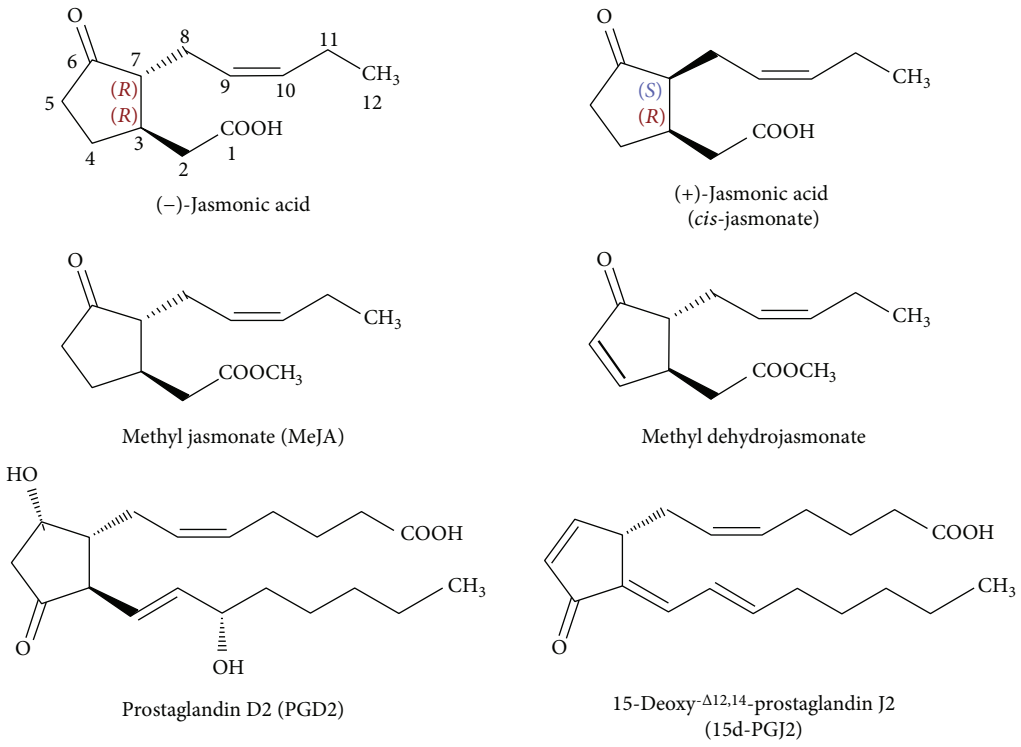

Figure 1: Chemical structures of jasmonates and anti-inflammatory prostaglandins. Jasmonic acid and *cis*-jasmonate differ by stereochemistry of R group at asymmetric center C-7. Methyl dehydrojasmonate is a synthetic analog of methyl jasmonate (MeJA) with an enone functional moiety. 15-Deoxy-$^{\Delta 12,14}$-prostaglandin J2 (15-deoxy-PGJ2) is formed by two consecutive dehydration reactions of prostaglandin D2 (PGD2). The images were modified from the original ones (Wikimedia Commons, the free media repository; Files: Enantiomers Jasmonic acid.svg and Prostaglandin D2.svg) using the program CorelDRAW® Graphics Suite X7 (Corel Corporation).

ATP depletion and finally cell death [1, 5, 6]. The association between cancer and chronic inflammation has been widely accepted and the anticancer activity of MeJA seems to be in addition related to anti-inflammatory actions [7]. Previous studies showed that MeJA inhibits the NFκB-mediated production of nitric oxide (NO), prostaglandin E, TNF-α, IL-1, and IL-6 in lipopolysaccharide (LPS)-activated murine macrophages (RAW264.7) [8–10].

Rheumatoid arthritis is an autoimmune and chronic inflammatory disease that affects primarily the joints and occurs in 0.5–1.0% of the adult population worldwide [11]. The pathophysiology of arthritis involves intense hyperplasia of the synovial membrane and cartilage with participation of proinflammatory cytokines and overproduction of reactive species, which act as mediators of tissue injury [12]. Rheumatoid arthritis is a systemic disease and in addition to the joints other organs are affected, such as brain, heart, and lungs [12]. In addition to inflammation, oxidative stress is increased in the joints and systemically [13].

Metabolic alterations are also prominent in rheumatoid arthritis, as the muscle wasting condition known as rheumatoid cachexia [14]. Metabolic modifications are equally significant in the liver of rats with adjuvant-induced arthritis, such as increased glycolysis, reduced gluconeogenesis and altered metabolism of xenobiotics [14–16]. Oxidative stress is also altered in the plasma, liver, heart, and brain of arthritic rats [17–20]. Particularly in the liver, where inflammation and metabolic alterations are prominent, oxidative stress is quite pronounced when compared to other organs [19, 20].

Considering the above-mentioned actions of MeJA, it seems reasonable to hypothesize that it could attenuate the articular and systemic inflammation that occurs in arthritis. Anti-inflammatory actions of MeJA were mainly demonstrated in isolated cells, but *in vivo* approaches have seldom been reported. A recent study showed that increased brain levels of prostaglandin E, TNF-α, and IL-1 in LPS-induced neuroinflammation in mice were reduced by intraperitoneally administered MeJA, which also suppressed COX-2, iNOS and NF-κB expression [21]. However, these actions refer specifically to neuroinflammation and so far no other systemic manifestation has been evaluated. Therefore, the present study aimed to investigate the action of orally administrated MeJA on the systemic inflammation and oxidative stress in rats with adjuvant-induced arthritis. The latter is an experimental immunopathology in rats which shares many features of rheumatoid arthritis and is often used as a model for evaluation of anti-inflammatory drugs [22]. Because MeJA has been reported to stimulate mitochondrial ROS production [1], this study has also evaluated the production of ROS and the respiratory activity in isolated hepatic mitochondria of healthy and arthritic rats. Furthermore, hexokinase catalyzes the first rate-limiting step of glycolysis and both glucose phosphorylation and the glycolytic flux are increased in the liver of arthritic rats [15]. These facts

make it of interest to search for possible effects of MeJA on hepatic hexokinase (glucokinase) and glycolysis.

The experimental model used in the present study is considered a severe arthritis model in rats [17]. Considering that rheumatoid arthritis can range from a mild form to other more severe and disseminated forms, the present study aims to provide data about the systemic effects of MeJA in rats with polyarthritis, which in turn should also allow extrapolations to patients with rheumatoid arthritis, particularly to those that manifest the more aggressive forms.

2. Materials and Methods

2.1. Chemicals. Methyl jasmonate, o-phthalaldehyde (OPT), 2,2′-azino-bis(3-ethylbenzothiazoline-6-sulfonic acid) diammonium salt (ABTS), 6-hydroxy-2,5,7,8-tetramethylchromane-2-carboxylic acid (Trolox), 5,5-dithiobis-2-nitrobenzoic acid (DTNB), 2,4-dinitrophenylhydrazine (DNPH), oxidized dichlorofluorescein (DCF), reduced glutathione (GSH), and oxidized glutathione (GSSG) were purchased from Sigma Chemical Co. (St. Louis, MO, USA). Commercial kits for AST, ALT, alkaline phosphatase, creatinine, albumin, and total proteins were purchased from Gold Analisa Diagnóstica Ltda (Belo Horizonte, MG, Brazil). All other chemicals were of analytical grade.

2.2. Animals and Induction of Arthritis. Male *Holtzman* rats weighting 170–180 g were obtained from the Center of Animal Breeding of the State University of Maringá (UEM) and maintained in an Animal Care Unit of our laboratory under standard conditions of temperature ($24 \pm 3^{\circ}C$) in a regulated 12 h light/dark cycle. The animals were kept in steel cages (3 rats/cage) and were fed ad libitum with laboratory diet (Nuvilab®, Colombo, Brazil). Arthritis was induced by means of a subcutaneous injection of Freund's adjuvant in the left hind paw (0.1 mL containing 500 μg of heat-inactivated *Mycobacterium tuberculosis* from H37Rv strain, suspended in Nujol®) [17]. Rats of similar weights and age served as controls. All procedures followed the guidelines of the Brazilian Council for the Control of Animal Experimentation (CONCEA) and were previously approved by the Ethics Committee for Animal Experimentation of the State University of Maringá (protocol number CEUA 6053280915).

2.3. Experimental Design. Forty-nine rats were randomly distributed into seven groups: controls (C), to which corn oil was administered; controls (C300) treated with MeJA at the dose of 300 $mg \cdot kg^{-1}$; arthritic rats (A), to which corn oil was administered; arthritic rats (A75, A150, and A300) treated with MeJA, respectively, at the doses of 75, 150, and 300 $mg \cdot kg^{-1}$; and arthritic rats (IBU) treated with ibuprofen at the dose of 30 $mg \cdot kg^{-1}$. This procedure was repeated three times (147 animals in total) to evaluate all parameters of this study. Animals were orally treated once a day with MeJA, corn oil, or ibuprofen for 5 days prior and by 18 days after the arthritis induction. Daily doses of MeJA were stipulated considering the effective dose that caused no toxicity as described elsewhere [23].

2.4. Evaluation of the Inflammatory Response. The volume of paws was measured daily by plethysmography (UGO BASILE SLR 21025). The severity of secondary lesions was assessed from the 10th to the 18th day as previously described [24]. Blood was collected by means of tail incision to obtain the total and differential count of circulating leukocytes. Total and differential counts of leukocytes recruited into the femorotibial joint cavity were additionally performed at the 19th day as previously described [25].

2.5. Blood Collection and Tissue Preparation. Fasted (12 h) rats were anesthetized with an overdose of sodium thiopental (100 $mg \cdot kg^{-1}$) plus lidocaine (10 $mg \cdot kg^{-1}$), and the peritoneal cavity was exposed. Blood was collected from the cava vein and placed into tubes with sodium heparin (100 IU mL^{-1}). Next, the liver was removed and divided into two parts: one was stored in liquid nitrogen for oxidative status measurements and the other was used for mitochondria isolation. Thereafter, the hind femorotibial joints were surgically exposed, articular cavities were washed with 40 μL of phosphate-buffered saline (PBS) solution containing 1 mM EDTA, and exudates were used for leukocyte count.

Blood was centrifuged (3000*g*/10 min) to separate the plasma fraction. The liver homogenate was prepared by the homogenization of a freeze-clamped tissue in a type Potter homogenizer with 10 volumes of 0.1 M potassium phosphate buffer (pH 7.4). A part of the homogenate was separated as total homogenate and the other was centrifuged (11,000*g*/15 min) for obtaining the soluble fraction of the homogenate. Fresh liver was used for mitochondria isolation by differential centrifugation as described elsewhere [26].

2.6. Plasma Analytical Assays. The myeloperoxidase (MPO) activity was measured spectrophotometrically with o-dianisidine (spectrophotometer Hitachi U-3000) [27]. The ferric reducing ability of plasma (FRAP) was measured by spectrophotometry (595 nm) using tripyridyltriazine (TPTZ) and ferric chloride ($FeCl_3$) [28].

Protein thiol groups were measured spectrophotometrically using DTNB (5,5′-dithiobis 2-nitrobenzoic acid) as described elsewhere [17]. The molar extinction coefficient (ε) of $1.36 \times 10^4\ M^{-1} \cdot cm^{-1}$ was used to calculate the thiol contents. Protein carbonyl groups were measured by spectrophotometry using 2,4-dinitrophenylhydrazine as previously described [29]. Calculations were done using the molar extinction coefficient (ε) of $2.20 \times 10^4\ M^{-1} \cdot cm^{-1}$.

Albumin, total protein, creatinine, and activities of alkaline phosphatase (ALP), aspartate aminotransferase (AST), and alanine aminotransferase (ALT) were measured in the plasma to evaluate liver and kidney damage using commercial kits (Gold Analisa®).

2.7. Liver Oxidative Stress Parameters. Carbonylated proteins were measured spectrophotometrically in the liver homogenate supernatant with 2,4-dinitrophenylhydrazine as above described for the plasma [29].

Lipoperoxide content was measured by means of the TBARS (thiobarbituric acid reactive substance) assay [30].

The levels of TBARS were calculated from the standard curve prepared with 1,1′,3,3′-tetraethoxypropane.

The total ROS content was quantified via the 2′-7′-dichlorofluorescein diacetate (DCFH-DA) assay [31], which quantifies the oxidation of DCFH-DA to the fluorescent 2′, 7′-dichlorofluorescein (DCF) in the presence of ROS. The formation of DCF was measured using a spectrofluorometer RF-5301 (Shimadzu; 504 nm for excitation and 529 nm for emission). The rate of mitochondrial ROS production (real-time ROS production) was estimated by measuring the linear fluorescence increase due to DCF formation as previously described [32]. The results were expressed as both $nmol \cdot min^{-1} \cdot (mg\ protein)^{-1}$ and the effective concentration of MeJA that stimulates ROS production half-maximally (EC_{50}). EC_{50} was calculated by numerical interpolation using Stineman's interpolation formula [33].

Reduced (GSH) and oxidized glutathione (GSSG) were measured spectrofluorimetrically (excitation at 350 nm and emission at 420 nm) by means of the *o*-phthalaldehyde (OPT) assay [34]. The activities of catalase, superoxide dismutase (SOD), and myeloperoxidase (MPO) were assayed by spectrophotometry in the supernatant of the liver homogenate. The catalase activity was estimated in 240 nm using H_2O_2 as substrate [35]. The activity of SOD was estimated according to the pyrogallol autoxidation method [36]. MPO activity was measured as above described for the plasma [27].

2.8. Hepatic Glucose Phosphorylation Capacity (Glucokinase Activity). The glucokinase activity was measured in the liquid fraction obtained by the additional high-speed centrifugation of the liver homogenate supernatant (1 h at 105,000*g*) [37]. The assay system, in a final volume of 1 mL, contained 100 mM Tris-HCl (pH 7.2), 20 mM glucose, 5 mM ATP, 10 mM $MgCl_2$, 1 mM NAD^+, 5 units of glucose 6-phosphate dehydrogenase from *Leuconostoc mesenteroides*, and 20 μl of high-speed centrifugation supernatant. The increase in absorbance at 340 nm, resulting from the production of NADH, was measured during 3 min. Rates were evaluated from the slopes of the recording traces and expressed as $nmol \cdot min^{-1} \cdot (mg\ protein)^{-1}$.

2.9. Mitochondrial Respiratory Activity. Two protocols were used to evaluate the mitochondrial respiratory activity: (1) mitochondria isolated from animals treated with MEJA and (2) mitochondria isolated from nontreated animals incubated with exogenously added MeJA.

Mitochondrial respiration was measured by polarography using a platinum electrode [26, 38]. Mitochondria were incubated in the closed oxygraph (acrylic chamber) with a medium (2.0 mL) containing 0.25 M mannitol, 10 mM KCl, 5 mM sodium diphosphate, and 10 mM Tris-HCl (pH 7.4). Succinate and α-ketoglutarate, both at a concentration of 10 mM, were used as substrates. When appropriate, MeJA was added at various concentrations in the range up to 10 mM. The slopes of recorder tracings were used to calculate the rates of oxygen uptake. The respiration rates were measured under three conditions: (a) before the addition of ADP (substrate respiration or basal), (b) just after 0.125 mM ADP addition (state III respiration), and (c) after cessation of the ADP stimulation (state IV). The respiratory control (RC) was calculated as the state III/state IV ratio, and the ADP/O ratio was determined according to Chance and Williams [39].

The activities of NADH oxidase and succinate oxidase were measured polarographically using freeze-thawing disrupted mitochondria [26]. The incubation medium contained 20 mM Tris-HCl (pH 7.4), and, when appropriate, MeJA was added at various concentrations in the range up to 10 mM. The reaction was started by the addition of substrates, 1 mM NADH and 1 mM succinate, for NADH oxidase and succinate oxidase, respectively. The couple TMPD-ascorbate was in addition used as electron donating substrate to cytochrome c/complex IV of the mitochondrial respiratory chain.

2.10. Liver Perfusion and Glycolysis. Glycolysis was measured in the perfused livers of 12 h fasted rats. Hemoglobin-free nonrecirculating liver perfusion was performed as previously described [38, 40]. Krebs/Henseleit-bicarbonate buffer (pH 7.4) was used as perfusion liquid, saturated with oxygen by means of a membrane oxygenator. The flow was maintained constant (30 and 33 $mL \cdot min^{-1}$) by a peristaltic pump (Minipuls 3, Gilson, France). Glucose (20 mM) was infused during 30 minutes. Samples of the effluent perfusion fluid were collected at 2-minute intervals and analyzed for their lactate and pyruvate content [35]. Glycolysis was estimated as the sum of lactate + pyruvate production. Oxygen concentration in the venous perfusate was constantly monitored by a platinum electrode.

2.11. Statistical Analysis. The parameters presented in graphs and tables are means ± standard errors of the means. Statistical analysis was done by means of the GraphPad Prism Software (version 5.0). Statistical significance of the data was inferred from ANOVA one-way with Newman-Keuls post hoc testing. The 5% level of significance was adopted ($p < 0.05$). Student's t test was used when comparing two means ($p < 0.05$).

3. Results

3.1. Effects of MeJA on Induction and Development of Adjuvant Arthritis. Table 1 shows the inflammatory parameters due to arthritis development and the effects of methyl jasmonate treatment. The initial volume of the hind paws before adjuvant injection was 1.60 ± 0.10 mL. Inflammatory reactions in the injected paw were observed on the first day, and they were equal in all groups (not shown). At day 18, the volume of the injected paw of arthritic rats had increased by 220% relative to its initial volume. This increase was considerably less pronounced in arthritic rats treated with 300 $mg \cdot kg^{-1}$ MeJA (only 71%) or ibuprofen (88%). Treatments with 75 and 150 $mg \cdot kg^{-1}$ MeJA, however, had no effect. Arthritis increased the volume of the contralateral paw by 125%. Treatment of arthritic rats with 300 $mg \cdot kg^{-1}$ MeJA or ibuprofen diminished these increases to 30% and 18%, respectively. Here also the doses of 75 and 150 $mg \cdot kg^{-1}$

Table 1: Inflammatory parameters and number of blood and articular leukocytes. The number of leukocytes in the peripheral blood was measured before adjuvant induction (initial, at day 0) for the arthritic group (A) and at day 18 for all groups. The number of articular leukocytes was measured in the femorotibial hind joints at day 18. The initial paw volume was 1.6 ± 0.1 ml; Δvol of paws (paw edema) = volume at day 18 − initial volume. The score of secondary lesions (arthritic score) is defined in Section 2.4. A: nontreated arthritic rats; A corn oil: arthritic rats treated with corn oil; A75, A150, and A300: arthritic rats treated with 75, 150, and 300 $mg \cdot kg^{-1}$ MeJA; IBU: arthritic rats treated with 30 $mg \cdot kg^{-1}$ ibuprofen.

Parameters	Initial	A	A corn oil	A75	A150	A300	IBU
Δvol – injected paw (mL)	—	4.0 ± 0.3^a	3.5 ± 0.2^a	4.4 ± 0.3^a	4.0 ± 0.2^a	1.3 ± 0.2^b	1.6 ± 0.2^b
Δvol – noninjected (mL)	—	2.1 ± 0.3^a	2.0 ± 0.2^a	2.9 ± 0.2^a	2.6 ± 0.1^a	0.5 ± 0.1^b	0.3 ± 0.1^b
Arthritic score	—	5.0 ± 0.0^a	5.0 ± 0.0^a	5.0 ± 0.0^a	4.4 ± 0.2^a	4.4 ± 0.4^a	3.5 ± 0.3^a
	(at day 0)	Blood leukocytes (at day 18)					
Total leukocytes ($\times 10^3$) $(mm^3)^{-1}$	13.1 ± 0.5^a	66.7 ± 9.9^b	47.2 ± 1.3^b	52.8 ± 6.4^b	52.8 ± 6.4^b	32.6 ± 2.4^c	34.6 ± 2.2^c
PMN cells (%)	15 ± 2^a	70 ± 3^b	64 ± 4^b	66 ± 3^b	66 ± 3^b	48 ± 6^c	62 ± 5^b
	Articular leukocytes (hind left joint)						
Total leukocytes ($\times 10^4$) $(mm^3)^{-1}$	—	16.8 ± 3.2^a	13.7 ± 1.7^a	16.1 ± 1.8^a	2.0 ± 0.7^b	0.9 ± 0.3^c	3.9 ± 1.1^b
PMN cells (%)	—	53 ± 3^a	69 ± 6^a	62 ± 2^a	58 ± 23^b	61 ± 3^b	65 ± 3^b
	Articular leukocytes (hind right joint)						
Total leukocytes ($\times 10^4$) $(mm^3)^{-1}$	—	6.9 ± 0.7^a	6.1 ± 1.5^a	6.5 ± 0.7^a	7.0 ± 1.5^a	2.3 ± 0.2^b	1.1 ± 0.4^b
PMN cells (%)	—	53 ± 1^a	61 ± 8^a	69 ± 2^a	60 ± 1^a	74 ± 3^a	69 ± 4^a

Data are mean ± SEM of 5 animals. Values with different superscript letters in the same line are different.

Table 2: Plasma parameters of inflammation and liver/renal damage. C, controls treated with corn oil; C300, controls treated with MeJA at the dose of 300 $mg \cdot kg^{-1}$; A: arthritic rats treated with corn oil; A300: arthritic rats treated with MeJA at the dose of 300 $mg \cdot kg^{-1}$; IBU: arthritic rats treated with ibuprofen at the dose of 30 $mg \cdot kg^{-1}$.

Parameter	Groups				
	C	C300	A	A300	IBU
AST ($U \cdot L^{-1}$)	37.6 ± 1.6^a	36.6 ± 3.9^a	77.4 ± 2.8^b	52.4 ± 1.6^a	60.6 ± 3.6^c
ALT ($U \cdot L^{-1}$)	18.9 ± 0.8^a	18.6 ± 0.6^a	16.5 ± 1.1^a	19.0 ± 0.6^a	26.1 ± 0.6^a
ALP ($U \cdot L^{-1}$)	60.7 ± 7.7^a	59.0 ± 5.4^a	139 ± 11^b	81.1 ± 8.1^a	151 ± 5.9^b
Total protein ($g \cdot dL^{-1}$)	5.9 ± 0.3^a	5.8 ± 0.3^a	5.9 ± 0.1^a	5.6 ± 0.1^a	5.8 ± 0.2^a
Albumin ($g \cdot dL^{-1}$)	2.3 ± 0.2^a	2.3 ± 0.1^a	1.3 ± 0.1^b	1.6 ± 0.1^b	2.1 ± 0.1^a
Globulin ($g \cdot dL^{-1}$)	3.5 ± 0.5^a	3.4 ± 0.1^a	4.6 ± 0.1^b	3.9 ± 0.2^a	3.7 ± 0.2^a
Albumin/globulin (A/G ratio)	0.7 ± 0.1^a	0.7 ± 0.1^a	0.3 ± 0.01^b	0.4 ± 0.04^b	0.6 ± 0.02^a
Creatinine ($mg \cdot dL^{-1}$)	0.4 ± 0.1^a	0.4 ± 0.1^a	0.6 ± 0.01^a	0.6 ± 0.02^a	0.8 ± 0.1^b
MPO activity ($nmol \cdot min^{-1} \cdot mg^{-1}$)	2.3 ± 0.3^a	3.1 ± 0.2^a	14.7 ± 1.4^b	8.4 ± 1.1^c	8.3 ± 0.8^c

The data are the mean ± standard error of the mean of 5 animals. Values with different superscript letters in the same line are different.

MeJA were totally ineffective. Secondary lesions appeared at day 10 and reached the highest scores at day 18. The scores at day 18 were not different in all groups.

At day 18, the number of total blood leukocytes in nontreated arthritic rats was four times higher than initially (day 0). Treatment of animals with corn oil and MeJA (75 and 150 $mg \cdot kg^{-1}$) did not modify the number of total leukocytes in blood, but treatment with ibuprofen and 300 $mg \cdot kg^{-1}$ MeJA caused a decrease by approximately 50%. The number of total leukocytes recruited into the articular cavity (joint of the injected paw) was three times higher when compared to that in the contralateral joint. Treatment of animals with ibuprofen, 150 $mg \cdot kg^{-1}$ MeJA, and 300 $mg \cdot kg^{-1}$ MeJA caused 77%, 89%, and 95% decreases, respectively. Only ibuprofen and 300 $mg \cdot kg^{-1}$ MeJA decreased the number of leukocytes recruited into the femorotibial right joint.

3.2. Biochemical Parameters in Plasma. Table 2 shows the levels of albumin, globulin, and creatinine, and the activities of MPO, AST, ALT, and ALP in the plasma. The MeJA doses of 75 and 150 $mg \cdot kg^{-1}$ did not affect inflammation and the corresponding data are not shown in Table 2 for simplicity. Arthritis induction increased the plasma activity of AST (+100%) and ALP (+130%). Treatment of arthritic rats with MeJA, but not with ibuprofen, maintained the AST and ALP activities at values close to the control ones. Plasma levels of creatinine were not different in rats treated or not with MeJA; however, they were 40% higher in animals treated with ibuprofen. Arthritis induction increased the activity of plasma MPO (+400%) and globulins (+30%) while it decreased the levels of albumin (−44%) and the albumin/globulin ratio (−60%). Treatment of arthritic rats with MeJA had no effects on plasma albumin, globulin, and the albumin/

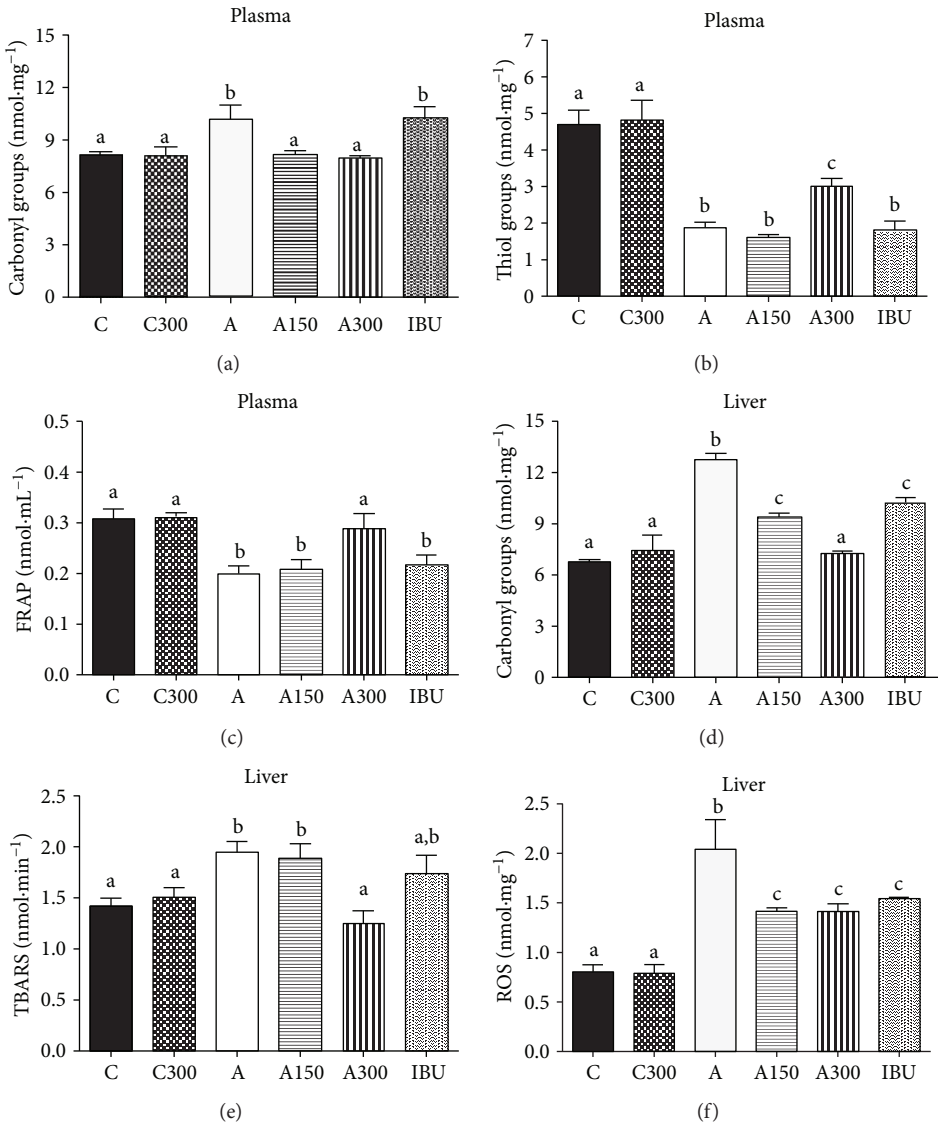

Figure 2: Effects of MeJA on the oxidative state of plasma and liver in arthritic rats. (a) Plasma protein carbonyl groups; (b) plasma thiol groups; (c) ferric reducing ability of plasma (FRAP); (d) hepatic protein carbonyl groups; (e) hepatic TBARS levels; (f) hepatic oxygen reactive species (ROS). C: controls treated with corn oil; C300: control treated with 300 mg·kg^{-1} MeJA; A: arthritic rats treated with corn oil; A150 and A300: arthritic rats treated with 150 and 300 mg·kg^{-1} MeJA; IBU: arthritic rats treated with ibuprofen (30 mg·kg^{-1}). Data represent the mean ± SEM of 5 animals. Values with different superscript letters are statistically different ($p < 0.05$).

globulin ratio. The MPO activity, however, was approximately 40% lower when arthritic rats were treated with 300 mg·kg^{-1} MeJA or ibuprofen.

3.3. Oxidative Status of the Plasma. The levels of protein carbonyl groups, a prooxidant parameter, were 25% higher in the plasma of nontreated arthritic rats (compared to the controls; Figure 2(a)). Treatment of arthritic rats with 150 and 300 mg·kg^{-1} MeJA maintained the protein carbonyl contents at levels close to the control ones. The concentration of thiol groups in arthritic rats, an antioxidant parameter, was only 40% of that in the controls (Figure 2(b)). In arthritic animals treated with 300 mg·kg^{-1} MeJA, this decrease was attenuated, the thiol levels being 60% above those found in nontreated arthritic rats. FRAP, an antioxidant parameter, was 33% lower in nontreated arthritic rats (compared to the controls; Figure 2(c)). In arthritic animals treated with 300 mg·kg^{-1} MeJA, this decrease was diminished, the FRAP levels being 44% above those found in nontreated arthritic rats.

3.4. Liver Oxidative Stress. The levels of protein carbonyl groups in the liver homogenate were 80% higher in arthritic rats (Figure 2(d)). The levels of carbonyl groups were 20, 26, and 43% lower in the liver of arthritic rats treated with ibuprofen, 150 mg·kg^{-1} MeJA, and 300 mg·kg^{-1} MeJA, respectively. The levels of TBARS were 36% higher in the liver of arthritic rats (Figure 2(e)). Treatment of arthritic animals with 300 mg·kg^{-1} MeJA maintained TBARS at levels close to the control ones. The concentrations of oxygen reactive species (ROS) were 155% higher in arthritic rats

Table 3: Effects of MeJA on antioxidant and inflammation parameters in the liver. C: controls treated with corn oil; C300: control treated with MeJA at the dose of 300 mg·kg^{-1}; A: arthritic rats treated with corn oil; A300: arthritic rats treated with MeJA at the dose of 300 mg·kg^{-1}; IBU: arthritic rats treated with ibuprofen at the dose of 30 mg·kg^{-1}, GSH: reduced glutathione; GSSG: oxidized glutathione; SOD: superoxide dismutase; MPO: myeloperoxidase.

Parameter	Groups				
	C	C300	A	A300	IBU
GSH (nmol·mg^{-1})	11.4 ± 0.6^{a}	12.0 ± 1.5^{a}	7.2 ± 0.3^{b}	12.3 ± 0.8^{a}	8.7 ± 0.7^{b}
GSSG (nmol·mg^{-1})	1.5 ± 0.2^{a}	1.3 ± 0.1^{a}	1.7 ± 0.2^{a}	1.4 ± 0.3^{a}	1.6 ± 0.2^{a}
GSH + 2GSSG (nmol GSH units·mg^{-1})	14.3 ± 0.8^{a}	14.6 ± 1.5^{a}	10.5 ± 0.3^{b}	14.1 ± 0.5^{a}	$12.0 \pm 0.4^{a,b}$
GSH/GSSG ratio	8.7 ± 0.2^{a}	10.8 ± 1.2^{a}	4.8 ± 0.4^{b}	8.2 ± 1.1^{a}	$6.5 \pm 1.0^{a,b}$
Catalase activity (mmol·min^{-1}·mg^{-1})	1.1 ± 0.09^{a}	1.0 ± 0.02^{a}	0.2 ± 0.02^{b}	0.4 ± 0.04^{c}	0.3 ± 0.03^{b}
SOD activity (U·mg^{-1})	1.9 ± 0.1^{a}	2.1 ± 0.2^{a}	1.7 ± 0.2^{a}	2.2 ± 0.2^{a}	2.4 ± 0.3^{a}
MPO activity (nmol·min^{-1}·mg^{-1})	16.7 ± 0.1^{a}	16.0 ± 0.1^{a}	23.1 ± 0.8^{b}	16.9 ± 0.1^{a}	18.4 ± 1.6^{a}

The data are the mean ± standard error of the mean of 5 animals. Values with different superscript letters in the same line are different.

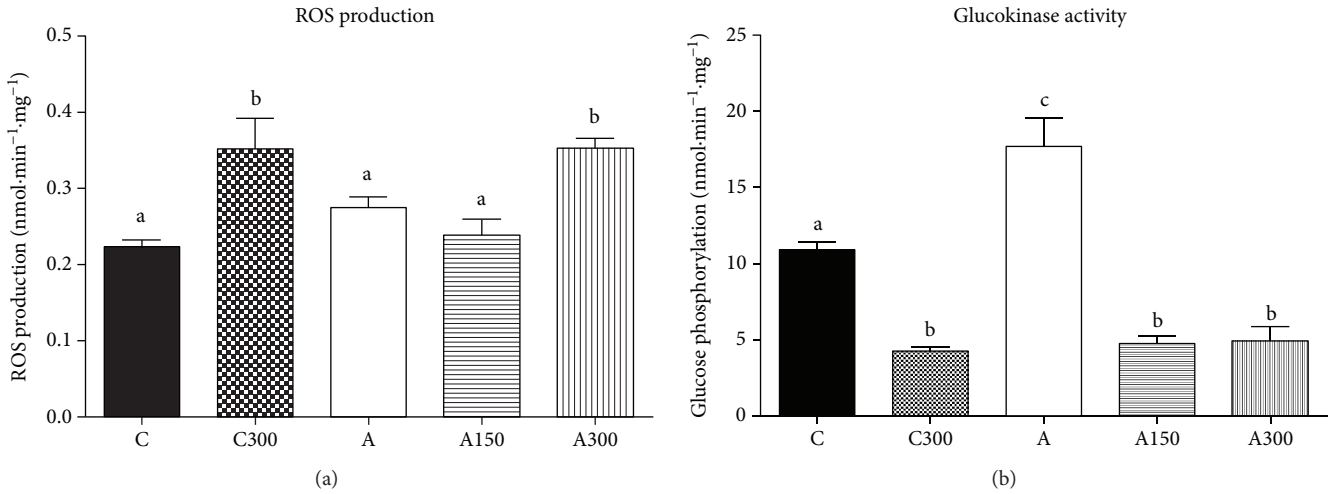

Figure 3: Effects of MeJA on mitochondrial ROS generation and glucokinase activity in the liver of treated rats. (a) ROS generation in isolated hepatic mitochondria and (b) glucokinase activity in liver homogenate. Isolated mitochondria and homogenate were obtained of livers from rats nontreated and treated with MeJA as described in Section 2.3. C: controls treated with corn oil; C300: control treated with 300 mg·kg^{-1} MeJA; A: arthritic rats treated with corn oil; A150 and A300: arthritic rats treated with 150 and 300 mg·kg^{-1} MeJA. Data represent the me an ± SEM of 5 animals. Values with different superscript letters in the same condition are statistically different ($p < 0.05$).

(Figure 2(f)). Treatment of arthritic rats with ibuprofen, 150 mg·kg^{-1} MeJA, and 300 mg·kg^{-1} MeJA maintained the ROS contents at levels that were approximately 30% lower than that found in nontreated arthritic rats.

3.5. Hepatic Antioxidant and Inflammatory Status. The hepatic levels of glutathione and the activities of catalase, SOD, and MPO are shown in Table 3. No effects were found with 150 mg·kg^{-1} MeJA, and therefore, data obtained with this dose were omitted. The levels of GSH in the liver of arthritic rats were 38% lower than those in the controls. Treatment of arthritic rats with 300 mg·kg^{-1} MeJA partly prevented this decrease. The GSSG levels were similar for all groups. The GSH/GSSG ratio was 45% lower in the arthritic condition, but treatment with 300 mg·kg^{-1} MeJA prevented the decrease. The catalase activity in the liver of arthritic rats was only 20% of that in control rats, an effect that was partially prevented by the 300 mg·kg^{-1} MeJA treatment. The MPO activity was 38% higher in arthritic rats, but treatment with 300 mg·Kg^{-1} MeJA and ibuprofen totally prevented this increase.

3.6. Mitochondrial ROS Generation and Glucokinase Activity. The rate of ROS production (real-time ROS production) was measured in freshly isolated hepatic mitochondria. Mitochondrial ROS production was 58 and 28% higher, respectively, in control and arthritic rats treated with 300 mg·kg^{-1} MeJA (Figure 3(a)). However, there was no difference between control and arthritic rats treated with corn oil. Figure 3(b) shows the effects of MeJA treatment on glucokinase activity, which was 60% higher in nontreated arthritic rats (compared to the controls). Glucokinase activity was 60% lower in control rats treated with 300 mg·kg^{-1} MeJA and approximately 70% lower in arthritic rats treated with all doses of MeJA.

3.7. Respiratory Activity in Isolated Liver Mitochondria from MeJA-Treated Rats. Considering that ROS production and

respiratory activity are associated phenomena in mitochondria, it was evaluated if MeJA affects the respiration of isolated hepatic mitochondria. Figure 4(a) outlines the experimental approach used to evaluate the respiratory activity of phosphorylating liver mitochondria. Basal respiration was 37% (with succinate) and 58% (with α-ketoglutarate) lower in mitochondria of nontreated arthritic rats (Figure 4(b)). Treatment with MeJA decreased basal respiration (−30%) in controls when succinate was the substrate but stimulated it (+110%) when α-ketoglutarate was the substrate. State III respiration was not modified in mitochondria from control rats treated with MeJA, but it was stimulated (+90%) in mitochondria from arthritic rats when α-ketoglutarate was the substrate (Figure 4(c)). State IV respiration, RC, and ADP/O ratio were not modified by MeJA treatment.

3.8. Glycolysis in the Perfused Liver of MeJA-Treated Rats. The diminution of the liver glucokinase activity by MeJA should lead to a decreased flux of glucose through the glycolytic pathway. To test this hypothesis, experiments with perfused livers were done to evaluate glycolysis and oxygen uptake. Figure 5 illustrates the time courses of oxygen consumption and lactate and pyruvate production from 20 mM glucose in livers of rats treated with saline or 300 $mg \cdot kg^{-1}$ MeJA. The basal rates (before glucose infusion) of lactate and pyruvate production were minimal and similar in all groups, but the basal rate of oxygen consumption was more elevated in arthritic rats treated with MeJA (Figure 5). Upon the introduction of 20 mM glucose, the productions of lactate and pyruvate increased to variable extents, whereas oxygen uptake suffered relatively small and similar increments. In order to compare the groups, numerical values for each parameter at a 38-minute perfusion time in Figure 5 (steady-state) are displayed in Table 4. Treatment of control or arthritic rats with corn oil produced no differences. Lactate and pyruvate production rates were approximately 100% higher in arthritic rats. Lactate production was 50% lower in the liver of control and arthritic rats treated with MeJA. Pyruvate production was 65 and 20% lower, respectively, in control and arthritic rats treated with MeJA. The glycolytic flux (lactate + pyruvate/2) was modified in the same proportion as lactate production.

3.9. Mitochondrial ROS Generation and Glucokinase Activity In Vitro. Figure 6(a) shows the concentration dependence of exogenously added MeJA on mitochondrial ROS generation *in real time*. These experiments were done in order to detect possible reversible short-term effects of MeJA that are no longer present once the mitochondria or the glucokinase of treated rats is isolated from the liver cells of the intact organism. Figure 6(a) reveals that in the absence of MeJA, ROS production was 23% higher in arthritic rats ($p = 0.014$). MeJA stimulated ROS production in both mitochondria from control and arthritic rats. The final increment was approximately the same, 0.116 and 0.124 $nmol \cdot mL^{-1} \cdot mg^{-1}$ for the control and arthritic conditions, respectively. However, at low concentrations mitochondria from control rats were more sensitive, as can be judged from the lower concentration producing 50% stimulation (see Figure 6(a)).

Figure 6(b) shows the effects of exogenously added MeJA on the glucokinase activity in the control and arthritic conditions. The glucokinase activity in the absence of MeJA was 33% higher in the arthritic condition ($p = 0.0225$). Addition of MeJA diminished glucokinase activity in both conditions, but only at the high concentration of 10 mM.

3.10. Mitochondrial Respiratory Activity In Vitro. The MeJA treatment of rats caused some minor modifications in the respiratory activity of mitochondria that persisted after isolation. Reversible and short-term effects can be detected in experiments where MeJA is added to mitochondria obtained from animals that were not treated with the compound. The experimental approach used to evaluate the respiratory activity of mitochondria was that one shown in Figure 4(a). MeJA was added in the range up to 10 mM. Basal respiration in the absence of MeJA was approximately 50% lower in mitochondria of arthritic rats ($p < 0.05$). MeJA decreased basal respiration only in the arthritic condition and with the substrate α-ketoglutarate (Figure 7(a)). State III respiration was diminished in a concentration-dependent manner irrespective of the substrate (succinate or α-ketoglutarate) and the conditions (healthy or arthritic; Figure 7(b)). EC_{50} of MeJA for the inhibition of state III respiration was 22% lower for arthritic rats when compared to the controls. The state IV respiration was inhibited to a lesser degree when compared to state III (Figure 7(c)). The mitochondrial respiratory control (RC), on the other hand, was diminished and even abolished with increasing MeJA concentrations for both conditions and substrates (Figure 7(d)).

Considering that the mitochondrial respiratory activity, especially state III respiration, was inhibited when incubated with MeJA, the NADH and succinate oxidase activities were further measured in disrupted mitochondria. The results are shown in Figure 7(e). Both NADH oxidase and succinate oxidase activities were progressively diminished with increasing MeJA concentrations in disrupted mitochondria from both control and arthritic rats. The EC_{50} values for succinate oxidase inhibition were similar for the control and arthritic condition, but the EC_{50} value for NADH oxidase inhibition for the control condition was only one third of that for the arthritic condition (Figure 7(e)). However, it is important to highlight that the NADH oxidase activity in the absence of MeJA was already 30% lower in arthritic rats ($p = 0.0036$; compared to the controls). Figure 7(f) shows the effects of MeJA on oxygen consumption of disrupted mitochondria using the combination TMPD-ascorbate as substrate. Under this condition, oxygen consumption was not modified by MeJA in both the control and arthritic conditions.

4. Discussion

4.1. The Anti-Inflammatory Action. Rats with adjuvant-induced arthritis present generalized inflammatory manifestations, particularly on the 18th day after arthritis induction, when an intense inflammatory response to the adjuvant is observed in all paws (polyarthritis) in addition to leukocytosis and high levels of systemic proinflammatory cytokines [17, 20]. In this study, MeJA was effective as anti-

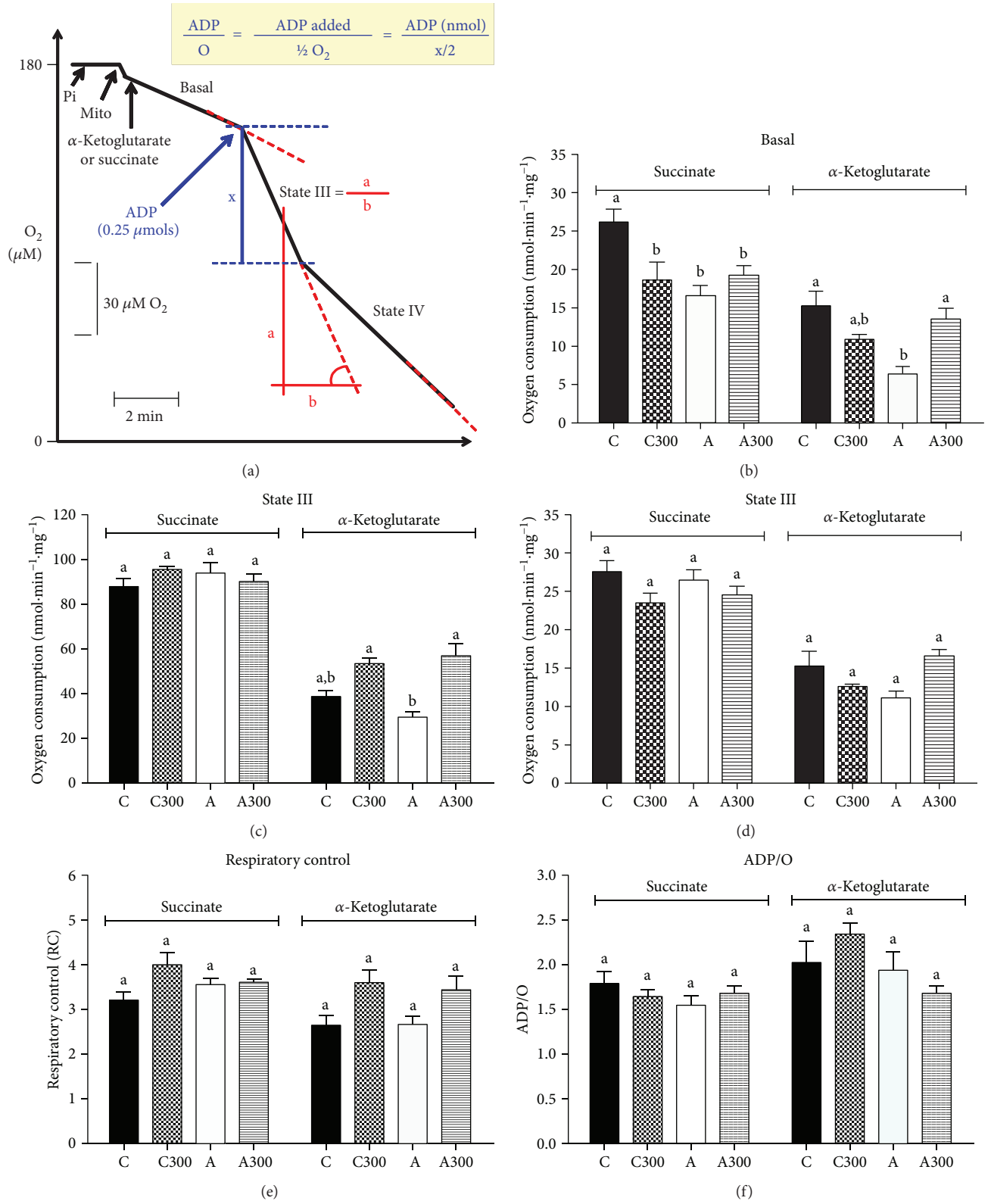

FIGURE 4: Effects of MeJA treatment on respiratory activity of intact isolated hepatic mitochondria. Hepatic mitochondria were isolated as described in Section 2.9. Succinate and alpha-ketoglutarate (10 mM) were used as respiratory substrates. Panel a shows the experimental protocol and calculation procedures. C: controls treated with corn oil; C300: control treated with 300 mg·kg^{-1} MeJA; A: arthritic rats treated with corn oil; A300: arthritic rats treated with 300 mg·kg^{-1} MeJA. Data represent the mean ± SEM of 5 animals. Values with different superscript letters are different ($p < 0.05$).

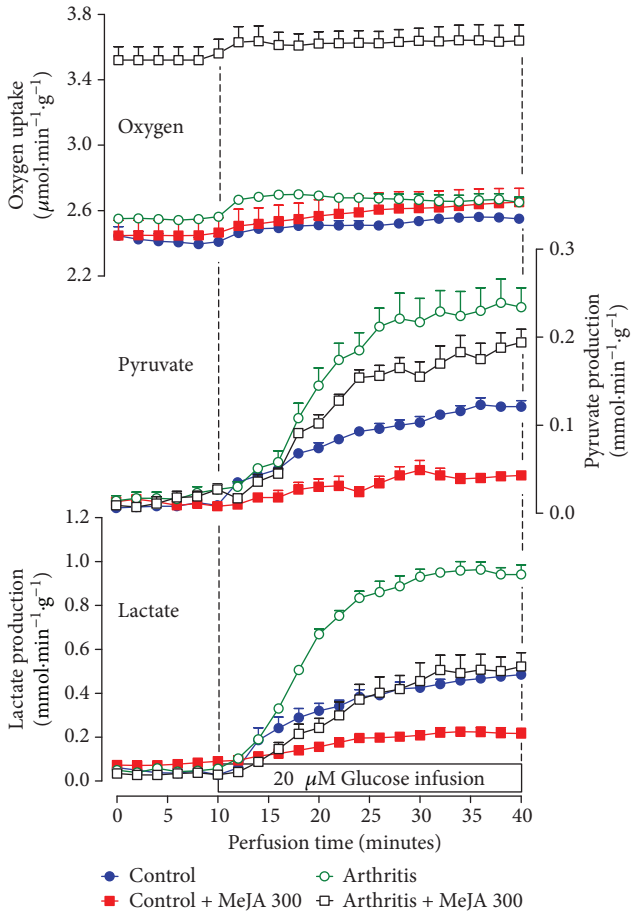

Figure 5: Effects of methyl jasmonate treatment on liver glycolysis and oxygen uptake. Control and arthritic rats were treated with MeJA at a dose of 300 mg·kg^{-1}, as described in Section 2.3. Livers from 12 h fasted rats were perfused with Krebs/Henseleit bicarbonate buffer and 20 mM glucose as indicated by the horizontal bar. The effluent perfusate was sampled in 2 min intervals and analyzed for lactate and pyruvate. Oxygen uptake was monitored by polarography. Data are mean ± SEM obtained with 4 animals.

inflammatory, notably at the dose of 300 mg·kg^{-1}. The anti-inflammatory activity of MeJA was already shown previously in LPS-activated murine macrophages (RAW264.7) [8–10] and *in vivo* in the brain of mice with LPS-induced neuroinflammation [21]. Our results reveal that MeJA is additionally effective on articular and systemic inflammation, especially in the liver of rats with adjuvant-induced arthritis. Several results of this study have been included in a Master Dissertation presented at the University of Maringá [41].

The anti-inflammatory mechanism of MeJA has not yet been completely clarified, but it is known that it suppresses NF-κB-mediated expression of proinflammatory enzymes and cytokines. MeJA inhibited the production of prostaglandin E, TNF-α, IL-1, and IL-6 as well as the expression of iNOS, COX-2, and NF-κB in the brain of mice with LPS-induced neuroinflammation and LPS-stimulated RAW267.4 cells [8, 21]. In addition, MeJA was reported to attenuate activation of NF-κB by suppressing degradation

Table 4: Effects of MeJA treatment on glycolysis and oxygen uptake in livers from control and arthritic rats. Livers from 12 h fasted rats were perfused with Krebs/Henseleit bicarbonate as described in Section 2.10. Glucose (20 mM) was infused as glycolytic substrate. The rates of lactate and pyruvate production were computed at a 38-minute perfusion time in Figure 5 (steady-state). Glycolysis was calculated as (lactate + pyruvate)/2 and expressed as μmol glucosyl units·min^{-1}·g^{-1}. ΔOxygen consumption is the increment in the oxygen consumption due to glucose infusion at a 38-minute perfusion time. C: controls treated with saline; C corn oil: controls treated with corn oil; C300: controls treated with 300 mg·kg^{-1} MeJA; A: arthritic rats treated with saline; A corn oil: arthritic rats treated with corn oil; A300: arthritic rats treated with 300 mg·kg^{-1} MeJA.

Groups	Parameter (μmol·min^{-1}·g^{-1})			
	Lactate production	Pyruvate production	Glycolysis	ΔOxygen consumption
C	0.48 ± 0.02^{a}	0.12 ± 0.01^{a}	0.30 ± 0.01^{a}	0.16 ± 0.03^{a}
C corn oil	0.36 ± 0.03^{a}	0.13 ± 0.02^{a}	0.26 ± 0.02^{a}	0.10 ± 0.05^{a}
C300	0.22 ± 0.03^{b}	0.04 ± 0.01^{b}	0.13 ± 0.01^{b}	0.13 ± 0.02^{a}
A	0.94 ± 0.03^{c}	0.24 ± 0.03^{c}	0.59 ± 0.03^{c}	0.12 ± 0.03^{a}
A corn oil	0.84 ± 0.07^{c}	$0.18 \pm 0.02^{a,c}$	0.50 ± 0.03^{c}	0.29 ± 0.07^{a}
A300	0.50 ± 0.06^{a}	$0.19 \pm 0.02^{a,c}$	0.35 ± 0.04^{a}	0.27 ± 0.09^{a}

The data are the mean ± standard error of the mean of 4 animals. Values with different superscript letters in the same line are different.

of its inhibitor I kappa B-alpha (IκB-α) [21]. Evidence from studies with methyl dehydrojasmonate, a structural analog of MeJA, suggests that MeJA may in addition downregulate miR-155, which is elevated in synovial fibroblasts from rheumatoid arthritis patients and LPS-stimulated RAW267.4 cells [9, 42].

Although the effective dose of MeJA (300 mg·kg^{-1}) may be considered elevated for clinical studies, it is similar to those previously used to evaluated the antitumoral properties (50–1000 mg·kg^{-1}) [2]. Moreover, a notable absence of MeJA toxicity was reported for doses of this range, including an intravenous dose of 236 mg·kg^{-1} in mice [2, 3, 23]. In addition, plasma markers of hepatic and renal damage were not modified by the treatment.

4.2. The Antioxidant Action. The oxidative stress is systemically altered in rats with adjuvant-induced arthritis [17–20] as confirmed in the present study for plasma and liver. In the plasma, higher levels of carbonyl groups indicate that oxidative stress is occurring in a place where antioxidant enzymes and glutathione contribute poorly and the antioxidant activity depends mainly on the thiol groups of albumin [17]. MeJA decreased oxidative stress in the plasma of arthritic rats, but it did not increase the albumin levels. On the other hand, it increased the thiol groups on albumin and, consequently, the plasma antioxidant capacity.

Oxidative stress in the liver has been reported to be more pronounced when compared to other tissues in arthritic rats [19, 20]. In this study and in previous reports higher levels of ROS, lipoperoxides and carbonyl groups in the arthritic liver were accompanied by a marked deficiency in catalase and a very low GSH/GSSG ratio [20, 38]. Altered oxidative stress

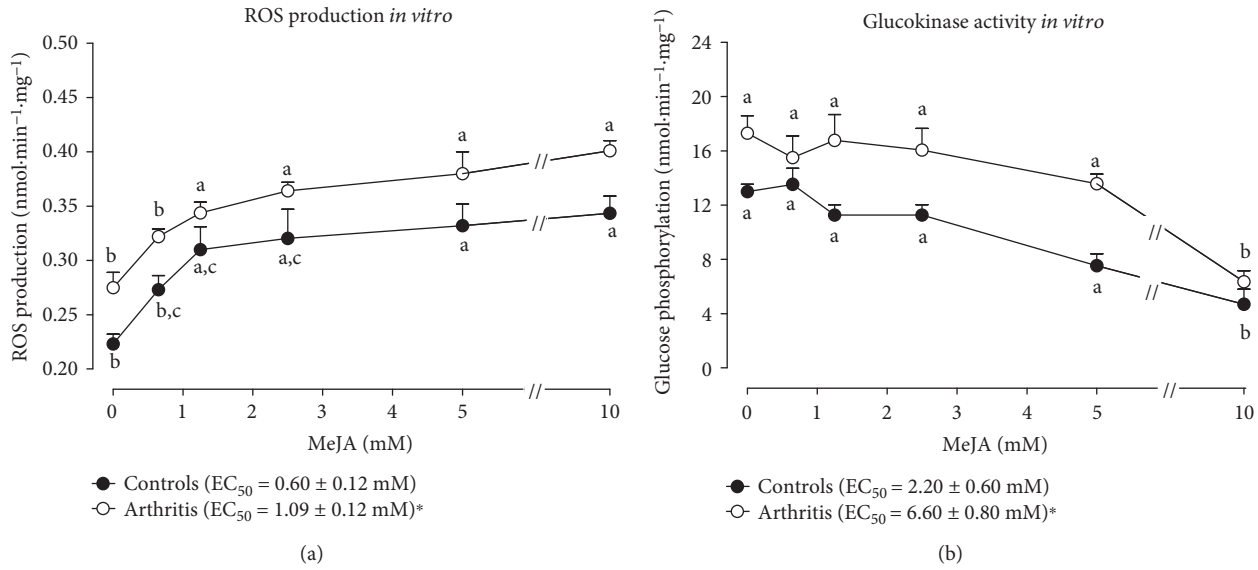

Figure 6: Effects of MeJA on mitochondrial ROS generation and hepatic glucokinase activity in vitro. (a) Concentration dependence of stimulation of mitochondrial ROS production by exogenously added MeJA; (b) concentration dependence of inhibition of glucokinase activity. ROS production was measured in isolated hepatic mitochondria and glucokinase activity in the supernatant of liver homogenate. EC_{50} was calculated by numerical interpolation. Data represent the mean ± SEM of 5 animals. Values with different superscript letters in the same condition are different ($p < 0.05$). EC_{50}: $^*p < 0.05$ for difference between control and arthritis.

has been attributed to both an impaired ROS scavenging system and an increased production of ROS. Both phenomena are probably mediated by proinflammatory cytokines. In fact, TNF-α and IL-1 were reported to stimulate mitochondrial ROS production and to diminish catalase activity in the liver [43, 44]. These cytokines, in addition, stimulate oxidative metabolism in the liver of arthritic rats, a phenomenon that generates a more oxidizing environment and more intense production of ROS [15, 16, 20]. The very low GSH/GSSG ratio reflects the more oxidized state of the arthritic liver. Figure 8 summarizes the key events determining oxidative stress in the arthritic liver (black arrows) and also suggests how MeJA could be acting to reverse them (red arrows). For the latter, there are two possible mechanisms: by decreasing the inflammatory process or by stimulating the endogenous antioxidant system. Both phenomena occurred in arthritic rats, as indicated, for example, by the lower MPO activity in the plasma and liver associated with the increased catalase activity and GSH/GSSG ratio in the liver, which can at least in part be attributed to an inhibition of proinflammatory cytokines. On the other hand, the cellular redox homeostasis is regulated mainly by nuclear factor erythroid 2-related 2 (Nfr2), a redox-sensible transcription factor which upregulates antioxidant defense genes, including catalase and enzymes required for GSH synthesis and regeneration [45]. Nfr2 in turn is regulated mainly by microRNAs (miRNAs), which mediate posttranscriptional gene modulation [46]. miR-155 is reported to downregulate Nfr2 while miR-101 upregulates it [46, 47]. Methyl dehydrojasmonate suppresses miR-155 induction in LPS-stimulated RAW264.7 cells and MeJA enhances the induction of miR-101 in human colorectal and bladder cancer cells [48, 49]. Therefore, MeJA may be improving the antioxidant status of arthritic rats by downregulating miR-155 and upregulating miR-101, which results in upregulation of the Nfr2 activity.

4.3. The Mitochondrial ROS Production and Metabolism. MeJA's cytotoxic activity against cancer cells is reported to occur as consequence of one or more of the following events: (I) increased ROS production in mitochondria of cancer cells, which are more sensitive than normal cells to higher ROS concentrations [2], and (II) modification of the mitochondrial respiration of cancer cells which provokes ATP depletion [1]; and (III) impaired glucose metabolism through glycolysis, due to hexokinase inhibition [50]. The results of this study show that hepatic cells of both healthy and arthritic rats respond to MeJA, at least partly, in the same way as cancer cells. In hepatic mitochondria of healthy and arthritic rats, the MeJA treatment stimulated ROS production over a concentration range that was similar to that in cancer cells [51]. This increased capacity of generating ROS in isolated mitochondria, however, did not result in increased oxidative stress in the healthy liver. In the liver of arthritic rats, a diminution of oxidative stress was even found upon MeJA treatment. This combination, the induction of a higher capacity of producing ROS in mitochondria and a diminished oxidative stress suggests strongly that the effects of MeJA as a stimulator of the ROS scavenging mechanisms predominate over its actions as a stimulator of ROS production in the liver of both arthritic and healthy rats. This is not what happens in cancer cells in which the net balance of the action of MeJA seems to favor ROS production [2].

Increased mitochondrial ROS production is normally associated with modifications in the mitochondrial respiration. The latter was slightly increased in mitochondria isolated after MeJA treatment of arthritic rats when α-ketoglutarate was the substrate in the absence and presence

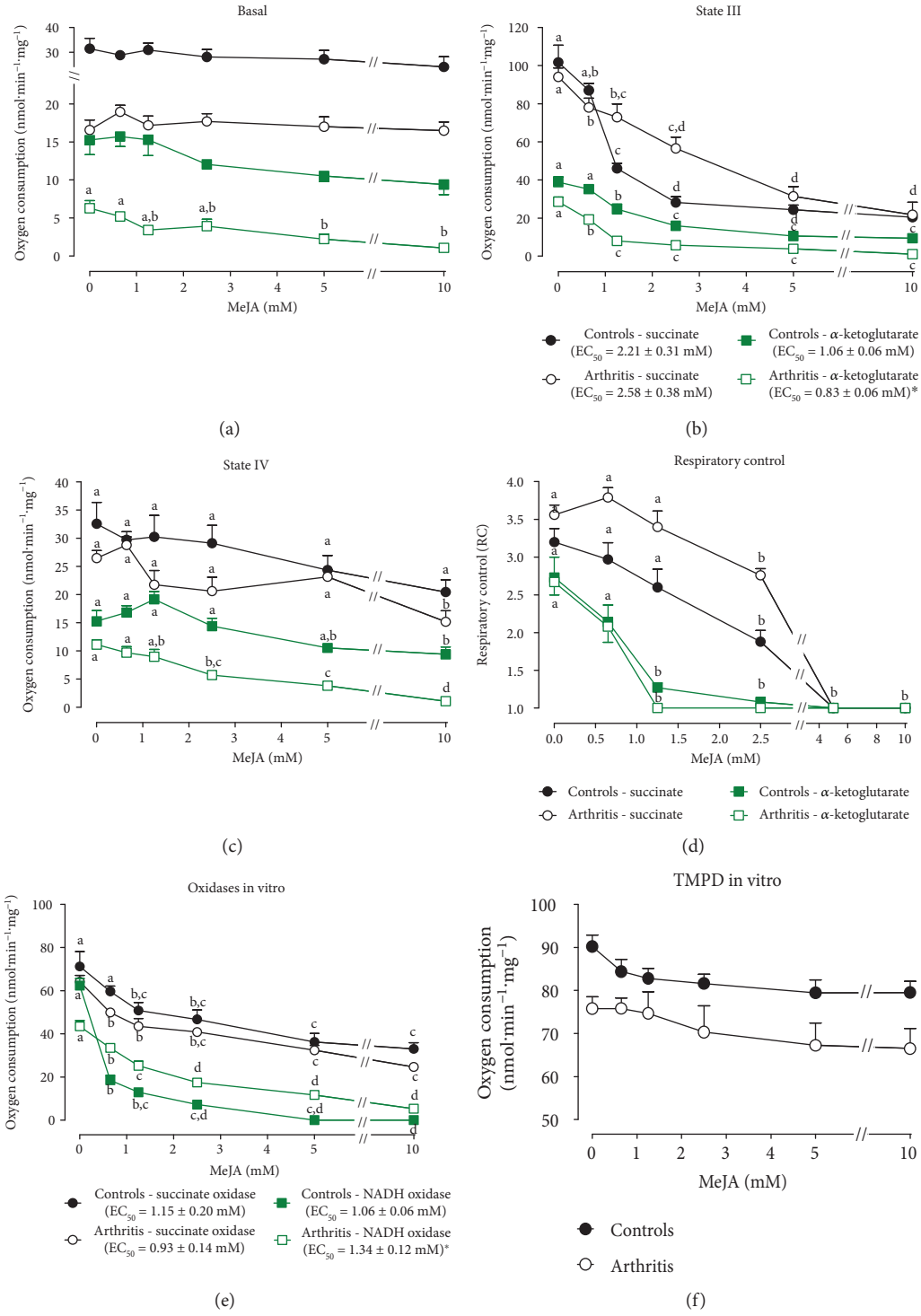

Figure 7: Effects of exogenous MeJA on respiratory activity of isolated hepatic mitochondria. Concentration dependence of the inhibition of basal respiration (a), state III (b), state IV (c), RC (d), mitochondrial membrane-bound enzyme activities (e), and mitochondrial respiration with TMPD-ascorbate (f) by exogenously added MeJA. Data represent the mean ± SEM of 5 animals. Values with different superscript letters in the same condition are different. EC_{50}: $^{*}p < 0.05$ for difference between control and arthritis.

of exogenously added ADP (Figures 4(b) and 4(c)), but not when succinate was the substrate. As the ADP/O ratio was not modified, the small increase in state III respiration may also represent a small increase in the rate of ADP phosphorylation under these conditions. It is unlikely, however, that this small stimulation of the α-ketoglutarate respiration and of possibly other NADH-dependent substrates within the cell can represent significant increases in ROS generation. Moreover, it should be recalled that when MeJA was added to liver mitochondria of healthy or arthritic

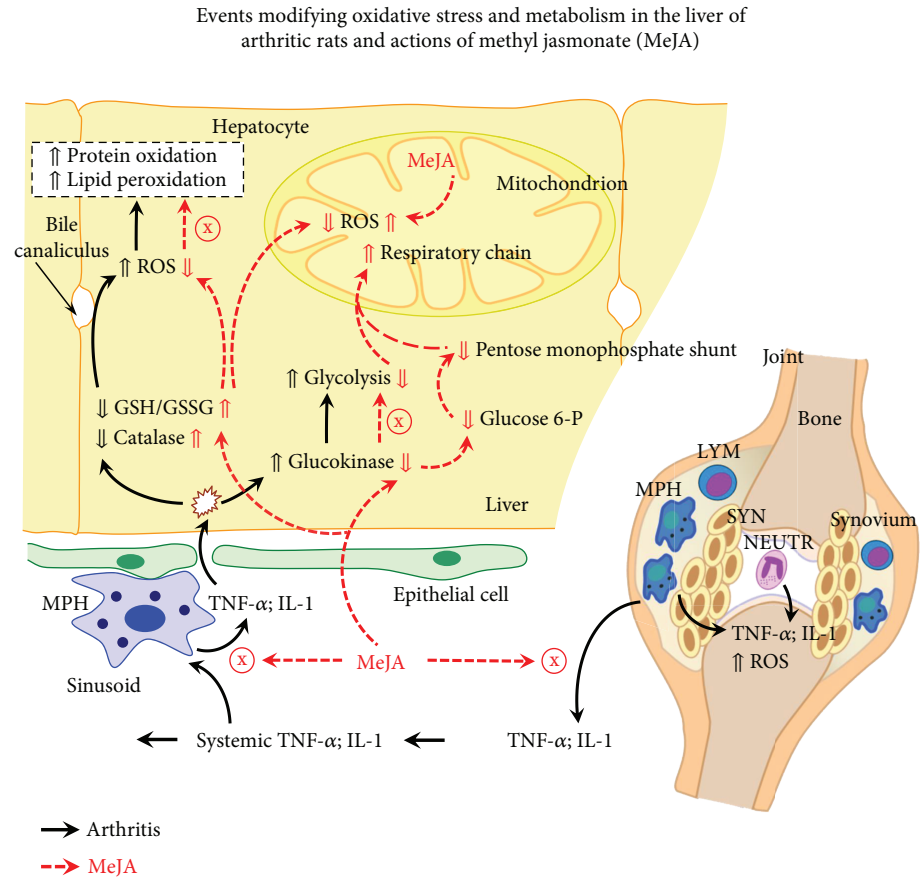

FIGURE 8: Schematic representation of the events modifying oxidative stress and metabolism in the liver of arthritic rats and actions of methyl jasmonate (MeJA). The scheme is discussed in the text and is based on the results of the current work and on previously published data. The symbol ⇑ means upregulation and ⇓ downregulation. Black arrows indicate events in the absence of MeJA, and red arrows indicate the effects of MeJA. TNF-α: tumor necrosis factor alpha; IL-1: interleukin 1; GSH: reduced glutathione; GSSG: oxidized glutathione; MPH: macrophages; LYM: lymphocytes; NEUTR: neutrophils; SYN: synoviocytes; ROS: reactive oxygen species.

rats not treated with this compound, a concentration-dependent inhibition of state III respiration was found (Figure 7(b)). It is difficult to infer if this short-term inhibition is significant *in vivo* as relatively high concentrations at the mitochondrial site are required (around or above 1 mM). If this effect also occurs *in vivo* with doses up to 300 mg·kg^{-1} MeJA, however, a situation may arise in which both stimulatory and inhibitory effects match each other so that the net effect is negligible. Consequently, stimulation of mitochondrial ROS generation by MeJA is likely to occur by another mechanism that is not dependent on the respiratory activity. In cancer cells, when attached to the mitochondrial outer membrane, hexokinase decreases the mitochondrial membrane potential ($\Delta\psi_m$) and suppresses ROS generation [52]. MeJA is reported to bind hexokinase and detach it from mitochondria, a condition that stimulates ROS production in cancer cells [6]. This is a mechanism that could explain, partly at least, the increased ROS production found in mitochondria from healthy and arthritic rats treated with MeJA.

Detachment of hexokinase from the mitochondrial outer membrane is associated with a reduced capacity of glucose phosphorylation and consequently reduced flux of glucosyl units through the glycolytic pathway. The MeJA-induced glucokinase inhibition is reported to be more harmful to cancer cells than to healthy cells because the former rely more on the glycolytic pathway [6, 50]. However, the inhibition of hexokinase and even glycolysis by MeJA was measured in isolated cells [6, 50]. In the present study, hepatic hexokinase was additionally inhibited in healthy and arthritic rats treated with MeJA. Moreover, the glucose flux through the glycolytic pathway was substantially decreased in perfused livers of healthy and arthritic rats, a phenomenon that may affect energy metabolism of these cells. Additionally, it may also lead to hyperglycemia, a possibility that remains to be verified in future experiments.

The accelerated oxygen consumption in perfused livers of MeJA-treated arthritic rats deserves additional comments. When glucose oxidation is decreased, an increase in oxygen consumption would not be a surprise because a compensatory increase in the oxidation of fatty acids and amino acids could be occurring. However, this phenomenon did not occur in healthy rats treated with MeJA, an observation that speaks against the expectation of a compensatory effect on respiration due to an inhibited glycolysis. On the other hand, the difference between livers from healthy and

arthritic rats could be related to different needs in terms of the corresponding antioxidant defenses. Phosphorylation of glucose is also essential for its oxidation in the pentose monophosphate shunt and to provide reducing equivalents as NADPH to the glutathione cycle. If the concentration of glucose 6-phosphate is decreased, the NADPH/$NADP^+$ and, consequently, the GSH/GSSG ratios will also decrease. However, oxidative stress was improved and the GSH/GSSG ratio was increased in MeJA-treated arthritic rats. This suggests the activation of a further source of reducing equivalents. NADPH generation can occur additionally via mitochondrial isocitrate dehydrogenase 1 (IDH1) and cytosolic $NADP^+$-dependent malic enzyme, which are both upregulated by Nfr2 [45]. Oxidation of fatty acids in the Krebs cycle can propel NADPH generation via isocitrate dehydrogenase and by consequence to increase hepatic oxygen uptake. In this sense, Nfr2 has been reported also to enhance mitochondrial fatty acid oxidation [45]. Thus, the accelerated oxygen uptake only in perfused livers of MeJA-treated arthritic rats could be representing an increased fatty acid oxidation for generating NADPH and not for compensating the inhibition of the glycolytic pathway.

5. Conclusions

In conclusion, MeJA decreased the articular and systemic inflammation in rats with severe adjuvant-induced arthritis and decreased the pronounced oxidative stress in the plasma and liver of arthritic rats. This latter effect occurs in consequence of reduced inflammation associated with an improvement of the antioxidant defenses. MeJA induced mitochondrial ROS production and inhibited the glucokinase activity in livers from healthy and arthritic rats, but it did not increase the hepatic oxidative stress. It is apparent that the effects of MeJA as a stimulator of the ROS scavenging mechanisms predominate over its actions as a stimulator of ROS production. However, the MeJA-induced glucokinase inhibition decreased substantially the flux through the glycolytic pathway of healthy and arthritic livers. In addition, the effective doses of MeJA in the present study were neither hepatotoxic nor nephrotoxic, a phenomenon that makes this compound a potentially important starting point for the development of anti-inflammatory and antirheumatic drugs. Finally, future approaches should consider the role of Nfr2 in the MeJA actions and possible modifications in systemic metabolism due to inhibition of hexokinase and hepatic glycolysis.

Abbreviations

MeJA:	Methyl jasmonate
ROS:	Reactive oxygen species
GSH:	Reduced glutathione
GSSG:	Oxidized glutathione
TNF-α:	Tumor necrosis factor alpha
IL-1:	Interleukin 1
COX-2:	Cyclooxygenase 2
iNOS:	Inducible nitric oxide synthase
NFκB:	Nuclear factor kappa B
Nfr2:	Nuclear factor erythroid 2-related 2
miR-101 and 155:	microRNAs 101 and 155
TBARS:	Thiobarbituric acid reactive substances
GK:	Glucokinase
G6Pase:	Glucose 6-phosphatase
SOD:	Superoxide dismutase
MPO:	Myeloperoxidase
IDH1:	Isocitrate dehydrogenase 1
FRAP:	Ferric reducing activity of plasma
ALT:	Alanine aminotransferase
AST:	Aspartate aminotransferase
MPH:	Macrophages
LYM:	Lymphocytes
NEUTR:	Neutrophils
SYN:	Synoviocytes.

Data Availability

The data used to support the findings of this study are available from the corresponding author upon request.

Conflicts of Interest

The authors declare no conflict of interest.

Authors' Contributions

Anacharis B. Sá-Nakanishi and Jamil Soni-Neto contributed equally and should be considered co-first authors.

Acknowledgments

This work was supported by the Conselho Nacional de Desenvolvimento Científico e Tecnológico (CNPq) (Grant no. 447876/2014-7). The authors wish to thank the financial support of the Coordenação de Aperfeiçoamento de Pessoal de Nível Superior (CAPES) and of the Conselho Nacional de Desenvolvimento Científico e Tecnológico (CNPq).

References

[1] Z. Raviv, S. Cohen, and D. Reischer-Pelech, "The anti-cancer activities of jasmonates," *Cancer Chemotherapy and Pharmacology*, vol. 71, no. 2, pp. 275–285, 2013.

[2] I. M. Cesari, E. Carvalho, M. Figueiredo Rodrigues, B. S. Mendonça, N. D. Amôedo, and F. D. Rumjanek, "Methyl jasmonate: putative mechanisms of action on cancer cells cycle, metabolism, and apoptosis," *International Journal of Cell Biology*, vol. 2014, Article ID 572097, 25 pages, 2014.

[3] O. Fingrut and E. Flescher, "Plant stress hormones suppress the proliferation and induce apoptosis in human cancer cells," *Leukemia*, vol. 16, no. 4, pp. 608–616, 2002.

[4] S. Klippel, J. Jakubikova, J. Delmore et al., "Methyljasmonate displays *in vitro* and *in vivo* activity against multiple myeloma cells," *British Journal of Haematology*, vol. 159, no. 3, pp. 340–351, 2012.

[5] M. Zhang, M. W. Zhang, L. Zhang, and L. Zhang, "Methyl jasmonate and its potential in cancer therapy," *Plant Signaling & Behavior*, vol. 10, no. 9, article e1062199, 2015.

[6] N. Goldin, L. Arzoine, A. Heyfets et al., "Methyl jasmonate binds to and detaches mitochondria-bound hexokinase," *Oncogene*, vol. 27, no. 34, pp. 4636–4643, 2008.

[7] S. Reuter, S. C. Gupta, M. M. Chaturvedi, and B. B. Aggarwal, "Oxidative stress, inflammation, and cancer: how are they linked?," *Free Radical Biology and Medicine*, vol. 49, no. 11, pp. 1603–1616, 2010.

[8] M. J. Kim, S. S. Kim, K. J. Park et al., "Methyl jasmonate inhibits lipopolysaccharide-induced inflammatory cytokine production via mitogen-activated protein kinase and nuclear factor-κB pathways in RAW 264.7 cells," *Die Pharmazie*, vol. 71, no. 9, pp. 540–543, 2016.

[9] H.-J. Lee, K. Maeng, H. T. Dang et al., "Anti-inflammatory effect of methyl dehydrojasmonate (J2) is mediated by the NF-κB pathway," *Journal of Molecular Medicine*, vol. 89, no. 1, pp. 83–90, 2011.

[10] H. T. Dang, H. J. Lee, E. S. Yoo et al., "New jasmonate analogues as potential anti-inflammatory agents," *Bioorganic & Medicinal Chemistry*, vol. 16, no. 24, pp. 10228–10235, 2008.

[11] T. Uhlig, R. H. Moe, and T. K. Kvien, "The burden of disease in rheumatoid arthritis," *PharmacoEconomics*, vol. 32, no. 9, pp. 841–851, 2014.

[12] I. B. McInnes and G. Schett, "The pathogenesis of rheumatoid arthritis," *New England Journal of Medicine*, vol. 365, no. 23, pp. 2205–2219, 2011.

[13] H. Lemarechal, Y. Allanore, C. Chenevier-Gobeaux, A. Kahan, O. G. Ekindjian, and D. Borderie, "Serum protein oxidation in patients with rheumatoid arthritis and effects of infliximab therapy," *Clinica Chimica Acta*, vol. 372, no. 1-2, pp. 147–153, 2006.

[14] R. Roubenoff, "Rheumatoid cachexia: a complication of rheumatoid arthritis moves into the 21st century," *Arthritis Research & Therapy*, vol. 11, no. 2, p. 108, 2009.

[15] Z. Fedatto Jr, E. L. Ishii-Iwamoto, C. Bersani-Amado, E. R. M. Maciel, A. Bracht, and A. M. Kelmer-Bracht, "Glucose phosphorylation capacity and glycolysis in the liver of arthritic rats," *Inflammation Research*, vol. 49, no. 3, pp. 128–132, 2000.

[16] Z. Fedatto Júnior, E. L. Ishii-Iwamoto, C. B. Amado et al., "Gluconeogenesis in the liver of arthritic rats," *Cell Biochemistry and Function*, vol. 17, no. 4, pp. 271–278, 1999.

[17] A. Bracht, S. S. Silveira, C. V. Castro-Ghizoni et al., "Oxidative changes in the blood and serum albumin differentiate rats with monoarthritis and polyarthritis," *SpringerPlus*, vol. 5, no. 1, p. 36, 2016.

[18] A. C. Schubert, M. M. N. Wendt, A. B. de Sá-Nakanishi et al., "Oxidative state and oxidative metabolism of the heart from rats with adjuvant-induced arthritis," *Experimental and Molecular Pathology*, vol. 100, no. 3, pp. 393–401, 2016.

[19] M. M. N. Wendt, A. B. de Sá-Nakanishi, C. V. de Castro Ghizoni et al., "Oxidative state and oxidative metabolism in the brain of rats with adjuvant-induced arthritis," *Experimental and Molecular Pathology*, vol. 98, no. 3, pp. 549–557, 2015.

[20] J. F. Comar, A. Babeto de Sá-Nakanishi, A. L. de Oliveira et al., "Oxidative state of the liver of rats with adjuvant-induced arthritis," *Free Radical Biology and Medicine*, vol. 58, pp. 144–153, 2013.

[21] U. Solomon and E. A. Taghogho, "Methyl jasmonate attenuates memory dysfunction and decreases brain levels of biomarkers of neuroinflammation induced by lipopolysaccharide in mice," *Brain Research Bulletin*, vol. 131, pp. 133–141, 2017.

[22] M. Hegen, J. C. Keith Jr, M. Collins, and C. L. Nickerson-Nutter, "Utility of animal models for identification of potential therapeutics for rheumatoid arthritis," *Annals of the Rheumatic Diseases*, vol. 67, no. 11, pp. 1505–1515, 2008.

[23] S. Umukoro and A. S. Olugbemide, "Antinociceptive effects of methyl jasmonate in experimental animals," *Journal of Natural Medicines*, vol. 65, no. 3-4, pp. 466–470, 2011.

[24] L. Bracht, C. P. Barbosa, S. M. Caparroz-Assef et al., "Effects of simvastatin, atorvastatin, ezetimibe, and ezetimibe + simvastatin combination on the inflammatory process and on the liver metabolic changes of arthritic rats," *Fundamental & Clinical Pharmacology*, vol. 26, no. 6, pp. 722–734, 2012.

[25] C. F. Estevão-Silva, F. Q. Ames, F. M. . S. Silva-Comar et al., "Fish oil and adjuvant-induced arthritis: inhibitory effect on leukocyte recruitment," *Inflammation*, vol. 39, no. 1, pp. 320–326, 2016.

[26] S. C. Saling, J. F. Comar, M. S. Mito, R. M. Peralta, and A. Bracht, "Actions of juglone on energy metabolism in the rat liver," *Toxicology and Applied Pharmacology*, vol. 257, no. 3, pp. 319–327, 2011.

[27] P. P. Bradley, R. D. Christensen, and G. Rothstein, "Cellular and extracellular myeloperoxidase in pyogenic inflammation," *Blood*, vol. 60, no. 3, pp. 618–622, 1982.

[28] I. F. F. Benzie and J. J. Strain, "The ferric reducing ability of plasma (FRAP) as a measure of "antioxidant power": the FRAP assay," *Analytical Biochemistry*, vol. 239, no. 1, pp. 70–76, 1996.

[29] R. L. Levine, D. Garland, C. N. Oliver et al., "[49] Determination of carbonyl content in oxidatively modified proteins," *Methods in Enzymology*, vol. 186, pp. 464–478, 1990.

[30] J. A. Buege and S. D. Aust, "[30] Microsomal lipid peroxidation," *Methods in Enzymology*, vol. 52, pp. 302–310, 1978.

[31] I. Rodrigues Siqueira, C. Fochesatto, I. L. da Silva Torres, C. Dalmaz, and C. Alexandre Netto, "Aging affects oxidative state in hippocampus, hypothalamus and adrenal glands of Wistar rats," *Life Sciences*, vol. 78, no. 3, pp. 271–278, 2005.

[32] A. C. B. Biazon, M. M. N. Wendt, J. R. Moreira et al., "The in vitro antioxidant capacities of hydroalcoholic extracts from roots and leaves of Smallanthus sonchifolius (Yacon) do not correlate with their in vivo antioxidant action in diabetic rats," *Journal of Biosciences and Medicines*, vol. 4, no. 2, pp. 15–27, 2016.

[33] R. W. Stineman, "A consistently well-behaved method of interpolation," *Creative Computing*, vol. 6, pp. 54–57, 1980.

[34] P. J. Hissin and R. Hilf, "A fluorometric method for determination of oxidized and reduced glutathione in tissues," *Analytical Biochemistry*, vol. 74, no. 1, pp. 214–226, 1976.

[35] H. U. Bergmeyer, *Methods of Enzymatic Analysis*, Verlag Chemie-Academic Press, London, 1974.

[36] S. Marklund and G. Marklund, "Involvement of the superoxide anion radical in the autoxidation of pyrogallol and a convenient assay for superoxide dismutase," *European Journal of Biochemistry*, vol. 47, no. 3, pp. 469–474, 1974.

[37] V. R. Vilela, A. L. de Oliveira, J. F. Comar, R. M. Peralta, and A. Bracht, "Tadalafil inhibits the cAMP stimulated glucose output in the rat liver," *Chemico-Biological Interactions*, vol. 220, pp. 1–11, 2014.

[38] C. V. Castro Ghizoni, A. P. Arssufi Ames, O. A. Lameira et al., "Anti-inflammatory and antioxidant actions of copaiba oil are related to liver cell modifications in arthritic rats," *Journal of Cellular Biochemistry*, vol. 118, no. 10, pp. 3409–3423, 2017.

[39] B. Chance and G. R. Williams, "A simple and rapid assay of oxidative phosphorylation," *Nature*, vol. 175, no. 4469, pp. 1120-1121, 1955.

[40] J. F. Comar, F. Suzuki-Kemmelmeier, and A. Bracht, "The action of oxybutynin on haemodynamics and metabolism in the perfused rat liver," *Pharmacology and Toxicology*, vol. 93, no. 3, pp. 147–152, 2003.

[41] J. Soni-Neto, *Anti-Inflammatory Action of Methyl Jasmonate Is Associated with Oxidative Modifications in the Liver of Arthritic Rats (Postgraduate Program in Biological Sciences) [M.S. thesis]*, State University of Maringá, PR, Brazil, 2017, http://nou-rau.uem.br/nou-rau/document/?code=vtls000227092.

[42] E. Sonkoly and A. Pivarcsi, "Advances in microRNAs: implications for immunity and inflammatory diseases," *Journal of Cellular and Molecular Medicine*, vol. 13, no. 1, pp. 24–38, 2009.

[43] L. Kastl, S. W. Sauer, T. Ruppert et al., "TNF-α mediates mitochondrial uncoupling and enhances ROS-dependent cell migration *via* NF-κB activation in liver cells," *FEBS Letters*, vol. 588, no. 1, pp. 175–183, 2014.

[44] W. G. Yasmineh, J. L. Parkin, J. I. Caspers, and A. Theologides, "Tumor necrosis factor/cachectin decreases catalase activity of rat liver," *Cancer Research*, vol. 51, no. 15, pp. 3990–3995, 1991.

[45] A. T. Dinkova-Kostova and A. Y. Abramov, "The emerging role of Nrf2 in mitochondrial function," *Free Radical Biology and Medicine*, vol. 88, Part B, pp. 179–188, 2015.

[46] Y. Guo, S. Yu, C. Zhang, and A. N. T. Kong, "Epigenetic regulation of Keap1-Nrf2 signaling," *Free Radical Biology and Medicine*, vol. 88, Part B, pp. 337–349, 2015.

[47] D.-S. Yu, Y. S. Wang, Y. L. Bi et al., "Salvianolic acid A ameliorates the integrity of blood-spinal cord barrier via miR-101/Cul3/Nrf2/HO-1 signaling pathway," *Brain Research*, vol. 1657, pp. 279–287, 2017.

[48] Z. Peng and Y. Zhang, "Methyl jasmonate induces the apoptosis of human colorectal cancer cells via downregulation of EZH2 expression by microRNA-101," *Molecular Medicine Reports*, vol. 15, no. 2, pp. 957–962, 2017.

[49] Y. Wang, W. Xiang, M. Wang et al., "Methyl jasmonate sensitizes human bladder cancer cells to gambogic acid-induced apoptosis through down-regulation of EZH2 expression by miR-101," *British Journal of Pharmacology*, vol. 171, no. 3, pp. 618–635, 2014.

[50] J. Li, K. Chen, F. Wang et al., "Methyl jasmonate leads to necrosis and apoptosis in hepatocellular carcinoma cells via inhibition of glycolysis and represses tumor growth in mice," *Oncotarget*, vol. 8, no. 28, pp. 45965–45980, 2017.

[51] E. Milrot, A. Jackman, T. Kniazhanski, P. Gonen, E. Flescher, and L. Sherman, "Methyl jasmonate reduces the survival of cervical cancer cells and downregulates HPV E6 and E7, and survivin," *Cancer Letters*, vol. 319, no. 1, pp. 31–38, 2012.

[52] R. J. Mailloux, T. Dumouchel, C. Aguer, R. deKemp, R. Beanlands, and M. E. Harper, "Hexokinase II acts through UCP3 to suppress mitochondrial reactive oxygen species production and maintain aerobic respiration," *Biochemical Journal*, vol. 437, no. 2, pp. 301–311, 2011.

Hindawi
Oxidative Medicine and Cellular Longevity
Volume 2018, Article ID 4596746, 15 pages
https://doi.org/10.1155/2018/4596746

Research Article

Taurine Attenuates Calpain-2 Induction and a Series of Cell Damage via Suppression of NOX-Derived ROS in ARPE-19 Cells

Yuanyuan Zhang, Shu Ren, Yanting Gu, Jiahong Wang, Zheng Liu, and Zhou Zhang

Department of Pharmacology, Shenyang Pharmaceutical University, Shenyang 110016, China

Correspondence should be addressed to Zheng Liu; zhengliu@syphu.edu.cn and Zhou Zhang; zhouzhang@syphu.edu.cn

Received 21 March 2018; Revised 24 May 2018; Accepted 7 June 2018; Published 29 July 2018

Academic Editor: Karolina Szewczyk-Golec

Nicotinamide adenine dinucleotide phosphate (NADPH) oxidases (NOXs) are key transmembrane proteins leading to reactive oxygen species (ROS) overproduction. However, the detailed roles of NOXs in retinal pigment epithelial (RPE) cell metabolic stress induced by Earle's balanced salt solution (EBSS) through starvation remain unclear. In this study, we investigated what roles NOXs play in regard to calpain activity, endoplasmic stress (ER), autophagy, and apoptosis during metabolic stress in ARPE-19 cells. We first found that EBSS induced an increase in NOX2, NOX4, p22phox, and NOX5 compared to NOX1. Secondly, suppression of NOXs resulted in reduced ER stress and autophagy, decreased ROS generation, and alleviated cell apoptosis. Thirdly, silencing of NOX4, NOX5, and p22phox resulted in reduced levels of cell damage. However, silencing of NOX1 was unaffected. Finally, taurine critically mediated NOXs in response to EBSS stress. In conclusion, this study demonstrated for the first time that NOX oxidases are the upstream regulators of calpain-2, ER stress, autophagy, and apoptosis. Furthermore, the protective effect of taurine is mediated by the reduction of NOX-derived ROS, leading to sequential suppression of calpain induction, ER stress, autophagy, and apoptosis.

1. Introduction

Reactive oxygen species (ROS) are signaling molecules that result in metabolic stress, changes in mitochondrial membrane permeability, DNA damage, and cell apoptosis [1–3]. ROS are generated by many cell types in the human body and are involved in the pathogenesis of various ocular diseases [4, 5], including glaucoma [6], age-related macular degeneration (AMD) [7], and retinopathy [8–10].

Nicotinamide adenine dinucleotide phosphate (NADPH) oxidase (NOX) is another key source of ROS besides mitochondria [11, 12]. NOX is the only enzyme group that produces ROS as its main function. Studies have shown that the NOX family is the inducer of ROS generation, ER stress, autophagy, and apoptosis [1, 13, 14]. There are different isoforms of NOXs in mammalian cells, containing NOX1–5 and DUOX1 and DUOX2 [15]. Of these homologues, we discovered that human retina expresses NOX1, NOX2, NOX4, and NOX5 [15–17]. Studies have shown that different homologues play different roles in retinal pathological processes. Some studies indicate that NOX1 is increased during eye disease and cardiac dysfunction [18, 19]. NOX2 is upregulated during ocular injury and diabetes [4, 16]. The expression level of NOX4 is increased during cardiomyocyte injury, diabetic retinopathy, and stroke [10, 13, 20]. The p22phox subunit is an essential part of the NOX compound. Except for NOX5 and DUOX1/2, p22phox is required for regulating NOX isoforms [3, 21]. Unlike other NOX homologues, NOX5 has the ability to bind and be activated by intracellular calcium directly and its function to produce ROS is regulated by intracellular calcium mobilization, influx, and phosphorylation [22, 23]. Calcium/calmodulin-dependent kinase II can activate NOX5 via direct phosphorylation [15]. Moreover, some studies show that crosstalk between ROS and calpain leads to the release of Ca^{2+} [24–27]. The nuclear translocation of calpain-2 can be activated by increased NOX-

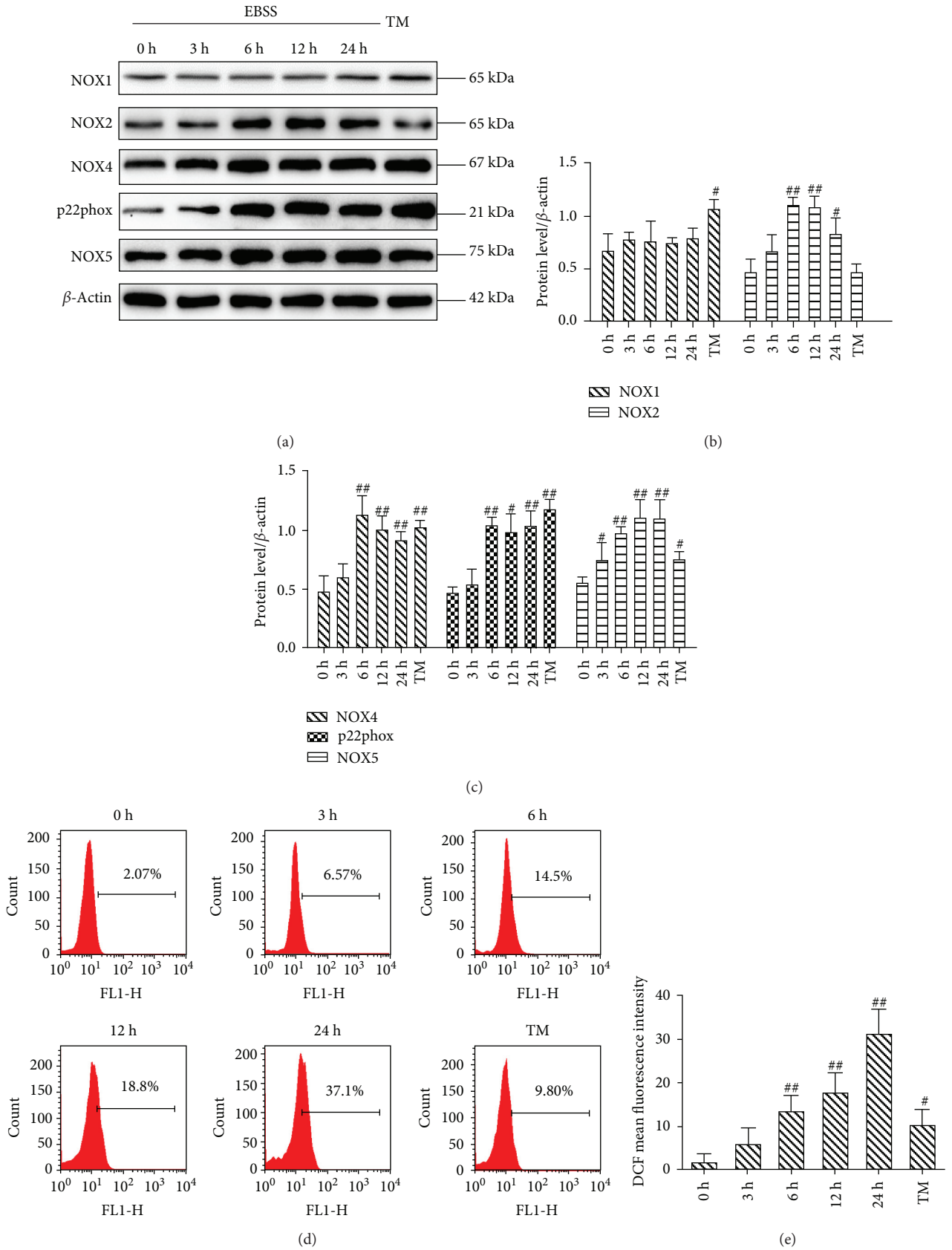

Figure 1: Continued.

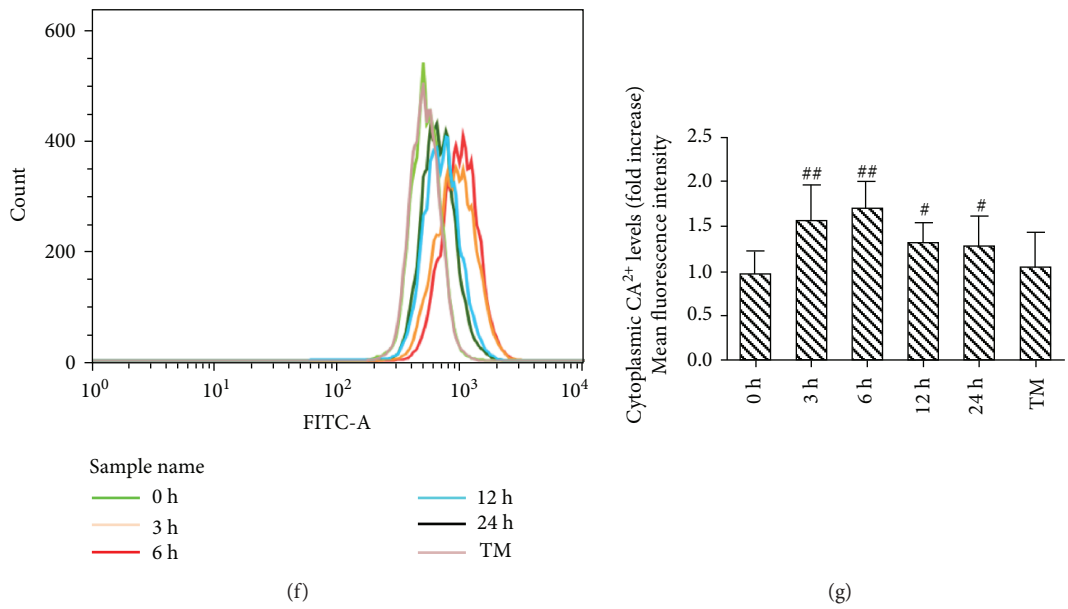

(f) (g)

Figure 1: Earle's balanced salt solution (EBSS) increases NADPH oxidative activity and ROS generation in ARPE-19 cells in a time-dependent manner. (a–c) A Western blot analysis was carried out to detect the expression levels of NOXs. (d, e) Intracellular ROS was determined by flow cytometry. (f, g) Earle's balanced salt solution (EBSS) increases cytoplasmic calcium in ARPE-19 cells. The intracellular calcium was detected with Fluo-3 AM. TM stands for tunicamycin. The data are presented as the means ± SEM of three independent experiments. $^{\#}p < 0.05$ and $^{\#\#}p < 0.01$ compared to control (0 h).

derived ROS. Furthermore, the ROS level and nuclear calpain-2 induction might be crucial pathogenic elements for apoptosis of cardiomyocyte [28].

There is growing evidence showing that NOXs are important sources of ROS during ER stress [29]. The increase of cellular stress and oxidative stress can lead to ER stress by activating the process of unfolded protein response and Ca^{2+} disturbances [30, 31]. Numerous studies have revealed that oxidative stress and ER stress are associated with neuronal cell death signaling after ischemia injury [32]. Oxidative stress plays an essential role in protective cell autophagy [33, 34]. ROS also leads to excessive autophagy and even apoptosis in cells [35]. It is known that apoptosis of ARPE-19 cells is the major cause of AMD-induced pathological changes [36]. In addition, a change in ROS balance is in charge of the execution of cell apoptosis [37, 38].

RPE cells are highly metabolically active cells that are located in the retina and play a vital role in maintaining normal visual function. Hence, RPE cells are vulnerable to oxidative stress [7, 39]. In addition, sunlight is one of the causes for ROS production that can damage RPE cells [40, 41]. The human cell line ARPE-19 has functional and structural characteristics similar to RPE cells. Therefore, we used an ARPE-19 cell line for our study.

In our previous study, we demonstrated that taurine inhibited starvation-triggered cell damage in ARPE-19 cells [24]. However, the detailed roles of NOX (one of the main ROS sources) in EBSS-induced cell injury remain unclear. We hypothesize that NOXs are the upstream regulators of calpains, ER stress, autophagy, and apoptosis. Furthermore, the protective effect of taurine is mediated by the reduction of NOX-derived ROS, leading to sequential suppression of calpain induction, ER stress, autophagy, and apoptosis. In this study, the potential roles of NOXs in EBSS-induced cell injury were studied in ARPE-19 cells.

2. Material and Methods

2.1. Cell Line and Cell Culture. ARPE-19 cells were procured from Shanghai GuanDao Biotech Co. Ltd. Cells were subcultured in Dulbecco's modified Eagle's medium (DMEM)/F-12 (Hyclone, Logan, UT, USA) containing 10% FBS (Gibco, Grand Island, NY, USA), penicillin (100 IU/mL), and streptomycin (100 μg/mL). Cells were maintained at 37°C and 5% CO_2.

2.2. Transfection Experiments. Human *NOX2*, *NOX4*, *p22phox*, and *NOX5* small interfering RNAs (siRNAs) were obtained from GenePharma (ShangHai, China). The siRNAs (two short sequences of siRNA specific for each one) were transfected into ARPE-19 cells using lipofectamine 2000 reagent (Invitrogen, Carlsbad, CA, USA) for 12 h. Next, cells were incubated for another 48 h in normal culture conditions. Protein expression was detected using Western blot, and the better siRNAs were chosen for subsequent experiments. The scrambled (nontargeting) siRNAs were used as the negative control.

2.3. Western Blotting. The protocol of the Western blot analysis is described in detail elsewhere [24]. Antibodies used and their dilutions were the following: NOX1 (1 : 500, Cambridge, MA, USA, Abcam, ab55831), NOX2/gp91phox (1 : 500, ABclonal Biotech, Wuhan, China, A1636), NOX4 (1 : 1000, Abcam, ab133303), p22phox (1 : 1000, Abcam, ab191512),

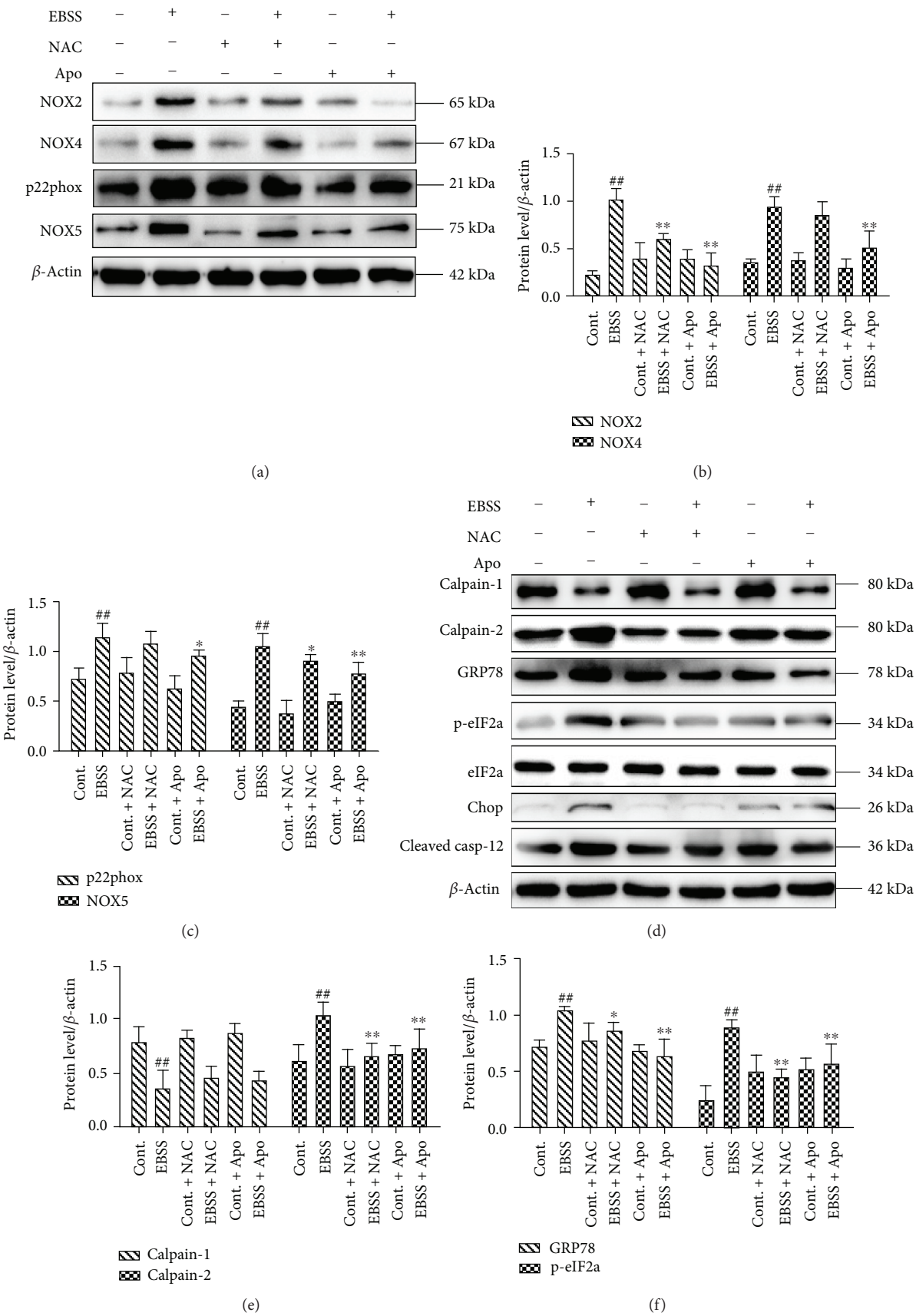

Figure 2: Continued.

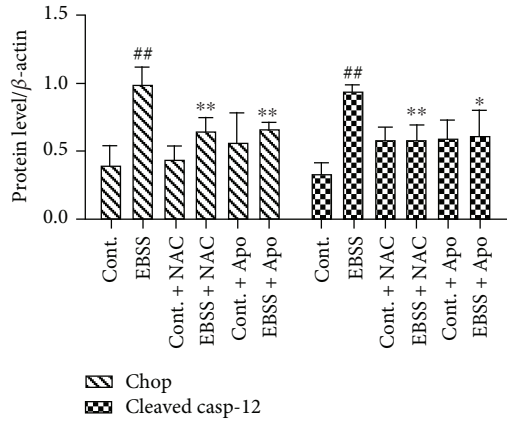

(g)

Figure 2: ROS scavenging and NOX suppression attenuate EBSS-induced loss of calcium homeostasis and ER stress in ARPE-19 cells. (a–c) The expression levels of NOX proteins were examined by Western blot. (d–g) The expression levels of calpains and the ER stress-related proteins were examined by Western blot. The data are presented as the means ± SEM of three independent experiments. $^{\#\#}p < 0.01$ compared to the control group. $^{*}p < 0.05$ and $^{**}p < 0.01$ compared to the EBSS group.

and NOX5 (1 : 500, ABclonal, A7136). Other antibodies are described in detail elsewhere [24].

2.4. Flow Cytometry. Cellular ROS levels were monitored using the fluorescent probe (DCFH-DA). Cells were seeded in 6-well plates overnight and treated with EBSS for 24 h with or without inhibitors/siRNA/taurine pretreatment. Next, cells were loaded with DCFH-DA (10 μM) in PBS for 30 min. Fluorescence was measured with a FACSCalibur flow cytometer (Becton, Dickinson and Company, San Jose, CA, USA). The protocol of the annexin V/PI staining is described in detail elsewhere [24]. The cytosolic-free calcium was detected using Fluo-3 AM. The protocol of the intracellular calcium detection is described in detail elsewhere [42].

2.5. Confocal Microscopy. Cells were cocultured with DCFH-DA (10 μM, Beyotime Biotech, ShangHai, China) for 30 min. Nuclei were stained with Hoechst for 20 min. The protocol of image analysis is described in detail elsewhere [24].

2.6. Statistics. Data was expressed as the mean ± standard error of the mean (SEM). Statistics were analyzed by SPSS 21.0 statistics program (SPSS Inc., Chicago, IL, USA). One-way ANOVA and Dunnett's posttest were used to determine the statistical significance. A p value of less than 0.05 ($p < 0.05$) was considered significant.

3. Results

3.1. Effects of EBSS Treatment on NOX Expression and ROS Generation. To evaluate the role of EBSS treatment in the activities of NOXs and ROS generation, the cells were cultured in EBSS for 0, 3, 6, 12, and 24 hours (h) or with tunicamycin (50 μM) as a positive control for 6 h. The expression of NOX proteins was examined by Western blot. The results show that the protein expression of NOX2, NOX4, p22phox, and NOX5 was dramatically increased from 6 h until 24 h after EBSS treatment. However, the expression of NOX1 was unchanged (Figures 1(a)–1(c)). The generation of ROS was markedly elevated between 6 h and 24 h after EBSS treatment (Figures 1(d) and 1(e)). Our results suggest that EBSS induces the activities of NOXs and ROS production. In addition, levels of NOXs were fully activated by 6 h posttreatment and subsequently this time point was chosen for our experiments. ER stress, autophagy, and apoptosis also could be induced at 6 and 12 h, respectively (data available online with this article; doi: 10.3390/ijms18102146, pages 4-5). We observed that the fluorescence intensity of the peaks shifted immediately after 3 h until 24 h post-EBSS treatment. Furthermore, EBSS induced the loss of calcium homeostasis in ARPE-19 cells (Figures 1(f) and 1(g)).

3.2. ROS Scavenging and NOX Suppression Attenuated EBSS-Induced Loss of Calcium Homeostasis and ER Stress. To investigate the possible roles of NOXs and ROS in EBSS-induced loss of calcium homeostasis and ER stress in ARPE-19 cells, the cells were pretreated for 2 h with the ROS scavenger compound, N-acetyl-cysteine (NAC, 10 mM), or the NOX inhibitor, apocynin (Apo, 1 mM), and then cultured with EBSS (6 or 12 h). We found that pretreatment with NAC or Apo strongly and significantly reduced the expression of NOX2, NOX4, p22phox, and NOX5 (Figures 2(a)–2(c)), suggesting that the activity of NOXs and the accumulation of ROS were inhibited by the two inhibitors. To assess the relationship between NOXs, ER stress, and calpains in ARPE-19 cells, calpains and ER stress-related proteins were examined by Western blot. The results show that the expression of calpain-2 and ER stress-related proteins was decreased. However, induction of calpain-1 was unchanged (Figures 2(d)–2(g)). Our findings suggest that the induction of NOXs can promote loss of calcium homeostasis and ER stress. Furthermore, NOXs may be critical upstream regulators of calcium homeostasis and ER stress.

3.3. NOX Suppression and ROS Scavenging Attenuated EBSS-Induced Autophagy, Apoptosis, and ROS Generation.

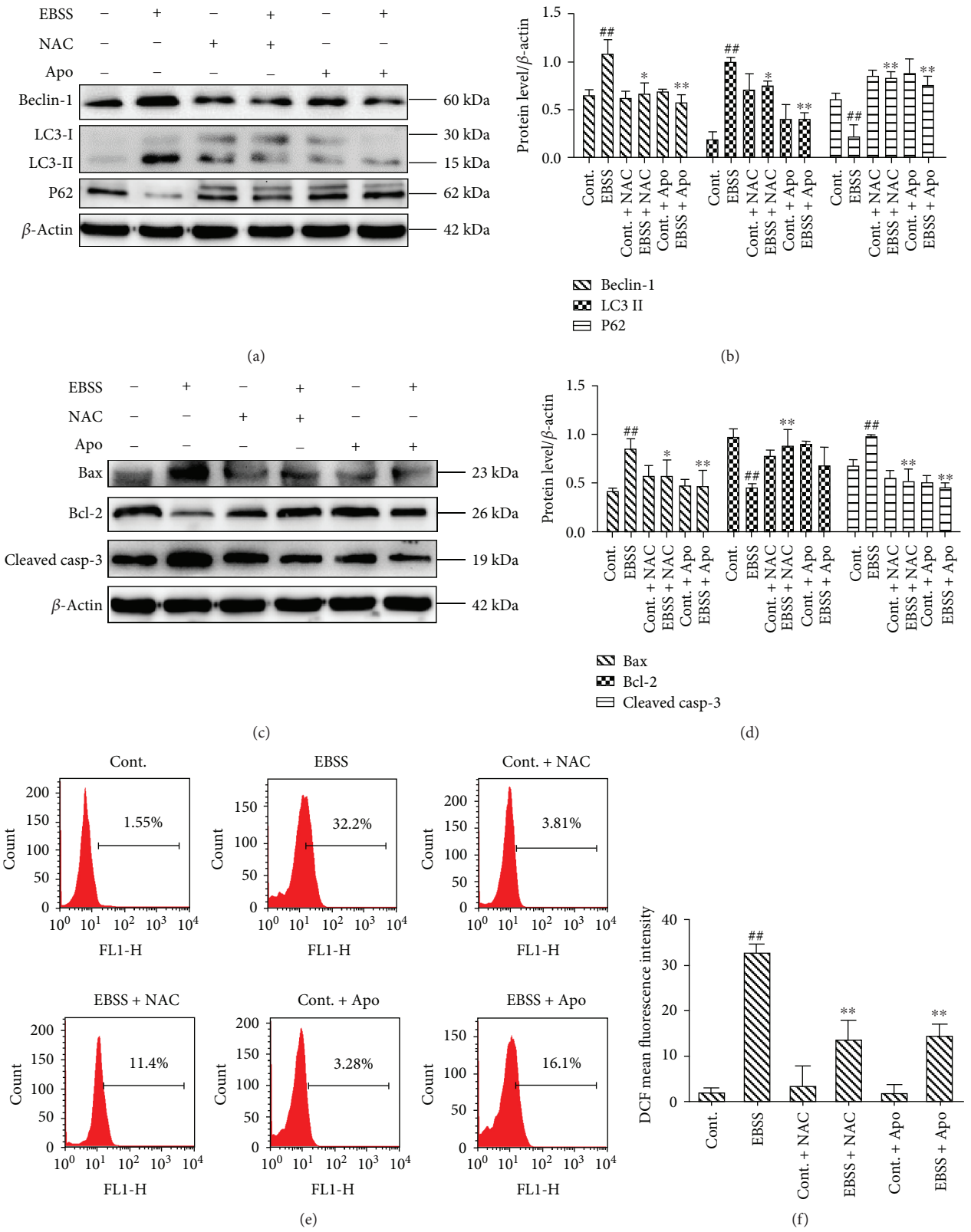

Figure 3: ROS scavenging and NOX suppression attenuate EBSS-induced autophagy, apoptosis, and ROS generation. (a–d) The expression of autophagy-related proteins and apoptosis-related proteins was detected by Western blot. (e, f) Intracellular ROS was evaluated by flow cytometry. The data are presented as the means ± SEM of three independent experiments. $^{\#\#}p < 0.01$ compared to the control group. $^{*}p < 0.05$ and $^{**}p < 0.01$ compared to the EBSS group.

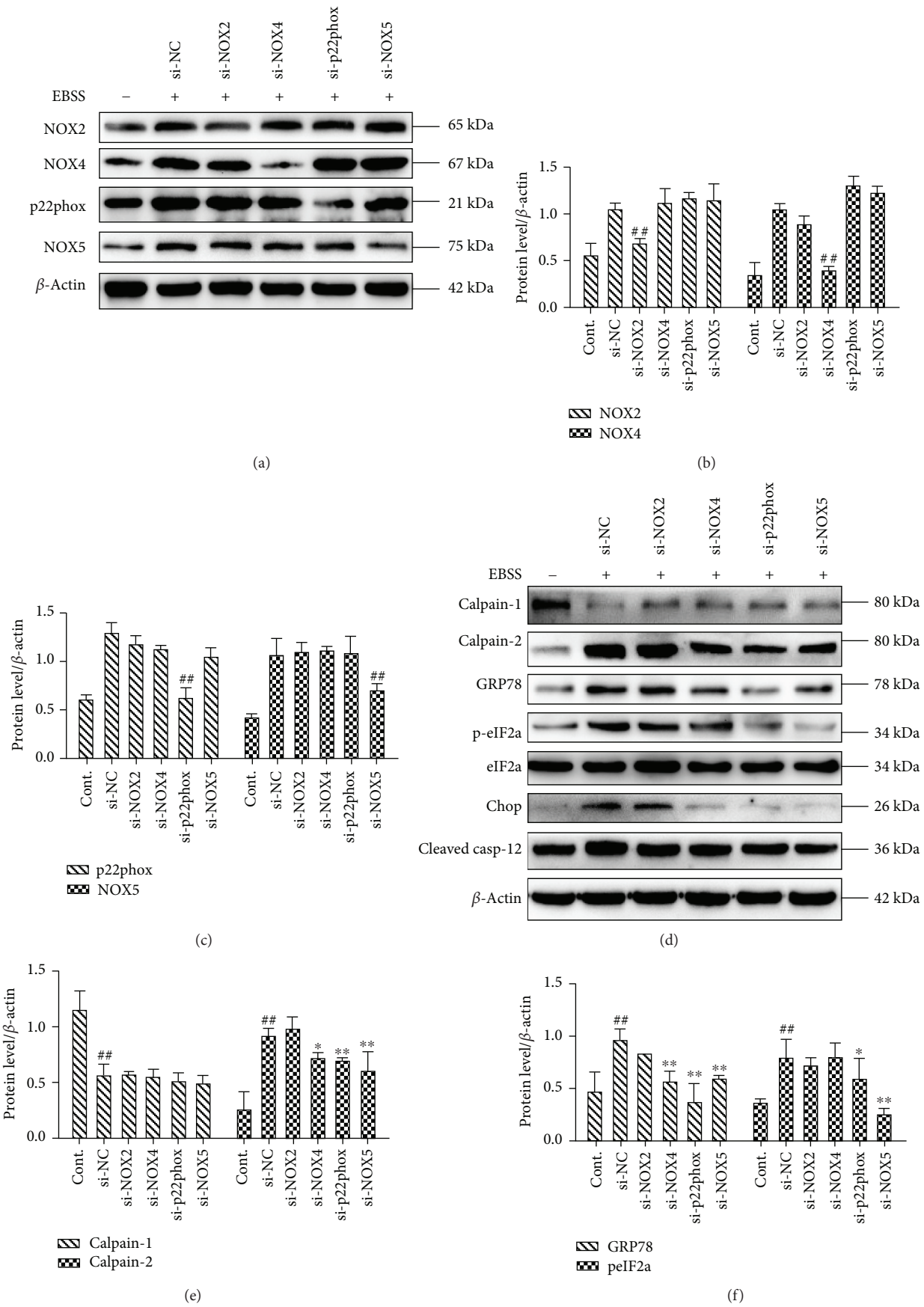

Figure 4: Continued.

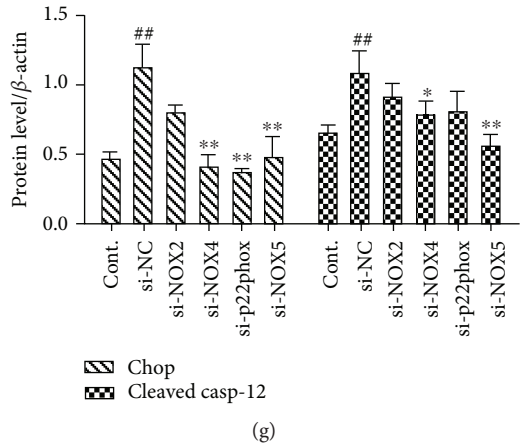

Figure 4: NOX4, p22phox, and NOX5 modulate loss of calcium homeostasis and ER stress in ARPE-19 cells. (a–c) Silencing of *NOX2*/*NOX4*/*p22phox*/*NOX5* decreases its protein level. (d–g) The activities of ER stress and calpain-2 were suppressed by siRNA knockdown of *NOX4*, *p22phox*, and *NOX5*. The data are presented as the means ± SEM of three independent experiments. $^{\#\#}p < 0.01$ compared to the control group. $^{*}p < 0.05$ and $^{**}p < 0.01$ compared with the EBSS group.

To further explore the possible roles of NOXs and ROS in EBSS-induced autophagy and apoptosis in ARPE-19 cells, we examined the expression of autophagy-related proteins and mitochondrial apoptotic proteins by Western blot. Our results suggest that both inhibitors, NAC and Apo, caused a significant decrease in the expression of beclin-1, LC3, Bax, and cleaved caspase-3. Meanwhile, levels of P62 and Bcl-2 were noticeably increased (Figures 3(a)–3(d)), indicating that the NOXs were related to the induction of autophagy and apoptosis. To evaluate the role of ROS, intracellular ROS was first evaluated by flow cytometry. The results show that pretreatment with NAC or Apo reverses the accumulation of ROS (Figures 3(e) and 3(f)). Our findings show that the suppression of NOX oxidases or ROS generation could decrease autophagy and apoptosis. Moreover, NOXs may be vital upstream regulators of ER stress, autophagy, and apoptosis.

3.4. NOX4, p22phox, and NOX5 Played Crucial Roles in EBSS-Induced Loss of Calcium Homeostasis and ER Stress. To test the involvement of NOXs in EBSS-induced calpain production and ER stress, we used specific interference RNA (siRNA) species leading to a marked decrease of NOX protein levels (Figures 4(a)–4(c)). To demonstrate the effect of NOXs on ER stress and calpain production, calpains and the ER stress-related proteins were examined by Western blot. The results show that *NOX4*, *p22phox*, and *NOX5* silencing resulted in lower levels of calpain-2 and ER stress-related proteins. However, induction of calpain-1 was unaffected (Figures 4(d)–4(g)). Our findings indicate that silencing *NOX4*, *p22phox*, and *NOX5* can prevent calpain induction and ER stress. Furthermore, NOX4, p22phox, and NOX5 may be essential upstream regulators of calcium homeostasis and ER stress.

3.5. NOX4, p22phox, and NOX5 Play Key Roles in EBSS-Induced Autophagy, Apoptosis, and ROS Generation. We next evaluated the effects of NOX2, NOX4, p22phox, and NOX5 on autophagy, apoptosis, and ROS production. The autophagy-related proteins and apoptosis-related proteins were examined by Western blot. The results show that *NOX4*, *p22phox*, and *NOX5* silencing downregulated the expression of beclin-1, LC3, Bax, and cleaved caspase-3. Meanwhile, the levels of P62 and Bcl-2 were increased (Figures 5(a)–5(d)). Moreover, the cell apoptosis rate was evaluated by flow cytometry, and our data show that apoptosis is inhibited with the reduction of NOX4, p22phox, and NOX5 expression (Figures 5(e) and 5(f)). The main sources of ROS are NOX enzymes, and our data suggest that the downregulation of NOX4, p22phox, and NOX5 is associated with significantly reduced production of ROS (Figures 5(g) and 5(h)). Our findings indicate that silencing of *NOX4*, *p22phox*, and *NOX5* can reduce autophagy, apoptosis, and ROS production. Furthermore, NOX4, p22phox, and NOX5 may be essential upstream regulators of autophagy and apoptosis.

3.6. Effects of Taurine on NOX Expression and ROS Generation Induced by EBSS. We also investigated the effects of taurine (30 mM) on NOXs and ROS. Our results suggest that the expression of NOX2, NOX4, p22phox, and NOX5 in the EBSS group was increased compared with the control group. The level of proteins was decreased after intervention with taurine. The expression of NOX1 levels was not influenced in models (EBSS treatment) and taurine + EBSS groups (Figures 6(a)–6(c)). Oxidative stress was evaluated by detecting ROS with flow cytometry. Intracellular ROS was decreased by taurine treatment (Figures 6(d) and 6(e)). Moreover, ROS accumulation was also determined with immunofluorescence. High fluorescence intensity was presented in the EBSS group. But it was weak in the control and EBSS + taurine groups (Figures 6(f) and 6(g)). These data suggest that taurine inhibited the activities of NOX enzymes and the accumulation of ROS. Therefore, taurine attenuates ER stress, autophagy, and apoptosis in ARPE-19 cells via suppression of the NADPH oxidase-derived reactive oxygen species-mediated calpain induction pathway (data

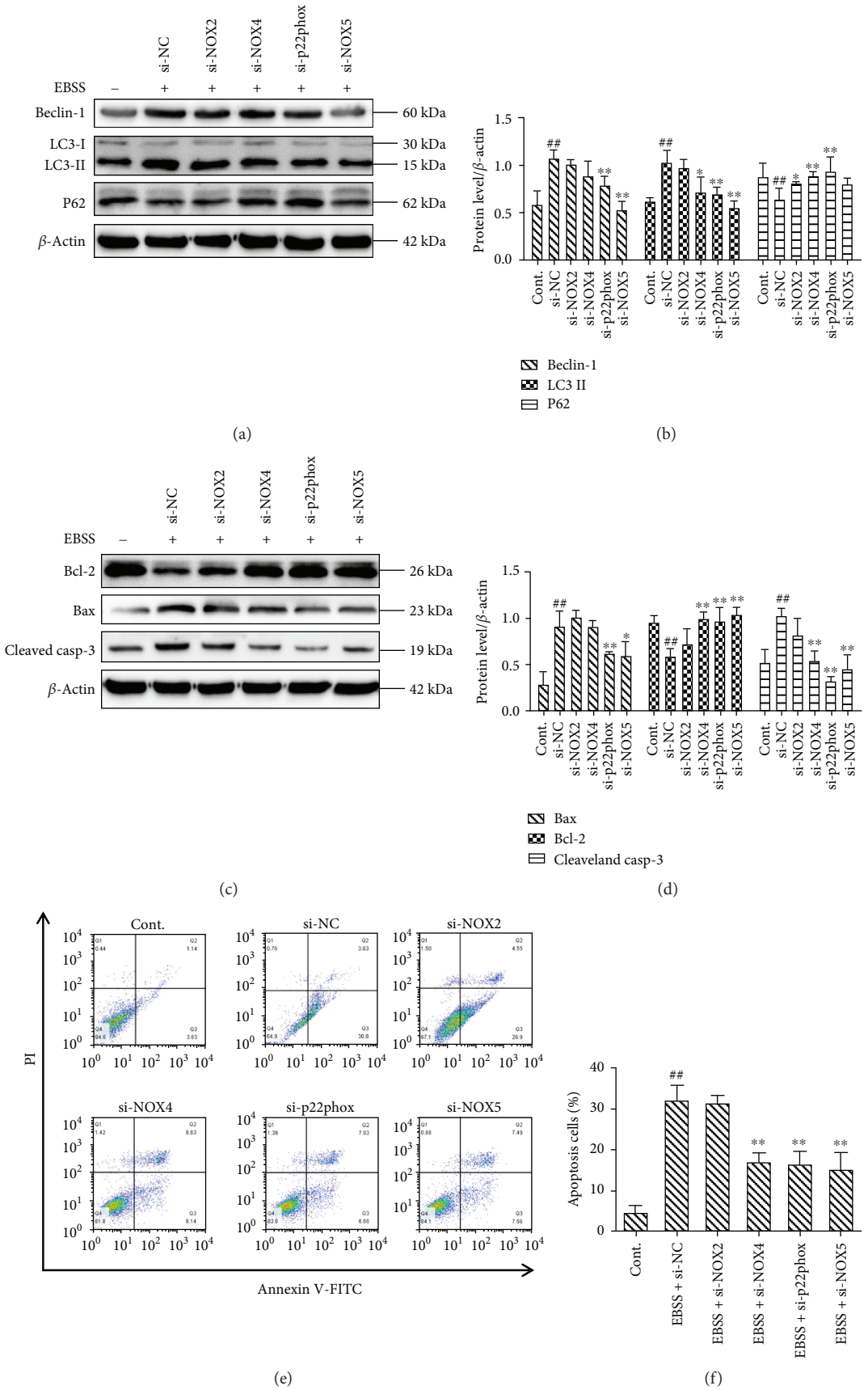

Figure 5: Continued.

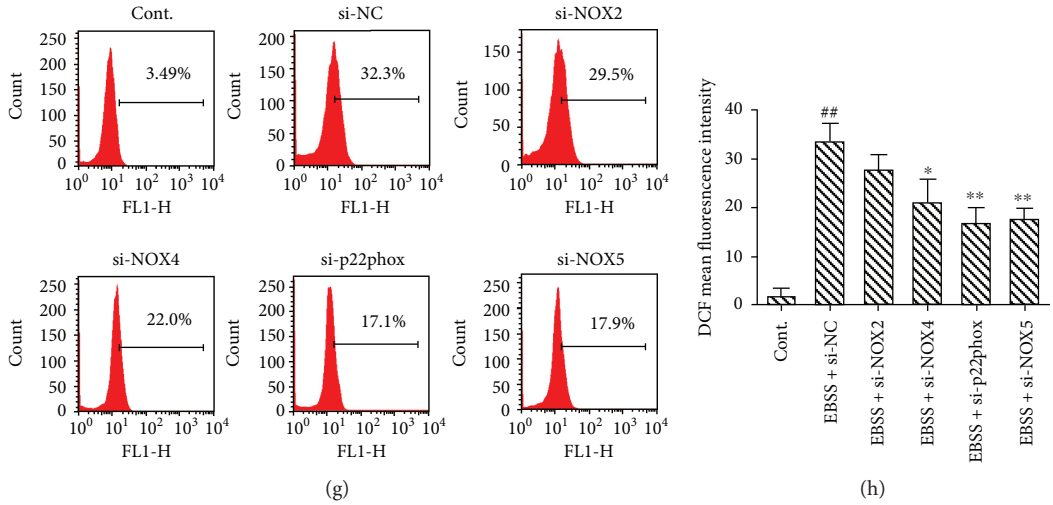

Figure 5: NOX4, p22phox, and NOX5 modulate autophagy and apoptosis in ARPE-19 cells. (a–d) NOX4, p22phox, or NOX5 silencing inhibits autophagy and apoptosis. (e, f) siRNA knockdown of *NOX4*, *p22phox*, or *NOX5* decreases cell apoptosis. (g, h) siRNA knockdown of *NOX4*, *p22phox*, or *NOX5* decreases ROS production. Intracellular ROS was evaluated by flow cytometry. The data are presented as the means ± SEM of three independent experiments. $^{\#\#}p < 0.01$ compared to the control group. $^{*}p < 0.05$ and $^{**}p < 0.01$ compared to the EBSS group.

available online with this article; doi:10.3390/ijms18102146, pages 8-9).

4. Discussion

Our study demonstrates the involvement of NOX-derived ROS in EBSS-induced RPE metabolic disorders. NOXs are upstream regulators of calpain-2, ER stress, autophagy, and apoptosis. Furthermore, NOXs are involved in calpain-2, ER stress, autophagy, and apoptosis regulation by NOX4, p22phox, and NOX5 but not by NOX1 or NOX2. Taurine alleviated cell injuries through regulation of NOX levels (Figure 7).

During metabolic stress (starvation), the balance of ROS level changes. NOXs are activated and result in excessive production of ROS (termed oxidative stress) (Figure 1). Furthermore, an excessive level of ROS interferes with lipids and proteins leading to functional and structural changes of target molecules [43, 44]. NOX1/NADPH oxidase plays a key role in endotoxin-induced cardiomyocyte apoptosis [19]. NOX1 does not influence vascular endothelial growth factor (VEGF) activation in HG-induced cell injuries [16]. NOX2 and NOX4 play physiological roles in homocysteine-induced endothelial cell apoptosis [45]. NOX5 and p22phox are involved in human monocyte differentiation into dendritic cells [3]. We demonstrate that NOX4 and p22phox play key roles in ARPE-19 cell injuries (Figure 1). NOX5 is expressed in cells of the cardiovascular system and in the retina [46]. However, NOX5 is absent in rodents and this may explain the lack of data on its expression and function in the retina in this model. Previous research indicated that NOX5 was predominantly expressed in RPE cells [15]. Our results show that NOX5 is a key factor of EBSS-induced cell damage (Figure 1).

The interaction of ROS and calcium signaling can be considered bidirectional; ROS can regulate cellular calcium signaling, while calcium signaling is crucial for ROS generation [25, 47, 48]. Increasing evidence suggests that this crosstalk plays a key role in many pathological conditions, including colorectal cancer, cardiomyocyte apoptosis, neuronal damage, and also renal cell injury [28, 49–51]. We revealed that suppression of NOX-mediated ROS production through the use of the NOX inhibitor (apocynin) or ROS scavenger (NAC) inhibited calpain-2 induction (Figure 2). During cellular stress, NOX-mediated ROS generation was observed. ROS levels correlate with cell survival. The decrease in ROS production also reduces the expression of NOX, which forms a feed-forward loop [52–55]. NOX is activated due to its notable ability to produce ROS. The ER is a major site of calcium storage [25]. The release of Ca^{2+} also leads to ROS accumulation [56, 57]. Overproduction of ROS activated ER-based calcium channels by triggering signaling molecules upstream of calpain-2 [58–60]. Induction of calpain-2 further mediates the subsequent ER-mitochondrial crosstalk [1, 28, 50]. ROS not only acts as an activator but can also be regulated by autophagy through macroautophagosomes [34, 61]. Bcl-2 is an integral membrane protein, and it can form homodimers to protect cells from apoptosis. In contrast, Bax is a proapoptotic gene and can cause mitochondria to release cytochrome C. Cytochrome C leads to caspase 3 activation which is an important mitochondrial apoptotic marker [62, 63]. We investigated the ROS-calcium crosstalk in the ER, autophagosome, and their influence on apoptosis in the mitochondria. Our results indicate that suppression of NOX oxidases or ROS generation could decrease calpain-2 induction, ER stress, autophagy, and apoptosis (Figures 2 and 3).

To elucidate the functional significance of NOXs, we examined ROS generation, ER stress, autophagy, and apoptosis in which NOX2/NOX4/p22phox/NOX5 was knocked down with siRNA. Although NOX4/p22phox/NOX5 was not completely knocked down, induction of NADPH oxidase was inhibited. The exact reasons for this are complex and

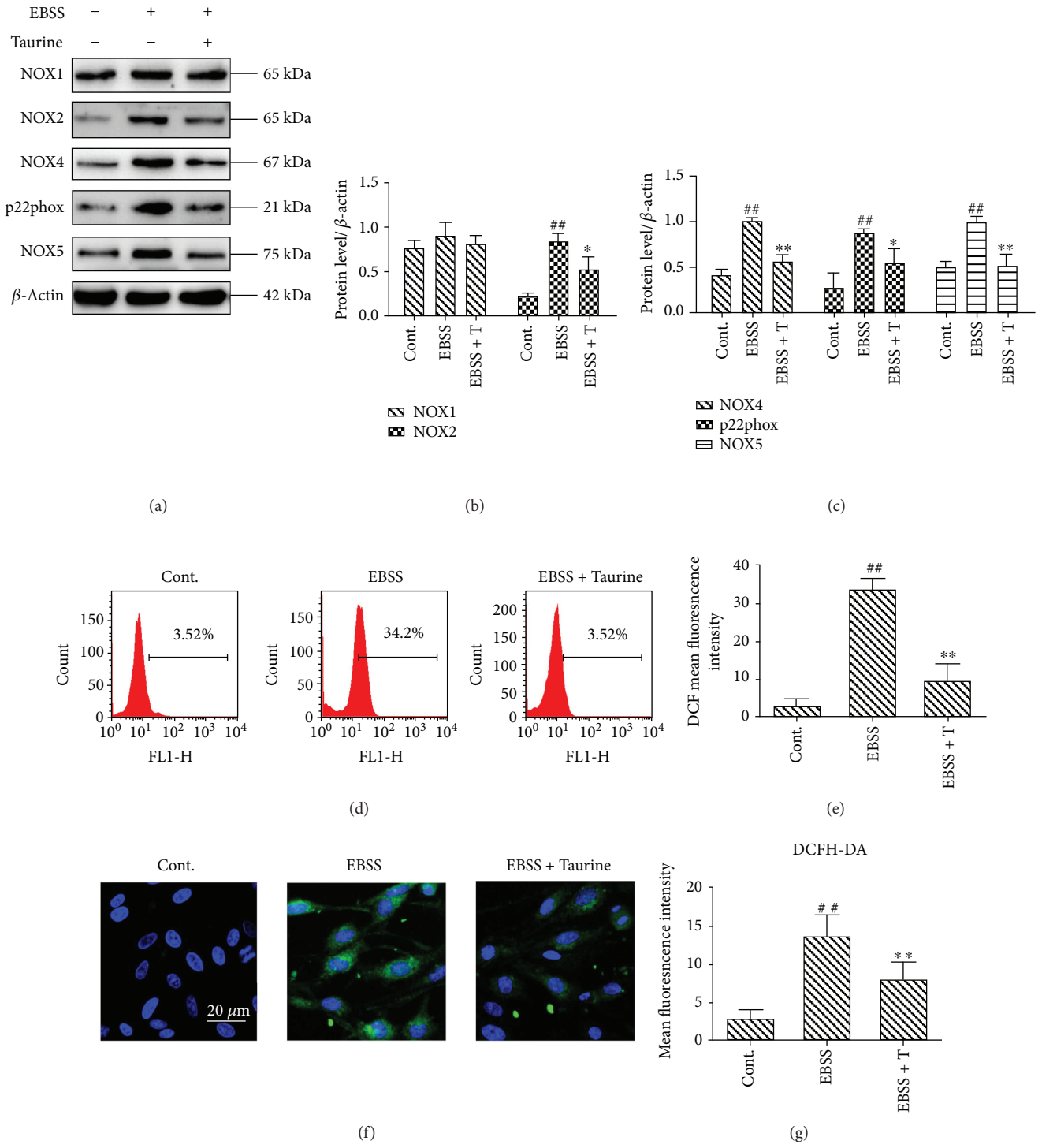

FIGURE 6: Effects of taurine on NOX expression and ROS generation induced by EBSS. (a–c) Western blot analysis was carried out to determine the expression of NOX proteins in ARPE-19 cells. (d, e) Intracellular ROS was evaluated by flow cytometry. (f, g) Confocal images of ROS labelled with DCFH-DA (green) and nuclear stained with DAPI (blue). Scale bar = 20 μm. The data are presented as the means ± SEM of three to five independent experiments. $^{\#\#}p < 0.01$ compared to the control group. $^{*}p < 0.05$ and $^{**}p < 0.01$ compared to the EBSS group. T: taurine.

not well-understood but relate to the fact that NOX4/p22phox/NOX5 downregulation influences other NADPH oxidase subunits that may have an impact on the induction of oxidases [45, 64]. It is also possible that NOX4/p22phox/NOX5 might interact with other NOX isoforms, which, in the context of NOX4/p22phox/NOX5 downregulation, inhibits NOX-associated NOX induction. Such considerations require further examinations. In NOX4/p22phox/

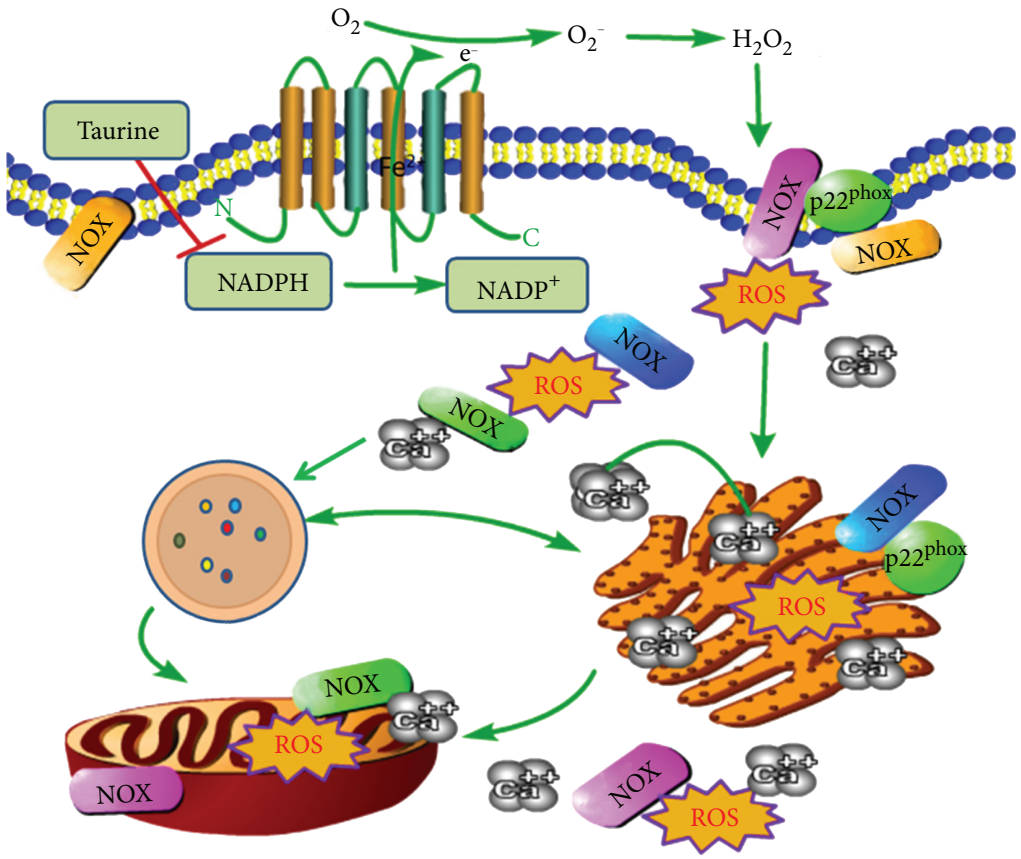

Figure 7: Schematic diagram of the effects of taurine in ARPE-19 cells. The protective effect of taurine is regulated by the reduction of intracellular ROS from NOXs, leading, in turn, to sequential suppression of calpain induction, ER stress, autophagy, and apoptosis. NADPH oxidases (NOXs) are transmembrane proteins that are localized either in intracellular granules and vesicles or on the cell surface membranes.

NOX5-downregulated cells, but not NOX2-downregulated cells, ROS generation, ER stress, autophagy, and apoptosis were significantly reduced, indicating the importance of NOX4/p22phox/NOX5 in redox signaling by EBSS. Moreover, these processes are Ca^{2+} sensitive, because calpain-2 induction was also inhibited. Hence, NOX influence generation of ROS also regulates ER stress, autophagy, and apoptosis. We showed that NOX4, p22phox, and NOX5 are critical for damage and cell death of ARPE-19 cells. In addition, we found for the first time that NOX5 induction is required for calpain-2 induction, ER stress, autophagy, and apoptosis in ARPE-19 cells (Figures 4 and 5).

The antioxidation of taurine may prevent disease progression [65]. The antioxidant properties are limited by the sulfonic group through neutralizing ROS production [41, 66]. In a previous study, we demonstrated that taurine inhibited starvation-triggered cell damage. In our study, our results suggest that taurine inhibited the activation of NOXs and ROS generation (Figure 6).

In conclusion, our data demonstrate that ROS generated via the NADPH oxidase system is the major contributing factor in RPE dysfunction induced by EBSS. NOX silencing or suppression partly protects cells from cell damage. NOX4, p22phox, and NOX5 play key roles in the production of ROS, ER stress, autophagy, and apoptosis. Our observations support the hypothesis that oxidative stress is the main causative for cell injury, and taurine attenuates ER stress, autophagy, and apoptosis in ARPE-19 cells via a suppression of the NADPH oxidase-derived reactive oxygen species-mediated calpain induction pathway. Our data provides novel insights into ocular diseases and mechanisms of taurine.

Data Availability

Previously reported research data were used to support this study and are available at doi: 10.3390/ijms18102146. These prior studies (and datasets) are cited at relevant places within the text as references. The data used to support the findings of this study are available from the corresponding author, Zhou Zhang, upon reasonable request.

Conflicts of Interest

The authors declare no conflict of interest.

Authors' Contributions

Yuanyuan Zhang conceived and designed the experiments. Yuanyuan Zhang and Shu Ren performed the experiments. Zhou Zhang, Yuanyuan Zhang, Yanting Gu, and Jiahong

Wang analyzed the data. Zheng Liu contributed reagents, materials, and analysis tools. Yuanyuan Zhang wrote the paper.

Acknowledgments

This research was funded by the National Natural Science Foundation of China (Grant no. 31270883) to Zhou Zhang.

References

[1] M. L. Sheu, C. C. Shen, Y. S. Chen, and C. K. Chiang, "Ochratoxin A induces ER stress and apoptosis in mesangial cells via a NADPH oxidase-derived reactive oxygen species-mediated calpain activation pathway," *Oncotarget*, vol. 8, no. 12, pp. 19376–19388, 2017.

[2] G. Ren, W. Luo, W. Sun et al., "Psoralidin induced reactive oxygen species (ROS)-dependent DNA damage and protective autophagy mediated by NOX4 in breast cancer cells," *Phytomedicine*, vol. 23, no. 9, pp. 939–947, 2016.

[3] V. Marzaioli, M. Hurtado-Nedelec, C. Pintard et al., "NOX5 and p22phox are 2 novel regulators of human monocytic differentiation into dendritic cells," *Blood*, vol. 130, no. 15, pp. 1734–1745, 2017.

[4] A. Kowluru and R. A. Kowluru, "Phagocyte-like NADPH oxidase [Nox2] in cellular dysfunction in models of glucolipotoxicity and diabetes," *Biochemical Pharmacology*, vol. 88, no. 3, pp. 275–283, 2014.

[5] J. L. Wilkinson-Berka, I. Rana, R. Armani, and A. Agrotis, "Reactive oxygen species, Nox and angiotensin II in angiogenesis: implications for retinopathy," *Clinical Science*, vol. 124, no. 10, pp. 597–615, 2013.

[6] S. Huang, P. Huang, Z. Lin et al., "Hydrogen sulfide supplement attenuates the apoptosis of retinal ganglion cells in experimental glaucoma," *Experimental Eye Research*, vol. 168, pp. 33–48, 2018.

[7] Y. Li, X. Liu, T. Zhou et al., "Inhibition of APE1/Ref-1 redox activity rescues human retinal pigment epithelial cells from oxidative stress and reduces choroidal neovascularization," *Redox Biology*, vol. 2, pp. 485–494, 2014.

[8] M. Sugai, A. Ohta, Y. Ogata et al., "Asymmetric dimethylarginine (ADMA) in the aqueous humor of diabetic patients," *Endocrine Journal*, vol. 54, no. 2, pp. 303–309, 2007.

[9] G. Mohammad, K. Alam, M. I. Nawaz, M. M. Siddiquei, A. Mousa, and A. M. Abu El-Asrar, "Mutual enhancement between high-mobility group box-1 and NADPH oxidase-derived reactive oxygen species mediates diabetes-induced upregulation of retinal apoptotic markers," *Journal of Physiology and Biochemistry*, vol. 71, no. 3, pp. 359–372, 2015.

[10] J. Li, J. J. Wang, Q. Yu, K. Chen, K. Mahadev, and S. X. Zhang, "Inhibition of reactive oxygen species by lovastatin downregulates vascular endothelial growth factor expression and ameliorates blood-retinal barrier breakdown in *db*/*db* mice: role of NADPH oxidase 4," *Diabetes*, vol. 59, no. 6, pp. 1528–1538, 2010.

[11] M. Sedeek, A. C. Montezano, R. L. Hebert et al., "Oxidative stress, Nox isoforms and complications of diabetes—potential targets for novel therapies," *Journal of Cardiovascular Translational Research*, vol. 5, no. 4, pp. 509–518, 2012.

[12] E. C. Vaquero, M. Edderkaoui, S. J. Pandol, I. Gukovsky, and A. S. Gukovskaya, "Reactive oxygen species produced by NAD(P)H oxidase inhibit apoptosis in pancreatic cancer cells," *Journal of Biological Chemistry*, vol. 279, no. 33, pp. 34643–34654, 2004.

[13] Y. Wang, L. Zhong, X. Liu, and Y. Z. Zhu, "ZYZ-772 prevents cardiomyocyte injury by suppressing Nox4-derived ROS production and apoptosis," *Molecules*, vol. 22, no. 2, 2017.

[14] J. E. Leadsham, G. Sanders, S. Giannaki et al., "Loss of cytochrome c oxidase promotes RAS-dependent ROS production from the ER resident NADPH oxidase, Yno1p, in yeast," *Cell Metabolism*, vol. 18, no. 2, pp. 279–286, 2013.

[15] J. C. Jha, A. M. D. Watson, G. Mathew, L. C. de Vos, and K. Jandeleit-Dahm, "The emerging role of NADPH oxidase NOX5 in vascular disease," *Clinical Science*, vol. 131, no. 10, pp. 981–990, 2017.

[16] R. Haque, P. M. Iuvone, L. He et al., "Prorenin receptor (PRR)-mediated NADPH oxidase (Nox) signaling regulates VEGF synthesis under hyperglycemic condition in ARPE-19 cells," *Journal of Receptor and Signal Transduction*, vol. 37, no. 6, pp. 560–568, 2017.

[17] Y. Qiu, L. Tao, C. Lei et al., "Downregulating p22phox ameliorates inflammatory response in angiotensin II-induced oxidative stress by regulating MAPK and NF-κB pathways in ARPE-19 cells," *Scientific Reports*, vol. 5, no. 1, article 14362, 2015.

[18] D. Deliyanti and J. L. Wilkinson-Berka, "Inhibition of NOX1/4 with GKT137831: a potential novel treatment to attenuate neuroglial cell inflammation in the retina," *Journal of Neuroinflammation*, vol. 12, no. 1, p. 136, 2015.

[19] K. Matsuno, K. Iwata, M. Matsumoto et al., "NOX1/NADPH oxidase is involved in endotoxin-induced cardiomyocyte apoptosis," *Free Radical Biology and Medicine*, vol. 53, no. 9, pp. 1718–1728, 2012.

[20] Y. Y. Qin, M. Li, X. Feng et al., "Combined NADPH and the NOX inhibitor apocynin provides greater anti-inflammatory and neuroprotective effects in a mouse model of stroke," *Free radical biology and medicine*, vol. 104, pp. 333–345, 2017.

[21] K. K. Prior, M. S. Leisegang, I. Josipovic et al., "CRISPR/Cas9-mediated knockout of p22phox leads to loss of Nox1 and Nox4, but not Nox5 activity," *Redox biology*, vol. 9, pp. 287–295, 2016.

[22] F. Chen, Y. Wang, S. Barman, and D. J. Fulton, "Enzymatic regulation and functional relevance of NOX5," *Current Pharmaceutical Design*, vol. 21, no. 41, pp. 5999–6008, 2015.

[23] S. Carnesecchi, A. L. Rougemont, J. H. Doroshow et al., "The NADPH oxidase NOX5 protects against apoptosis in ALK-positive anaplastic large-cell lymphoma cell lines," *Free Radical Biology and Medicine*, vol. 84, pp. 22–29, 2015.

[24] Y. Zhang, S. Ren, Y. Liu, K. Gao, Z. Liu, and Z. Zhang, "Inhibition of starvation-triggered endoplasmic reticulum stress, autophagy, and apoptosis in ARPE-19 cells by taurine through modulating the expression of calpain-1 and calpain-2," *International Journal of Molecular Sciences*, vol. 18, no. 10, 2017.

[25] A. Gorlach, K. Bertram, S. Hudecova, and O. Krizanova, "Calcium and ROS: a mutual interplay," *Redox biology*, vol. 6, pp. 260–271, 2015.

[26] S. Limbu, T. M. Hoang-Trong, B. L. Prosser, W. J. Lederer, and M. S. Jafri, "Modeling local X-ROS and calcium signaling in the heart," *Biophysical Journal*, vol. 109, no. 10, pp. 2037–2050, 2015.

[27] S. Javadov, "The calcium-ROS-pH triangle and mitochondrial permeability transition: challenges to mimic cardiac ischemia-reperfusion," *Frontiers in Physiology*, vol. 6, p. 83, 2015.

[28] H. Chang, J. J. Sheng, L. Zhang et al., "ROS-induced nuclear translocation of calpain-2 facilitates cardiomyocyte apoptosis in tail-suspended rats," *Journal of Cellular Biochemistry*, vol. 116, no. 10, pp. 2258–2269, 2015.

[29] F. R. Laurindo, T. L. Araujo, and T. B. Abrahao, "Nox NADPH oxidases and the endoplasmic reticulum," *Antioxidants & Redox Signaling*, vol. 20, no. 17, pp. 2755–2775, 2014.

[30] H. Y. Lee, H. J. Chae, S. Y. Park, and J. H. Kim, "Porcine placenta hydrolysates enhance osteoblast differentiation through their antioxidant activity and effects on ER stress," *BMC Complementary and Alternative Medicine*, vol. 16, no. 1, p. 291, 2016.

[31] C. X. Santos, A. A. Nabeebaccus, A. M. Shah, L. L. Camargo, S. V. Filho, and L. R. Lopes, "Endoplasmic reticulum stress and Nox-mediated reactive oxygen species signaling in the peripheral vasculature: potential role in hypertension," *Antioxidants & Redox Signaling*, vol. 20, no. 1, pp. 121–134, 2014.

[32] S. Hong, J. Kwon, D. W. Kim, H. J. Lee, D. Lee, and W. Mar, "Mulberrofuran G protects ischemic injury-induced cell death via inhibition of NOX4-mediated ROS generation and ER stress," *Phytotherapy Research*, vol. 31, no. 2, pp. 321–329, 2017.

[33] E. J. Song, S. J. Lee, H. S. Lim et al., "*Vibrio vulnificus* VvhA induces autophagy-related cell death through the lipid raft-dependent c-Src/NOX signaling pathway," *Scientific Reports*, vol. 6, no. 1, article 27080, 2016.

[34] S. Sciarretta, P. Zhai, D. Shao et al., "Activation of NADPH oxidase 4 in the endoplasmic reticulum promotes cardiomyocyte autophagy and survival during energy stress through the protein kinase RNA-activated-like endoplasmic reticulum kinase/eukaryotic initiation factor 2α/activating transcription factor 4 pathway," *Circulation research*, vol. 113, no. 11, pp. 1253–1264, 2013.

[35] X. Wen, J. Wu, F. Wang, B. Liu, C. Huang, and Y. Wei, "Deconvoluting the role of reactive oxygen species and autophagy in human diseases," *Free Radical Biology and Medicine*, vol. 65, pp. 402–410, 2013.

[36] L. Palanza, R. Nuzzi, M. Repici, and A. Vercelli, "Ganglion cell apoptosis and increased number of NADPH-d-positive neurones in the rodent retina in an experimental model of glaucoma," *Acta Ophthalmologica Scandinavica*, vol. 80, pp. 47-48, 2002.

[37] J. Dong, K. K. Sulik, and S. Y. Chen, "The role of NOX enzymes in ethanol-induced oxidative stress and apoptosis in mouse embryos," *Toxicology letters*, vol. 193, no. 1, pp. 94–100, 2010.

[38] P. Sancho, E. Bertran, L. Caja, I. Carmona-Cuenca, M. M. Murillo, and I. Fabregat, "The inhibition of the epidermal growth factor (EGF) pathway enhances TGF-β-induced apoptosis in rat hepatoma cells through inducing oxidative stress coincident with a change in the expression pattern of the NADPH oxidases (NOX) isoforms," *Biochimica et Biophysica Acta (BBA) - Molecular Cell Research*, vol. 1793, no. 2, pp. 253–263, 2009.

[39] S. H. Kim, H. Kim, H. J. Ku et al., "Oxalomalate reduces expression and secretion of vascular endothelial growth factor in the retinal pigment epithelium and inhibits angiogenesis: implications for age-related macular degeneration," *Redox biology*, vol. 10, pp. 211–220, 2016.

[40] X. Zhu, K. Wang, K. Zhang, F. Zhou, and L. Zhu, "Induction of oxidative and nitrosative stresses in human retinal pigment epithelial cells by all-*trans*-retinal," *Experimental cell research*, vol. 348, no. 1, pp. 87–94, 2016.

[41] Y. Li, J. M. Arnold, M. Pampillo, A. V. Babwah, and T. Peng, "Taurine prevents cardiomyocyte death by inhibiting NADPH oxidase-mediated calpain activation," *Free radical biology and medicine*, vol. 46, no. 1, pp. 51–61, 2009.

[42] S. Lv, Q. Y. Xu, E. C. Sun, J. K. Zhang, and D. L. Wu, "Dissection and integration of the autophagy signaling network initiated by bluetongue virus infection: crucial candidates ERK1/2, Akt and AMPK," *Scientific Reports*, vol. 6, no. 1, article 23130, 2016.

[43] U. Weyemi, C. E. Redon, T. Aziz et al., "Inactivation of NADPH oxidases NOX4 and NOX5 protects human primary fibroblasts from ionizing radiation-induced DNA damage," *Radiation Research*, vol. 183, no. 3, pp. 262–270, 2015.

[44] S. Hu, X. Yang, and J. He, "NADPH oxidase-induced macrophage autophagy mediated by reactive oxygen species in Aspergillus fumigatus infection," *Xi bao yu fen zi mian yi xue za zhi = Chinese journal of cellular and molecular immunology*, vol. 31, no. 2, pp. 190–193, 2015.

[45] J. A. Sipkens, N. Hahn, C. S. van den Brand et al., "Homocysteine-induced apoptosis in endothelial cells coincides with nuclear NOX2 and peri-nuclear NOX4 activity," *Cell biochemistry and biophysics*, vol. 67, no. 2, pp. 341–352, 2013.

[46] T. J. Guzik, W. Chen, M. C. Gongora et al., "Calcium-dependent NOX5 nicotinamide adenine dinucleotide phosphate oxidase contributes to vascular oxidative stress in human coronary artery disease," *Journal of the American College of Cardiology*, vol. 52, no. 22, pp. 1803–1809, 2008.

[47] C. Mazars, P. Thuleau, O. Lamotte, and S. Bourque, "Cross-talk between ROS and calcium in regulation of nuclear activities," *Molecular Plant*, vol. 3, no. 4, pp. 706–718, 2010.

[48] A. Di, D. Mehta, and A. B. Malik, "ROS-activated calcium signaling mechanisms regulating endothelial barrier function," *Cell Calcium*, vol. 60, no. 3, pp. 163–171, 2016.

[49] M. Chocry, L. Leloup, and H. Kovacic, "Reversion of resistance to oxaliplatin by inhibition of p38 MAPK in colorectal cancer cell lines: involvement of the calpain / Nox1 pathway," *Oncotarget*, vol. 8, no. 61, pp. 103710–103730, 2017.

[50] B. Paramo, T. Montiel, D. R. Hernandez-Espinosa, M. Rivera-Martinez, J. Moran, and L. Massieu, "Calpain activation induced by glucose deprivation is mediated by oxidative stress and contributes to neuronal damage," *The international journal of biochemistry & cell biology*, vol. 45, no. 11, pp. 2596–2604, 2013.

[51] L. Yu, X. Gan, X. Liu, and R. An, "Calcium oxalate crystals induces tight junction disruption in distal renal tubular epithelial cells by activating ROS/Akt/p38 MAPK signaling pathway," *Renal Failure*, vol. 39, no. 1, pp. 440–451, 2017.

[52] D. Hernandez-Saavedra, L. Sanders, M. J. Perez et al., "RTP801 amplifies nicotinamide adenine dinucleotide phosphate oxidase-4–dependent oxidative stress induced by cigarette smoke," *American Journal of Respiratory Cell and Molecular Biology*, vol. 56, no. 1, pp. 62–73, 2017.

[53] C. Wilson, E. Munoz-Palma, D. R. Henriquez et al., "A feed-forward mechanism involving the NOX complex and RyR-mediated Ca^{2+} release during axonal specification," *Journal of Neuroscience*, vol. 36, no. 43, pp. 11107–11119, 2016.

[54] Y. Cai, L. Yang, G. Hu et al., "Regulation of morphine-induced synaptic alterations: role of oxidative stress, ER stress, and autophagy," *Journal of Cell Biology*, vol. 215, no. 2, pp. 245–258, 2016.

[55] G. L. Semenza and N. R. Prabhakar, "Neural regulation of hypoxia-inducible factors and redox state drives the pathogenesis of hypertension in a rodent model of sleep apnea," *Journal of Applied Physiology*, vol. 119, no. 10, pp. 1152–1156, 2015.

[56] R. K. Srivastava, C. Li, A. Ahmad et al., "ATF4 regulates arsenic trioxide-mediated NADPH oxidase, ER-mitochondrial crosstalk and apoptosis," *Archives of Biochemistry and Biophysics*, vol. 609, pp. 39–50, 2016.

[57] Y. S. Kim, S. J. Birge, L. V. Avioli, and R. Miller, "Cell density-dependent vitamin D effects on calcium accumulation in rat osteogenic sarcoma cells (ROS 17/2)," *Calcified Tissue International*, vol. 41, no. 4, pp. 218–222, 1987.

[58] M. S. Sharaf, D. Stevens, and C. Kamunde, "Zinc and calcium alter the relationship between mitochondrial respiration, ROS and membrane potential in rainbow trout (*Oncorhynchus mykiss*) liver mitochondria," *Aquatic Toxicology*, vol. 189, pp. 170–183, 2017.

[59] L. Minasyan, P. G. Sreekumar, D. R. Hinton, and R. Kannan, "Protective mechanisms of the mitochondrial-derived peptide Humanin in oxidative and endoplasmic reticulum stress in RPE cells," *Oxidative Medicine and Cellular Longevity*, vol. 2017, Article ID 1675230, 11 pages, 2017.

[60] U. Siegmund, J. Heller, J. A. van Kan, and P. Tudzynski, "The NADPH oxidase complexes in *Botrytis cinerea*: evidence for a close association with the ER and the tetraspanin Pls1," *PLoS One*, vol. 8, no. 2, article e55879, 2013.

[61] J. Huang, V. Canadien, G. Y. Lam et al., "Activation of antibacterial autophagy by NADPH oxidases," *Proceedings of the National Academy of Sciences of the United States of America*, vol. 106, no. 15, pp. 6226–6231, 2009.

[62] A. Beberok, D. Wrzesniok, J. Rok, Z. Rzepka, M. Respondek, and E. Buszman, "Ciprofloxacin triggers the apoptosis of human triple-negative breast cancer MDA-MB-231 cells via the p53/Bax/Bcl-2 signaling pathway," *International journal of oncology*, vol. 52, no. 5, pp. 1727–1737, 2018.

[63] P. F. Hu, W. P. Chen, J. P. Bao, and L. D. Wu, "Paeoniflorin inhibits IL-1β-induced chondrocyte apoptosis by regulating the Bax/Bcl-2/caspase-3 signaling pathway," *Molecular Medicine Reports*, vol. 17, no. 4, pp. 6194–6200, 2018.

[64] R. Accetta, S. Damiano, A. Morano et al., "Reactive oxygen species derived from NOX3 and NOX5 drive differentiation of human oligodendrocytes," *Frontiers in cellular neuroscience*, vol. 10, 2016.

[65] C. Bucolo, A. Fidilio, C. B. M. Platania, F. Geraci, F. Lazzara, and F. Drago, "Antioxidant and osmoprotecting activity of taurine in dry eye models," *Journal of Ocular Pharmacology and Therapeutics*, vol. 34, no. 1-2, pp. 188–194, 2017.

[66] N. Froger, L. Moutsimilli, L. Cadetti et al., "Taurine: the comeback of a neutraceutical in the prevention of retinal degenerations," *Progress in Retinal and Eye Research*, vol. 41, pp. 44–63, 2014.

Hindawi
Oxidative Medicine and Cellular Longevity
Volume 2018, Article ID 9658230, 10 pages
https://doi.org/10.1155/2018/9658230

Research Article

Renoprotective Effect of Platelet-Rich Plasma on Cisplatin-Induced Nephrotoxicity in Rats

Neveen Salem,[1,2] **Nawal Helmi**,[1] **and Naglaa Assaf**[3]

[1]*Department of Applied Biochemistry, Faculty of Science, University of Jeddah, Jeddah, Saudi Arabia*
[2]*Narcotics, Ergogenic Aids and Poisons Department, Medical Research Division, National Research Centre, Giza, Egypt*
[3]*Department of Pharmacology and Toxicology, Faculty of Pharmacy, Misr University for Science and Technology, Cairo, Egypt*

Correspondence should be addressed to Neveen Salem; dr_nsalem@yahoo.com

Received 12 April 2018; Accepted 27 June 2018; Published 18 July 2018

Academic Editor: Jolanta Czuczejko

Platelet-rich plasma (PRP) has grown as an attractive biologic instrument in regenerative medicine for its powerful healing properties. It is considered as a source of growth factors that may induce tissue repairing and improve fibrosis. This product has proven its efficacy in multiple studies, but its effect on cisplatin-induced nephrotoxicity has not yet been elucidated. The present investigation was performed to estimate the protective impact of platelet-rich plasma against cisplatin- (CP-) evoked nephrotoxicity in male rats. Nephrotoxicity was induced in male Wistar rats by right uninephrectomy followed by CP administration. Uninephrectomized rats were assigned into four groups: (1) control group, (2) PRP group, (3) CP group, and (4) CP + PRP group. PRP was administered by subcapsular renal injection. Renal function, inflammatory cytokines, and growth factor level as well as histopathological investigation were carried out. Treatment with PRP attenuated the severity of CP-induced nephrotoxicity as evidenced by suppressed creatinine, blood urea nitrogen (BUN), and N-acetyl glucosaminidase (NAG) levels. Moreover, PRP depressed intercellular adhesion molecule-1 (ICAM-1), kidney injury molecule-1 (KIM-1), caspase-3, and transforming growth factor-beta 1 (TGF-β1) levels, while enhanced the epidermal growth factor (EGF) level. These biochemical results were reinforced by the histopathological investigation, which revealed restoration of normal renal tissue architectures. These findings highlight evidence for the possible protective effects of PRP in a rat model of CP-induced nephrotoxicity, suggesting a new avenue for using PRP to improve the therapeutic index of cisplatin.

1. Introduction

Cisplatin or *cis*-diamminedichloroplatinum (II) is one of the most potent antineoplastic agents used to treat a wide assortment of solid tumors, including cancers of the ovaries, testes, head, neck, bladder, cervix, and lung, children's cancers, and some cancers of the blood. It is usually given along with other anticancer drugs [1]. However, nephrotoxicity is a major adverse effect spotted after cisplatin administration. This adverse effect has restricted the clinical use of cisplatin in 25–30% of patients, even after the first dose [2].

Ognjanović et al. [3] demonstrated that cisplatin accumulates in the tubular epithelial cells of the renal proximal tubule, where it is converted to a platinum-glutathione conjugate which is a toxic metabolite and then to a cysteinyl-glycine-platinum conjugate. The latter is further transformed to metabolically reactive thiol a cysteine conjugate that acts as a promoter of cellular kidney injury. The clinical benefits of CP have been restricted due to its nephrotoxic adverse effects [4]. Therefore, creating new agents to alleviate the nephrotoxic effect of cisplatin remains a major goal.

Platelet-rich plasma (PRP) has grown as an attractive biologic instrument in regenerative medicine for its powerful healing properties. PRP is an autologous derivative of whole blood rich in active growth factors. PRP is obtained by centrifuging the blood sample and isolating the platelet-rich supernatant. Then, products such as calcium chloride or fibrinogen are used to activate PRP before application [5]. PRP can include different quantities of plasma, white blood cells, erythrocytes, and platelets according to the device and technique used. The platelet concentration should exceed baseline for whole blood concentration with a minimum

fivefold to be considered "platelet rich" [6]. PRP was found to promote tissue regeneration by enhancing cell recruitment, proliferation, and differentiation [7].

Growth factors (GFs) were found to control cell migration, differentiation, proliferation [8], and physiological functions, thereby promotes angiogenesis and tissue regeneration [9]. These GFs include platelet-derived growth factor (PDGF) which promotes type I collagen formation and enhances angiogenesis; transforming growth factor-beta 1 (TGF-β1) initiates mesenchymal stem cell proliferation and differentiation and also promotes angiogenesis. Administration of exogenous EGF enhances the regeneration and repair of renal tubule cells and accelerates the restoration of renal function [10]; vascular endothelial growth factor (VEGF) triggers chemotaxis and proliferation of endothelial cells, boosting angiogenesis, vascular hyperpermeability, and renal stem cell differentiation; basic fibroblast growth factor (b-FGF), insulin-like growth factor (IGF), adenosine triphosphate (ATP), angioprotein-2, fibronectin, osteocalcin, and thrombospondin-1 (TSP-1) are among growth factors which are released by PRP [11]. EGF promotes the growth of renal tubular cells that curbs tubular necrosis [12]. IGF is a hormone that alleviates acute tubular necrosis [13]. TGF-β1 elevates antiapoptotic Bcl-2 expression, preserves epithelial homeostasis, and prevents renal cell apoptosis [14]. VEGF protects peritubular endothelium, enhances the proliferation of tubular epithelial cells, induces angiogenesis, and promotes renal healing after ischemia [15]. Some studies demonstrated that HGF promotes renal tubular cell regeneration and leads to the repair of kidney structure and function after damage [16]. These growth factors enhance renal tubule cell regeneration, accelerate the recovery of renal function, and repair kidney structure and function after damage [10]. So, it could be anticipated that the administration of PRP as a natural cocktail of GFs to cisplatin-injured kidney would improve its recovery.

Administering growth factors in the form of PRP is better than any other ways as it is a cheap product, easily obtained, and being autologous diminishes the hazards of rejection or immune reaction. Moreover, PRP possesses an antimicrobial action as it contains leukocytes, thus lowering the risk of infection [17].

Despite the fact that PRP has demonstrated to be helpful as a regenerative product as it releases growth factors known to improve tissue damage, its impact on cisplatin-induced renal toxicity has not been previously explored. Therefore, this study was performed to estimate the protective impact of PRP on CP-evoked nephrotoxicity.

2. Materials and Methods

2.1. Experimental Animals. Fifty adult male Wistar rats (180–220 g) were obtained from the Animal House Colony of the National Research Centre (Cairo, Egypt). The animals were kept in adjusted laboratory conditions (temperature = 25 ± 1°C, humidity = 60 ± 10%, and a 12/12 h light/dark cycle). Animals had free access to standard rat chow and water. Guidelines of the Ethical Committee of National Research Centre, Egypt, were followed, which conform to the recommendations of the National Institutes of Health Guide for Care and Use of Laboratory Animals (publication number 85-23, revised 1996).

2.2. Chemicals. Cisplatin (CP) was purchased from Sigma-Aldrich (USA), whereas sodium citrate was from Egyptian International Pharmaceutical Industries Company, Cairo, Egypt.

2.3. Preparation of Platelet-Rich Plasma. 10 age-matched healthy male Wistar rats were used as PRP donors. The whole blood of rats was drawn through cardiac puncture and mixed with 3.2% sodium citrate at a blood/citrate ratio of 9/1, centrifuged at 400 ×g for 10 minutes, and the supernatant was separated and centrifuged again at 800 ×g for 10 minutes. The top 2/3 which consisted of platelet-poor plasma (PPP) was removed. The remaining layer (1/3) was separated as PRP [18]. PRP was allocated and frozen at −80°C for use. The average PRP was evaluated using a Sysmex XT-1600i system. The platelet count was 2410×10^3 platelets/μL. $CaCl_2$ 10% (0.8 mL of PRP + 0.2 mL of $CaCl_2$ 10%) was used to activate PRP immediately before its application.

2.4. Surgical Procedure. Rats were anesthetized by sodium phenobarbital (50 mg/kg IP) [19]. A right abdominal incision was done; the right renal pedicle was ligated, and a right nephrectomy was performed.

2.5. Induction of Nephrotoxicity. Ten days after nephrectomy, renal toxicity was induced in uninephrectomized rats utilizing CP (10 mg/kg) that was administered once intraperitoneally (IP) [20, 21].

2.6. Application of PRP in Uninephrectomized Nephrotoxic Rats. 24 hours after CP administration, animals were anesthetized by sodium phenobarbital (50 mg/kg IP) and a left abdominal incision was performed. The left kidney was exposed, and activated PRP was directly injected into the kidneys. Five subscapular punctures were performed distributing activated PRP (1 mL) equally over the renal surface. Following the same protocol, other groups were injected with 1 mL of saline and served as saline and positive control groups [22]. It is agreed upon that growth factors are released mainly during the first week after PRP application [11]. Two weeks was set as the end point of the experiment.

2.7. Experimental Design. 40 adult male uninephrectomized rats were gathered into four groups, 10 rats each: group (1): rats received saline (1 mL, once in the kidney), served as a normal saline control group; group (2): rats received PRP (1 mL, once in the kidney); group (3): rats received CP (10 mg/kg, once IP) to induce nephrotoxicity + saline (1 mL, once in the kidney); and group (4): rats received CP (10 mg/kg, once IP) + PRP (1 mL, once in the kidney).

2.8. Sample Collection. After two weeks, blood samples were collected through retroorbital bleeding, centrifuged at 3000 ×g for 15 min (4°C), for serum separation, and stored at −20°C as aliquots for further determinations of renal function: creatinine, blood urea nitrogen (BUN), and N-acetyl-glucosaminidase (NAG). Then, the animals were rapidly

decapitated, and the left kidneys of the rats were dissected and rinsed with 0.9% NaCl. Part of the harvested kidneys was homogenized with 0.1 M phosphate-buffered saline at pH 7.4, to give a final concentration of 10% *w*/*v*, and kept at −20°C for the biochemical determinations of intercellular adhesion molecule-1 (ICAM-1), kidney injury molecule-1 (KIM-1), caspase-3, transforming growth factor-beta 1 (TGF-β1), and epidermal growth factor (EGF). The other parts of the kidneys were stored in 10% formol-saline at 4°C for subsequent histopathological investigation.

2.9. Biochemical Analysis. Serum creatinine concentration was determined kinetically by following the method of [23]. Serum BUN was estimated using the modified Searcey method [24]. Serum NAG was measured according to Luqmani et al. [25]. Renal tissue ICAM-1, KIM-1, EGF (Assaypro, USA), caspase-3, and TGF-β1 (Glory Science, USA) were determined by utilizing the methods of solid phase enzyme-linked immunosorbent assay using rat kits according to the manufacturer's instructions.

2.10. Histopathological Investigation. Kidney samples were fixed in 10% formalin saline. The specimens were processed and stained with hematoxylin and eosin (H&E), and examined sections (10 fields for each slide) were investigated blindly under the light microscope (Leica, USA) with magnification 400x. The photos were taken by using the AmScope microscopy camera (USA). The renal sections were graded by semiquantitative scale to evaluate the degree of tubular changes. These parameters were evaluated under a 4-point scale: (−) = no alteration, (+) = 10–25% mild altered tubules, (++) = 25 to 50% moderate altered tubules, and (+++) = more than 50% severe altered tubules.

2.11. Statistical Analysis. The obtained data were statistically analyzed using SPSS statistical package V. 16 (SPSS Inc., IL, USA). Statistical analysis was performed using one-way analysis of variance (ANOVA) followed by a Tukey post hoc multiple comparison test. Difference was considered significant at $p \leq 0.05$. Results are shown as median and interquartile range (IQR).

3. Results

Three rats died during the experiment and were excluded. Two died after uninephrectomy due to postoperative complications, and the other rat which died after CP administration showed unexpected respiratory distress and reduced mobility.

3.1. PRP Ameliorates Kidney Dysfunction and Proximal Tubular Damage in CP Nephrotoxic Rats. CP administration triggered a significant elevation in serum creatinine, BUN levels, and NAG activity (700%, 203 %, and 263%, resp.) versus the control group. PRP administration depressed the levels of the aforementioned parameters (Figure 1). These data indicate the boosting effect of PRP treatment on kidney function and damage.

3.2. PRP Alleviates Kidney Injury and Suppresses Apoptotic Markers. CP injection resulted in a significant elevation in renal ICAM-1, KIM-1, and caspase-3 levels by (300%, 310%, and 512%, resp.) as compared to the control group. Meanwhile, PRP treatment counteracted these changes as indicated by significant reduction in these markers (Figure 2). These results suggest that PRP can significantly suppress inflammatory reactions and apoptotic pathway in CP-injected rats.

3.3. PRP Downregulates Renal Tissue TGF-β1 with Restoration of EGF. CP significantly elevated the renal TGF-β1 level by 2.2 folds, in addition to the significant depression of the EGF level as compared to the control group (Figure 3).

3.4. Histological Investigation. Microscopic examination of rat's kidney sections was scored and represented in Table 1. The examined sections of the control group and PRP group revealed normal structure, normal glomerular, and tubular architecture (Figures 4(a) and 4(b)). While kidney sections of rats treated with CP showed necrotic and shrunken glomeruli (20%), and some glomeruli were lobulated. Moreover, other necrotic glomeruli containing mesangial proliferative glomerulonephritis were observed (Figure 4(c)). Nephritic changes varied from degenerative to necrotic changes in some tubular epithelium besides the fact that heavy casts in the lumina of injured renal tubules were prominent (Figure 4(d)). Endotheliosis and vacuolated media of some renal blood vessels besides interstitial fibrous strands which extend to the neighboring tissue were noticed. Extravasated erythrocytes in some examined sections were seen (Figure 4(e)). Investigation of kidney sections of rat treated with CP + PRP showed that majority of renal parenchyma were apparently normal morphological structure with delicate albuminous casts within some tubules (Figure 4(f)).

4. Discussion

The present study investigates for the first time the beneficial impact of PRP on CP-induced nephrotoxicity. CP is a potent and highly effective anticancer agent used nowadays [26]. But its clinical use is limited due to its nephrotoxic side effect [27]. Increasing evidence indicates that oxidative stress, inflammatory cytokines, and apoptosis play some pivotal roles in its pathogenesis [28].

PRP is a powerful therapeutic option for its ability to deliver a great variety of biologically active GFs to the site of injury and is characterized by its simplicity, effectiveness, safety, and constant availability [29]. PRP enhances healing via the secretion of different cytokines and GFs from the alpha granules present in platelets [30]. PRP has an 8-fold increase in GF concentrations as compared to whole blood [31]. So, it could be anticipated that PRP administration as a natural cocktail of GFs with cisplatin would improve kidney recovery.

In the present study, CP administration resulted in impaired glomerular function and renal tubular damage manifested in elevated serum urea and creatinine versus the

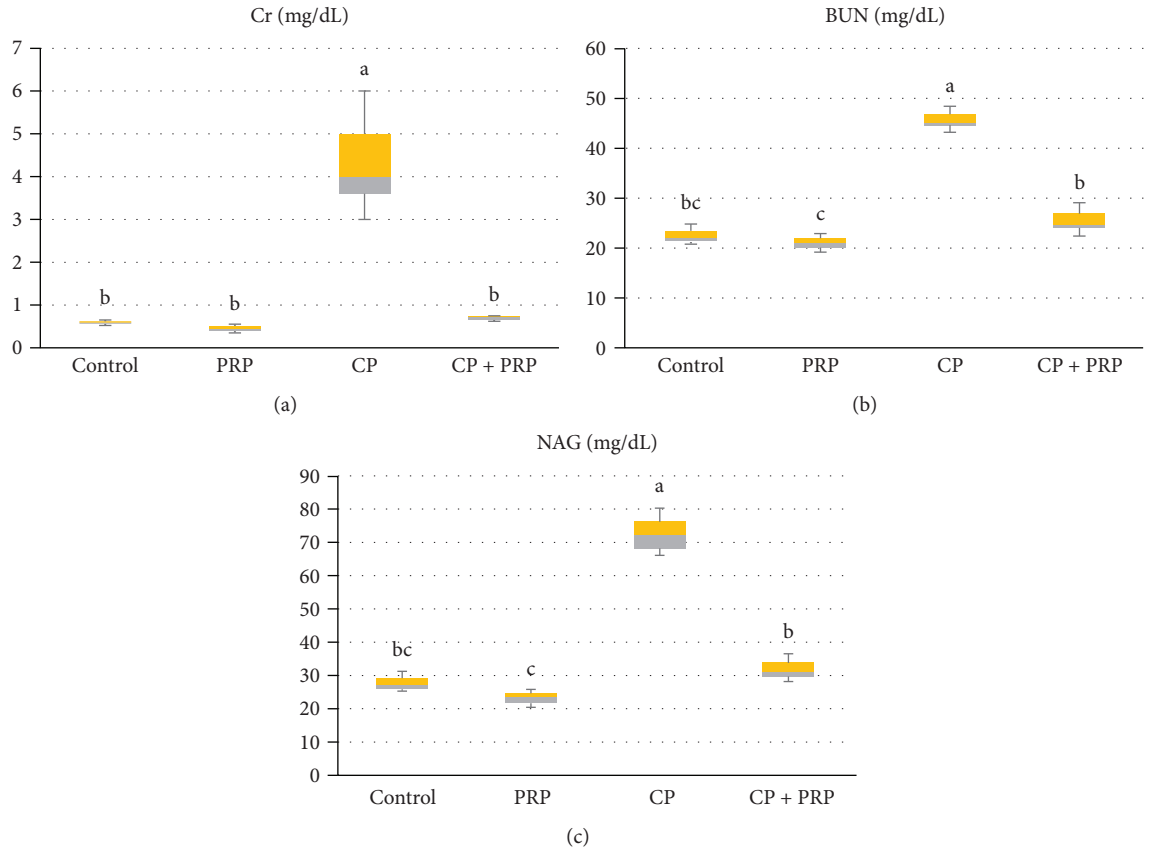

Figure 1: Box and whisker plots showing the effect of PRP administration on serum Cr, BUN, and NAG levels in CP nephrotoxic rats. (a) Creatinine level. (b) Blood urea nitrogen (BUN). (c) N-acetyl-glucosaminidase (NAG). Data are expressed as median and interquartile range. Boxes refer to the 25th (bottom) and 75th (up) percentiles, and the median is the horizontal line inside. PRP: platelet-rich plasma (2410×10^3 platelets/μL); CP: cisplatin (10 mg/kg). Treatments with different letters are significantly different at $p \leq 0.05$.

control group associated with an augmentation in the serum NAG level, which is a proximal epithelium intralysosomal membrane-bound enzyme, released when lysosomal membranes are disrupted. These data agreed with the studies of Saad and Al-Rikabi [32] and Ekor et al. [33]. CP binds to DNA, resulting in the formation of inter- and intrastrand cross-links, hence inhibiting DNA, RNA, protein synthesis, and replication in rapidly proliferating cells. These events enhance tubular damage, especially proximal tubule which receives the highest concentration of cisplatin thereby exacerbating renal insult and leading to renal toxicity, tubular injury, and cell death [34]. Cisplatin interacts with SH groups causing GSH depletion, thereby reducing the cellular antioxidant system and accumulating ROS or its products. Thus, CP initially evokes oxidative renal damage which progresses with a reduced glomerular filtration rate (GFR) and enhances tubular damage followed by morphological architectural deterioration which eventually leads to release of tissue markers in the blood [35]. PRP treatment attenuated renal dysfunction and tubular enzyme leakage as evidenced by suppression of serum creatinine, BUN, and NAG levels via activating intracellular antioxidant enzymes, mainly glutathione peroxidase enzyme (GPx). PRP releases considerable quantities of growth factors (GFs), such as hepatocyte growth factor (HGF), adenosine diphosphate (ADP), adenosine triphosphate (ATP), insulin-like growth factor-1 (IGF-1), and epidermal growth factor (EGF) [16]. These growth factors enhance renal tubule cell regeneration and renal function restoration and repair kidney structure and function after damage [10].

The current data revealed that CP ingestion upregulated inflammatory responses, kidney injury indicators, and apoptotic cascades as evidenced by elevated intercellular adhesion molecule-1 (ICAM-1), kidney injury molecule-1 (KIM-1), and apoptotic marker caspase-3. Overproduction of radicals instigates proinflammatory processes by endothelial cell injury which promotes leukocyte adhesion and infiltration. Generated ROS activates the transcription factor NF-κB, resulting in the synthesis of various proinflammatory adhesion molecules, cytokines, and chemokines such as ICAM-1 and MCP-1 which promote and activate inflammatory cell migration [36] Moreover, kidney injury molecule-1 (KIM-1) is highly expressed in proximal tubular cells following kidney injury as it is considered a specific blood biomarker for acute and chronic kidney injuries [37]. The present results also revealed a significant upregulation in apoptotic markers in the CP-treated renal tissue as indicated by elevation in caspase-3 which belongs to a family of cell death proteases involved in the activation and execution phase of apoptosis. Inflammatory signals together with

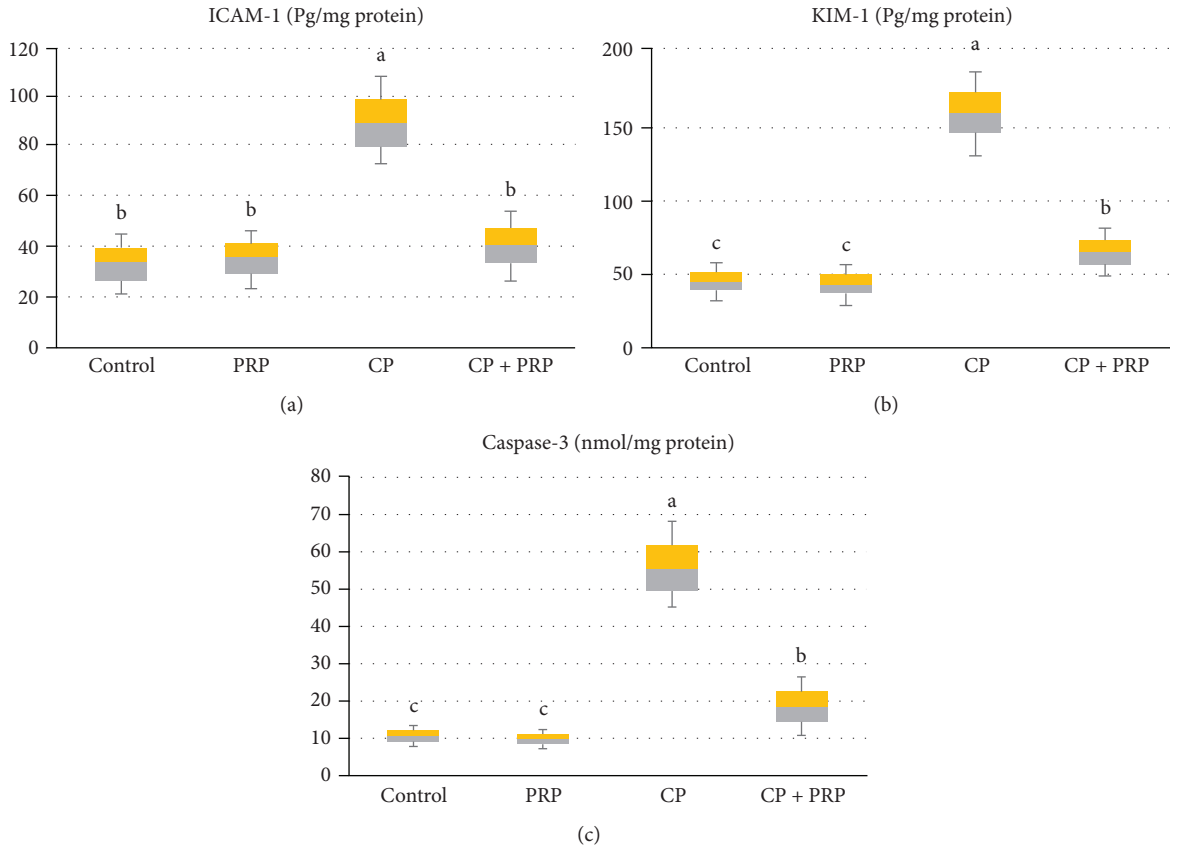

FIGURE 2: Box and whisker plots showing the effect of PRP administration on renal ICAM-1, KIM-1, and caspase-3 levels in CP nephrotoxic rats. (a) ICAM-1: intercellular adhesion molecule-1. (b) KIM-1: kidney injury molecule-1. (c) Caspase-3. Data are expressed as median and interquartile range. Boxes refer to the 25th (bottom) and 75th (up) percentiles, and the median is the horizontal line inside. PRP: platelet-rich plasma (2410×10^3 platelets/μL); CP: cisplatin (10 mg/kg). Treatments with different letters are significantly different at $p \leq 0.05$.

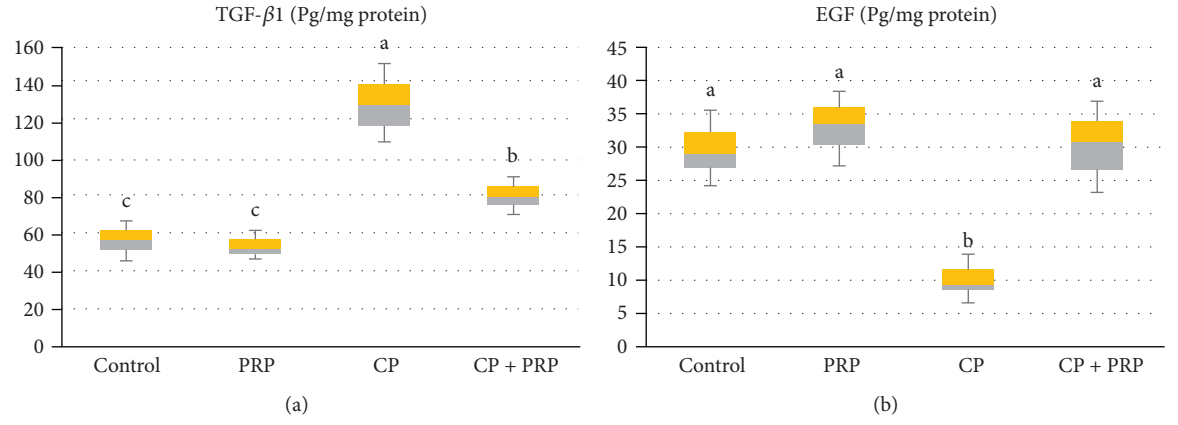

FIGURE 3: Box and whisker plots showing the effect of PRP administration on renal TGF-β1 and EGF levels in CP nephrotoxic rats. (a) TGF-β1: transforming growth factor-beta 1; EGF: epidermal growth factor. Data are expressed as median and interquartile range. Boxes refer to the 25th (bottom) and 75th (up) percentiles, and the median is the horizontal line inside. PRP: platelet-rich plasma (2410×10^3 platelets/μL); CP: cisplatin (10 mg/kg). Treatments with different letters are significantly different at $p \leq 0.05$.

oxidative stress associated with CP administration have been documented to trigger the upregulation of several genes responsible for cellular death by apoptosis [38]. Interestingly, PRP suppressed renal ICAM-1, KIM-1, and caspase-3 by enhancing the PI3K/Akt pathway which curbs ROS generation, thereby downregulating NF-κB activation and increasing resistance to oxidation [39]. Also, PRP was reported to increase the intracellular expression of the anti-inflammatory mediators (IL-4, IL-10, and IL-13) known to play a major role in inhibiting inflammation and decreasing

Table 1: Semi-quantitative scoring for renal injury in different experimental groups.

Lesion	Control	PRP	CP	CP + PRP
Necrosis of glomerular tufts	−	−	+++	−
Necrosis of renal tubules	−	−	++	−
Acute cell selling of epithelial renal tubule	−	−	+++	+
Congestion of renal blood vessels	−	−	++	−
Hemorrhages	−	−	+	−
Fibrosis	−	−	++	−
Tubular casts	−	−	+++	++

− = no alteration; + = 10–25% mild altered tubules; ++ = 25 to 50% moderate altered tubules; +++ = more than 50% severe altered tubules.

IL-1β-mediated catabolic effect [40]. Moreover, IGF-1 is one of the growth factors in PRP which activates tubular cell regeneration in acute renal failure probably by stimulating the release of growth hormones, which help in tissue repair [41], thus decreases tubular damage and preserves the integrity of the renal parenchyma, glomerular filtration rate, renal blood flow, and renal excretory function [42]. Furthermore, PRP showed antiapoptotic activities via downregulating the expression of apoptotic genes as DAPK1 and BIM mRNA [43] and inhibiting p53, Bax, and caspase-3 levels [44]. Also, HGF in PRP has been shown to interfere in the Fas pathway, thereby rescuing apoptosis in renal cells [45].

Data of the current study demonstrated that CP enhanced the level of renal TGF-β1 while lowered the EGF level. These findings coincide with previous studies [46]. The involvement of inflammatory processes has been greatly evidenced in renal injury, including expression of genes that encode proinflammatory cytokines, such as TNF-α, interleukin 6 (IL-6), IL-1β, and transforming growth factor β, which potentiate inflammation [47]. TGF-β1 causes renal fibrosis through the production of collagen-rich matrix, starting myofibroblast activation, and epithelial-myofibroblast transdifferentiation [48, 49]. TGF-β1 induces apoptosis in renal tubule cells in vitro [50] and in the kidney of transgenic mice in vivo [51]. TGF-β1 level has been observed to be augmented in ischemia/reperfusion [52]. Kidney diseases are associated with an alteration in the expression of growth factors and their receptors. For example, the level of EGF was found to be decreased following ischemia and restores its basal level during the recovery phase of ischemia/reperfusion injury [53]. Comparable alterations in the EGF level were observed in patients suffering from acute renal failure [54]. Ledeganck et al. [55] reported that cisplatin resulted in suppression in the epidermal growth factor/epidermal growth factor receptor pathway.

Conversely, PRP administration attenuated TGF-β1, while enhanced EGF. PRP possesses powerful mitogenic and chemotactic growth factors involved in initiating the healing process. HGF mediates cellular proliferation, migration, survival, and tissue regeneration. HGF and its receptor c-met are present in the liver, lung, heart, kidney, and brain [56]. HGF possesses a potent antifibrotic ability in the kidney via antagonizing TGF-beta receptor-dependent expression and other profibrotic mediators such as collagen type 1 and fibronectin. Moreover, HGF induced expression of Smad7, an inhibitor of TGF-β signaling, in a mitogen-activated protein kinase-dependent manner [57]. HGF prevents activation of interstitial fibroblasts and suppresses tubular epithelial to mesenchymal transition [41]. Epidermal growth factor (EGF) is one of the distinguished growth factors present in PRP and released upon injury. EGF enhances chemotaxis and angiogenesis of endothelial cells and mitosis of mesenchymal cells [58]. Different studies have proven that EGF promotes epithelization and markedly accelerates the healing process. Also, following EGF secretion, cytokine secretion by mesenchymal and epithelial cells is increased. EGF, HGF, and IGF-I boost DNA synthesis in regenerating proximal tubule [59].

Histopathological investigation in this study confirmed the abovementioned biochemical analysis which demonstrated that nephrotic changes varied from degenerative to necrotic changes in some tubular epithelium besides lobulation of glomerular tuft which was common after CP treatment. Moreover, intense albuminous or hyaline casts were detected inside the lumina of the collecting tubules. These findings were confirmed in [60] which revealed CP-induced massive degenerative changes in 50–75% of glomeruli and renal tubules by mechanisms such as oxidative stress and apoptosis. While the CP + PRP-treated group in this study showed that majority of renal parenchyma restore apparently normal renal tissues (accelerated regeneration) with few delicate albuminous casts as compared to the CP group.

Concerning PRP clinical feasibility, PRP therapy is safe given its autologous nature and long-term usage without any reported major complications. For this reason, in addition to its easy availability, it is readily used in clinical and surgical settings such as plastic and maxillofacial surgery, dentistry, and orthopedics [61]. Moreover, it is routinely used in some centers to treat bone fractures, as an aid in dental implants and prosthesis, and to treat diabetic ulcers and dry eye in Sjögren's syndrome [62]. However, limitation in evaluating the clinical effects of PRP is variation in established preparation protocols. An additional variation in the PRP product results from patient differences in age, medical comorbidities, and healing capabilities [63]. Continued basic science research elucidating the downstream effects of PRP can help drive clinical research and develop clinical recommendations for the use of PRP.

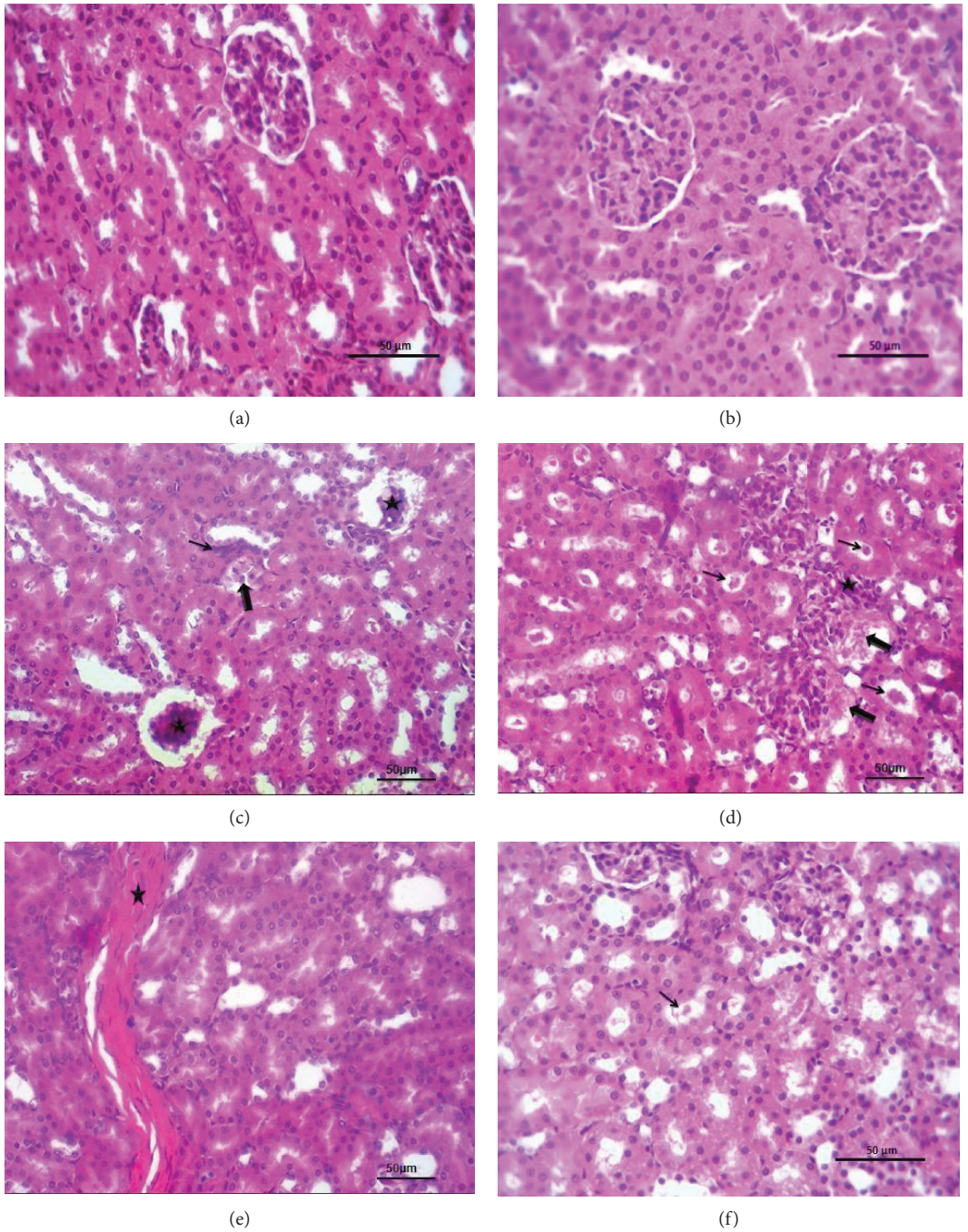

Figure 4: Effect of PRP administration on renal histopathology in CP nephrotoxic rats. Photomicrographs of sections from rat renal tissues. (a) Control group rats received saline showing normal histomorphological architectures. (b) PRP group rats received 1 m PRP elicited no histologic modification. (c, d, e) CP group rats received CP (10 mg/kg) showing (c) necrotic and shrunken glomerular tufts (star), minute peritubular spindle cells (thin arrow) beside sloughed tubular epithelium (thick arrow). (d) Necrotic areas (thick arrow) beside mesangial proliferative glomerulonephritis (star) and numerous casts in injured renal tubule lumina (thin arrow). (e) Interstitial fibrous streaks in corticomedullary junctions (star). (f) CP + PRP group showing a few delicate tubular casts (arrow) within the apparently normal renal tissues. Hematoxylin and eosin staining. Scale bar = 50 μm.

5. Conclusions

Our findings highlight evidences for the protective effects of PRP in a rat model of CP-induced nephrotoxicity. These effects were mediated through suppressing inflammatory mediators, boosting renal antioxidant defense, curbing apoptosis, accelerating the recovery of renal function, and repairing kidney structures after damage. Collectively, this study could open a new avenue for using PRP to improve the therapeutic index of cisplatin.

Data Availability

The data used to support the findings of this study are available from the corresponding author upon request.

Additional Points

Highlights. (i) Platelet-rich plasma protects against cisplatin-induced nephrotoxicity in a rat model. (ii) PRP suppresses inflammatory mediators, boosts renal antioxidant defense, and curbs apoptosis. (iii) Also, it accelerates the recovery of renal function and repairs kidney structure after damage induced by cisplatin.

Conflicts of Interest

The authors declare that there are no competing interests associated with the manuscript.

Authors' Contributions

Neveen Salem contributed to the conceptualization of the study, study design, manuscript editing, and resources and supervised the experiment and manuscript writing. Naglaa Assaf and Nawal Helmi contributed to the conceptualization of the study, study design, and manuscript editing.

Acknowledgments

The authors would like to thank Abdelmoniem A. Ali, prof. of pathology, and Naif A. Algabri, assistant lecturer of pathology in Faculty of Veterinary Medicine, Zagazig University, for their cooperation.

References

[1] Z. Rajaei, Z. Keshavarzi, M. G. Shirazi, V. Toosi, and M.-A.-R. Hadjzadeh, "Effect of aqueous extract of *Rheum ribes* on cisplatin-induced nephrotoxicity in rat," *Journal of Pharmacy & Bioallied Sciences*, vol. 5, no. 4, pp. 309–313, 2013.

[2] M. S. El-Gerbed, "Ameliorative effect of fish oil on the cisplatin induced hepatotoxicity and nephrotoxicity in rats," *Research Journal of Pharmaceutical, Biological and Chemical Sciences*, vol. 4, pp. 479–491, 2013.

[3] B. I. Ognjanović, N. Z. Djordjević, M. M. Matić et al., "Lipid peroxidative damage on cisplatin exposure and alterations in antioxidant defense system in rat kidneys: a possible protective effect of selenium," *International Journal of Molecular Sciences*, vol. 13, no. 2, pp. 1790–1803, 2012.

[4] A. Naqshbandi, W. Khan, S. Rizwan, and F. Khan, "Studies on the protective effect of flaxseed oil on cisplatin-induced hepatotoxicity," *Human & Experimental Toxicology*, vol. 31, no. 4, pp. 364–375, 2012.

[5] J. W. Lee, O. H. Kwon, T. K. Kim et al., "Platelet-rich plasma: quantitative assessment of growth factor levels and comparative analysis of activated and inactivated groups," *Archives of Plastic Surgery*, vol. 40, no. 5, pp. 530–535, 2013.

[6] L. Brass, "Understanding and evaluating platelet function," *Hematology*, vol. 2010, no. 1, pp. 387–396, 2010.

[7] A. Nurden, "Platelets, inflammation and tissue regeneration," *Thrombosis and Haemostasis*, vol. 105, Supplement 6, pp. S13–S33, 2011.

[8] D. J. Sánchez-González, C. A. Sosa-Luna, and I. Vásquez-Moctezuma, "Transfer factors in medical therapy," *Medicina Clínica*, vol. 137, no. 6, pp. 273–277, 2011.

[9] D. N. Lyras, K. Kazakos, D. Verettas et al., "The influence of platelet-rich plasma on angiogenesis during the early phase of tendon healing," *Foot & Ankle International*, vol. 30, no. 11, pp. 1101–1106, 2009.

[10] J. Norman, Y. K. Tsau, A. Bacay, and L. G. Fine, "Epidermal growth factor accelerates functional recovery from ischaemic acute tubular necrosis in the rat: role of the epidermal growth factor receptor," *Clinical Science*, vol. 78, no. 5, pp. 445–450, 1990.

[11] D. J. Sánchez-González, E. Méndez-Bolaina, and N. I. Trejo-Bahena, "Platelet-rich plasma peptides: key for regeneration," *International Journal of Peptides*, vol. 2012, Article ID 532519, 10 pages, 2012.

[12] S. He, N. Liu, G. Bayliss, and S. Zhuang, "EGFR activity is required for renal tubular cell dedifferentiation and proliferation in a murine model of folic acid-induced acute kidney injury," *American Journal of Physiology-Renal Physiology*, vol. 304, no. 4, pp. F356–F366, 2013.

[13] Y. Yang, M. Song, Y. Liu et al., "Renoprotective approaches and strategies in acute kidney injury," *Pharmacology & Therapeutics*, vol. 163, pp. 58–73, 2016.

[14] Q. Guan, C. Y. C. Nguan, and C. Du, "Expression of transforming growth factor-β1 limits renal ischemia-reperfusion injury," *Transplantation*, vol. 89, no. 11, pp. 1320–1327, 2010.

[15] F. Liu, Y.-L. Lou, J. Wu et al., "Upregulation of microRNA-210 regulates renal angiogenesis mediated by activation of VEGF signaling pathway under ischemia/perfusion injury in vivo and in vitro," *Kidney & Blood Pressure Research*, vol. 35, no. 3, pp. 182–191, 2012.

[16] K. Matsumoto and T. Nakamura, "Hepatocyte growth factor: renotropic role and potential therapeutics for renal diseases," *Kidney International*, vol. 59, no. 6, pp. 2023–2038, 2001.

[17] A. Cieslik-Bielecka, T. Bielecki, T. S. Gazdzik, J. Arendt, W. Krol, and T. Szczepanski, "Autologous platelets and leukocytes can improve healing of infected high-energy soft tissue injury," *Transfusion and Apheresis Science*, vol. 41, no. 1, pp. 9–12, 2009.

[18] J. M. Pazzini, A. B. De Nardi, R. R. Huppes et al., "Method to obtain platelet-rich plasma from rabbits (*Oryctolagus cuniculus*)," *Pesquisa Veterinária Brasileira*, vol. 36, no. 1, pp. 39–44, 2016.

[19] M. Tomita, H. Sogabe, S. Nakazato et al., "Monoclonal antibody 1-22-3-induced glomerulonephritis in uninephrectomized rats as a model of progressive renal failure," *Nephrology Dialysis Transplantation*, vol. 20, no. 11, pp. 2358–2367, 2005.

[20] E. A. Salem, N. A. Salem, A. M. Maarouf, E. C. Serefoglu, and W. J. G. Hellstrom, "Selenium and lycopene attenuate cisplatin-induced testicular toxicity associated with oxidative stress in Wistar rats," *Urology*, vol. 79, no. 5, pp. 1184.e1–1184.e6, 2012.

[21] H.-J. Kim, D. J. Park, J. H. Kim et al., "Glutamine protects against cisplatin-induced nephrotoxicity by decreasing cisplatin accumulation," *Journal of Pharmacological Sciences*, vol. 127, no. 1, pp. 117–126, 2015.

[22] O. Martín-Solé, J. Rodó, L. García-Aparicio, J. Blanch, V. Cusí, and A. Albert, "Effects of platelet-rich plasma (PRP) on a model of renal ischemia-reperfusion in rats," *PLoS One*, vol. 11, no. 8, article e0160703, 2016.

[23] R. J. Henry, "Clinical chemistry, principles and technique," Harper and Row, New York, NY, USA, 2nd edition, 1974.

[24] R. I. Searcey, J. I. Reardon, and J. A. Forenam, "Enzymatic urea kits," *The American Journal of Medical Technology*, vol. 33, pp. 15–20, 1967.

[25] Y. Luqmani, L. Temmim, A. Memon et al., "Measurement of serum N-acetyl β-glucosaminidase activity in patients with breast cancer," *Acta Oncologica*, vol. 38, no. 5, pp. 649–653, 1999.

[26] T. Boulikas and M. Vougiouka, "Recent clinical trials using cisplatin, carboplatin and their combination chemotherapy drugs (review)," *Oncology Reports*, vol. 11, no. 3, pp. 559–595, 2004.

[27] G. Mattheolabakis, E. Taoufik, S. Haralambous, M. L. Roberts, and K. Avgoustakis, "In vivo investigation of tolerance and antitumor activity of cisplatin-loaded PLGA-mPEG nanoparticles," *European Journal of Pharmaceutics and Biopharmaceutics*, vol. 71, no. 2, pp. 190–195, 2009.

[28] Q. Huang, Dunn RT2nd, S. Jayadev et al., "Assessment of cisplatin-induced nephrotoxicity by microarray technology," *Toxicological Sciences*, vol. 63, no. 2, pp. 196–207, 2001.

[29] J. P. Frechette, I. Martineau, and G. Gagnon, "Platelet-rich plasmas: growth factor content and roles in wound healing," *Journal of Dental Research*, vol. 84, no. 5, pp. 434–439, 2005.

[30] R. E. Marx, "Platelet-rich plasma (PRP): what is PRP and what is not PRP?," *Implant Dentistry*, vol. 10, no. 4, pp. 225–228, 2001.

[31] B. L. Eppley, J. E. Woodell, and J. Higgins, "Platelet quantification and growth factor analysis from platelet-rich plasma: implications for wound healing," *Plastic and Reconstructive Surgery*, vol. 114, no. 6, pp. 1502–1508, 2004.

[32] S. Y. Saad and A. C. Al-Rikabi, "Protection effects of taurine supplementation against cisplatin-induced nephrotoxicity in rats," *Chemotherapy*, vol. 48, no. 1, pp. 42–48, 2002.

[33] M. Ekor, G. O. Emerole, and E. O. Farombi, "Phenolic extract of soybean (*Glycine max*) attenuates cisplatin-induced nephrotoxicity in rats," *Food and Chemical Toxicology*, vol. 48, no. 4, pp. 1005–1012, 2010.

[34] D. Wang and S. J. Lippard, "Cellular processing of platinum anticancer drugs," *Nature Reviews Drug Discovery*, vol. 4, no. 4, pp. 307–320, 2005.

[35] A. Karadeniz, N. Simsek, E. Karakus et al., "Royal jelly modulates oxidative stress and apoptosis in liver and kidneys of rats treated with cisplatin," *Oxidative Medicine and Cellular Longevity*, vol. 2011, Article ID 981793, 10 pages, 2011.

[36] H. Zhou, A. Kato, T. Miyaji et al., "Urinary marker for oxidative stress in kidneys in cisplatin-induced acute renal failure in rats," *Nephrology Dialysis Transplantation*, vol. 21, no. 3, pp. 616–623, 2006.

[37] V. S. Sabbisetti, S. S. Waikar, D. J. Antoine et al., "Blood kidney injury molecule-1 is a biomarker of acute and chronic kidney injury and predicts progression to ESRD in type I diabetes," *Journal of the American Society of Nephrology*, vol. 25, no. 10, pp. 2177–2186, 2014.

[38] G. P. Kaushal, V. Kaushal, X. Hong, and S. V. Shah, "Role and regulation of activation of caspases in cisplatin-induced injury to renal tubular epithelial cells," *Kidney International*, vol. 60, no. 5, pp. 1726–1736, 2001.

[39] S. Lee, S.-O. Moon, W. Kim et al., "Protective role of L-2-oxothiazolidine-4-carboxylic acid in cisplatin-induced renal injury," *Nephrology Dialysis Transplantation*, vol. 21, no. 8, pp. 2085–2095, 2006.

[40] M. Moussa, D. Lajeunesse, G. Hilal et al., "Platelet rich plasma (PRP) induces chondroprotection via increasing autophagy, anti-inflammatory markers, and decreasing apoptosis in human osteoarthritic cartilage," *Experimental Cell Research*, vol. 352, no. 1, pp. 146–156, 2017.

[41] A. Moghadam, T. T. Khozani, A. Mafi, M. R. Namavar, and F. Dehghani, "Effects of platelet-rich plasma on kidney regeneration in gentamicin-induced nephrotoxicity," *Journal of Korean Medical Science*, vol. 32, no. 1, pp. 13–21, 2017.

[42] P. D. Sanchez-Gonzalez, F. J. Lopez-Hernandez, F. Perez-Barriocanal, A. I. Morales, and J. M. Lopez-Novoa, "Quercetin reduces cisplatin nephrotoxicity in rats without compromising its anti-tumour activity," *Nephrology Dialysis Transplantation*, vol. 26, no. 11, pp. 3484–3495, 2011.

[43] Y. Fukaya, M. Kuroda, Y. Aoyagi et al., "Platelet-rich plasma inhibits the apoptosis of highly adipogenic homogeneous preadipocytes in an in vitro culture system," *Experimental & Molecular Medicine*, vol. 44, no. 5, pp. 330–339, 2012.

[44] C. Jia, Y. Lu, B. Bi et al., "Platelet-rich plasma ameliorates senescence-like phenotypes in a cellular photoaging model," *RSC Advances*, vol. 7, no. 6, pp. 3152–3160, 2017.

[45] J. B. Kopp, "Hepatocyte growth factor: mesenchymal signal for epithelial homeostasis," *Kidney International*, vol. 54, no. 4, pp. 1392-1393, 1998.

[46] Y. Topcu-Tarladacalisir, M. Sapmaz-Metin, and T. Karaca, "Curcumin counteracts cisplatin-induced nephrotoxicity by preventing renal tubular cell apoptosis," *Renal Failure*, vol. 38, no. 10, pp. 1741–1748, 2016.

[47] M. R. Daha and C. van Kooten, "Is the proximal tubular cell a proinflammatory cell?," *Nephrology Dialysis Transplantation*, vol. 15, Supplement 6, pp. 41–43, 2000.

[48] E. P. Böttinger and M. Bitzer, "TGF-β signaling in renal disease," *Journal of the American Society of Nephrology*, vol. 13, no. 10, pp. 2600–2610, 2002.

[49] J. M. Pérez-Rojas, C. Cruz, P. García-López et al., "Renoprotection by α-mangostin is related to the attenuation in renal oxidative/nitrosative stress induced by cisplatin nephrotoxicity," *Free Radical Research*, vol. 43, no. 11, pp. 1122–1132, 2009.

[50] G. Nowak and R. G. Schnellmann, "Autocrine production and TGF-beta 1-mediated effects on metabolism and viability in renal cells," *American Journal of Physiology-Renal Physiology*, vol. 271, no. 3, pp. F689–F697, 1996.

[51] N. Sanderson, V. Factor, P. Nagy et al., "Hepatic expression of mature transforming growth factor beta 1 in transgenic mice results in multiple tissue lesions," *Proceedings of the National Academy of Sciences of the United States of America*, vol. 92, no. 7, pp. 2572–2576, 1995.

[52] R. Hirschberg and H. Ding, "Growth factors and acute renal failure," *Seminars in Nephrology*, vol. 18, pp. 191–207, 1998.

[53] R. P. Schaudies, D. Nonclercq, L. Nelson et al., "Endogenous EGF as a potential renotrophic factor in ischemia-induced acute renal failure," *American Journal of Physiology-Renal Physiology*, vol. 265, no. 3, pp. F425–F434, 1993.

[54] T. Taira, A. Yoshimura, K. Iizuka, S. Iwasaki, T. Ideura, and S. Koshikawa, "Urinary epidermal growth factor levels in

patients with acute renal failure," *American Journal of Kidney Diseases*, vol. 22, no. 5, pp. 656–661, 1993.

[55] K. J. Ledeganck, G. A. Boulet, J. J. Bogers, G. A. Verpooten, and B. Y. de Winter, "The TRPM6/EGF pathway is downregulated in a rat model of cisplatin nephrotoxicity," *PLoS One*, vol. 8, no. 2, article e57016, 2013.

[56] R. A. Hurle, G. Davies, C. Parr et al., "Hepatocyte growth factor/scatter factor and prostate cancer: a review," *Histology and Histopathology*, vol. 20, no. 4, pp. 1339–1349, 2005.

[57] M. N. Shukla, J. L. Rose, R. Ray, K. L. Lathrop, A. Ray, and P. Ray, "Hepatocyte growth factor inhibits epithelial to myofibroblast transition in lung cells via Smad7," *American Journal of Respiratory Cell and Molecular Biology*, vol. 40, no. 6, pp. 643–653, 2009.

[58] S. Barrientos, O. Stojadinovic, M. S. Golinko, H. Brem, and M. Tomic-Canic, "Perspective article: growth factors and cytokines in wound healing," *Wound Repair and Regeneration*, vol. 16, no. 5, pp. 585–601, 2008.

[59] J. Berlanga-Acosta, J. Gavilondo-Cowley, P. López-Saura et al., "Epidermal growth factor in clinical practice – a review of its biological actions, clinical indications and safety implications," *International Wound Journal*, vol. 6, no. 5, pp. 331–346, 2009.

[60] S. K. Nigam and W. Lieberthal, "Acute renal failure. III. The role of growth factors in the process of renal regeneration and repair," *American Journal of Physiology-Renal Physiology*, vol. 279, no. 1, pp. F3–F11, 2000.

[61] W. Li, M. Enomoto, M. Ukegawa et al., "Subcutaneous injections of platelet-rich plasma into skin flaps modulate proangiogenic gene expression and improve survival rates," *Plastic and Reconstructive Surgery*, vol. 129, no. 4, pp. 858–866, 2012.

[62] U. Sheth, N. Simunovic, G. Klein et al., "Efficacy of autologous platelet-rich plasma use for orthopaedic indications: a meta-analysis," *The Journal of Bone and Joint Surgery-American Volume*, vol. 94, no. 4, pp. 298–307, 2012.

[63] E. L. Matz, A. M. Pearlman, and R. P. Terlecki, "Safety and feasibility of platelet rich fibrin matrix injections for treatment of common urologic conditions," *Investigative and Clinical Urology*, vol. 59, no. 1, pp. 61–65, 2018.

Hindawi
Oxidative Medicine and Cellular Longevity
Volume 2018, Article ID 7671850, 9 pages
https://doi.org/10.1155/2018/7671850

Research Article

Analysis of Plasma MicroRNAs as Predictors and Biomarkers of Aging and Frailty in Humans

Iryna Rusanova,[1,2] **María E. Diaz-Casado**,[1] **Marisol Fernández-Ortiz**,[1] **Paula Aranda-Martínez**,[1] **Ana Guerra-Librero**,[1] **Francisco J. García-García**,[3] **Germaine Escames**,[1,2] **Leocadio Mañas**,[4] **and Darío Acuña-Castroviejo**[1,2,5]

[1]*Departamento de Fisiología, Facultad de Medicina, Centro de Investigación Biomédica, Parque Tecnológico de Ciencias de la Salud, Universidad de Granada, Granada, Spain*
[2]*CIBERfes, ibs.Granada, Granada, Spain*
[3]*CIBERfes, División de Medicina Geriátrica, Hospital Virgen del Valle, Complejo Hospitalario de Toledo, Toledo, Spain*
[4]*CIBERfes, Servicio de Geriatría, Hospital Universitario de Getafe, Madrid, Spain*
[5]*UGC de Laboratorios Clínicos, Complejo Hospitalario de Granada, Granada, Spain*

Correspondence should be addressed to Iryna Rusanova; irusanova@ugr.es and Darío Acuña-Castroviejo; dacuna@ugr.es

Received 15 April 2018; Accepted 26 June 2018; Published 18 July 2018

Academic Editor: Przemko Tylzanowski

Although circulating microRNAs (miRNAs) can modulate gene expression and affect immune system response, little is known about their participation in age-associated frailty syndrome and sarcopenia. The aim of this study was to determine miRNAs as possible biomarkers of age and frailty and their correlation with oxidative and inflammatory state in human blood. Three inflammation-related miRNAs (miR-21, miR-146a, and miR-223) and one miRNA related with the control of melatonin synthesis (miR-483) were analyzed. Twenty-two healthy adults, 34 aged robust, and 40 aged fragile patients were selected for this study. The expression of plasma miRNAs was assessed by RT-qPCR; plasma cytokines (IL-6, IL-8, IL-10, and TNFα) were analyzed by commercial kits, and plasma advanced oxidation protein products (AOPP) and lipid oxidation (LPO) were spectrophotometrically measured. Fragile subjects had higher miR-21 levels than control subjects, whereas miR-223 and miR-483 levels increased at a similar extend in both aged groups. All cytokines measured increased in aged groups compared with controls, without differences between robust and fragile subjects. The fragile group had a TNFα/IL-10 ratio significantly higher than robust and control groups. Aged groups also had higher AOPP and LPO levels than controls. Women presented higher AOPP and LPO levels and increased expression of miR-483 compared with men. Positive correlations between miR-21 and AOPP and between miR-483 and IL-8 were detected. The expression of miR-21 and the TNFα/IL-10 ratio were correlated positively with the presence of frailty, which suggests that these markers can be considered as possible biomarkers for age-related frailty.

1. Introduction

One reason that aging is emerging as a key policy issue is that both the proportion and absolute number of older people in populations around the world are increasing dramatically. Aging is a global problem affecting both developed and developing countries. According with the World Health Organization report of 2015, the older adult population in sub-Saharan Africa is expected to grow faster than anywhere else, increasing from 46 million in 2015 to 157 million by 2050 [1]. In terms of life expectancy at birth, the EU is a world leader, and according to "*The 2015 Ageing Report*" by European Commission, the life expectancy at birth for males is expected to increase by 7.1 years from 2013 to 2060 period, reaching 84.8 in 2060 [2]. For females, it is projected to increase by 6.0 years, reaching 89.1 in 2060. As a result, the demographic old-age dependency ratio (people aged 65 or above relative to those aged 15–64) is projected to

Table 1: Characteristics of the studied subjects.

Item	Control group	Aged without frailty	Aged with frailty
Number of subjects	22	34	40
Age	20.5 ± 2.4	76.6 ± 5.3	84.4 ± 5.6
Gender (male/female)			
Male	19 (86%)	12 (35%)	13 (33%)
Female	3 (14%)	22 (65%)	27 (67%)
<80 years old (M/F)	0	24 (10/14)	8 (2/6)
≥80 years old (M/F)	0	10 (2/8)	32 (11/21)
Physical activity	n.m.	79.69 ± 8.05	$10.77 \pm 2.76^{\#\#\#}$
Physical dependence	0%	$12\%^{***}$	$75\%^{\#\#\#}$
Hypertension	0%	$38\%^{***}$	$32\%^{***}$

Age and physical activity are expressed as the means ± SEM. M/F: male/female; n.m.: not measured. $^{***}P < 0.001$ versus the control group; $^{\#\#\#}P < 0.001$ versus aged without frailty.

increase from 27.8% to 50.1% in the EU as a whole over the mentioned period. Similar changes are expected in many other countries.

Apart from the usual age-related diseases, progressive loss of muscle mass and function associated with aging limits the physical capabilities of the older population and increases the cost of health care by the public health system. This age-related muscle wasting has been termed sarcopenia. The preliminary concept of sarcopenia as an age-related loss of muscle mass and function [3] was updated in 2010 by the European Working Group on Sarcopenia in Older People (EWGSOP) focus on a generalized loss of muscle mass and strength with the risk of physical disability, poor quality of life, and death [4].

Sarcopenia is one of the manifestations of frailty, a clinical condition of aged adults that increases risk for poor health outcomes including falls, disabilities, hospitalization, and death [5]. Clinical features of frailty are related to chronic inflammation associated to the age (inflammaging), oxidative stress, mitochondrial dysfunction, insulin resistance, aging-related loss of anabolic hormones, diminished strength, and tolerance to physical activity [6]. The prevalence of frailty of adults aged 65 and older is 12% in the USA, increasing up 25% in the group of 85 years or older [7]. Similar data have been reported in other countries including the European Union [2].

Circulating noncoding RNAs (miRNAs) are small RNA molecules that, depending upon base pairing to mRNA, mediate mRNA cleavage, translational repression, or mRNA destabilization [8, 9]. miRNAs or miRs are involved in crucial cellular processes, and their deregulation has been described in different diseases, including aging, sarcopenia, and age-related musculoskeletal impairments [10–12]. Due to the role of some miRNAs to promote inflammation, changes in expression of miRNAs throughout life, and their easily measurement in blood, it is suggested that miRNAs may be candidates for an early diagnosis of frailty in the elderly.

Thus, as a potential noninvasive method to study frailty, we consider it worthwhile the determination of some miRNA levels in blood and analyze whether changes in circulating miRNAs correlate with oxidative stress and inflammation during aging and frailty. We determined miR-21, miR-146a, and miR-223, three miRNAs related with inflammation, and miR-483, which is related with the control of melatonin synthesis, the hormone with anti-aging properties [13].

2. Materials and Methods

2.1. Participants. Control samples were collected from healthy volunteers. Samples from frailty and nonfrailty aged groups of subjects were obtained from the cohort of the Toledo study for healthy aging, whose characterization was published elsewhere [14]. The participants in the study were classified into three groups: young healthy group (control), aged healthy group (robust), and aged fragile group (fragile) (Table 1). Informed consent was obtained from all subjects and from the Hospital Ethical Committee, according to the 1983 revised Helsinki Declaration of 1975. The final study was approved by the Andalusian Ethical Committee (ref. CEEA: 462-CEEA-2013). The diagnosis of frailty in aged population was based on the Fried criteria (weakness, low speed, low physical activity, exhaustion, and weight loss) [15]. As an indirect measurement of sarcopenia, a hand grip strength test was used [16].

2.2. Assessment of Frailty and Physical Performance. The Fried criteria used for diagnosis of frailty are described as follows [15]: weakness is defined as the worse quintile of maximum strength on the dominant hand adjusted for sex and body mass index (kg/m^2), strength was measured with a Jaymar hydraulic dynamometer, according to the standards of the Hispanic EPESE, weight was measured with a SECA precision scale, and height was measured with a stadiometer on a wall without a skirting board [17]. Physical performance was assessed with the following criteria: (1) low energy, subjects were classified as having "low energy" when they provided a positive answer to any of the following two questions from the CES-D (Center for Epidemiologic Studies Depression Scale) [18]: "I felt that anything I did was a big effort" and "I felt that I could not keep on doing things" at least 3 to 4 days a week; (2) slowness, defined as the worse

quintile in the three-meter walking speed test, adjusted for sex and height according to the standards of the Short Physical Performance Battery [19]; and (3) weight loss, defined as unintentional weight loss of 4.5 kg or more in the last year. One point was assigned to each variable and built a score as the sum of points for all of them. According to this score, aged subjects were classified as nonfrail or robust (0 points), prefrail (1-2 points), and fragile (≥3 points). For this study, we used samples of robust and fragile patients only. The data of physical activity of the patients were obtained with the Physical Activity Scale for the Elderly (PASE). This questionnaire was specifically developed to assess the physical activity in epidemiological studies in people ≥ 65 years [20]. Physical dependence was evaluated based on measures reflecting the personal persuasion of need of help for the accomplishment of activities of daily living. The information about the presence of hypertension was based on medical diagnosis.

2.3. Samples. Blood samples (10 mL) were collected from the antecubital vein between 8:00 and 9:00 a.m. after 8–10 hours of fasting. The samples were collected in vacutainer tubes with EDTA-K_2. Blood was centrifuged at 1900 ×g for 10 min at 4°C, and plasma and erythrocytes were separated. Aliquots of plasma were transferred into RNase-free microcentrifuge tubes and stored at −80°C until the assays were performed. Once thawed, 250 μL of all plasma samples was centrifuged at 16000 ×g at 4°C for 10 min to remove cryoprecipitates. 100 μL of plasma supernatants was used for miRNA isolation.

2.4. Plasma miRNA Profiling and Data Analysis. Plasma miRNAs were extracted using the miRNeasy Serum/Plasma Kit (Qiagen, Werfen España, Barcelona, Spain) by following the manufacturer's instructions. Reverse transcription of the microRNAs into cDNA was done with the TaqMan MicroRNA Reverse Transcription Kit (Life Technologies, Thermo Fisher Scientific, Madrid, Spain) and TaqMan microRNA assays specific for miR-21, miR-146a, miR-223, miR-483, and U6 (Applied Biosystems, Thermo Fisher Scientific, Madrid, Spain) according to the manufacturer's recommendations. PCR was performed in 15 μL reaction mixtures using the MJ Mini Personal Thermal Cycler (Bio-Rad Laboratories, S.A., Madrid, Spain). The samples were subjected to thermal cycling parameters of 30 min at 16°C, 30 min at 42°C, and 5 min at 85°C and then kept at 4°C. Real-time PCR reaction was performed in a final volume of 20 μL, containing 1.33 μL of cDNA, 10 μL of TaqMan Universal Master Mix II with no UNG (Life Technologies, Thermo Fisher Scientific, Madrid, Spain), 7.67 μL of RNase-free water, and 1 μL of TaqMan microRNA probe specific for each examined microRNAs (Life Technologies). The cycling conditions were as follows: initial denaturation at 50°C for 2 minutes, followed by enzyme activation at 95°C for 10 minutes, and 40 cycles of 95°C for 15 seconds and 60°C for 1 minute. PCR was performed using an Agilent Technologies Stratagene Mx3005P System (Life Technologies, Thermo Fisher Scientific, Madrid, Spain). All real-time PCR reactions were performed in triplicate. After the reaction, the threshold cycle values were determined using fixed threshold settings. When the average of miRNA expression was ≥35 C_t, it was not included in analysis. Data were analyzed using the SDS 2.3 and RQ Manager 1.2 software packages (Life Technologies), and relative gene expression was generated using the $2^{-\Delta\Delta CT}$ method (ΔC_t target gene − ΔC_t control gene). All miRNAs were calibrated against spike-in control miR-39 (external control). As there is no consensus on endogenous stable miRNAs in the circulation for normalization and quantification of circulating miRNAs, the expression levels were normalized both against U6 snRNA (internal control) and against the average C_t of the control group (general normalization) [21, 22].

2.5. Determination of Advanced Oxidation Protein Products. Advanced oxidation protein products (AOPPs) were measured spectrophotometrically on a microplate reader. Samples were calibrated with chloramine-T solution that in the presence of potassium iodide absorb at 340 nm [23]. 200 μL of plasma diluted 1/5 in PBS, 10 μL of PBS, and 20 μL of concentrated acetic acid were added to sample wells. The standard curve was made with 10 μL of 1.16 M potassium iodide, 200 μL of chloramine-T solution (0–100 nmol/mL), and 20 μL acetic acid. The absorbance of the reaction mixture was immediately read at 340 nm on a microplate reader against a blank containing 200 μL PBS, 10 μL potassium iodide, and 20 μL of acetic acid. The AOPP concentration was expressed in nmol/mL of chloramine-T equivalents.

2.6. Determination of Lipid Peroxidation. Plasma samples were thawed and centrifuged at 5000g x 5 min at 5°C, and 200 μL of the supernatants were used for lipid peroxidation (LPO) measurement. For this purpose, a commercial LPO assay kit that estimates both malondialdehyde and 4-hydroxyalkenals was used (Bioxytech LPO-586 assay kit, Oxis Research, CA, USA). Absorbance was read at 586 nm, and lipid peroxidation concentration was expressed in nmol/mL [24].

2.7. Measurement of Plasma Cytokines. The Affymetrix's ProcartaPlex Simplex Kits refs EPX010-10213-901 for IL-6, EPX010-10204-901 for IL-8, EPX010-10215-901 for IL-10, and EPX010-10223-901 for TNFα (Labclinics, S.A., Barcelona, Spain) were used to profile expression of these cytokines. The assay was performed according to the manufacturer's instructions. Briefly, 50 μL of working solution containing multiple microbeads labeled with specific antibodies against each cytokine was added into each well, washed twice with 200 μL of wash buffer, and filtered to dryness. Then, 25 μL thawed plasma aliquots diluted 1 : 4 with the specific LINCOplex sample diluent was added to each well and incubated for 60 min at room temperature. After a wash step (twice) with 200 μL wash buffer, the beads were incubated with 25 μL of the detection antibody cocktail containing a specific antibody to each cytokine for 30 min at room temperature. The mixture was washed twice with 200 μL wash buffer; the beads were incubated with 25 μL of the streptavidin-phycoerythrin solution for 30 min at room temperature and washed twice again. The beads were resuspended with 100 μL of buffer and the concentration of each

cytokine was determined using the array reader (Bio-Rad Laboratories, Madrid, Spain). A parallel standard curve was constructed for each cytokine. Cytokine levels were expressed in pg/mL.

2.8. Statistical Analysis. Data were analyzed using SPSS version 20.0 (WPSS Ltd., Surrey, UK), and graphs were generated using GraphPad Prism 6 scientific software (GraphPad Software Inc., La Jolla, CA, USA). Data were assessed for normal distribution with the Shapiro-Wilk test, and most of them do not have normal distribution. Nonparametric tests (Mann–Whitney rank test) were used to examine any differences among groups. Correlations between 2 parameters were assessed using simple linear regression. Binomial logistic regression analysis was used to explore the association between plasma miRNAs, oxidative biomarker levels, and the presence of frailty. Results are displayed as odds ratios ($\mathrm{Exp}(B)$) and 95% confidence intervals (CI). Differences were considered statistically significant at P values < 0.05. Data are expressed as means ± standard error of the mean (SEM).

3. Results

3.1. Characteristics of the Studied Subjects. Table 1 shows the profile of the subjects of the study. The control group was constituted by 22 healthy adults, 15 males, and 7 females, with a mean age of 20.5 ± 2.4 years. Two groups of aged subjects, robust and fragile, aged 76.6 ± 5.3 and 84.4 ± 5.6 years, respectively, were also enrolled in the study. As expected, fragile patients have a lower index of daily physical activity and higher physical dependency than those robust patients. Hypertension was present in a similar extent in both aged groups of subjects.

3.2. Plasma miRNA Expression in Studied Samples. The relative cycle threshold (C_t) for U6 small nuclear RNA was used as an endogenous control for normalizing the respective miRNAs C_t as previously described [22]. Because some are concerned with the use of this method for circulating miRNAs, we also normalized with the average C_t of the control group. Both normalization methods, however, yield similar results and statistical differences between groups. Compared with the control group, the robust group had higher expression of miR-146a, miR-223, and miR-483, while the fragile group showed higher expression of miR-21, miR-223, and miR-483 (Figures 1(a), 1(c), and 1(d)). So, except for miR-21 in the robust group and miR-146a in the fragile group, age courses with enhanced expression of miRNAs were analyzed (correlation between miR-223 expression and age ($r = 0.359$; $P < 0.001$) and between miR-483 expression and age ($r = 0.2461$; $P < 0.01$) was significant, data not shown). Women had increased expression of miR-483 compared with men (2.12 ± 1.18 versus 1.44 ± 0.99, $P < 0.001$, data not shown). Thus, the results from both methods of normalization guarantee the identification of these miRNAs in our samples, and then, we used normalization for U6. Positive correlations between miR-223 and miR-21 ($r = 0.608$, $P < 0.001$) and between miR-483 and miR-146a ($r = 0.504$, $P < 0.001$) were found (Figures 1(e) and 1(f), respectively).

3.3. Markers of Inflammation and Oxidative Stress in Studied Samples. Regarding the inflammatory markers, here measured, we found that IL-6, IL-8, and IL-10 levels increased significantly in both aged groups compared with those in the young control (Figures 2(a)–2(c)), with a trend to display higher levels of IL-8 in the fragile group. In addition, TNFα becomes significantly higher in the fragile group compared with that in control and robust ones (Figure 2(c)). Regarding inflammatory/anti-inflammatory balance measured by the index TNFα/IL-10, we detected significant difference between fragile subjects and controls, as well as between fragile and robust subjects (Figure 2(e)). No differences between men and women were detected in the levels of the cytokines measured. Because of the connection between miRNAs and inflammation, we next studied the existence of any correlation between these miRNAs and proinflammatory cytokines. Our data show only positive correlation between miR-483 and IL-8 ($r = 0.430$, $P < 0.05$) (data not shown). As expected, age was accompanied with increased oxidative stress, which is reflected in significantly higher levels of LPO and AOPP in plasma of all aged patients compared with youngers (Figures 3(a) and 3(b)). No significant differences were found between aged robust and fragile groups. Gender comparison of plasma levels of LPO and AOPP reported that women have significantly higher levels of these biomarkers than men (Figures 3(c) and 3(d)). Additionally, we found that miR-21 and AOPP correlated significantly ($r = 0.251$, $P < 0.05$) (Figure 3(e)). Logistic regression analysis suggested that the expression of miR-21 and index TNFα/IL-10 correlates positively with frailty ($\mathrm{Exp}(B) = 1.423$, 95% CI: 1.079–1.878, $P = 0.013$ for miR-21 and $\mathrm{Exp}(B) = 2.433$, 95% CI: 1.019–5.810, $P = 0.045$ for TNFα/IL-10).

4. Discussion

We present data that support that oxidative stress and cytokines, as well as subclinical inflammation, measured through miRs (miR-223 and miR-483), increase with age. Also, miR-21 become significantly higher in the group of fragile patients. We show here the association between miR-21 with frailty and AOPP and between miR-483 with frailty and IL-8; moreover, index TNFα/IL-10 was significantly elevated in the fragile group. These results point to the utility and feasibility of the determination of miRNAs together with parameters of inflammation and oxidative stress in a routine blood analysis to detect early signs of frailty during aging.

It has been suggested that low miR-21 expression is related with a healthier aging [25]. Different mechanisms of action of miR-21 in age have been reported. Circulating miR-21 can bind to toll-like receptors (TLRs) in surrounding immune cells, leading to NF-κB pathway activation and increased secretion of proinflammatory cytokines including IL-6 and TNFα [26]. Moreover, miR-21 directly modulates TGF-β signaling by targeting the TGF-βR2 in different

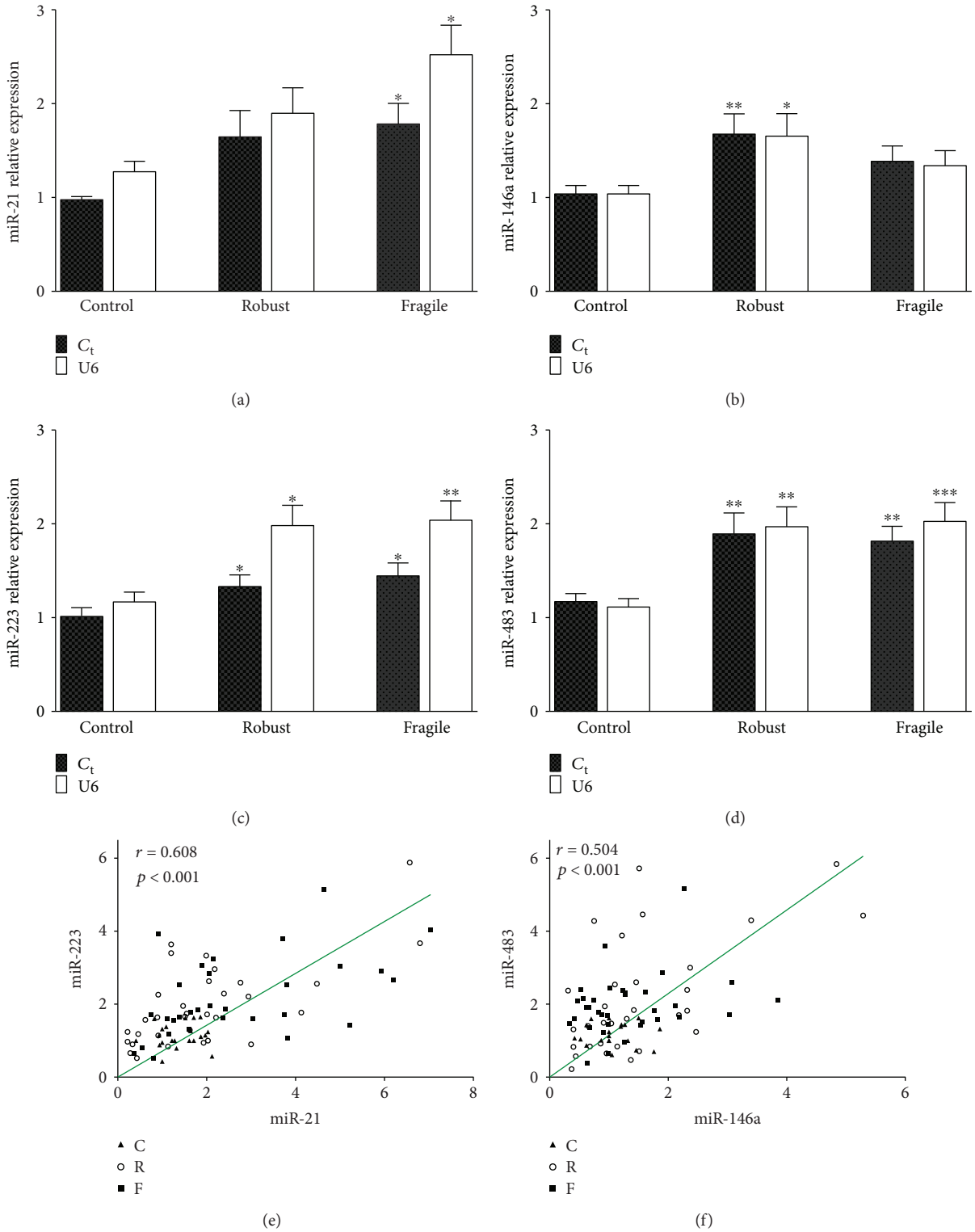

FIGURE 1: miRNA levels in control and aged groups (a)–(d). Relative expression of these miRNAs was calculated using the $2^{-\Delta\Delta Ct}$ method. The expression levels were normalized against U6 snRNA and against the average of the control group (C_t, general normalization). Data are presented as means ± SEM. $^{*}P < 0.05$, $^{**}P < 0.01$, and $^{***}P < 0.001$ versus the control group. Regression and correlation analysis with relative expression of miRNAs, calculated using analysis of the Spearman correlation coefficient. Only those miRNAs that had significant correlation are shown (e) and (f). C: control group; R: robust group; F: fragile group.

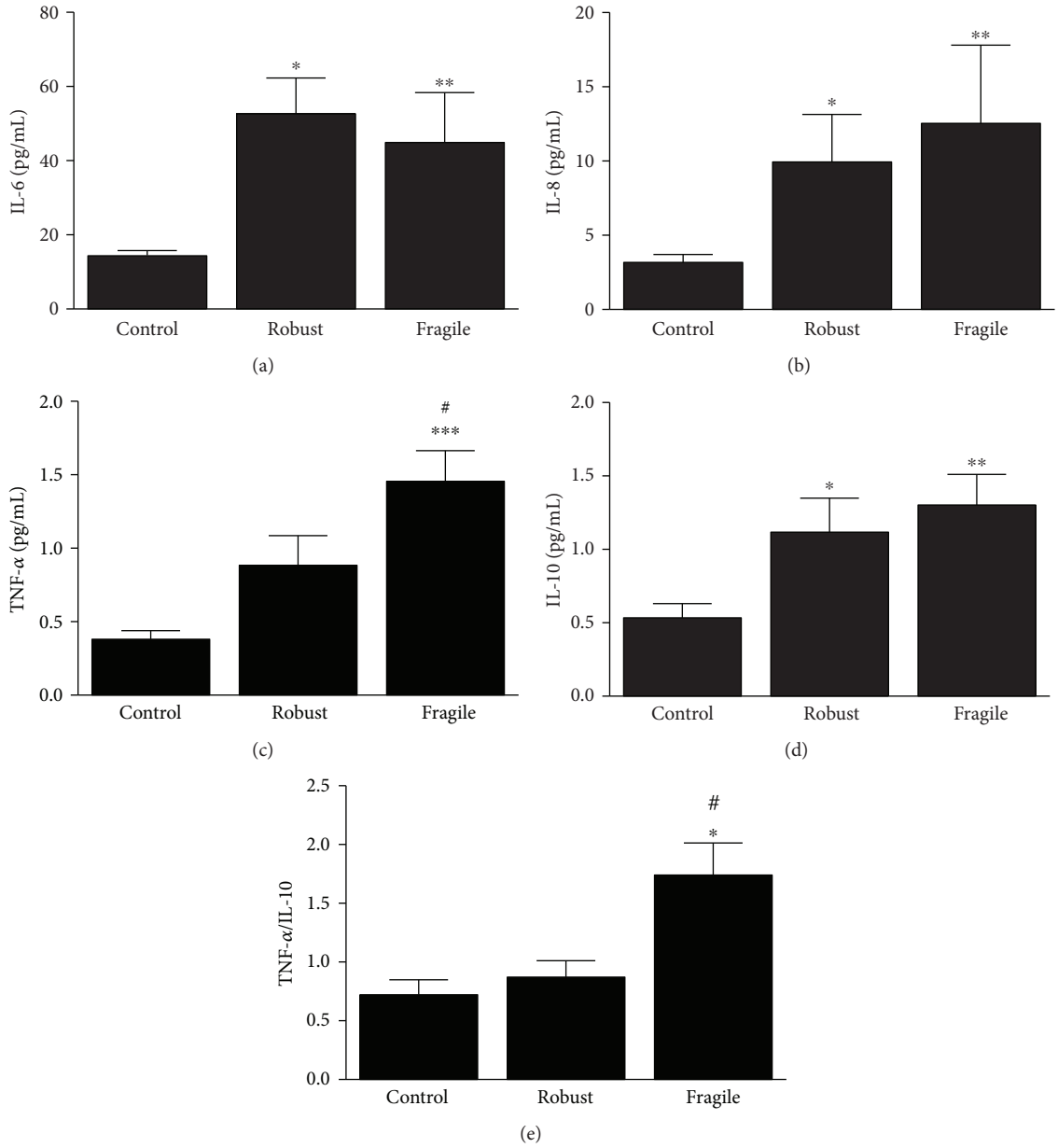

Figure 2: Plasma levels of IL-6, IL-8, TNFα, and IL-10 in control and aged groups of subjects ((a)–(d)). TNFα/IL-10 ratio in the three studied groups (e). Data are presented as means ± SEM. $^{*}P < 0.05$, $^{**}P < 0.01$ and $^{***}P < 0.001$ versus the control group. $^{\#}P < 0.05$ versus the robust group.

cellular models. This signaling pathway can interconnect inflammation, senescence, and cancer [27]. The increase in serum miR-21 in response to an acute exhaustive exercise in congestive heart failure patients further supports its relationship also with muscle condition and, thus, sarcopenia [28]. Here, we report a significant increase in plasma levels of miR-21with frailty, supporting its relation with inflammaging and age-related diseases.

Regarding miR-146a and unlike miR-21, the former increase with age but not with frailty. miR-146a/b is a component of a negative feedback loop that downregulates the levels of IRAK1 by repressing TNF receptor-associated factor 6 (TRAF6) and interleukin-1 receptor-associated kinase 1 (IRAK1) expression [29]. An upregulation of miR-146a in cells with high senescence-associated secretory phenotype (SASP) leads to increase IL-1α levels enhancing IRAK1 and NF-κB-dependent production of IL-6, IL-8, and also miR-146a/b [30]. Hence, miR-146a can prevent an excessive production of inflammatory mediators, thus limiting some of the potentially deleterious effect of SASP [30]. Our results showed that miR-146a was lower in fragile subjects that in robust aged subjects, which may trigger the proinflammatory pathway. In fact, fragile patients tend to have higher levels of IL-8 and high levels of TNFα than healthy aged subjects.

Initially described as a key modulator of hematopoietic lineage differentiation, miR-223 is one of the most abundant miRNAs in plasma. miR-223 regulates the pathways related with immune responses by affecting different targets; these

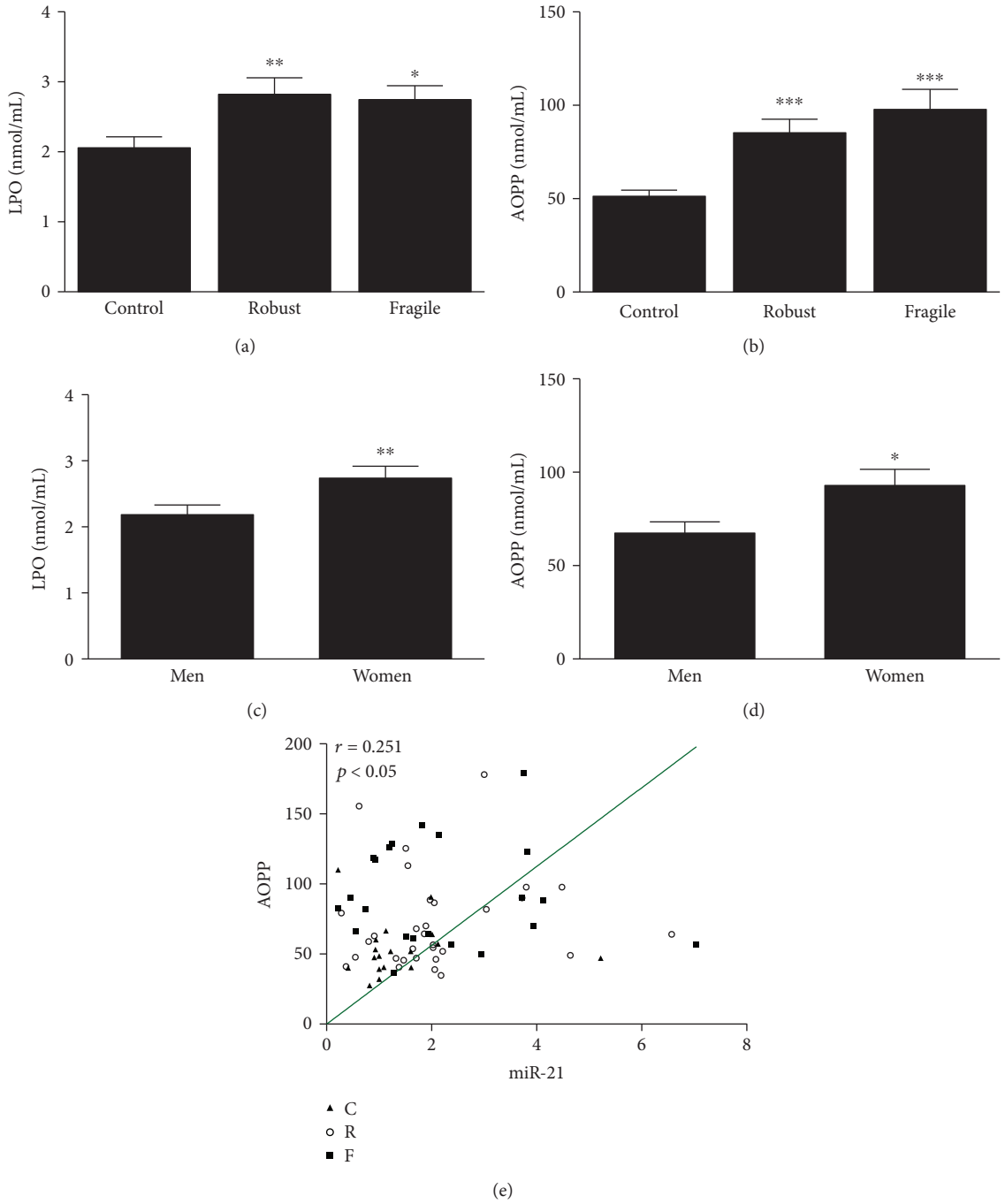

Figure 3: Lipid peroxidation (LPO) and advanced oxidation protein product (AOPP) levels in plasma of subjects of three studied groups ((a) and (b)). LPO and AOPP levels in plasma were also classified according to gender ((c) and (d)). Data are presented as means ± SEM. $^{*}P < 0.05$, $^{**}P < 0.01$, and $^{***}P < 0.001$ versus the control group. Correlation analysis between miR-21 relative expression and AOPP levels (e), calculated using analysis of the Spearman correlation coefficient. C: control group; R: robust group; F: fragile group.

include insulin-like growth factor 1 receptor (IGF-R1), IKKα, STAT3, FOXO1, NLRP3, and Roquin, and it may induce the activation of NF-κB in macrophages during their differentiation [29]. Circulating miR-223 has been positively associated with inflammation and fibrosis muscle-deficient mice [31]. Our results shown that miR-223 expression increased in both groups of aged patients, and thus, miR-223 could be considered a biomarker of aging but not of frailty. This assumption coincides with recent investigation of the epigenetic network involved in human aging [32]. Nevertheless, newest findings suggest that miRNAs do not act individually but rather exert a cooperative control over different signaling pathways. Here, we found a positive correlation between miR-21 and miR-223. Whereas both of them are related with aging, the former is also related with frailty and AOPP. Thus, miR-21 could be used to detect a risk of frailty in the patients.

With regard to miR-483, different targets have been described. Clokie et al. demonstrated that miR-483 extracted from the rat pineal gland act as suppressor of *arylalkylamine-N-acetyltransferase (aanat)* mRNA expression, the key enzyme in melatonin synthesis [33]. High levels of miR-483 suppress N-acetylserotonin production, the melatonin precursor, leading to a reduction in melatonin synthesis. Our data showed that miR-483 correlated with IL-8 and its expression levels significantly increased with age. Since melatonin production decays with age, the increased expression of miR-483 in aged patients could underlie the age-dependent melatonin decay. Nevertheless, this affirmation requires further confirmation because we did not measure the levels of melatonin in the groups of subjects here studied.

Human aging can be considered as a complex process that combines inflammation and oxidative stress. In our study, we found a significant increase in the levels of the proinflammatory cytokines IL-6, IL-8, and TNFα with age, Moreover, some studies proved that elevated levels of TNFα can increase muscle catabolism by suppressing the Akt/mTOR pathway [34]. The tendency to increase IL-6, IL-8, and significantly high levels of TNFα in the group with frailty here reported, as well as increased inflammatory/anti-inflammatory balance measured by the index TNFα/IL-10, suggests a role for these cytokines in muscle deterioration. Together with inflammation, we report here the increase in LPO and AOPP levels, reflecting the lipid and protein oxidative damage. Again, these ROS did not show differences with frailty, although women have significantly higher levels of LPO and AOPP than men.

The use of different animal models for the study of changes in aged muscle confirms that circulating miRNAs indicate that while muscle and serum have distinct age-related changes in miRNA expression, some miRNAs showed the same directionality in expression changes [35]. Together, our data suggest a relationship between c-miRNAs and aged patients with and without frailty. Elevated levels of miR-21 in frailty indicate an activation of innate immunity associated with age, and it suggests miR-21 as a biomarker of human muscle frailty. On the other hand, the reduction in miR-146a levels in frailty can promote NF-κB-dependent inflammation. The increased expression of circulating miR-483 in the experimental group may contribute to the decreased production of melatonin due to age. All these changes are accompanied by increased levels of inflammatory and ROS markers, indicating the presence of chronic inflammation associated with age. Women, who have increased AOPP, LPO, and miR-483 compared with men, can be considered as the population most vulnerable to frailty.

5. Summary and Conclusions

We confirmed that aging and frailty are companied with higher oxidative and inflammation states, such as increasing expression of c-miR-21, c-miR-223, and c-miR-483, reflecting the changes that occur at the molecular level in the aging process.

Our results point that the miR-21 and TNFα/IL-10 ratio may be considered as possible biomarkers for age-related frailty. Enhanced understanding of alterations in c-miRNA expression with aging and in different pathological condition may result in a relevant diagnostic tool and offers more information on mechanisms involved in the aging process. Detection and identification of stable miRNAs in blood has opened a new possibility in systemic biomarker research directed at improving clinical diagnosis and prognosis.

Data Availability

The datasets generated during and/or analysed during the current study are available from the corresponding author on reasonable request.

Ethical Approval

Informed consent was obtained from all subjects and from the Hospital Ethical Committee, according to the 1983 revised Helsinki Declaration of 1975. The final study was approved by the Andalusian Ethical Committee (ref. CEEA: 462-CEEA-2013).

Conflicts of Interest

The authors declared that they have no conflicts of interest to this work.

Acknowledgments

This work was partially supported by grants from the Ministerio de Economía, Industria y Competitividad y por el Fondo de Desarrollo Regional Feder, Spain nos. RD12/0043/0005, PI13-00981, and CB16-10-00238 and from the Universidad de Granada, Spain no. CEI2014-MPBS31.

References

[1] J. R. Beard, A. Officer, I. A. de Carvalho et al., "The world report on ageing and health: a policy framework for healthy ageing," *Lancet*, vol. 387, no. 10033, pp. 2145–2154, 2016.

[2] European Commission Directorate-General for Economic and Financial Affairs, *The 2015 Ageing Report Economic and budgetary projections for the 28 EU Member States (2013-2060)*, European Economy, Brussels, 2015.

[3] I. H. Rosenberg, "Sarcopenia: origins and clinical relevance," *The Journal of Nutrition*, vol. 127, no. 5, pp. 990S-991S, 1997.

[4] A. Cruz-Jentoft, J. Baeyens, J. Bauer et al., "Sarcopenia: European consensus on definition and diagnosis: report of the European Working Group on Sarcopenia in Older People," *Age and Ageing*, vol. 39, no. 4, pp. 412–423, 2010.

[5] Q. L. Xue, "The frailty syndrome: definition and natural history," *Clinics in Geriatric Medicine*, vol. 27, no. 1, pp. 1–15, 2011.

[6] N. Montero-Fernández and J. A. Serra-Rexach, "Role of exercise on sarcopenia in the elderly," *European Journal of Physical and Rehabilitation Medicine*, vol. 49, no. 1, pp. 131–143, 2013.

[7] K. Bandeen-Roche, C. L. Seplaki, J. Huang et al., "Frailty in older adults: a nationally representative profile in the United States," *The Journals of Gerontology: Series A*, vol. 70, no. 11, pp. 1427–1434, 2015.

[8] V. Ambros, "The functions of animal microRNAs," *Nature*, vol. 431, no. 7006, pp. 350–355, 2004.

[9] J. Winter, S. Jung, S. Keller, R. I. Gregory, and S. Diederichs, "Many roads to maturity: microRNA biogenesis pathways and their regulation," *Nature Cell Biology*, vol. 11, no. 3, pp. 228–234, 2009.

[10] S. Weilner, R. Grillari-Voglauer, H. Redl, J. Grillari, and T. Nau, "The role of microRNAs in cellular senescence and age-related conditions of cartilage and bone," *Acta Orthopaedica*, vol. 86, no. 1, pp. 92–99, 2015.

[11] Y. T. Li, S. Y. Chen, C. R. Wang et al., "Brief report: amelioration of collagen-induced arthritis in mice by lentivirus-mediated silencing of microRNA-223," *Arthritis and Rheumatism*, vol. 64, no. 10, pp. 3240–3245, 2012.

[12] J. Fan, X. Kou, Y. Yang, and N. Chen, "MicroRNA-regulated proinflammatory cytokines in sarcopenia," *Mediators of Inflammation*, vol. 2016, Article ID 1438686, 9 pages, 2016.

[13] F. E. Martin-Cano, C. Camello-Almaraz, D. Acuña-Castroviejo, M. J. Pozo, and P. J. Camello, "Age-related changes in mitochondrial function of mouse colonic smooth muscle: beneficial effects of melatonin," *Journal of Pineal Research*, vol. 56, no. 2, pp. 163–174, 2014.

[14] F. J. Garcia-Garcia, G. Gutierrez Avila, A. Alfaro-Acha et al., "The prevalence of frailty syndrome in an older population from Spain. The Toledo study for healthy aging," *The Journal of Nutrition, Health & Aging*, vol. 15, no. 10, pp. 852–856, 2011.

[15] L. P. Fried, C. M. Tangen, J. Walston et al., "Frailty in older adults: evidence for a phenotype," *The Journals of Gerontology: Series A*, vol. 56, no. 3, pp. M146–M157, 2001.

[16] F. Lauretani, C. R. Russo, S. Bandinelli et al., "Age-associated changes in skeletal muscles and their effect on mobility: an operational diagnosis of sarcopenia," *Journal of Applied Physiology*, vol. 95, no. 5, pp. 1851–1860, 2003.

[17] K. J. Ottenbacher, L. G. Branch, L. Ray, V. A. Gonzales, M. K. Peek, and M. R. Hinman, "The reliability of upper- and lower-extremity strength testing in a community survey of older adults," *Archives of Physical Medicine and Rehabilitation*, vol. 83, no. 10, pp. 1423–1427, 2002.

[18] J. G. Orme, J. Reis, and E. J. Herz, "Factorial and discriminant validity of the center for epidemiological studies depression (CES-D) scale," *Journal of Clinical Psychology*, vol. 42, no. 1, pp. 28–33, 1986.

[19] J. M. Guralnik, L. Ferrucci, C. F. Pieper et al., "Lower extremity function and subsequent disability: consistency across studies, predictive models, and value of gait speed alone compared with the short physical performance battery," *The Journals of Gerontology: Series A*, vol. 55, no. 4, pp. M221–M231, 2000.

[20] R. A. Washburn, K. W. Smith, A. M. Jette, and C. A. Janney, "The physical activity scale for the elderly (PASE): development and evaluation," *Journal of Clinical Epidemiology*, vol. 46, no. 2, pp. 153–162, 1993.

[21] X. Chen, H. Liang, D. Guan et al., "A combination of Let-7d, Let-7g and Let-7i serves as a stable reference for normalization of serum microRNAs," *PLoS One*, vol. 8, no. 11, article e79652, 2013.

[22] M. R. Zile, S. M. Mehurg, J. E. Arroyo, R. E. Stroud, S. M. DeSantis, and F. G. Spinale, "Relationship between the temporal profile of plasma microRNA and left ventricular remodeling in patients after myocardial infarction," *Circulation. Cardiovascular Genetics*, vol. 4, no. 6, pp. 614–619, 2011.

[23] V. Witko-Sarsat, M. Friedlander, C. Capeillère-Blandin et al., "Advanced oxidation protein products as a novel marker of oxidative stress in uremia," *Kidney International*, vol. 49, no. 5, pp. 1304–1313, 1996.

[24] H. Esterbauer and K. H. Cheeseman, "[42] Determination of aldehydic lipid peroxidation products: malonaldehyde and 4-hydroxynonenal," *Methods in Enzymology*, vol. 186, pp. 407–421, 1990.

[25] F. Olivieri, L. Spazzafumo, G. Santini et al., "Age-related differences in the expression of circulating microRNAs: miR-21 as a new circulating marker of inflammaging," *Mechanisms of Ageing and Development*, vol. 133, no. 11-12, pp. 675–685, 2012.

[26] M. Fabbri, A. Paone, F. Calore, R. Galli, and C. M. Croce, "A new role for microRNAs, as ligands of Toll-like receptors," *RNA Biology*, vol. 10, no. 2, pp. 169–174, 2014.

[27] F. Olivieri, M. Capri, M. Bonafè et al., "Circulating miRNAs and miRNA shuttles as biomarkers: Perspective trajectories of healthy and unhealthy aging," *Mechanisms of Ageing and Development*, vol. 165, Part B, pp. 162–170, 2017.

[28] T. Xu, Q. Zhou, L. Che et al., "Circulating miR-21, miR-378, and miR-940 increase in response to an acute exhaustive exercise in chronic heart failure patients," *Oncotarget*, vol. 7, no. 11, pp. 12414–12425, 2016.

[29] T. Li, M. J. Morgan, S. Choksi, Y. Zhang, Y. S. Kim, and Z. G. Liu, "MicroRNAs modulate the noncanonical transcription factor NF-κB pathway by regulating expression of the kinase IKKα during macrophage differentiation," *Nature Immunology*, vol. 11, no. 9, pp. 799–805, 2010.

[30] D. Bhaumik, G. K. Scott, S. Schokrpur et al., "MicroRNAs miR-146a/b negatively modulate the senescence-associated inflammatory mediators IL-6 and IL–8," *Aging*, vol. 1, no. 4, pp. 402–411, 2009.

[31] J. Holmberg, A. Alajbegovic, K. I. Gawlik, L. Elowsson, and M. Durbeej, "Laminin α2 chain-deficiency is associated with microRNA deregulation in skeletal muscle and plasma," *Frontiers in Aging Neuroscience*, vol. 6, p. 155, 2014.

[32] C. W. Li, W. H. Wang, and B. S. Chen, "Investigating the specific core genetic-and-epigenetic networks of cellular mechanisms involved in human aging in peripheral blood mononuclear cells," *Oncotarget*, vol. 7, no. 8, pp. 8556–8579, 2016.

[33] S. J. H. Clokie, P. Lau, H. H. Kim, S. L. Coon, and D. C. Klein, "MicroRNAs in the pineal gland: miR-483 regulates melatonin synthesis by targeting arylalkylamine N-acetyltransferase," *The Journal of Biological Chemistry*, vol. 287, no. 30, pp. 25312–25324, 2012.

[34] D. T. Wang, Y. Yin, Y. J. Yang et al., "Resveratrol prevents TNF-α-induced muscle atrophy via regulation of Akt/mTOR/FoxO1 signaling in C2C12 myotubes," *International Immunopharmacology*, vol. 19, no. 2, pp. 206–213, 2014.

[35] H. J. Jung, K.-P. Lee, B. Milholland et al., "Comprehensive miRNA profiling of skeletal muscle and serum in induced and normal mouse muscle atrophy during aging," *The Journals of Gerontology: Series A*, vol. 72, no. 11, pp. 1483–1491, 2017.

Hindawi
Oxidative Medicine and Cellular Longevity
Volume 2018, Article ID 6857190, 11 pages
https://doi.org/10.1155/2018/6857190

Research Article

Resistance-Trained Individuals Are Less Susceptible to Oxidative Damage after Eccentric Exercise

Ypatios Spanidis,[1] Dimitrios Stagos,[1] Christina Papanikolaou,[1] Konstantina Karatza,[1] Andria Theodosi,[1] Aristidis S. Veskoukis,[1] Chariklia K. Deli,[2] Athanasios Poulios,[2] Sofia D. Koulocheri,[3] Athanasios Z. Jamurtas,[2] Serkos A. Haroutounian,[3] and Demetrios Kouretas[1]

[1]*Laboratory of Animal Physiology, Department of Biochemistry and Biotechnology, University of Thessaly, 41500 Viopolis, Larissa, Greece*
[2]*Laboratory of Exercise Biochemistry, Exercise Physiology and Sports Nutrition (SmArT Lab), Department of Physical Education and Sport Science, University of Thessaly, 42100 Trikala, Greece*
[3]*Department of Nutritional Physiology and Feeding, Faculty of Animal Science and Aquaculture, Agricultural University of Athens, Iera Odos 75, 11855 Athens, Greece*

Correspondence should be addressed to Demetrios Kouretas; dkouret@uth.gr

Received 9 March 2018; Accepted 21 June 2018; Published 17 July 2018

Academic Editor: Joanna Lecka

It has been proposed that exercise-induced oxidative stress and adaptations are dependent on training status. In this study, we examined the effects of training background on free radical generation and adaptations after eccentric exercise. Forty volunteers were divided into two groups (trained and untrained) and were asked to perform eccentric exercise. Then, their blood samples were collected pre, 24, 48, and 72 hours postexercise. Biomarkers indicating oxidative damage and the antioxidant profiles of the participants were measured in plasma and erythrocyte lysate both spectrophotometrically and chromatographically. The results revealed that the untrained group depicted more severe oxidative damage (protein carbonyls, malondialdehyde), weaker antioxidant status (reduced glutathione, static and capacity oxidation-reduction potential), and weaker radical-scavenging activity (superoxide radical scavenging and reducing power) compared to the trained participants. Our findings show that trained individuals are less susceptible to oxidative damage and suggest that generalized nutritional recommendations regarding recovery after exercise should be avoided.

1. Introduction

The association between physical exercise and free radical generation has been established in the literature and is attributed to diverse mechanisms [1]. Numerous studies have reported that reactive oxygen species (ROS) generation post-exercise leads to severe muscle damage and oxidative stress [2]. Moreover, it has been proposed that the magnitude of ROS production is directly related to exercise intensity, resulting therefore to an excessive increase in ROS production after an intense and demanding exercise [3].

Eccentric exercise is considered to be a quite demanding exercise modality. It is characterized by an active contraction and lengthening of skeletal muscle inducing severe tissue damage characterized by decreased muscle force production, increased serum creatine kinase activity, and inflammation [4]. Thus, eccentric exercise leads to cellular disruption, loss of normal function, and soreness [5]. However, despite the fact that eccentric exercise is related to severe oxidative stress induction, significant differences in oxidation levels after eccentric exercise, as well as the presence of reductive stress among individuals, have also been observed [6]. Such

diversity could be possibly attributed to the training background of each individual, since, according to the literature, ROS produced during regular exercise induce adaptations by improving antioxidant capacity, mitochondrial biogenesis, insulin sensitivity, cytoprotection, and aerobic capacity of skeletal muscle [2].

Since there was a need to find a parameter that may affect individuals' response after performing eccentric exercise, the primary purpose of the present study was to examine the effects of muscle-damaging eccentric exercise on blood redox profile and to shed light on the impact of training load on redox adaptations. Furthermore, we attempted to clarify whether training background affects changes in redox biomarkers after an arduous and demanding exercise modality, such as eccentric exercise. The idea for the present study emerged from past works of our scientific team and others that correlated oxidative damage (protein carbonyls (PC), thiobarbituric acid reactive substances (TBARS)) and the weaker redox status of individuals with muscle soreness after bouts of eccentric exercise. In addition, the diversity among participants is highlighted [6–9].

It is evident that this approach will try to fill the gaps in literature regarding the response of trained and untrained people after performing eccentric exercise and examine whether an individual or group approach should be conducted. This would also help to improve the response of exercising individuals regarding recovery and health status after specific interventions (e.g., nutrition or administration of antioxidant supplements). We hypothesized that untrained people may display a compromised antioxidant profile and, therefore, will be more susceptible to oxidative and muscle damage compared to the trained ones as they are less adapted in performing bouts of exercise.

2. Materials and Methods

2.1. Subjects. Twenty-four male and sixteen female volunteers (age 22.5 ± 0.58 years, height 175.1 ± 1.6 cm, and weight 75.4 ± 2.3 kg) participated in the present study. The selection of the participants was based on their athletic (i.e., training) background. In order to cluster the participants into two groups, they were asked to provide details about their athletic background. According to them, the trained group consisted of 15 males and 7 females. Seventeen participants regularly performed resistance exercise (i.e., weightlifting) recreationally at least 4 times per week, while the remaining 5 mostly performed a combination of aerobic and resistance exercises. The untrained group comprised 18 participants (9 males and 9 females), who had never been in contact with any kind of exercise.

Subjects have not suffered any musculoskeletal injuries to the lower limbs that would limit their ability to perform the exercise protocol. Additionally, the participants were asked to abstain from smoking and from consuming alcohol and nutritional supplements, as well as from engaging in any kind of exercise for over a week before the study and during the experiment. However, there were no limitations regarding food intake before or during blood sampling. Body mass was measured to the nearest 0.5 kg (BeamBalance 710, Seca, United Kingdom), while the subjects were lightly dressed and barefoot. Standing height was measured to the nearest 0.5 cm (Stadiometer 208, Seca). A written informed consent to participate in the study was provided to and was signed by all participants after they had been informed of all benefits, risks, and discomforts of the investigation.

2.2. Study Design. The participants of the present study were divided into two groups (i.e., trained and untrained) according to their athletic background, as mentioned in Section 2.1. Blood samples were collected before and 24 h, 48 h, and 72 h after performing the eccentric exercise protocol described in the next paragraph. Plasma and erythrocyte lysate samples were isolated after blood collection and stored at −80°C until the biochemical analyses were performed.

2.3. Eccentric Exercise Protocol. An eccentric exercise session was performed on an isokinetic dynamometer (Cybex Norm, Ronkonkoma, NY) and exercise protocols were undertaken from the seated position (120° hip angle) with the lateral femoral condyle aligned with the axis of rotation of the dynamometer. Participants were coupled to the dynamometer by an ankle cuff, attached proximal to the lateral malleolus, and finally stabilized according to the manufacturer's instructions. Participants completed 5 sets of 15 eccentric maximal voluntary contractions (knee range, 0° full extension to 90° flexion) at an angular velocity of 60°/s. A 2 min rest interval was used between sets and the total workout time was 15 min. Before the exercise session, subjects performed a 10 min warmup consisting of cycling on a Monark cycle ergometer (Vansbro, Sweden) at 70–80 rpm and 50 W.

2.4. Blood Sample Preparation. The blood samples were drawn from a forearm vein in ethylenediaminetetraacetic acid (EDTA) and heparin tubes at four different time points, namely, before exercise and 24, 48, and 72 h postexercise. Subsequently, they were centrifuged (1370g, 10 min, and 4°C) and the supernatant (i.e., plasma) was collected. The remaining packed erythrocytes were lysed with 1 : 1 (v/v) distilled water (dH_2O), inverted vigorously, and centrifuged (4020g, 15 min, and 4°C). The supernatant, which is the erythrocyte lysate, was then collected. The plasma and erythrocyte lysate samples were then stored at −80°C until further biochemical analysis.

2.5. Biochemical Analyses. PC were determined in plasma as described in a previous work of our team [10]. Briefly, 50 μl of 20% trichloroacetic acid (TCA) was added to 50 μl of plasma, and this mixture was incubated in an ice bath for 15 min and centrifuged (15,000g, 5 min, and 4°C). The supernatant was discarded and 500 μl of 10 mM 2,4-dinitrophenylhydrazine (in 2.5 N HCl) for the sample, or 500 μl of 2.5 N HCl for the blank, was added to the pellet. The samples were incubated in the dark at room temperature (RT) for 1 h with intermittent vortexing every 15 min and centrifuged (15,000g, 5 min, and 4°C). The supernatant was discarded, and 1 ml of 10% TCA was added. Then, the samples were vortexed and centrifuged (15,000g, 5 min, and 4°C). The supernatant was discarded, and 1 ml of ethanol-ethyl acetate

mixture (1 : 1 *v*/*v*) was added. Then, the samples were vortexed and centrifuged (15,000*g*, 5 min, and 4°C). This step was repeated twice. The supernatant was discarded, and 1 ml of 5 M urea (pH = 2.3) was added. Then, the samples were vortexed and incubated at 37°C for 15 min. The samples were then centrifuged (15,000*g*, 3 min, and 4°C), and the absorbance was monitored at 375 nm. Total plasma protein was determined using Bradford's method via a standard curve of solutions with known bovine serum albumin concentrations.

For plasma malondialdehyde (MDA) assessment as a biomarker of lipid peroxidation, one spectrophotometric (TBARS) and one chromatographic (high-performance liquid chromatography with diode-array detector, HPLC-DAD) method was applied. For TBARS determination, 100 μl of plasma was mixed with 500 μl of 35% TCA and 500 μl of Tris-HCl (200 mM, pH = 7.4) and incubated for 10 min at RT. A total of 1 ml of 2 M sodium sulfate (Na_2SO_4) and 55 mM thiobarbituric acid (TBA) (2.84 g of Na_2SO_4 and 0.08 g of TBA diluted in 10 ml of dH_2O) was added and the samples were incubated at 95°C for 45 min. The samples were cooled on ice for 5 min, vortexed after adding 1 ml of 70% TCA, and centrifuged (15,000*g*, 3 min, and 20°C). Then, the absorbance of the supernatant was monitored at 530 nm. TBARS concentration was calculated on the basis of the molar extinction coefficient of MDA [10].

Regarding plasma MDA determination by chromatography (HPLC-DAD), a method described by Spirlandeli et al., [11] was used. Briefly, 100 μl of plasma was added to 700 μl of 1% phosphoric acid and 200 μl of 42 mM TBA. The mixture was vortexed and heated for 40 min in a water bath at 100°C. Afterwards, 250 μl of the mixture was added to 250 μl of 1 M sodium hydroxide in methanol (1 : 6), centrifuged (10,000*g*, 5 min, and 20°C), filtered through a Milli-RO 10 Plus and a Milli-Q Plus plant (final pore size 0.2 mm; Millipore, Bedford, MA). Then, 20 μl of the supernatant was injected in the HPLC apparatus at a flow rate of 1 ml/min. The absorbance was monitored at 532 nm. For the MDA standard curve, a stock solution of 100 μM MDA was prepared in 0.01 mM HCl. Dilutions from stock MDA solutions of 2–14 μM were then performed. The same treatment described for plasma was used for the standard. The method was carried out by using a 5 μm C18 reverse-phase column (4.6 mm × 250 mm) in a Hewlett Packard HP1100 Series HPLC Value System (Agilent Technologies, Waldbronn, Germany) equipped with a quaternary pump, autosampler, degasser, and diode array detector (DAD). Retrieval and processing of chromatographic data was performed with Chemstation Software.

In total antioxidant capacity (TAC) determination, 20 μl of plasma was added to 480 μl of 10 mM sodium potassium phosphate (pH = 7.4) and 500 μl of 0.1 mM 2,2-diphenyl-1-picrylhydrazyl ($DPPH^{\bullet}$). The samples were incubated in the dark for 30 min at RT and centrifuged (20,000*g*, 3 min, and 20°C). Then, the absorbance was monitored at 520 nm [10]. In GSH, 20 μl of erythrocyte lysate treated with 5% TCA was mixed with 660 μl of 67 mM sodium potassium phosphate (pH = 8.0) and 330 μl of 1 mM 5,5-dithiobis (2 nitrobenzoic acid) (DTNB). The samples were incubated in the dark at RT for 45 min and the absorbance was monitored at 412 nm. GSH concentration was calculated relative to a calibration curve made using commercial standards [10].

Catalase (CAT) activity in the erythrocyte lysate was measured as previously described [10]. Specifically, 4 μl of erythrocyte lysate (diluted 1 : 10) was added to 2991 μl of 67 mM sodium potassium phosphate (pH = 7.4) and the samples were incubated at 37°C for 10 min. Five microliters of 30% hydrogen peroxide (H_2O_2) was added to the samples and the absorbance was monitored at 240 nm for 130 sec. CAT activity was calculated on the basis of the molar extinction coefficient of H_2O_2.

The superoxide anion radical-scavenging ability of plasma was measured using a slightly modified protocol of Ak and Gülçin, [12]. In this method, superoxide anion ($O_2^{\bullet-}$) is generated in a phenazine methosulfate and reduced nicotinamide adenine dinucleotide (PMS-NADH) system by NADH oxidation and it reduces the yellow dye of nitroblue tetrazolium (NBT^{2+}) to the blue colored formazan. More specifically, 125 μl of 300 μM NBT^{2+}, 125 μl of 468 μM NADH, and 50 μl of plasma were added into 625 μl of 16 mM Tris-HCl (pH = 8.0). The reaction is initiated by the addition of 125 μl of 60 μM PMS to the mixture. The samples were incubated for 5 min and the absorbance was monitored at 560 nm. Plasma antioxidants are acting as inhibitors to the blue colored formazan formation. The $O_2^{\bullet-}$ radical-scavenging activity was calculated according to (1):

$$\% \text{ Superoxide radical scavenging activity} = \left[\frac{\left(\text{Abs}_{\text{control}} - \text{Abs}_{\text{sample}}\right)}{\text{Abs}_{\text{control}}}\right] \times 100, \quad (1)$$

where $\text{Abs}_{\text{control}}$ and $\text{Abs}_{\text{sample}}$ are the absorbance values of the control and the tested sample, respectively.

In the reducing power assay, a plasma sample was dissolved in phosphate buffer (0.2 M, pH = 6.6) at different concentrations. An aliquot (250 μl) of the sample solution was added to 250 μl of 1% potassium ferricyanide and incubated at 50°C for 20 min. The samples were cooled on ice for 5 min. Then, 250 μl of 10% TCA was added and the samples were centrifuged (1700*g*, 10 min, and 25°C). Subsequently, 250 μl of dH_2O and 50 μl of 0.1% ferric chloride were added to the supernatant and the samples were incubated at RT for 10 min. The absorbance was monitored at 700 nm [13].

Regarding the assay for hydroxyl radical- ($OH^{\bullet}$-) scavenging activity, 75 μl of plasma dissolved in dH_2O at different concentrations was added to 450 μl of 0.2 M sodium phosphate buffer (pH = 7.4), 150 μl of 10 mM 2-deoxyribose, 150 μl of 10 mM $FeSO_4$-EDTA, 525 μl of dH_2O, and 150 μl of 10 mM H_2O_2. Then, the samples were incubated at 37°C for 4 h. Afterwards, 750 μl of 2.8% TCA and 750 μl of 1% TBA were added, and the samples were incubated at 95°C for 10 min. Then, the samples were cooled on ice for 5 min, centrifuged (1700*g*, 10 min, and 25°C), and the absorbance was monitored at 520 nm. In each experiment, the sample without H_2O_2 was considered as blank and the sample

Table 1: Delayed onset muscle soreness (DOMS) pre- and postexercise.

	Pre	Immediately after	24 h	48 h	72 h
Trained					
DOMSw	1.00 ± 0.00	4.49 ± 0.67*	3.52 ± 0.48*	4.52 ± 0.48*	3.00 ± 0.46*
DOMSsq	1.00 ± 0.00	3.58 ± 0.37*	4.08 ± 0.51*	4.33 ± 0.48*	3.17 ± 0.51*
Untrained					
DOMSw	1.00 ± 0.00	3.44 ± 0.38*	4.21 ± 0.44*	5.34 ± 0.53*	4.43 ± 0.33*
DOMSsq	1.00 ± 0.00	3.44 ± 0.50*	4.84 ± 0.44*	5.71 ± 0.55*	5.05 ± 0.53*

DOMSw: DOMS assessed during walking; DOMSsq: DOMS assessed after performing a squat movement. Values are expressed as mean ± SEM. *Statistically significant compared with preexercise values ($p < 0.05$).

without protein as control. The $OH^{\bullet}$ scavenging activity was calculated according to (2):

$$\%\ \text{Hydroxyl radical scavenging activity} = \left[\frac{\left(\text{Abs}_{\text{control}} - \text{Abs}_{\text{sample}}\right)}{\text{Abs}_{\text{control}}}\right] \times 100, \quad (2)$$

where $\text{Abs}_{\text{control}}$ and $\text{Abs}_{\text{sample}}$ are the absorbance values of the control and the tested sample, respectively [14].

Oxidation-reduction potential (ORP) in plasma was determined by a novel method using the RedoxSYS Diagnostic System (Luoxis Diagnostics Inc., Englewood, CO, USA). Specifically, ORP is an integrated measure of the balance between the pool of oxidants (e.g., oxidized thiols, $O_2^{\bullet-}$, $OH^{\bullet}$, H_2O_2, $NO^{\bullet}$, $ONOO^{\bullet}$, and transition metal ions) and the pool of reductants (e.g., free thiols, ascorbate, α-tocopherol, β-carotene, and uric acid). It has been shown that this is an effective, fast, and accurate method for the determination of oxidative stress induced by an ultramarathon mountain race, eccentric exercise, and a strenuous basketball season [6, 10, 15]. The system consists of a battery-powered reader and small sensors that require limited sample manipulation, as it measures ORP within 4 min in 20 μl of heparinized mammalian plasma samples. Static oxidation-reduction potential (sORP) value displays the integrated balance of oxidants and reductants in a sample and is expressed in millivolts (mV). Capacity oxidation-reduction potential (cORP) is the amount of the antioxidant pool in the human body and is expressed in microcoulombs (μC). High sORP values and low cORP values indicate the presence of oxidative stress [10].

2.6. Assessment of Delayed Onset Muscle Soreness (DOMS). Perceived soreness of the participants as a measure of DOMS was rated by them on a scale ranging from 1 (i.e., no pain), 5 (i.e., moderate pain), to 10 (i.e., very strong pain) during walking (DOMSw) and the squat movement (DOMSsq).

2.7. Statistical Analysis. The distribution of the biomarker values in each sample was examined by the Shapiro-Wilk test and was found not to differ significantly from normality. Data were analyzed using two-way ANOVA followed by Dunnett's test for multiple pairwise comparisons. Correlations between oxidative stress biomarkers were examined by Spearman's correlation analysis. The level of significance was set at $p < 0.05$. Data are presented as mean ± SEM. For all statistical analyses, SPSS version 20.0 (SPSS, Inc., Chicago, IL, USA) was used.

3. Results

3.1. Muscle Soreness. Eccentric exercise resulted in significant increases in DOMS levels of the trained group ranging between 3.49- and 4.52-fold during walking and between 3.58- and 4.33-fold after squatting. The corresponding data collected by the untrained group after walking and the squat movement increased significantly from 3.44- to 5.34-fold and from 3.44- to 5.00-fold, respectively (Table 1). Moreover, the correlation between DOMS levels and oxidative stress markers exhibited significant negative correlations between DOMS, cORP, and reducing power in the untrained group. Specifically, there was a negative correlation between DOMS squat and cORP 48 h postexercise while negative correlations were also obtained between DOMS walking, cORP, and reducing power at the 72 h postexercise time point (Table 2).

3.2. Oxidative Stress Biomarkers

3.2.1. Protein Oxidation. Protein carbonyl levels in the untrained group were significantly increased 48 h postexercise by 14.67% compared with the preexercise value and were also significantly higher compared with the corresponding results of the trained group (Table 3). On the contrary, protein carbonylation of the trained group was slightly, but not significantly, decreased at all time points (Table 3).

3.2.2. Lipid Peroxidation Measured by Spectrophotometry. TBARS levels were increased in the trained group by 10.25%, 8.50%, and 14.98% at 24, 48, and 72 h, respectively, while the corresponding results in the untrained individuals revealed significant increases by 18.29%, 26.89%, and 13.49%, respectively (Table 3). The TBARS levels of the untrained group were significantly higher compared to the trained group 48 h postexercise (Table 3).

3.2.3. Lipid Peroxidation Measured by Chromatography

(1) Validation (Linearity, Precision, and Recovery). After choosing the pretreatment procedure and establishing the chromatographic conditions for the analysis, the method was validated. Firstly, a pooled human plasma sample, spiked

Table 2: Statistical correlation between DOMS and the examined oxidative stress biomarkers 24 h, 48 h, and 72 h postexercise in both trained and untrained groups.

	PC	TBARS	TAC	GSH	CAT	sORP	cORP	SRS	RP	HRS	MDA
						Trained					
24 hours											
DOMS sq.	0.074	0.423	0.141	0.182	0.164	0.191	−0.268	−0.154	0.349	0.336	0.390
DOMS w.	0.093	0.173	0.202	0.122	0.174	0.332	−0.252	−0.136	.301	−0.50	0.202
48 hours											
DOMS sq.	−0.272	−0.016	0.311	0.356	0.012	−0.216	0.060	−0.066	0.011	0.104	0.059
DOMS w.	0.027	0.061	0.221	0.217	0.001	−0.284	0.045	0.023	0.151	0.050	0.064
72 hours											
DOMS sq.	−0.286	−0.334	0.120	0.284	0.380	−0.057	0.136	0.369	0.084	0.108	−0.28
DOMS w.	−0.039	−0.372	0.039	0.078	0.389	−0.262	0.410	0.187	0.198	0.132	−0.25
						Untrained					
24 hours											
DOMS sq.	−0.120	0.376	−0.357	0.156	0.029	0.075	−0.234	−0.018	−0.041	−0.13	0.193
DOMS w.	−0.168	0.164	−0.326	0.085	−0.05	−0.085	−0.170	−0.003	0.085	−0.03	0.123
48 hours											
DOMS sq.	−0.202	0.296	0.070	0.285	−0.306	−0.085	−0.463*	0.176	−0.084	0.301	0.252
DOMS w.	−0.050	0.368	−0.281	0.227	−0.352	−0.308	−0.330	0.350	0.053	0.087	0.312
72 hours											
DOMS sq.	−0.269	−0.194	−0.118	0.146	−0.003	−0.188	−0.164	0.243	0.273	0.244	−0.12
DOMS w.	0.130	0.130	0.072	0.134	0.216	0.018	−0.484*	0.078	−0.440*	0.098	0.132

DOMSw: DOMS assessed during walking; DOMSsq: DOMS assessed after performing a squat movement; PC: protein carbonyls; TBARS: thiobarbituric acid reactive substances (malondialdehyde measured spectrophotometrically); TAC: total antioxidant capacity; GSH: reduced glutathione; CAT: catalase; sORP: static oxidation-reduction potential; cORP: capacity oxidation-reduction potential; SRS: superoxide radical scavenging; HRS: hydroxyl radical scavenging; RP: reducing power; MDA: malondialdehyde (measured by HPLC-DAD). *Statistically significant correlation ($p < 0.05$).

Table 3: Percentage (%) alterations of the oxidative stress biomarkers postexercise compared to baseline.

	Trained			Untrained		
	24 h	48 h	72 h	24 h	48 h	72 h
PC	−0.93 ± 3.51	−7.45 ± 4.21$^{\#}$	−8.04 ± 3.80	8.64 ± 4.27	14.67 ± 3.16*	2.32 ± 3.16
TBARS	10.25 ± 2.93*	8.50 ± 2.85*$^{\#}$	14.98 ± 5.92*	18.29 ± 7.86*	26.89 ± 6.48*	13.49 ± 6.98*
TAC	1.59 ± 1.56	0.04 ± 1.51	0.91 ± 1.92	1.14 ± 1.38	1.50 ± 1.52	0.67 ± 1.20
GSH	12.63 ± 5.44*	23.09 ± 7.17*$^{\#}$	3.83 ± 3.19	−2.98 ± 3.91	1.11 ± 5.47	−9.64 ± 4.75*
CAT	1.82 ± 3.68	10.22 ± 4.05	4.13 ± 4.14	6.09 ± 4.86	5.75 ± 4.58	2.58 ± 5.28
sORP	−2.11 ± 0.73$^{\#}$	−3.31 ± 1.11$^{\#}$	−0.64 ± 1.14$^{\#}$	4.65 ± 1.43*	4.01 ± 1.61*	7.45 ± 1.45*
cORP	30.57 ± 7.02*$^{\#}$	27.15 ± 7.55*$^{\#}$	15.84 ± 8.18	−9.31 ± 6.41	−4.87 ± 7.11	−8.57 ± 11.28
SRS	12.16 ± 3.17*$^{\#}$	7.45 ± 2.69*$^{\#}$	5.79 ± 2.79	−1.16 ± 3.21	−3.95 ± 3.67	0.65 ± 3.09
HRS	1.14 ± 11.22	−11.42 ± 9.28	15.72 ± 13.74	−9.29 ± 6.06	−12.66 ± 9.60	0.23 ± 9.01
RP	3.14 ± 2.82	4.21 ± 3.32	5.74 ± 3.22$^{\#}$	−7.08 ± 4.95	0.13 ± 5.41	−10.37 ± 5.58
MDA	14.07 ± 3.21*	14.70 ± 4.30*	21.79 ± 3.59*	15.83 ± 3.81*	14.55 ± 3.71*	23.65 ± 4.87*

PC: protein carbonyls; TBARS: thiobarbituric acid reactive substances (malondialdehyde measured spectrophotometrically); TAC: total antioxidant capacity; GSH: reduced glutathione; CAT: catalase; sORP: static oxidation-reduction potential; cORP: capacity oxidation-reduction potential; SRS: superoxide radical scavenging; HRS: hydroxyl radical scavenging; RP: reducing power; MDA: malondialdehyde (measured by HPLC-DAD). Values are expressed as mean ± SEM. *Statistically significant compared with preexercise values ($p < 0.05$). $^{\#}$Statistically significant between trained and untrained at the same time point.

with 2, 4, 6, 8, 10, and 12 μM of MDA, and a calibration curve was obtained. A similar procedure was also followed for the determination of the aqueous curve by using the same concentrations of MDA. Linearity and reproducibility were evaluated by linear regression. The equations obtained by the least squared regression were $y = 3.863x + 11.651$ for plasma curves and $y = 4.4151x - 4.1043$ for aqueous curves, and the values to R^2 were 0.9952 and 0.9982 for plasma and

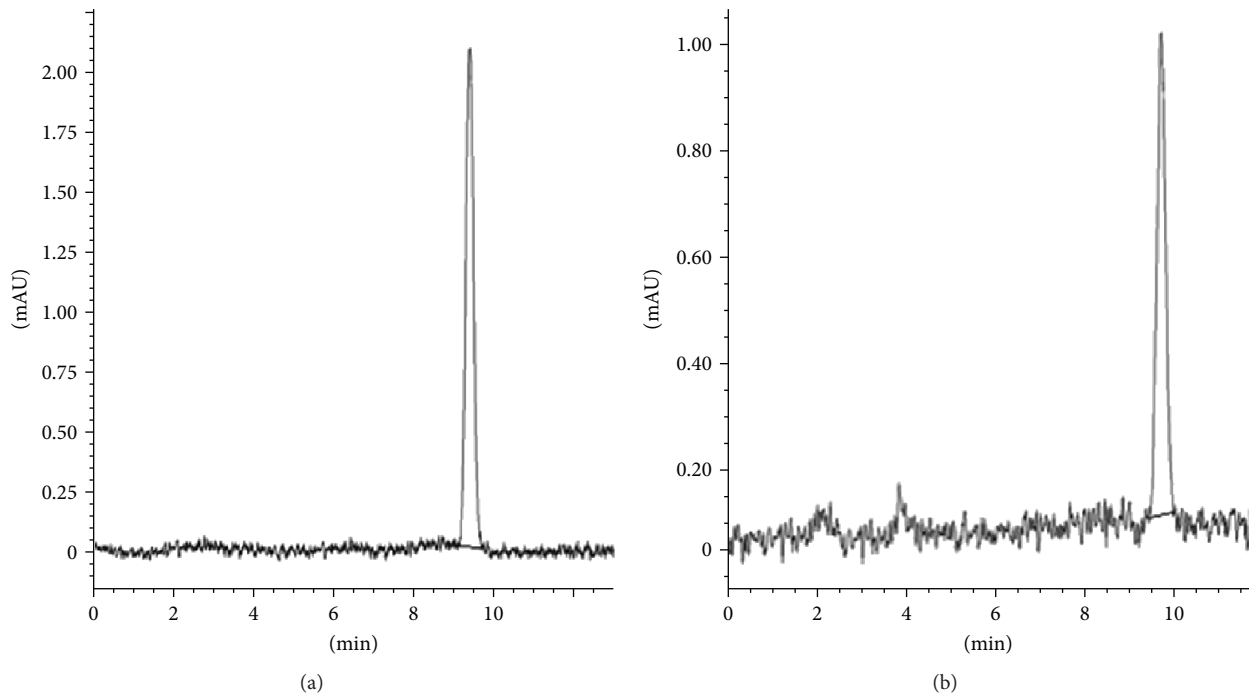

Figure 1: Representative chromatograms of plasma spiked with 12 μM MDA (a) and a plasma sample of a volunteer containing 3.79 μM MDA (b).

aqueous curves, respectively. Moreover analytical curves (i.e., peak area of each concentration from spiked plasma against area from aqueous MDA standards) exhibited an excellent linearity having a correlation coefficient more than 0.995. The relative recovery for the MDA-TBA complex was assessed at three concentrations of 0.5, 1.0, and 1.5 μM, and the average recovery was counted at 98.06% (ranged from 97.54% to 98.58%). The intra- and interday precision of this specific proposed method was determined by counting standard spiked plasma solutions. Specifically, regarding the interday precision, three different spiked plasma solutions (0.5, 1.0, and 1.5 μM MDA) were analyzed in triplicate for 5 consecutive days each. Intraday precision was counted by measuring a plasma solution spiked with 1.7 μM of MDA plasma sample for seven times within the same day. The precisions were expressed in % RSD and calculated at 0.43% and 0.31% for the inter- and intraday tests, respectively, which are in the range of acceptability and accuracy [16]. It is worth mentioning that the average retention time was at 9.55 min (Figure 1).

(2) Malondialdehyde Levels. As far as the chromatographic determination of MDA levels is concerned, the results were similar in both trained (i.e., MDA levels increased at all time points by 14.07%, 14.70%, and 21.79%) and untrained groups (i.e., MDA levels increased at all time points by 15.83%, 14.55%, and 23.65%) (Table 3).

(3) Comparison between the MDA Concentrations Measured by Spectrophotometry and Chromatography. All tested groups exhibited a 2.5-fold increase in MDA concentration measured by spectrophotometry (ranged from 5.5 to 9.2 μM) compared with chromatography (ranged from 2.2 to 4.7 μM, resp.) (Figure 2). The percentage alterations of MDA concentrations postexercise compared to preexercise were also similar between the two methods (Table 3). This similarity was also confirmed by the significant correlation between the percentage alterations of MDA values obtained by the two analytical techniques ($r = 0.703$, $p < 0.01$) (Figure 3).

3.2.4. GSH Levels. As depicted in Table 3, GSH was significantly increased in the trained group 24 and 48 h postexercise by 12.63% and 23.09%, respectively. Furthermore, there was also a significant increase in the trained group compared with the untrained participants 48 h postexercise. On the contrary, GSH levels were significantly decreased in the untrained group by 9.64% 72 h postexercise compared to preexercise (Table 3).

3.2.5. Catalase Activity. Regarding catalase activity, no significant effects were observed (Table 3).

3.2.6. ORP Markers. The results from ORP marker analysis as estimated by the RedoxSYS system showed significant differences between the two groups at all time points (Table 3). In particular, the untrained group displayed significant increases at all time points postexercise by 4.65%, 4.01%, and 7.45%, respectively, compared to preexercise, indicating induced oxidative status (Table 3). The cORP analysis indicated induced reductive status postexercise compared to preexercise in the trained group (Table 3). In fact, cORP levels were significantly increased by 30.57% and 27.15% 24 and 48 h postexercise, respectively, compared with preexercise values (Table 3).

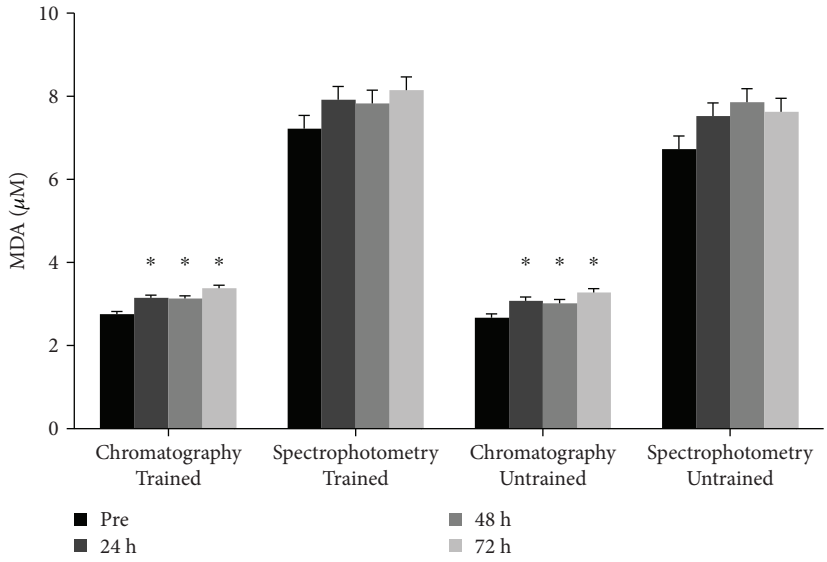

Figure 2: Comparison of malondialdehyde (MDA) concentrations measured chromatographically (HPLC) and spectrophotometrically (TBARS). *Statistically significant compared with preexercise value.

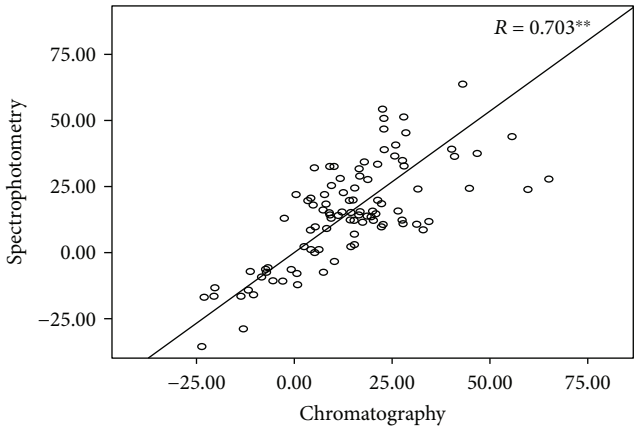

Figure 3: Spearman's correlation coefficient (R) and solid line for percentage (%) alterations of MDA concentrations measured chromatographically (HPLC) and spectrophotometrically (TBARS). **Significant correlation ($p < 0.01$).

3.2.7. Determination of Antioxidant and Free Radical Scavenging Capacity. Regarding TAC, no significant differences were observed either between pre- and postexercise or between trained and untrained groups (Table 3). In the reducing power assay, there was only a significant increase 72 h postexercise in the trained group compared to the untrained individuals (Table 3). Regarding superoxide radical-scavenging activity in the trained group, an increase 24 and 48 h postexercise by 12.16% and 7.45%, respectively, compared to preexercise was displayed (Table 3). The participants of the trained group also exhibited increased superoxide radical-scavenging capacity compared with the untrained group 24 and 48 h postexercise (Table 3). However, no significant alteration was observed in the hydroxyl radical-scavenging capacity either between pre- and postexercise or between trained and untrained groups (Table 3).

Moreover, a Spearman correlation analysis was conducted for examining the possibility of a potential correlation between the above four biomarkers (Table 4). No significant correlations were observed in any of the tested groups, apart from a moderate significant correlation ($R = 0.514$) between superoxide radical-scavenging capacity and reducing power levels in the trained group.

4. Discussion

In the present study, the effects of eccentric exercise on oxidative stress and inflammation between trained and untrained individuals were examined. A first approach in the evaluation of exercise-induced muscle damage was the assessment of muscle pain, as eccentric exercise has been shown to cause delayed onset muscle soreness (DOMS) [6]. DOMS has been considered the major cause of reduced exercise performance, impaired muscle strength, and psychological discomfort for both trained and untrained humans [17]. In the present study, DOMS levels in the trained group were lower than those in the untrained group. It is also worth mentioning that the peak muscle soreness was detected 48 h postexercise in both groups, being in accordance with other studies [18]. Eccentric exercise-induced inflammation may be the main cause of ROS production after a bout of exercise as it leads to migration of phagocytic cells to the damaged tissue. The forthcoming respiratory burst results in the production of ROS, such as superoxide and hydroxyl radicals [6]. Statistical analysis confirmed the aforementioned hypothesis, as DOMS in the untrained group displayed a significant negative correlation with cORP and reducing power, which depict the antioxidants' reserves and scavenging activity, respectively. However, a "preconditioning" of muscle during exercise may reduce susceptibility to inflammation response after performing a new bout of eccentric exercise, and consequently

Table 4: Correlation analysis between superoxide radical-scavenging (SRS) activity, hydroxyl radical-scavenging (HRS) activity, reducing power (RP), and total antioxidant capacity (TAC).

	24 h			48 h			72 h	
	HRS	SRS	RP	HRS	SRS	RP	HRS	SRS	RP
Trained									
HRS		−0.153	0.514*		−0.081	0.253		0.155	0.336
SRS			−0.107			0.137			−0.068
TAC	0.178	−0.126	0.061	−0.248	0.008	−0.214	−0.137	0.077	−0.327
Untrained									
HRS		0.352	−0.117		−0.385	0.166		−0.412	−0.328
SRS			−0.127			−0.069			0.130
TAC	0.230	0.325	−0.199	−0.007	−0.117	0.346	0.356	−0.069	−0.123

*Significant correlation ($p < 0.05$).

the inflammatory response is not so extended, resulting in weaker muscle pain. The latter confirms the notion regarding the relationship between inflammatory and pain response and may account for the difference in muscle pain between the two examined groups of our study [19].

As regard to protein carbonylation, it typically occurs several hours after eccentric exercise and generates a substantial amount of ROS via multiple mechanisms [20]. Our results indicated a more effective protection of proteins from oxidation (i.e., reduction of PC concentration) in the trained group compared to the untrained individuals postexercise assuring the impact of training background [19]. Interestingly, another study has shown an increase in protein oxidation levels of "nonresistance" trained women after eccentric exercise [20]. Considering that in this experiment the majority of trained individuals (17/22) were accustomed to resistance training, it seems that the type of exercise may affect the range of muscle injury and the forthcoming protein carbonylation.

Lipid peroxidation did not show any significant alterations between the tested groups when measured spectrophotometrically using the TBARS assay. However, increased MDA concentrations were observed in both groups at all time points compared with preexercise samples. This is usually observed several hours to days after acute resistance exercise probably triggered by leukocyte and macrophage infiltration and/or xanthine oxidase activation due to the ischemia-reperfusion process [21]. Since the TBARS assay has received criticism due to a lack of specificity that increases the noise of the measurements [22, 23], we also performed HPLC-DAD, a more specific method for MDA determination in plasma, in order to compare these two methods. The results indicated an approximately 2.5-fold increase in the absolute values of MDA concentration measured spectrophotometrically compared with the chromatographic results in both groups. This finding confirmed that MDA is determined in a more sensitive manner by HPLC than by spectrophotometry, since in TBARS assay, TBA reacts apart from MDA with other compounds such as sugars, amino acids, and aldehydes [11]. Interestingly, a similar difference between the two performed assays has also been previously reported [11, 23]. However, the TBARS assay exhibited a good matching with chromatography regarding the postexercise percentage alterations of MDA concentrations, a fact that was also verified by the significant correlation between the two assays (Figure 3). Therefore, regardless of the obtained overestimated absolute values, alterations of MDA concentration can be reliably described using spectrophotometry (i.e., TBARS). Thus, (3) can be used by researchers for the accurate spectrophotometric calculation of MDA concentration:

$$\text{Chromatographic [MDA] } (\mu\text{M}) = 0.4 \text{ spectrophotometric [MDA] } (\mu\text{M}). \quad (3)$$

Regarding GSH levels, they increased in the trained compared to the untrained individuals at all tested time points and especially 48 h postexercise. In that sense, it has been proposed that regular exercise induces adaptations due to the repeated activation of antioxidant genes and proteins leading to a higher antioxidant capacity and, therefore, to a more effective neutralization of ROS [2]. GSH-related antioxidant enzymes play a significant role in GSH synthesis and regeneration and, therefore, this explains the GSH increase in trained participants [24].

Similarly, ORP markers also indicated that oxidative stress was lower in the trained individuals. Specifically, sORP levels in the untrained group were found not only significantly higher postexercise compared with preexercise values but also elevated compared to the trained participants suggesting oxidative stress induction. Our group has previously reported that this marker was increased and associated with oxidative stress induction after endurance and strenuous exercise [6, 10]. The obtained result of the cORP assay, which indicates antioxidant capacity, was also in accordance with sORP, as it was higher in the trained participants. Thus, it becomes evident that untrained individuals are more vulnerable to ROS generation and inflammation response after muscle injury. The improved capability of trained people to decrease ROS levels imply that they are better protected from exercise-induced oxidative damage.

The increased antioxidant capacity of the trained participants was also confirmed by the significant increase in $O_2^{\bullet -}$ scavenging capacity postexercise compared to

preexercise as well as compared to their untrained counterparts. According to the literature, SOD plays a predominant role in scavenging $O_2^{\bullet -}$ in plasma [25]. Interestingly, studies have shown that trained individuals exhibited high SOD levels, thus coping with $O_2^{\bullet -}$ more effectively [26]. Similarly, reduction of Fe(III) to Fe(II) as determined by the reducing power assay was higher in the trained in comparison with the untrained individuals. It is apparent that the concentrations of plasma antioxidant molecules, such as uric acid, α-tocopherol, bilirubin, and ascorbic acid are elevated in individuals with an athletic background [27]. The high GSH levels in the trained group may account for their higher reducing capacity, since GSH acts as an antioxidant by donating hydrogen atoms in the regeneration of the antioxidant vitamins E and C [28]. On the other hand, no significant alterations were observed in $OH^{\bullet}$ scavenging levels after exercise compared with preexercise samples, whereas trained individuals were again more efficient in neutralizing $OH^{\bullet}$ 72 h postexercise compared to untrained individuals.

Finally, the lack of significant correlations between the examined biomarkers is worth mentioning (apart from RP and $OH^{\bullet}$ in the trained group at 72 h). This fact confirms the notion that oxidative stress induction and the following adaptations based on the activation of the antioxidant mechanisms is a complex process depending on various physiological, biochemical, and genetic factors that vary considerably between individuals [29]. This particular conclusion is very important as it suggests a personalized approach for counteracting eccentric exercise-induced oxidative stress. Undoubtedly, it suggests that a specific formulation of each person's diet, according to his oxidative status and based on supplementation with the appropriate antioxidants days after performing bouts of exercise, may lead to a faster and more efficient recovery. Regarding the present study, the nutritional intake of the participants was not thoroughly examined. However, according to their report, they did not consume higher amounts of proteins through their normal diet. Furthermore, we suggested that they should abstain from any unusual nutritional as well as antioxidant supplementation a week before, until the end of the experiment. Therefore, we believe that their nutrition did not affect our results. Nevertheless, supplementation is considered a double-edge sword, as it should only be applied in a severe oxidative stress condition after strenuous exercise. Otherwise, it can interfere with muscle adaptations and damaged-tissue regeneration [30, 31].

Taking the above data into consideration, it is clear that eccentric exercise induced reductive stress or no stress instead of oxidative stress in trained individuals, contrary to what is expected after such a demanding exercise bout. Indeed, reductive stress has also been observed by our research group in athletes who participated in top level basketball competitions as well as in individuals who have undergone a 103 km ultramarathon mountain race [10, 15]. Nikolaidis et al. [19] have reported that a repeated bout of lengthening contractions induced much less muscle damage and blood exercise oxidative stress than the first bout, a key information in our effort to analyze our findings. It seems therefore that trained individuals regularly performing eccentric contractions have performed muscle adaptations limiting in that way the exercise-induced inflammation and the subsequent free radical production generated by neutrophil and macrophage infiltration to the injury point [32].

In general, regularly performed exercise may lead to well-described adaptations of the cardiovascular and muscular system. Important responses at the intramyocellular level include increases in size and number of mitochondria as well as induction of the antioxidant enzyme activities [33, 34]. It has been proposed that exercise causes an activation of mitogen-activated protein kinases (MAPKs: p38, ERK 1, and ERK 2) that subsequently activates nuclear factor κB (NF-κB) in rat gastrocnemius muscle and consequently the expression of important enzymes associated with defense against ROS (i.e., Mn-SOD and Cu, Zn-SOD, CAT, and GPX1) and adaptation to exercise [35, 36]. For example, GSH-related antioxidant enzymes including glutathione reductase (GR) and GSH synthetase are also such products of the above factors' activation [24], explaining abundantly the increase of GSH in the trained participants of our study. Similarly, the activation of the mechanisms referred above, as a result of the frequent exercise, may tone up the antioxidant status of the regularly trained individuals and therefore lead to a better protection against oxidative damage and an enhanced scavenging activity against free radicals The hypothesis regarding exercise-induced responses of the trained individuals, also relies on a study, which reported that regular exercise appears to gradually increase the adaptation levels by the repeated activation of antioxidant proteins and genes [37]. However, increased free radical production may be desired or even required for normal muscle function and/or muscle regeneration [32]. Free radicals generated by neutrophils and macrophages are crucial for removing muscle tissue that has been damaged after eccentric exercise. Furthermore, they are also important as they act as signaling molecules to regulate muscle cell growth, differentiation, and proliferation in the context of damaged tissue repair [38].

5. Conclusion

Previous studies of our group with respect to the individualized monitoring of exercise-induced oxidative stress have suggested that each individual is a unique biological entity and that generalized recommendations concerning recovery after exercise should be avoided. Supporting this notion, the present study demonstrated that the training background is an important factor with high impact on eccentric exercise-induced oxidative stress and the subsequent adaptations. We expect that our findings will help the endeavor to identify the ideal approach in terms of type, duration, and intensity of conducted exercise, in conjunction to the training background of an individual and may help to better understand the phenomenon of oxidative or reductive stress after exercise. Moreover, as suggested by our work, individualized nutritional approach could help to fine-tune the recovery process and consequently improve health status and performance after eccentric exercise.

Data Availability

All data, tables, and figures in this manuscript are original and are available upon request.

Ethical Approval

All procedures performed in this study involving human participants were in accordance with the ethical standards of the institutional and/or national research committee and with the 1964 Helsinki declaration and its later amendments or comparable ethical standards, and approval was received by the "Human Subjects Committee" of the University of Thessaly (Reference no.: 1074, date: 10/02/2016).

Conflicts of Interest

The authors had no financial, consultant, or other relations that might lead to bias or a conflict of interest. The results of the present study are presented clearly, honestly, and without fabrication, falsification, or inappropriate data manipulation.

Acknowledgments

The study was funded by the Hellenic General Secretariat for Research and Technology (GSRT) and the Hellenic Foundation for Research and Innovation (HFRI) (Grant no. 5450).

References

[1] C. E. Cooper, N. B. J. Vollaard, T. Choueiri, and M. T. Wilson, "Exercise, free radicals and oxidative stress," *Biochemical Society Transactions*, vol. 30, no. 2, pp. 280–285, 2002.

[2] P. Steinbacher and P. Eckl, "Impact of oxidative stress on exercising skeletal muscle," *Biomolecules*, vol. 5, no. 2, pp. 356–377, 2015.

[3] M. G. Nikolaidis, A. Kyparos, M. Hadziioannou et al., "Acute exercise markedly increases blood oxidative stress in boys and girls," *Applied Physiology, Nutrition, and Metabolism*, vol. 32, no. 2, pp. 197–205, 2007.

[4] D. H. Serravite, A. Perry, K. A. Jacobs, J. A. Adams, K. Harriell, and J. F. Signorile, "Effect of whole-body periodic acceleration on exercise-induced muscle damage after eccentric exercise," *International Journal of Sports Physiology and Performance*, vol. 9, no. 6, pp. 985–992, 2014.

[5] M. A. Brentano and L. F. Martins Kruel, "A review on strength exercise-induced muscle damage: applications, adaptation mechanisms and limitations," *Journal of Sports Medicine and Physical Fitness*, vol. 51, no. 1, pp. 1–10, 2011.

[6] D. Stagos, N. Goutzourelas, A.-M. Ntontou et al., "Assessment of eccentric exercise-induced oxidative stress using oxidation-reduction potential markers," *Oxidative Medicine and Cellular Longevity*, vol. 2015, Article ID 204615, 10 pages, 2015.

[7] J. Lee, A. H. Goldfarb, M. H. Rescino, S. Hegde, S. Patrick, and K. Apperson, "Eccentric exercise effect on blood oxidative-stress markers and delayed onset of muscle soreness," *Medicine and Science in Sports and Exercise*, vol. 34, no. 3, pp. 443–448, 2002.

[8] J. Kim and J. Lee, "A review of nutritional intervention on delayed onset muscle soreness. Part I," *Journal of Exercise Rehabilitation*, vol. 10, no. 6, pp. 349–356, 2014.

[9] N. V. Margaritelis, A. Kyparos, V. Paschalis et al., "Reductive stress after exercise: the issue of redox individuality," *Redox Biology*, vol. 2, pp. 520–528, 2014.

[10] Y. Spanidis, D. Stagos, M. Orfanou et al., "Variations in oxidative stress levels in 3 days follow-up in ultramarathon mountain race athletes," *Journal of Strength and Conditioning Research*, vol. 31, no. 3, pp. 582–594, 2017.

[11] A. L. Spirlandeli, R. Deminice, and A. A. Jordao, "Plasma malondialdehyde as biomarker of lipid peroxidation: effects of acute exercise," *International Journal of Sports Medicine*, vol. 35, no. 1, pp. 14–18, 2014.

[12] T. Ak and İ. Gülçin, "Antioxidant and radical scavenging properties of curcumin," *Chemico-Biological Interactions*, vol. 174, no. 1, pp. 27–37, 2008.

[13] G. C. Yen and P. D. Duh, "Scavenging effect of methanolic extracts of peanut hulls on free-radical and active-oxygen species," *Journal of Agricultural and Food Chemistry*, vol. 42, no. 3, pp. 629–632, 1994.

[14] S.-K. Chung, T. Osawa, and S. Kawakishi, "Hydroxyl radical-scavenging effects of spices and scavengers from brown mustard (*Brassica nigra*)," *Bioscience, Biotechnology, and Biochemistry*, vol. 61, no. 1, pp. 118–123, 2014.

[15] Y. Spanidis, N. Goutzourelas, D. Stagos et al., "Variations in oxidative stress markers in elite basketball players at the beginning and end of a season," *Experimental and Therapeutic Medicine*, vol. 11, no. 1, pp. 147–153, 2016.

[16] H. Z. Rofael and M. S. Abdel-Rahman, "Development and validation of a high-performance liquid chromatography method for the determination of cocaine, its metabolites and ketamine," *Journal of Applied Toxicology*, vol. 22, no. 2, pp. 123–128, 2002.

[17] M. A. Serinken, C. Gencoglu, and B. M. Kayatekin, "The effect of eccentric exercise-induced delayed-onset muscle soreness on positioning sense and shooting percentage in wheelchair basketball players," *Balkan Medical Journal*, vol. 30, no. 4, pp. 382–386, 2013.

[18] J. E. Hilbert, G. A. Sforzo, and T. Swensen, "The effects of massage on delayed onset muscle soreness," *British Journal of Sports Medicine*, vol. 37, no. 1, pp. 72–75, 2003.

[19] M. G. Nikolaidis, V. Paschalis, G. Giakas et al., "Decreased blood oxidative stress after repeated muscle-damaging exercise," *Medicine and Science in Sports and Exercise*, vol. 39, no. 7, pp. 1080–1089, 2007.

[20] A. H. Goldfarb, R. J. Bloomer, and M. J. Mckenzie, "Combined antioxidant treatment effects on blood oxidative stress after eccentric exercise," *Medicine and Science in Sports and Exercise*, vol. 37, no. 2, pp. 234–239, 2005.

[21] N. G. Avery, J. L. Kaiser, M. J. Sharman et al., "Effects of vitamin E supplementation on recovery from repeated bouts of resistance exercise," *Journal of Strength and Conditioning Research*, vol. 17, no. 4, pp. 801–809, 2003.

[22] D. Grotto, L. D. Santa Maria, S. Boeira et al., "Rapid quantification of malondialdehyde in plasma by high performance liquid chromatography-visible detection," *Journal of Pharmaceutical and Biomedical Analysis*, vol. 43, no. 2, pp. 619–624, 2007.

[23] H. F. Moselhy, R. G. Reid, S. Yousef, and S. P. Boyle, "A specific, accurate, and sensitive measure of total plasma malondialdehyde by HPLC," *Journal of Lipid Research*, vol. 54, no. 3, pp. 852–858, 2013.

[24] C. Espinosa-Diez, V. Miguel, D. Mennerich et al., "Antioxidant responses and cellular adjustments to oxidative stress," *Redox Biology*, vol. 6, pp. 183–197, 2015.

[25] V. Lobo, A. Patil, A. Phatak, and N. Chandra, "Free radicals, antioxidants and functional foods: impact on human health," *Pharmacognosy Reviews*, vol. 4, no. 8, pp. 118–126, 2010.

[26] N. Ortenblad, K. Madsen, and M. S. Djurhuus, "Antioxidant status and lipid peroxidation after short-term maximal exercise in trained and untrained humans," *The American Journal of Physiology*, vol. 272, 4, Part 2, pp. R1258–R1263, 1997.

[27] P. E. Reddy, S. M. Manohar, S. V. Reddy, A. R. Bitla, S. Vishnubhotla, and P. V. L. N. Srinivasa Rao, "Ferric reducing ability of plasma and lipid peroxidation in hemodialysis patients: intradialytic changes," *International Journal of Nephrology & Urology*, vol. 2, no. 3, pp. 414–421, 2010.

[28] J. M. May, Z. C. Qu, R. R. Whitesell, and C. E. Cobb, "Ascorbate recycling in human erythrocytes: role of GSH in reducing dehydroascorbate," *Free Radical Biology & Medicine*, vol. 20, no. 4, pp. 543–551, 1996.

[29] T. Rankinen and C. Bouchard, "Gene-physical activity interactions: overview of human studies," *Obesity*, vol. 16, Supplement 3, pp. S47–S50, 2008.

[30] M.-C. Gomez-Cabrera, C. Borrás, F. V. Pallardó, J. Sastre, L. L. Ji, and J. Viña, "Decreasing xanthine oxidase-mediated oxidative stress prevents useful cellular adaptations to exercise in rats," *The Journal of Physiology*, vol. 567, no. 1, pp. 113–120, 2005.

[31] L. L. Ji, M.-C. Gomez-Cabrera, N. Steinhafel, and J. Vina, "Acute exercise activates nuclear factor (NF)-κB signaling pathway in rat skeletal muscle," *The FASEB Journal*, vol. 18, no. 13, pp. 1499–1506, 2004.

[32] I. G. Fatouros and D. Kouretas, "Exercise, oxidative stress, and inflammation," in *Exercise Physiology: From a Cellular to an Integrative Approach*, vol. 75, p. 245, IOS Press, 2010.

[33] I. Irrcher, P. J. Adhihetty, T. Sheehan, A. M. Joseph, and D. A. Hood, "PPARγ coactivator-1α expression during thyroid hormone- and contractile activity-induced mitochondrial adaptations," *American Journal of Physiology. Cell Physiology*, vol. 284, no. 6, pp. C1669–C1677, 2003.

[34] Z. Yan, M. Okutsu, Y. N. Akhtar, and V. A. Lira, "Regulation of exercise-induced fiber type transformation, mitochondrial biogenesis, and angiogenesis in skeletal muscle," *Journal of Applied Physiology*, vol. 110, no. 1, pp. 264–274, 2011.

[35] L. L. Ji, M.-C. Gomez-Cabrera, and J. Vina, "Exercise and hormesis: activation of cellular antioxidant signaling pathway," *Annals of the New York Academy of Sciences*, vol. 1067, no. 1, pp. 425–435, 2006.

[36] M.-C. Gomez-Cabrera, E. Domenech, and J. Vina, "Moderate exercise is an antioxidant: upregulation of antioxidant genes by training," *Free Radical Biology & Medicine*, vol. 44, no. 2, pp. 126–131, 2008.

[37] Z. Radak, Z. Zhao, E. Koltai, H. Ohno, and M. Atalay, "Oxygen consumption and usage during physical exercise: the balance between oxidative stress and ROS-dependent adaptive signaling," *Antioxidants & Redox Signaling*, vol. 18, no. 10, pp. 1208–1246, 2013.

[38] J. Vina, C. Borras, M.-C. Gomez-Cabrera, and W. C. Orr, "Part of the series: from dietary antioxidants to regulators in cellular signalling and gene expression. Role of reactive oxygen species and (phyto)oestrogens in the modulation of adaptive response to stress," *Free Radical Research*, vol. 40, no. 2, pp. 111–119, 2009.

Hindawi
Oxidative Medicine and Cellular Longevity
Volume 2018, Article ID 7496936, 18 pages
https://doi.org/10.1155/2018/7496936

Research Article

Solid Lipid Nanoparticles of Myricitrin Have Antioxidant and Antidiabetic Effects on Streptozotocin-Nicotinamide-Induced Diabetic Model and Myotube Cell of Male Mouse

Akram Ahangarpour,[1] Ali Akbar Oroojan,[2] Layasadat Khorsandi,[3] Maryam Kouchak,[4] and Mohammad Badavi[5]

[1]*Department of Physiology, Faculty of Medicine, Diabetes Research Center, Health Research Institute, Ahvaz Jundishapur University of Medical Sciences, Ahvaz, Iran*
[2]*Department of Physiology, Faculty of Medicine, Cellular and Molecular Research Center, Student Research Committee, Ahvaz Jundishapur University of Medical Sciences, Ahvaz, Iran*
[3]*Department of Anatomical Sciences, Faculty of Medicine, Cellular and Molecular Research Center, Ahvaz Jundishapur University of Medical Sciences, Ahvaz, Iran*
[4]*Department of Pharmaceutical Sciences, Faculty of Pharmacy, Nanotechnology Research Center, Ahvaz Jundishapur University of Medical Sciences, Ahvaz, Iran*
[5]*Department of Physiology, Faculty of Medicine, Physiology Research Center, Ahvaz Jundishapur University of Medical Sciences, Ahvaz, Iran*

Correspondence should be addressed to Ali Akbar Oroojan; aliakbar_oroojan@yahoo.com

Received 17 February 2018; Revised 12 May 2018; Accepted 31 May 2018; Published 17 July 2018

Academic Editor: Joanna Lecka

Type 2 diabetes mellitus (T2DM) may occur via oxidative stress. Myricitrin is a plant-derived antioxidant, and its solid lipid nanoparticle (SLN) may be more potent. Hence, the present study was conducted to evaluate the effects of myricitrin SLN on streptozotocin-nicotinamide- (STZ-NA-) induced T2DM of the mouse and hyperglycemic myotube. In this experimental study, cold homogenization method was used to prepare SLN. Then, 120 adult male NMRI mice were divided into 7 groups: control, vehicle, diabetes (received STZ 65 mg/kg 15 min after injected NA 120 mg/kg), diabetes + SLN containing myricitrin 1, 3, and 10 mg/kg, and diabetes + metformin. For in vitro study, myoblast (C2C12) cell line was cultured and divided into 6 groups ($n = 3$): control, hyperglycemia, hyperglycemia + SLN containing myricitrin 1, 3, and, 10 μM, and hyperglycemia + metformin. After the last nanoparticle treatment, plasma samples, pancreas and muscle tissues, and myotubes were taken for experimental assessments. Diabetes increased lipid peroxidation and reduced antioxidant defense along with the hyperglycemia, insulin resistance, and pancreas apoptosis. Hyperglycemia induced oxidative stress, antioxidant impairment, and cellular apoptosis. Myricitrin SLN improved diabetes and hyperglycemia complications in the in vivo and in vitro studies. Therefore, SLN of myricitrin showed antioxidant, antidiabetic, and antiapoptotic effects in the mouse and myotube cells.

1. Introduction

Diabetes mellitus is characterized by a group of metabolic disorders such as hyperglycemia over a long period, impaired carbohydrate, lipid, and protein metabolism caused by pancreas's failure to produce enough insulin, and insufficiency of the cells responding properly to the produced insulin. Type 2 diabetes mellitus (T2DM) is the most common form of diabetes mellitus, which making up to about 90% to 95% of all diabetes cases and is predicted to increase to 439 million by 2030. This is equivalent to about 6% of the world's population. It is estimated that this type of diabetes increase in the developing countries which more than 70% of the patients being 45–64 years old suffer from this disease [1, 2].

Glucose transporter type 4 (Glut-4), as a major insulin-stimulated glucose transporter, is expressed predominantly in skeletal muscle and facilitates the glucose transport into the skeletal muscle during insulin-stimulated glucose uptake. Glut-4 is sequestered in intracellular vesicles, and upon the plasma level of insulin increased during the postprandial period in response to the ingested carbohydrates and fat, Glut-4 vesicles translocate to and fuse with the plasma membrane, permitting increased glucose flux. Glut-4 is a rate-controlling transporter of glucose transport into muscle, and this disposal is diminished in insulin-resistant states. Also, a disruption in the normal insulin stimulated-glucose uptake into the skeletal muscle indicates a decrease or defect of Glut-4 expression and function caused by peripheral insulin resistance associated with T2DM [1–3]. Two main methods to evaluate glucose homeostasis in subjects at risk of diabetes are homeostasis model assessment of insulin resistance (HOMA-IR) and homeostasis model assessment of β-cell function (HOMA-β) that measuring quantifies insulin resistance and β-cell function, based on fasting insulin and glucose levels. These variables have been widely applied as an index of insulin resistance in individuals with both normal glucose tolerance and impaired glucose tolerance and have been used to document insulin resistance for patients at risk for T2DM [4, 5]. Metformin, belonging to the biguanide drug group, represents the first-line treatment of T2DM. This drug exerts its therapeutic effects via decreasing glucose production in the liver and reducing the intestinal absorption of glucose. These events lead to improving insulin sensitivity by increasing peripheral glucose uptake and utilization in muscles and other tissues. Metformin, along with antihyperglycemic properties, has several effects such as improvements in endothelial dysfunction, homeostasis and oxidative stress, insulin resistance, lipid profiles, and fat redistribution [6, 7].

There is a growing scientific evidence that oxidative stress and free radicals play an important role in the pathogenesis of T2DM and its complications through the induced damage in lipids, proteins, and nucleic acids. More recent studies indicated that oxidative stress could accelerate or contribute to the development of β-cell's dysfunction and insulin resistance. Hyperglycemia induces free radicals and impairs both enzymatic and nonenzymatic pathways of endogenous antioxidant defense. This condition can stimulate imbalance between the production and elimination of reactive oxygen species (ROS). Superoxide dismutase (SOD) and catalase (CAT) are enzymatic endogenous antioxidants that play synergistic actions in scavenging of free radicals by transforming them to less deleterious molecules. SOD catalyzes the dismutation from the superoxide anion (O_2^-), as a major ROS, into hydrogen peroxide (H_2O_2), and CAT converts H_2O_2 into H_2O. Hence, a harmful free radical could be converting to the innocuous molecules. The main indicators of oxidative stress are polyunsaturated fatty acid peroxidation end products known as malondialdehyde (MDA). Higher levels of MDA and lower levels of antioxidant enzymes were observed in T2DM patients [8].

Bax and Bcl-2 are two proteins that regulate apoptosis in muscle cells. It was demonstrated that Bcl-2 expression could significantly elevate during hydrogen peroxide-induced apoptosis in myotubes and other muscle cells. Further, overexpression of Bcl-2 can decrease the level of proapoptotic Bax in myotubes, without significant changes in the levels of other proapoptotic agents such as Bak and Bad. It was generally approved that Bax and Bcl-2 serve to control the release of mitochondrial apoptotic factors in C2C12 myotubes following oxidative stress treatment. So, these genes are more important for apoptosis assessment than the others in the muscle cells [9].

Antioxidant therapy may inhibit the risk of developing diabetes and its complications in type 2 diabetic patients. A variety of antioxidants including plant-derived active substances interact with the free radicals through the binding of the metals which stimulate the production of free radicals, scavenge, or reduce their formation. These plants which contain antioxidant agents such as flavonoids have therapeutic effects on the treatment of T2DM [10]. Myricitrin (myricetin-3-O-α-rhamnoside), a botanical flavonol glycoside, belonging to the flavonol subgroup, was extracted from some plants (*Myrica rubra*, *Pouteria gender*, *Manilkara zapota*, and *Eugenia uniflora*). It has anxiolytic, antinociceptive, anti-inflammatory, and antioxidant effects [11]. Since this flavonoid glycoside has a high antioxidative activity, it is used as an important supplement in medicines. Further, myricitrin was shown to be a stronger free radical scavenger than other flavonol rhamnosides or quercetin. It was revealed that myricitrin inhibits ROS-induced vein endothelial cell dysfunction through the reducing of MDA, H_2O_2-induced oxidative damage, and regulation of antioxidant enzyme activity [12]. Also, the results of one study indicated that myricitrin showed higher hepatoprotective activity than silymarin and improved toxic liver damage via several mechanisms including antioxidant defense system preservation, inhibitors of inflammation, suppressors of profibrotic response, and enhancers of liver regeneration [13]. The bioavailability and metabolism of flavonoids, especially flavonoid glycoside, are the main properties to be considered. This compound is large and highly polar that cannot cross the membranes easily. Moreover, flavonoids have been extensive metabolism and hydrolysis by glycosidases in the cells of the liver, kidney, and gastrointestinal mucosa. So, these events may lead to reduce biological activity of myricitrin [14]. In recent researches, various nanoparticles have been created as carriers for drug and gene delivery such as solid lipid nanoparticles (SLNs). SLN may be a novel drug carrier system for oral delivery. This type of nanoparticle has several advantages, including high storage stability, reduces drug side effects concurrent with increase in bioavailability, and minimizes erratic absorption through its properties such as oral administration stability in the body fluids or plasma and decreased reticuloendothelial system uptake in the spleen and liver by induced hydrophilic molecule coating and altering surface characteristics [15].

The streptozotocin-nicotinamide (STZ-NA) model of T2DM is designed from the protective effects of NA against β-cell cytotoxic effects of STZ and was first introduced by Masiello et al. [16]. The severity of diabetic condition belongs to the administration of NA dosage in this model. It was

revealed that 120 mg/kg of NA could induce a chronic hyperglycemia and its related metabolic disorders. This model of diabetes characterized by several properties such as stable hyperglycemia without exogenous insulin requirement reduced 40% of pancreatic β-cells and 60% of insulin stores, glucose intolerance, impaired glucose-stimulated insulin secretion, and the stability of metabolic alterations. STZ-NA model, as a nonobese model of T2DM, is reported to be more suitable for elucidation of the potential mechanisms of diabetic complications and biochemical or pharmacological assessment of antidiabetic drugs and natural compounds on the course of blood glucose-lowering and insulin-secretory properties and regenerative capacity of the endocrine pancreas [16, 17]. Also, this experimental model appears closer to human T2DM compare to other commonly used animal model [16]. Based on the previous considerations about the therapeutic effects of antioxidant component such as bioflavonoids on T2DM or hyperglycemic condition, and according to the low bioavailability of these agents, and since myotube cell is an important site of glucose utilization, the aim of this present study was conducted to evaluate the antidiabetic effect of SLN containing myricitrin on STZ-NA-induced diabetes and C2C12 cell of male mouse.

2. Materials and Methods

2.1. Reagents. The reagents are as follows: myricitrin (purity 98%) (AvaChem Scientific, USA), C2C12 (Pasteur Institute, Iran), Compritol®888 ATO (Sigma-Aldrich, France), oleic acid, propylene glycol, citrate buffer (citric acid monohydrate ($C_6H_8O_7{\cdot}H_2O$)), trisodium citrate dihydrate ($C_6H_5O_7Na_3{\cdot}2H_2O$; pH 4.5), potassium hydroxide (KOH), sodium sulfate (Na_2SO_4), D-glucose, saline 0.9%, phenol, sulfuric acid (Merck, Germany), Tween 80 (Sinopharm Chemical Reagent Co. Ltd., China), phosphate-buffered saline (Pharmaceutical Technology Development Center of Ahvaz Jundishapur University of Medical Sciences, Iran; pH 7.4), proteinase K (Invitrogen, Thermo Fisher Scientific, Germany), fetal bovine serum (FBS), Dulbecco's modified eagle's medium (DMEM) (Solar Bio, South Korea), Trypsin-EDTA (Gibco, Canada), thiazolyl blue tetrazolium bromide (MTT), penicillin-streptomycin (Sigma-Aldrich, Canada), and dimethyl sulphoxide (DMSO) (Bio Idea, Iran).

2.2. Preparation of SLN. Since myricitrin is susceptible to the high temperature, cold homogenization method has been used in the present research. This method has been used to prepare SLNs loaded with myricitrin. Briefly, compritol was indirectly heated up to 65°C, then oleic acid as liquid lipid was added. The surfactant containing a mixture of Tween 80 and Span 20 (1 : 1) and myricitrin was dissolved in distilled water and added to the melt lipid phase. This mixture was sonicated at 90 W and 37°C for 2 min. The congelation was performed by adding a mixture of water/propylene glycol at 4°C (4 : 1) to reach 50 mL of volume, and this mixture was simultaneously homogenized using high-speed homogenizer (IKA® T25 digital ULTRA-TURRAX®, Germany) at 12000 ×g for 20 min.

2.3. Determination of Particle Size. After diluting SLN with myricitrin in double-distilled water, the particle size of nanoparticles was analyzed by Particle Size Analyzer instrument (Scatteroscope 1 Qudix, Korea). Each sample was assessed in triplicate (three-time readings were taken), and the average of the results was calculated.

2.4. Zeta Potential Assessment. The prepared myricitrin SLN zeta potential has been measured to determine the surface charge and stability of nanoparticles using the particle electrophoretic mobility procedure and the Zetasizer (Malvern Instruments Ltd., Worcestershire, UK) at 25°C. Myricitrin SLNs were dispersed in double-distilled water as dispersing medium (dispersant dielectric constant 80.0, viscosity 0.9781 cP, and dispersant refractive index 1.330). Each sample was measured in three-time readings.

2.5. Scanning Electron Microscopy (SEM) Imaging. Particle size and surface morphology of myricitrin SLNs were determined by SEM (Leo 1455 VP, Germany). Approximately 2 mg SLN containing myricitrin was dispersed in deionized water. A low amount of this suspension was dried on metal stub to form a thin uniform layer of nanoparticles. The metal stub was coated with 50 nm gold/palladium alloy. Finally, the gold-coated myricitrin SLNs were observed under SEM, and photographs were taken triplicate for each sample.

2.6. Determination of Encapsulation Efficiency and Encapsulation Capacity. Encapsulation efficiency (EE%) of myricitrin nanoparticles was determined by ultracentrifugation method. 2 mL of each sample was centrifuged (Vision Scientific Co. Ltd., Korea) 2 times at 30000 ×g for 25 min at 4°C to separate the SLN containing myricitrin from the unloaded drug. The amount of myricitrin in supernatant was determined by ultraviolet (UV) spectrophotometrical method (Analytik Jena AG, Germany) at 256 nm. The encapsulation efficiency was calculated by the following formula, which means that the amount of entrapped myricitrin was determined by subtracting the amount of unentrapped drug from the total amount of drug: EE% = (total drug − un − entrapped drug)/total drug × 100. The percentage of encapsulation capacity (EC%) was calculated by following formula: EC% = amount of drug loaded in lipid nanoparticles/weight of lipid (compritol) in SLN × 100 [18, 19].

2.7. In Vitro Release of Myricitrin. In vitro release of myricitrin was determined by dialysis membrane (12000 Dalton, Sigma-Aldrich, USA) method using ethanol and water (70–30%) (pH 7.4) as release medium. 1 mL of diluted myricitrin-loaded SLN suspensions with Tween 80 (3%) + normal saline (97%), as myricitrin solvent, containing 1 mg myricitrin was put into the dialysis membrane bags. The bags were suspended into 50 mL of distilled water, pH 7.4, and stirred at 80 ×g (37°C). At the intervals of 15, 30, and 45 min and 1, 2, 3, 4, 5, 6, 7, 8, and 24 h from the start of the experiment, 1 mL of dissolution medium was withdrawn and replaced by 1 mL of receptor medium. The concentration of released myricitrin was assessed by a UV spectrophotometer at 256 nm,

and the cumulative percentage of drug release was calculated against time [20].

2.8. In Vivo Test

2.8.1. Animals. In this experimental study, 120 adult (3-month-old) male NMRI mice weighing 25–30 g were obtained from the Ahvaz Jundishapur University of Medical Sciences (AJUMS) animal facility and were treated in accordance with the principles and guidelines on animal care of AJUMS as reviewed by an ethics committee (IR.AJUMS.REC.1395.136) and kept at a 20°C ± 4°C temperature with a 12-hour light/12-hour dark cycle. They had access to tap water and commercial chow ad libitum.

2.8.2. Induction of Diabetes and Experimental Design. After one week of animal's acclimatization, for the sake of induce T2DM, a single dose of STZ (65 mg/kg) (Solar Bio, South Korea) dissolved in a citrate buffer (pH 4.5) was intraperitoneally injected 15 min after an intraperitoneal administration of NA (120 mg/kg) (Sigma-Aldrich, USA) dissolved in normal saline. Diabetes induction was confirmed by assaying blood glucose levels more than 200 mg/dL at 3 days after STZ-NA injection [21]. SLNs containing myricitrin, vehicle, and metformin (Alfa Aesar, Canada) (as a standard drug for T2DM treatment) were orally gavaged for 4 weeks in the treatment groups. So, animals were divided into 7 groups ($n = 12$): control, vehicle (injected one dose of STZ and NA solvent and gavaged Tween 80 (3%) + normal saline (97%) as myricitrin and its SLN solvent) [22], diabetes, diabetes + SLN containing myricitrin 1 mg/kg, diabetes + SLN containing myricitrin 3 mg/kg, diabetes + SLN containing myricitrin 10 mg/kg [23], and diabetes + metformin 200 mg/kg [24].

Since the half-life of myricitrin is about 12 h [25], 6 h after the last drug administration, the overnight fasted mice were anesthetized by ketamine/xylazine (70 mg/kg/10 mg/kg) (Alfasan, Netherlands), and the plasma samples were taken by cardiac puncture blood collection and centrifuging at 3500 ×g for 20 min. Then, the pancreas and muscle of all animals were immediately removed for histopathological and real-time PCR assessment, respectively. All plasma and tissue samples were kept at −80°C until experimental assessments were performed.

2.9. In Vitro Test

2.9.1. Cell Culture. Skeletal myoblast (C2C12) cell line was purchased from the cellular bank of Pasteur Institute of Iran, Tehran, Iran. This cell was cultured in DMEM, supplemented with 10% FBS, 4 mM glutamine, penicillin-streptomycin (100 U/mL and 100 μg/mL, resp.), under a humidified atmosphere of 5% CO_2 at 37°C. The cells were cultured in 75 cm^2 and divided into 25 cm^2 cell culture flasks for SLN containing myricitrin treatment. The medium was replaced every 3 days until cultured cells arriving at 80% confluence [26, 27].

2.9.2. Experimental Design. The grown C2C12 cells in 25 cm^2 cell culture flasks were divided into 5 groups ($n = 3$): control (received medium containing D-glucose 5 mM), hyperglycemia (maintained in medium containing D-glucose 100 mM without any drug assessment), hyperglycemia + SLN containing myricitrin 1 μM, hyperglycemia + SLN containing myricitrin 3 μM, hyperglycemia + SLN containing myricitrin 10 μM [28], and hyperglycemia + metformin 400 μM [28]. The period of hyperglycemia only and concomitant with SLN of myricitrin administration was 48 h, and all administered flasks were incubated in the normal cell-cultured condition [29–31]. After the treating period, all cultured cells were collected by trypsin-EDTA (0.05%) and centrifuged at 1300 ×g for 15 min, resuspended in 0.5 mL of PBS (pH 7.4), and lysed using a Teflon homogenizer. All the samples were centrifuged at 2000 ×g for 10 min and kept at −80°C until experimental and real-time PCR measurements were performed [32].

2.10. Lipid Peroxidation and Antioxidant Enzyme Assessment. Pancreas tissue was removed, cut into small pieces on ice, and homogenized in 1/5 (w/v) PBS (pH 7.4) with a Teflon homogenizer. The supernatant of pancreas tissue and cultured cell homogenate were prepared via sample centrifuging at 2000 ×g for 10 min, and the levels of MDA, TAC, CAT (ZellBio, Germany), and SOD (Randox Laboratories Ltd., United Kingdom) were measured by specific commercial kits.

2.11. Diabetic Variable Measurement. At the end of experiment, fasting blood glucose was measured in overnight fasted mice by putting a drop of blood from the tip of the tail and using a digital glucometer (Elegance, Germany). A quantitative of plasma insulin level was performed by insulin ELISA kit (Monobind, USA). HOMA-IR and HOMA-β were carried out by homeostasis model assessment methods and were calculated using the following formula [33]:

$$\begin{aligned}\text{HOMA-IR} &= \text{fasting insulin}(\mu\text{IU/mL}) \\ &\quad \times \frac{\text{fasting glucose}(\text{mg/dL})}{405}, \\ \text{HOMA-}\beta &= \frac{\text{fasting insulin}(\mu\text{IU/mL}) \times 360}{\text{fasting glucose}(\text{mg/dL}) - 63}.\end{aligned} \tag{1}$$

2.12. Glycogen Content of Skeletal Muscle. For muscle glycogen content measurement, 100 mg of mouse soleus and gastrocnemius muscles and C2C12 cells cultured in 25 cm^2 flasks were removed, and 0.5 mL of 30% KOH solution saturated with Na_2SO_4 was added to the sample tubes, and the samples were heated at 100°C for 30 min and incubated on ice and added 1.2 volume of 95% ethanol to the tubes. All samples stood on ice for 30 min before centrifugation at 840 ×g for 30 min. The supernatants were removed, and the glycogen precipitates were resuspended in (1 mL for skeletal muscle and 50 μL for C2C12 cells) distilled water. Then, 1 mL for skeletal muscle and 50 μL for C2C12 cells of 5% phenol solution were added to the aliquots of glycogen solution, and 5 mL for skeletal muscle and 250 μL for C2C12 cells of 98% sulfuric acid were rapidly added, and the absorbance was measured with a plate reader at 490 nm. The glycogen content in the muscle and C2C12 cells was calculated from the standard curve of D-glucose and expressed as mg/g wet muscle weight and percent of control, respectively [34].

2.13. MTT Assay Experiment. The concentration of MTT 5 mg/mL was prepared in PBS to determine the cellular viability. Live cells convert the MTT compound to the formed formazan crystals. These crystals were dissolved by DMSO. So, removed cultured cells were incubated in medium containing 0.5 mg/mL of 3-(4,5-dimethylthiazol-2-yl)-2,5-diphenyltetrazolium bromide for 4 h (at 5% CO_2 and 37°C). The purple formazan crystals were dissolved in 100 μL DMSO and shacked for 15 min, and the absorbance MTT assessment was read at 540 nm using an ELISA reader (ELx808 Absorbance Microplate Reader, ELISA Technologies Inc., USA) [35, 36].

2.14. Glut-4 and Apoptotic Gene Expression Assessment. Total RNA was purified from the muscle and C2C12 cells using the commercial instruction of RNeasy mini kit (Qiagen, Valencia, CA). cDNA was synthesized using Reverse Transcriptase kit (Takara, Japan) according to the manufacturer's instructions. Real-time PCR was performed with SYBR green Master Mix (Takara, Japan) in ABI StepOnePlus instrument (Thermo Fisher, USA) and was prepared in duplicate. The protocol of real-time PCR was conducted under the following conditions: 2 min at 60°C and 10 min at 95°C, followed by 40 cycles at 95°C for 15 seconds and 60°C for 60 seconds, 1 cycle of 95°C for 15 seconds, 60°C for 30 seconds, and 95°C for 15 seconds. The relative Glut-4, Bax, and Bcl-2 gene expression levels to the expression level of GAPDH, as the endogenous reference gene, were calculated using a comparative 2-delta delta cycle threshold ($2^{-\Delta\Delta CT}$) method ($2^{-\Delta\Delta CT}$ = [(Ct Glut-4 of treated mice − Ct GAPDH of treated mice) − (Ct Glut-4 of untreated mice − Ct GAPDH of untreated mice)]). Before using this method for quantitation, a primer efficiency investigation was conducted to validate our experiment. The primer sequences of the forward and reverse regarding Glut-4, Bax, Bcl-2, and GAPDH gene (Microsynth, Switzerland) were [27] as follows:

Glut-4 forward primer, 5′-CGCACTAGCTGAGCTG AAGG-3′ and Glut-4 reverse primer, 5′-GCAGCACCACT GCGATGATA-3′; Bax forward primer, 5′-GCTGGACAT TGGACTTCCTC-3′ and Bax reverse primer, 5′-ACCACT GTGACCTGCTCCA-3′; Bcl-2 forward primer, 5′-GCTG GACATTGGACTTCCTC-3′ and Bcl-2 reverse primer, 5′-GCTGGACATTGGACTTCCTC-3′; and GAPDH forward primer, 5′-ACCCAGAAGACTGTGGATGG-3′ and GAPDH reverse primer, 5′-TTCTAGACGGCAGGTC AGGT-3′.

2.15. Histological Assessment of Pancreas Tissue. The pancreas tissue samples of animals were fixed in formalin solution (10%). All tissues were embedded in paraffin after dehydrated in graded alcohol concentrations. Pancreatic sections of 5–7 μm were prepared and stained with hematoxylin and eosin (H&E) (Sigma-Aldrich, USA). Eight microscopic stained slides per mouse were examined for the assessment of islet diameters. This measurement was analyzed using Motic Images Plus 2.0 image analysis software. The slide reading was conducted under a blind method [37].

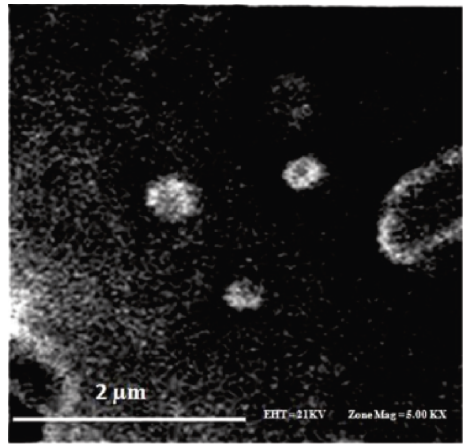

Figure 1: Scanning electron microscope (SEM) image of myricitrin SLNs.

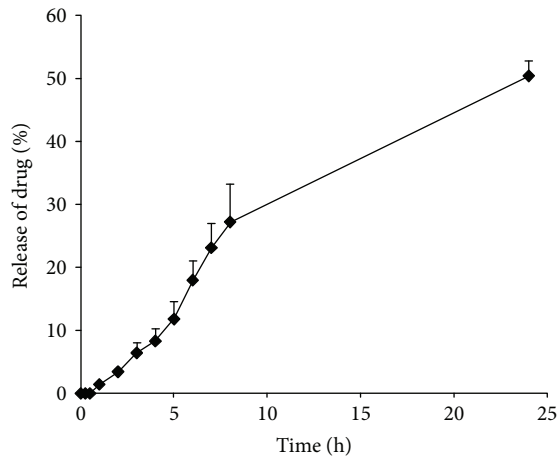

Figure 2: In vitro release of myricitrin from its SLN.

2.16. Pancreatic Tissue Apoptosis Assessment. TUNEL staining was carried out based on labeling of the DNA strand breaks by the In Situ Cell Death Detection Kit, POD (Roche Applied Science, Germany). The paraffin sections of pancreas tissue were dewaxed and incubated with Proteinase K for 0.5 h at 24°C. After washing with PBS, the sections were incubated with TUNEL reaction mixture in a humidity chamber at 37°C for 1 h. The sections were incubated with antifluorescein-AP for 30 min at 37°C after washing with PBS. The slides were washed in deionized water and incubated with DAB substrate for 5 min. Intense, dark brown stained nucleus was considered as TUNEL-positive cells. Percentage of TUNEL-positive cells (apoptotic index) was calculated randomly in 10 fields for each slide. Three slides per animal were used for this method [38].

2.17. Statistical Assessment. The results were statistically analyzed using SPSS software (version 16) with one-way analysis of variance (ANOVA), followed by post hoc least significant difference (LSD) tests. Further, data were represented as

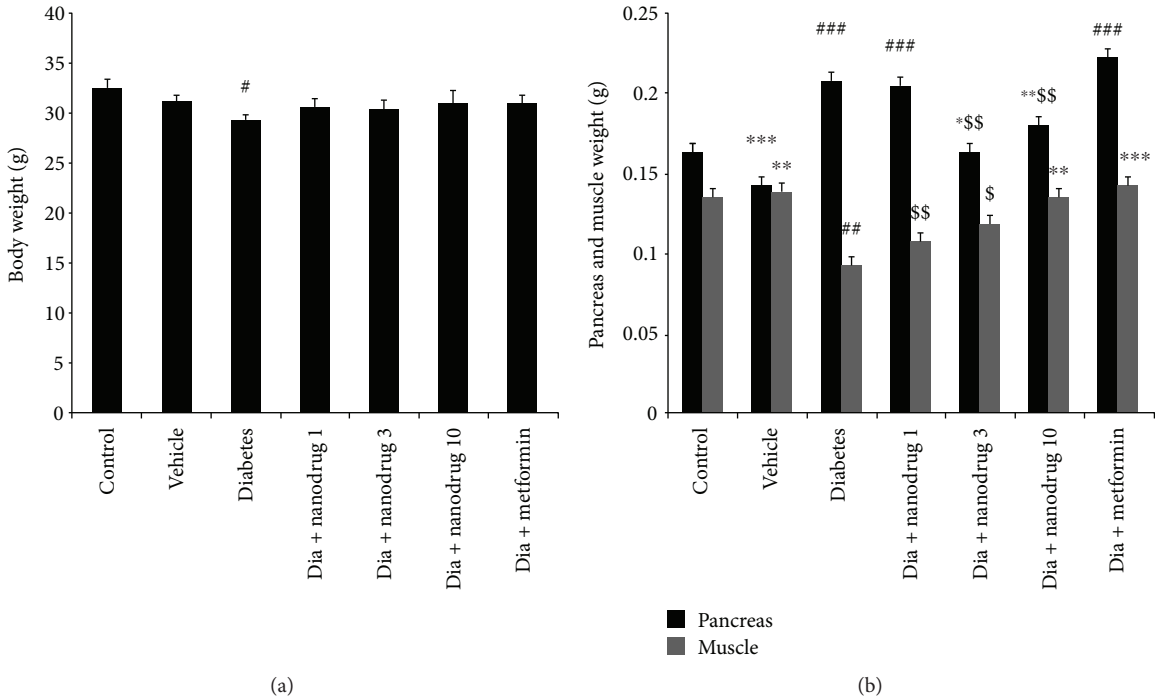

Figure 3: Effect of myricitrin SLN on body and tissue weight. Data are presented as mean ± SE; $n = 12$; $^{\#}p < 0.05$, $^{\#\#}p < 0.01$, and $^{\#\#\#}p < 0.001$ compared with control; $^{*}p < 0.05$, $^{**}p < 0.01$, and $^{***}p < 0.001$ compared with diabetes; $^{\$}p < 0.05$, $^{\$\$}p < 0.01$, and $^{\$\$\$}p < 0.001$ compared with diabetes + metformin (one-way analysis of variance (ANOVA), followed by post hoc least significant difference (LSD) tests). (a) Body weight; (b) tissue weight.

mean ± standard error (SE) and differences were considered statistically significant at $p < 0.05$.

3. Results

3.1. Characterization of Myricitrin SLNs. The mean particle size and zeta potential were 76.1 nm and− 5.51 mV, respectively. Encapsulation efficiency (EE) and encapsulation capacity (EC) were 56.2% and 5.62%, respectively. The nanoparticles showed spherical shapes under SEM, and the particle size ranged from 50 to 150 nm (Figure 1). The release of myricitrin from SLNs occurred in two phases. The release of myricitrin from its SLNs did not occur at the intervals of 15, 30, and 45 min, because the lipid skeleton of the SLN as part of the drug was absorbing water. Next, the release of myricitrin from its SLNs was 1.435, 3.435, 6.432, 8.318, 11.789, 17.972, 23.1, 27.184, and 50.339% at 1, 2, 3, 4, 5, 6, 7, 8, and 24 h, respectively (Figure 2).

3.2. Role of SLN Containing Myricitrin on Body and Tissue Weight. The body weight reduced in the untreated diabetic group compared to the control ($p < 0.05$) (Figure 3(a)). The pancreas weight increased in diabetes, diabetic SLN of myricitrin 1 mg/kg, and metformin-administered mice compared to control ($p < 0.001$). This variable decreased in vehicle ($p < 0.001$), diabetes + SLN containing myricitrin 3 mg/kg ($p < 0.05$), and 10 mg/kg ($p < 0.01$) when compared to the diabetes group. Further, the weight of the pancreas in diabetes + SLN containing myricitrin 3 ($p < 0.01$) and 10 mg/kg ($p < 0.001$) showed a significant decrease versus the metformin group. The weight of mouse muscle showed a significant decrease in the untreated diabetic group when compared to the control group ($p < 0.01$). This variable increased in the vehicle ($p < 0.01$), diabetes + SLN containing myricitrin 10 mg/kg ($p < 0.01$), and diabetes + metformin groups ($p < 0.001$) compared with the diabetes group. Also, there was a significant muscle weight reduction in the diabetes + SLN containing myricitrin 1 ($p < 0.01$) and 3 mg/kg ($p < 0.05$) compared to diabetes + metformin (Figure 3(b)).

3.3. Malondialdehyde and Antioxidant Enzyme Level. Pancreatic level of malondialdehyde increased in the diabetes group ($p < 0.01$) compared to the control. Also, compared with the diabetes group, this lipid peroxidation marker decreased in the vehicle ($p < 0.05$), diabetes + SLN containing myricitrin 1 ($p < 0.05$), 3 ($p < 0.01$), and 10 mg/kg ($p < 0.01$), and diabetes + metformin groups ($p < 0.001$). Metformin administered in diabetic mice reduced more the level of MDA than SLN containing myricitrin 1 mg/kg ($p < 0.05$) (Figure 4(a)). The results of total antioxidant capacity (TAC) showed a remarkable increase in the diabetes + SLN containing myricitrin 1 mg/kg and diabetes + metformin groups ($p < 0.05$) compared with the diabetes group (Figure 4(b)). Pancreatic level of SOD increased in the diabetes + SLN containing myricitrin 1 mg/kg group versus the untreated diabetic mice and diabetes + metformin groups ($p < 0.01$) (Figure 4(c)). CAT measurement revealed a significant decrease in the diabetes ($p < 0.001$) and diabetes + SLN containing myricitrin 1 mg/kg ($p < 0.05$) groups when

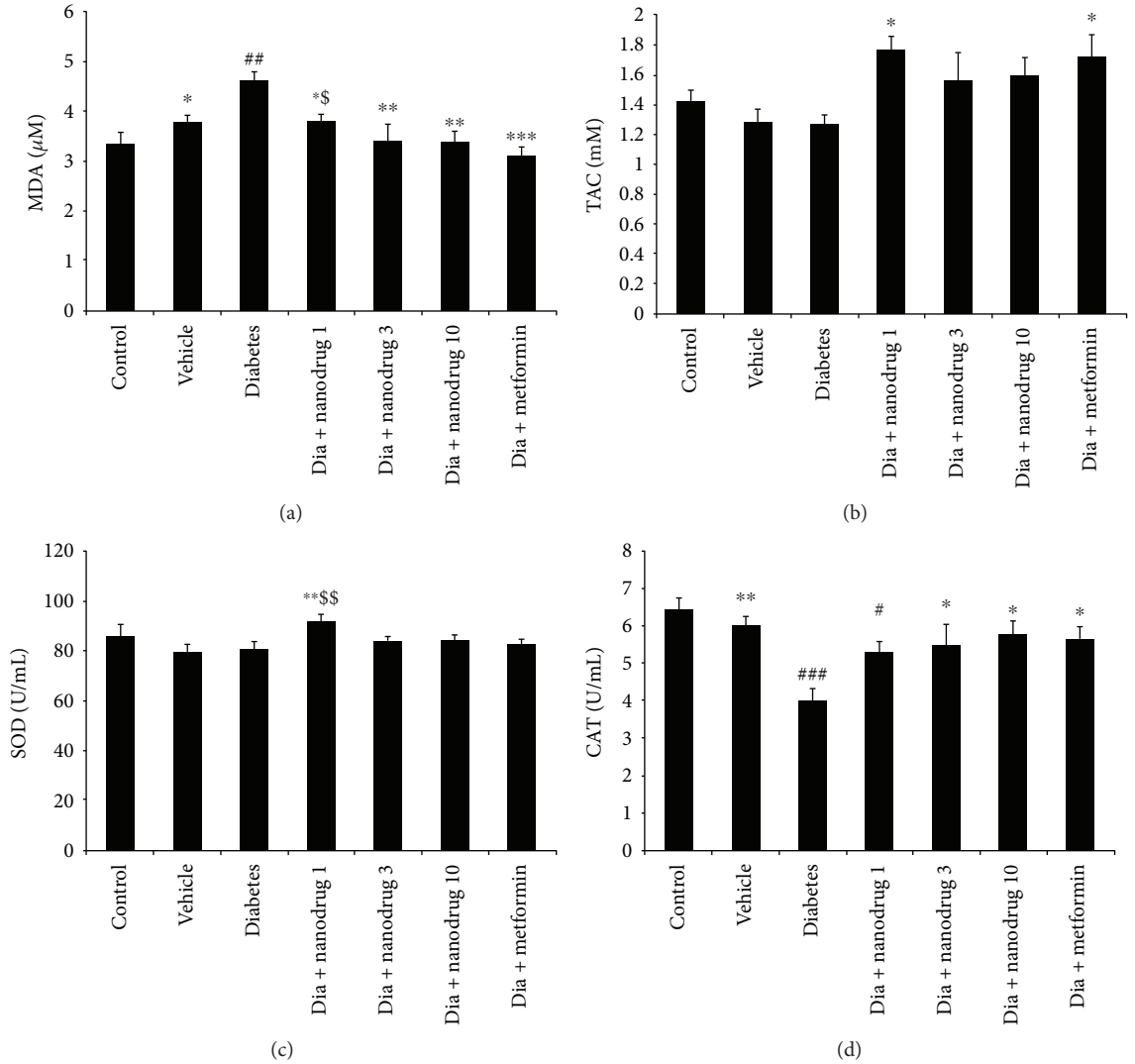

Figure 4: Effect of myricitrin SLN on MDA, TAC, and antioxidant enzyme level of the pancreas. Data are presented as mean ± SE; $n = 12$; $^{\#}p < 0.05$, $^{\#\#}p < 0.01$, and $^{\#\#\#}p < 0.001$ compared with control; $^{*}p < 0.05$, $^{**}p < 0.01$, and $^{***}p < 0.001$ compared with diabetes; $^{\$}p < 0.05$ and $^{\$\$}p < 0.01$ compared with diabetes + metformin (one-way analysis of variance (ANOVA), followed by post hoc least significant difference (LSD) tests). (a) MDA, (b) TAC, (c) SOD, and (d) CAT.

compared to the control. Further, this enzyme level increased in the vehicle ($p < 0.01$), diabetes + SLN containing myricitrin 3 and 10 mg/kg and diabetes + metformin groups ($p < 0.05$) compared to the diabetes group (Figure 4(d)). In vitro results indicated that a significant increase of MDA has occurred in the hyperglycemia group compared to the control ($p < 0.05$) (Figure 5(a)). TAC assessment showed an increased in all groups with $p < 0.001$ and hyperglycemia + metformin with $p < 0.05$ compared with the control. This variable increased in the hyperglycemia + SLN containing myricitrin 1 ($p < 0.01$), 3 ($p < 0.001$), and 10 μM ($p < 0.05$) groups and decreased in the hyperglycemia + metformin group ($p < 0.001$) compared to the hyperglycemia group. TAC increased significantly in the hyperglycemia + SLN containing 1, 3, and 10 μM groups ($p < 0.001$) versus the hyperglycemia + metformin group (Figure 5(b)). SOD enzyme level in myotubes reduced in the hyperglycemia ($p < 0.01$), hyperglycemia + SLN containing 3 ($p < 0.05$) and 10 μM ($p < 0.01$), and hyperglycemia + metformin groups ($p < 0.001$) compared to the control. This antioxidant enzyme increased in the hyperglycemia + SLN containing myricitrin 1 μM ($p < 0.01$) and decreased in hyperglycemia + metformin ($p < 0.01$) groups versus the untreated hyperglycemic exposed myotubes. The results of metformin administration showed a significant decrease in SOD when compared to the hyperglycemia + SLN containing myricitrin 1, 3, and 10 μM groups ($p < 0.001$, $p < 0.01$, and $p < 0.05$, resp.) (Figure 5(c)). CAT assessment demonstrated a remarkable reduction in the hyperglycemia group compared to the control group ($p < 0.01$). Further, a significant increase was observed in all treated groups when compared with the hyperglycemia group ($p < 0.001$) (Figure 5(d)).

3.4. Antidiabetic Effects of Myricitrin SLNs. The blood glucose level at the first day of experiment increased in all groups except the vehicle group compared to the control group

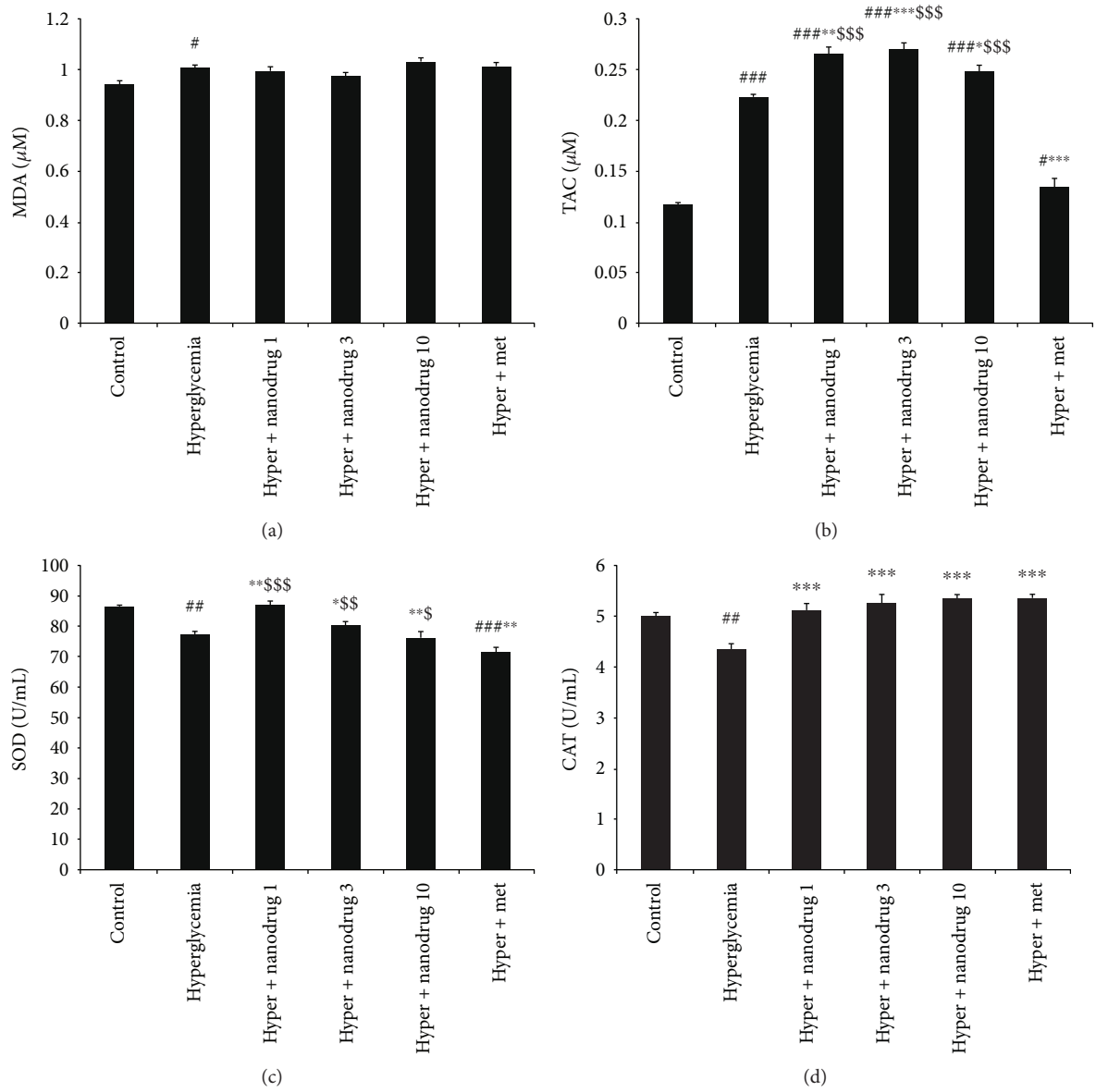

Figure 5: Effect of myricitrin SLN on MDA, TAC, and antioxidant enzyme level of C2C12 cell. Data are presented as mean ± SE; $n = 3$; $^{\#}p < 0.05$, $^{\#\#}p < 0.01$, and $^{\#\#\#}p < 0.001$ compared with control; $^{*}p < 0.05$, $^{**}p < 0.01$, and $^{***}p < 0.001$ compared with hyperglycemia; $^{\$}p < 0.05$, $^{\$\$}p < 0.01$, and $^{\$\$\$}p < 0.001$ compared with hyperglycemia + metformin (one-way analysis of variance (ANOVA), followed by post hoc least significant difference (LSD) tests). (a) MDA, (b) TAC, (c) SOD, and (d) CAT.

($p < 0.001$). This variable increased in all treated groups compared to the control and increased in that groups versus the diabetes group at the fourteenth day of the experiment ($p < 0.01$). The blood glucose level increased in the diabetes group compared to the control and decreased in the vehicle group and all drug-administered mice versus the diabetes group at the end of experimental period ($p < 0.001$) (Figure 6). Insulin measurement showed a significant increase in the diabetes ($p < 0.05$), diabetes + SLN containing myricitrin, and diabetes + metformin-administered mice ($p < 0.001$) when compared to the control. Further, this hormone level decreased in the vehicle ($p < 0.05$) and increased in the diabetes + SLN containing myricitrin 3 ($p < 0.05$) and 10 mg/kg ($p < 0.01$) and diabetes + metformin groups ($p < 0.001$) compared to the diabetes group. Plasma level of insulin decreased in mice administered with diabetic SLN containing myricitrin 1, 3, and 10 mg/kg when compared to the diabetes + metformin group ($p < 0.01$, $p < 0.01$, and $p < 0.05$, resp.). HOMA-IR increased in the diabetes, diabetes + SLN containing myricitrin, and diabetes + metformin-treated mice when compared to the control ($p < 0.001$). This insulin resistance index reduced in the vehicle ($p < 0.001$), diabetes + SLN containing myricitrin 1, 3, ($p < 0.05$) and 10 mg/kg- ($p < 0.01$) administered animals versus the diabetes group. HOMA-β decreased in the diabetes ($p < 0.001$) and increased in diabetes + SLN containing

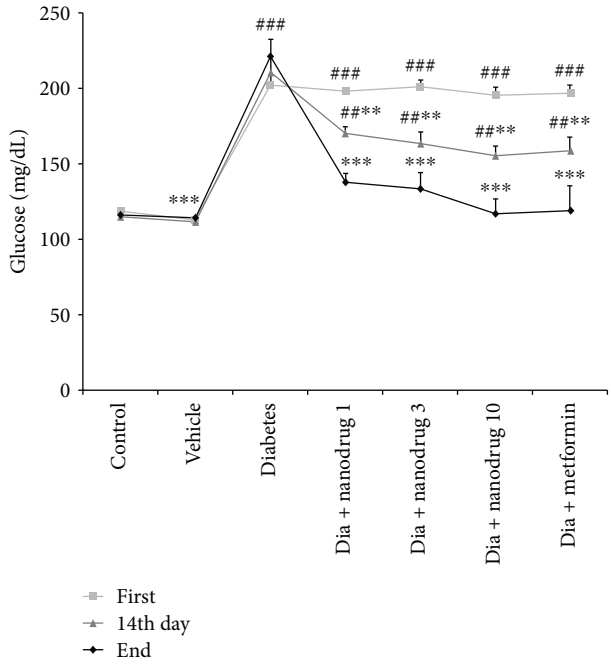

Figure 6: Effect of myricitrin SLN on blood glucose level at the first day, 14th day, and end of experimental period. Data are presented as mean ± SE; $n = 12$; $^{\#\#}p < 0.01$ and $^{\#\#\#}p < 0.001$ compared with control; $^{**}p < 0.01$ and $^{***}p < 0.001$ compared with diabetes (one-way analysis of variance (ANOVA), followed by post hoc least significant difference (LSD) tests).

myricitrin 1 ($p < 0.05$), 3, and 10 mg/kg, and diabetes + metformin ($p < 0.001$) groups compared with the control. Furthermore, the assessment of the vehicle, diabetes + SLN containing all dose of myricitrin, and diabetes + -metformin groups revealed a significant increase in this variable when compared to the untreated diabetic mice ($p < 0.001$). This β-cell function index showed a significant decrease in the diabetes + SLN containing myricitrin 1, 3, and 10 mg/kg in comparison with the diabetes + metformin group ($p < 0.001$, $p < 0.001$, and $p < 0.01$, resp.) (Table 1).

3.5. Glycogen Content of Skeletal Muscle and C2C12. As shown in Figure 7(a), muscle's glycogen decreased in the diabetes ($p < 0.05$) and increased in diabetic SLN 1 ($p < 0.01$), 3, and 10 mg/kg ($p < 0.001$) and metformin- ($p < 0.01$) treated groups when compared to the control. Also, SLN containing myricitrin 1, 3, and 10 mg/kg and metformin administration increased the storage of muscle's glycogen compared with the diabetes group ($p < 0.001$). SLN containing myricitrin 10 mg/kg in diabetic mice indicated a significant increase in this variable versus the diabetes + metformin group ($p < 0.01$). C2C12 glycogen content measurement revealed a significant decrease in untreated hyperglycemic cells when compared to the control ($p < 0.05$). Further, this variable increased in the hyperglycemia + SLN containing myricitrin 10 μM- ($p < 0.05$) treated groups compared with the control. Myotube glycogen content increased in the hyperglycemia + SLN containing myricitrin 1, 3, and 10 μM ($p < 0.01$) and hyperglycemia + metformin groups ($p < 0.05$) versus the untreated hyperglycemic cells. Also, SLN containing myricitrin 10 μM ($p < 0.05$) administration increased the content of glycogen in hyperglycemic C2C12 cells compared to metformin (Figure 7(b)).

3.6. Glut-4 Gene Expression. The results of gene assessment indicated that muscle's Glut-4 gene expression significantly decreased in the diabetes ($p < 0.001$) and diabetes + SLN containing myricitrin 1 and 3 mg/kg groups and increased in the diabetes + SLN containing myricitrin 10 mg/kg compared to the control ($p < 0.05$). This variable increased in the vehicle ($p < 0.001$), diabetes + SLN containing myricitrin 1, 3 ($p < 0.01$), and 10 mg/kg, and diabetes + metformin groups ($p < 0.001$) when compared with the untreated diabetic mice (Figure 8(a)). Glut-4 gene expression was significantly reduced in all treated C2C12 cell groups compared to the control ($p < 0.001$). This gene expression increased in all treated groups when compared to the hyperglycemia group ($p < 0.001$). The comparison between metformin and SLN administration revealed a significant increase of this gene expression in the hyperglycemia + metformin group versus the hyperglycemia + SLN containing myricitrin 1 ($p < 0.001$) and 3 μM groups ($p < 0.001$) (Figure 8(b)).

3.7. Cellular Viability. The results of MTT assessment demonstrated that this variable decreased in the hyperglycemia, hyperglycemia + SLN containing myricitrin 1, 3 ($p < 0.001$), and 10 μM groups ($p < 0.05$) compared to the control. This variable revealed an increase in SLN containing myricitrin 3 ($p < 0.05$), 10 μM ($p < 0.01$), and hyperglycemia + metformin ($p < 0.001$) groups when compared to the untreated hyperglycemic C2C12 cells. Further, metformin treatment showed a significant increase in cellular viability compared with hyperglycemia + SLN containing myricitrin 1 and 3 μM groups ($p < 0.01$) (Figure 9).

3.8. Myotube Cell Apoptotic Gene Expression. The level of Bax gene expression revealed a significant increase in the hyperglycemia group compared to the control ($p < 0.001$). This variable decreased in the hyperglycemia + SLN containing myricitrin 1, 3 ($p < 0.01$), and 10 μM and hyperglycemia + metformin ($p < 0.001$) groups versus the hyperglycemia group (Figure 10(a)). Bcl-2 assessment showed a remarkable decrease in the hyperglycemia ($p < 0.001$), hyperglycemia + SLN containing myricitrin 1 ($p < 0.01$) and 3 μM ($p < 0.05$) groups when compared to the control. This gene expression increased in the SLN containing all doses of myricitrin ($p < 0.001$) and metformin- ($p < 0.05$) treated groups versus the hyperglycemia group. Further, there were significant differences between metformin and SLN containing myricitrin 3 ($p < 0.05$) and 10 μM ($p < 0.01$) administration in Bcl-2 levels (Figure 10(b)). Bax to Bcl-2 ratio level showed an enhancement in the hyperglycemia ($p < 0.001$) and hyperglycemia + SLN containing myricitrin 1 μM ($p < 0.05$) groups compared to the control. Also, this ratio decreased in all treated groups compared with the hyperglycemia group ($p < 0.001$) (Figure 10(c)).

Table 1: Effects of myricitrin SLNs on plasma level of insulin, HOMA-IR, and HOMA-β.

Experimental groups	Insulin (μIU/mL)	HOMA-IR	HOMA-β
Control	17.22 ± 0.65	4.90 ± 0.21	119.69 ± 8.07
Vehicle	$15.79 \pm 1.97^{*}$	$4.38 \pm 0.39^{***}$	$118.06 \pm 6.25^{***}$
Diabetes	$24.31 \pm 0.97^{\#}$	$13.19 \pm 0.52^{\#\#\#}$	$56.12 \pm 3.58^{\#\#\#}$
Diabetes + SLN of myricitrin 1 mg/kg	$30.99 \pm 2.25^{\#\#\#\$\$}$	$10.51 \pm 0.44^{\#\#\#*}$	$150.963 \pm 5.01^{\#***}$
Diabetes + SLN of myricitrin 3 mg/kg	$33.36 \pm 3.02^{\#\#\#*\$\$}$	$10.95 \pm 0.90^{\#\#\#*}$	$172.363 \pm 7.93^{\#\#\#***}$
Diabetes + SLN of myricitrin 10 mg/kg	$36.02 \pm 3.41^{\#\#\#**\$}$	$10.35 \pm 1.18^{\#\#\#**}$	$260.163 \pm 15.30^{\#\#\#***}$
Diabetes + metformin 200 mg/kg	$42.95 \pm 2.62^{\#\#\#***}$	$12.45 \pm 0.30^{\#\#\#}$	$293.625 \pm 10.30^{\#\#\#***}$

Data are presented as mean ± SE; $n = 12$; $^{\#}p < 0.05$ and $^{\#\#\#}p < 0.001$ compared with control; $^{*}p < 0.05$, $^{**}p < 0.01$, and $^{***}p < 0.001$ compared with diabetes; $^{\$}p < 0.05$ and $^{\$\$}p < 0.01$ compared with diabetes + metformin (one-way analysis of variance (ANOVA), followed by post hoc least significant difference (LSD) tests).

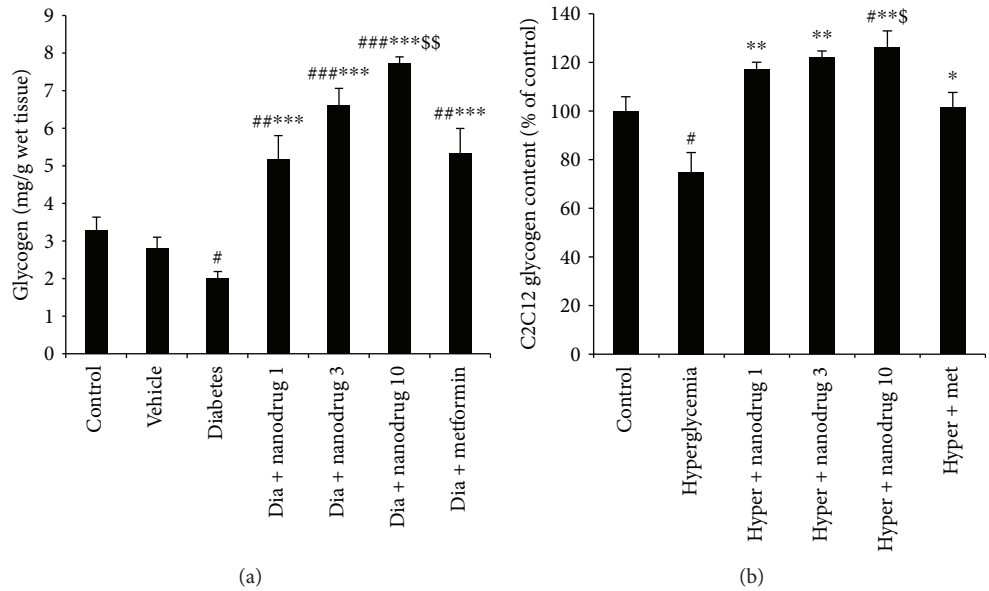

Figure 7: Effect of myricitrin SLN on glycogen content of skeletal muscle and C2C12 cell. Data are presented as mean ± SE; $n = 12$ for skeletal muscle and $n = 3$ for C2C12 cell; $^{\#}p < 0.05$, $^{\#\#}p < 0.01$, and $^{\#\#\#}p < 0.001$ compared with control; $^{*}p < 0.05$, $^{**}p < 0.01$, and $^{***}p < 0.001$ compared with diabetes or hyperglycemia; $^{\$}p < 0.05$ and $^{\$\$}p < 0.01$ compared with diabetes + metformin or hyperglycemia + metformin (one-way analysis of variance (ANOVA), followed by post hoc least significant difference (LSD) tests). (a) Glycogen content in skeletal muscle; (b) glycogen content in C2C12 cell.

3.9. Histological Changes of Pancreas Tissue. As demonstrated in Figure 11, the islet diameter decreased in diabetes ($p < 0.001$) and increased in diabetes + metformin and diabetes + SLN containing myricitrin 1 ($p < 0.05$), 3 ($p < 0.01$), and 10 mg/kg ($p < 0.001$) groups compared to the control. SLN containing myricitrin 1, 3, and 10 mg/kg and metformin ($p < 0.001$) administered in diabetic animals improved this diameter reducing when compared to the diabetes group. Similar effect was observed in the vehicle group compared to the diabetes group ($p < 0.001$).

3.10. Role of Myricitrin SLNs on Pancreatic Apoptosis. Pancreatic cell apoptosis was significantly increased in the diabetes ($p < 0.001$) and diabetes + SLN containing myricitrin 1 mg/kg groups ($p < 0.05$) compared with the control group. This variable improved in all diabetic treated mice when compared to the diabetes group ($p < 0.001$) (Figure 12).

4. Discussion

Some of the nanoparticle advantages are drug protection from the rapid metabolism and nonspecific recognition or distribution. It does appear that two important variables which affect the cellular nanoparticle uptake are the size and shape. The cellular uptake of nanoparticles (100 nm) was 2.5 and 6 times more than microparticles (1 μm and 10 μm), respectively. Nanoparticles less than 10 nm were eliminated by renal rapidly, and if the diameter arrived at 200 nm, the vascular permeability decreases; hence, it is quickly removed by the activation of a complementary system in the bloodstream. It was revealed that the spherical

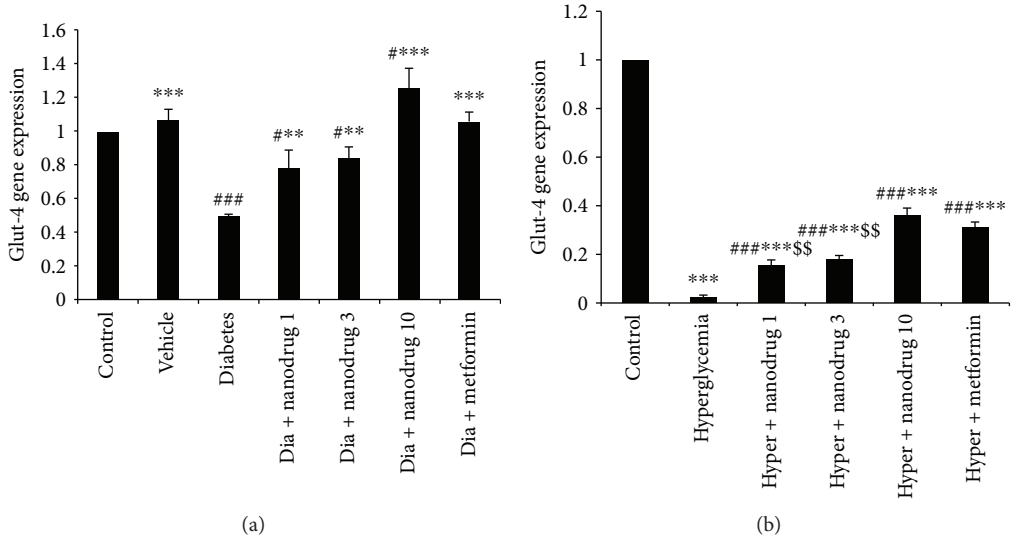

Figure 8: Glut-4 gene expression in skeletal muscle and C2C12 cell. Data are presented as mean ± SE; $n = 12$ for skeletal muscle and $n = 3$ for C2C12 cell; $^{\#}p < 0.05$ and $^{\#\#\#}p < 0.001$ compared with control; $^{**}p < 0.01$ and $^{***}p < 0.001$ compared with diabetes or hyperglycemia; $^{\$\$}p < 0.01$ compared with diabetes + metformin or hyperglycemia + metformin (one-way analysis of variance (ANOVA), followed by post hoc least significant difference (LSD) tests). (a) Glut-4 gene expression in skeletal muscle; (b) Glut-4 gene expression in C2C12 cell.

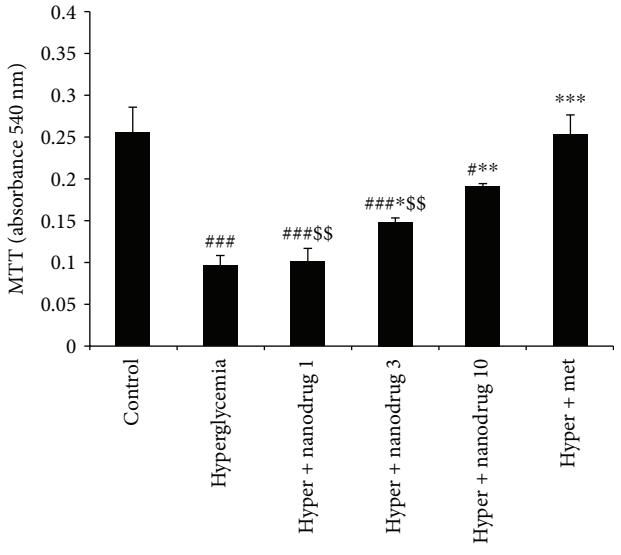

Figure 9: C2C12 cell survival. Data are presented as mean ± SE; $n = 5$; $^{\#}p < 0.05$ and $^{\#\#\#}p < 0.001$ compared with control; $^{*}p < 0.05$, $^{**}p < 0.01$, and $^{***}p < 0.001$ compared with hyperglycemia; $^{\$\$}p < 0.01$ compared with hyperglycemia + metformin (one-way analysis of variance (ANOVA), followed by post hoc least significant difference (LSD) tests).

nanoparticle uptake is 5 times greater than rod-shaped particles. The nanoparticle surface properties such as hydrophobicity and hydrophilicity are important for blood component absorbance including opsonins. Surface charge is the main factor for surface properties because less opsonization occurs in neutrally charged particles than charged particles [39]. The administration of Tween 80 as a surfactant in the construction of SLNs gives them an added advantage of hydrophilicity. Further, this agent increased permeability across the intestinal membrane by a high affinity between lipid particles and intestinal membrane, and it may improve bioadhesion to the gastrointestinal tract wall. Zeta potential is another important factor for stable dispersing of nanoparticles. So, having zeta potential about −5 mV produced a stable dispersion with little or no chance of aggregation [40].

According to the present results, myricitrin SLNs revealed the optimum size, zeta potential, good stability, and release. This event indicated high entrapment of myricitrin in the solid lipid matrix, preventing from the aggregate or opsonization, maintaining the effective therapeutic drug concentrations, and leads to a longer half-life. So, drug released from its SLNs was about 50% during 24 h in the present study. A slow release in initial 1 h could be explained as the slow diffusion of the drug from the inside of the solid lipid matrix. A controlled 1release pattern was depicted during 1–24 h, and it could be conducted by drug desorption from the outer surface of the SLNs and the larger specific surface of the smaller particles [41]. Since myricitrin is susceptible to the high temperature, cold homogenization has been used in our research. This method was developed to resolve various problems such as temperature-induced drug degradation, drug distribution into the aqueous phase during homogenization, and complexity of the crystallization step of the nanoemulsion [42].

Consistent with the present results, previous studies demonstrated that STZ-NA-induced diabetes is characterized by significant body weight loss due to the insulin resistance, which causes the excessive breakdown of protein as an energy source due to the inability of the body to administer glucose for producing energy [43]. An alteration in the internal organ weights may indicate toxicity or pathology occurring to them. It was revealed that pancreas weight increased in type 2 diabetic patients and STZ-induced diabetic rats [44–46]. Also, the loss of muscle weight has

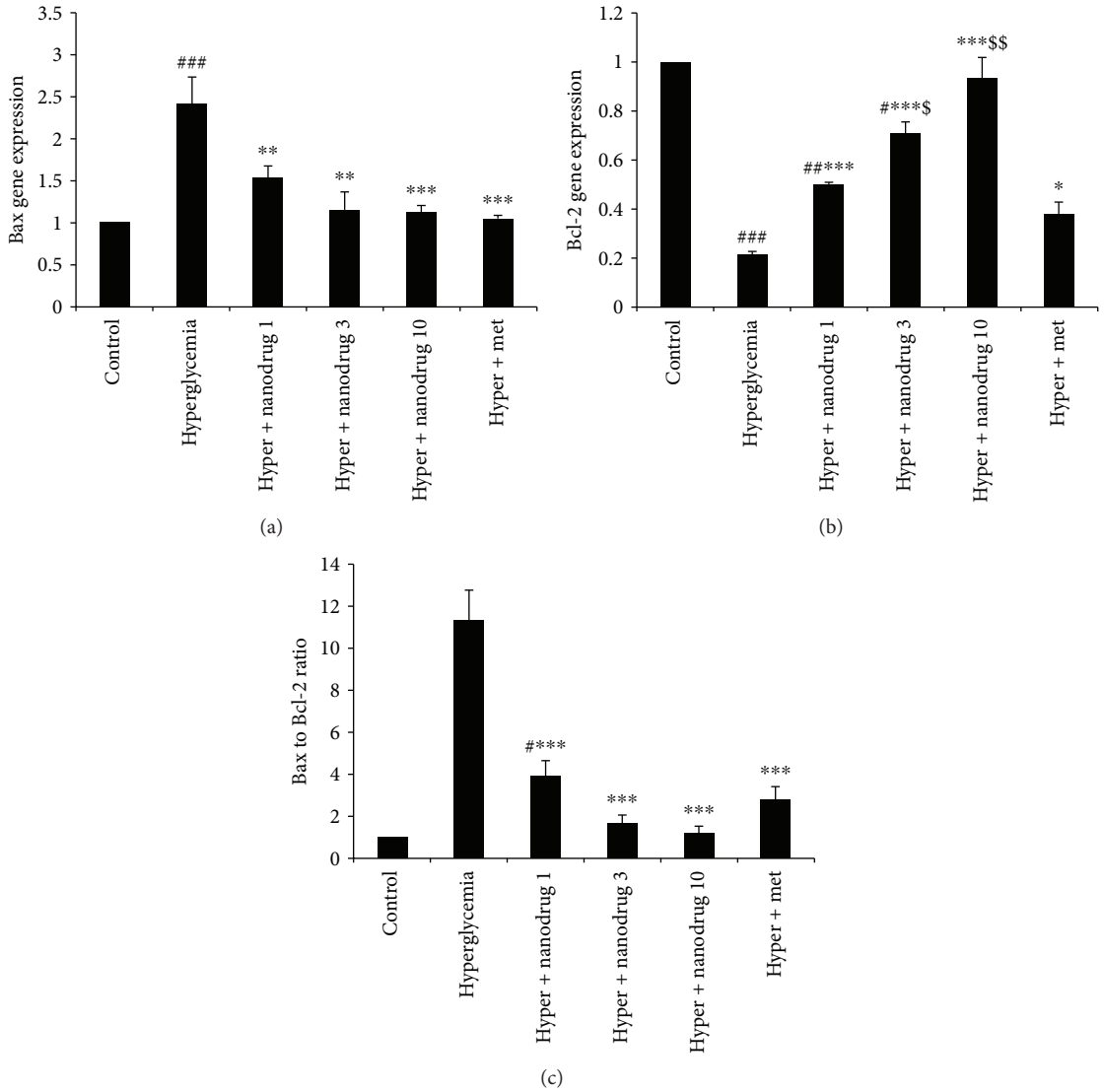

Figure 10: Effect of myricitrin SLN on C2C12 apoptosis gene expression. Data are presented as mean ± SE; $n = 3$; $^{\#}p < 0.05$, $^{\#\#}p < 0.01$, and $^{\#\#\#}p < 0.001$ compared with control; $^{*}p < 0.05$, $^{**}p < 0.01$, and $^{***}p < 0.001$ compared with hyperglycemia; $^{\$}p < 0.05$ and $^{\$\$}p < 0.01$ compared with hyperglycemia + metformin (one-way analysis of variance (ANOVA), followed by post hoc least significant difference (LSD) tests).

occurred in diabetic cases [47]. The results of myricitrin SLN administration in diabetic mice improved these alterations due to the protection from the damage of the pancreatic and muscle tissues. So, the mechanism of its action may occur through the enhancement of glycemic control and decreased catabolism of muscle's protein [48].

Lipid peroxidation has occurred in chronic diabetic condition, and MDA level increased in diabetic cases. It demonstrated that the mean activities of SOD and CAT are lower in pancreatic tissue of untreated diabetic rats. Hyperglycemia caused cellular damage through the several pathways such as increased nonenzymatic glycation and increased oxidative stress [49]. This condition elevates lipid peroxidation and reduces antioxidant defense, which leads to the increased expression of cellular damage gene products [50]. Antioxidant therapy by several compounds could prevent the lipid peroxidation [51]. Therefore, present results showed that STZ-NA-induced T2DM increased MDA and decreased CAT in the pancreas. Hence, it could be suggested that this model of diabetes may create pancreatic disorders via the increase of lipid peroxidation and H_2O_2. Further, the same effect in hyperglycemic exposed myotubes was observed in addition to the decrease of SOD level. SLN of myricitrin could enhance plasma antioxidant capacity in conjunction with reduced lipid peroxidation and results in maintaining redox balance in the pancreas. These effects were more evident in C2C12 cells due to the direct administration of myricitrin SLNs in the culture medium. Excessive production of antioxidant agents during oxidative stress and lipid peroxidation can exacerbate the cellular function disorders [52]. Hence, it seems hyperglycemic medium may induce more damages in muscle cells by the enhanced level of both TAC and MDA in the present study. Also, administered myricitrin at a low dose was more potent on the improvement of

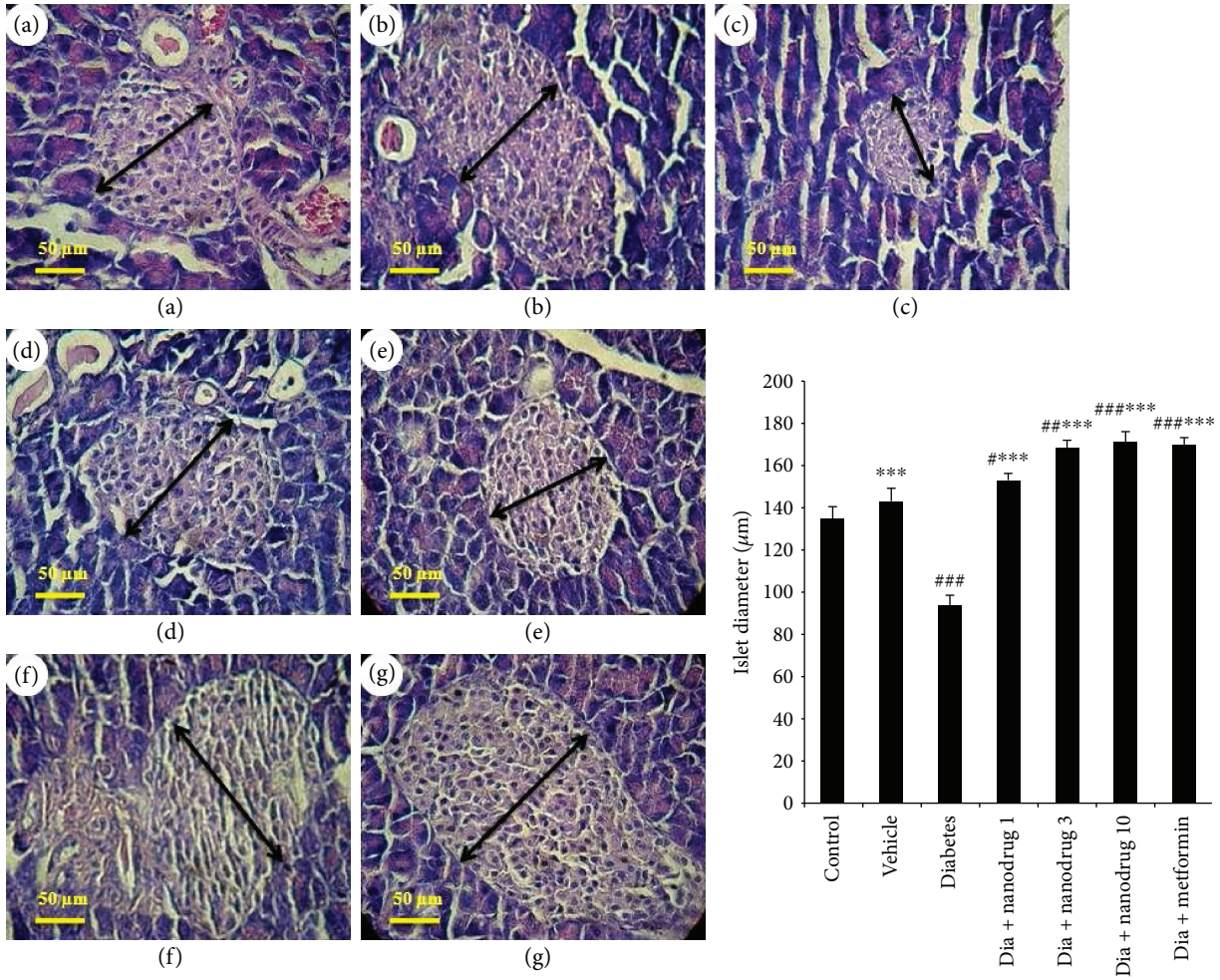

FIGURE 11: Role of myricitrin SLN on islet diameter (hematoxylin and eosin; ×40 magnification). Data are presented as mean ± SE; $n = 8$; $^{\#}p < 0.05$, $^{\#\#}p < 0.01$, and $^{\#\#\#}p < 0.001$ compared with control; $^{***}p < 0.001$ compared with diabetes (one-way analysis of variance (ANOVA), followed by post hoc least significant difference (LSD) tests). (a) Control; (b) vehicle; (c) diabetes; (d) diabetes + SLN containing myricitrin 1 mg/kg; (e) diabetes + SLN containing myricitrin 3 mg/kg; (f) diabetes + SLN containing myricitrin 10 mg/kg; (g) diabetes + metformin.

hyperglycemia-induced oxidative stress through increased antioxidant enzyme levels in myotubes, and this effect was more evident than metformin administration.

T2DM causes the insulin resistance that leads to hyperglycemia and reduces β-cell mass or secretory effectiveness [53]. The synthesis of glycogen is the main pathway for glucose uptake in the myotubes, which is regulated by hexokinase II and glucose-6-phosphate amidotransferase activity [54, 55]. In diabetic condition, the normal capacity of skeletal muscle gets impaired to synthesize of glycogen. In STZ-NA-induced diabetes model, the activation of glycogen synthase was decreased, and the activity of glycogen phosphorylase increased [56]. The Glut-4 transporter is a major site for glucose uptake which is specifically expressed in insulin-sensitive tissue such as skeletal muscles. Impaired glucose transport by a defect in insulin-mediated Glut-4 translocation induces insulin resistance [57]. Further, the impairment of glucose uptake due to the decrease Glut-4 level in skeletal muscle tissue has occurred through hyperglycemia [54, 55]. Therefore, the present study revealed that STZ-NA, as a model of type 2 diabetes, induced hyperglycemia, increased HOMA-IR, reduced HOMA-β, and decreased glycogen content of skeletal muscle and Glut-4 gene expression. A similar effect was evident in glycogen content and Glut-4 gene expression of untreated hyperglycemic C2C12 cells.

Flavonoids play an insulin-mimetic action, stimulate glucose uptake in peripheral tissue, and regulate the activity or expression of the rate-limiting enzymes involved in carbohydrate metabolism such as hexokinase [58]. Present results indicated that myricitrin SLN administration improved STZ-NA-induced diabetic alterations such as hyperglycemia, hyperinsulinemia, and β-cell's function index. However, SLN containing myricitrin consumption increased plasma level of insulin compared to untreated diabetic mice, but it could be suggested that this effect may occur through the more improved insulin secretion as a compensatory function of β-cell which is evident in islet diameter (as an increased β-cell secretory activity).

Hyperinsulinemia associated with increased insulin resistance is a demand for insulin secretion, and this event thought

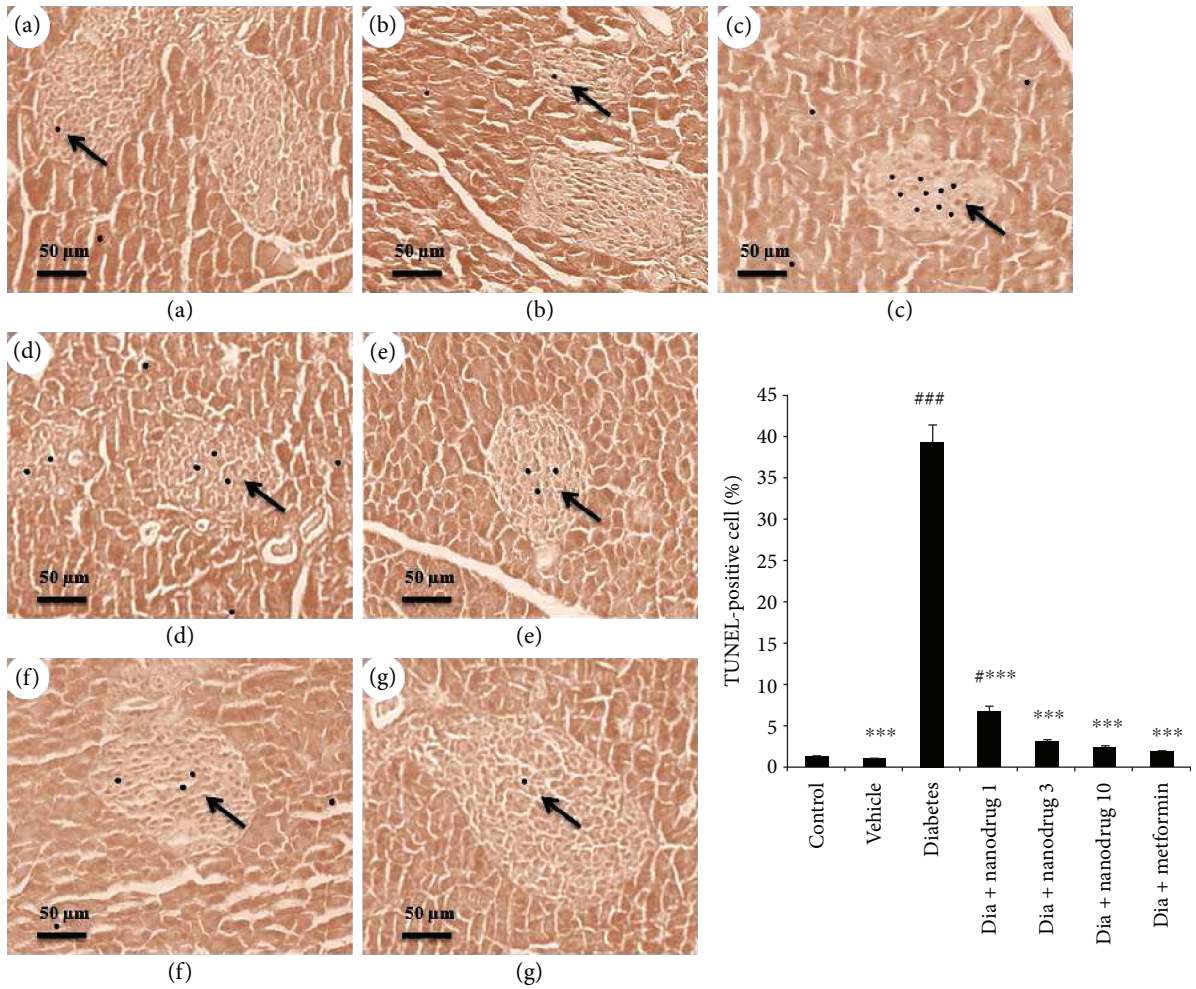

Figure 12: Effect of myricitrin SLN on pancreas apoptosis (TUNEL) (×40 magnification). Data are presented as mean ± SE; $n = 3$; $^{\#}p < 0.05$ and $^{\#\#\#}p < 0.001$ compared with control; $^{***}p < 0.001$ compared with diabetes (one-way analysis of variance (ANOVA), followed by post hoc least significant difference (LSD) tests). (a) Control; (b) vehicle; (c) diabetes; (d) diabetes + SLN containing myricitrin 1 mg/kg; (e) diabetes + SLN containing myricitrin 3 mg/kg; (f) diabetes + SLN containing myricitrin 10 mg/kg; (g) diabetes + metformin.

to reflect increased secretory capacity from the β-cells as a compensatory response for reducing blood glucose level during T2DM [59, 60]. Also, several studies have suggested that the T2DM process should be divided into the following three phases: hyperinsulinemia stage, prediabetes stage (impaired fasting glucose), and diabetes stage. Thus, hyperinsulinemia exists long before T2DM occurs. According to the WHO, prediabetes was typically defined as blood glucose level higher than the normal, but lower than diabetes thresholds (about 100–130 mg/dL) along with hyperinsulinemia. Hence, if physicians can provide an intervention treatment during the earlier stages of hyperinsulinemia, patients may have a better opportunity to prevent or delay the occurrence or development of T2DM. Moreover, several studies have reported that prediabetes can convert back to normoglycemia by an intervention in lifestyle and drug-based [61, 62]. So, according to the results of SLN containing myricitrin in the present study, it could be suggested that this compound increased the compensatory action of β-cells and improved hyperglycemia concomitant with increased plasma level of insulin and was able to restore the STZ-NA-induced diabetes to a prediabetes stage, which may be a promising new treatment for the recovery and treatment of T2DM.

Glucose uptake in skeletal muscle was mediated by mobilizing Glut-4 to the plasma membrane which stimulates insulin action. Insulin initiates glycogen synthesis in muscle via the entrance glucose into the cells. This process is the majority of whole-body glucose uptake and nonoxidative glucose metabolism [63] which was destroyed during T2DM [64]. Also, it was revealed that quercetin as a flavonoid compound improved the utilization of glucose through the increase Glut-4 gene expression and glycogen synthesis in myotubes [64]. So, the present results indicated STZ-NA-induced diabetes increased insulin resistance and decreased Glut-4 level that leads to hyperglycemia and reduced glycogen content in muscles and C2C12 cells. Moreover, myricitrin SLN administration recovered muscle's glycogen decreasing through the improved Glut-4 gene expression, insulin resistance, and glucose uptake in diabetic animals and muscle cells.

Anion superoxide level elevates during hyperglycemia and induces mitochondrial dysfunction or cellular apoptosis [65]. It was revealed that hyperglycemic condition reduced

adrenal medulla and osteoblast cell viability by a decrease in MTT levels [66, 67]. The mechanism of apoptosis is regulated by Bcl-2 family of proteins including Bax and Bcl-2. Bax protein expression promotes cell death, and the increase in Bcl-2 level leads to enhancement of cell survival. One studyshowed that Bax inactivated Bcl-2 proteins via heterodimerization [68]. Bax to Bcl-2 ratio increased during the apoptosis induction and exacerbates the susceptibility of apoptotic stimuli in the hematopoietic cell [68]. One study demonstrated that hyperglycemia significantly reduces Bcl-2 and enhances Bax levels in beta-cells [69]. The administration of antioxidants such as kaempferol improves hyperglycemia-induced apoptotic changes in cells [70, 71]. Therefore, according to the previous study, the present results demonstrated that hyperglycemic medium reduced C2C12 cell viability through the decreased MTT and Bcl-2 and increased Bax gene expression and Bax to Bcl-2 ratio. Further, SLN containing myricitrin treatment improved cell viability and apoptosis via the inversion of hyperglycemic changes in a dose-dependent manner.

Beta-cell apoptosis depends on the severity and time coursing of progression T2DM, oxidative stress, and antioxidant defenses. Consistent with the results of our study, Adam et al. revealed that STZ-NA-induced T2DM could decrease islet diameter and reduce β-cell through increased apoptosis in them [72]. It was demonstrated that antioxidant therapy could protect β-cells against glucose toxicity as a beneficial treatment for T2DM [73]. Therefore, the present results indicated that myricitrin SLN utilization increased islet diameter via improved hyperglycemic induced pancreas toxicity and apoptosis.

Metformin, belonging to the biguanide, has an insulinotropic effect, reduces blood glucose level concomitant with MDA concentration, and improved the altered activities of the antioxidant enzyme [74]. It was revealed that skeletal muscle glycogen synthase activity and glycogen content were increased in diabetic metformin-treated mice [75]. Concomitant with the previous studies, and similar to the results of SLN containing myricitrin administration, metformin could improve lipid peroxidation, antioxidant defense, hyperglycemia, β-cell function index, glycogen content, and islet diameter or apoptosis in STZ-NA-induced diabetic mice. Also, the comparison between metformin and myricitrin SLN utilization revealed that SLN of myricitrin is more potent than metformin in the improvement of SOD level, muscle and myotube glycogen content, Glut-4 gene expression in skeletal muscle and C2C12 cells, Bcl-2 gene expression, and Bax to Bcl-2 ratio of myotubes as an apoptosis index.

5. Conclusion

In conclusion, SLN containing myricitrin showed antidiabetic and antioxidant effects through the recovered body and tissue weight, oxidative stress, hyperglycemia, skeletal muscle glycogen content, insulin resistance, β-cell's function index, Glut-4 gene expression, and pancreas apoptosis which have been altered by STZ-NA-induced T2DM. In vitro assessment revealed that SLNs of myricitrin improved the antioxidant defense, amount of glycogen, and cellular survival in myotube cells exposed to the hyperglycemic condition. Also, some of these effects were more evident in SLN-administered groups compared to the metformin group.

Data Availability

The data used to support the findings of this study are available from the corresponding author upon request.

Ethical Approval

All the experimental procedures and protocols involving animals were approved by the Ethical Committee of Ahvaz Jundishapur University of Medical Sciences animal facility and were conducted in accordance with the principles and guidelines on the animal care of AJUMS as reviewed by an ethics committee (IR.AJUMS.REC.1395.136).

Disclosure

This study is a part of the Ph.D. thesis of Ali Akbar Oroojan and was labeled Cellular and Molecular Research Center project (CMRC-9509).

Conflicts of Interest

The authors have no conflicts of interest to report with respect to this paper.

Acknowledgments

This study was supported financially by the vice-chancellor of research affairs of Ahvaz Jundishapur University of Medical Sciences, Ahvaz, Iran.

References

[1] B. H. Goodpaster, A. Bertoldo, J. M. Ng et al., "Interactions among glucose delivery, transport, and phosphorylation that underlie skeletal muscle insulin resistance in obesity and type 2 diabetes: studies with dynamic PET imaging," *Diabetes*, vol. 63, no. 3, pp. 1058–1068, 2014.

[2] M. Mueckler, "Insulin resistance and the disruption of Glut4 trafficking in skeletal muscle," *Journal of Clinical Investigation*, vol. 107, no. 10, pp. 1211–1213, 2001.

[3] M. A. Herman and B. B. Kahn, "Glucose transport and sensing in the maintenance of glucose homeostasis and metabolic harmony," *The Journal of Clinical Investigation*, vol. 116, no. 7, pp. 1767–1775, 2006.

[4] P. Xu, D. Cuthbertson, C. Greenbaum, J. P. Palmer, J. P. Krischer, and for the Diabetes Prevention Trial Type 1 Study Group, "Role of insulin resistance in predicting progression to type 1 diabetes," *Diabetes Care*, vol. 30, no. 9, pp. 2314–2320, 2007.

[5] L. J. Holm, M. Haupt-Jorgensen, J. Larsen, J. D. Giacobini, M. Bilgin, and K. Buschard, "L-Serine supplementation lowers diabetes incidence and improves blood glucose homeostasis in NOD mice," *PLoS One*, vol. 13, no. 3, article e0194414, 2018.

[6] L. Brunetti and J. Kalabalik, "Management of type-2 diabetes mellitus in adults: focus on individualizing non-insulin therapies," *Pharmacy and Therapeutics*, vol. 37, no. 12, pp. 687–696, 2012.

[7] L. B. A. Rojas and M. B. Gomes, "Metformin: an old but still the best treatment for type 2 diabetes," *Diabetology & Metabolic Syndrome*, vol. 5, no. 1, p. 6, 2013.

[8] M. E. Zujko, A. M. Witkowska, M. Górska, J. Wilk, and A. Krętowski, "Reduced intake of dietary antioxidants can impair antioxidant status in type 2 diabetes patients," *Polskie Archiwum Medycyny Wewnętrznej*, vol. 124, no. 11, pp. 599–607, 2014.

[9] A. Ahangarpour, A. A. Oroojan, L. Khorsandi, M. Kouchak, and M. Badavi, "Antioxidant effect of myricitrin on hyperglycemia-induced oxidative stress in C2C12 cell," *Cell Stress and Chaperones*, pp. 1–9, 2018.

[10] S. R. Zatalia and H. Sanusi, "The role of antioxidants in the pathophysiology, complications, and management of diabetes mellitus," *Acta Medica Indonesiana*, vol. 45, no. 2, pp. 141–147, 2013.

[11] M. Pereira, I. P. Siba, L. R. Chioca et al., "Myricitrin, a nitric oxide and protein kinase C inhibitor, exerts antipsychotic-like effects in animal models," *Progress in Neuro-Psychopharmacology and Biological Psychiatry*, vol. 35, no. 7, pp. 1636–1644, 2011.

[12] G.-b. Sun, M. Qin, J.-x. Ye et al., "Inhibitory effects of myricitrin on oxidative stress-induced endothelial damage and early atherosclerosis in ApoE−/− mice," *Toxicology and Applied Pharmacology*, vol. 271, no. 1, pp. 114–126, 2013.

[13] R. Domitrović, K. Rashed, O. Cvijanović, S. Vladimir-Knežević, M. Škoda, and A. Višnić, "Myricitrin exhibits antioxidant, anti-inflammatory and antifibrotic activity in carbon tetrachloride-intoxicated mice," *Chemico-Biological Interactions*, vol. 230, pp. 21–29, 2015.

[14] S. P. Fernandez, M. Nguyen, T. T. Yow et al., "The flavonoid glycosides, myricitrin, gossypin and naringin exert anxiolytic action in mice," *Neurochemical Research*, vol. 34, no. 10, pp. 1867–1875, 2009.

[15] M. Üner and G. Yener, "Importance of solid lipid nanoparticles (SLN) in various administration routes and future perspectives," *International Journal of Nanomedicine*, vol. 2, no. 3, pp. 289–300, 2007.

[16] P. Masiello, C. Broca, R. Gross et al., "Experimental NIDDM: development of a new model in adult rats administered streptozotocin and nicotinamide," *Diabetes*, vol. 47, no. 2, pp. 224–229, 1998.

[17] A. Ghasemi, S. Khalifi, and S. Jedi, "Streptozotocin-nicotinamide-induced rat model of type 2 diabetes (review)," *Acta Physiologica Hungarica*, vol. 101, no. 4, pp. 408–420, 2014.

[18] M. A. Karami, B. Sharif Makhmal Zadeh, M. Koochak, and E. Moghimipur, "Superoxide dismutase-loaded solid lipid nanoparticles prepared by cold homogenization method: characterization and permeation study through burned rat skin," *Jundishapur Journal of Natural Pharmaceutical Products*, vol. 11, no. 4, 2016.

[19] P. T. Nandini, R. C. Doijad, H. N. Shivakumar, and P. M. Dandagi, "Formulation and evaluation of gemcitabine-loaded solid lipid nanoparticles," *Drug Delivery*, vol. 22, no. 5, pp. 647–651, 2013.

[20] E. Moghimipour, M. Kargar, Z. Ramezani, and S. Handali, "The potent in vitro skin permeation of archaeosome made from lipids extracted ofsulfolobus acidocaldarius," *Archaea*, vol. 2013, Article ID 782012, 7 pages, 2013.

[21] A. Ahangarpour, A. A. Oroojan, L. Khorsandi, G. Arzani, and G. Afshari, "Effects of betulinic acid on the male reproductive system of a streptozotocin-nicotinamide-induced diabetic mouse model," *The World Journal of Men's Health*, vol. 34, no. 3, pp. 209–216, 2016.

[22] F. C. Meotti, T. Posser, F. C. Missau, M. G. Pizzolatti, R. B. Leal, and A. R. S. Santos, "Involvement of p38MAPK on the antinociceptive action of myricitrin in mice," *Biochemical Pharmacology*, vol. 74, no. 6, pp. 924–931, 2007.

[23] R. C. Schwanke, R. Marcon, F. C. Meotti et al., "Oral administration of the flavonoid myricitrin prevents dextran sulfate sodium-induced experimental colitis in mice through modulation of PI3K/Akt signaling pathway," *Molecular Nutrition & Food Research*, vol. 57, no. 11, pp. 1938–1949, 2013.

[24] J. Yang, P. Zhao, D. Wan et al., "Antidiabetic effect of methanolic extract from *Berberis julianae* Schneid. via activation of AMP-activated protein kinase in Type 2 diabetic mice," *Evidence-based Complementary and Alternative Medicine*, vol. 2014, Article ID 106206, 12 pages, 2014.

[25] Z. Sun, L. Zhao, L. Zuo, C. Qi, P. Zhao, and X. Hou, "A UHPLC-MS/MS method for simultaneous determination of six flavonoids, gallic acid and 5,8-dihydroxy-1,4-naphthoquinone in rat plasma and its application to a pharmacokinetic study of Cortex Juglandis Mandshuricae extract," *Journal of Chromatography B*, vol. 958, pp. 55–62, 2014.

[26] C. J. Botha, S. J. Clift, G. C. H. Ferreira, and M. G. Masango, "Geigerin-induced cytotoxicity in a murine myoblast cell line (C2C12)," *The Onderstepoort Journal of Veterinary Research*, vol. 84, no. 1, pp. e1–e7, 2017.

[27] M. J. Son, Y. Miura, and K. Yagasaki, "Mechanisms for antidiabetic effect of gingerol in cultured cells and obese diabetic model mice," *Cytotechnology*, vol. 67, no. 4, pp. 641–652, 2015.

[28] P. Senesi, A. Montesano, L. Luzi, R. Codella, S. Benedini, and I. Terruzzi, "Metformin treatment prevents sedentariness related damages in mice," *Journal of Diabetes Research*, vol. 2016, Article ID 8274689, 11 pages, 2016.

[29] Q. Huang, B. Gao, L. Wang et al., "Protective effects of myricitrin against osteoporosis via reducing reactive oxygen species and bone-resorbing cytokines," *Toxicology and Applied Pharmacology*, vol. 280, no. 3, pp. 550–560, 2014.

[30] J. Kang, K. Boonanantanasarn, K. Baek et al., "Hyperglycemia increases the expression levels of sclerostin in a reactive oxygen species- and tumor necrosis factor-alpha-dependent manner," *Journal of Periodontal & Implant Science*, vol. 45, no. 3, pp. 101–110, 2015.

[31] S. Karbach, T. Jansen, S. Horke et al., "Hyperglycemia and oxidative stress in cultured endothelial cells – a comparison of primary endothelial cells with an immortalized endothelial cell line," *Journal of Diabetes and its Complications*, vol. 26, no. 3, pp. 155–162, 2012.

[32] I. Dimauro, T. Pearson, D. Caporossi, and M. J. Jackson, "A simple protocol for the subcellular fractionation of skeletal muscle cells and tissue," *BMC Research Notes*, vol. 5, no. 1, pp. 513–513, 2012.

[33] Y. Onishi, T. Hayashi, K. K. Sato et al., "Fasting tests of insulin secretion and sensitivity predict future prediabetes in Japanese with normal glucose tolerance," *Journal of Diabetes Investigation*, vol. 1, no. 5, pp. 191–195, 2010.

[34] A. Uruno, Y. Yagishita, F. Katsuoka et al., "Nrf2-mediated regulation of skeletal muscle glycogen metabolism," *Molecular and Cellular Biology*, vol. 36, no. 11, pp. 1655–1672, 2016.

[35] R. Hosseinzadeh and K. Khorsandi, "Methylene blue, curcumin and ion pairing nanoparticles effects on photodynamic

therapy of MDA-MB-231 breast cancer cell," *Photodiagnosis and Photodynamic Therapy*, vol. 18, pp. 284–294, 2017.

[36] M. Gomez Perez, L. Fourcade, M. A. Mateescu, and J. Paquin, "Neutral red versus MTT assay of cell viability in the presence of copper compounds," *Analytical Biochemistry*, vol. 535, pp. 43–46, 2017.

[37] A. Ahangarpour, A. A. Oroojan, L. Khorsandi, and S. A. Najimi, "Pancreatic protective and hypoglycemic effects of *Vitex agnus-castus* L. fruit hydroalcoholic extract in D-galactose-induced aging mouse model," *Research in Pharmaceutical Sciences*, vol. 12, no. 2, pp. 137–143, 2017.

[38] L. S. Khorsandi, M. Hashemitabar, M. Orazizadeh, and N. Albughobeish, "Dexamethasone effects on fas ligand expression in mouse testicular germ cells," *Pakistan Journal of Biological Sciences*, vol. 11, no. 18, pp. 2231–2236, 2008.

[39] N. Hoshyar, S. Gray, H. Han, and G. Bao, "The effect of nanoparticle size on in vivo pharmacokinetics and cellular interaction," *Nanomedicine*, vol. 11, no. 6, pp. 673–692, 2016.

[40] V. Kakkar, S. K. Muppu, K. Chopra, and I. P. Kaur, "Curcumin loaded solid lipid nanoparticles: an efficient formulation approach for cerebral ischemic reperfusion injury in rats," *European Journal of Pharmaceutics and Biopharmaceutics*, vol. 85, no. 3, Part A, pp. 339–345, 2013.

[41] J. Shaji and D. Varkey, "Silica-coated solid lipid nanoparticles enhance antioxidant and antiradical effects of meloxicam," *Journal of Pharmaceutical Investigation*, vol. 43, no. 5, pp. 405–416, 2013.

[42] G. Singhal, R. Patel, and B. Prajapati, "Solid lipid nanoparticles: a review. Scientific reviews and chemical communications," *International Research Journal of Pharmacy*, vol. 2, no. 2, pp. 40–52, 2011.

[43] A. Ahangarpour, H. Heidari, M. S. Junghani, R. Absari, M. Khoogar, and E. Ghaedi, "Effects of hydroalcoholic extract of *Rhus coriaria* seed on glucose and insulin related biomarkers, lipid profile, and hepatic enzymes in nicotinamide-streptozotocin-induced type II diabetic male mice," *Research in Pharmaceutical Sciences*, vol. 12, no. 5, pp. 416–424, 2017.

[44] T. Rodriguez-Calvo, O. Ekwall, N. Amirian, J. Zapardiel-Gonzalo, and M. G. von Herrath, "Increased immune cell infiltration of the exocrine pancreas: a possible contribution to the pathogenesis of type 1 diabetes," *Diabetes*, vol. 63, no. 11, pp. 3880–3890, 2014.

[45] S.-S. Roh, O. J. Kwon, J. H. Yang et al., "*Allium hookeri* root protects oxidative stress-induced inflammatory responses and β-cell damage in pancreas of streptozotocin-induced diabetic rats," *BMC Complementary and Alternative Medicine*, vol. 16, no. 1, p. 63, 2016.

[46] M. Choudhary, N. Choudhary, P. Gupta, N. Aggarwal, and V. Budhwaar, "Effect of aqueous and alcoholic extract of *Sesbania sesban* (Linn) Merr. Root on glycemic control in streptozotocin-induced diabetic mice," *Drug Development and Therapeutics*, vol. 5, no. 2, p. 115, 2014.

[47] L. Mohapatra, S. K. Bhattamishra, R. Panigrahy, S. Parida, and P. Pati, "Antidiabetic effect of *Sargassum wightii* and *Ulva fasciata* in high fat diet and multi low dose streptozotocin induced type 2 diabetic mice," *UK Journal of Pharmaceutical and Biosciences*, vol. 4, no. 2, pp. 13–23, 2016.

[48] V. Kumar, F. Anwar, D. Ahmed et al., "*Paederia foetida* Linn. leaf extract: an antihyperlipidemic, antihyperglycaemic and antioxidant activity," *BMC Complementary and Alternative Medicine*, vol. 14, no. 1, p. 76, 2014.

[49] S. K. Jain, R. McVie, and J. A. Bocchini Jr, "Hyperketonemia (ketosis), oxidative stress and type 1 diabetes," *Pathophysiology*, vol. 13, no. 3, pp. 163–170, 2006.

[50] J. L. Evans, I. D. Goldfine, B. A. Maddux, and G. M. Grodsky, "Are oxidative stress-activated signaling pathways mediators of insulin resistance and β-Cell dysfunction?," *Diabetes*, vol. 52, no. 1, pp. 1–8, 2003.

[51] T. Annadurai, A. R. Muralidharan, T. Joseph, M. J. Hsu, P. A. Thomas, and P. Geraldine, "Antihyperglycemic and antioxidant effects of a flavanone, naringenin, in streptozotocin-nicotinamide-induced experimental diabetic rats," *Journal of Physiology and Biochemistry*, vol. 68, no. 3, pp. 307–318, 2012.

[52] L. Lorente, M. M. Martín, A. Pérez-Cejas et al., "Association between total antioxidant capacity and mortality in ischemic stroke patients," *Annals of Intensive Care*, vol. 6, no. 1, p. 39, 2016.

[53] M. Novelli, B. Bonamassa, M. Masini et al., "Persistent correction of hyperglycemia in streptozotocin-nicotinamide-induced diabetic mice by a non-conventional radical scavenger," *Naunyn-Schmiedeberg's Archives of Pharmacology*, vol. 382, no. 2, pp. 127–137, 2010.

[54] M. Kato, A. Suwa, and T. Shimokawa, "Glucose catabolic gene mRNA levels in skeletal muscle exhibit non-coordinate expression in hyperglycemic mice," *Hormone and Metabolic Research*, vol. 36, no. 8, pp. 513–518, 2004.

[55] Y. B. Kim, O. D. Peroni, W. G. Aschenbach et al., "Muscle-specific deletion of the Glut4 glucose transporter alters multiple regulatory steps in glycogen metabolism," *Molecular and Cellular Biology*, vol. 25, no. 21, pp. 9713–9723, 2005.

[56] G. B. Kavishankar and N. Lakshmidevi, "Anti-diabetic effect of a novel N-trisaccharide isolated from *Cucumis prophetarum* on streptozotocin-nicotinamide induced type 2 diabetic rats," *Phytomedicine*, vol. 21, no. 5, pp. 624–630, 2014.

[57] A. Rezaei Farimani, M. Saidijam, M. T. Goodarzi et al., "Effect of resveratrol supplementation on the SNARE proteins expression in adipose tissue of stroptozotocin-nicotinamide induced type 2 diabetic rats," *Iranian Journal of Medical Sciences*, vol. 40, no. 3, pp. 248–255, 2015.

[58] R. Gupta, M. Mathur, V. K. Bajaj et al., "Evaluation of antidiabetic and antioxidant activity of *Moringa oleifera* in experimental diabetes," *Journal of Diabetes*, vol. 4, no. 2, pp. 164–171, 2012.

[59] A. Clark, L. Jones, E. de Koning, B. C. Hansen, and D. R. Matthews, "Decreased insulin secretion in type 2 diabetes: a problem of cellular mass or function?," *Diabetes*, vol. 50, Supplement 1, pp. S169–S171, 2001.

[60] V. Grill and A. Björklund, "Type 2 diabetes—effect of compensatory oversecretion as a reason for β-cell collapse," *International Journal of Experimental Diabetes Research*, vol. 3, no. 3, pp. 153–158, 2002.

[61] G. Yang, C. Li, Y. Gong et al., "Assessment of insulin resistance in subjects with normal glucose tolerance, hyperinsulinemia with normal blood glucose tolerance, impaired glucose tolerance, and newly diagnosed type 2 diabetes (prediabetes insulin resistance research)," *Journal of Diabetes Research*, vol. 2016, Article ID 9270768, 11 pages, 2016.

[62] A. G. Tabák, C. Herder, W. Rathmann, E. J. Brunner, and M. Kivimäki, "Prediabetes: a high-risk state for diabetes development," *The Lancet*, vol. 379, no. 9833, pp. 2279–2290, 2012.

[63] R. B. Ceddia, R. Somwar, A. Maida, X. Fang, G. Bikopoulos, and G. Sweeney, "Globular adiponectin increases GLUT4 translocation and glucose uptake but reduces glycogen synthesis in rat skeletal muscle cells," *Diabetologia*, vol. 48, no. 1, pp. 132–139, 2005.

[64] R. Dhanya, A. D. Arya, P. Nisha, and P. Jayamurthy, "Quercetin, a lead compound against type 2 diabetes ameliorates glucose uptake via AMPK pathway in skeletal muscle cell line," *Frontiers in Pharmacology*, vol. 8, p. 336, 2017.

[65] B.-J. Pyun, Y. S. Kim, I.-S. Lee, and J. S. Kim, "*Homonoia riparia* and its major component, myricitrin, inhibit high glucose-induced apoptosis of human retinal pericytes," *Integrative Medicine Research*, vol. 6, no. 3, pp. 300–309, 2017.

[66] A. Mohammadi-Farani, M. Ghazi-Khansari, and M. Sahebgharani, "Glucose concentration in culture medium affects mRNA expression of TRPV1 and CB1 receptors and changes capsaicin toxicity in PC12 cells," *Iranian Journal of Basic Medical Sciences*, vol. 17, no. 9, pp. 673–378, 2014.

[67] N. Ogawa, T. Yamaguchi, S. Yano, M. Yamauchi, M. Yamamoto, and T. Sugimoto, "The combination of high glucose and advanced glycation end-products (AGEs) inhibits the mineralization of osteoblastic MC3T3-E1 cells through glucose-induced increase in the receptor for AGEs," *Hormone and Metabolic Research*, vol. 39, no. 12, pp. 871–875, 2007.

[68] P. Magistrelli, R. Coppola, G. Tonini et al., "Apoptotic index or a combination of Bax/Bcl-2 expression correlate with survival after resection of pancreatic adenocarcinoma," *Journal of Cellular Biochemistry*, vol. 97, no. 1, pp. 98–108, 2006.

[69] J. Hasnan, M. I. Yusof, T. D. Damitri, A. R. Faridah, A. S. Adenan, and T. H. Norbaini, "Relationship between apoptotic markers (Bax and Bcl-2) and biochemical markers in type 2 diabetes mellitus," *Singapore Medical Journal*, vol. 51, no. 1, pp. 50–55, 2010.

[70] D. Verzola, M. B. Bertolotto, B. Villaggio et al., "Oxidative stress mediates apoptotic changes induced by hyperglycemia in human tubular kidney cells," *Journal of the American Society of Nephrology*, vol. 15, no. 90010, Supplement 1, pp. S85–S87, 2004.

[71] Y. Zhang and D. Liu, "Flavonol kaempferol improves chronic hyperglycemia-impaired pancreatic beta-cell viability and insulin secretory function," *European Journal of Pharmacology*, vol. 670, no. 1, pp. 325–332, 2011.

[72] S. H. Adam, N. Giribabu, P. V. Rao et al., "Rhinacanthin C ameliorates hyperglycaemia, hyperlipidemia and pancreatic destruction in streptozotocin-nicotinamide induced adult male diabetic rats," *European Journal of Pharmacology*, vol. 771, pp. 173–190, 2016.

[73] Y. Kajimoto and H. Kaneto, "Role of oxidative stress in pancreatic β-cell dysfunction," *Annals of the New York Academy of Sciences*, vol. 1011, no. 1, pp. 168–176, 2004.

[74] B. Chukwunonso Obi, T. Chinwuba Okoye, V. E. Okpashi, C. Nonye Igwe, and E. Olisah Alumanah, "Comparative study of the antioxidant effects of metformin, glibenclamide, and repaglinide in alloxan-induced diabetic rats," *Journal of Diabetes Research*, vol. 2016, Article ID 1635361, 5 pages, 2016.

[75] A. S. Reddi and G. N. Jyothirmayi, "Effect of chronic metformin treatment on hepatic and muscle glycogen metabolism in KK mice," *Biochemical Medicine and Metabolic Biology*, vol. 47, no. 2, pp. 124–132, 1992.

Hindawi
Oxidative Medicine and Cellular Longevity
Volume 2018, Article ID 8354747, 8 pages
https://doi.org/10.1155/2018/8354747

Research Article

The Associations between Infertility and Antioxidants, Proinflammatory Cytokines, and Chemokines

Dorota Chyra-Jach,[1] Zbigniew Kaletka,[2] Michał Dobrakowski,[1] Anna Machoń-Grecka,[1] Sławomir Kasperczyk,[1] Ewa Birkner,[1] and Aleksandra Kasperczyk[1]

[1]*Department of Biochemistry, School of Medicine with the Division of Dentistry in Zabrze, Medical University of Silesia, ul. Jordana 19, 41-808 Zabrze, Poland*
[2]*Department and Clinic of Urology, School of Medicine with the Division of Dentistry in Zabrze, Medical University of Silesia, ul. 3 Maja 13-15, 41-800 Zabrze, Poland*

Correspondence should be addressed to Anna Machoń-Grecka; anna.machon-grecka@med.sum.edu.pl

Received 18 April 2018; Accepted 19 June 2018; Published 16 July 2018

Academic Editor: Karolina Szewczyk-Golec

The aim of the study was to evaluate the parameters of oxidative stress and antioxidant defense in relation to the levels of proinflammatory cytokines and chemokines in patients diagnosed with oligozoospermia and asthenozoospermia. Based on the basic parameters of the spermogram, the examined group ($n = 243$) was divided into three groups: oligospermic group (sperm count less than 15×10^6/ml) consisting of 152 men, astenozoospermic group (less than 40% of progressively moving sperm cells) consisting of 142 men, and oligoastenozoospermic group (both criteria met) consisting of 90 men. The control group consisted of 103 males with normal semen profile according to the WHO criteria. Total superoxide dismutase (SOD) activity in seminal plasma and spermatozoa lysate was significantly lower by 12% and 22%, respectively, in males with oligospermia than in the control group. Analogically, Mn-SOD activity in spermatozoa lysate was significantly lower in males with oligospermia, asthenospermia, and oligoasthenospermia by 44%, 32%, and 45%, respectively. By contrast, CuZn-SOD activity in spermatozoa lysate was significantly higher in males with oligospermia by 60%. The activity of glutathione peroxidase (GPx) in seminal plasma was also significantly higher in males with oligospermia and oligoasthenospermia by 56% and 78%, respectively. The level of malondialdehyde (MDA) in seminal plasma was significantly higher in males with asthenospermia than in the control group by 12%. By contrast, the level of MDA in spermatozoa lysate was significantly lower in males with oligospermia, asthenospermia, and oligoasthenospermia by 26%, 20%, and 26%, respectively. The level of interleukin- (IL-) 8 in seminal plasma was significantly higher in males with asthenospermia and oligoasthenospermia by 64% and 67%, respectively. Abnormalities in spermogram, such as oligospermia, asthenospermia, and oligoasthenospermia, may be related to a decreased activity of Mn-SOD in spermatozoa and increased levels of chemokines in seminal plasma.

1. Introduction

The failure to conceive after one year of regular, unprotected intercourse with the same partner is defined as infertility [1]. The male factor is the cause of infertility in couples in approximately 30–40% of cases [2]. Defective sperm function is the most common cause of male infertility. Abnormal semen parameters include decreased sperm concentration, impaired motility, and altered morphology. There are many possible endogenous and exogenous factors that influence sperm quality. Many studies indicate that oxidative stress should be regarded as a plausible cause of idiopathic male infertility [3].

In spermatozoa, the NADPH oxidase at the level of the sperm plasma membrane and the NADH-dependent oxidoreductase at the mitochondrial level are the two major sources of reactive oxygen species (ROS). In seminal plasma, the main exogenous sources of ROS are radiation and toxins, including tobacco smoke and alcohol, while the main endogenous sources of ROS include the pathophysiologic effects of varicocele, accumulation of damaged spermatozoa with excess residual cytoplasm, and immune cells. Various intracellular or extracellular stimuli, such as infection or inflammation, may recruit and activate peroxidase-positive leukocytes, including polymorphonuclear leukocytes and macrophages that originate from the prostate and seminal vesicles. These cells are able to discharge up to 100 times more ROS than normal as a result of a respiratory burst. Consistently, many studies indicate a correlation between decreased sperm function and elevated levels of proinflammatory cytokines [4].

At low concentrations, ROS play an important role in capacitation, hyperactivation, acrosome reaction, and spermatozoa-oocyte fusion. However, elevated levels of ROS override antioxidant defenses and lead to a damage to biomolecules such as lipids, proteins, and nucleic acids [5]. Human spermatozoa are extremely vulnerable to oxidative attack because they contain high amounts of polyunsaturated fatty acids and little cytoplasm sequestering antioxidants. Therefore, human seminal plasma serves as a source of antioxidants. In this microenvironment, antioxidant enzymes, such as superoxide dismutase (SOD) and catalase (CAT), can be found. Besides, seminal plasma contains high levels of nonenzymatic antioxidants, such as ascorbate or thiol groups [6].

Oxidative stress-induced loss of membrane integrity, increased cell permeability, enzyme inactivation, structural damage of DNA, and cell death may be associated with decreased sperm count and motility [1, 4]. In light of this, we decided to evaluate the parameters of oxidative stress and antioxidant defense in relation to the levels of proinflammatory cytokines and chemokines in males diagnosed with oligospermia and asthenospermia.

2. Materials

The study group consisted of 346 males living in Upper Silesia (Poland) who had attended an andrology clinic to diagnose infertility. Information about the fertile abilities of men was provided by the spermogram test. The seminal samples were collected by masturbation after 3 days of abstinence on the same day in the morning before the first meal. All of the semen specimens were analyzed according to WHO standards [7], including the assessment of seminal volume, sperm cell density, total sperm cell count, motility, supravital eosin staining (for percentage of live spermatozoa), and number of peroxidase-positive cells. Additively, we analyzed percentages of motile spermatozoa after 24 hours and progressive motile spermatozoa after 24 hours.

Based on the basic parameters of the spermogram, the examined group was selected ($n = 243$). Subjects in that group were divided into three groups: oligospermic group (sperm count less than 15×10^6/ml) consisting of 152 men, astenozoospermic group (less than 40% of progressively moving sperm cells) consisting of 142 men, and oligoastenozoospermic group (both criteria met) consisting of 90 men. The control group consisted of 103 males with normal semen profile according to the WHO criteria [7]. The exclusion criteria were defined as follows: drug consumption (including antioxidant medications), smoking habits, alcohol abuse, and a history of any chronic disease, such as diabetes, coronary artery disease, or malignant neoplasm.

The experimental set-up has been approved by the Bioethics Committee of the Medical University of Silesia in Katowice (KNW/0022/KB1/I/13/09).

3. Methods

3.1. Sample Preparation and Semen Analysis. The semen specimens were analyzed according to WHO standards [7].

After complete liquefaction, seminal plasma was separated from the spermatozoa by centrifugation at 6000g for 10 minutes. The supernatants obtained were stored at −75°C until required for the biochemical analysis. In addition, a 10% spermatozoa lysate in bidistilled water was made.

3.2. Biochemical Analysis

3.2.1. Antioxidant Enzymes. The method of Oyanagui [8] was used to measure the activities of SOD, CuZn-SOD, and Mn-SOD in seminal plasma and spermatozoa. The enzymatic activity of SOD was expressed in nitric units. The activity of SOD is equal to 1 nitric unit (NU) when it inhibits nitric ion production by 50%. Activities of SOD and isoenzymes, Mn-SOD and CuZn-SOD, in seminal plasma were expressed in NU/ml and in NU/dl packed spermatozoa. The seminal plasma glutathione peroxidase (GPx) activity was measured by the kinetic method of Paglia and Valentine [9]. The GPx activity was expressed in U/l. The activity of seminal plasma glutathione-S-transferase (GST) was measured according to the kinetic method of Habig and Jakoby [10]. The GST activity was expressed as moles of thioether produced per minute per liter of seminal plasma (U/l). The activities of glucose-6-phosphate dehydrogenase (G6PD) and glutathione reductase (GR) in seminal plasma were measured according to Richterich [11]. G6PD and GR activity was expressed as μmol of NADPH produced and utilized, respectively, per minute per liter of seminal plasma (U/l). CAT activity in seminal plasma was measured by the method of Johansson and Borg [12]. The activity of catalase was expressed as U/l.

3.2.2. Nonenzymatic Antioxidants. Total antioxidant capacity (TAC) was measured according to Erel [13]. Data were shown as mmol/l. The levels of uric acid (UA), bilirubin, and albumin were determined in seminal plasma by colorimetric methods. For uric acid and bilirubin, concentrations are provided in mg/dl, and albumin is expressed in g/ml. The concentration of thiol groups (SH) in seminal plasma was determined by Koster et al. [14]. The results were shown as μmol/l.

3.2.3. Markers of Oxidative Stress. The level of malondialdehyde (MDA) in seminal plasma and spermatozoa lysate according to Ohkawa et al. [15]. TBARS values are expressed as malondialdehyde (MDA) equivalents. Concentrations were given in μmol/l in seminal plasma and μmol/dl in packed spermatozoa. The lipofuscin (LPS) concentration was determined in seminal plasma according to Jain [16]. Values were presented as relative units (relative fluorescence lipid extract, RF). Total oxidant status (TOS) was measured in seminal plasma according to Erel [17]. Data were shown in μmol/l.

3.2.4. Cytokines. The levels of IL-1β, IL-6, IL-8, IL-12, TNF-α, MCP-1, and MIP-1β were measured in seminal plasma using a Bio-Plex 200 System (Bio-Rad Laboratories Inc., USA) according to the manufacturer's instructions. Data were presented in pg/ml.

3.3. Statistical Analysis. A database was created in MS Excel 2007. Statistical analysis was performed using Statistica 10.0 PL software. Statistical methods included mean and standard deviation (SD) for normal distribution and median and interquartile range (IQR) for abnormal distribution. Shapiro-Wilk's test was used to verify normality and Levene's test to verify homogeneity of variances. Statistical comparisons between groups were made by a t-test, t-test with a separate variance, or Mann–Whitney U test (nonparametric test). Spearman's coefficient R for nonparametric correlation was calculated. A value of $p < 0.05$ was considered significant.

4. Results

Mean age in the control and examined groups did not differ significantly (Table 1). Differences between the control group and examined groups in terms of the semen volume, pH, count, and motility are presented in Table 1. The numbers of peroxidase-positive cells were within the normal ranges ($<1 \times 10^6$/ml) in all examined groups and did not differ among them.

Total SOD activity in seminal plasma and spermatozoa lysate was significantly lower by 12% and 22%, respectively, in males with oligospermia than in the control group. Analogically, Mn-SOD activity in spermatozoa lysate was significantly lower in males with oligospermia, asthenospermia, and oligoasthenospermia by 44%, 32%, and 45%, respectively. By contrast, CuZn-SOD activity in spermatozoa lysate was significantly higher in males with oligospermia by 60%. The activity of GPx in seminal plasma was also significantly higher in males with oligospermia and oligoasthenospermia by 56% and 78%, respectively (Table 2).

The level of UA in seminal plasma was significantly higher in males with oligoasthenospermia than in the control group by 19%, while the level of albumin in seminal plasma was significantly lower in males with oligospermia by 12% (Table 3).

The level of MDA in seminal plasma was significantly higher in males with asthenospermia than in the control group by 12%. By contrast, the level of MDA in spermatozoa lysate was significantly lower in males with oligospermia, asthenospermia, and oligoasthenospermia by 26%, 20%, and 26%, respectively (Table 4).

The level of IL-12 in seminal plasma was significantly lower in males with oligoasthenospermia than in the control group by 50%. At the same time, the level of IL-8 in seminal plasma was significantly higher in males with asthenospermia and oligoasthenospermia by 64% and 67%, respectively. Analogically, the level of MCP-1 in seminal plasma was significantly higher by 47% and 64%, respectively. The level of MIP-1β in seminal plasma was significantly higher in males with oligospermia, asthenospermia, and oligoasthenospermia than in the control group by 57%, 47%, and 49%, respectively (Table 5).

Spearman correlations showed positive correlations between the sperm cell count and motility and spermatozoa Mn-SOD activity ($R = 0.26 - 0.51$, $p < 0.05$) and spermatozoa MDA ($R = 0.23 - 0.44$, $p < 0.05$) as well as albumin concentration in seminal plasma ($R = 0.15 - 0.25$, $p < 0.05$). By contrast, the level of MDA, MCP-1, and IL-8 in seminal plasma negatively correlated with motility (R between −0.11 and −0.21, $p < 0.05$) (Table 6).

5. Discussion

The activity of the antioxidant defense system in spermatozoa is limited by the low amount of their cytoplasm [18]. Nevertheless, human seminal plasma is considered as an important source of antioxidants. SOD is believed to be the first enzymatic line of antioxidant defense [1]. SOD prevents lipid peroxidation of plasma membrane through superoxide anion utilization by converting it into hydrogen peroxide. In order to prevent the toxic action of hydrogen peroxide, SOD should be conjugated with CAT or GPx [18]. Utilization of hydrogen peroxide by GPx depletes GSH pool, a cofactor which is converted to oxidized glutathione (GSSG). The recycling of GSSG into its reduced form depends on the activity of GR which needs NADPH as a reducing cofactor. The main source of NADPH is the pentose phosphate cycle in which G6PD transforms glucose-6-phosphate into phospho-6-gluconolactone releasing NADPH [19].

It has been established that SOD plays a major role in maintaining sperm viability and its activity in spermatozoa is positively correlated with duration of sperm motility [2]. Consistently, we showed positive correlations between SOD activity in spermatozoa lysate and sperm volume, sperm cell count, rapid progressive motility after 1 hour, and motile spermatozoa after 24 hours. At the same time, the percentages of nonlinear progressive and unprogressive motile spermatozoa after 1 hour correlated negatively with SOD activity in spermatozoa lysate. We reported also lower activities of SOD in seminal plasma and spermatozoa lysate of males with oligospermia than in the controls. These results confirm the proposed protective role of SOD against oxidative stress in semen. In this context, the activity of manganese isoenzyme of SOD seems to be crucial for sperm quality maintenance because we reported lower activities of Mn-SOD in spermatozoa lysate of males with oligospermia, asthenospermia, and oligoasthenospermia than in the control group. Additively,

Table 1: Age, semen analysis in control and study groups; p value—t-test.

	Control $n = 107$		Oligospermia $n = 155$				Asthenospermia $n = 146$				Oligoasthenospermia $n = 91$			
	Mean	SD	Mean	SD	Relative change	p value	Mean	SD	Relative change	p value	Mean	SD	Relative change	p value
Age (years)	33	6	34	5	2%	0.432	34	6	3%	0.256	34	5	2%	0.403
Sperm volume (ml)	3.70	1.73	3.58	1.53	−3%	0.541	3.42	1.63	−8%	0.186	3.41	1.58	−8%	0.214
pH value	7.56	0.08	7.57	0.09	0%	0.646	7.57	0.08	0%	0.783	7.56	0.09	0%	0.915
Sperm cells count in 1 ml (mln/ml)	79.5	60.1	4.39	4.51	**−94%**	**<0.001**	25.4	42.8	**−68%**	**<0.001**	3.81	4.68	**−95%**	**<0.001**
Total sperm cells count (mln)	269	189	15.5	19.9	**−94%**	**<0.001**	73.9	122	**−73%**	**<0.001**	12.5	19.8	**−95%**	**<0.001**
Total motility after 1 hour (% motile)	58.1	9.48	32.4	20.6	**−44%**	**<0.001**	22.9	14.0	**−61%**	**<0.001**	18.3	14.1	**−69%**	**<0.001**
Rapid progressive motility (a) after 1 hour (%)	26.0	9.96	9.16	7.82	**−65%**	**<0.001**	6.75	5.97	**−74%**	**<0.001**	5.14	5.55	**−80%**	**<0.001**
Slow progressive motility (b) after 1 hour (%)	18.0	6.81	9.53	8.11	**−47%**	**<0.001**	6.76	7.13	**−62%**	**<0.001**	4.77	4.98	**−73%**	**<0.001**
Progressive motility (a + b) after 1 hour (%)	44.0	9.74	18.7	14.22	**−57%**	**<0.001**	13.5	10.66	**−69%**	**<0.001**	9.9	9.41	**−77%**	**<0.001**

$p < 0.001$.

Table 2: Antioxidant enzyme activity in seminal plasma and spermatozoa (SOD: superoxide dismutase; CAT: catalase; GR: glutathione reductase; GPx: glutathione peroxidase; GST: glutathione-S-transferase; G6PD: glucose-6-phosphate dehydrogenase; p value—t-test.

	Control		Oligospermia				Asthenospermia				Oligoasthenospermia			
	Mean	SD	Mean	SD	Relative change	p value	Mean	SD	Relative change	p value	Mean	SD	Relative change	p value
Total SOD activity (NU/ml)	183	55.5	162	55.6	**−12%**	**0.004**	169	53.3	−8%	0.062	170	50.8	−7%	0.087
Mn-SOD activity (NU/ml)	37.6	44.0	31.7	36.1	−16%	0.317	37.1	43.6	−1%	0.935	32.9	34.2	−12%	0.504
CuZn SOD activity (NU/ml)	143	49.8	129	52.2	−10%	0.063	133	52.0	−7%	0.210	138	43.6	−3%	0.555
CAT activity (U/l)	607	460	573	336	−6%	0.547	608	413	0%	0.986	579	352	−5%	0.685
GR activity (U/l)	78.8	85.7	70.0	71.2	−11%	0.378	69.0	73.3	−12%	0.341	70.3	74.9	−11%	0.474
GPx activity (U/l))	118	210	184	276	**56%**	**0.039**	187	301	58%	0.051	210	284	**78%**	**0.007**
GST activity (U/l)	3.75	2.96	3.34	2.05	−11%	0.837	3.29	2.18	−12%	0.187	3.64	2.30	−3%	0.787
G6PD activity (U/l)	64.8	53.0	63.7	45.9	−2%	0.701	55.2	44.9	−15%	0.251	58.8	46.0	−9%	0.531
Total SOD activity (NU/dl packed spermatozoa)	152	75.4	119	75.3	**−22%**	**0.045**	128	78.8	−16%	0.198	118	75.8	−22%	0.106
Mn-SOD activity (NU/dl packed spermatozoa)	135	66.7	75.3	51.5	**−44%**	**<0.001**	90.9	57.7	**−32%**	**0.007**	73.9	51.8	**−45%**	**0.001**
CuZn SOD activity (NU/dl packed spermatozoa)	33.7	19.4	53.9	42.0	**60%**	**0.019**	46.2	35.9	37%	0.095	48.6	41.6	44%	0.093

$p < 0.05$.

the activity of Mn-SOD positively correlated with sperm volume, sperm cell count, and sperm motility in the examined population. Consistently, in our previous study, we showed a negative association between SOD activities, including Mn-SOD, in spermatozoa and oxidative stress measured as a TOS level [20]. Mn-SOD is localized in the mitochondrial matrix. Mitochondria are responsible for energy production via the oxidative phosphorylation pathway and are one of the major sources of chronic ROS production under physiological conditions and compromised by severe and prolonged oxidative stress. Decreased Mn-SOD activity promotes generation of oxidants which inactivate enzymes and damage mtDNA leading to the disruption of mitochondrial integrity [21]. Ultimately, mitochondrial dysfunction may lead to ATP pool depletion and sperm motility impairment. Mitochondrial dysfunction associated with decreased oxidative metabolism may be an explanation for observed simultaneously paradoxically lower MDA level in spermatozoa

Table 3: Antioxidant reserves in seminal plasma and spermatozoa (thiol group concentration (SH concentration), total antioxidant capacity (TAC); p value—t-test.

	Control		Oligospermia				Asthenospermia				Oligoasthenospermia			
	Mean	SD	Mean	SD	Relative change	p value	Mean	SD	Relative change	p value	Mean	SD	Relative change	p value
SH concentration (μmol/l)	211	86.6	198	84.6	−6%	0.304	196	91.6	−7%	0.279	199	87.7	−6%	0.432
TAC (mmol/l)	1.33	0.24	1.31	0.30	−1%	0.785	1.34	0.28	1%	0.814	1.35	0.33	2%	0.690
Uric acid concentration (mg/dl)	4.39	1.40	4.96	2.35	13%	0.079	4.90	2.54	12%	0.142	5.20	2.89	**19%**	**0.045**
Bilirubin (mg/dl)	0.12	0.17	0.10	0.13	−15%	0.445	0.14	0.23	17%	0.567	0.12	0.16	3%	0.906
Albumin (g/ml)	0.49	0.16	0.43	0.15	**−12%**	**0.007**	0.45	0.16	−8%	0.052	0.44	0.17	−10%	0.118

$p < 0.05$.

Table 4: Parameters related to oxidative stress intensity in seminal plasma and spermatozoa (MDA: malondialdehyde; TOS: total oxidant status); p value—t-test.

	Control		Oligospermia				Asthenospermia				Oligoasthenospermia			
	Mean	SD	Mean	SD	Relative change	p value	Mean	SD	Relative change	p value	Mean	SD	Relative change	p value
MDA concentration (μmol/dl packed spermatozoa)	0.56	0.19	0.41	0.09	**−26%**	**<0.001**	0.45	0.12	**−20%**	**0.006**	0.42	0.09	**−26%**	**0.002**
MDA concentration (μmol//l)	2.41	0.98	2.63	1.18	9%	0.125	2.71	1.13	**12%**	**0.031**	2.69	1.20	11%	0.087
Lipofuscin (RF)	3.92	1.57	3.84	1.35	−2%	0.705	3.86	1.26	−1%	0.786	3.91	1.33	0%	0.971
TOS (μmol/l)	11.0	13.8	8.23	13.2	−25%	0.248	9.72	13.5	−12%	0.591	8.62	14.8	−22%	0.409

$p < 0.05$.

Table 5: Concentrations of cytokines in seminal plasma (IL-1β: interleukin 1β; IL-6: interleukin 6; IL-8: interleukin 8; IL-12 interleukin 12; MCP-1: monocyte chemoattractant protein-1; MIP-1β: macrophage inflammatory protein 1-β; TNF-α: tumor necrosis factor α; p-value—Mann–Whitney U test.

	Control		Oligospermia				Asthenospermia				Oligoasthenospermia			
	Median	IQR	Median	IQR	relative change	p value	Median	IQR	relative change	p value	Median	IQR	relative change	p value
IL-1β (pg/ml)	1.21	2.61	1.98	10.52	64%	0.164	1.66	9.90	37%	0.134	1.65	9.93	36%	0.198
IL-6 (pg/ml)	9.97	13.0	13.5	18.7	35%	0.161	15.90	16.4	59%	0.177	17.0	17.4	71%	0.064
IL-8 (pg/ml)	155	157	242	371	56%	0.092	254	437	**64%**	**0.017**	259	423	**67%**	**0.038**
IL-12 (pg/ml)	2.80	3.72	1.56	3.40	−44%	0.108	2.22	3.74	−21%	0.296	1.39	2.99	**−50%**	**0.041**
MCP-1 (pg/ml)	992	1181	1347	1411	36%	0.221	1457	1387	**47%**	**0.038**	1624	1467	**64%**	**0.041**
MIP-1β (pg/ml)	50.9	31.0	79.8	111	**57%**	**0.006**	74.9	76.7	**47%**	**0.013**	75.8	72.2	**49%**	**0.016**
TNF-α (pg/ml)	4.13	3.39	3.73	4.16	−10%	0.326	3.88	3.68	−6%	0.361	3.67	4.16	−11%	0.318

IQR: interquartile range, $p < 0.05$.

lysate of males with oligospermia, asthenospermia, and oligoasthenospermia than in the control group. The second explanation for lower MDA level in spermatozoa is its possible leakage form damaged sperm cells due to oxidative stress and peroxidation of cell membrane lipids. Additively, in males with oligospermia, lower MDA level may be also due to a higher activity of CuZn-SOD in spermatozoa lysate. This SOD isoenzyme is localized in the cytosol with a smaller fraction in the intermembrane space of mitochondria [21]. Elevation of its activity might be a result of a compensatory defense mechanism. Higher activities of GPx in seminal plasma of males with oligospermia and oligoasthenospermia than in the control group should be interpreted in the same way. At the same time, in males with asthenospermia, antioxidant defense in seminal plasma seems to be insufficient because an elevated level of MDA in that group was observed. The levels and activities of remaining parameters of oxidative stress and antioxidant enzymes did not differ between the control and examined groups.

Results of other studies on this topic are only partially in concordance with our observations. Marzec-Wróblewska et al. [2] reported lower SOD activity in males with

Table 6: Spearman correlations between semen parameters and oxidative stress and cytokines.

	Seminal plasma								Spermatozoa			
	Total SOD	Mn-SOD	GPx	MDA	Albumin	IL-8	IL-12 (p70)	MCP-1	Total SOD	Mn-SOD	CuZn-SOD	MDA
Sperm cell count in 1 ml	0.17	0.15			0.22		0.19		0.31	0.51		0.44
Total sperm cell count	0.12	0.15			0.21		0.18		0.33	0.51		0.44
Total motility after 1 hour				−0.14		−0.18		−0.21		0.26		0.23
Rapid progressive motility (a) after 1 hour								−0.24	0.25	0.47		0.36
Slow progressive motility (b) after 1 hour				−0.21	0.20		0.20	−0.18			−0.27	
Progressive motility (a + b) after 1 hour				−0.11	0.15			−0.22		0.31	−0.24	0.34
Motile spermatozoa after 24 hours			−0.18		0.29				0.30	0.44		0.26
Progressive motility after 24 hours			−0.16	−0.11	0.25					0.39		0.31

R, $p < 0.05$.

pathological spermogram than in the normozoospermic males. SOD activity was also negatively associated with semen volume and positively associated with rapid progressive motility, nonprogressive motility, and sperm concentration. Similarly, in a study of Zelen et al. [5], the activities of SOD and CAT were significantly lower in the seminal plasma of the oligozoospermic, astenozoospermic, and teratozoospermic patients compared to the fertile controls, while the level of MDA was higher in the infertile subjects. Analogical results were shown in a study of Shiva et al. [18] who reported a significant increase in the MDA levels in asthenozoospermics and teratozoospermics as compared to progressively motile and morphologically normal groups, respectively. A positive correlation between SOD activity and sperm count and total progressive motility was also found. Authors concluded that decline in SOD activity might be involved in the abnormal semen quality. On the other hand, Abdallah et al. [6] reported elevated activity of SOD in azoospermic, oligoasthenozoospermic, and asthenozoospermic males compared to normozoospermic ones postulating that SOD expression is upregulated in response to defective spermatogenesis or hormonal deficiency. In other analogous studies, unchanged, elevated, and decreased activities of SOD, CAT, and GPx were found in semen of infertile males compared to the fertile controls [6]. The discrepancies between studies may be due to the different study protocols and a result of action of many factors influencing antioxidant enzyme expression and activities. In light of this, as proposed Tavilani et al. [22], lack of protection against lipid peroxidation in semen of infertile males may be not due to the alteration in the activity of a particular antioxidant enzyme but rather due to a noncoordination between several of them. Consistently, Micheli et al. [23] suggested that the alteration of a single parameter of oxidative stress/antioxidant system does not have enough clinical value to estimate the male fertilizing potential.

The associations between fertility impairment and seminal nonenzymatic antioxidant defense seem to be as complex as those between antioxidant enzyme activities and spermogram parameters. Seminal plasma and spermatozoa contain nonenzymatic ROS scavengers, such vitamins, glutathione, uric acid, and albumin [24]. The antioxidant properties of albumin are attributed to the thiol groups of its cysteine residues. Albumin is believed also to sequester prooxidant molecules and redox-active metals [25]. Consistently, bovine serum albumin has been shown to protect membrane integrity of sperm cells from heat shock during freezing thawing of canine semen [26]. In light of this, significantly lower seminal plasma albumin level in males with oligospermia than in the controls should be interpret as attenuation of antioxidant defense. The antioxidant properties of uric acid are less unequivocal. On the one hand, uric acid acts as a scavenger of ROS being regarded as a main antioxidant in human plasma. On the other hand, uric acid may be a prooxidant under conditions of oxidative stress [27]. Lahnsteiner et al. [28] reported that uric acid is the primary antioxidant in semen of brown trout. Therefore, higher levels of uric acid in males diagnosed with oligoasthenospermia than in the controls may be interpret as an effect of compensatory defense mechanism; however, elevation of this metabolite level may be also due to increased purine degradation.

The inflammatory process within the male genitourinary tract was found to reduce fertilizing potential of mature spermatozoa. Recruitment of immune cells to the site of inflammation results in the release of reactive oxygen intermediates and proinflammatory cytokines by activated neutrophils and macrophages [29]. Consistently, we reported higher levels of IL-8, MCP-1, and MIP-1β in males with asthenospermia, oligoasthenospermia, and oligospermia than in the control group. All of these compounds play a role in chemokines [30]. On the other hand, the levels of proinflammatory cytokines were not simultaneously higher in males with abnormal spermogram. Camejo et al. [31] reported higher IL-6 concentration in seminal plasma of infertile men compared to fertile men, while the level of TNF-α did not differ between studied groups. At the same time, there

was a positive correlation between the levels of IL-6 in seminal plasma and the levels of lipid peroxidation of the sperm membranes. However, TNF-α and IL-6 concentrations did not correlate with sperm parameters, such as normal morphology, sperm concentration, and motility, in that study. Consistently, Frączek et al. [29] concluded that proinflammatory cytokines per se are unable to cause oxidative stress in semen to the level of membrane oxidative damage. The discrepancies between studies are probably due to the complex dependences between cytokines which act inhibitory or synergistic in an array [32].

6. Conclusions

Abnormalities in spermogram, such as oligospermia, asthenospermia, and oligoasthenospermia, may be related to decreased activity of Mn-SOD in spermatozoa and increased levels of chemokines in seminal plasma.

Data Availability

The data used to support the findings of this study are available from the corresponding author upon request.

Conflicts of Interest

The authors have no conflicts of interest to declare.

Acknowledgments

This work was supported by the Medical University of Silesia (KNW-1-103/N/7/O). The data used to support the findings of this study are available from the corresponding author upon request.

References

[1] F. Atig, M. Raffa, H. B. Ali, K. Abdelhamid, A. Saad, and M. Ajina, "Altered antioxidant status and increased lipid per-oxidation in seminal plasma of tunisian infertile men," *International Journal of Biological Sciences*, vol. 8, no. 1, pp. 139–149, 2012.

[2] U. Marzec-Wróblewska, P. Kamiński, P. Łakota et al., "Zinc and iron concentration and SOD activity in human semen and seminal plasma," *Biological Trace Element Research*, vol. 143, no. 1, pp. 167–177, 2011.

[3] S. A. Sheweita, A. M. Tilmisany, and H. Al-Sawaf, "Mechanisms of male infertility: role of antioxidants," *Current Drug Metabolism*, vol. 6, no. 5, pp. 495–501, 2005.

[4] A. Agarwal, G. Virk, C. Ong, and S. S. du Plessis, "Effect of oxidative stress on male reproduction," *World Journal Mens Health*, vol. 32, no. 1, pp. 1–17, 2014.

[5] I. Zelen, M. Mitrović, A. Jurisic-Skevin, and S. Arsenijević, "Activity of superoxide dismutase and catalase and content of malondialdehyde in seminal plasma of infertile patients," *Medicinski Pregled*, vol. 63, no. 9-10, pp. 624–629, 2010.

[6] F. Ben Abdallah, I. Dammak, H. Attia, B. Hentati, and L. Ammar-Keskes, "Lipid peroxidation and antioxidant enzyme activities in infertile men: correlation with semen parameter," *Journal of Clinical Laboratory Analysis*, vol. 23, no. 2, pp. 99–104, 2009.

[7] WHO, *The Laboratory Manual for the Examination of Human Semen*, Cambridge University Press, 5 edition, 2010.

[8] Y. Oyanagui, "Reevaluation of assay methods and establishment of kit for superoxide dismutase activity," *Analytical Biochemistry*, vol. 142, no. 2, pp. 290–296, 1984.

[9] D. E. Paglia and W. N. Valentine, "Studies on the quantitative and qualitative characterization of erythrocyte glutathione peroxidase," *The Journal of Laboratory and Clinical Medicine*, vol. 70, no. 1, pp. 158–169, 1967.

[10] W. H. Habig and W. B. Jakoby, "Assays for differentiation of glutathione S-Transferases," *Methods in Enzymology*, vol. 77, pp. 398–405, 1981.

[11] R. Richterich, *Chemia kliniczna*, PZWL, Warszawa, 1971.

[12] L. H. Johansson and L. A. Håkan Borg, "A spectrophotometric method for determination of catalase activity in small tissue samples," *Analytical Biochemistry*, vol. 74, no. 1, pp. 331–336, 1988.

[13] O. Erel, "A novel automated direct measurement method for total antioxidant capacity using a new generation, more stable ABTS radical cation," *Clinical Biochemistry*, vol. 37, no. 4, pp. 277–285, 2004.

[14] J. F. Koster, P. Biemond, and A. J. Swaak, "Intracellular and extracellular sulphydryl levels in rheumatoid arthritis," *Annals of the Rheumatic Diseases*, vol. 45, no. 1, pp. 44–46, 1986.

[15] H. Ohkawa, N. Ohishi, and K. Yagi, "Assay for lipid peroxides in animal tissues by thiobarbituric acid reaction," *Analytical Biochemistry*, vol. 95, no. 2, pp. 351–358, 1979.

[16] S. K. Jain, "In vivo externalization of phosphatidylserine and phosphatidylethanolamine in the membrane bilayer and hypercoagulability by the lipid peroxidation of erythrocytes in rats," *The Journal of Clinical Investigation*, vol. 76, no. 1, pp. 281–286, 1985.

[17] O. Erel, "A new automated colorimetric method for measuring total oxidant status," *Clinical Biochemistry*, vol. 38, no. 12, pp. 1103–1111, 2005.

[18] M. Shiva, A. K. Gautam, Y. Verma, V. Shivgotra, H. Doshi, and S. Kumar, "Association between sperm quality, oxidative stress, and seminal antioxidant activity," *Clinical Biochemistry*, vol. 44, no. 4, pp. 319–324, 2011.

[19] J. F. Griveau, E. Dumont, P. Renard, J. P. Callegari, and D. Le Lannou, "Reactive oxygen species, lipid peroxidation and enzymatic defence systems in human spermatozoa," *Journal of Reproduction and Fertility*, vol. 103, no. 1, pp. 17–26, 1995.

[20] M. Dobrakowski, S. Kasperczyk, S. Horak, D. Chyra-Jach, E. Birkner, and A. Kasperczyk, "Oxidative stress and motility impairment in the semen of fertile males," *Andrologia*, vol. 49, no. 10, 2017.

[21] T. Fukai and M. Ushio-Fukai, "Superoxide dismutases: role in redox signaling, vascular function, and diseases," *Antioxidants & Redox Signaling*, vol. 15, no. 6, pp. 1583–1606, 2011.

[22] H. Tavilani, M. T. Goodarzi, A. Vaisi-raygani, S. Salimi, and T. Hassanzadeh, "Activity of antioxidant enzymes in seminal plasma and their relationship with lipid peroxidation of spermatozoa," *International Braz J Urol*, vol. 34, no. 4, pp. 485–491, 2008.

[23] L. Micheli, D. Cerretani, G. Collodel et al., "Evaluation of enzymatic and non-enzymatic antioxidants in seminal plasma of men with genitourinary infections, varicocele and idiopathic infertility," *Andrology*, vol. 4, no. 3, pp. 456–464, 2016.

[24] E. de Lamirande, H. Jiang, A. Zini, H. Kodama, and C. Gagnon, "Reactive oxygen species and sperm physiology," *Reviews of Reproduction*, vol. 2, no. 1, pp. 48–54, 1997.

[25] M. Dobrakowski, J. Zalejska-Fiolka, T. Wielkoszyński, E. Świętochowska, and S. Kasperczyk, "The effect of occupational exposure to lead on the non-enzymatic antioxidant system," *Medycyna Pracy*, vol. 65, no. 4, pp. 443–451, 2014.

[26] O. Uysal and M. N. Bucak, "Effects of oxidized glutathione, bovine serum albumin, cysteine and lycopene on the quality of frozen-thawed ram semen," *Acta Veterinaria Brno*, vol. 76, no. 3, pp. 383–390, 2007.

[27] C. Gersch, S. P. Palii, K. M. Kim, A. Angerhofer, R. J. Johnson, and G. N. Henderson, "Inactivation of nitric oxide by uric acid," *Nucleosides, Nucleotides & Nucleic Acids*, vol. 27, no. 8, pp. 967–978, 2008.

[28] F. Lahnsteiner, N. Mansour, and K. Plaetzer, "Antioxidant systems of brown trout (Salmo trutta f. fario) semen," *Animal Reproduction Science*, vol. 119, no. 3-4, pp. 314–321, 2010.

[29] M. Frączek, D. Sanocka, M. Kamieniczna, and M. Kurpisz, "Proinflammatory cytokines as an intermediate factor enhancing lipid sperm membrane peroxidation in in vitro conditions," *Journal of Andrology*, vol. 29, no. 1, pp. 85–92, 2008.

[30] J. A. Politch, L. Tucker, F. P. Bowman, and D. J. Anderson, "Concentrations and significance of cytokines and other immunologic factors in semen of healthy fertile men," *Human Reproduction*, vol. 22, no. 11, pp. 2928–2935, 2007.

[31] M. I. Camejo, L. Abdala, G. Vivas-Acevedo, R. Lozano-Hernández, M. Angeli-Greaves, and E. D. Greaves, "Selenium, copper and zinc in seminal plasma of men with varicocele, relationship with seminal parameters," *Biological Trace Element Research*, vol. 143, no. 3, pp. 1247–1254, 2011.

[32] P. Martínez, F. Proverbio, and M. I. Camejo, "Sperm lipid peroxidation and pro-inflammatory cytokines," *Asian Journal of Andrology*, vol. 9, no. 1, pp. 102–107, 2007.

Hindawi
Oxidative Medicine and Cellular Longevity
Volume 2018, Article ID 3795070, 12 pages
https://doi.org/10.1155/2018/3795070

Research Article

Antioxidant Status in the Soleus Muscle of Sprague-Dawley Rats in Relation to Duodenal-Jejunal Omega Switch and Different Dietary Patterns

Bronisława Skrzep-Poloczek,[1] **Dominika Stygar**,[1] **Elżbieta Chełmecka**,[2] **Katarzyna Nabrdalik**,[3] **Ewa Romuk**,[4] **Jakub Poloczek**,[5] **Tomasz Sawczyn**,[1] **Konrad W. Karcz**,[6] **and Janusz Gumprecht**[3]

[1]*Department of Physiology, School of Medicine with the Division of Dentristy in Zabrze, Medical University of Silesia, Katowice, Poland*
[2]*Department of Statistics, Department of Instrumental Analysis, School of Pharmacy with the Division of Laboratory Medicine in Sosnowiec, Medical University of Silesia, Katowice, Poland*
[3]*Department of Internal Medicine, Diabetology and Nephrology in Zabrze, Medical University of Silesia, Katowice, Poland*
[4]*Department of Biochemistry, School of Medicine with the Division of Dentistry in Zabrze, Medical University of Silesia, Katowice, Poland*
[5]*Department of Rehabilitation, 3rd Specialist Hospital in Rybnik, Rybnik, Poland*
[6]*Clinic of General, Visceral, Transplantation and Vascular Surgery, Hospital of the Ludwig Maximilian University, Munich, Germany*

Correspondence should be addressed to Dominika Stygar; dstygar@gmail.com

Received 24 February 2018; Accepted 5 June 2018; Published 8 July 2018

Academic Editor: Jolanta Czuczejko

Background. Obesity and chronic ingestion of lipid-rich meals are related to an enhanced oxidative stress (OS). *Aims.* To examine the influence of duodenal-jejunal omega switch surgery in combination with different diets on the antioxidative status in the soleus muscle of rats. *Methods.* After 8 weeks on a high-fat diet (HF) or control diet (CD), rats underwent duodenal-jejunal omega switch (DJOS) or SHAM (control) surgery. After surgery, for the next 8 weeks, half of DJOS/SHAM animals were kept on the same diet as before, and half had a changed diet. The total superoxide dismutase (SOD), catalase (CAT), glutathione peroxidase (GPx), glutathione-S-transferase (GST), and glutathione reductase (GR) activity as well as malondialdehyde (MDA) concentration were measured in the soleus of rats. *Results.* CAT and GPx activity were significantly lower after DJOS surgery versus SHAM, regardless of the type of diet. The activity of CAT, SOD, GR, CuZnSOD, and GPx was altered in the CD/HF or HF/CD groups. After DJOS, the lowest muscle concentration of MDA was observed in the CD/CD group and the highest in CD/HF. *Conclusions.* DJOS surgery significantly decreases the antioxidative system in soleus muscles of rats. CD/HF and HF/CD dietary patterns lead to an increase in antioxidative activity, while remaining on unchanged diet (CD or HF) is associated with a reduced oxidative stress.

1. Introduction

Obesity and comorbidities related to it pose a major challenge to public health systems and affected individuals worldwide. Even though there are many treatment methods available, the one that leads to sustained and clinically relevant body weight loss is bariatric surgery [1, 2]. What is even more important is that it is also currently the only obesity treatment modality with a proven mortality benefit [1]. Surgical treatment of obesity became a metabolic surgery because it not only leads to a reduction in body weight but also influences different metabolic pathways, with incretin hormones and diabetes type 2 resolution being two of the most studied areas up to date [3]. However, one must

remember that obesity as well as chronic ingestion of lipid-rich meals are related also to an enhanced oxidative stress which in turn causes many unfavourable health consequences [4–7]. Oxidative stress (OS) is just a general term for the cellular damage being caused by an imbalance between prooxidants such as reactive oxygen species (ROS) and antioxidants in favour of the first one mentioned [8]. ROS are necessary for many physiological functions; however, to maintain a physiologically beneficial level of ROS antioxidants, which are enzymatic and nonenzymatic molecules, is crucial [9]. Markers indicative of oxidative stress include elevated measures of reactive oxygen species (ROS) and diminished antioxidant defence, associated with lower antioxidant enzyme levels [4, 5]. OS is also related to direct damage to lipids, with the production of end products of lipid peroxidation with malondialdehyde (MDA) being the most mutagenic one [10]. One of many organs that can be affected by OS associated with obesogenic conditions like obesity itself and high-fat diet (HFD) is the skeletal muscle. The high abundance of fat exceeds the ability of the muscle to oxidize this substrate, which leads to intramyocellular deposition and intermission of normal muscle function, with lipotoxicity as a consequence [11]. Scientists are trying to understand the influence of various aspects related to different treatment methods like diets or metabolic surgery procedures on humans using animal models. Regarding HFD diet, bariatric surgery, and OS, there have been only single studies related to models of oxidative stress markers performed; however, neither one took into consideration all three mentioned aspects in one experiment. In relation to HF diet, Auberval et al. proved the increase of tissue but not plasma oxidative stress among the studied animals [12] and Pinho et al. revealed that HFD induces skeletal muscle OS in rats [13]. Similarly, bariatric surgery procedures have been linked to a reduction in oxidative stress in rats [14]. DJOS is a relatively new technique; thus, an animal model, for exploring the long-term physiological effects and pathophysiological outcomes of this procedure, is still needed [15, 16]. DJOS is a type of bypass-like procedure, with proximal loop duodenoenterostomy, where the pylorus of the patients is saved. This type of surgery allows for direct hindgut stimulation [17, 18]. The biochemical mechanisms responsible for the pathophysiological traits of obesity, insulin resistance, and type 2 diabetes mellitus are incompletely understood. In the presented study, we aimed to assess the influence of duodenal-jejunal omega switch (DJOS) surgery in combination with different types of diet on antioxidant status in the soleus skeletal muscles of rats, which to our best knowledge have not been studied up to date, neither in humans nor in animals.

2. Materials and Methods

2.1. Animals and Diets. The study was performed in accordance with the Guide for the Care and Use of Laboratory Animals. Male Sprague-Dawley rats (Charles River Breeding Laboratories, Wilmington, Mass) aged 7 weeks, 200 ± 7 g, were housed in a 12 h light-dark cycle, 22°C, and 40–60% humidity. All rats had free access to water and rat food (Provimi Kliba AG, Kaiseraugst, Switzerland). The control group was maintained on ssniff® EF R/M. Obesity was induced by placing the animals on a high-fat diet (HF; 23.0 kJ/g, 59% fat, 27% carbohydrate, and 14% protein (EF RAT/E15744/ssniff Spezialdiäten GmbH) for an average of two months. Animals maintained on the HF diet were pair-fed (kcal) with the animals exposed to an ad libitum control diet. The energy content of the high-fat and standard diets were 5.04 and 3.59 kcal/g (20.1 and 15.0 kJ/g), respectively.

2.2. Experimental Design. This individual study is based on an experimental design applied and described in an earlier work by Stygar et al. [19]. After one week of acclimatisation, the animals were assigned to the CD ($n = 28$) and HF groups ($n = 28$). After 8 weeks, both groups underwent the two different types of surgery SHAM, which is a control type of surgery ($n = 14$), and DJOS ($n = 14$), presented in Figure 1(a). After the surgery, the two groups of animals fed previously with CD or HF diets were divided further into 8 groups, depending on the postoperation diet regimen. In each surgery group, that is, SHAM and DJOS, 7 animals were kept on the same diet as before the surgery, and another 7 had the diet changed (Figure 1(a)). A number of rats were kept as small as possible in consideration of the "3Rs" for the humane treatment of animals [20]. All 7 rats survived in 7 out of 8 experimental groups. In HF/SHAM/CD, 6 out of 7 rats survived the experiment.

A DJOS and SHAM surgery was performed according to Karcz et al.'s methodology [16], described in the aforementioned study [19]. To perform DJOS surgery, the animals were anaesthetised with 2% isoflurane (AbbVie Deutschland GmbH & Co. KG, Ludwigshafen, Germany) and oxygen flow at 2 l/min under spontaneous breathing. Analgesia with xylazine (5 mg/kg, ip; Xylapan, Vetoquinol Biovet, Poland) and antibiotic prophylaxis with gentamicin were applied. The gastric volume was left intact, whereas the entire duodenum and the proximal jejunum were bypassed. The stomach was separated from the duodenum below the pylorus. The distal part of the transected duodenum was closed using Prolene 6/0 (Ethicon). The position of the duodenoenterostomy was determined to be at the aboral of the Treitz ligament, located approximately at one-third of the total small bowel length for DJOS. The duodenojejunostomy was performed as a simple antecolic, continuous end-to-side, hand-sewn, extramucosal anastomosis using 6-0 sutures. Postoperative analgesia was performed using carprofen (4 mg/kg, sc; Rimadyl, Pfizer, Switzerland) for 3 consecutive days after the surgery.

For the type of control operation called SHAM, transections and reanastomosis of the gastrointestinal tract were performed at the corresponding sites where enterotomies were performed for the duodenojejunostomy, thereby maintaining the physiological conduit of food passage through the bowel (Figures 1(b) and 1(c)).

2.3. Tissue Collection. After 16 weeks of the experiment and 8 weeks after the surgery, the tissue of the soleus muscle was harvested and the animals were euthanized. 100 mg of muscle tissue was homogenized in 1 ml of a homogenising buffer. All samples were snap frozen in liquid nitrogen and stored at −80°C until further analysis. All experimental procedures

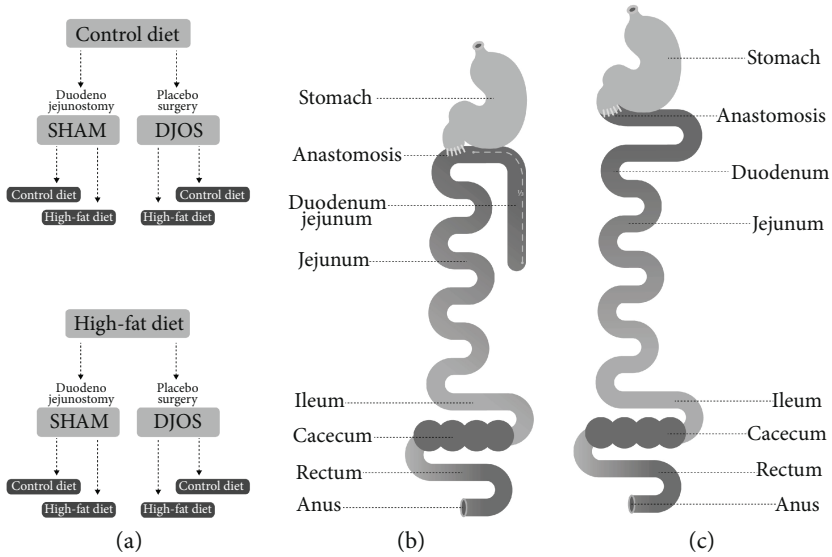

Figure 1: (a) Schematic illustration of DJOS and (b) SHAM surgery, respectively, and (c) scheme of experimental groups.

were approved by the Ethical Committee for Animal Experimentation of the Medical University of Silesia (58/2014). All applicable institutional and/or national guidelines for the care and use of animals were followed (Directive 2010/63/EU).

2.4. Oxidative Stress Marker Analysis

2.4.1. Oxidative Enzyme Analysis. 8 weeks after DJOS and SHAM surgery, an antioxidant system was analysed determining the activity of the following antioxidant enzymes in soleus muscle homogenates: glutathione reductase (glutathione-disulfide reductase, GR, and GSR), catalase (CAT), glutathione peroxidase (GPx), glutathione-S-transferase (GST), and total superoxide dismutase activity (SOD) and the nonenzymatic antioxidant system—lipid peroxidation by determining the malondialdehyde concentration.

2.4.2. Glutathione Reductase Activity (EC 1.8.1.7). GR enzymatic activity in the muscle homogenates was evaluated by a decrease in the concentration of NADPH in the samples using GR buffer (200 mM sodium phosphate pH 7.5, 6.3 mm EDTA), and kinetic reading was performed at a wavelength of 340 nm for 10 minutes [21].

2.4.3. Catalase Activity (EC 1.11.1.6). The catalase activity in muscle homogenates was measured using Aebi's methods. Briefly, 50 mM TRIS/HCl buffer, pH 7.4, and perhydrol were mixed with 50 μl of homogenate. After 10 seconds, the absorbance was read at $\lambda = 240$ nm, every 30 seconds for 2 minutes. Enzymatic activity was expressed in IU/mg protein [22].

2.4.4. Glutathione Peroxidase Activity (EC 1.11.1.9). To measure the activity of glutathione peroxidase, the muscle homogenates were incubated with a GPx buffer (100 mM potassium phosphate with 1 mM EDTA pH 7.7), 40 mM sodium azide, GSH (diluted in 5% metaphosphoric acid), GR (GPx diluted in the buffer), NADPH (diluted with sodium bicarbonate 5%), and 0.5 mM tert-butyl. The decay of NADPH concentration was evaluated for 10 minutes in a spectrophotometer, at 340 nm [23].

2.4.5. Glutathione-S-transferase Activity (EC 2.5.1.18). Transferase activity of glutathione-S-transferase in muscle homogenates was estimated by the kinetic method, previously described by Habig and Jakoby [24]. 1-Chloro-2,3-dinitrobenzene was used as a substrate, and results are expressed in IU/g protein.

2.4.6. Superoxide Dismutase Analysis (EC 1.15.1.1). SOD isoenzyme activity was determined with the use of the spectrophotometric method by Oyanagui [25]. KCN was used as the inhibitor of the CuZnSOD isoenzyme. CuZnSOD activity was calculated as the difference between total SOD activity and MnSOD activity. SOD activity was calculated against a blank probe (containing bidistilled water). Enzyme activity was expressed as nitrite units (NU) per mg of protein in tissue. One NU exhibits 50% inhibition of formation of nitrite ion under the method's condition [25].

2.4.7. Lipid Peroxidation. Malondialdehyde (MDA) concentration was measured in samples of muscle homogenates based on Ohkawa et al.'s method, using the reaction with thiobarbituric acid, with spectrophotometric detection employing 515 nm excitation and 552 nm emission wavelengths. MDA concentration was calculated from the standard curve, prepared from 1,1,3,3-tetraethoxypropane [26].

2.4.8. Protein Concentration. Protein concentration was determined by Lowry methods using bovine serum albumin as the standard [27].

3. Statistical Analysis

Statistical analysis was performed using STATISTICA 12.5 PL (StatSoft, Cracow, Poland). Statistical significance was set at a p value below 0.05. All tests were two-tailed. Interval data were expressed as mean value ± standard deviation in

the case of a normal distribution or as median/lower–upper quartile range in the case of data with skewed or nonnormal distribution. Distribution of variables was evaluated by the Shapiro-Wilk test and the quantile-quantile plot; homogeneity of variances was assessed by the Levene test. For comparison of data, the two-way parametric ANOVA with post hoc contrast analysis or nonparametric Kruskal-Wallis test or Mann–Whitney U test were used. In case of skewed data distribution, logarithmic transformation was done before analysis.

4. Results

The results of body weight change after DJOS and SHAM surgery in all experimental groups were previously presented by Stygar et al. [19]. The values of antioxidative systems for DJOS- and SHAM-operated groups are presented in Table 1. Table 2 presents results of multiple comparisons in contrast analysis of DJOS- and SHAM-operated groups in relation to diet used before and after surgery. Column one presents a comparison between DJOS and SHAM surgery associated with different diets, column two shows comparisons between dietary groups of DJOS-operated animals, and column three shows comparisons between dietary groups of SHAM-operated animals.

4.1. Oxidative Enzyme Systems

4.1.1. Glutathione Reductase. GR muscle's activity in DJOS-operated animals compared to SHAM-operated ones was significantly different among HF/HF, HF/CD, and CD/CD diet groups (Figure 2(a), Tables 1 and 2). In the DJOS surgery group, GR muscle's activity in the HF/HF group was significantly lower when compared to the SHAM-operated HF/HF diet group. Oppositely, in the DJOS surgery group, GR muscle's activity in the HF/CD and CD/CD diet groups were significantly higher when compared to the SHAM-operated HF/CD and CD/CD diet groups of animals. There was no difference among the CD/HF diet group of DJOS- and SHAM-operated animals in relation to GR muscle's activity.

Taking into consideration DJOS surgery, there was a significant difference in terms of GR muscle's activity in the studied diet groups, namely, HF/HF and HF/CD, HF/HF and CD/HF, HF/HF and CD/CD, HF/CD and CD/HF, HF/CD and CD/CD, and CD/HF and CD/CD (Figure 2(a), Tables 1 and 2). The lowest GR muscle's activity was observed among the HF/HF diet group and the highest among the CD/CD group (Figure 2(a), Tables 1 and 2).

There were no significant differences in terms of GR muscle's activity in the studied diet groups in SHAM-operated animals.

4.1.2. Catalase. CAT muscle's activity in DJOS-operated animals compared to SHAM-operated ones was significantly different among the HF/HF, HF/CD, CD/HF, and CD/CD diet groups (Figure 2(b), Tables 1 and 2). In the DJOS group, CAT activity was significantly lower in HF/HF, HF/CD, and CD/HF when compared to the HF/HF, HF/CD, and CD/HF diet groups of SHAM-operated animals. Oppositely, in the DJOS group, CAT activity was significantly higher in the CD/CD diet group when compared to the SHAM CD/CD diet group (Figure 2(b); Tables 1 and 2).

For the DJOS surgery, a significant difference in terms of CAT activity among the studied diet groups, namely, HF/HF and CD/HF, HF/CD and CD/HF, and CD/HF and CD/CD, was observed. The lowest CAT muscle activity was observed in the HF/HF diet group and the highest among the CD/HF diet group (Figure 2(b); Tables 1 and 2).

There was a significant difference in terms of CAT activity among the SHAM-operated studied diet groups, namely, HF/HF and CD/HF, HF/HF and CD/CD, HF/CD and CD/HF, and CD/HF and CD/CD (Figure 2(b); Tables 1 and 2), with the lowest value observed among the CD/CD group and the highest value among the CD/HF studied group (Figure 2(b); Tables 1 and 2).

4.1.3. Glutathione Peroxidase Activity. GPx muscle's activity in DJOS-operated animals compared to SHAM-operated ones was significantly lowered among all analysed diet groups, namely, HF/HF, HF/CD, CD/HF, and CD/CD (Figure 2(c), Tables 1 and 2).

In DJOS-operated animals, there were significant differences in terms of GPx muscle's activity between each of the four diet groups, namely, HF/HF and HF/CD, HF/HF and CD/HF, HF/HF and CD/CD, HF/CD and CD/HF, HF/CD and CD/CD, and CD/HF and CD/CD, with the lowest value observed in the CD/CD group and the highest value in the CD/HF diet group (Figure 2(c), Tables 1 and 2).

In SHAM-operated animals, there were significant differences in terms of GPx muscle's activity between three out of four diet groups, namely, HF/HF and CD/HF, HF/HF and CD/CD, HF/CD and CD/CD, and CD/HF and CD/CD, with the lowest value observed among the CD/CD diet group and the highest one among the CD/HF diet group (Figure2(c); Tables 1 and 2).

4.1.4. Glutathione-S-transferase Activity. GST muscle's activity in DJOS-operated animals compared to SHAM-operated ones was significantly lowered in HF/HF and CD/CD diet groups (Figure 2(d), Tables 1 and 2).

After DJOS surgery, there were significant differences in terms of GST muscle's activity between studied diet groups, namely, the HF/HF and CD/HF, HF/HF and CD/CD, HF/CD and CD/CD, and CD/HF and CD/CD diet study groups, with the lowest value observed among the CD/CD diet group and the highest ones among the CD/HF diet group (Figure 2(d), Tables 1 and 2).

There were no significant differences in terms of GST muscle's activity among any diet groups in SHAM-operated rats (Figure 2(d), Tables 1 and 2).

4.1.5. Total Superoxide Dismutase Activity. SOD muscle's activity in DJOS-operated animals compared to SHAM-operated ones was significantly lowered in the HF/CD and CD/HF study diet groups (Figure 3(a), Tables 1 and 2).

After DJOS surgery, there were significant differences in terms of SOD muscle's activity between the studied diet groups, namely, HF/HF and CD/HF, HF/HF and CD/CD, HF/CD and CD/HF, and CD/HF and CD/CD, with the

Table 1: Antioxidant activity and concentration levels in soleus muscle 8 weeks after DJOS (1st column) and SHAM (2nd column) surgery, subjected to 16 weeks of different dietary patterns, and intergroup comparison between DJOS and SHAM study groups (3rd column) using descriptive statistics and results of two-way analysis of variance. Statistical significance was set at $p < 0.05$.

	DJOS				SHAM				*p* ANOVA		
Parameter	HF/HF	HF/CD	CD/HF	CD/CD	HF/HF	HF/CD	CD/HF	CD/CD	Group	Op.	Int.
GR (IU/g)	3.61 ± 0.80	14.32 ± 2.94	7.72 ± 1.18	29.90 ± 8.98	9.96 ± 0.81	9.95 ± 0.93	6.57 ± 1.28	8.05 ± 2.63	<0.001	<0.001	<0.001
CAT (IU/g)	31.95 ± 4.57	34.65 ± 3.15	47.31 ± 3.45	39.28 ± 6.63	56.38 ± 13.99	58.93 ± 3.68	63.91 ± 2.19	29.00 ± 3.33	<0.001	<0.001	<0.001
GPX (IU/g)	2.37 ± 0.64	3.27 ± 0.87	4.44 ± 1.27	1.34 ± 0.14	3.26 ± 0.78	5.14 ± 1.02	8.84 ± 0.42	4.43 ± 0.25	<0.001	<0.001	<0.001
GST (IU/g)	1.12 ± 0.08	1.42 ± 0.26	1.47 ± 0.34	0.78 ± 0.09	1.57 ± 0.34	1.38 ± 0.32	1.49 ± 0.34	1.30 ± 0.11	<0.01	<0.01	<0.05
Total SOD (NU/mg)	85.59 ± 2.90	80.72 ± 6.0	105.64 ± 17.55	74.33 ± 1.69	93.16 ± 7.01	93.87 ± 3.24	91.53 ± 4.40	75.55 ± 1.27	<0.001	0.359	<0.001
MnSOD (NU/mg)	24.50 ± 4.05	36.00 ± 3.02	37.67 ± 11.22	27.59 ± 3.36	30.25 ± 2.93	40.93 ± 8.56	38.72 ± 8.33	39.44 ± 5.17	<0.001	<0.01	0.246
CuZnSOD (NU/mg)	55.49 ± 3.42	48.73 ± 1.63	43.30 ± 2.04	35.00 ± 2.92	72.19 ± 8.47	39.97 ± 4.56	53.93 ± 5.64	42.44 ± 5.61	<0.001	<0.001	<0.001
MDA (μmol/g)	4.56 ± 0.24	5.49 ± 1.34	5.57 ± 0.24	3.41 ± 0.30	4.76 ± 0.57	6.82 ± 0.67	5.92 ± 0.36	4.45 ± 0.30	<0.001	<0.001	0.083

GR: glutathione reductase; CAT: catalase; GPX: glutathione peroxidase; SOD: total superoxide dismutase; GST: glutathione-S-transferase; MnSOD: Mn superoxide dismutase; ZnSOD: Zn superoxide dismutase; MDA: malondialdehyde; DJOS: duodenal-jejunal omega switch surgery; HF: high-fat diet; CD: control diet; HF/HF, CD/HF, HF/CD, CD/CD: type of diet 8 weeks before/8 weeks after surgery; Op.: operation type; Int.: interaction between group and operation type. Mean ± standard deviation or median (lower – upper quartile).

Table 2: Multiple comparisons in contrast analysis. Column 1: Inter-group comparisons between HF/HF, CD/HF, HF/CD, CD/CD groups DJOS versus SHAM; Column 2: Intragroup comparisons between HF/HF, CD/HF, HF/CD, CD/CD groups after DJOS surgery; Column 3: Intragroup comparisons between HF/HF, CD/HF, HF/CD, CD/CD groups after SHAM surgery. Post hoc analysis, statistical significance was set at a $p < 0.05$.

Post hoc	DJOS versus SHAM					DJOS					SHAM					
	1: HF/HF	2: HF/CD	3: CD/HF	4: CD/CD	1 versus 2	1 versus 3	1 versus 4	2 versus 3	2 versus 4	3 versus 4	1 versus 2	1 versus 3	1 versus 4	2 versus 3	2 versus 4	3 versus 4
GR (IU/g)	<0.01	<0.05	0.573	<0.001	<0.001	<0.05	<0.001	<0.01	<0.001	<0.001	0.993	0.090	0.333	0.104	0.355	0.472
CAT (IU/g)	<0.001	<0.001	<0.001	<0.01	0.479	<0.001	0.059	<0.01	0.227	<0.05	0.488	<0.05	<0.001	0.195	<0.001	<0.001
GPX (IU/g)	<0.05	<0.001	<0.001	<0.01	<0.05	<0.001	<0.05	<0.05	<0.001	<0.001	<0.001	<0.001	<0.01	<0.001	0.118	<0.001
GST (IU/g)	<0.01	0.799	0.909	<0.01	0.068	<0.05	<0.05	0.721	<0.001	<0.001	0.145	0.559	0.070	0.469	0.622	0.227
Total SOD (NU/mg)	0.072	<0.01	<0.01	0.776	0.259	<0.001	<0.05	<0.001	0.141	<0.001	0.862	0.694	<0.001	0.585	<0.001	<0.001
MnSOD (NU/mg)	0.118	0.193	0.780	<0.01	<0.01	<0.01	0.413	0.656	<0.05	<0.01	<0.01	<0.05	<0.05	0.557	0.692	0.848
CuZnSOD (NU/mg)	<0.001	<0.01	<0.001	<0.05	<0.05	<0.001	<0.001	0.062	<0.001	<0.01	<0.001	<0.001	<0.001	<0.001	0.389	<0.001
MDA (μmol/g)	0.559	<0.001	0.329	<0.01	<0.05	<0.01	<0.01	0.821	<0.001	<0.001	<0.001	<0.01	0.372	<0.05	<0.001	<0.001

GR: glutathione reductase; CAT: catalase; GPX: glutathione peroxidase; SOD: total superoxide dismutase; GST: glutathione-S-transferase; MnSOD: Mn superoxide dismutase; ZnSOD: Zn superoxide dismutase; MDA: malondialdehyde; DJOS: duodenal-jejunal omega switch surgery; HF: high-fat diet; CD: control diet; HF/HF, CD/HF, HF/CD, CD/CD: type of diet 8 weeks before/8 weeks after surgery.

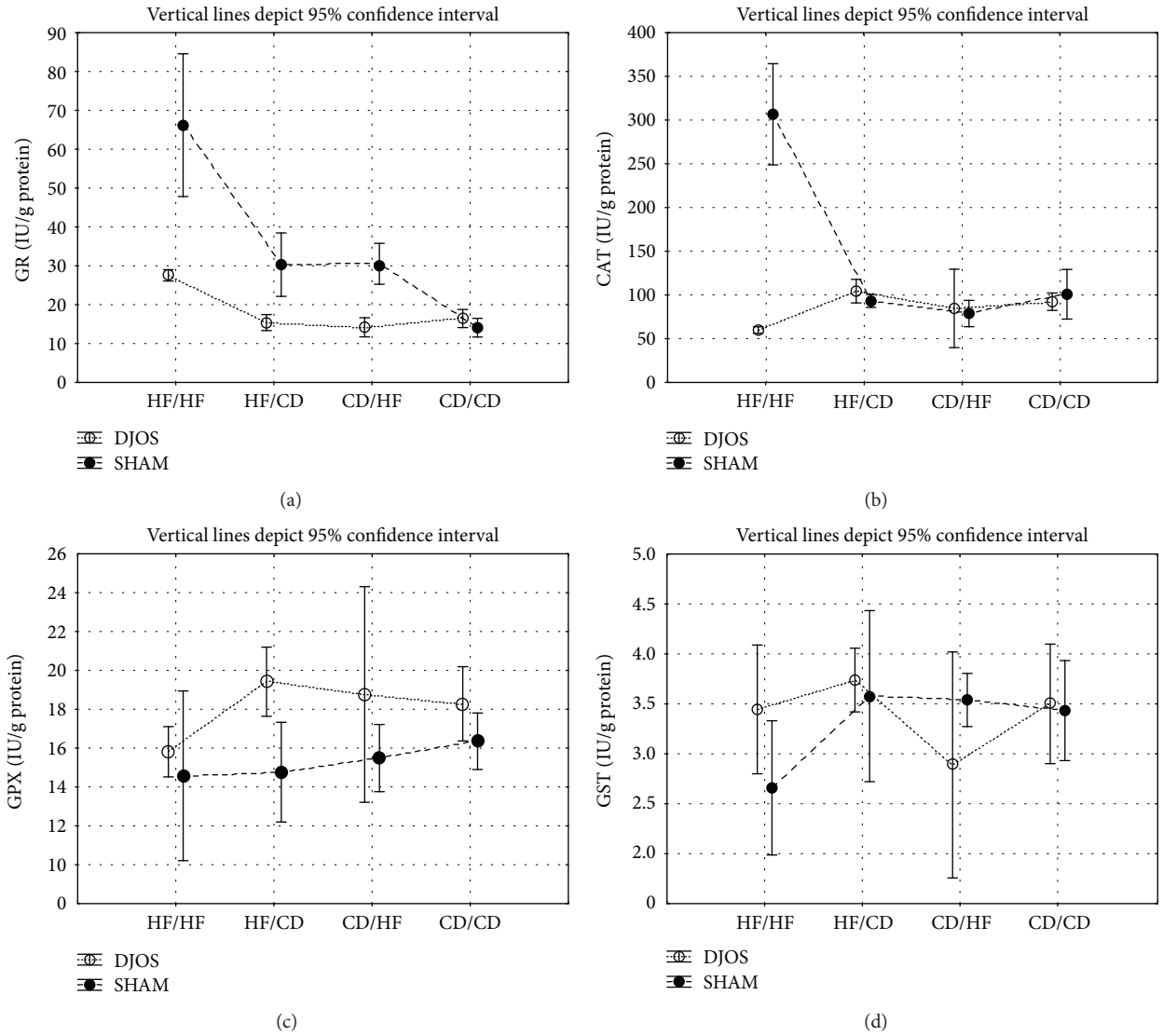

Figure 2: (a) Mean values of GR (IU/g) activity in four groups subjected to different dietary patterns, according to the DJOS and SHAM operation type. Statistical significance was set at $p < 0.05$. Vertical lines depict 95% confidence interval. DJOS: duodenal-jejunal omega switch surgery; HF: high-fat diet; CD: control diet; HF/HF, CD/HF, HF/CD, CD/CD: type of diet 8 weeks before/8 weeks after surgery. (b) Mean values of CAT (IU/g) activity in four groups subjected to different dietary patterns, according to the DJOS and SHAM operation type. Statistical significance was set at $p < 0.05$. Vertical lines depict 95% confidence interval. DJOS: duodenal-jejunal omega switch surgery; HF: high-fat diet; CD: control diet; HF/HF, CD/HF, HF/CD, CD/CD: type of diet 8 weeks before/8 weeks after surgery. (c) Mean values of GPX (IU/g) activity in four groups subjected to different dietary patterns, according to the DJOS and SHAM operation type. Statistical significance was set at $p < 0.05$. Vertical lines depict 95% confidence interval. DJOS: duodenal-jejunal omega switch surgery; HF: high-fat diet; CD: control diet; HF/HF, CD/HF, HF/CD, CD/CD: type of diet 8 weeks before/8 weeks after surgery. (d) Mean values of GST (IU/g) activity in four groups subjected to different dietary patterns, according to the DJOS and SHAM operation type. Statistical significance was set at $p < 0.05$. Vertical lines depict 95% confidence interval. DJOS: duodenal-jejunal omega switch surgery; HF: high-fat diet; CD: control diet; HF/HF, CD/HF, HF/CD, CD/CD: type of diet 8 weeks before/8 weeks after surgery.

lowest value observed among the CD/CD diet group and the highest ones among the CD/HF diet group (Figure 3(a), Tables 1 and 2).

In SHAM-operated animals, there were significant differences in terms of SOD muscle's activity between four diet groups, namely, HF/HF and CD/CD, HF/CD and CD/CD, CD/HF, and CD/CD, with the lowest value observed among the CD/CD diet group (Figure 3(a), Tables 1 and 2).

4.1.6. Mn Superoxide Dismutase Activity. MnSOD muscle's activity in DJOS-operated animals compared to SHAM-operated ones was significantly lowered in the CD/CD study diet group (Figure 3(b), Tables 1 and 2).

After DJOS, there were significant differences in terms of MnSOD muscle's activity between studied groups, namely, HF/HF and CD/HF, HF/HF and CD/HF, HF/CD and CD/HF, and CD/HF and CD/CD studied diet

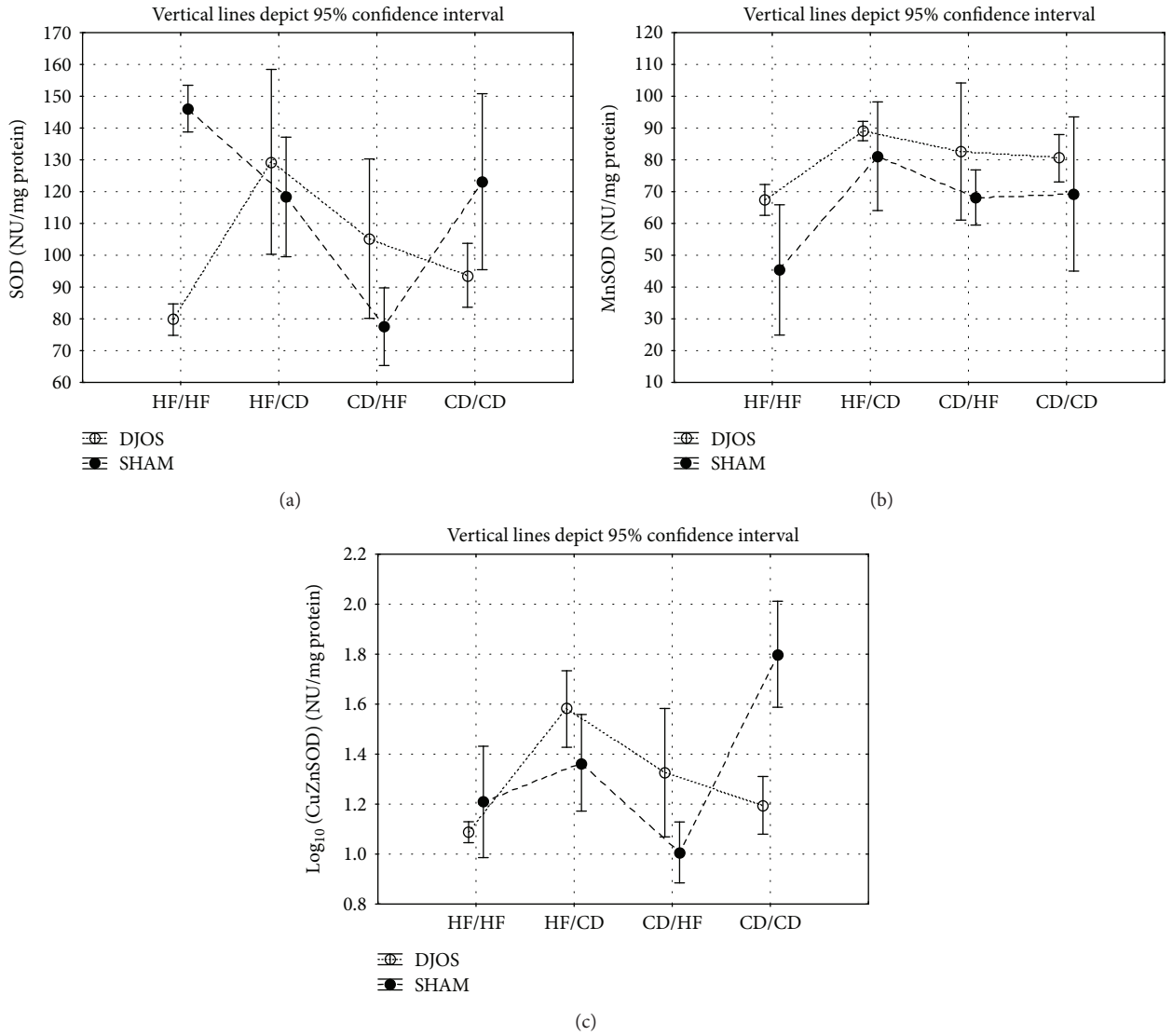

Figure 3: (a) Mean values of SOD (NU/mg) activity in four groups subjected to different dietary patterns, according to the DJOS and SHAM operation type. Statistical significance was set at $p < 0.05$. Vertical lines depict 95% confidence interval. DJOS: duodenal-jejunal omega switch surgery; HF: high-fat diet; CD: control diet; HF/HF, CD/HF, HF/CD, CD/CD: type of diet 8 weeks before/8 weeks after surgery. (b) Mean values of MnSOD (NU/mg) activity in four groups subjected to different dietary patterns, according to the DJOS and SHAM operation type. Statistical significance was set at $p < 0.05$. Vertical lines depict 95% confidence interval. DJOS: duodenal-jejunal omega switch surgery; HF: high-fat diet; CD: control diet; HF/HF, CD/HF, HF/CD, CD/CD: type of diet 8 weeks before/8 weeks after surgery. (c) Mean values of CuZnSOD (NU/mg) activity in four groups subjected to different dietary patterns, according to the DJOS and SHAM operation type. Statistical significance was set at $p < 0.05$. Vertical lines depict 95% confidence interval. DJOS: duodenal-jejunal omega switch surgery; HF: high-fat diet; CD: control diet; HF/HF, CD/HF, HF/CD, CD/CD: type of diet 8 weeks before/8 weeks after surgery.

groups, with the lowest value observed among the HF/HF diet group (Figure 3(b), Table 2).

In SHAM-operated animals, there were significant differences in terms of SOD muscle's activity between the studied groups, namely, HF/HF and HF/CD, HF/HF and CD/HF, HF/HF and CD/CD, HF/CD and CD/HF, and CD/HF and CD/CD, with the lowest value observed among the HF/HF one (Figure 3(b), Tables 1 and 2).

4.1.7. CuZn Superoxide Dismutase Activity. CuZnSOD muscle's activity in DJOS-operated animals compared to SHAM-operated ones was significantly different in all studied diet groups. Among HF/HF, CD/HF, and CD/CD diet groups of DJOS-operated animals, ZnCuSOD activity was significantly lower when compared to the HF/HF, CD/HF, and CD/CD diet groups of SHAM-operated animals (Figure 3(c), Tables 1 and 2). In the HF/CD diet group of DJOS-operated animals, ZnCuSOD activity was significantly higher when compared to the HF/CD diet group of SHAM-operated animals (Figure 3(c), Tables 1 and 2).

After DJOS surgery, there were significant differences in terms of CuZnSOD muscle's activity between the studied diet

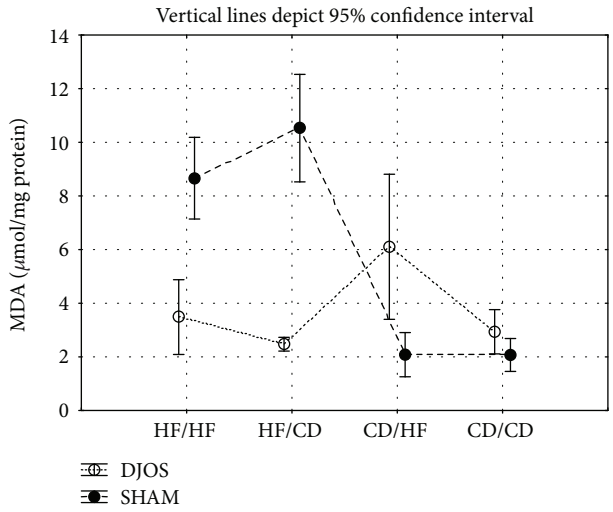

Figure 4: Mean values of MDA (μmol/g) concentration in four groups subjected to different dietary patterns, according to the DJOS and SHAM operation type. Statistical significance was set at $p < 0.05$. Vertical lines depict 95% confidence interval. DJOS: duodenal-jejunal omega switch surgery; HF: high-fat diet; CD: control diet; HF/HF, CD/HF, HF/CD, CD/CD: type of diet 8 weeks before/8 weeks after surgery.

groups, namely, HF/HF and HF/CD, HF/HF and CD/HF, HF/HF and CD/CD, HF/CD and CD/CD, and CD/HF and CD/CD, with the lowest two values observed in the CD/CD diet group and the highest value in the HF/HF group (Figure 3(c), Tables 1 and 2).

After SHAM surgery, there were significant differences in terms of CuZnSOD muscle's activity between the studied diet groups, namely, HF/HF and HF/CD, HF/HF and CD/HF, HF/HF and CD/CD, HF/CD and CD/HF, and CD/HF and CD/CD, with the lowest value observed among the HF/CD diet group and the highest among the HF/HF studied group (Figure 3(c), Tables 1 and 2).

4.1.8. Lipid Peroxidation

(1) Malondialdehyde Concentration. MDA muscle's activity in DJOS-operated animals compared to SHAM-operated ones was significantly lowered in the HF/CD and CD/CD study diet groups (Figure 4, Tables 1 and 2).

After DJOS surgery, there were significant differences in terms of MDA muscle's concentrations between the studied groups, namely, HF/HF and HF/CD, HF/HF and CD/HF, HF/HF and CD/CD, HF/CD and CD/CD, and CD/HF and CD/CD, with the lowest value observed in the CD/CD diet group and the highest in the CD/HF diet group (Figure 4, Tables 1 and 2).

After SHAM surgery, there were significant differences in terms of MDA muscle's activity between the studied groups, namely, HF/HF and HF/CD, HF/HF and CD/HF, HF/CD and CD/HF, HF/CD and CD/CD, and CD/HF and CD/CD, with the lowest value observed in the CD/CD diet group and the highest value in the HF/CD diet group (Figure 4, Tables 1 and 2).

5. Discussion

It is already known that both high-fat diet and/or obesity lead to an increased OS [28]. It is however not known whether different types of diet combined with bariatric surgery decrease the skeletal muscles' OS. In this study, we have, for the first time, proven that DJOS surgery positively reduced the redox state of the rat's soleus muscle cells in comparison to the SHAM procedure. It was also noticed that the type of diet applied before and after DJOS and SHAM surgery is associated with the different levels of OS status, antioxidant enzymatic activity, and nonenzymatic system in the soleus muscle of rats. Thus, the antioxidant activity was related to the type of diet before and after the surgery and the studied enzyme. Treatment with the control dietary pattern or HF diet, both before and after surgery, was associated with the lowest antioxidants' activity, while changing the diet from CD to HF or the reverse significantly increased the ROS generation and lipid peroxidation measured by MDA concentration. Because there were no studies performed up to date that took under consideration the association of bariatric surgery in relation to diet with skeletal muscle's antioxidant system activity, we will refer to studies examining single components of our experiment in this discussion section.

Metabolic disorders are associated with alterations in lipid and glucose metabolism in skeletal muscle. Some of those alterations are explained by defects in insulin signalling, glucose transport, or glycogen synthesis in skeletal muscles [29, 30]. This leads to deterioration of metabolic function and is associated with mitochondrial dysfunction [31–33]. It is known that altered mitochondrial function in skeletal muscle leads to reduced fatty acid oxidation and reduction of insulin-stimulated glucose transport. This may be understood as a hallmark of insulin resistance and diabetes mellitus type 2 [34]. Under obesogenic conditions, for example, high-fat diet, the ability of muscle tissue to oxidize the fat content is highly reduced and may lead to an increased level of ROS; thus, ROS production is intensified under inflammatory conditions characteristic for obesity. ROS, by its dual nature, may play a pathogenic role in many muscular diseases or lead to further injury by oxidatively damaging differentiating myoblasts and myotubes [31]. Conversely, together with other factors such as growth factors and chemokines, ROS takes part in a process of muscle regeneration and repair [31]. ROS also stimulates signalling pathways relevant to skeletal muscle metabolism, homeostasis, and adaptation [35]. The muscle cellular antioxidant capacity is the main factor, which can curb the negative activity of ROS, and the modulation of muscle sensitivity to ROS depends on the ROS level. The antioxidant enzymes keep ROS on the physiological level, where they can act as defence systems, signalling molecules, and mitochondrial function modulators [35, 36].

In our study, the CAT and GPx activity was significantly lower after DJOS surgery in comparison with the SHAM one in all diet study groups. It was not dependent on diet; nevertheless, the redox state of the muscle cells and activity of CAT, SOD, and GPx was altered in the groups maintained on the mixed CD/HF diet. GR and CuZnSOD activity was

increased after DJOS surgery compared to the SHAM one among animals fed with the HF diet before the surgery and CD following the procedure. These enzymatic antioxidants are the main force of prevention mechanisms, controlling the formation of ROS [37, 38]. Apart from ATP production, mitochondrial areas are major sites for ROS production. Characteristic of rat soleus muscles are mitochondria-rich slow-twitch type I fibres, which exhibit oxidative metabolism and fatigue resistance [39]. Long-term exposure to an HF diet increases the muscle rates of fatty acid oxidation regardless of the fibre type [13]. Chronic disturbances in energy metabolism caused by excessive food intake and obesity lead to an increase in ROS production and mitochondrial dysfunction [34]. The changes in the structure and functions of mitochondria in the skeletal muscles of obese mice favour the generation of ROS, the development of oxidative stress, and insulin resistance [40, 41]. Chronic oxidative stress and inflammation mainly derived from reduced mitochondrial mass, changed morphology, and mitochondrial metabolic dysfunction are proven to induce lipid accumulation and insulin resistance in muscle tissue [34, 42–44]. Recent laboratory findings prove that a high-fat diet changes the mitochondrial structure in mice and the optimal mitochondrial function is obtained only under the condition of caloric restriction or regular diet [34]. Our findings show that DJOS surgery reduces the deleterious impact of an HF/HF diet on OS but does not act efficiently under the condition of a change in dietary pattern. Other studies confirm the reduction in oxidative stress and a downregulation of antioxidant enzymes after duodenojejunostomy in the insulin resistance and diabetic animal models [14].

In this study, the HF diet, applied before and after surgery, stimulated antioxidative activity less than the CD/HF and HF/CD ones. Here, rats were exposed to an HF diet for 16 weeks, and this could have allowed enough time for the antioxidant system to adapt to a proinflammatory diet and quench ROS production. In this manner, it may be interpreted as an increase in the oxidative capacity of the soleus muscle. After DJOS surgery the activity of Mn SOD, CAT, GPx, GR, and GST was reduced in the presence of the HF/HF diet when compared to the HF/CD and CD/HF dietary groups. Significant differences in the activity of all studied enzymes were observed between the HF/HF and CD/HF groups, with higher activity of CAT, GPx, GST, Mn SOD, and SOD and MDA concentration after the change of the diet from CD to HF. The activity of studied enzymes and MDA concentration was significantly higher also in the CD/HF dietary pattern when compared to CD/CD, with the exception of GR. The different activity profile of ZnCu SOD, GR, and total SOD, when compared to other studied enzymes and MDA concentration, could have been understood as a compensation mechanism, reducing the potentially deleterious impact of ROS production on soleus muscle metabolism and function under obesogenic conditions. It can also reflect on the intrinsic differences between the studied dietary patterns, in relation to the activity of antioxidative/prooxidative systems.

The change of the diet from CD to HF or HF to CD caused more disturbances in oxidative stress, measured by enzymatic activity and MDA concentration, than remaining on the same nutritional profile. We suggest that the change of a diet after 8 weeks, and hence the consumption of a different type of nutrients, influenced the biochemical pathways, causing perturbations and irregularities in substrate catabolism, which is also manifested in ROS production and antioxidative activity. Therefore, in relation to the general data presented above, it can be hypothesised that the way DJOS influences the soleus muscle's antioxidative enzyme activity is related to the type of diet implemented before and after the surgery and the type of enzyme studied. Changing the diet from CD to HF or vice versa seems to be the less preferable method of treatment, and remaining on the stable diet, preferably the control one, which is more favourable in terms of antioxidative enzyme activity following bariatric surgery would be the better option.

To our best knowledge, there has been no study performed to date that examined MDA skeletal muscles' activity following a bariatric surgery procedure in relation neither to HF or CD nor to animals or humans. Reduction of MDA skeletal muscle's activity following the bariatric surgery procedure stays in line with the recently performed study in humans by Monzo-Beltran et al. However, the MDA activity was measured in serum, not in skeletal muscle [45]. These authors observed that MDA progressively decreased in patients undergoing laparoscopic sleeve gastrectomy [45]. Even though bariatric surgery procedures have an advantage in decreasing lipid peroxidation measured with MDA skeletal muscle's concentration, the changes in the dietary pattern (CD/HF; HF/CD) are less favourable in comparison with HF/HF and CD/CD patterns. In the light of the presented studies, it might be reflected that bariatric procedure has an advantageous effect in terms of mobilisation of antioxidative systems and OS reduction. To our knowledge, the phenomenon of diverse responses to OS amplified by HF diet across different muscle types has been studied [13]. Therefore, the observations coming from soleus muscle are not necessarily reflective of the redox response to diet and bariatric procedures in all skeletal muscles. Thus, further studies are needed to more widely explore our initial findings.

6. Conclusions

The dietary patterns applied for this research included combinations of the same diet before and after surgery (HF/HF, CD/CD) as well as different ones (HF/CD, CD/HF). After 16 weeks of the experiment and 8 weeks after DJOS and SHAM surgery, we observed the following: (i) Enzymatic systems represented by GPX, CAT, CuZnSOD, and nonenzymatic MDA showed a significantly lower level of activity and concentration in muscle after DJOS surgery in comparison to SHAM-operated animals. (ii) GR showed a significantly increased activity after DJOS in relation to SHAM operation. This may suggest a strong beneficial impact of DJOS surgery on the dynamics of antioxidative/oxidative processes. (iii) A change in diet, regardless of the type of diet, stimulated OS in DJOS-operated rats. (iv) For most of the analysed parameters, we observed that the same type of diet before and after surgery, which was HF/HF and CD/CD,

induced OS less than a change in dietary pattern from HF to CD or from CD to HF.

We conclude that metabolic surgery together with mixed dietary patterns may be potentially used as a strategy to modulate oxidative stress under pathological conditions. Long-term application of mixed control and obesogenic dietary patterns led to significant changes after DJOS surgery, many times reducing its beneficial effect, measured by selected antioxidants.

Data Availability

The data used to support the findings of this study are available from the corresponding author upon request.

Ethical Approval

All applicable institutional and/or national guidelines for the care and use of animals were followed. All animal experimental protocols were approved by the Local Ethics Committee, Poland.

Conflicts of Interest

The authors declare that they have no conflict of interest.

Authors' Contributions

Bronisława Skrzep-Poloczek, Dominika Stygar, and Konrad W Karcz conceived the idea of the experiment; Bronisława Skrzep-Poloczek, Dominika Stygar, and Tomasz Sawczyn maintained the animals; Dominika Stygar and Jakub Poloczek conducted the surgery; Bronisława Skrzep-Poloczek, Dominika Stygar, Katarzyna Nabrdalik, and Janusz Gumprecht worked on the manuscript; Bronisława Skrzep-Poloczek and Elżbieta Chełmecka analysed the data and performed the statistical analysis; Bronisława Skrzep-Poloczek and Ewa Romuk carried out the analysis. All authors had final approval of the submitted and published version.

Acknowledgments

The authors would like to thank Anna Dulska for the Figure 1 graphic design. The authors would like to express their special gratitude to Scott Richards for the scientific English language correction. This work was supported by Medical University of Silesia.

References

[1] L. Sjöström, K. Narbro, C. D. Sjöström et al., "Effects of bariatric surgery on mortality in Swedish obese subjects," *The New England Journal of Medicine*, vol. 357, no. 8, pp. 741–752, 2007.

[2] L. Sjöström, M. Peltonen, P. Jacobson et al., "Bariatric surgery and long-term cardiovascular events," *Journal of the American Medical Association*, vol. 307, no. 1, pp. 56–65, 2012.

[3] L. Sjöström, M. Peltonen, P. Jacobson et al., "Association of bariatric surgery with long-term remission of type 2 diabetes and with microvascular and macrovascular complications," *Journal of the American Medical Association*, vol. 311, no. 22, pp. 2297–2304, 2014.

[4] G. Fruhbeck, "Bariatric and metabolic surgery: a shift in eligibility and success criteria," *Nature Reviews. Endocrinology*, vol. 11, no. 8, pp. 465–477, 2015.

[5] S. O. Olusi, "Obesity is an independent risk factor for plasma lipid peroxidation and depletion of erythrocyte cytoprotectic enzymes in humans," *International Journal of Obesity*, vol. 26, no. 9, pp. 1159–1164, 2002.

[6] J. F. Keaney, M. G. Larson, R. S. Vasan et al., "Obesity and systemic oxidative stress: clinical correlates of oxidative stress in the Framingham study," *Arteriosclerosis, Thrombosis, and Vascular Biology*, vol. 23, no. 3, pp. 434–439, 2003.

[7] R. J. Bloomer, M. M. Kabir, K. E. Marshall, R. E. Canale, and T. M. Farney, "Postprandial oxidative stress in response to dextrose and lipid meals of differing size," *Lipids in Health and Disease*, vol. 9, no. 1, p. 79, 2010.

[8] P. Manna and S. K. Jain, "Obesity, oxidative stress, adipose tissue dysfunction, and the associated health risks: causes and therapeutic strategies," *Metabolic Syndrome and Related Disorders*, vol. 13, no. 10, pp. 423–444, 2015.

[9] A. C. Montezano and R. M. Touyz, "Reactive oxygen species and endothelial function-role of nitric oxide synthase uncoupling and Nox family nicotinamide adenine dinucleotide phosphate oxidases," *Basic & Clinical Pharmacology & Toxicology*, vol. 110, no. 1, pp. 87–94, 2012.

[10] A. Kunwar and I. K. Priyadarsini, "Free radicals, oxidative stress and importance of antioxidants in human health," *Journal of Medical & Allied Sciences*, vol. 1, pp. 53–60, 2011.

[11] S. Blankenberg, H. J. Rupprecht, C. Bickel et al., "Glutathione peroxidase 1 activity and cardiovascular events in patients with coronary artery disease," *The New England Journal of Medicine*, vol. 349, no. 17, pp. 1605–1613, 2003.

[12] N. Auberval, S. Dal, W. Bietiger et al., "Metabolic and oxidative stress markers in Wistar rats after 2 months on a high-fat diet," *Diabetology and Metabolic Syndrome*, vol. 6, no. 1, p. 130, 2014.

[13] R. A. Pinho, D. M. Sepa-Kishi, G. Bikopoulos et al., "High-fat diet induces skeletal muscle oxidative stress in a fiber type-dependent manner in rats," *Free Radical Biology & Medicine*, vol. 110, pp. 381–389, 2017.

[14] C. R. Wietzycoski, J. C. D. Marchesini, S. Al-Themyat, F. S. Meyer, and M. R. M. Trindade, "Improvement in oxidative stress after duodenojejunostomy in an experimental model of type 2 diabetes mellitus," *ABCD. Arquivos Brasileiros de Cirurgia Digestiva (São Paulo)*, vol. 29, Supplement 1, pp. 3–7, 2016.

[15] J. M. Grueneberger, I. Karcz-Socha, G. Marjanovic et al., "Pylorus preserving loop duodeno-enterostomy with sleeve gastrectomy - preliminary results," *BMC Surgery*, vol. 14, no. 1, p. 20, 2014.

[16] W. K. Karcz, S. Kuesters, G. Marjanovic, and J. M. Grueneberger, "Duodeno-enteral omega switches—more physiological techniques in metabolic surgery," *Videosurgery and Other Miniinvasive Techniques*, vol. 4, no. 4, pp. 273–279, 2013.

[17] M. A. Nauck, "Unraveling the science of incretin biology," *The American Journal of Medicine*, vol. 122, no. 6, pp. S3–10, 2009.

[18] F. Rubino and M. Gagner, "Potential of surgery for curing type 2 diabetes mellitus," *Annals of Surgery*, vol. 236, no. 5, pp. 554–559, 2002.

[19] D. Stygar, T. Sawczyn, B. Skrzep-Poloczek et al., "The effects of duodenojejunal omega switch in combination with high-fat diet and control diet on incretins, body weight, and glucose tolerance in Sprague-Dawley rats," *Obesity Surgery*, vol. 28, no. 3, pp. 748–759, 2018.

[20] W. M. S. Russell and R. L. Burch, *The Principles of Humane Experimental Technique the Principles of Humane Experimental Technique*, Methuen Co., LTD, London, 1959.

[21] I. Carlberg and B. Mannervik, "[59] Glutathione reductase," *Methods in Enzymology*, vol. 113, pp. 484–490, 1985.

[22] H. Aebi, "[13] Catalase in vitro," *Methods in Enzymology*, vol. 105, pp. 121–126, 1984.

[23] B. Mannervik, "[60] Glutathione peroxidase," *Methods in Enzymology*, vol. 113, pp. 490–495, 1985.

[24] W. H. Habig and W. B. Jakoby, "[51] Assays for differentiation of glutathione S-Transferases," *Methods in Enzymology*, vol. 77, pp. 398–405, 1981.

[25] Y. Oyanagui, "Reevaluation of assay methods and establishment of kit for superoxide dismutase activity," *Analytical Biochemistry*, vol. 142, no. 2, pp. 290–296, 1984.

[26] H. Ohkawa, N. Ohishi, and K. Yagi, "Assay for lipid peroxides in animal tissues by thiobarbituric acid reaction," *Analytical Biochemistry*, vol. 95, no. 2, pp. 351–358, 1979.

[27] O. Lowry, N. Rosebrough, A. Farr, and R. Randall, "Protein measurement with the Folin phenol reagent," *The Journal of Biological Chemistry*, vol. 193, no. 1, pp. 265–275, 1951.

[28] A. Fernández-Sánchez, E. Madrigal-Santillán, M. Bautista et al., "Inflammation, oxidative stress, and obesity," *International Journal of Molecular Sciences*, vol. 12, no. 5, pp. 3117–3132, 2011.

[29] R. A. DeFronzo and D. Tripathy, "Skeletal muscle insulin resistance is the primary defect in type 2 diabetes," *Diabetes Care*, vol. 32, Supplement_2, pp. S157–S163, 2009.

[30] S. Fröjdö, H. Vidal, and L. Pirola, "Alterations of insulin signaling in type 2 diabetes: a review of the current evidence from humans," *Biochimica et Biophysica Acta (BBA) - Molecular Basis of Disease*, vol. 1792, no. 2, pp. 83–92, 2009.

[31] J. G. Tidball, "Inflammatory processes in muscle injury and repair," *American Journal of Physiology-Regulatory, Integrative and Comparative Physiology*, vol. 288, no. 2, pp. R345–R353, 2005.

[32] A. Krook, H. Wallberg-Henriksson, and J. R. Zierath, "Sending the signal: molecular mechanisms regulating glucose uptake," *Medicine & Science in Sports & Exercise*, vol. 36, no. 7, pp. 1212–1217, 2004.

[33] V. B. Schrauwen-Hinderling, M. Roden, M. E. Kooi, M. K. C. Hesselink, and P. Schrauwen, "Muscular mitochondrial dysfunction and type 2 diabetes mellitus," *Current Opinion in Clinical Nutrition and Metabolic Care*, vol. 10, no. 6, pp. 698–703, 2007.

[34] A. Hernández-Aguilera, A. Rull, E. Rodríguez-Gallego et al., "Mitochondrial dysfunction: a basic mechanism in inflammation-related non-communicable diseases and therapeutic opportunities," *Mediators of Inflammation*, vol. 2013, Article ID 135698, 13 pages, 2013.

[35] E. Barbieri and P. Sestili, "Reactive oxygen species in skeletal muscle signaling," *Journal of Signal Transduction*, vol. 2012, Article ID 982794, 17 pages, 2012.

[36] P. J. Adhihetty, I. Irrcher, A. M. Joseph, V. Ljubicic, and D. A. Hood, "Plasticity of skeletal muscle mitochondria in response to contractile activity," *Experimental Physiology*, vol. 88, no. 1, pp. 99–107, 2003.

[37] E. Birben, U. M. Sahiner, C. Sackesen, S. Erzurum, and O. Kalayci, "Oxidative stress and antioxidant defense," *World Allergy Organization Journal*, vol. 5, no. 1, pp. 9–19, 2012.

[38] K. Brieger, S. Schiavone, J. Miller, and K. H. Krause, "Reactive oxygen species: from health to disease," *Swiss Medical Weekly*, vol. 142, pp. 1–14, 2012.

[39] M. J. Gillespie, T. Gordon, and P. R. Murphy, "Motor units and histochemistry in rat lateral gastrocnemius and soleus muscles: evidence for dissociation of physiological and histochemical properties after reinnervation," *Journal of Neurophysiology*, vol. 57, no. 4, pp. 921–937, 1987.

[40] H. F. Jheng, P. J. Tsai, S. M. Guo et al., "Mitochondrial fission contributes to mitochondrial dysfunction and insulin resistance in skeletal muscle," *Molecular and Cellular Biology*, vol. 32, no. 2, pp. 309–319, 2011.

[41] H. F. Jheng, S. H. Huang, H. M. Kuo, M. W. Hughes, and Y. S. Tsai, "Molecular insight and pharmacological approaches targeting mitochondrial dynamics in skeletal muscle during obesity," *Annals of the New York Academy of Sciences*, vol. 1350, no. 1, pp. 82–94, 2015.

[42] C. Tang, K. Koulajian, I. Schuiki et al., "Glucose-induced beta cell dysfunction in vivo in rats: link between oxidative stress and endoplasmic reticulum stress," *Diabetologia*, vol. 55, no. 5, pp. 1366–1379, 2012.

[43] C. Aguer and M. E. Harper, "Skeletal muscle mitochondrial energetics in obesity and type 2 diabetes mellitus: endocrine aspects," *Best Practice & Research Clinical Endocrinology & Metabolism*, vol. 26, no. 6, pp. 805–819, 2012.

[44] A. Zorzano, M. Liesa, and M. Palacín, "Role of mitochondrial dynamics proteins in the pathophysiology of obesity and type 2 diabetes," *The International Journal of Biochemistry & Cell Biology*, vol. 41, no. 10, pp. 1846–1854, 2009.

[45] L. Monzo-Beltran, A. Vazquez-Tarragón, C. Cerdà et al., "One-year follow-up of clinical, metabolic and oxidative stress profile of morbid obese patients after laparoscopic sleeve gastrectomy. 8-oxo-dG as a clinical marker," *Redox Biology*, vol. 12, pp. 389–402, 2017.

Hindawi
Oxidative Medicine and Cellular Longevity
Volume 2018, Article ID 3407375, 9 pages
https://doi.org/10.1155/2018/3407375

Review Article

Metallic Nanoantioxidants as Potential Therapeutics for Type 2 Diabetes: A Hypothetical Background and Translational Perspectives

Oleh Lushchak,[1] **Alina Zayachkivska**,[1] **and Alexander Vaiserman**[2]

[1]*Department of Biochemistry and Biotechnology, Vasyl Stefanyk Precarpathian National University, 57 Shevchenko, Ivano-Frankivsk 76018, Ukraine*
[2]*Laboratory of Epigenetics, Institute of Gerontology, 67 Vyshgorodska, Kyiv 04114, Ukraine*

Correspondence should be addressed to Oleh Lushchak; olehl@pu.if.ua and Alexander Vaiserman; vaiserman23@gmail.com

Received 6 February 2018; Revised 4 May 2018; Accepted 20 May 2018; Published 27 June 2018

Academic Editor: Karolina Szewczyk-Golec

Hyperglycemia-induced overproduction of reactive oxygen species (ROS) is an important contributor to type 2 diabetes (T2D) pathogenesis. The conventional antioxidant therapy, however, proved to be ineffective for its treatment. This may likely be due to limited absorption profiles and low bioavailability of orally administered antioxidants. Therefore, novel antioxidant agents that may be delivered to specific target organs are actively developed now. Metallic nanoparticles (NPs), nanosized materials with a dimension of 1–100 nm, appear very promising for the treatment of T2D due to their tuned physicochemical properties and ability to modulate the level of oxidative stress. An excessive generation of ROS is considered to be the most common negative outcome related to the application of NPs. Several nanomaterials, however, were shown to exhibit enzyme-like antioxidant properties in animal models. Such NPs are commonly referred to as "nanoantioxidants." Since NPs can provide specifically targeted or localized therapy, their use is a promising therapeutic option in addition to conventional therapy for T2D. NP-based therapies should certainly be used with caution given their potential toxicity and risk of adverse health outcomes. However, despite these challenges, NP-based therapeutic approaches have a great clinical potential and further translational studies are needed to confirm their safety and efficacy.

1. Introduction

Diabetes mellitus is one the leading causes of death in most countries across the globe. Over the last few decades, diabetes has emerged as an epidemic worldwide. Today 415 million people, about 9% of the adult population, have diabetes and this number is expected to increase to 642 million people during the next decade [1]. Type 2 diabetes (T2D), also called noninsulin-dependent or adult-onset diabetes, accounts for roughly 90% of all diabetes cases worldwide. The pathophysiology of this disease is characterized by peripheral insulin resistance, declining β-cell function, and impaired glucose metabolism in the liver [2]. The causes and manner of the development of T2D are associated with numerous factors, including genetic predisposition, age, unhealthy nutritional habits, decreased physical activity, and stressful life conditions. Lifestyle factors contributing to this disease (e.g., diet and exercise) may be controlled through lifestyle changes [3]. However, in some cases, impairments in insulin secretion and/or sensitivity are too severe to be corrected by lifestyle changes. In these cases, the use of oral hypoglycaemic drugs or even insulin injections is the next treatment option to control blood sugar levels [4].

2. Treatment of T2D: Old Problems and New Solutions

T2D patients usually receive oral or injectable medications to improve the production and function of insulin. However, antidiabetic therapies are still far from perfect. Indeed, currently used antidiabetic medicines, which act primarily by suppressing hepatic gluconeogenesis and improving insulin

sensitivity, have many side effects. For example, oral hypoglycemics including the first-line antidiabetic drug, metformin, often cause gastric distress leading to nausea and diarrhea [4]. Moreover, oral drugs may stop working for T2D patients and they may ultimately require insulin therapy to achieve and maintain adequate glycemic control. In addition, even though considerable technological advances have been made over the past years in the treatment of T2D, it remains difficult to maintain proper glucose levels using conventional treatment options. Indeed, about half of diabetic patients fail to achieve target blood glucose levels when using common therapeutic modalities [5]. Therefore, many attempts have been made in recent years to develop alternative treatment options for management of T2D [6].

The use of natural health products is one of the most promising tools in T2D management. Among them, there are several trace metals, such as chromium, selenium, vanadium, molybdenum, and magnesium, which are known to exert hypoglycemic activity possibly due to their insulin-mimetic effects [7–10]. For example, chromium has shown the benefit in the treatment of T2D, particularly in conditions of chromium deficiency or when diabetes is poorly controlled [11]. From these findings, it can be assumed that dietary supplementation with well-studied trace metals can be a promising treatment option for T2D patients, complementary to approved pharmacological therapies. In this context, the use of metal nanoparticles (NPs) seems highly attractive for biomedical applications. NPs, nanosized materials with a dimension of 1–100 nm, exhibit unique size-related optical, electronic, and catalytic properties that differ significantly from those observed in the corresponding bulk materials due to their high surface area and nanoscale size [12, 13]. One important advantage of artificially engineered nanomaterials is that they may be well controlled for appropriate usage due to their tuned physicochemical properties; it provides an opportunity to directly influence interactions between nanomaterials and cells [14]. Finally, with respect to the biomedical applicability of NPs, a crucial point is that the interaction of NPs with proteins may influence both protein structure and function providing a means to influence the enzyme response to disease states [12, 15].

Nanotechnology-based systems provide apparent benefits in terms of increased bioavailability, decreased dosing frequency, prevention from degradation in the harsh gastric environment, high site specificity and minimal side effects [6]. NP drug delivery systems have attracted considerable attention due to their ability to overcome multiple biological barriers and release a therapeutic load in the optimal dose range [16]. Currently, numerous NP formulations including liposomes, nanostructures, polymer and metallic NPs, stimuli-responsive NPs, and nanofabricated devices are extensively used to deliver both small-molecule therapeutic agents and different classes of biomacromolecules, such as proteins, DNA, and RNA. These formulations are also used to diagnose and monitor the onset and progression of diseases [17]. Over the past two decades, clinical implementation of nanotechnology has led to both diagnostic and therapeutic advances in treatment of various chronic pathologies, including cardiovascular diseases [18], neurodegenerative disorders including Alzheimer's and Parkinson's diseases [19], and cancer [20], as well as diabetes [21, 22].

Currently, naked (not loaded with therapeutics) metallic NPs are increasingly used in a variety of biomedical applications [23, 24]. Metallic NPs may be synthesized and/or modified with diverse surface functionalities, thereby allowing them to be conjugated with different ligands, antibodies, vesicles, and drugs therefore increasing their potential clinical utility [25]. In this opinion paper, we focus on the potential therapeutic applications of metallic NPs in T2D management.

3. Role of Reactive Oxygen Species in Pathogenesis of T2D

Oxidative stress levels and associated chronic inflammation are known to be significantly increased in patients with metabolic syndrome and T2D [26, 27]. A potential means of using NPs for therapeutic purposes is related to their ability to modulate the level of oxidative stress, thus making them especially important in the context of the topic under consideration [28]. Free radicals such as reactive oxygen species (ROS), which are generated in the mitochondria during normal metabolic processes, are important second messengers that support signal transduction pathways implicated in normal cell functions including survival, proliferation, differentiation, and apoptosis [29]. Under normal physiological conditions, cellular ROS levels are strongly controlled by specific antioxidant enzymes, including superoxide dismutase (SOD), catalase (CAT), and glutathione peroxidase (GPX) and by exogenous antioxidants such as flavonoids, vitamin E, ascorbic acids, and glutathione (GSH) [30]. Under pathological conditions such as T2D, abnormally large ROS concentrations may damage a wide variety of biomolecules including lipids, proteins, and nucleic acids. ROS can also result in permanently disturbed patterns of gene expression and signal transduction [31]. Chronic extracellular hyperglycemia causes elevated production of ROS by the mitochondrial electron-transport chain and thus leads to disturbed cell redox state and abnormal expression of genes of insulin sensitivity [32]. Oxidative stress thereby plays a crucial role in hyperglycemia-triggered tissue damage and is regarded as one of the key initial events in T2D onset and progression. Chronic hyperglycemia also results in an increase of the generation of advanced glycation end products (AGEs), a group of modified lipids and/or proteins with damaging potential [33]. Overproduction of AGEs leads to an enhanced ROS formation and impaired antioxidant defense which results in a detrimental cycle since the generation of AGEs can be induced under oxidative conditions [33]. Therefore, AGEs are thought to play a significant role in the pathogenesis of T2D. Another important contributing factor in pathogenesis of T2D is accelerated telomere shortening. Telomeres are nucleotide repeated sequences that cap the chromosome ends and shorten with every cell division in absence of the telomerase activity. Age-associated telomere attrition, however, depends not only on the replicative shortening but also on the level of oxidative stress (known to be, in turn,

contributing to most age-related chronic diseases), because of a deficiency in the repair of telomere-specific damage [34]. Shortened telomere lengths were revealed in pancreatic beta cells in T2D patients, thus potentially resulting in an impaired capability for proliferation, secretion of insulin, and in accelerated cell death [35]. There is evidence from animal models that insulin resistance can be induced through telomere attrition in adipose tissue as well. Telomere attrition depends on the level of oxidative stress [34]. Taken together, currently available data suggest that hyperglycemia, oxidative stress, and telomere attrition in both pancreatic beta cells and adipocytes may cumulatively form a vicious cycle contributing to the pathogenesis of T2D. Therefore, modulating these processes by innovative nanotechnology-based therapeutics could provide a promising approach for the prevention and progression of T2D and its complications.

In the last few decades, much hope was placed on the prevention and therapy of T2D with antioxidants owing to their ability to counteract oxidative stress by scavenging ROS. Oxidative stress occurs when ROS production exceeds the endogenous antioxidant defense capacity. Therefore, given that T2D-associated conditions are generally accompanied by a higher oxidative stress level, it was believed that patients suffering from this disease would benefit from exogenous antioxidant supplementation as adjunct therapy [36]. However, clinical antioxidant trials have been largely ineffective so far in preventing and managing T2D. Most of them gave inconclusive or even negative results [31, 37, 38]. Although there is robust experimental evidence for beneficial outcomes of the dietary antioxidant consumption, most interventional studies have failed to demonstrate any health benefits of antioxidants. This contradiction is commonly referred to as the "antioxidant paradox" [37, 39]. One possible explanation for this is that oxidative stress and inflammation accompanying T2D are closely linked to pathophysiological conditions which can mutually induce each other. From this, it can be assumed that the failure of clinical antioxidant trials could result from an inability to develop medications that specifically target both oxidative stress and inflammation or from failure to apply both anti-inflammatory agents and antioxidants simultaneously [39]. Moreover, it might result from the use of substances that block several inflammatory and/or prooxidative pathways but strengthen others. In addition, most orally administered antioxidants have limited absorption profiles and consequently have low bioavailability resulting in insufficient concentrations at the target site [40, 41]. Therefore, novel agents with antioxidant capabilities that have improved bioavailability and that may be delivered to specific target tissues have been actively developed in recent years.

4. Metallic NPs as Potential Modulators of T2D-Induced Oxidative Stress

Metallic NPs such as magnetic, silver, and gold NPs seem to have promising potential for use in prevention and treatment of disorders caused by excessive generation of ROS [25]. NPs, among other nanomaterials, are increasingly used for various biomedical applications owing to their exceptional and tunable biophysical properties dependent on their size and shape [22, 42]. Indeed, NPs differ substantially from their bulk analogs since their surface areas are significantly greater and contain a larger fraction of atoms [43]. Moreover, the surface-to-volume ratio is inversely related to particle size. Smaller NPs have larger ratio; therefore, the number of reactive sites on the surface of a NP is regulated by the particle size [44].

The NP-induced effects are mediated by their enhanced catalytic activity, which is likely related to the high ratio of electrons remaining on the particle's surface, increasing the ability of the NP to transform the substrate. Smaller NPs have higher catalytic activity than larger NPs owing to their greater surface area [45]. In addition, chemical reactivity substantially increases with decreasing particle size [43]. High chemical reactivity of NPs is commonly attributed to dangling bonds (unsatisfied valences on immobilized atoms located on the surface of NP) which consequently make their surface unstable and highly reactive [46]. Due to these unique properties of NPs, their clinical implementation would likely provide many benefits compared to conventional treatment modalities with drugs which have multiple side effects because of their insufficient and off-target activity.

4.1. NP-Induced ROS Generation. The most common negative outcome related to the therapeutic application of NPs is the excessive generation of ROS which is regarded as a key factor in NP-induced toxicity [25, 47, 48]. Both large surface areas and reactive surfaces contribute to the oxidizing capacities of the NPs. The mitochondrion is an organelle crucially involved in the NP-induced generation of cellular ROS due to the capacity of NPs to depolarize mitochondrial membrane potential and to interfere with the electron-transport chain via the activation of nicotinamide adenine dinucleotide phosphate- (NADPH-) related enzymes [49]. NP exposure can thus lead to blocking the mitochondrial electron-transport chain, consequently increasing the cellular levels of superoxide radicals through electron transfer from respiratory carriers to molecular oxygen. Other mechanisms involved in the generation of intracellular ROS by NPs include the catalysis of free-radical reactions, the interaction of NPs with different cellular components of redox active proteins (e.g., NADPH oxidase), as well as the interplay with cellular surface receptors and activation of various intracellular signaling pathways [49]. The NP-induced toxic state can cause elevated expression of proinflammatory cytokines and activation of inflammatory cells, including neutrophils and macrophages, which can result in an increased generation of ROS. The potential of different metallic NPs for generating ROS depends on their chemical composition, particle size, surface area, and shape [25], as well as on the mode of interaction with cells, aggregation, inflammation, and pH of the medium [50]. Importantly, on the cellular level, the amount of ROS generated is dependent on the concentration of NPs to which the cell is exposed. Exposure to low concentrations results in an improvement of the endogenous antioxidant defense system to combat the

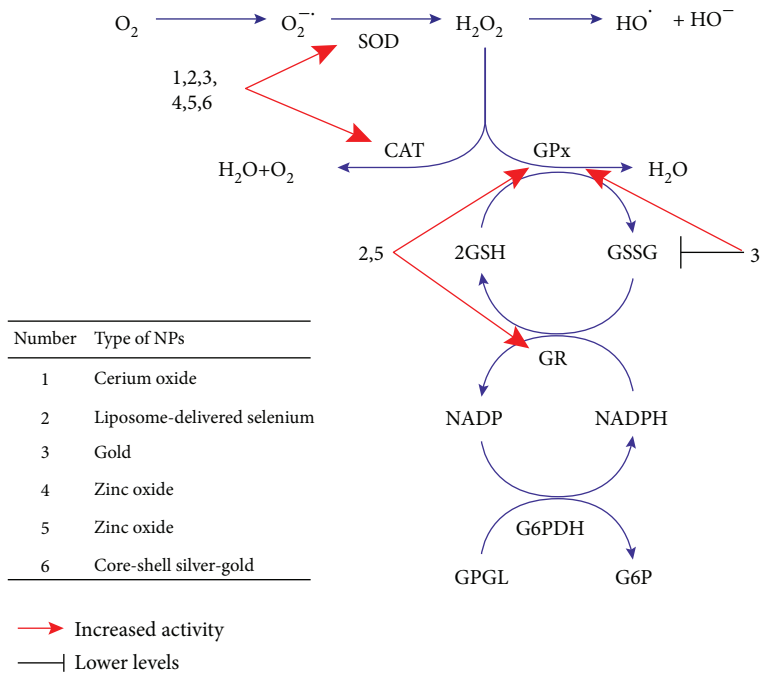

Number	Type of NPs
1	Cerium oxide
2	Liposome-delivered selenium
3	Gold
4	Zinc oxide
5	Zinc oxide
6	Core-shell silver-gold

Figure 1: NPs can prevent diabetes-induced oxidative stress by affecting different steps of free-radical metabolism. Many NPs including all of those presented in Table 1 are able to restore the activities of superoxide dismutase (SOD) and catalase (CAT) that are often decreased under diabetic conditions. Lower oxidative damages to cellular macromolecules are achieved by decreasing the levels of superoxide anion (O_2^-) or preventing the generation of hydroxyl radical from hydrogen peroxide (H_2O_2). Additionally, t*he liposome-delivered selenium and zinc oxide* NPs can affect the activities of glutathione peroxidase (GPx) and glutathione reductase (GR), thereby increasing the H_2O_2 detoxification by glutathione-dependent system. Decreased concentration of oxidized glutathione (GSH) and increased activity of GPx are also observed under treatment with the gold NPs.

damaging consequences of oxidative stress and recover the redox balance, while exposure to high NP concentrations provokes excess ROS formation, overwhelming antioxidant systems and causing cytotoxicity and inflammation [51]. Determination of maximal effective doses therefore is critical to avoid negative outcomes.

4.2. Nanoantioxidants. Recently, some nanomaterials, including metallic NPs, were unexpectedly shown to exhibit enzyme-like antioxidant properties by being able to scavenge free radicals and decrease ROS concentrations [52, 53]. Such NPs are commonly referred to as "nanoantioxidants." Nanoantioxidants include both NPs functionalized with antioxidants or antioxidant enzymes for functioning as an antioxidant delivery system and nonorganic NPs with intrinsic antioxidant properties. Significant antioxidant properties such as SOD-, CAT-, oxidase-, and peroxidase-mimicking activities have been demonstrated for metallic NPs produced from cerium oxide (nanoceria) [54–56], iron oxide [57, 58], cobalt oxide [59], copper oxide [60], manganese dioxide [61], and vanadium pentoxide [62], as well as from noble metals such as gold [63, 64], silver [65], and platinum [66].

The precise molecular mechanisms determining the antioxidant capabilities of metallic NPs remain largely unclear. The antioxidant capabilities of these NPs can likely be attributed to their high surface-to-volume ratio, electronic configuration, catalytic and redox properties, and oxygen vacancy defects [52, 53]. The antioxidative behavior of metallic NMs may to a large extent depend on their capacity to oscillate between different multioxidation states. For example, antioxidant properties of nanoceria NPs, which are considered to be one of the most promising nanomaterials due to their catalytic properties, are thought to be related to the presence of oxygen vacancies on their surfaces and also to the autoregenerative cycle of their two oxidation states, Ce^{3+} and Ce^{4+} [67]. Indeed, as shown by X-ray absorption near edge spectroscopy and X-ray photoelectron spectroscopy, the concentration of Ce^{3+} relative to Ce^{4+} can be substantially increased as the particle size decreases, and such loss of oxygen due to reduction of Ce^{4+} to Ce^{3+} is accompanied by the formation of an oxygen vacancy on the surface of the NP [52, 67]. Such ability of this NP to oscillate among these multioxidation states can definitely contribute to its ROS-scavenging ability. Moreover, there is persuasive evidence that NPs including, for example, CeO_2 NPs, can modulate key antioxidant pathways such as Nrf2 [53]. Furthermore, interactions of NPs with cellular macromolecules including proteins, lipids, and nucleic acids could be of great importance for these processes. A wide variety of sites of the NP protein interaction is expected through the diversity of protein structure, and the kinetics of NP protein interaction can significantly depend on the NP structure, as well as protein availability and duration of interaction [53]. Due to these properties, NPs can largely affect the cellular redox environment by either stimulating or inhibiting ROS generation under certain conditions. In addition, the hormetic phenomenon

Table 1: An overview of NP-induced metabolic outcomes and markers of oxidative status in streptozotocin-induced diabetic rats.

NP formulation	NP dose; route of administration	Metabolic outcomes	Markers of oxidative status	Ref.
Cerium oxide NPs	60 mg/kg per day for 2 wk; intraperitoneal injection	Increase of high density lipoprotein level; decrease of adenosine diphosphate/adenosine triphosphate (ADP/ATP) ratio, cholesterol, triglyceride, and low-density lipoprotein levels	Recovery in normal antioxidant enzyme activity and oxidative stress level	[80]
Cerium oxide NPs	65 or 85 mg/kg; intraperitoneal injection	Recovery in body weight, total thiol molecules, lipid peroxidation levels, and ADP/ATP ratio	Recovery in antioxidant enzyme activity	[81]
Liposome-delivered selenium NPs	0.1 mg/kg per day for 21 days; oral administration	Recovery in serum glucose and insulin and pancreatic malondialdehyde, nitric oxide, tumor necrosis factor-α, and prostaglandin F2α levels; improvement in immunohistochemical indices (insulin and glucagon)	Recovery in pancreatic SOD, CAT, glutathione, glutathione peroxidase, and glutathione reductase levels	[82]
Gold NPs	2.5 mg/kg for 7 days; intraperitoneal injection	Improved lipid profile and kidney functions; no evidence of separation of nuclear membrane in euchromatic nuclei of beta cells	Increased SOD, CAT, and glutathione peroxidase activities; lowered oxidized glutathione levels	[83]
Core-shell silver-gold NPs	0.5 or 1 ml per day for 21 days; oral administration by gastric intubation	Restoring the normal glucose and serum insulin levels and glucokinase activity; reducing the lipid profile; anti-inflammatory effect assessed using inflammatory markers IL-α and C-reactive protein; decreased level of necrosis of hepatocytes	Suppressing the oxidative stress and elevating the antioxidant defense system	[84]
Zinc oxide NPs	1, 3, and 10 mg/kg per day for 56 days; oral administration by gavage	Improved glucose disposal, insulin levels, and zinc status compared to rats supplemented with zinc sulfate	Altered activities of erythrocyte antioxidant enzymes, raised levels of lipid peroxidation, and a marked reduction of total antioxidant capacity in rats administered with high dose of NPs	[85]
Zinc oxide NPs	10 mg/kg per day for 30days; oral administration	Increased sperm count and motility	Increased activity of SOD, CAT, glutathione peroxidase, glutathione reductase, and glutathione-S-transferase; decreased malondialdehyde and increased glutathione levels in testicular tissue	[86]

referred to as a "biphasic dose-response relationship characterized by a low-dose stimulation and high-dose inhibition" may likely play an important role in redox-modulating effects of NPs [68]. Under the conditions of oxidative stress, particular NPs could likely prevent key biomolecules from oxidative damage, thereby causing health benefits and disease prevention. The hypothetical mechanisms through which NPs can prevent diabetes-induced oxidative stress are presented in Figure 1.

The capability of metallic NPs to scavenge free radicals was repeatedly shown in *in vitro* studies [69–71], as well as in animal models such as *Drosophila melanogaster* [72, 73], mice [74], and rats [75–78]. Most compelling evidence for the ability of metallic NPs to protect against diabetes-related oxidative stress was obtained in the streptozotocin-induced diabetic rat model. Streptozotocin is known to destroy insulin-producing pancreatic beta cells, thereby leading to hypoinsulinemia and hyperglycemia in exposed animals. Since in this model hyperglycemia arises owing to the hypoinsulinemia in the absence of peripheral insulin resistance, it most closely mimics type 1 diabetes but can also be used for induction of T2D under certain conditions [79]. A summary of the main findings from these studies is provided in Table 1. As we can see from the table, administration of metallic NPs, independently on the route of administration, in most cases led to an improvement of metabolic indices and protection from diabetes-induced oxidative stress in streptozotocin-treated rats. These findings demonstrate that catalytic NPs could represent a promising therapeutic approach for patients with pathological conditions related to elevated levels of oxidative stress, including T2D.

5. Conclusion

The use of metallic NPs in clinical practice has many advantages, including their superior biocompatibility and stability, low operational and capital expenses, and reduced environmental impacts [87]. The development of metallic NPs with antioxidant properties seems a particularly promising therapeutic option, since it might provide specifically targeted or localized therapy [88]. The unique opportunities from the clinical application of nanoantioxidants are related to the fact that they may be made larger than the cutoff size for kidney filtration (~10 nm), thereby prolonging the circulation period

in comparison with small molecules [28]. They may also be further designed to avoid rapid clearance by phagocytes or to target specific sites and organs. This allows them to be used in smaller but more effective doses, thus minimizing potential adverse impacts. Due to these properties, treatment with nanoantioxidants might represent a promising therapeutic option, in addition to conventional therapy, in patients with T2D. Finally, NP-based therapeutic approaches have a great clinical potential and certainly further translational studies are needed to confirm their safety and efficacy and overcome the known risks of toxicity and potential for adverse health outcomes at higher doses.

Abbreviations

AGEs: Advanced glycation end products
GSH: Glutathione
GPx: Glutathione peroxidase
GR: Glutathione reductase
GSSG: Oxidized glutathione
G6P: Glucose-6-phosphate
G6PDH: Glucose-6-phosphate dehydrogenase
CAT: Catalase
NP: Nanoparticle
NADPH: Nicotinamide adenine dinucleotide phosphate
ROS: Reactive oxygen species
SOD: Superoxide dismutase
T2D: Type 2 diabetes
6PGL: 6-phosphogluconate.

Conflicts of Interest

The authors declare that there is no conflict of interest regarding the publication of this article.

Authors' Contributions

Oleh Lushchak and Alexander Vaiserman conceived the idea for the manuscript and produced the first draft. Alina Zayachkivska was involved in critical review and rewriting of subsequent drafts. All authors read and approved the final manuscript.

Acknowledgments

The work was partially supported by the Science and Technology Center in Ukraine (STCU) (Grant no. 6274).

References

[1] L. M. Jaacks, K. R. Siegel, U. P. Gujral, and K. M. V. Narayan, "Type 2 diabetes: a 21st century epidemic," *Best Practice & Research Clinical Endocrinology & Metabolism*, vol. 30, no. 3, pp. 331–343, 2016.

[2] J. S. Skyler, G. L. Bakris, E. Bonifacio et al., "Differentiation of diabetes by pathophysiology, natural history, and prognosis," *Diabetes*, vol. 66, no. 2, pp. 241–255, 2017.

[3] E. M. Venditti, "Behavior change to prevent or delay type 2 diabetes: psychology in action," *The American Psychologist*, vol. 71, no. 7, pp. 602–613, 2016.

[4] E. A. Nyenwe, T. W. Jerkins, G. E. Umpierrez, and A. E. Kitabchi, "Management of type 2 diabetes: evolving strategies for the treatment of patients with type 2 diabetes," *Metabolism*, vol. 60, no. 1, pp. 1–23, 2011.

[5] H. E. Resnick, G. L. Foster, J. Bardsley, and R. E. Ratner, "Achievement of American Diabetes Association clinical practice recommendations among U.S. adults with diabetes, 1999–2002: the National Health and Nutrition Examination Survey," *Diabetes Care*, vol. 29, no. 3, pp. 531–537, 2006.

[6] V. K. Rai, N. Mishra, A. K. Agrawal, S. Jain, and N. P. Yadav, "Novel drug delivery system: an immense hope for diabetics," *Drug Delivery*, vol. 23, no. 7, pp. 2371–2390, 2016.

[7] B. M. Rovenko, N. V. Perkhulyn, O. V. Lushchak, J. M. Storey, K. B. Storey, and V. I. Lushchak, "Molybdate partly mimics insulin-promoted metabolic effects in *Drosophila melanogaster*," *Comparative Biochemistry and Physiology Part C: Toxicology & Pharmacology*, vol. 165, pp. 76–82, 2014.

[8] N. V. Perkhulyn, B. M. Rovenko, T. V. Zvarych et al., "Sodium chromate demonstrates some insulin-mimetic properties in the fruit fly *Drosophila melanogaster*," *Comparative Biochemistry and Physiology Part C: Toxicology & Pharmacology*, vol. 167, pp. 74–80, 2015.

[9] C. Necyk and L. Zubach-Cassano, "Natural health products and diabetes: a practical review," *Canadian Journal of Diabetes*, vol. 41, no. 6, pp. 642–647, 2017.

[10] S. K. Panchal, S. Wanyonyi, and L. Brown, "Selenium, vanadium, and chromium as micronutrients to improve metabolic syndrome," *Current Hypertension Reports*, vol. 19, no. 3, p. 10, 2017.

[11] R. V. Yin and O. J. Phung, "Effect of chromium supplementation on glycated hemoglobin and fasting plasma glucose in patients with diabetes mellitus," *Nutrition Journal*, vol. 14, no. 1, 2015.

[12] M. Zaman, E. Ahmad, A. Qadeer, G. Rabbani, and R. H. Khan, "Nanoparticles in relation to peptide and protein aggregation," *International Journal of Nanomedicine*, vol. 9, pp. 899–912, 2014.

[13] P. N. Navya and H. K. Daima, "Rational engineering of physicochemical properties of nanomaterials for biomedical applications with nanotoxicological perspectives," *Nano Convergence*, vol. 3, no. 1, p. 1, 2016.

[14] L. C. Cheng, X. Jiang, J. Wang, C. Chen, and R. S. Liu, "Nano-bio effects: interaction of nanomaterials with cells," *Nanoscale*, vol. 5, no. 9, pp. 3547–3569, 2013.

[15] Y. Kim, S. M. Ko, and J. M. Nam, "Protein-nanoparticle interaction-induced changes in protein structure and aggregation," *Chemistry – An Asian Journal*, vol. 11, no. 13, pp. 1869–1877, 2016.

[16] F. Alexis, E. Pridgen, L. K. Molnar, and O. C. Farokhzad, "Factors affecting the clearance and biodistribution of polymeric nanoparticles," *Molecular Pharmaceutics*, vol. 5, no. 4, pp. 505–515, 2008.

[17] O. Veiseh, B. C. Tang, K. A. Whitehead, D. G. Anderson, and R. Langer, "Managing diabetes with nanomedicine: challenges and opportunities," *Nature Reviews Drug Discovery*, vol. 14, no. 1, pp. 45–57, 2015.

[18] V. M. Martín Giménez, D. E. Kassuha, and W. Manucha, "Nanomedicine applied to cardiovascular diseases: latest developments," *Therapeutic Advances in Cardiovascular Disease*, vol. 11, no. 4, pp. 133–142, 2017.

[19] D. Silva Adaya, L. Aguirre-Cruz, J. Guevara, and E. Ortiz-Islas, "Nanobiomaterials' applications in neurodegenerative diseases," *Journal of Biomaterials Applications*, vol. 31, no. 7, pp. 953–984, 2017.

[20] Y. Huang, C. Q. Fan, H. Dong, S. M. Wang, X. C. Yang, and S. M. Yang, "Current applications and future prospects of nanomaterials in tumor therapy," *International Journal of Nanomedicine*, vol. 12, pp. 1815–1825, 2017.

[21] R. M. DiSanto, V. Subramanian, and Z. Gu, "Recent advances in nanotechnology for diabetes treatment," *Wiley Interdisciplinary Reviews: Nanomedicine and Nanobiotechnology*, vol. 7, no. 4, pp. 548–564, 2015.

[22] J. Jeevanandam, M. Danquah, S. Debnath, V. Meka, and Y. Chan, "Opportunities for nano-formulations in type 2 diabetes mellitus treatments," *Current Pharmaceutical Biotechnology*, vol. 16, no. 10, pp. 853–870, 2015.

[23] R. Bhattacharya and P. Mukherjee, "Biological properties of "naked" metal nanoparticles," *Advanced Drug Delivery Reviews*, vol. 60, no. 11, pp. 1289–1306, 2008.

[24] B. Song, Y. Zhang, J. Liu, X. L. Feng, T. Zhou, and L. Q. Shao, "Is neurotoxicity of metallic nanoparticles the cascades of oxidative stress?," *Nanoscale Research Letters*, vol. 11, no. 1, p. 291, 2016.

[25] A. Abdal Dayem, M. Hossain, S. Lee et al., "The role of reactive oxygen species (ROS) in the biological activities of metallic nanoparticles," *International Journal of Molecular Sciences*, vol. 18, no. 1, p. 120, 2017.

[26] S. Tangvarasittichai, "Oxidative stress, insulin resistance, dyslipidemia and type 2 diabetes mellitus," *World Journal of Diabetes*, vol. 6, no. 3, pp. 456–480, 2015.

[27] S. Rovira-Llopis, C. Bañuls, N. Diaz-Morales, A. Hernandez-Mijares, M. Rocha, and V. M. Victor, "Mitochondrial dynamics in type 2 diabetes: pathophysiological implications," *Redox Biology*, vol. 11, pp. 637–645, 2017.

[28] J. Morry, W. Ngamcherdtrakul, and W. Yantasee, "Oxidative stress in cancer and fibrosis: opportunity for therapeutic intervention with antioxidant compounds, enzymes, and nanoparticles," *Redox Biology*, vol. 11, pp. 240–253, 2017.

[29] E. Georgieva, D. Ivanova, Z. Zhelev, R. Bakalova, M. Gulubova, and I. Aoki, "Mitochondrial dysfunction and redox imbalance as a diagnostic marker of "free radical diseases"," *Anticancer Research*, vol. 37, no. 10, pp. 5373–5381, 2017.

[30] H. Wu, J. J. Yin, W. G. Wamer, M. Zeng, and Y. M. Lo, "Reactive oxygen species-related activities of nano-iron metal and nano-iron oxides," *Journal of Food and Drug Analysis*, vol. 22, no. 1, pp. 86–94, 2014.

[31] P. Pérez-Matute, M. A. Zulet, and J. A. Martínez, "Reactive species and diabetes: counteracting oxidative stress to improve health," *Current Opinion in Pharmacology*, vol. 9, no. 6, pp. 771–779, 2009.

[32] D. Zephy and J. Ahmad, "Type 2 diabetes mellitus: role of melatonin and oxidative stress," *Diabetes & Metabolic Syndrome: Clinical Research & Reviews*, vol. 9, no. 2, pp. 127–131, 2015.

[33] K. Nowotny, T. Jung, A. Höhn, D. Weber, and T. Grune, "Advanced glycation end products and oxidative stress in type 2 diabetes mellitus," *Biomolecules*, vol. 5, no. 1, pp. 194–222, 2015.

[34] A. K. Koliada, D. S. Krasnenkov, and A. M. Vaiserman, "Telomeric aging: mitotic clock or stress indicator?," *Frontiers in Genetics*, vol. 6, no. 82, 2015.

[35] Y. Tamura, K. Takubo, J. Aida, A. Araki, and H. Ito, "Telomere attrition and diabetes mellitus," *Geriatrics & Gerontology International*, vol. 16, no. 1, pp. 66–74, 2016.

[36] E. C. Opara, "Role of oxidative stress in the etiology of type 2 diabetes and the effect of antioxidant supplementation on glycemic control," *Journal of Investigative Medicine*, vol. 52, no. 1, pp. 19–23, 2004.

[37] M. Sheikh-Ali, J. M. Chehade, and A. D. Mooradian, "The antioxidant paradox in diabetes mellitus," *American Journal of Therapeutics*, vol. 18, no. 3, pp. 266–278, 2011.

[38] L. Rochette, M. Zeller, Y. Cottin, and C. Vergely, "Diabetes, oxidative stress and therapeutic strategies," *Biochimica et Biophysica Acta*, vol. 1840, no. 9, pp. 2709–2729, 2014.

[39] S. K. Biswas, "Does the interdependence between oxidative stress and inflammation explain the antioxidant paradox?," *Oxidative Medicine and Cellular Longevity*, vol. 2016, Article ID 5698931, 9 pages, 2016.

[40] V. Hajhashemi, G. Vaseghi, M. Pourfarzam, and A. Abdollahi, "Are antioxidants helpful for disease prevention?," *Research in Pharmaceutical Sciences*, vol. 5, no. 1, pp. 1–8, 2010.

[41] E. B. Souto, P. Severino, R. Basso, and M. H. A. Santana, "Encapsulation of antioxidants in gastrointestinal-resistant nanoparticulate carriers," *Methods in Molecular Biology*, vol. 1028, pp. 37–46, 2013.

[42] A. Majdalawieh, M. C. Kanan, O. El-Kadri, and S. M. Kanan, "Recent advances in gold and silver nanoparticles: synthesis and applications," *Journal of Nanoscience and Nanotechnology*, vol. 14, no. 7, pp. 4757–4780, 2014.

[43] C. Buzea, I. I. Pacheco, and K. Robbie, "Nanomaterials and nanoparticles: sources and toxicity," *Biointerphases*, vol. 2, no. 4, pp. MR17–MR71, 2007.

[44] M. Auffan, J. Rose, J. Y. Bottero, G. V. Lowry, J. P. Jolivet, and M. R. Wiesner, "Towards a definition of inorganic nanoparticles from an environmental, health and safety perspective," *Nature Nanotechnology*, vol. 4, no. 10, pp. 634–641, 2009.

[45] H. Katsumi, K. Fukui, K. Sato et al., "Pharmacokinetics and preventive effects of platinum nanoparticles as reactive oxygen species scavengers on hepatic ischemia/reperfusion injury in mice," *Metallomics*, vol. 6, no. 5, pp. 1050–1056, 2014.

[46] J. Fan, J.-J. Yin, B. Ning et al., "Direct evidence for catalase and peroxidase activities of ferritin-platinum nanoparticles," *Biomaterials*, vol. 32, no. 6, pp. 1611–1618, 2011.

[47] R. K. Pandey and V. K. Prajapati, "Molecular and immunological toxic effects of nanoparticles," *International Journal of Biological Macromolecules*, vol. 107, pp. 1278–1293, 2018.

[48] J. K. Tee, C. N. Ong, B. H. Bay, H. K. Ho, and D. T. Leong, "Oxidative stress by inorganic nanoparticles," *Wiley Interdisciplinary Reviews: Nanomedicine and Nanobiotechnology*, vol. 8, no. 3, pp. 414–438, 2016.

[49] S. J. Soenen, P. Rivera-Gil, J.-M. Montenegro, W. J. Parak, S. C. de Smedt, and K. Braeckmans, "Cellular toxicity of inorganic nanoparticles: common aspects and guidelines for improved nanotoxicity evaluation," *Nano Today*, vol. 6, no. 5, pp. 446–465, 2011.

[50] P. P. Fu, Q. Xia, H. M. Hwang, P. C. Ray, and H. Yu, "Mechanisms of nanotoxicity: generation of reactive oxygen species," *Journal of Food and Drug Analysis*, vol. 22, no. 1, pp. 64–75, 2014.

[51] A. Nel, T. Xia, L. Mädler, and N. Li, "Toxic potential of materials at the nanolevel," *Science*, vol. 311, no. 5761, pp. 622–627, 2006.

[52] G. Mohammad, V. K. Mishra, and H. P. Pandey, "Antioxidant properties of some nanoparticle may enhance wound healing in T2DM patient," *Digest Journal of Nanomaterials and Biostructures*, vol. 3, no. 4, pp. 159–162, 2008.

[53] M. J. Akhtar, M. Ahamed, H. A. Alhadlaq, and A. Alshamsan, "Mechanism of ROS scavenging and antioxidant signalling by redox metallic and fullerene nanomaterials: potential implications in ROS associated degenerative disorders," *Biochimica et Biophysica Acta (BBA) - General Subjects*, vol. 1861, no. 4, pp. 802–813, 2017.

[54] L. L. Wong and J. F. McGinnis, "Nanoceria as bona fide catalytic antioxidants in medicine: what we know and what we want to know…," *Advances in Experimental Medicine and Biology*, vol. 801, pp. 821–828, 2014.

[55] D. Dutta, R. Mukherjee, M. Patra et al., "Green synthesized cerium oxide nanoparticle: a prospective drug against oxidative harm," *Colloids and Surfaces B: Biointerfaces*, vol. 147, pp. 45–53, 2016.

[56] H. Nadaroglu, H. Onem, and A. Alayli Gungor, "Green synthesis of Ce_2O_3 NPs and determination of its antioxidant activity," *IET Nanobiotechnology*, vol. 11, no. 4, pp. 411–419, 2017.

[57] Z. Chen, J. J. Yin, Y. T. Zhou et al., "Dual enzyme-like activities of iron oxide nanoparticles and their implication for diminishing cytotoxicity," *ACS Nano*, vol. 6, no. 5, pp. 4001–4012, 2012.

[58] L. Gao, K. Fan, and X. Yan, "Iron oxide nanozyme: a multifunctional enzyme mimetic for biomedical applications," *Theranostics*, vol. 7, no. 13, pp. 3207–3227, 2017.

[59] J. Mu, Y. Wang, M. Zhao, and L. Zhang, "Intrinsic peroxidase-like activity and catalase-like activity of CO_3O_4 nanoparticles," *Chemical Communications*, vol. 48, no. 19, pp. 2540–2542, 2012.

[60] W. Chen, J. Chen, A.-L. Liu, L. M. Wang, G. W. Li, and X. H. Lin, "Peroxidase-like activity of cupric oxide nanoparticle," *ChemCatChem*, vol. 3, no. 7, pp. 1151–1154, 2011.

[61] Y. Wan, P. Qi, D. Zhang, J. Wu, and Y. Wang, "Manganese oxide nanowire-mediated enzyme-linked immunosorbent assay," *Biosensors and Bioelectronics*, vol. 33, no. 1, pp. 69–74, 2012.

[62] R. André, F. Natálio, M. Humanes et al., "V_2O_5 nanowires with an intrinsic peroxidase-like activity," *Advanced Functional Materials*, vol. 21, no. 3, pp. 501–509, 2011.

[63] S. Wang, W. Chen, A. L. Liu, L. Hong, H. H. Deng, and X. H. Lin, "Comparison of the peroxidase-like activity of unmodified, amino-modified, and citrate-capped gold nanoparticles," *Chemphyschem*, vol. 13, no. 5, pp. 1199–1204, 2012.

[64] Y. Lin, J. Ren, and X. Qu, "Nano-gold as artificial enzymes: hidden talents," *Advanced Materials*, vol. 26, no. 25, pp. 4200–4217, 2014.

[65] R. S. Priya, D. Geetha, and P. S. Ramesh, "Antioxidant activity of chemically synthesized AgNPs and biosynthesized Pongamia pinnata leaf extract mediated AgNPs - a comparative study," *Ecotoxicology and Environmental Safety*, vol. 134, Part 2, pp. 308–318, 2016.

[66] D. Pedone, M. Moglianetti, E. De Luca, G. Bardi, and P. P. Pompa, "Platinum nanoparticles in nanobiomedicine," *Chemical Society Reviews*, vol. 46, no. 16, pp. 4951–4975, 2017.

[67] I. Celardo, E. Traversa, and L. Ghibelli, "Cerium oxide nanoparticles: a promise for applications in therapy," *Journal of Experimental Therapeutics & Oncology*, vol. 9, no. 1, pp. 47–51, 2011.

[68] I. Iavicoli, V. Leso, L. Fontana, and E. J. Calabrese, "Nanoparticle exposure and hormetic dose-responses: an update," *International Journal of Molecular Sciences*, vol. 19, no. 3, 2018.

[69] G. Ciofani, G. G. Genchi, B. Mazzolai, and V. Mattoli, "Transcriptional profile of genes involved in oxidative stress and antioxidant defense in PC12 cells following treatment with cerium oxide nanoparticles," *Biochimica et Biophysica Acta*, vol. 1840, no. 1, pp. 495–506, 2014.

[70] H. Ghaznavi, R. Najafi, S. Mehrzadi et al., "Neuro-protective effects of cerium and yttrium oxide nanoparticles on high glucose-induced oxidative stress and apoptosis in undifferentiated PC12 cells," *Neurological Research*, vol. 37, no. 7, pp. 624–632, 2015.

[71] L. Rubio, B. Annangi, L. Vila, A. Hernández, and R. Marcos, "Antioxidant and anti-genotoxic properties of cerium oxide nanoparticles in a pulmonary-like cell system," *Archives of Toxicology*, vol. 90, no. 2, pp. 269–278, 2016.

[72] M. Alaraby, A. Hernández, B. Annangi et al., "Antioxidant and antigenotoxic properties of CeO_2 NPs and cerium sulphate: studies with Drosophila melanogaster as a promising in vivo model," *Nanotoxicology*, vol. 9, no. 6, pp. 749–759, 2015.

[73] M. Alaraby, A. Hernández, and R. Marcos, "Copper oxide nanoparticles and copper sulphate act as antigenotoxic agents in Drosophila melanogaster," *Environmental and Molecular Mutagenesis*, vol. 58, no. 1, pp. 46–55, 2017.

[74] S. M. Hirst, A. Karakoti, S. Singh et al., "Bio-distribution and in vivo antioxidant effects of cerium oxide nanoparticles in mice," *Environmental Toxicology*, vol. 28, no. 2, pp. 107–118, 2013.

[75] A. Arya, N. K. Sethy, S. K. Singh, M. Das, and K. Bhargava, "Cerium oxide nanoparticles protect rodent lungs from hypobaric hypoxia-induced oxidative stress and inflammation," *International Journal of Nanomedicine*, vol. 8, pp. 4507–4520, 2013.

[76] A. Hosseini, A. M. Sharifi, M. Abdollahi et al., "Cerium and yttrium oxide nanoparticles against lead-induced oxidative stress and apoptosis in rat hippocampus," *Biological Trace Element Research*, vol. 164, no. 1, pp. 80–89, 2015.

[77] B. C. Nelson, M. E. Johnson, M. L. Walker, K. R. Riley, and C. M. Sims, "Antioxidant cerium oxide nanoparticles in biology and medicine," *Antioxidants*, vol. 5, no. 2, p. 15, 2016.

[78] M. R. Khaksar, M. Rahimifard, M. Baeeri et al., "Protective effects of cerium oxide and yttrium oxide nanoparticles on reduction of oxidative stress induced by sub-acute exposure to diazinon in the rat pancreas," *Journal of Trace Elements in Medicine and Biology*, vol. 41, pp. 79–90, 2017.

[79] S. Gheibi, K. Kashfi, and A. Ghasemi, "A practical guide for induction of type-2 diabetes in rat: incorporating a high-fat diet and streptozotocin," *Biomedicine & Pharmacotherapy*, vol. 95, pp. 605–613, 2017.

[80] N. Pourkhalili, A. Hosseini, A. Nili-Ahmadabadi et al., "Biochemical and cellular evidence of the benefit of a combination of cerium oxide nanoparticles and selenium to diabetic rats," *World Journal of Diabetes*, vol. 2, no. 11, pp. 204–210, 2011.

[81] R. Najafi, A. Hosseini, H. Ghaznavi, S. Mehrzadi, and A. M. Sharifi, "Neuroprotective effect of cerium oxide nanoparticles

in a rat model of experimental diabetic neuropathy," *Brain Research Bulletin*, vol. 131, pp. 117–122, 2017.

[82] H. H. Ahmed, M. D. Abd El-Maksoud, A. E. Abdel Moneim, and H. A. Aglan, "Pre-clinical study for the antidiabetic potential of selenium nanoparticles," *Biological Trace Element Research*, vol. 177, no. 2, pp. 267–280, 2017.

[83] M. E. Selim, Y. M. Abd-Elhakim, and L. Y. Al-Ayadhi, "Pancreatic response to gold nanoparticles includes decrease of oxidative stress and inflammation in autistic diabetic model," *Cellular Physiology and Biochemistry*, vol. 35, no. 2, pp. 586–600, 2015.

[84] T. I. Shaheen, M. E. El-Naggar, J. S. Hussein et al., "Antidiabetic assessment*; in vivo* study of gold and core-shell silver-gold nanoparticles on streptozotocin-induced diabetic rats," *Biomedicine & Pharmacotherapy*, vol. 83, pp. 865–875, 2016.

[85] A. Nazarizadeh and S. Asri-Rezaie, "Comparative study of antidiabetic activity and oxidative stress induced by zinc oxide nanoparticles and zinc sulfate in diabetic rats," *AAPS PharmSciTech*, vol. 17, no. 4, pp. 834–843, 2016.

[86] M. Afifi, O. A. Almaghrabi, and N. M. Kadasa, "Ameliorative effect of zinc oxide nanoparticles on antioxidants and sperm characteristics in streptozotocin-induced diabetic rat testes," *BioMed Research International*, vol. 2015, Article ID 153573, 6 pages, 2015.

[87] A. Schröfel, G. Kratošová, I. Šafařík, M. Šafaříková, I. Raška, and L. M. Shor, "Applications of biosynthesized metallic nanoparticles - a review," *Acta Biomaterialia*, vol. 10, no. 10, pp. 4023–4042, 2014.

[88] R. Sandhir, A. Yadav, A. Sunkaria, and N. Singhal, "Nano-antioxidants: an emerging strategy for intervention against neurodegenerative conditions," *Neurochemistry International*, vol. 89, pp. 209–226, 2015.

Hindawi
Oxidative Medicine and Cellular Longevity
Volume 2018, Article ID 1725191, 12 pages
https://doi.org/10.1155/2018/1725191

Research Article

Propofol Protects Hippocampal Neurons from Hypoxia-Reoxygenation Injury by Decreasing Calcineurin-Induced Calcium Overload and Activating YAP Signaling

Xiaojun Li,[1] Li Yao,[2] Qianlei Liang,[3] Hangyin Qu,[4] and Hui Cai[2]

[1]*The Second Department of Thoracic Surgery, The First Affiliated Hospital of Xi'an Jiaotong University, Xi'an, Shaanxi 710061, China*
[2]*Department of Vascular Surgery, The First Affiliated Hospital of Xi'an Jiaotong University, Xi'an, Shaanxi 710061, China*
[3]*The Second Department of Neurosurgery, China-Japan Union Hospital of Jilin University, Changchun 130033, China*
[4]*Shaanxi University of Chinese Medicine, Xianyang, Shaanxi 712000, China*

Correspondence should be addressed to Hui Cai; caihui9@stu.xjtu.edu.cn

Received 26 January 2018; Accepted 9 May 2018; Published 26 June 2018

Academic Editor: Jolanta Czuczejko

Objectives. Propofol is a popular anesthetic drug that is neuroprotective. However, the mechanisms of propofol for hippocampal neuroprotection remain elusive. This study is aimed at investigating the neuroprotective effect and mechanism of propofol in hippocampal neurons exposed to ischemia-reperfusion (I/R) injury. *Methods*. Hypoxia-reoxygenated (H/R) HT-22 cells were used to mimic I/R injury of the hippocampus in vitro. An MTT assay was used to determine cell viability. Cell apoptosis was detected by a TUNEL assay and a flow cytometry cell apoptosis assay. Expression levels of proteins were measured by Western blotting. Intracellular calcium was assessed by Fura-2/AM staining. Flow cytometry was used to determine the mitochondrial membrane potential (MMP). Coimmunoprecipitation was used to evaluate the stability of the FKBP-RyR complex. Calcineurin enzymatic activity was measured with a colorimetric method. YAP nuclear translocation was tested by immunofluorescence staining. *Results*. H/R induced HT-22 cell viability depression, and apoptosis was reversed by propofol treatment. Propofol could alleviate H/R-induced intracellular calcium accumulation and MMP loss by inhibiting calcineurin activity and FKBP12.6-RyR disassociation in a concentration-dependent manner. In addition, YAP expression was crucial for propofol to protect HT-22 cell apoptosis from H/R injury. Propofol could activate YAP through dephosphorylation. Activated YAP stimulated the transcription of the Bcl2 gene, which promotes cellular survival. Our data also demonstrated that propofol activated YAP through the RhoA-Lats1 pathway without large G proteins or MST involvement. In addition, we showed that there was no interaction between calcineurin signaling and YAP activation in HT-22 cells. *Conclusions*. Propofol protected hippocampal neurons from I/R injury through two independent signaling pathways, including the calcineurin/FKBP12.6-RyR/calcium overload pathway and the RhoA/Lats1/YAP/Bcl-2 pathway.

1. Introduction

Ischemic stroke has become one of the leading causes of morbidity and mortality worldwide [1]. To treat ischemic injury, reestablishment of blood supply for the ischemic region is the most effective approach [2]. However, cerebral ischemia-reperfusion (I/R) injury after sudden recovery of blood supply, causing dysfunction of neurons, glia cells, and cerebral blood vessels, still threatens the survival of stroke patients [3]. Previous studies indicated that neuronal apoptosis was the associated mechanism of I/R injury, and the pyramidal neurons were found to be the most vulnerable neurocytes to I/R injury-induced apoptosis [4]. Over recent decades, numerous studies were conducted to prevent hippocampal neurons from I/R injury. Among them, anesthetic drugs have been suggested to have neuroprotective effects on cerebral I/R injury via inhibiting cell apoptosis [5–7].

Propofol, also known as 2,6-disopropylphenol, has been a widely used intravenous short-acting anesthetic agent since the late 1980s. It was reported that, except for its benefits as an anesthetic agent, propofol also exerts many nonanesthetic effects, including immunomodulatory effects, analgesia effects, anxiolytic effects, and neuroprotective properties [8]. Previous studies indicated that propofol could reduce hypoxia/reoxygenation- (H/R-) induced cell apoptosis of myocytes, epithelial cells, and neurons [9, 10]. Several mechanisms were mentioned, such as mitochondrial dysfunction, apoptosis-inducing factor translocation, and the m-TOR pathway [7, 11]. Recently, propofol was also shown to inhibit rat hippocampal neuronal apoptosis by depressing calcium overload [6]. Of note, propofol could regulate multiple intracellular signaling pathways [8]. The mechanisms involved in the propofol's neuroprotective role in hippocampal neurons need more exploration.

YAP (Yes-associated protein) is a transcriptional coactivator that is negatively regulated by the Hippo pathway, which originally was identified for the function in the regulation of organ development and size [12]. Subsequent studies verified the effects of YAP in neuronal proliferation, survival, differentiation, and neurogenesis in both the central and peripheral nervous systems [13–17]. Meanwhile, the intracellular signaling that regulates YAP activation was widely discussed [18–21]. However, the extracellular regulators and detailed mechanisms of YAP signaling in hippocampal neurons are essentially unknown. At present, activation of YAP is best known to be regulated by multiple phosphokinases and phosphatases [22, 23]. Since propofol could regulate activation of phosphokinases and phosphatases [5, 24], we hypothesized that propofol would have neuroprotective effects in I/R injury, perhaps through activating YAP signaling.

In this study, we used hypoxia-reoxygenated hippocampal neurons in vitro to mimic I/R injury of the hippocampus and then aimed to confirm that propofol could prevent hippocampal neurons from hypoxia/reoxygenation- (H/R-) induced apoptosis by decreasing calcineurin-induced calcium overload. Furthermore, the roles and mechanism of YAP signaling in propofol alleviating H/R-induced hippocampal neuronal apoptosis were also explored. Meanwhile, we aimed to clarify whether there is cross-talk between the calcineurin-calcium pathway and YAP signaling in hippocampal neurons.

2. Materials and Methods

2.1. Reagents. Propofol was purchased from Sigma-Aldrich (St. Louis, MO, USA). The following inhibitors were used in this study: pertussis toxin (PTX; Invitrogen, Grand Island, NY, USA), Y27632 (BioVision, Milpitas, CA, USA), C3-exoenzyme (Cytoskeleton, Denver, CO, USA), and cyclosporine A (Selleckchem, Houston, TX, USA). YAP, phospho-YAP (Ser127), phosphoLats1 (Ser909), and phospho-MST1 (Thr183)/MST2 (Thr180) antibodies were purchased from Cell Signaling (Boston, MA, USA). GAPDH, Bax, caspase-3, caspase-9, survivin, and Bcl2 antibodies were purchased from Santa Cruz Biotechnology (Santa Cruz, CA, USA). Alexa Fluor secondary antibodies were purchased from Life Technologies, Grand Island, NY, USA. The dominant negatives (dn) of large and small G protein constructs were from UMR cDNA Resource Center (Rolla, MO, USA).

2.2. Cell Culture and Treatment. HT-22 cells, which were derived from immortalized mouse hippocampal neuron cultures, were provided by ATCC. Cells were cultured with Dulbecco's modified Eagle's medium (DMEM, Gibco, Thermo Fisher Scientific, Shanghai, China) supplemented with 10% fetal bovine serum (FBS, Gibco, Thermo Fisher Scientific, Shanghai, China) and an antibiotics mix (HyClone, GE Healthcare, Pittsburgh, PA, USA) in a humidified cell incubator with 5% CO_2 and 95% fresh air at 37°C.

2.3. Hypoxia-Reoxygenation Protocol. The protocol performed was in accordance with previous studies [25]. Briefly, the culture plates were transferred to a humidified hypoxia-controlled incubator chamber (1% O_2, 5% N_2, 94% CO_2) at 37°C for 6 hours. Then, these cells were exposed to reoxygenation in a humidified incubator providing atmosphere containing 5% CO_2 and 95% fresh air at 37°C for 6 hours.

2.4. Cell Viability Assay. An MTT assay was used in this study to assess the viability of the neurons. Briefly, after treatment, cells were seeded in the wells of 96-well culture plates. MTT was added to the cells at a final concentration of 0.5 mg/ml and incubated for 4 hours at 37°C. DMSO was added to dissolve the formed formazan crystals. A microplate reader (Bio-Rad, Hercules, California, USA) was used to determine the absorbance values at 490 nm.

2.5. Cell Apoptosis Assessment. Cell apoptosis was evaluated by terminal deoxynucleotidyl transferase- (TdT-) mediated dUTP nick end labeling (TUNEL) assay in this study. After treatment, cells were fixed with paraformaldehyde (4%) at room temperature for 30 minutes. Then, Triton X-100 (0.1%, Solarbio) was used to permeabilize the cells at room temperature for 30 minutes. A TUNEL assay kit (Roche, Indianapolis, IN, USA) was used to visualize the apoptotic cells. All procedures performed were in accordance with the manufacturer's instructions. A fluorescence microscope was used to observe the TUNEL-positive cells.

2.6. Flow Cytometry Cell Apoptosis Assay. For the cell apoptosis assay, cells were harvested after designated treatments, washed twice with PBS, and resuspended in binding buffer (BioLegend, San Diego, CA, USA). Cells were incubated with PI and FITC-Annexin V (BioLegend, San Diego, CA, USA) for 30 min, and the percentage of apoptotic cells was analyzed by flow cytometry. Three independent repeated experiments were performed.

2.7. Coimmunoprecipitation. After treatment, lysis buffer (0.1 Triton X-100, 100 mmol/l NaCl, 50 mmol/l Tris HCl, 10 mmol/l EDTA, 10 mmol/l NaF, 10% glycerol, 0.5 mmol/l phenylmethylsulfonyl fluoride, 1 mmol/l dithiothreitol, and 10 mmol/l sodium pyrophosphate) was used to lyse the cells. After centrifugation at 12000g for 5 minutes, protein-G agarose (Beyotime, Shanghai, China) was incubated with a

specific antibody against RyR (Cell Signaling, Boston, MA, USA) in the supernatants and rotated for 12 hours. The specific antibody for FKBP12.6 (Cell Signaling, Boston, MA, USA) was used for immunoblotting. Recruitments of molecules were calculated based on density detection.

2.8. Intracellular Calcium Assessment. The calcium indicator, Fura-2/AM (Invitrogen, Grand Island, NY, USA), was used in this study. After treatment, cells were incubated with Fura-2/AM at 10 μmol/l at room temperature for 30 minutes. After washing, a fluorescent inverse microscope was used to observe the cells at 510 nm after excited at 340 nm and the images were analyzed by Zeiss Physiology software (v3.2, Zeiss). Mean fluorescent intensity (MFI) was used to analyze intracellular calcium concentrations.

2.9. Mitochondrial Membrane Potential (MMP) Determination. MMP was determined by detection of the MMP indicator, rhodamine 123, by flow cytometry in accordance with the descriptions from previous studies. After treatment, cells were washed and incubated with rhodamine 123 solution (Beyotime, Shanghai, China) at a final concentration of 1 μmol/l at 37°C in a dark chamber for 30 minutes. A FACS cytometer (BD Biosciences, CA, USA) was used to detect the fluorescent signal of rhodamine 123 at 529 nm.

2.10. Plasmids and shRNA Transfection. 6-Well plates were seeded with 5×104 cells/well in 2 ml media 24 hr before transfection; cells were 80%–90% confluent. Cells were transfected with shRNA (100 pmol/well) or plasmid DNA (4 μg/well) using Lipofectamine 2000 Reagent (Life Technologies, Grand Island, NY, USA) according to the manufacturer's instructions. After 48 hr of transfection, cells were used for further experiments. All shRNAs were purchased from Santa Cruz Biotechnology (Santa Cruz, CA, USA).

2.11. Immunofluorescence Staining. Cells were seeded in chamber slides. After treatment, cells were fixed with 4% paraformaldehyde-PBS for 15 min. Following blocking in 5% goat serum with 0.3% Triton X-100 in PBS for 60 min, cells were incubated with YAP primary antibody (1 : 100 dilution) overnight at 4°C. After three washes with PBS, cells were incubated with Alexa Fluor 488- or 555-conjugated secondary antibodies (Invitrogen, 1 : 500 dilution) for 2 hr at room temperature. Slides were then washed three times and mounted. Immunofluorescence was detected using a QImaging Retiga 2000R camera (Surrey, BC, Canada) at 40x magnification. For frozen tissues, 5 μm sections were prepared and subjected to immunostaining as described.

2.12. Western Blotting. After treatment, RIPA cell lysis buffer (Santa Cruz, CA, USA) was used to lyse the cells. Total protein was extracted with a Protein Extraction Kit (Beyotime, Shanghai, China), and nuclear and cytosolic protein was extracted using the Nuclear-Cytosol Extraction Kit (TDY, Biotech Co. Ltd., Beijing) according to the manufacturer's instructions. After the protein samples were subjected to SDS-PAGE, the separated proteins were transferred to polyvinylidene difluoride (PVDF) membranes. Nonspecific binding was eliminated by incubation with blocking buffer. Then, specific antibodies against Bax, caspase-3, caspase-9, YAP, pYAP, MST1/2, pMST1/2, Lats1, pLats1, and GAPDH were used to incubate the membranes, which were then incubated with fluorescent secondary antibodies (IRDye800CW-conjugated or IRDye680-conjugated antispecies IgG, LI-COR Biosciences, Lincoln, NE, USA). The fluorescent signals were captured by an Odyssey Infrared Imaging System (LI-COR Biosciences, Lincoln, NE, USA) with both 700 and 800 nm channels. Boxes were manually placed around each band of interest, and the software returned near-infrared fluorescent values of raw intensity with background subtraction (Odyssey 3.0 analytical software, LI-COR Biosciences, Lincoln, NE, USA).

2.13. Calcineurin Activity Assay. Enzymatic activity of calcineurin was measured and calculated with a colorimetric method with the total protein extraction from treated cells. A calcineurin Activity Assay Kit (Merck) was used, as per the manufacturer's instructions.

2.14. Quantitative Real-Time PCR. After shRNA transfection for 48 hr, cells were washed with cold PBS and collected in the Qiagen RLT lysis buffer (Qiagen, Valencia, CA, USA). RNA was extracted with an RNeasy mini kit (Qiagen, Valencia, CA, USA) and reverse transcribed by M-MLV reverse transcriptase. Quantitative real-time PCR was performed on a Light Cycler 480 (Roche, Indianapolis, IN) with a SYBR Green I Master Mix (Roche, Indianapolis, IN). mRNA abundance was normalized to GAPDH. Negative controls contained no transcripts or reverse transcriptase. RNA from three separate cell pellets per treatment was analyzed. Relative gene expression was calculated using the method provided by Applied Biosystems User Bulletin Number 2 (P/N 4303859B), with nontargeting shRNA-treated cells acting as the control in each data set. Primer pairs used in this study were as follows: GAPDH: F, 50-GAAGGTGAAGG TCGGAGT-30/R, 50-GAAGATGGTGATGGGATTTC-30; survivin: F, 5′-GGACCACCGCATCTCTACAT-3′/R, 5′-G CACTTTGCCAGTTTCC-3′; and Bcl2: F, 5′-TTCTTTGAG TTCGGTGGGGTC-3′/R, 5′-TGCATATTTGTTTGGGGC AGG-3′.

2.15. Statistics. Data acquired in this study are presented as mean ± SEM. Data were analyzed by SPSS software (v17.0, SPSS). Differences between groups were evaluated by ANOVA or Student's t-tests. P values < 0.05 were considered statistically significant.

3. Results

3.1. Propofol Alleviated Hypoxia-Reoxygenation- (H/R-) Induced Hippocampal Neuronal Viability Depression and Apoptosis. MTT was used to assess cell viability. After H/R treatment, the cell viability of hippocampal neurons was significantly inhibited. However, propofol pretreatment dramatically improved the viability of HT-22 cells in a concentration-dependent manner (Figure 1(a)). We further tested the effects of propofol in cell apoptosis induced by H/R. As shown in Figures 1(b) and 1(c), H/R significantly

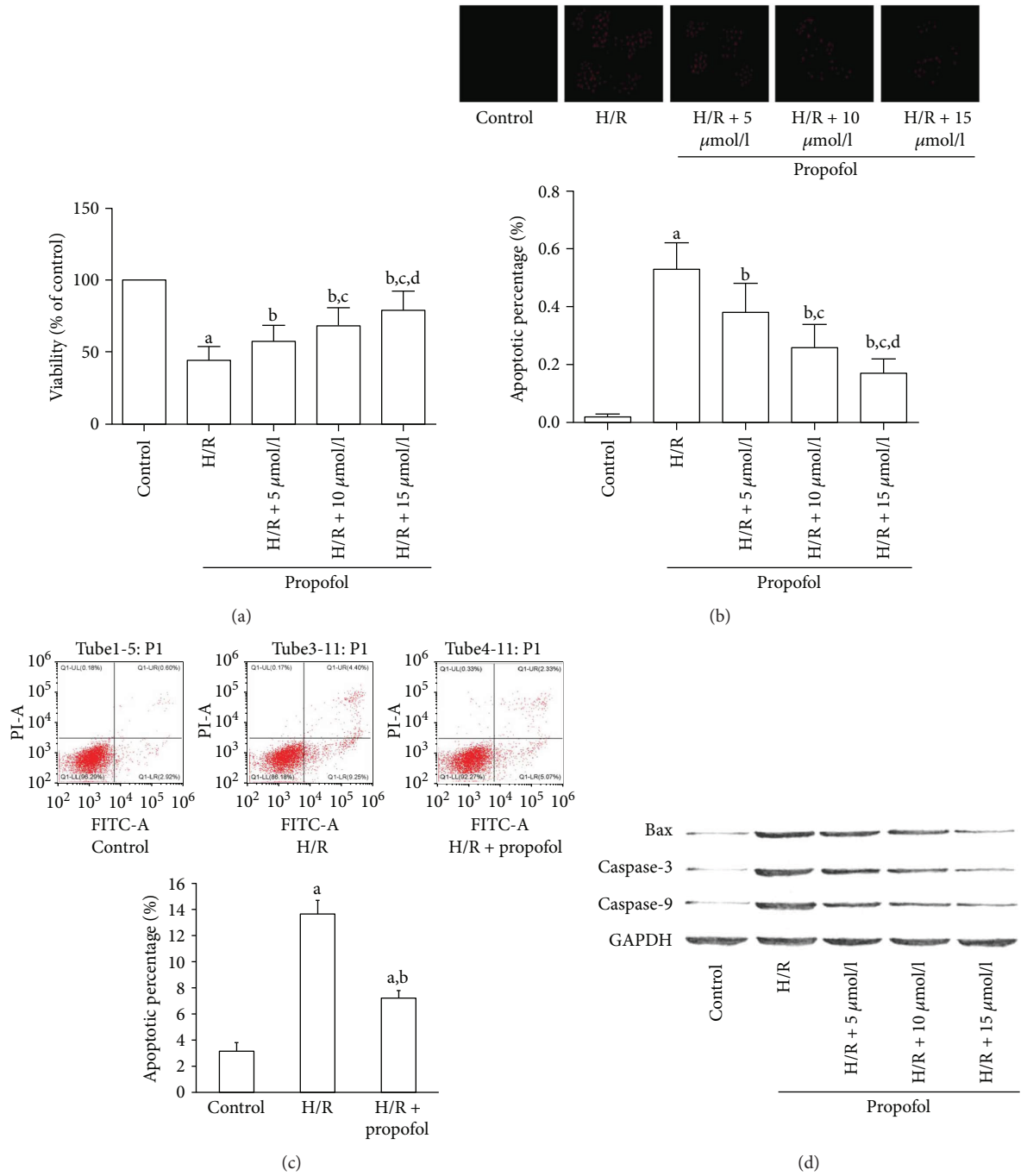

Figure 1: Propofol attenuated hypoxia-reoxygenation, suppressed viability, and induced apoptosis of HT-22 cells. (a, b, and c) HT-22 cells were pretreated without or with different concentrations of propofol for 2 hr prior to stimulation with hypoxia-reoxygenation (H/R). Cell viability was analyzed by MTT (a). Cell apoptosis was tested by TUNEL assay (b) and flow cytometry cell apoptosis assay (c, 15 μmol/l propofol). (d) Expression levels of Bax, caspase-3 (cleaved), and caspase-9 in HT-22 cells with different treatments were analyzed by Western blots. ([a]Differences were significant when compared with "control," $P < 0.05$. [b]Differences were significant when compared with "H/R," $P < 0.05$. [c]Differences were significant when compared with "H/R + 5 μmol/l," $P < 0.05$. [d]Differences were significant when compared with "H/R + 10 μmol/l," $P < 0.05$.)

elevated the apoptotic rate of hippocampal neurons by using the TUNEL assay (Figure 1(b)) and flow cytometry cell apoptosis assay (Figure 1(c)). However, apoptosis was suppressed in neurons that received propofol treatment. Consistently, protein expression levels of the apoptosis markers, namely, Bax, caspase-3, and caspase-9, were dramatically elevated in H/R neurons and restored when pretreated with propofol (Figure 1(d)).

3.2. Propofol Alleviated H/R-Induced Intracellular Calcium Accumulation and MMP Loss by Inhibiting Calcineurin Activity and FKBP12.6-RyR Disassociation. Since intracellular

calcium overload was recognized as an initiator of cell apoptosis [26], we detected the changes of intracellular calcium content in HT-22 cells that suffered from H/R with or without propofol. As shown in Figures 2(a) and 2(b), H/R treatment significantly increased intracellular calcium and impaired MMP. However, in propofol-treated neurons, both calcium accumulation and MMP loss were attenuated in a concentration-dependent manner. We further studied the mechanism of propofol-inhibited H/R-induced intracellular calcium accumulation. As a result, H/R treatment significantly increased the calcineurin activity, which was reversed by propofol in a concentration-dependent manner (Figure 2(c)). Furthermore, the co-IP assay found more FKBP12.6 disassociated from RyR3 after H/R treatment. However, when neurons were treated with propofol, FKBP12.6 molecules were recruited to bind with RyR3 (Figure 2(d)).

3.3. Downregulation of YAP Impaired Protective Effects of Propofol in Hippocampal Neuronal Apoptosis Induced by H/R. The potential involvement of YAP in propofol protecting hippocampal neurons from H/R-induced apoptosis was tested. Stable HT-22 cells with low expression of YAP were established using shRNA (Figure 3(a)). As a result, YAP knockdown significantly impaired propofol inhibiting HT-22 cell apoptosis induced by H/R (Figure 3(b)).

3.4. Propofol-Induced Dephosphorylation and Nuclear Translocation of YAP in HT-22 Cells. We tested whether propofol affected the dephosphorylation of YAP (dpYAP) at Ser127 in hippocampal neurons. Propofol induced dpYAP in a dose- and time-dependent manner in HT-22 cells, with the maximal effect at 4 hr and at 15 μM (Figure 4(a)). Concomitantly, propofol also induced YAP nuclear translocation (Figure 4(b)). Activated YAP stimulates the transcription of genes that promote cellular survival, such as survivin and Bcl2 [12, 27, 28]. We further tested the roles of propofol in expression of survivin and Bcl2. As shown in Figure 4(c), propofol significantly increased Bcl2 expression in both mRNA and protein levels. However, there was no change of survivin expression after propofol treatment in HT-22 cells.

3.5. Propofol Activated YAP through RhoA-Lats1. To determine whether propofol acts through the Hippo pathway core components to regulate YAP phosphorylation, we examined the effect of propofol on phosphorylation of MST1/2 (phospho-MST1 (Thr183)/MST2 (Thr180)) and Lats1 (phospho-LATS1 (Ser909)). We found that propofol had no detectable effect on MST1/2 phosphorylation in HT-22 cells. However, propofol dephosphorylated Lats1 (Figure 5(a)). Since G protein signaling has been proved to regulate Lats activation, we further tested the roles of G proteins in propofol-induced dephosphorylation of Lats1 (dpLats1) and YAP (dpYAP) by specific pharmacological inhibitors and dominant negative (dn) forms of G proteins. As shown in Figure 5(b), pertussis toxin (PTX, inhibitor of Gi protein), dn-Gq, dn-G_{12}, and dn-G_{13} did not affect propofol-induced dpLats1 and dpYAP. Interestingly, propofol-induced dpLats1 and dpYAP were abolished by the Rho inhibitor, C3 transferase, as well as by the Rho kinase (ROCK) inhibitor, Y27632, in HT-22 cells. We further determined which Rho kinases were involved. The results from cells transfected with different dn forms of Rho showed that RhoA was necessary for LPA-induced dpLats1 (Figure 5(c)).

3.6. No Interaction Was Observed between Calcineurin and YAP Activation in Hippocampal Neurons. Calcineurin is a member of the protein phosphatases (PP), also named protein phosphatase 2B (PP2B). Previous studies indicated that YAP activation could be mediated by PP, such as PP1 and PP2A [29, 30]. Thus, we aimed to clarify whether there is cross-talk between calcineurin and YAP activation in hippocampal neurons. As shown in Figure 6, inhibition of expression and activation of calcineurin did not affect YAP activation with or without propofol treatment, which indicated independent roles of calcineurin and YAP in propofol protection of hippocampal neurons from H/R-induced apoptosis.

4. Discussion

The hippocampus is functionally important in the central nervous system due to its vital role in memory and learning abilities of humans. Thus, hippocampal nerve cells damaged by I/R injury could lead to critical neurological dysfunction [31]. Recently, neuroprotective roles of propofol have been proved in an I/R model. However, fewer studies were designed to explore whether propofol could protect hippocampal neurons from I/R injury. In this study, a hypoxia-reoxygenation model stimulating I/R injury was used to treat hippocampal neurons. The results showed that treatment of propofol significantly suppressed apoptosis of hypoxia-reoxygenated hippocampal neurons.

Intracellular calcium overload is recognized as an initiator of cell apoptosis [26]. It is believed that I/R injury could induce the accumulation of intracellular calcium [32]. A recent study indicated that propofol could alleviate hippocampal neuronal injury induced by I/R through depressing calcium overload [6]. Consistently, our results showed a similar mechanism of propofol in protecting hippocampal neurons from I/R injury. The intracellular calcium concentration was regulated by calcium ion channels such as sarcoplasmic reticulum calcium ATPase (SERCA), ryanodine receptors (RyRs), and L-type calcium channel (LTCC). Calcineurin activity change was implicated in regulating the intracellular calcium by adjusting the opening of RyR via affecting FK506-binding protein 12.6 (FKBP12.6) [33, 34]. When encountering specific stimuli, the activity of calcineurin is upregulated to facilitate the splitting of the FKBP-RyR complex [35]. As a result, RyR channel opens to release calcium to induce calcium overload. In the present study, propofol was shown to decrease the enzymatic activity of calcineurin in hypoxia-reoxygenated hippocampal neurons, resulting in disassociating FKBP12.6 from RyR3 to close the channel, which reduced the intracellular calcium overload.

Propofol, as a widely used intravenous short-acting anesthetic, has been proved to regulate multiple intracellular signaling pathways [8]. Thus, we presented the hypothesis that

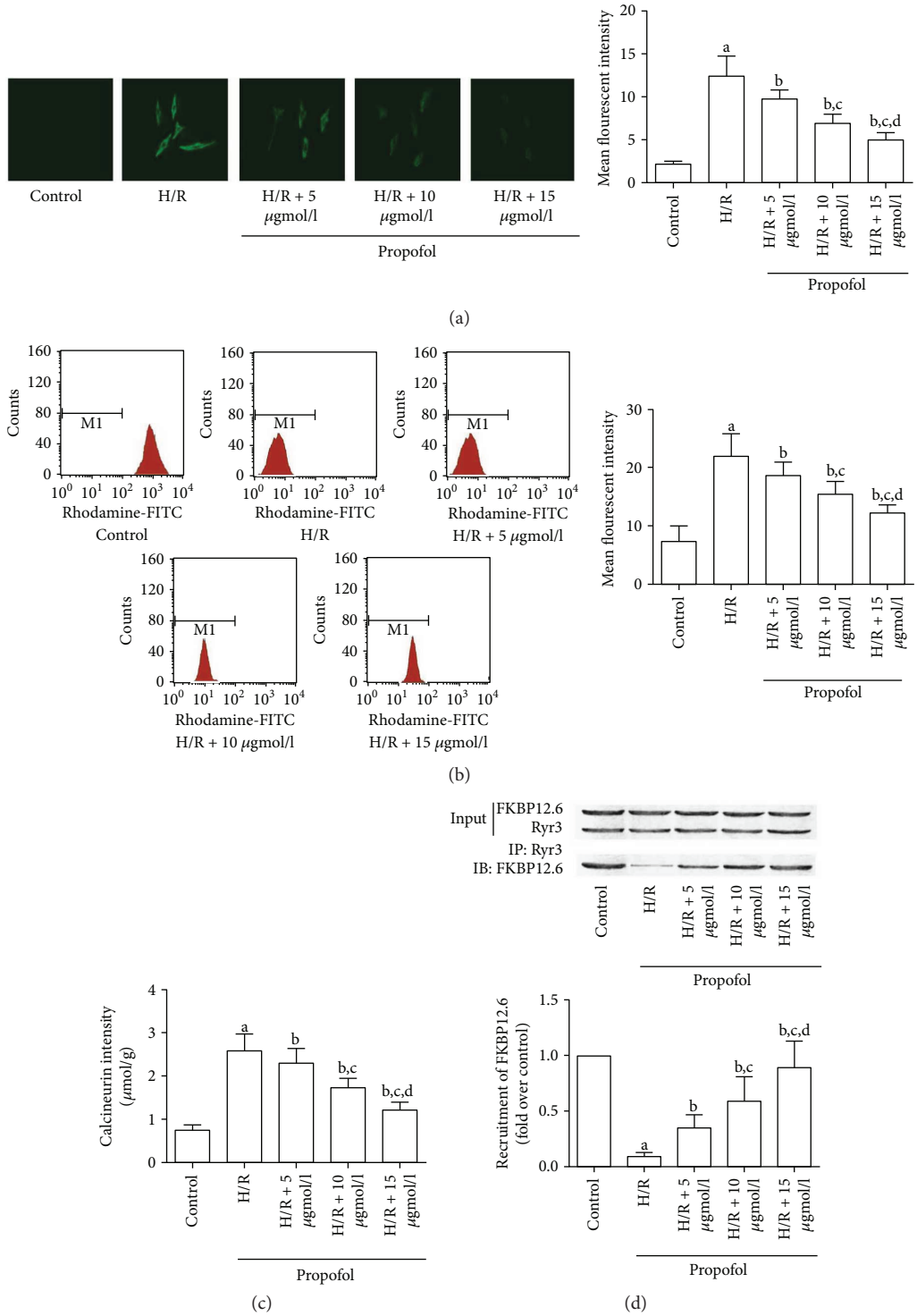

Figure 2: Propofol reversed H/R-induced intracellular calcium accumulation and MMP loss by inhibiting calcineurin activity and FKBP12.6-RyR disassociation. HT-22 cells were pretreated without or with different concentrations of propofol for 2 hr prior to stimulation by H/R. (a) Intracellular calcium was assessed by the calcium indicator, Fura-2/AM. Typical images of Fura-2A/M staining were captured. Columns indicate the measured mean fluorescent intensities of Fura-2A/M staining in HT-22 cells. (b) MMP measurements were detected by flow cytometry. Columns indicated the measured mean fluorescent intensities of rhodamine 123 staining in HT-22 cells. (c) Columns demonstrated the detected enzymatic activity of calcineurin in HT-22 cells. (d) FKBP12.6-RyR disassociation in HT-22 cells was detected by coimmunoprecipitation. RyR3 was immunoprecipitated with FKBP12.6 antibody and immunoblotted with FKBP12.6 antibody. Columns indicate the molecular recruitment of FKBP12.6. ([a]Differences were significant when compared with "control," $P < 0.05$. [b]Differences were significant when compared with "H/R," $P < 0.05$. [c]Differences were significant when compared with "H/R + 5 μmol/l," $P < 0.05$. [d]Differences were significant when compared with "H/R + 10 μmol/l," $P < 0.05$.)

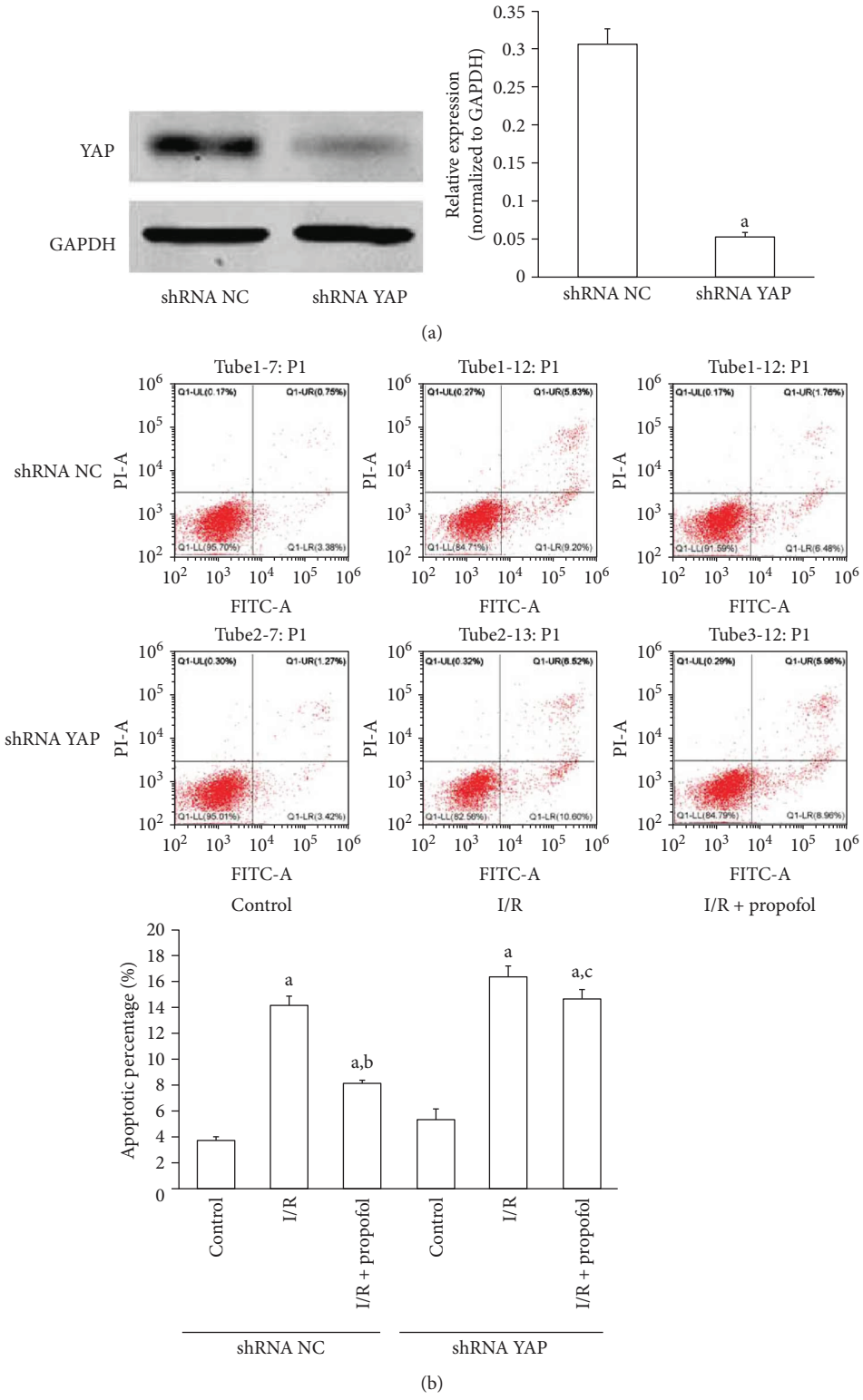

Figure 3: Suppression of YAP impaired protective effects of propofol in HT-22 cell apoptosis induced by H/R. (a) Reduced YAP expression by YAP shRNA in HT-22 cells detected by Western blots. [a]$P < 0.001$ versus shRNA NC. (b) The effect of downregulation of YAP on cell apoptosis induced by H/R with or without propofol (15 μmol/l) pretreatment in HT-22 cells (conducted 48 hr post shRNA treatment). The results are from three independent experiments. ([a]Differences were significant when compared with "control," $P < 0.05$. [b]Differences were significant when compared with "H/R," $P < 0.05$. [c]Differences were not significant when compared with "H/R," $P > 0.05$.)

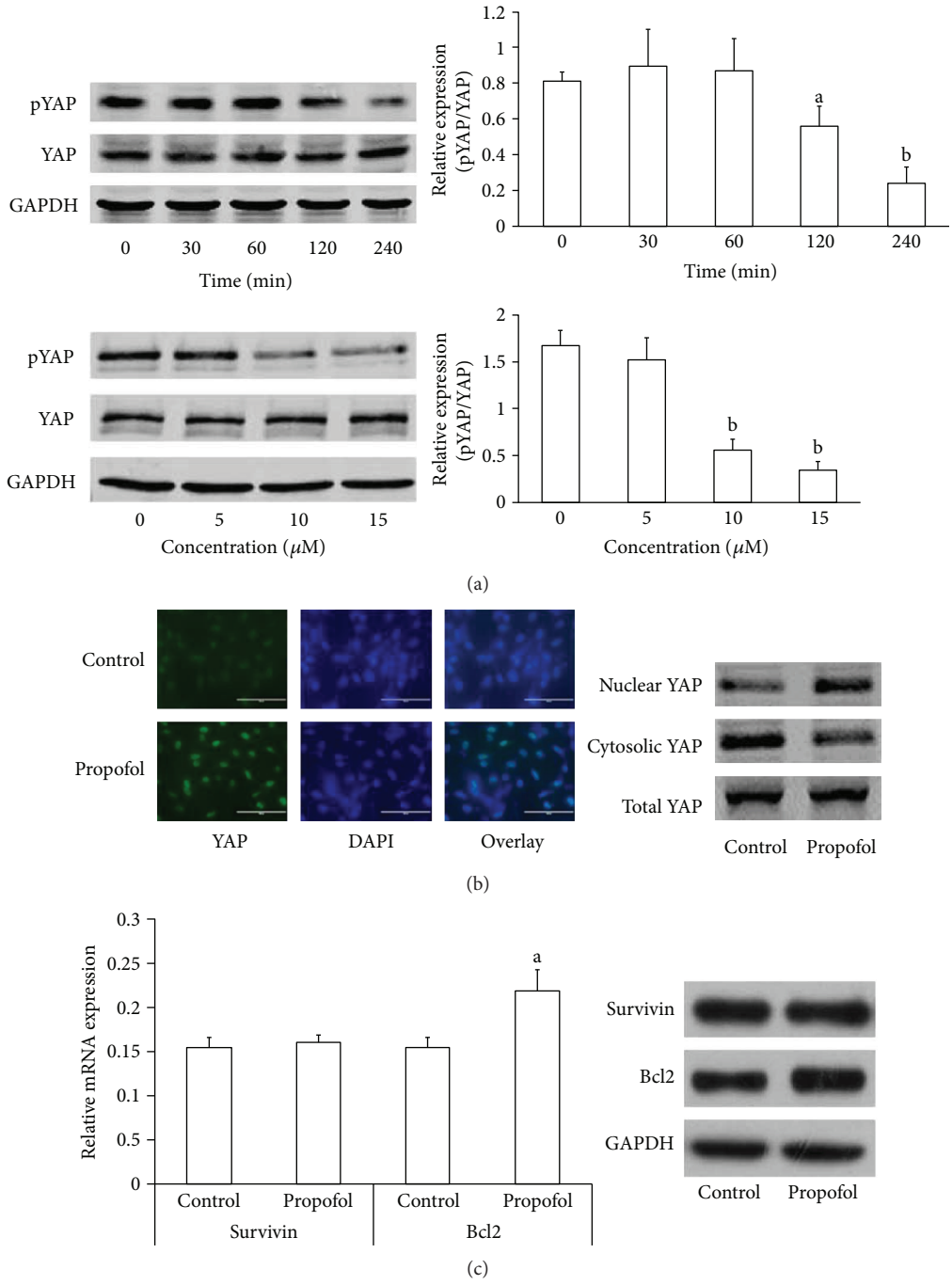

Figure 4: Propofol induced dephosphorylation and nuclear translocation of YAP in HT-22 cells. (a) HT-22 cells were starved for 16 hr, then treated with propofol (15 μmol/l) for different times or with different concentrations of propofol for 4 hr. Western blots were used to analyze the expression of phosphorylated YAP and total YAP. Representative results are shown from three independent experiments. $^{a}P < 0.01$ versus 0 min, $^{b}P < 0.001$ versus 0 min. (b) Propofol-induced (15 μmol/l for 4 hr) YAP nuclear translocation is shown in starved HT-22 cells by immunofluorescence staining and Western blots. Green: YAP; blue: DAPI. (c) Starved HT-22 cells treated with 15 μmol/l propofol for 12 hr, then mRNA and protein levels of survivin and Bcl2 were detected by real-time PCR and Western blot. $^{a}P < 0.05$ versus control.

other signaling pathways may also be involved in propofol's neuroprotective roles. Interestingly, we demonstrated that expression of YAP was crucial for propofol to protect hippocampal neuronal apoptosis from H/R injury. In addition, propofol could activate YAP by dephosphorylating YAP and promoting nuclear translocation. As a transcriptional coactivator, activated YAP can promote stem/progenitor cell self-renewal, drive cell migration and proliferation, and suppress cell apoptosis mainly through binding with TEAD in the nucleus [27]. Recent deep genome-wide sequencing led to multiple target genes of YAP. Among them, survival genes (e.g., survivin and Bcl2), proliferation-associated genes (e.g.,

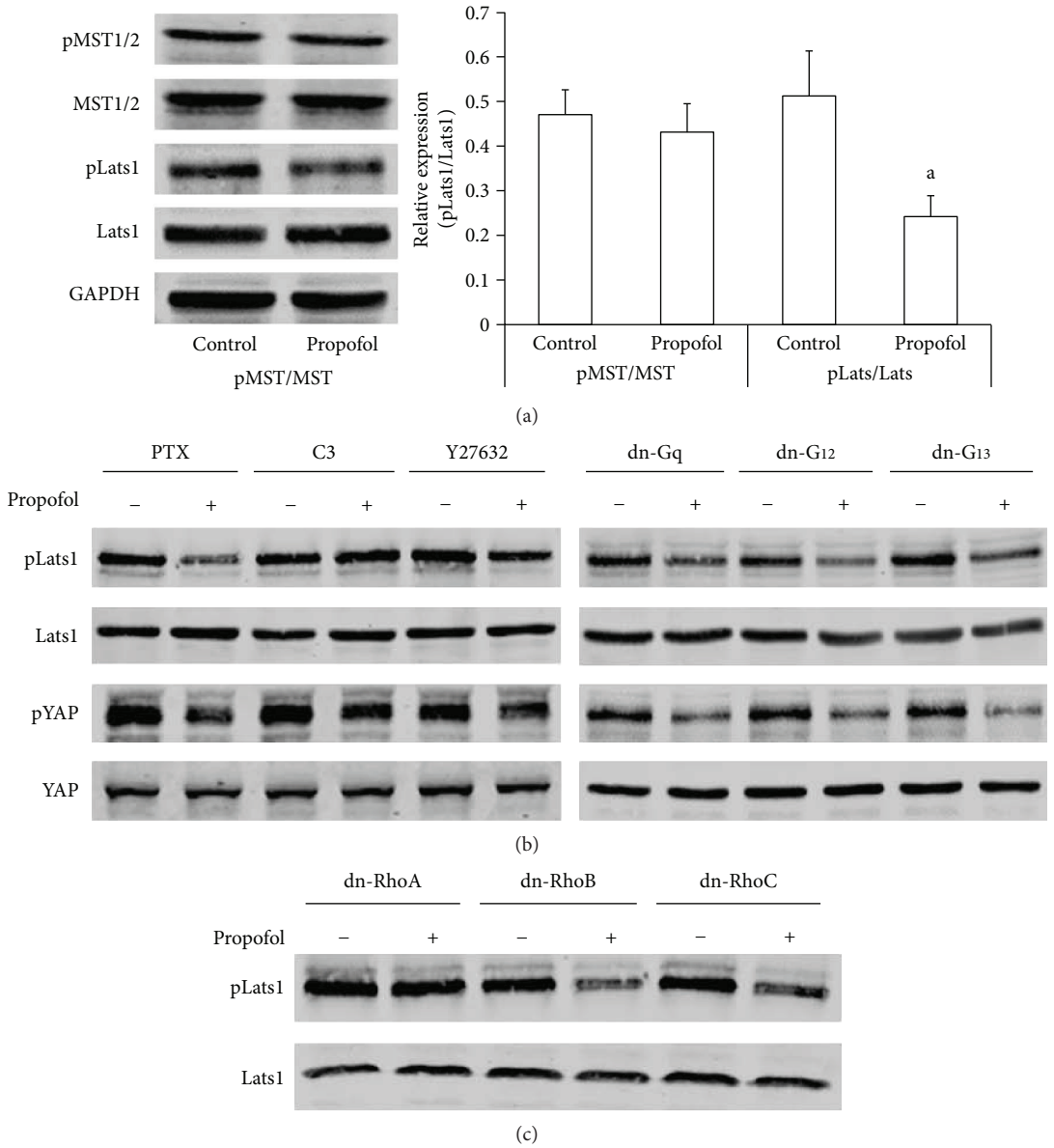

Figure 5: Propofol dephosphorylated YAP through the RhoA-Lats1 signaling pathway. (a) Starved HT-22 cells were treated with propofol (15 μmol/l) for 4 hr, and pMST1/2, total MST1/2, pLats1, and Lats1 were analyzed by Western blot. Representative results are shown from three independent experiments. $^{a}P < 0.001$ versus control. (b) Cells were pretreated with PTX (100 ng/ml, 16 hr), C3 transferase (1 μg/ml for 2 hr), and Y27632 (10 μmol/l for 2 hr) or transfected with different dn plasmids for 48 hr, then starved and treated with propofol (15 μmol/l for 4 hr). Cell lysates were analyzed by Western blot. Representative results are shown. (c) HT-22 cells were transfected with different dn-Rho plasmids, then starved and treated with propofol (15 μmol/l for 4 hr). Expression of pLats1 and Lats1 was analyzed by Western blot.

Ctgf, Cyr61, c-Myc, Foxm1, and miR-130), differentiation-associated genes (e.g., Oct4, Nanog, Cdx2, and Pax3), and migration/invasion-associated genes (e.g., Ctgf, Cyr61, and Zeb2) were sorted [27]. Since propofol has been proved to promote hippocampal neuronal survival and inhibit apoptosis in our research, herein, we further found that propofol could induce expression of Bcl2 (rather than survivin), which is specifically considered as an important antiapoptotic protein.

YAP is a type of transcriptional coactivator with a PDZ-binding motif. Its dephosphorylated morphology could translocate into the nucleus to bind the TEAD transcription factor family and induce expression of a wide range of genes [27]. YAP activation was initially identified to be negatively regulated by Hippo pathway kinases via phosphorylation of Ser127, which results in YAP 14-3-3 binding, cytoplasmic retention, and degradation [36]. Previous studies showed that YAP phosphorylation could be mediated by cell contact, mechanical signals, stress signals, cell polarity/architecture, and cell cycle. However, the extracellular soluble regulators of YAP were barely known, until Yu et al. found bioactive lipids, LPA, and sphingosine-1-phosphate

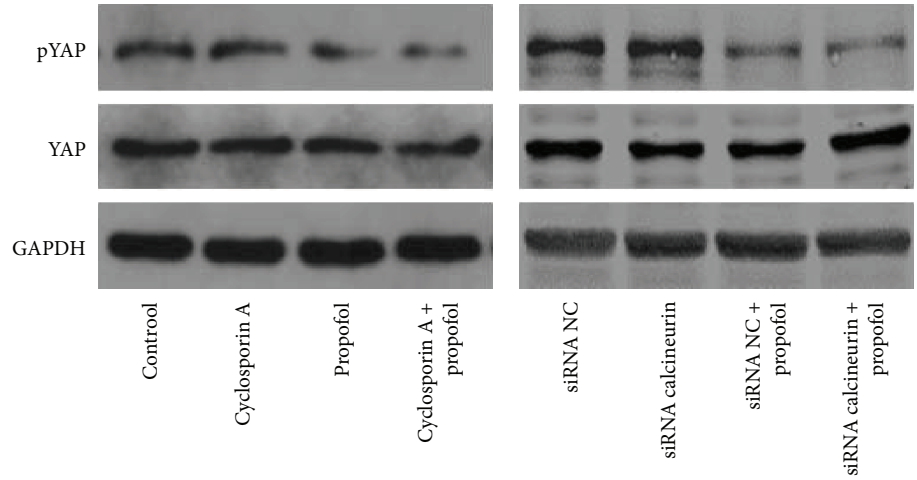

Figure 6: Calcineurin did not affect YAP activation in hippocampal neurons. HT-22 cells were pretreated with cyclosporin (1 μmol/l for 2 hr) or transfected with different calcineurin shRNAs for 48 hr, then starved and treated with propofol (15 μmol/l for 4 hr). Cell lysates were analyzed by Western blot to detect expression of YAP and pYAP.

(S1P) as extracellular regulators of YAP in mammary cell lines [37]. In addition, several hormones have been proved to regulate YAP, such as epinephrine, estrogen, and glucagon [38]. In the present study, we demonstrated that propofol acted as another extracellular soluble regulator of YAP. Propofol could dephosphorylate Ser127 of YAP, which resulted in YAP activation and nuclear translocation. Mostly, soluble factors regulate YAP via the Hippo pathway by their cognate G-protein-coupled receptors and associated G-protein subunits to engage the small GTPases, RhoA, and ROCK, leading to alterations of activation of Lats1/2 [38]. Consistently, our data indicated propofol dephosphorylated Lats1/2 and YAP partly through RhoA and ROCK. However, the large G proteins, neither Gi, Gq, nor $G_{12/13}$, were not involved, indicating that propofol acted independently of the G-protein-coupled receptor to regulate YAP activity. Thus, the details of propofol in regulation of small GTPases in hippocampal neurons need more exploration.

In the classical Hippo pathway, Lats1/2 is directly regulated by MST1/2. Recently, studies found that several phosphokinases and phosphatases were considered as upstream regulators of Lats1, which is parallel to MST1/2, such as PKA, NF2, MAP4K4, and AMPK. Interestingly, one study quantitatively analyzed global phosphoproteome alterations of HT-22 cells after propofol treatment revealed that propofol could mediate phosphorylation of NF2 and MAP4K4 [39]. Our data showed that propofol-induced dephosphorylation of Lats1/2 and YAP was partly absorbed by inhibition of RhoA. Thus, we speculated that propofol could also activate YAP through the NF2-Lats1/2 and MAP4K4-Lats1/2 pathways.

5. Conclusion

Our results indicate that propofol could protect hippocampal neurons from I/R injury through two independent signaling pathways, including the calcineurin/FKBP12.6-RyR/calcium overload pathway and the RhoA/Lats1/YAP/Bcl-2 pathway. This work further supports the potential therapeutic role of propofol against I/R in the nervous system.

Data Availability

The data used to support the findings of this study are included within the article. Alternatively, the data are also available from the corresponding author upon request (caihui9@stu.xjtu.edu.cn).

Conflicts of Interest

The authors have no conflicts of interest to declare.

Authors' Contributions

Xiaojun Li and Li Yao contributed equally to this work.

Acknowledgments

This study was supported by a grant from the National Natural Science Foundation of China (no. 81502295).

References

[1] G. J. Hankey, "Stroke," *The Lancet*, vol. 389, no. 10069, pp. 641–654, 2017.

[2] L. K. Sevick, S. Ghali, M. D. Hill et al., "Systematic review of the cost and cost-effectiveness of rapid endovascular therapy for acute ischemic stroke," *Stroke*, vol. 48, no. 9, pp. 2519–2526, 2017.

[3] X. R. Han, X. Wen, Y. J. Wang et al., "Protective effects of microRNA-431 against cerebral ischemia-reperfusion injury in rats by targeting the Rho/Rho-kinase signaling pathway," *Journal of Cellular Physiology*, vol. 233, no. 8, pp. 5895–5907, 2018.

[4] Y. Yang, X. Li, L. Zhang, L. Liu, G. Jing, and H. Cai, "Ginsenoside Rg1 suppressed inflammation and neuron apoptosis by activating PPARγ/HO-1 in hippocampus in rat model of

cerebral ischemia-reperfusion injury," *International Journal of Clinical and Experimental Pathology*, vol. 8, no. 3, pp. 2484–2494, 2015.

[5] Y. Lu, W. Chen, C. Lin et al., "The protective effects of propofol against $CoCl_2$-induced HT22 cell hypoxia injury via PP2A/CAMKIIα/nNOS pathway," *BMC Anesthesiology*, vol. 17, no. 1, p. 32, 2017.

[6] H. Wang, S. Zheng, M. Liu et al., "The effect of propofol on mitochondrial fission during oxygen-glucose deprivation and reperfusion injury in rat hippocampal neurons," *PLoS One*, vol. 11, no. 10, article e0165052, 2016.

[7] T. Tao, C. L. Li, W. C. Yang et al., "Protective effects of propofol against whole cerebral ischemia/reperfusion injury in rats through the inhibition of the apoptosis-inducing factor pathway," *Brain Research*, vol. 1644, pp. 9–14, 2016.

[8] I. Vasileiou, T. Xanthos, E. Koudouna et al., "Propofol: a review of its non-anaesthetic effects," *European Journal of Pharmacology*, vol. 605, no. 1-3, pp. 1–8, 2009.

[9] J. Zhang, Y. Xia, Z. Xu, and X. Deng, "Propofol suppressed hypoxia/reoxygenation-induced apoptosis in HBVSMC by regulation of the expression of Bcl-2, Bax, Caspase3, Kir6.1, and p-JNK," *Oxidative Medicine and Cellular Longevity*, vol. 2016, Article ID 1518738, 11 pages, 2016.

[10] S. Lemoine, L. Zhu, S. Gress, J.-L. Gérard, S. Allouche, and J.-L. Hanouz, "Mitochondrial involvement in propofol-induced cardioprotection: an in vitro study in human myocardium," *Experimental Biology and Medicine*, vol. 241, no. 5, pp. 527–538, 2016.

[11] H. S. Noh, I. W. Shin, J. H. Ha, Y. S. Hah, S. M. Baek, and D. R. Kim, "Propofol protects the autophagic cell death induced by the ischemia/reperfusion injury in rats," *Molecules and Cells*, vol. 30, no. 5, pp. 455–460, 2010.

[12] B. Zhao, L. Li, Q. Lei, and K. L. Guan, "The Hippo-YAP pathway in organ size control and tumorigenesis: an updated version," *Genes & Development*, vol. 24, no. 9, pp. 862–874, 2010.

[13] M. Hoshino, M. L. Qi, N. Yoshimura et al., "Transcriptional repression induces a slowly progressive atypical neuronal death associated with changes of YAP isoforms and p73," *The Journal of Cell Biology*, vol. 172, no. 4, pp. 589–604, 2006.

[14] N. Morimoto, M. Nagai, K. Miyazaki et al., "Progressive decrease in the level of YAPdeltaCs, prosurvival isoforms of YAP, in the spinal cord of transgenic mouse carrying a mutant SOD1 gene," *Journal of Neuroscience Research*, vol. 87, no. 4, pp. 928–936, 2009.

[15] X. Cao, S. L. Pfaff, and F. H. Gage, "YAP regulates neural progenitor cell number via the TEA domain transcription factor," *Genes & Development*, vol. 22, no. 23, pp. 3320–3334, 2008.

[16] Y. T. Lin, J. Y. Ding, M. Y. Li, T. S. Yeh, T. W. Wang, and J. Y. Yu, "YAP regulates neuronal differentiation through Sonic hedgehog signaling pathway," *Experimental Cell Research*, vol. 318, no. 15, pp. 1877–1888, 2012.

[17] H. Zhang, M. Deo, R. C. Thompson, M. D. Uhler, and D. L. Turner, "Negative regulation of Yap during neuronal differentiation," *Developmental Biology*, vol. 361, no. 1, pp. 103–115, 2012.

[18] A. Lavado, Y. He, J. Pare et al., "Tumor suppressor Nf2 limits expansion of the neural progenitor pool by inhibiting Yap/Taz transcriptional coactivators," *Development*, vol. 140, no. 16, pp. 3323–3334, 2013.

[19] S. Moleirinho, C. Patrick, A. M. Tilston-Lünel et al., "Willin, an upstream component of the hippo signaling pathway, orchestrates mammalian peripheral nerve fibroblasts," *PLoS One*, vol. 8, no. 4, article e60028, 2013.

[20] X. F. Jia, F. Ye, Y. B. Wang, and D. X. Feng, "ROCK inhibition enhances neurite outgrowth in neural stem cells by upregulating YAP expression in vitro," *Neural Regeneration Research*, vol. 11, no. 6, pp. 983–987, 2016.

[21] F. Yan, X. Tan, W. Wan et al., "ErbB4 protects against neuronal apoptosis via activation of YAP/PIK3CB signaling pathway in a rat model of subarachnoid hemorrhage," *Experimental Neurology*, vol. 297, pp. 92–100, 2017.

[22] C. Zhu, L. Li, and B. Zhao, "The regulation and function of YAP transcription co-activator," *Acta Biochimica et Biophysica Sinica*, vol. 47, no. 1, pp. 16–28, 2015.

[23] G. Santinon, A. Pocaterra, and S. Dupont, "Control of YAP/TAZ activity by metabolic and nutrient-sensing pathways," *Trends in Cell Biology*, vol. 26, no. 4, pp. 289–299, 2016.

[24] X. Chen, Y. M. Du, F. Xu, D. Liu, and Y. L. Wang, "Propofol prevents hippocampal neuronal loss and memory impairment in cerebral ischemia injury through promoting PTEN degradation," *Journal of Molecular Neuroscience*, vol. 60, no. 1, pp. 63–70, 2016.

[25] M. Chen, H. Y. Sun, P. Hu et al., "Activation of BKca channels mediates hippocampal neuronal death after reoxygenation and reperfusion," *Molecular Neurobiology*, vol. 48, no. 3, pp. 794–807, 2013.

[26] Y. Meng, W.-Z. Li, Y.-W. Shi, B.-F. Zhou, R. Ma, and W.-P. Li, "Danshensu protects against ischemia/reperfusion injury and inhibits the apoptosis of H9c2 cells by reducing the calcium overload through the p-JNK-NF-κB-TRPC6 pathway," *International Journal of Molecular Medicine*, vol. 37, no. 1, pp. 258–266, 2016.

[27] Z. Meng, T. Moroishi, and K. L. Guan, "Mechanisms of Hippo pathway regulation," *Genes & Development*, vol. 30, no. 1, pp. 1–17, 2016.

[28] Z. Zhang, H. Wang, Z. Jin et al., "Downregulation of survivin regulates adult hippocampal neurogenesis and apoptosis, and inhibits spatial learning and memory following traumatic brain injury," *Neuroscience*, vol. 300, pp. 219–228, 2015.

[29] Y. Zheng, B. Liu, L. Wang, H. Lei, K. D. Pulgar Prieto, and D. Pan, "Homeostatic control of Hpo/MST kinase activity through autophosphorylation-dependent recruitment of the STRIPAK PP2A phosphatase complex," *Cell Reports*, vol. 21, no. 12, pp. 3612–3623, 2017.

[30] H. Cai and Y. Xu, "The role of LPA and YAP signaling in long-term migration of human ovarian cancer cells," *Cell Communication and Signaling: CCS*, vol. 11, no. 1, p. 31, 2013.

[31] R. Wei, R. Zhang, Y. Xie, L. Shen, and F. Chen, "Hydrogen suppresses hypoxia/reoxygenation-induced cell death in hippocampal neurons through reducing oxidative stress," *Cellular Physiology and Biochemistry*, vol. 36, no. 2, pp. 585–598, 2015.

[32] E. R. Vasques, J. E. M. Cunha, A. M. M. Coelho et al., "Trisulfate disaccharide decreases calcium overload and protects liver injury secondary to liver ischemia/reperfusion," *PLoS One*, vol. 11, no. 2, 2016.

[33] M.-T. Matsoukas, Á. Aranguren-Ibáñez, T. Lozano et al., "Identification of small-molecule inhibitors of calcineurin-NFATc signaling that mimic the PxIxIT motif of calcineurin binding partners," *Science Signaling*, vol. 8, no. 382, p. ra63, 2015.

[34] B. Liao, Y. M. Zheng, V. R. Yadav, A. S. Korde, and Y. X. Wang, "Hypoxia induces intracellular Ca2+ release by causing

reactive oxygen species-mediated dissociation of FK506-binding protein 12.6 from ryanodine receptor 2 in pulmonary artery myocytes," *Antioxidants & Redox Signaling*, vol. 14, no. 1, pp. 37–47, 2011.

[35] Z. Liu, H. Cai, H. Zhu et al., "Protein kinase RNA-like endoplasmic reticulum kinase (PERK)/calcineurin signaling is a novel pathway regulating intracellular calcium accumulation which might be involved in ventricular arrhythmias in diabetic cardiomyopathy," *Cellular Signalling*, vol. 26, no. 12, pp. 2591–2600, 2014.

[36] K. Wang, C. Degerny, M. Xu, and X. J. Yang, "YAP, TAZ, and Yorkie: a conserved family of signal-responsive transcriptional coregulators in animal development and human disease," *Biochemistry and Cell Biology*, vol. 87, no. 1, pp. 77–91, 2009.

[37] F. X. Yu, B. Zhao, N. Panupinthu et al., "Regulation of the Hippo-YAP pathway by G-protein-coupled receptor signaling," *Cell*, vol. 150, no. 4, pp. 780–791, 2012.

[38] K. I. Watt, K. F. Harvey, and P. Gregorevic, "Regulation of tissue growth by the mammalian Hippo signaling pathway," *Frontiers in Physiology*, vol. 8, p. 942, 2017.

[39] H. Zhang, J. Ye, Z. Shi, C. Bu, and F. Bao, "Quantitative analyses of the global proteome and phosphoproteome reveal the different impacts of propofol and dexmedetomidine on HT22 cells," *Scientific Reports*, vol. 7, article 46455, 2017.

Hindawi
Oxidative Medicine and Cellular Longevity
Volume 2018, Article ID 7365490, 9 pages
https://doi.org/10.1155/2018/7365490

Research Article

Decreased Oxidative Stress in Male Patients with Active Phase Ankylosing Spondylitis Who Underwent Whole-Body Cryotherapy in Closed Cryochamber

Agata Stanek[1], **Armand Cholewka**[2], **Tomasz Wielkoszyński**[3], **Ewa Romuk**[3] and **Aleksander Sieroń**[1]

[1]*Department of Internal Medicine, Angiology and Physical Medicine, School of Medicine with the Division of Dentistry in Zabrze, Medical University of Silesia, Batorego Street 15, 41-902 Bytom, Poland*
[2]*Department of Medical Physics, Chelkowski Institute of Physics, University of Silesia, 4 Uniwersytecka St., 40-007 Katowice, Poland*
[3]*Department of Biochemistry, School of Medicine with the Division of Dentistry in Zabrze, Medical University of Silesia, Jordana 19 St., 41-808 Zabrze, Poland*

Correspondence should be addressed to Agata Stanek; astanek@tlen.pl

Received 14 January 2018; Accepted 10 April 2018; Published 2 May 2018

Academic Editor: Karolina Szewczyk-Golec

Objective. The aim of the study was to estimate the impact of whole body cryotherapy (WBC) on oxidative stress when performed in a closed cryochamber on patients with ankylosing spondylitis (AS). *Material and methods*. The effect of ten WBC procedures lasting 3 minutes a day with a subsequent 60-minute session kinesiotherapy on oxidative stress in male AS patients (WBC group $n = 16$) was investigated. To assess the disease activity, the Bath Ankylosing Spondylitis Diseases Activity Index (BASDAI) and Bath Ankylosing Spondylitis Functional Index (BASFI) were calculated. The WBC group was compared to the kinesiotherapy only (KT; $n = 16$) group. The routine parameters of oxidative stress (antioxidant enzymatic and nonenzymatic antioxidant status, lipid peroxidation products, total oxidative status (TOS), and oxidative stress index (OSI)) were estimated one day before the beginning and one day after the completion of the research program. *Results*. After the completion of the treatment in the WBC group, a significant decrease of oxidative stress markers (TOS and OSI) and a significant increase of total antioxidant status were observed. The erythrocyte activity of glutathione peroxidase, glutathione reductase decreased significantly in both groups, but the differences of activity of that enzymes prior to post treatment values (Δ) in the KT group were significantly higher as compared to the WBC group. The activity of erythrocyte catalase and plasma ZnCu isoenzyme of superoxide dismutase showed a decreased tendency; erythrocyte total superoxide dismutase activity showed an increased tendency in the WBC group after the completion of the treatment. The BASDAI and BASFI decreased significantly in both groups, but the differences of value indexes prior to post treatment (Δ) were significantly higher in the WBC than KT group. *Conclusion*. WBC performed in a closed cryochamber decreases oxidative stress and improves BASDAI and BASFI indexes in male patients during the active phase of ankylosing spondylitis.

1. Introduction

Ankylosing spondylitis (AS) is a chronic, usually progressive inflammatory rheumatic disease with severe complications that include sacroiliitis, spondylodesis, peripheral arthritis, and a range of extra-articular manifestations, ultimately leading to impacts upon mobility and societal functioning [1]. The pathogenesis of AS is still unknown, but lately it has been postulated that oxidative stress might be involved in the disease [2–6]. Oxidative stress can induce acute or chronic inflammation through the activation of multiple pathways. When oxidative stress appears as a primary disorder, inflammation develops as a secondary disorder and further enhances oxidative stress [7].

In addition to pharmacological treatment, physiotherapy plays an important role in the treatment of AS patients. They

are commonly used to maintain spinal mobility, decrease spinal deformity, and reduce pain as well as improve patient's functioning and quality of life [8, 9].

More and more frequently, whole-body cryotherapy (WBC), as a method of physical medicine, is used in the treatment of rheumatic and inflammatory diseases and muscle spasticity [10]. During WBC treatment, the subject is exposed to extreme cold temperatures (below −100°C) for a short period of time (maximum up to 3 minutes) [11, 12]. The action of cryogenic temperatures causes several favorable physiological reactions such as an analgesic, anti-inflammatory, and a circulatory effect [12–15]. Cryogenic temperatures applied to the whole body, apart from the aforementioned effects, also have significant influence on the psyche, the immune, and endocrine systems [15–18].

However, little is still known about the mechanisms of WBC treatment in AS patients. So far, it has been showed that WBC procedures with subsequent kinesiotherapy may help to decrease pain and inflammatory parameters, improve BASDAI (Bath Ankylosing Spondylitis Diseases Activity Index) and BASFI (Bath Ankylosing Spondylitis Functional Index) indexes, and some spinal mobility parameters [19–21]. It has been also proven that in AS patients, WBC treatment performed in a cryochamber with cold retention may decrease oxidative stress and lipid profile parameters [22].

However, the effect of WBC treatment may depend on the type of cryochamber in which procedures are performed [21, 22]. The most popular cryochambers are chambers with cold retention and closed ones (called Wroclawski type or two-step cryochamber).

In the cryochamber with cold retention, in order to make use of the "cold deposit" phenomenon, the cryogenic chamber is placed about 2.5 m under floor level. It is cooled by synthetic liquid air. The subjects enter the therapy chamber by stairs which constitute a mild adaptive area. An open antechamber (vestibule) is located at the base of the stairs. The vestibule and the proper chamber are separated by double swing doors [23, 24].

The closed Wroclawski-type cryochamber is placed at floor level. It is usually cooled by liquid nitrogen. The vestibule and the proper chamber are located on the same level and separated by a lockable door [24].

But until now, there are no papers in available literature on the impact of WBC treatment performed in a closed cryochamber (Wroclawski type) on oxidative stress in AS patients.

In light of the above findings, and taking account that WBC treatment may be performed in different types of cryochambers, the primary aim of the study was to assess the influence of WBC performed in a closed cryochamber (Wroclawski type) on oxidative stress in AS patients during the active phase.

2. Materials and Methods

2.1. Subjects. The research was conducted with the consent of the Bioethical Committee of the Medical University of Silesia in Katowice (permission number NN-6501-93/I/07), Poland. All examined subjects provided written informed consent. All investigations were conducted according to the principles expressed in the Declaration of Helsinki (1964).

The research involved a group of 32 nonsmoking male patients with ankylosing spondylitis who were divided randomly by a physician into two groups with an allocation ratio 1 : 1. The first group consisted of 16 AS patients exposed to whole-body cryotherapy procedures with subsequent kinesiotherapy (WBC group, mean age 46.63 ± 1.5 years). The second group consisted of 16 AS patients exposed only to kinesiotherapy procedures (KT group, mean age 45.94 ± 1.24 years). There was no significant difference in the mean age, BMI, BASDAI, BASFI, and treatment between these groups.

Male patients who were successfully enrolled in the research had a definite diagnosis of AS, did not suffer from any other diseases, had no associated pathologies, and had no treatment with disease-modifying antirheumatic drugs (DMARDs), biologic agents, or steroids. The AS patients were treated with doses of nonsteroidal anti-inflammatory drugs (NSAIDs), which were not altered within one month before the beginning of the study and during it. All the patients included in the trial fulfilled the modified New York Criteria for definite diagnosis of AS, which serves as the basis for the ASAS/EULAR recommendations [25]. The final selection for the study included only HLA B27 positive patients, who exhibited II and III radiographic grades of sacroiliac joint disease and attended a consulting unit in a health resort in the period of subsidence of acute clinical symptoms, in order to qualify for physiotherapy treatment. The demographic characteristics of the subjects is shown in Table 1.

Before the research, each patient was examined by a physician to exclude any coexisting diseases as well as any contraindications for WBC procedures. Prior to the research, a resting electrocardiogram was performed in all the patients, and before each session of WBC, the blood pressure was measured for each patient [24].

The patients from both groups were asked to abstain from alcohol, drugs, and any immunomodulators, immunostimulators, hormones, vitamins, minerals, or other substances with antioxidant properties for 4 weeks before the study. All the patients were also asked to refrain from the consumption of caffeine 12 hours prior to laboratory analyses. The diet of the patients was not modified.

2.2. Scheme of Whole-Body Cryotherapy and Kinesiotherapy Procedures. Depending on the group, the AS patients were exposed either to a cycle of WBC procedures lasting 3 minutes a day with a subsequent 60-minute session of kinesiotherapy or 60-minute session of kinesiotherapy only for 10 consecutive days excluding the weekend at the same time in the morning.

The WBC procedures were performed in a cryochamber Wroclawski type (closed cryochamber) cooled by liquid nitrogen (produced by Creator, Poland), which consisted of separated two compartments: the antechamber (vestibule) and the proper chamber. The temperature in the antechamber was −60°C, whereas in the proper chamber, it reached −120°C. The subjects entered the chamber in groups of four. Each

Table 1: Demographic characteristics of the research subjects.

Characteristic	WBC group ($n = 16$)	Kinesiotherapy group ($n = 16$)	p value
Age, years, mean (SD)	46.63 ± 1.5	45.94 ± 1.24	0.114
Sex M/F	16/0	16/0	—
BMI, kg/m^2, mean (SD)	24.35 ± 4.4	23.76 ± 6.8	0.968
BASDAI	5.34 ± 1.72	5.28 ± 1.71	0.880
BASFI	5.17 ± 2.28	5.01 ± 2.06	0.940
Smoking (yes/no)	0/16	0/16	—
Medication			
NSAID (yes/no)	16/0	16/0	—
DMARD (yes/no)	0/16	0/16	—
Biological agents (yes/no)	0/16	0/16	—

SD: standard deviation; BMI: body mass index; BASDAI: the Bath Ankylosing Spondylitis Diseases Activity Index; BASFI: the Bath Ankylosing Spondylitis Functional Index; NSAID: nonsteroidal anti-inflammatory drug; DMARD: disease-modifying antirheumatic drug.

entry to the cryochamber was preceded by a 30-second adaptation period in the vestibule at −60°C. After adaptation, the subjects stepped into the proper chamber, where they were exposed to cryogenic temperatures for 3 minutes. During the WBC procedure, all the patients were dressed in swimsuits, they wore cotton socks and gloves and wooden shoes, and their mouths and noses were protected by dust masks and their ears by ear-protectors. No jewelry, glasses, and contact lenses were allowed. Each subject was informed about the rules: the need for slow, shallow breathing (short nasal inhalation and longer oral exhalation), and the way to move about (slow walking in circles, one after the other). During the WBC procedure, they were also not allowed to touch each other.

Immediately after leaving the cryogenic chamber, the AS patients underwent kinesiotherapy lasting for one hour. The program of kinesiotherapy was the same for all the patients in both groups. Kinesiotherapy procedures included range-of-motion exercises of the spine and major joints (including the hip, knee, ankle, shoulder, elbow, and wrist). Chest expansion and breathing exercises were also included. Apart from range-of-motion exercise, the AS patients received strengthening exercises of the muscles of the major body parts (spine, arms, and thighs) as well as aerobic exercise (including cycling and fast walking). All the exercises were carried out under the supervision of physiotherapists [22].

All the patients completed the research program and no complications or side effects related to the WBC procedures were observed.

2.3. Blood Sample Collection. Blood samples of all the subjects were collected in the morning before the first meal one day before the beginning and one day after the completion of the research program. Samples of whole blood (5 ml) were drawn from the basilic vein and then collected into tubes containing ethylenediaminetetraacetic acid (Sarstedt, S-Monovette with 1.6 mg/ml EDTA-K_3) and into tubes with a clot activator (Sarstedt, S-Monovette). The blood samples were centrifuged (10 min., 900g 4°C) and then the plasma and serum were immediately separated and stored at the temperature of −75°C, until biochemical analyses could be performed. The red blood cells retained from the removal of EDTA plasma were rinsed with isotonic salt solution, and then 10% of the hemolysates were prepared for further analyses. The hemoglobin concentration in the hemolysates was determined by the standard cyanmethemoglobin method. The inter- and intra-assay coefficients of variations (CV) were 1.1% and 2.4%, respectively.

2.4. Biochemical Analysis

2.4.1. Oxidative Stress Analysis

(1) Determination of Activity of Antioxidant Enzymes. The plasma and erythrocytes superoxide dismutase (SOD-E.C.1.15.1.1) activity was assayed by the Oyanagui method [26]. Enzymatic activity was expressed in nitrite unit (NU) in each mg of hemoglobin (Hb) or ml of blood plasma. One nitrite unit (1 NU) means a 50% inhibition of nitrite ion production by SOD in this method. SOD isoenzymes (SOD-Mn and SOD-ZnCu) were measured using potassium cyanide as the inhibitor of the SOD-ZnCu isoenzyme. The inter- and intra-assay coefficients of variations (CV) were 2.8% and 5.4%, respectively.

The catalase (CAT-E.C.1.11.1.6.) activity in erythrocytes was measured by the Aebi [27] kinetic method and expressed in [IU/mgHb]. The inter- and intra-assay coefficients of variations (CV) were 2.6% and 6.1%, respectively.

The activity of erythrocyte glutathione peroxidase (GPx-E.C.1.11.1.9.) was assayed by Paglia and Valentine's kinetic method [28], with t-butyl peroxide as a substrate and expressed as micromoles of NADPH oxidized per minute and normalized to one gram of hemoglobin [IU/gHb]. The inter- and intra-assay coefficients of variations (CV) were 3.4% and 7.5%, respectively.

The glutathione reductase in erythrocytes (GR-E.C.1.6.4.2) activity was assayed by Richterich's kinetic method [29], expressed as micromoles of NADPH utilized per minute and normalized to one gram of hemoglobin [IU/g Hb]. The inter- and intra-assay coefficients of variations (CV) were 2.1% and 5.8%, respectively.

(2) Determination of Nonenzymatic Antioxidant Status. The total antioxidant capacity of plasma was measured as the ferric reducing ability of plasma (FRAP) according to Benzie and Strain [30] and calibrated using Trolox and expressed in [μmol/l]. The inter- and intra-assay coefficients of variations (CV) were 1.1% and 3.8%, respectively.

The serum concentration of protein sulfhydryl (PSH) was measured by Koster et al.'s method [31] using dithionitrobenzoic acid (DTNB) and expressed in [μmol/l]. The inter- and intra-assay coefficients of variations (CV) were 2.6% and 5.4%, respectively.

The serum concentration of uric acid (UA) was assayed by a uricase-peroxidase method [32] on the Cobas Integra 400 plus analyzer and expressed as [mg/dl]. The inter- and intra-assay coefficients of variations (CV) were 1.4% and 4.4%, respectively.

(3) Determination of Lipid Peroxidation Products, Total Oxidatative Status, and Oxidative Stress Index. The intensity of lipid peroxidation in the plasma and the erythrocytes was measured spectrofluorimetrically as thiobarbituric acid-reactive substances (TBARS) according to Ohkawa et al. [33]. The TBARS concentrations were expressed as malondialdehyde (MDA) equivalents in [μmol/l] in plasma or [nmol/gHb] in erythrocytes. The inter- and intra-assay coefficients of variations (CV) were 2.1% and 8.3%, respectively.

The serum total oxidant status (TOS) was determined with the method described by Erel [34] and expressed in [μmol/l]. The inter- and intra-assay coefficients of variations (CV) were 2.2% and 6.4%, respectively.

The oxidative stress index (OSI), an indicator of the degree of oxidative stress, was expressed as the ratio of total oxidant status (TOS) to total antioxidant capacity (FRAP) in arbitrary units [35].

2.5. Assessment of Activity of Ankylosing Spondylitis. The activity of ankylosing spondylitis was measured by the Bath Ankylosing Spondylitis Diseases Activity Index (BASDAI) and the Bath Ankylosing Spondylitis Functional Index (BASFI).

The BASDAI has six questions related to fatigue, back pain, peripheral pain, peripheral swelling, local tenderness, and morning stiffness (degree and length). Other than the issues relating to morning stiffness, all questions were scored from 0 (none) to 10 (very severe) using a visual analogue scale (VAS). The sum was calculated as the mean of two morning stiffness issues and the four remaining issues [36].

The BASFI is the mean score of ten questions addressing functional limitations and the level of physical activity at home and work, assessed on VAS scales (0 = easy, 10 = impossible) [37].

2.6. Statistical Analysis. For statistical analysis, the statistical package of Statistica 10 Pl software was used. For each parameter, the indicators of the descriptive statistics were determined (mean value and standard deviation SD). The normality of the data distribution was checked using the Shapiro–Wilk test, while the homogeneity of the variance was checked by applying the Levene's test. In order to compare the differences between the groups, an independent sample Student t-test was used or alternatively the Mann–Whitney U test. In the case of dependent samples, the Student t-test was used or alternatively the Wilcoxon test. Differences at the significance level of $p < 0.05$ were considered as statistically significant.

3. Results

3.1. Antioxidants Enzymes. AS patients in the WBC group had, after the completion of treatment, a statistically significant decrease in the erythrocyte activity of GPx (20.6 ± 5.07 and 18.3 ± 4.15 [IU/gHb]—before and after therapy, respectively, $p = 0.002$) and GR (1.21 ± 0.29 and 0.93 ± 0.37 [IU/gHb] [IU/gHb]—before and after therapy, respectively, $p = 0.007$). The erythrocyte activity of CAT (423.0 ± 61.6 and 380.0 ± 102.0 [IU/mgHb]—before and after therapy, respectively, $p = 0.079$) and plasma SOD-CuZn (7.05 ± 1.92 and 5.76 ± 2.36 [NU/ml]—before and after therapy, respectively, $p = 0.063$) showed a decreased tendency. The erythrocyte activity of total SOD (104.0 ± 15.0 and 112.0 ± 11.2 [NU/mgHb]—before and after therapy, respectively, $p = 0.056$) showed an increased tendency.

However, the activity of plasma total SOD (12.4 ± 1.89 and 11.5 ± 3.19 [NU/ml]—before and after therapy, respectively, $p = 0.501$) and SOD-Mn (5.31 ± 1.03 and 6.32 ± 2.16 [NU/ml]—before and after therapy, respectively, $p = 0.098$) did not change significantly in the WBC group after treatment. Similarly, as in the WBC group, the activity of plasma total SOD (12.3 ± 1.85 and 11.7 ± 2.49 [NU/ml]—before and after therapy, respectively, $p = 0.301$) and SOD-Mn (4.56 ± 1.86 and 5.02 ± 1.64 [NU/ml]—before and after therapy, respectively, $p = 0.642$) did not change significantly in the KT group after treatment. In the KT group, the erythrocyte activity of total SOD (128.0 ± 11.2 and 111.0 ± 15.6 [NU/mgHb]—before and after therapy, respectively, $p = 0.001$), GPx (29.9 ± 2.84 and 20.4 ± 5.05 [IU/gHb]—before and after therapy, respectively, $p = 0.001$) and GR (2.07 ± 0.52 and 1.65 ± 0.59 [IU/gHb]—before and after therapy, respectively, $p = 0.002$), similar to the WBC group of patients, decreased significantly after treatment. Additionally, the differences of activity of erythrocyte total SOD (-17.1 ± 11.8 [NU/mgHb] in the KT group versus 7.77 ± 17.2 [NU/mgHb] in the WBC group, $p < 0.001$) and GPx (-9.49 ± 6.74 [IU/gHb] in the KT group versus -2.27 ± 1.98 [IU/gHb] in the WBC group, $p = 0.001$) prior to post-treatment values (Δ) in the KT group were significantly higher as compared to the WBC group. In the KT group, the activity of erythrocyte CAT (425.0 ± 53.6 and 412.0 ± 58.6 [IU/mgHb]—before and after therapy, respectively, $p = 0.352$) and plasma SOD-CuZn (7.80 ± 2.21 and 7.05 ± 3.09 [NU/ml]—before and after therapy, respectively, $p = 0.326$) did not change significantly after treatment in comparison to the WBC group (Table 2).

3.2. Nonenzymatic Antioxidant Status. In the WBC group FRAP values (514.1 ± 63.2 and 587.9 ± 50.9 [μmol/l]—before and after therapy, respectively, $p = 0.001$) increased significantly after treatment. The UA level showed an increased

Table 2: Activities of antioxidant enzymes (mean value ± standard deviation SD) in AS patients before and after the completion of a cycle of ten whole-body cryotherapy procedures with subsequent kinesiotherapy (WBC group) or a cycle of ten kinesiotherapy procedures only (KT group), with statistical analyses. (p): plasma; (e): erythrocyte lysates; Δ: difference prior to post treatment.

Parameters		WBC group	KT group	p
Total SOD (p) [NU/ml]	Before	12.4 ± 1.89	12.3 ± 1.85	0.927
	After	11.5 ± 3.19	11.7 ± 2.49	0.884
	P^*	0.501	0.301	
	Δ	−0.81 ± 3.08	−0.60 ± 2.65	0.837
SOD-Mn (p) [NU/ml]	Before	5.31 ± 1.03	4.56 ± 1.86	0.170
	After	6.32 ± 2.16	5.02 ± 1.64	0.066
	P^*	0.098	0.642	
	Δ	1.01 ± 2.15	0.46 ± 2.46	0.509
SOD-CuZn (p) [NU/ml]	Before	7.05 ± 1.92	7.80 ± 2.21	0.310
	After	5.76 ± 2.36	7.05 ± 3.09	0.194
	P^*	0.063	0.326	
	Δ	−1.29 ± 2.46	−0.75 ± 2.72	0.166
Total SOD (e) [NU/mgHb]	Before	104.0 ± 15.0	128.0 ± 11.2	**<0.001**
	After	112.0 ± 11.2	111.0 ± 15.6	0.759
	P^*	0.056	**0.001**	
	Δ	7.77 ± 17.2	−17.1 ± 11.8	**<0.001**
CAT (e) [IU/mgHb]	Before	423.0 ± 61.6	425.0 ± 53.6	0.914
	After	380.0 ± 102.0	412.0 ± 58.6	0.294
	P^*	0.079	0.352	
	Δ	−42.3 ± 109.0	−13.0 ± 54.0	0.347
GPx (e) [IU/gHb]	Before	20.6 ± 5.07	29.9 ± 2.84	<0.001
	After	18.3 ± 4.15	20.4 ± 5.05	0.207
	P^*	**0.002**	**0.001**	
	Δ	−2.27 ± 1.98	−9.49 ± 6.74	**0.001**
GR (e) [IU/gHb]	Before	1.21 ± 0.29	2.07 ± 0.52	**<0.001**
	After	0.93 ± 0.37	1.65 ± 0.59	**<0.001**
	P^*	**0.007**	**0.002**	
	Δ	−0.28 ± 0.34	−0.42 ± 0.41	0.275

P: statistical significance of differences between both groups of patients; P^*: statistical significance of differences between values before and after treatment in particular groups of subjects.

tendency in WBC group of patients (4.44 ± 1.43 and 4.75 ± 1.08 [mg/dl]—before and after therapy, respectively, $p = 0.066$). After completion of the treatment FRAP values were significantly higher in the WBC group (587.9 ± 50.9 [μmol/l] when compared to the KT group (499.3 ± 74.6 [μmol/l]) ($p = 0.001$). The level of PSH (627.6 ± 248.0 and 616.5 ± 279.1 [μmol/l]—before and after therapy, respectively, $p = 0.918$) in the WBC group of patients did not change significantly after treatment. In turn, FRP values (550.0 ± 91.3 and 499.3 ± 74.6 [μmol/l]—before and after therapy, respectively, $p = 0.001$) and PSH concentration (393.2 ± 90.0 and 364.7 ± 28.4 [μmol/l]—before and after therapy, respectively, $p = 0.017$) decreased significantly, in the KT group, but the level of UA (4.34 ± 1.15 and 4.61 ± 1.25 [mg/dl]—before and after therapy, respectively, $p = 0.196$) did not change significantly after treatment (Table 3).

Table 3: Levels of nonenzymatic antioxidants (mean value ± standard deviation SD) in AS patients before and after the completion of a cycle of ten whole-body cryotherapy procedures with subsequent kinesiotherapy (WBC group) or a cycle of ten kinesiotherapy procedures only (KT group), with statistical analyses. (p): plasma; (s): serum; Δ: difference prior to post treatment.

Parameters		WBC group	KT group	p
FRAP [μmol/l	Before	514.1 ± 63.2	550.0 ± 91.3	0.206
	After	587.9 ± 50.9	499.3 ± 74.6	**0.001**
	P^*	**0.001**	**0.001**	
	Δ	73.9 ± 55.0	−50.8 ± 39.4	**<0.001**
PSH (s) [μmol/l]	Before	627.6 ± 248.0	393.2 ± 90.0	0.772
	After	616.5 ± 279.1	364.7 ± 28.4	0.239
	P^*	0.918	**0.017**	
	Δ	−11.1 ± 281.7	−28.5 ± 92.6	0.605
UA (s) [mg/dl]	Before	4.44 ± 1.43	4.34 ± 1.15	0.838
	After	4.75 ± 1.08	4.61 ± 1.25	0.738
	P^*	0.066	0.196	
	Δ	0.31 ± 1.02	0.27 ± 0.70	0.885

P: statistical significance of differences between both groups of patients; P^*: statistical significance of differences between values before and after treatment in particular groups of patients.

3.3. Lipid Peroxidation Products, Total Oxidative Status, and Oxidative Stress Index. AS patients in the WBC group had, after the completion of the treatment, a statistically significant decrease in serum TOS (30.49 ± 13.35 and 14.56 ± 9.01[μmol/l]—before and after therapy, respectively, $p = 0.003$) and value of OSI index (64.19 ± 65.93 and 10.20 ± 3.79—before and after therapy, respectively, $p = 0.001$) in comparison to initial values. The differences of these parameters prior to posttreatment values in the WBC group were significantly higher in comparison to the KT group (ΔTOS −15.93 ± 17.04 [μmol/l] in the WBC group versus 0.46 ± 9.11[μmol/l] in the KT group, $p = 0.003$; Δ OSI −53.99 ± 66.83 in WBC group versus 4.78 ± 13.88 in the KT group, $p = 0.003$). The levels of MDA in plasma (2.66 ± 0.73 and 2.48 ± 0.57 [μmol/l]—before and after therapy, respectively, $p = 0.215$) and in erythrocyte (0.16 ± 0.01 and 0.15 ± 0.02 [nmol/gHb]—before and after therapy, respectively, $p = 0.098$) did not change significantly in the WBC group. In the KT group, no significant changes in the levels of plasma MDA (2.32 ± 0.60 and 2.41 ± 0.83 [μmol/l]—before and after therapy, respectively, $p = 0.959$) and erythrocyte MDA (0.18 ± 0.02 and 0.18 ± 0.04 [nmol/gHb]—before and after therapy, $p = 0.642$) as well as serum TOS (23.94 ± 11.60 and 24.41 ± 6.24 [μmol/l]—before and after therapy, respectively, $p = 0.605$) and OSI index (18.87 ± 11.30 and 23.65 ± 15.68—before and after therapy, respectively, $p = 0.301$) were observed after the completion of treatment, in comparison to the initial values before the beginning of the kinesiotherapy cycle (Table 4).

Table 4: Levels of lipid peroxidation parameters, total oxidative status (TOS), and oxidative stress (OSI) index (mean value ± standard deviation SD) in AS patients before and after the completion of a cycle of ten whole-body cryotherapy procedures with subsequent kinesiotherapy (WBC group) or a cycle of ten kinesiotherapy procedures only (KT group), with statistical analyses. (p): plasma; (s): serum; (e): erythrocyte lysates; Δ: difference prior to post treatment.

Parameters		WBC group	KT group	p
MDA (p) [μmol/l]	Before	2.66 ± 0.73	2.32 ± 0.60	0.157
	After	2.48 ± 0.57	2.41 ± 0.83	0.783
	P^*	0.215	0.959	
	Δ	−0.19 ± 0.72	0.09 ± 1.04	0.391
MDA (e) [nmol/gHb]	Before	0.16 ± 0.01	0.18 ± 0.02	**0.001**
	After	0.15 ± 0.02	0.18 ± 0.04	**0.001**
	P^*	0.098	0.642	
	Δ	−0.01 ± 0.03	0.00 ± 0.04	0.155
TOS (s) [μmol/l]	Before	30.49 ± 13.35	23.94 ± 11.60	0.149
	After	14.56 ± 9.01	24.41 ± 6.24	**0.001**
	P^*	**0.003**	0.605	
	Δ	−15.93 ± 17.04	0.46 ± 9.11	**0.003**
OSI (p/s) [arbitrary unit]	Before	64.19 ± 65.93	18.87 ± 11.30	0.016
	After	10.20 ± 3.79	23.65 ± 15.68	**0.004**
	P^*	**0.001**	0.301	
	Δ	−53.99 ± 66.83	4.78 ± 13.88	**0.003**

P: statistical significance of differences between both groups of patients; P^*: statistical significance of differences between values before and after treatment in particular groups of patients.

3.4. BASDAI and BASFI Indexes. The BASDAI (5.34 ± 1.72 and 3.19 ± 0.91 in the WBC group—before and after therapy, respectively, $p = 0.001$; 5.28 ± 1.71 and 4.53 ± 1.62 in the KT group—before and after therapy, respectively, $p < 0.001$) and BASFI (5.17 ± 2.28 and 3.79 ± 2.21 in the WBC group—before and after therapy, respectively, $p < 0.001$; 5.01 ± 2.06 and 4.35 ± 2.23 in the KT group—before and after therapy, respectively, $p < 0.001$) indexes decreased significantly in both groups, but in the WBC group, with subsequent kinesiotherapy after the completion of the treatment, the decrease of these parameters was significantly higher in comparison to the KT group (Δ BASDAI −2.16 ± 1.29 in the WBC group versus −0.74 ± 0.38 in the KT group, $p < 0.001$; Δ BASFI −1.38 ± 1.07 in the WBC group versus −0.66 ± 0.39 in the KT group, $p = 0.007$). The value of both BASDAI and BASFI indexes was below 4 (inactive phase of AS disease) only in the WBC group after the completion of treatment (Table 5).

Table 5: The value of BASDAI and BASFI indexes (mean value ± standard deviation SD) in AS patients before and after the completion of a cycle of ten whole-body cryotherapy procedures with subsequent kinesiotherapy (WBC group) or a cycle of ten kinesiotherapy procedures only (KT group), with statistical analyses. (p): plasma; (s): serum; Δ: difference prior to post treatment.

Parameters		WBC group	KT group	p
BASDAI index	Before	5.34 ± 1.72	5.28 ± 1.71	0.880
	After	3.19 ± 0.91	4.53 ± 1.62	**0.030**
	P^*	**0.001**	**<0.001**	
	Δ	−2.16 ± 1.29	−0.74 ± 0.38	**0.001**
BASFI index	Before	5.17 ± 2.28	5.01 ± 2.06	0.940
	After	3.79 ± 2.21	4.35 ± 2.23	0.406
	P^*	**<0.001**	**<0.001**	
	Δ	−1.38 ± 1.07	−0.66 ± 0.39	**0.007**

P: statistical significance of differences between both groups of patients; P^*: statistical significance of differences between values before and after treatment in particular groups of patients.

4. Discussion

After the completion of the treatment, a significant decrease in markers of oxidative stress was achieved in the WBC group of AS patients who underwent a ten-day long cycle of WBC procedures with subsequent kinesiotherapy. In that group of patients, a significant decrease in levels of TOS and OSI values as well as in activity of erythrocyte GPx and GR was observed. A decreased tendency was also noticed in the activity of plasma SOD-CuZn and erythrocyte CAT. Contrary, an increased tendency was seen in the activity of erythrocyte total SOD and the level of UA after the completion of treatment in the WBC group. The FRAP value was increased significantly after the completion of treatment in the WBC group. No significant changes were noted in the activity of plasma total SOD and SOD-Mn, as well as levels of PSH and both plasma and erythrocyte MDA after the completion of treatment in the WBC group.

These findings are similar to our previous research, in which a beneficial impact on oxidative stress from ten WBC procedures performed in a cryochamber with cold retention (temperature: −120°C, time: 3 min, liquid air coolant) both in healthy subjects and AS patients was observed [22, 38]. It has been suggested by Mila-Kierzenkowska et al. [23] that even a single application of cryotherapy prior to exercise may have a beneficial impact on antioxidant system of organism and alleviate the signs of exercise-induced oxidative stress (a single session of WBC, temperature: −130°C, time: 1-2 min., cryochamber with cold retention, liquid air coolant).

However, it has been shown by Lubkowska et al. [39] that a single session of WBC (temperature: −130°C, time: 3 minutes, two-step cryochamber, liquid nitrogen coolant) could induce disturbances in prooxidant-antioxidant balance, in the form of lowering TOS and a temporary decrease in TAS, with a subsequent elevation of those parameters on the following day, resulting in an intensification of oxidative stress.

In another study by the same team [39], healthy men have been exposed to a single WBC session (temperature: −130 ° C, time 3 minutes, two-step cryochamber, liquid nitrogen coolant) without subsequent kinesiotherapy. A significant increase in GPx and GR activities, with a simultaneous decrease in CAT and glutathione S-transferase activities, was observed. A significant increase in the concentration

of glutathione, uric acid, albumins, and extra-erythrocyte hemoglobin was also observed in the serum of the subjects. It was concluded by the authors that a single stimulation with cryogenic temperatures results in oxidative stress in a healthy body, but the level of this stress is not very high.

It has been suggested that repeated exposure to cryogenic temperatures may cause adaptative changes in the form of an increase in antioxidant status and antioxidant enzyme activity, resulting in the formation of a prooxidant-antioxidant balance at a higher level (according to hormesis theory) [40].

A beneficial impact of WBC on prooxidant-antioxidant balance has been observed in both male and female kayak athletes when WBC procedures were included into the training regime [40, 41]. The increase in total antioxidant status and the level of UA as a result of a series of short-term whole-body cryotherapy (10 WBC sessions, temperature: −130°C, time: 3 minutes, without subsequent kinesiotherapy) has been also observed by Miller et al. [42] in healthy subjects. However, in other study [43], the authors have shown that the activity of antioxidant enzymes in healthy men depends on the number of WBC procedures (temperature: −130°C, time: 3 minutes). It was also suggested that WBC intensifies oxidative stress and causes an accompanying decrease in antioxidant enzyme activity after 10 sessions, with a subsequent compensatory increase after the completion of a cycle of 20 sessions. In a different study [44], patients with seropositive rheumatoid were observed by the authors to have only a short-term increase in TRAP during the first treatment session of WBC (the temperature− 110°C, three times daily for 7 consecutive days), and no significant oxidative stress or adaptation were caused by the cold treatment.

In our research a significant decrease in BASDAI and BASFI indexes in the WBC group after the completion of treatment was observed. These results are similar to our previous research, in which WBC procedures were performed in a cryochamber with cold retention and two-step cryochamber (Wroclawski type) [19, 22]. In both studies, after the completion of a cycle of WBC procedures consisting of ten 3 minute long WBC procedures daily with subsequent kinesiotherapy (temperature− 120°C, time 3 min, 10 sessions with a weekend break), a decreased of the BASDAI and BASFI index below 4 was observed, which suggests that the AS disease turned into an inactive phase after the completion of treatment. Similar results in AS patients have also been observed by Romanowski et al. [20] (8 daily WBC procedures, the temperature −110°C, time 3 min).

The differences in the results of various studies may be related to the type of cryochamber being used and the coolant medium, in addition to the time of exposure to cryogenic temperatures. Further studies are necessary to estimate whether the number of WBC procedures and type of cryochamber may have an influence on prooxidant-antioxidant balance in subjects who underwent WBC treatment. Comparability of the results obtained by different research teams could be improved through standardization of exposure times and the number of treatments during each cycle. In an attempt to optimise treatment, sexually dimorphism, body fat percentage, and BMI differences should be also taken into account [45, 46].

The present study has some limitations. Firstly, the study did not provide long-term follow-up (at least 3 months), and thus we are not sure how long the beneficial effect of WBC with subsequent kinesiotherapy would be maintained after the completion of a WBC cycle. Secondly, the cycle of WBC with subsequent kinesiotherapy consisted of ten procedures only. A greater number of procedures (e.g., 20–30) could probably intensify the treatment effect. Thirdly, the next studies should involve a larger number of AS patients in different stages of the disease. Females should be also included.

5. General Conclusion

Whole-body cryotherapy procedures performed in a closed cryochamber (Wroclawski type) with subsequent kinesiotherapy decrease oxidative stress as well as BASDAI and BASFI indexes in AS patients during the active phase of the disease.

Data Availability

All data are included in the tables within the article.

Conflicts of Interest

The authors declare that there are no conflicts of interests regarding the publication of this paper.

Acknowledgments

This work was supported by a grant from the Medical University of Silesia (KNW-1-045/K/7/K).

References

[1] C. Stolwijk, I. Essers, A. van Tubergen et al., "The epidemiology of extra-articular manifestations in ankylosing spondylitis: a population-based matched cohort study," *Annals of the Rheumatic Diseases*, vol. 74, no. 7, pp. 1373–1378, 2015.

[2] M. Karakoc, O. Altindag, H. Keles, N. Soran, and S. Selek, "Serum oxidative–antioxidative status in patients with ankylosing spondilitis," *Rheumatology International*, vol. 27, no. 12, pp. 1131–1134, 2007.

[3] S. Ozgocmen, S. Sogut, O. Ardicoglu, E. Fadillioglu, I. Pekkutucu, and O. Akyol, "Serum nitric oxide, catalase, superoxide dismutase, and malondialdehyde status in patients with ankylosing spondylitis," *Rheumatology International*, vol. 24, no. 2, pp. 80–83, 2004.

[4] D. Solmaz, D. Kozaci, I. Sari et al., "Oxidative stress and related factors in patients with ankylosing spondylitis," *European Journal of Rheumatology*, vol. 3, no. 1, pp. 20–24, 2016.

[5] A. Stanek, G. Cieślar, E. Romuk et al., "Decrease in antioxidant status of plasma and erythrocytes from patients with ankylosing spondylitis," *Clinical Biochemistry*, vol. 43, no. 6, pp. 566–570, 2010.

[6] A. Stanek, A. Cholewka, T. Wielkoszyński, E. Romuk, K. Sieroń, and A. Sieroń, "Increased levels of oxidative stress markers, soluble CD40 ligand and carotid intima - media thickness reflect acceleration of atherosclerosis in male patients with ankylosing spondylitis in active phase and

without the classical cardiovascular risk factors," *Oxidative Medicine and Cellular Longevity*, vol. 2017, Article ID 9712536, 8 pages, 2017.

[7] D. van der Heijde, S. Ramiro, R. Landewé et al., "2016 update of the ASAS-EULAR management recommendations for axial spondyloarthritis," *Annals of the Rheumatic Diseases*, vol. 76, no. 6, pp. 978–991, 2017.

[8] S. K. Biswas, "Does the interdependence between oxidative stress and inflammation explain the antioxidant paradox," *Oxidative Medicine and Cellular Longevity*, vol. 2016, Article ID 5698931, 9 pages, 2016.

[9] L. A. Passalent, "Physiotherapy for ankylosing spondylitis: evidence and application," *Current Opinion in Rheumatology*, vol. 23, no. 2, pp. 142–147, 2011.

[10] B. Skrzep-Poloczek, E. Romuk, B. Wiśnowiska et al., "Effect of whole-body cryotherapy on antioxidant systems in experimental rat model," *Oxidative Medicine and Cellular Longevity*, vol. 2017, Article ID 8158702, 10 pages, 2017.

[11] G. Lombardi, E. Ziemann, and G. Banfi, "Whole-body cryotherapy in athletes: from therapy to stimulation. An updated review of the literature," *Frontiers in Physiology*, vol. 8, no. 258, 2017.

[12] K. Kerschan-Schindl, E. M. Uher, A. Zauner-Dungl, and V. Fialka-Moser, "Cold and cryotherapy. A review of the literature on general principles and practical applications," *Acta Medica Austriaca*, vol. 25, no. 3, pp. 73–78, 1998.

[13] J. Bauer, P. Hurnik, J. Zdziarski et al., "Thermovision evaluation of cryotherapy effects," *Acta Bio-Optica et Informatica Médica*, vol. 3, no. 2–4, pp. 133–140, 1997.

[14] J. Bauer and A. Skrzek, "Physiological principles of cryotherapy," in *Whole body cryotherapy*, H. Podbielska, W. Stręk, and D. Biały, Eds., pp. 21–26, Kriotechnika Medyczna, Wrocław, 2006.

[15] R. Bouzigon, F. Grappe, G. Ravier, and B. Dugue, "Whole- and partial-body cryostimulation/cryotherapy: current technologies and practical applications," *Journal of Thermal Biology*, vol. 61, pp. 67–81, 2016.

[16] J. Rymaszewska, D. Ramsey, and S. Chładzińska-Kiejna, "Whole-body cryotherapy as adjunct treatment of depressive and anxiety disorders," *Archivum Immunologiae et Therapiae Experimentalis*, vol. 56, no. 1, pp. 63–68, 2008.

[17] I. Korzonek-Szlacheta, T. Wielkoszyński, A. Stanek, E. Swietochowska, J. Karpe, and A. Sieroń, "Effect of whole body cryotherapy on the levels of some hormones in professional soccer players," *Polish Journal of Endocrinology*, vol. 58, no. 1, pp. 27–32, 2007.

[18] J. Leppäluoto, T. Westerlund, P. Huttunen et al., "Effects of long-term whole-body cold exposures on plasma concentrations of ACTH, beta-endorphin, cortisol, catecholamines and cytokines in healthy females," *Scandinavian Journal of Clinical and Laboratory Investigation*, vol. 68, no. 2, pp. 145–153, 2008.

[19] A. Stanek, A. Cholewka, J. Gadula, Z. Drzazga, A. Sieron, and K. Sieron-Stoltny, "Can whole-body cryotherapy with subsequent kinesiotherapy procedures in closed type cryogenic chamber improve BASDAI, BASFI, and some spine mobility parameters and decrease pain intensity in patients with ankylosing spondylitis?," *BioMed Research International*, vol. 2015, Article ID 404259, 11 pages, 2015.

[20] M. W. Romanowski, W. Romanowski, P. Keczmer, M. Majchrzycki, W. Samborski, and A. Straburzynska-Lupa, "Whole body cryotherapy in rehabilitation of patients with ankylosing spondylitis. A randomised controlled study," *Physiotherapy*, vol. 101, article e1294, 2015.

[21] A. Stanek, G. Cielar, J. Strzelczyk et al., "Influence of cryogenic temperatures on inflammatory markers in patients with ankylosing spondylitis and healthy volunteers," *Polish Journal of Environmental Study*, vol. 19, no. 1, pp. 167–175, 2010.

[22] A. Stanek, A. Cholewka, T. Wielkoszyński, E. Romuk, and A. Sieroń, "Whole-body cryotherapy decreases the levels of inflammatory, oxidative stress, and atherosclerosis plaque markers in male patients with active phase ankylosing spondylitis in the absence of classical cardiovascular risk factors," *Mediators of Inflammation*, vol. 2018, Article ID 8592532, 11 pages, 2018.

[23] C. Mila-Kierzenkowska, A. Jurecka, A. Woźniak, M. Szpinda, B. Augustyńska, and B. Woźniak, "The effect of submaximal exercise preceded by single whole-body cryotherapy on the markers of oxidative stress and inflammation in blood of volleyball players," *Oxidative Medicine and Cellular Longevity*, vol. 2013, Article ID 409567, 10 pages, 2013.

[24] A. Sieroń, G. Cieślar, and A. Stanek, Eds., *Cryotherapy*, alpha-medica-press, Bielsko-Biała, 2010.

[25] S. Van Der Linden, H. A. Valkenburg, and A. Cats, "Evaluation of diagnostic criteria for ankylosing spondylitis a proposal for modification of the New York criteria," *Arthritis & Rheumatism*, vol. 27, no. 4, pp. 361–368, 1984.

[26] Y. Oyanagui, "Reevaluation of assay methods and establishment of kit for superoxide dismutase activity," *Analytical Biochemistry*, vol. 142, no. 2, pp. 290–296, 1984.

[27] H. Aebi, "[13] Catalase in vitro," *Methods in Enzymology*, vol. 105, pp. 121–126, 1984.

[28] D. Paglia and W. Valentine, "Studies on the quantitative and qualitative characterization of erythrocyte glutathione peroxidase," *Journal of Laboratory and Clinical Medicine*, vol. 70, no. 1, pp. 158–169, 1967.

[29] R. Richterich, *Clinical Chemistry: Theory and Practice*, Academic Press, New York, 1969.

[30] I. F. F. Benzie and J. J. Strain, "The ferric reducing ability of plasma (FRAP) as a measure of "antioxidant power": the FRAP assay," *Analytical Biochemistry*, vol. 239, no. 1, pp. 70–76, 1996.

[31] J. F. Koster, P. Biemond, and A. J. Swaak, "Intracellular and extracellular sulphydryl levels in rheumatoid arthritis," *Annals of the Rheumatic Diseases*, vol. 45, no. 1, pp. 44–46, 1986.

[32] Y. Zhao, X. Yang, W. Lu, H. Liao, and F. Liao, "Uricase based methods for determination of uric acid in serum," *Microchimica Acta*, vol. 164, no. 1-2, pp. 1–6, 2009.

[33] H. Ohkawa, N. Ohishi, and K. Yagi, "Assay for lipid peroxides in animal tissues by thiobarbituric acid reaction," *Analytical Biochemistry*, vol. 95, no. 2, pp. 351–358, 1979.

[34] O. Erel, "A new automated colorimetric method for measuring total oxidant status," *Clinical Biochemistry*, vol. 38, no. 12, pp. 1103–1111, 2005.

[35] M. Harma, M. Harma, and O. Erel, "Increased oxidative stress in patients with hydatidiform mole," *Swiss Medical Weekly*, vol. 133, no. 41-42, pp. 563–566, 2003.

[36] S. Garrett, T. Jenkinson, L. G. Kennedy, H. Whitelock, P. Gaisford, and A. Calin, "A new approach to defining disease status in ankylosing spondylitis: the bath ankylosing spondylitis disease activity index," *Journal of Rheumatology*, vol. 21, no. 12, pp. 2286–2291, 1994.

[37] A. Calin, S. Garrett, H. Whitelock et al., "A new approach to defining functional ability in ankylosing spondylitis: the development of the bath ankylosing spondylitis functional index," *The Journal of Rheumatology*, vol. 21, no. 12, pp. 2281–2285, 1994.

[38] A. Stanek, K. Sieroń-Stołtny, E. Romuk et al., "Whole-body cryostimulation as an effective method of reducing oxidative stress in healthy men," *Advances in Clinical and Experimental Medicine*, vol. 25, no. 6, pp. 1281–1291, 2016.

[39] A. Lubkowska, M. Chudecka, A. Klimek, Z. Szygula, and B. Fraczek, "Acute effect of a single whole-body cryostimulation on prooxidant–antioxidant balance in blood of healthy, young men," *Journal of Thermal Biology*, vol. 33, no. 8, pp. 464–467, 2008.

[40] A. Wozniak, B. Wozniak, G. Drewa, and C. Mila-Kierzenkowska, "The effect of whole-body cryostimulation on the prooxidant—antioxidant balance in blood of elite kayakers after training," *European Journal of Applied Physiology*, vol. 101, no. 5, pp. 533–537, 2007.

[41] P. Sutkowy, B. Augustyńska, A. Woźniak, and A. Rakowski, "Physical exercise combined with whole-body cryotherapy in evaluating the level of lipid peroxidation products and other oxidant stress indicators in kayakers," *Oxidative Medicine and Cellular Longevity*, vol. 2014, Article ID 402631, 7 pages, 2014.

[42] E. Miller, Ł. Markiewicz, J. Saluk, and I. Majsterek, "Effect of short-term cryostimulation on antioxidative status and its clinical applications in humans," *European Journal of Applied Physiology*, vol. 112, no. 5, pp. 1645–1652, 2012.

[43] A. Lubkowska, B. Dolegowska, and Z. Szygula, "Whole-body cryostimulation - potential beneficial treatment for improving antioxidant capacity in healthy men - significance of the number of sessions," *PLoS One*, vol. 7, no. 10, article e46352, 2012.

[44] H. Hirvonen, H. Kautiainen, E. Moilanen, M. Mikkelsson, and M. Leirisalo-Repo, "The effect of cryotherapy on total antioxidative capacity in patients with active seropositive rheumatoid arthritis," *Rheumatology International*, vol. 37, no. 9, pp. 1481–1487, 2017.

[45] S. Cuttell, L. Hammond, D. Langdon, and J. Costello, "Individualising the exposure of −110°C whole body cryotherapy: the effects of sex and body composition," *Journal of Thermal Biology*, vol. 65, pp. 41–47, 2017.

[46] A. Cholewka, A. Stanek, A. Sieroń, and Z. Drzazga, "Thermography study of skin response due to whole-body cryotherapy," *Skin Research and Technology*, vol. 18, no. 2, pp. 180–187, 2012.

Hindawi
Oxidative Medicine and Cellular Longevity
Volume 2018, Article ID 1271864, 12 pages
https://doi.org/10.1155/2018/1271864

Research Article

Losartan Ameliorates Calcium Oxalate-Induced Elevation of Stone-Related Proteins in Renal Tubular Cells by Inhibiting NADPH Oxidase and Oxidative Stress

Baolong Qin, Qing Wang, Yuchao Lu, Cong Li, Henglong Hu, Jiaqiao Zhang, Yufeng Wang, Jianning Zhu, Yunpeng Zhu, Yang Xun, and Shaogang Wang

Department of Urology, Tongji Hospital, Tongji Medical College, Huazhong University of Science and Technology, Wuhan, China

Correspondence should be addressed to Shaogang Wang; sgwangtjm@163.com

Received 28 October 2017; Revised 8 February 2018; Accepted 18 February 2018; Published 24 April 2018

Academic Editor: Karolina Szewczyk-Golec

Calcium oxalate (CaOx) is the most common type of urinary stone. Increase of ROS and NADPH oxidase gives rise to inflammation and injury of renal tubular cells, which promotes CaOx stone formation. Recent studies have revealed that the renin-angiotensin system might play a role in kidney crystallization and ROS production. Here, we investigated the involvement of Ang II/AT1R and losartan in CaOx stone formation. NRK-52E cells were incubated with CaOx crystals, and glyoxylic acid-induced hyperoxaluric rats were treated with losartan. Oxidative stress statuses were evaluated by detection of ROS, oxidative products (8-OHdG and MDA), and antioxidant enzymes (SOD and CAT). Expression of NADPH oxidase subunits (Nox2 and Nox4), NF-κB pathway subunits (p50 and p65), and stone-related proteins such as OPN, CD44, and MCP-1 was determined by Western blotting. The results revealed upregulation of Ang II/AT1R by CaOx treatment. CaOx-induced ROS and stone-related protein upregulation were mediated by the Ang II/AT1R signaling pathway. Losartan ameliorated renal tubular cell expression of stone-related proteins and renal crystallization by inhibiting NADPH oxidase and oxidative stress. We conclude that losartan might be a promising preventive and therapeutic candidate for hyperoxaluria nephrolithiasis.

1. Introduction

Calcium oxalate (CaOx) is the major constituent of most urinary stones, and hyperoxaluria is one of the primary risk factors for idiopathic kidney stone [1]. Renal tubular cells are notably injured in states of high levels of oxalate or CaOx crystals, which is associated with the development of oxidative stress (OS) and overproduction of reactive oxygen species (ROS) [2]. Intracellular ROS are generated mainly by nicotinamide adenine dinucleotide phosphate (NADPH) oxidase and mitochondria and involved in a variety of signaling pathways.

NADPH oxidase has emerged as a major source of receptor-mediated ROS production during exposure to high levels of oxalate or CaOx crystals [3, 4]. Activation of NADPH oxidase increases generation of ROS that modulate the expression of several stone-related macromolecules that promote or inhibit the formation of kidney stones [5]. The NADPH oxidase inhibitor apocynin has been proven to inhibit crystal deposition by regulating oxidative stress levels and stone-related protein expression [6]. Osteopontin (OPN), monocyte chemotactic protein 1 (MCP-1), and CD44 are very common stone-related proteins in urolithiasis research.

Recent studies have revealed that the renin-angiotensin system (RAS) might play an important role in kidney crystallization and ROS production in hyperoxaluric rats [7]. Angiotensin II (Ang II) type 1 receptor (AT1R) inhibitors were able to reduce renal injury and crystal deposition [8]. However, the mechanism underlying Ang II/AT1R in CaOx stone formation remains unclear. This study was designed to investigate Ang II/AT1R involvement in CaOx-induced

activation of NADPH oxidase and expression of subsequent stone-related proteins and to identify new promising drug targets for prevention and treatment of CaOx stones.

2. Materials and Methods

2.1. Reagents. Calcium oxalate monohydrate (COM) crystals were purchased from Macklin (Shanghai, China). COM crystals were weighed and suspended in sterile phosphate buffer solution at 1 mM and then were diluted into different concentrations. Ang II was purchased from Sangon Biotech (Shanghai, China). Anti-AT1R, anti-NADPH oxidase 2 (Nox2), anti-p50, and anti-p65 antibodies were purchased from Proteintech (Wuhan, China). Losartan and apocynin were purchased from Sigma Aldrich (St. Louis, MO, USA). 2′,7′-Dichlorofluorescein diacetate (DCF-DA) and Fluo-3AM were purchased from Beyotime Institute of Biotechnology (Shanghai, China). Anti-NADPH oxidase 4 (Nox4), anti-OPN, and anti-MCP-1 antibodies were purchased from Abcam (Cambridge, MA, USA). An anti-CD44 antibody was purchased from Cell Signaling Technology (Boston, MA, USA). Malondialdehyde (MDA), superoxide dismutase (SOD), and catalase (CAT) assay kits were purchased from Nanjing Jiancheng Bioengineering Institute (Jiangsu, China). An 8-OHdG assay kit was purchased from Elabscience (Wuhan, China). The transfection reagent Lipofectamine™ 2000 was purchased from Invitrogen (Carlsbad, CA, USA).

2.2. Animal Model. Eight-week-old male Sprague-Dawley rats (200–220 g) were purchased from the Experimental Animal Center of Tongji Hospital, Tongji Medical College, Huazhong University of Science and Technology. All animal experiments were performed according to the Guide for the Care and Use of Laboratory Animals (published by National Academy Press, Washington, DC, 2011) and were approved by the Ethical Committee of Tongji Hospital (permit number: TJ-A20151202). Hyperoxaluria was induced by daily intraperitoneal injections of glyoxylic acid (80 mg/kg) for 2 weeks. Angiotensin type 1 receptor blocker losartan (80 mg/kg) dissolved in saline was administrated by gavage for 2 weeks simultaneously. Four groups of eight rats each were used in the study: group A, untreated control animals; group B, hyperoxaluria induction only; group C, hyperoxaluria with losartan treatment; and group D, losartan treatment only.

2.3. Cell Culture and Treatments. The normal rat kidney proximal tubular epithelial cell line, NRK-52E, was obtained from the Type Culture Collection of the Chinese Academy of Sciences (Shanghai, China). Cells were maintained in Dulbecco's modified Eagle's medium (DMEM) (Hyclone; USA) supplemented with 10% fetal bovine serum (FBS) (Gibco; Grand Island, NY, USA) at 37°C in a humidified atmosphere with 5% CO_2. NRK-52E cells were stimulated with COM at a series of concentrations (0, 0.1, 0.5, 1, 5, or 10 mM) for 3–48 h. Cells were pretreated with NADPH oxidase inhibitor apocynin (30 μM) or AT1R inhibitor losartan (10 μM) for 1 h and then exposed to COM.

2.4. Small Interfering RNA (siRNA) Transfection. Three different siRNAs targeting specific sequences of the AT1R gene and a negative control siRNA were designed and synthesized by GenePharma Co. Ltd. (Shanghai, China). Sequences of siRNAs are shown in Table 1. NRK-52E cells were seeded in 24-well plates (5×10^4 cells/well) and cultured in DMEM containing 10% FBS until 60%–70% confluence. After starvation for 6 hours, the siRNA transfection was performed according to manufacturer's instructions. The culture medium was replaced with serum-free DMEM 6 hours after transfection. Then, COM or Ang II (1 μM) were added to stimulate the cells for subsequent assays.

2.5. Detection of Intracellular ROS by Flow Cytometry. Intracellular ROS production was detected using the probe DCF-DA. Cells were seeded in a 6-well plate and stimulated by COM and other drugs as aforementioned, followed by incubation with 10 μM DCF-DA for 30 min at 37°C. Then, cells were collected and washed with PBS. After resuspending the pellet in 200 μl PBS, fluorescence was detected by a flow cytometer (BD Biosciences).

2.6. Measurement of Oxidative and Antioxidative Biomarkers. MDA was measured as a product of lipid peroxidation, and 8-OHdG was regarded as a marker of oxidative DNA damage. SOD and CAT activities as well as MDA content were determined by chemiluminescence methods. The concentration of 8-OHdG considered as a marker of oxidative DNA damage was measured using a commercial ELISA kit according to the manufacturer's instructions.

2.7. Quantitative Polymerase Chain Reaction (PCR). Total RNA was extracted from kidney tissues and NRK-52E cells using TRIzol reagent (Invitrogen). Total cDNA was synthesized using the PrimeScript® RT reagent kit (Takara Biotechnology, Dalian, China). Real-time PCR was performed using an ABI Prism 7500 system (Applied Biosystems, Foster City, CA, USA) according to manufacturer's instructions. Sequences of primers are as follows: AT1R, forward CACCATCTGCATAGCGTATT and reverse TTC GTAGACAGGCTTGAGTG; β-actin, forward CACGAT GGAGGGGCCGGACTCATC and reverse TAAAGACCT CTATGCCAACACAGT. PCR thermal cycling conditions were as follows: denaturation at 95°C for 30s, followed by 40 cycles of 95°C for 30 s and 60°C for 30 s. Relative changes of gene expression were calculated using $2^{-\Delta\Delta Ct}$ and expressed as fold changes relative to the control group.

2.8. Western Blotting Analysis. Kidney tissues and NRK-52E cells were lysed with RIPA buffer containing 1% protease inhibitor PMSF. The supernatant was gathered after centrifugation. All lysates were diluted with SDS loading buffer and boiled for 5 minutes. Equal amounts of protein (40 μg) were loaded into each lane of a 10% SDS-PAGE gel for electrophoresis. Proteins were then transferred onto a PVDF membrane. Then, the membranes were blocked with 5% BSA for 2 h and incubated with primary rabbit polyclonal antibodies against AT1R (1 : 1000), Nox2 (1 : 1000), Nox4 (1 : 2000), p50 (1 : 1000), p65 (1 : 2000), OPN (1 : 1000), MCP-1 (1 : 2000), or GAPDH (1 : 1000) or a mouse polyclonal antibody against CD44 (1 : 1000) at 4°C overnight, followed by incubation with a secondary antibody (anti-rabbit or anti-

Table 1: Sequences of the siRNAs.

siRNA	Forward	Reverse
AT1R siRNA-1	GCGUCUUUCUUCUCAAUCUTT	AGAUUGAGAAGAAAGACGCTT
AT1R siRNA-2	GCCAGUGUGUUCCUUCUCATT	UGAGAAGGAACACACUGGCTT
AT1R siRNA-3	CAGCUGUCAUCCACCGAAATT	UUUCGGUGGAUGACAGCUGTT
Scrambled siRNA	UUCUCCGAACGUGUCACGUTT	ACGUGACACGUUCGGAGAATT

mouse IgG) for 1 h at 37°C. Membranes were developed using an enhanced chemiluminescence Bio-Rad Clarity Western ECL kit. Band intensities were analyzed using ImageJ software. Protein levels were normalized to GAPDH expression.

2.9. Morphological Staining. Paraffin-embedded kidney tissue sections were subjected to Von Kossa staining to identify CaOx crystal depositions, according to manufacturer's instructions.

2.10. Statistical Analysis. Results are presented as the mean ± SEM. One-way ANOVA was used to test significant differences among groups with SPSS version 18.0. A value of $P < 0.05$ was considered as statistically significant.

3. Results

3.1. Effects of Various Concentrations of Ang II on ROS Generation in NRK-52E Cells. Confluent NRK-52E cells were treated with Ang II at a series of concentrations (0.1, 1, 10, 100, and 1000 nM) for 6 h to determine the effect of Ang II on intracellular ROS generation. Treatment with 1 nM Ang II or lower did not influence ROS generation (Figure 1(a)). Therefore, 1 nM Ang II was added to the medium as a supplement in subsequent experiments to simulate the physiological state.

3.2. Effects of COM on ROS Generation in NRK-52E Cells Are Concentration- and Time-Dependent. NRK-52E cells were exposed to various COM concentrations (0, 0.1, 0.5, 1, 5, and 10 mM) for various periods of time (0, 3, 6, 12, 24, and 48 h) to identify the appropriate concentration and time for treatment. ROS generation in response to COM was both concentration- and time-dependent (Figures 1(b) and 1(c)). And exposure to 1 mM COM for 6 h was adopted as the appropriate treatment condition.

3.3. Ang II/AT1R Expression Was Increased during Exposure to CaOx Crystals In Vitro and In Vivo. Expression of Ang II and AT1R was detected *in vitro* and *in vivo* to evaluate the activation of RAS. NRK-52E cells showed upregulation of AT1R after exposure to COM at both mRNA (Figure 2(a)) and protein (Figure 2(b)) levels. The serum concentration of Ang II was also increased in the hyperoxaluria group compared with the untreated control group (Figure 2(c)). Western blotting examination of experimental rat kidneys indicated upregulation of AT1R expression in the hyperoxaluria group compared with the untreated control group (Figure 2(d)).

3.4. ROS and NADPH Oxidase Were Upregulated under Stimulation of CaOx Crystals. High concentrations of Ang II had been proven to increase ROS production [9, 10]. Apocynin was used as an inhibitor of NADPH oxidase. Expression of Nox2 and Nox4 was detected to reflect the activity of NADPH oxidase. Activities of SOD and CAT and levels of MDA and 8-OHdG were measured to evaluate the intracellular oxidative stress.

The results showed that COM markedly increased intracellular ROS production in accordance with the high concentration of the Ang II group (Figure 3(a)). Expression of NADPH oxidase subunits (Nox2 and Nox4) was upregulated in both CaOx-induced NRK-52E cells and rat kidneys in the hyperoxaluria group by Western blotting analysis (Figures 3(b) and 3(c)). In addition, COM reduced cellular SOD and CAT activities and increased MDA and 8-OHdG levels, prompting a state of oxidative stress (Figure 3(d)). In contrast, preincubation of NRK-52E cells with apocynin reversed the ROS overproduction and activation of NADPH oxidase induced by COM (Figures 3(a)–3(d)). These results suggested that the activity of NADPH oxidase was enhanced by CaOx crystals and might be involved in the CaOx-induced ROS overproduction and oxidative stress.

3.5. CaOx Activated the ROS-Mediated Nuclear Factor-κB (NF-κB) Pathway and Expression of Stone-Related Proteins. The NF-κB pathway is involved in the production of many stone-related proteins in response to oxidative stress [11, 12]. We examined NF-κB pathway activity and expression of stone-related proteins (OPN, CD44, and MCP-1) in response to CaOx treatment. The results of Western blotting analysis showed that treatment with CaOx crystals significantly increased protein expression of NF-κB subunits (p50 and p65) (Figure 4(a)) and stone-related proteins (OPN, CD44, and MCP-1) (Figure 4(b)). Apocynin partially reversed the increased NF-κB pathway activity and expression of stone-related proteins (Figures 4(a) and 4(b)).

3.6. CaOx-Induced ROS Generation and Overproduction of Stone-Related Proteins Were Activated via Ang II/AT1R. In the above results, we showed that both Ang II/AT1R and ROS levels were increased by COM treatment and high Ang II promoted ROS generation. Next, we tried to determine whether CaOx-induced ROS overproduction was activated via Ang II/AT1R. The mRNA levels of AT1R in NRK-52E cells transfected with AT1R siRNA-1, siRNA-2, or siRNA-3 were decreased compared with the negative control group (NC group, scrambled siRNA transfected) and the mock group (transfection reagent treated only) (Figure 5(a)). The AT1R siRNA-3-transfected group achieved the best silencing and was used in subsequent experiments. The protein level of AT1R was downregulated in the COM + Ang

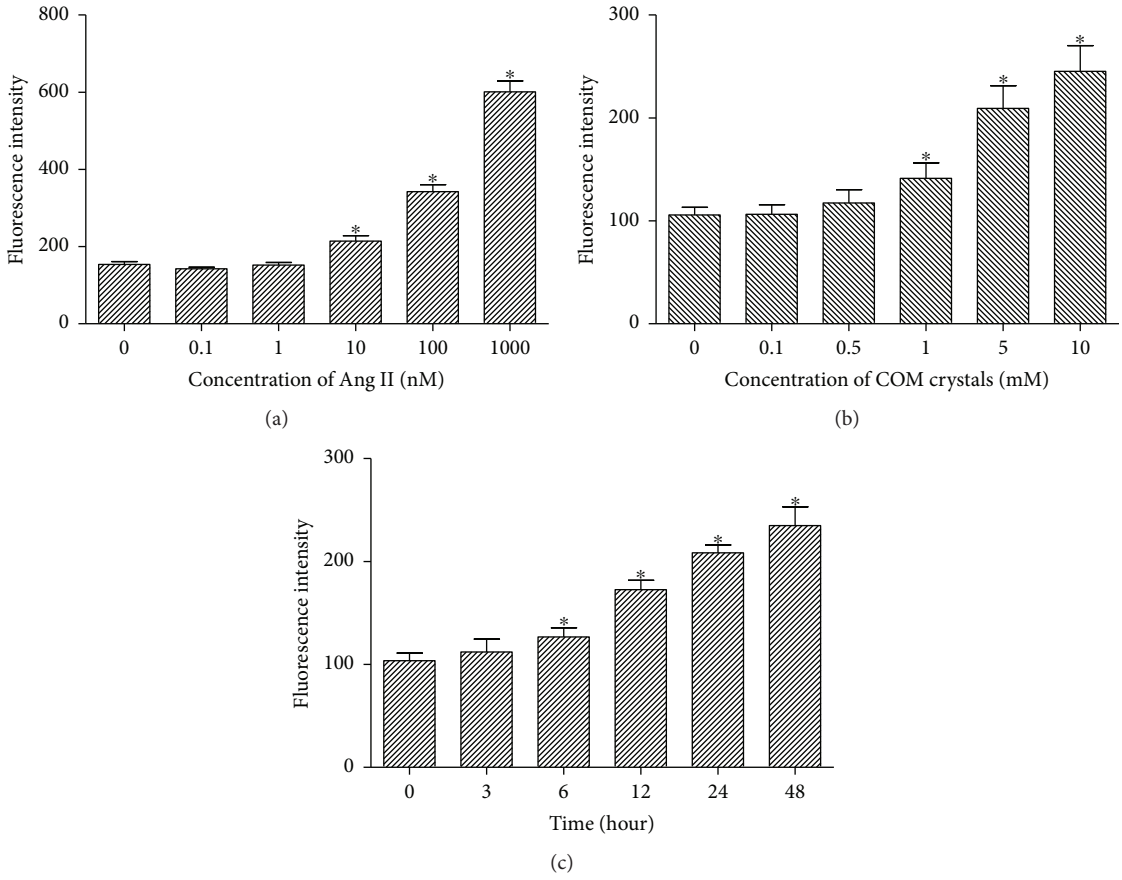

Figure 1: Effects of Ang II and COM on ROS generation in NRK-52E cells. (a) Cells were treated with various Ang II (0.1, 1, 10, 100, and 1000 nM) for 6 h, and then intracellular ROS was detected by flow cytometry. (b) Cells were treated with various COM (0, 0.1, 0.5, 1, 5, and 10 mM) for 6 h, and then intracellular ROS was detected by flow cytometry. (c) Cells were treated with COM (1 mM) for 0, 3, 6, 12, 24, and 48 h, and then intracellular ROS was detected by flow cytometry. The data are expressed as mean ± SEM. $^*P < 0.05$ compared with the control group.

II + AT1R siRNA-3 group compared with the COM + Ang II group, which validated the silencing effect of the siRNA (Figure 5(b)). These results showed that downregulation of AT1R remarkably inhibited the activation of ROS (Figure 5(c)) and expression of NADPH oxidase subunits (Nox2 and Nox4) (Figure 5(d)). Furthermore, expression of NF-κB subunits (p50 and p65) (Figure 5(e)) and stone-related proteins (OPN, CD44, and MCP-1) (Figure 5(f)) was decreased in the AT1R siRNA-3-transfected group.

3.7. Losartan Downregulated NF-κB Pathway Activity and Stone-Related Protein Expression by Attenuation of Renal Tubular Cell Oxidative Stress. To elucidate the effect of losartan on NF-κB pathway activity and stone-related protein expression in renal tubular cells as well as its association with ROS production, NRK-52E cells were preincubated with losartan for 1 h and then treated with COM for 6 h. As shown in Figure 6, losartan attenuated ROS production (Figure 6(a)) and NADPH oxidase activity (Figure 6(b)) in the presence of COM, meanwhile the NF-κB pathway activity (p50 and p65) (Figure 6(c)) and expression of stone-related proteins (OPN, CD44, and MCP-1) (Figure 6(d)) were decreased at protein levels. As a proof, renal crystal depositions were also significantly ameliorated in rat kidneys of the losartan group compared with the hyperoxaluria group, as examined by Von Kossa staining (Figure 6(e)).

4. Discussion

Over the past decades, mechanisms in regard to formation of kidney stones are poorly understood. CaOx is the major mineral constituent of most kidney stones. The formation of CaOx stones involves crystal nucleation, growth, aggregation, and finally retention within the kidneys. Many hypotheses such as Randall's plaques or plugs theory, renal tubular cell inflammatory injury theory, were proposed to explain the origin and formation of kidney stones [13, 14]. Crystal-cell interaction is thought as one of the earliest processes in the formation of urinary stone disease [15]. Exposure to high levels of oxalate or CaOx crystals results in excess production of cellular ROS, followed by inflammation and injury of renal tubular cells [2]. Increasing evidence indicates that ROS is involved in the formation of CaOx stones by regulating multiple signaling pathways including NF-κB and mitogen-activated protein kinase (MAPK) [16–18]. Activation of these transduction pathways leads to elevation of many

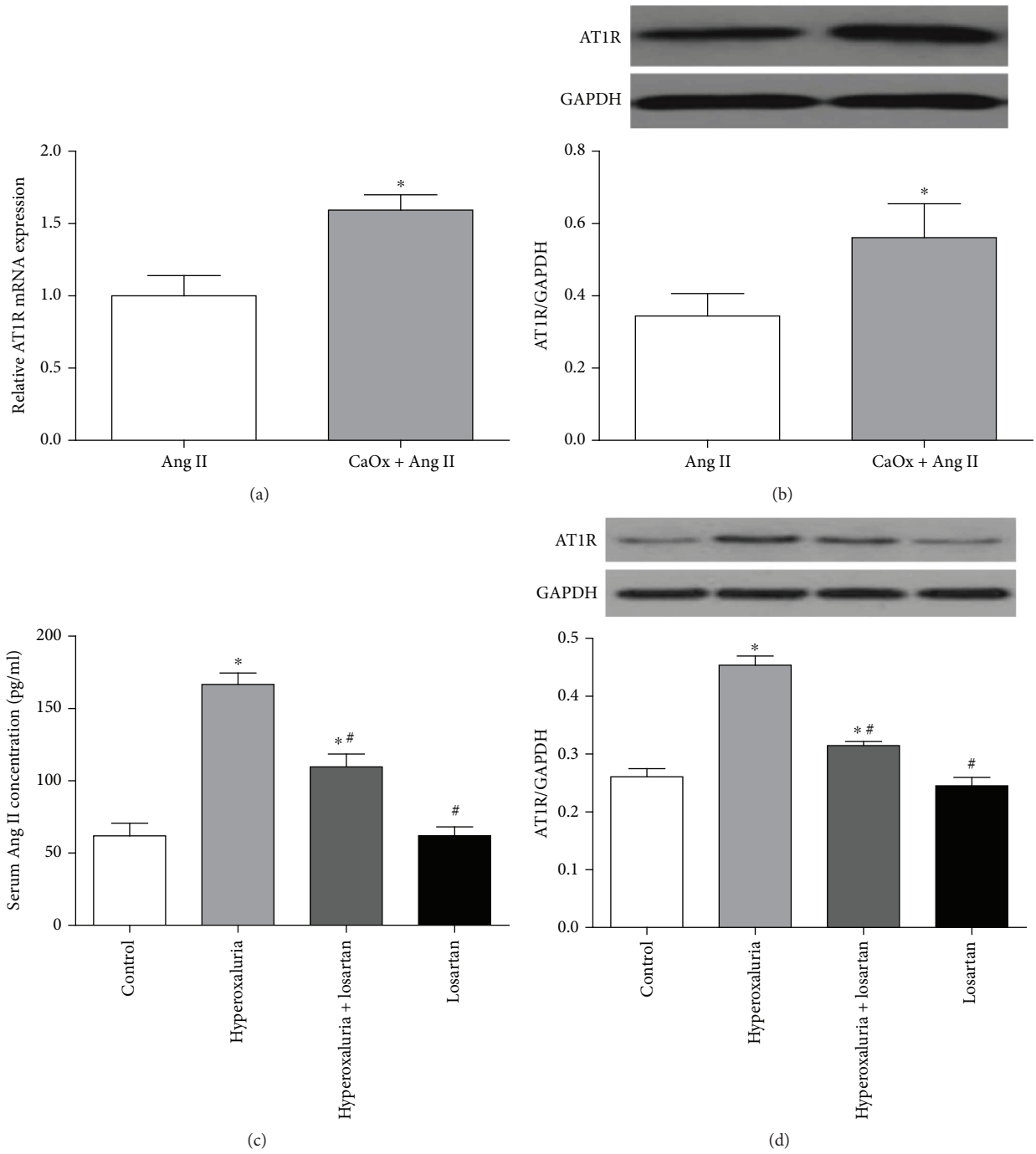

Figure 2: Ang II/AT1R expression was increased during exposure to CaOx crystals which was alleviated by losartan. NRK-52E cells were cultivated with COM (1 mM) for 6 h; the expression of AT1R was increased at both mRNA (a) and protein (b) levels. $^{*}P < 0.05$ compared with the Ang II group. (c) The serum concentration of Ang II was increased in the hyperoxaluria group compared with the untreated control group which was alleviated by losartan administration. (d) AT1R expression of the hyperoxaluria group was upregulated compared with the untreated control group which was also alleviated by losartan administration, as determined by Western blotting. The data are expressed as mean ± SEM. $^{*}P < 0.05$ compared with the control group and $^{\#}P < 0.05$ compared with the hyperoxaluria group.

stone-related proteins such as OPN, CD44, MCP-1, and Tamm-Horsfall protein, which affects cell-crystal interactions and stone formation [3].

NADPH oxidase is one of the major sources of ROS in response to oxalate or CaOx crystals [14]. According to the Nox catalytic subunit, NADPH oxidases are divided into seven isoforms consisting of Nox1–5, Duox1, and Duox2. Among these Nox isoforms, Nox4 and Nox2 are abundantly expressed in the kidney and have attracted broad investigations [4, 19, 20]. Apocynin, a common NADPH oxidase

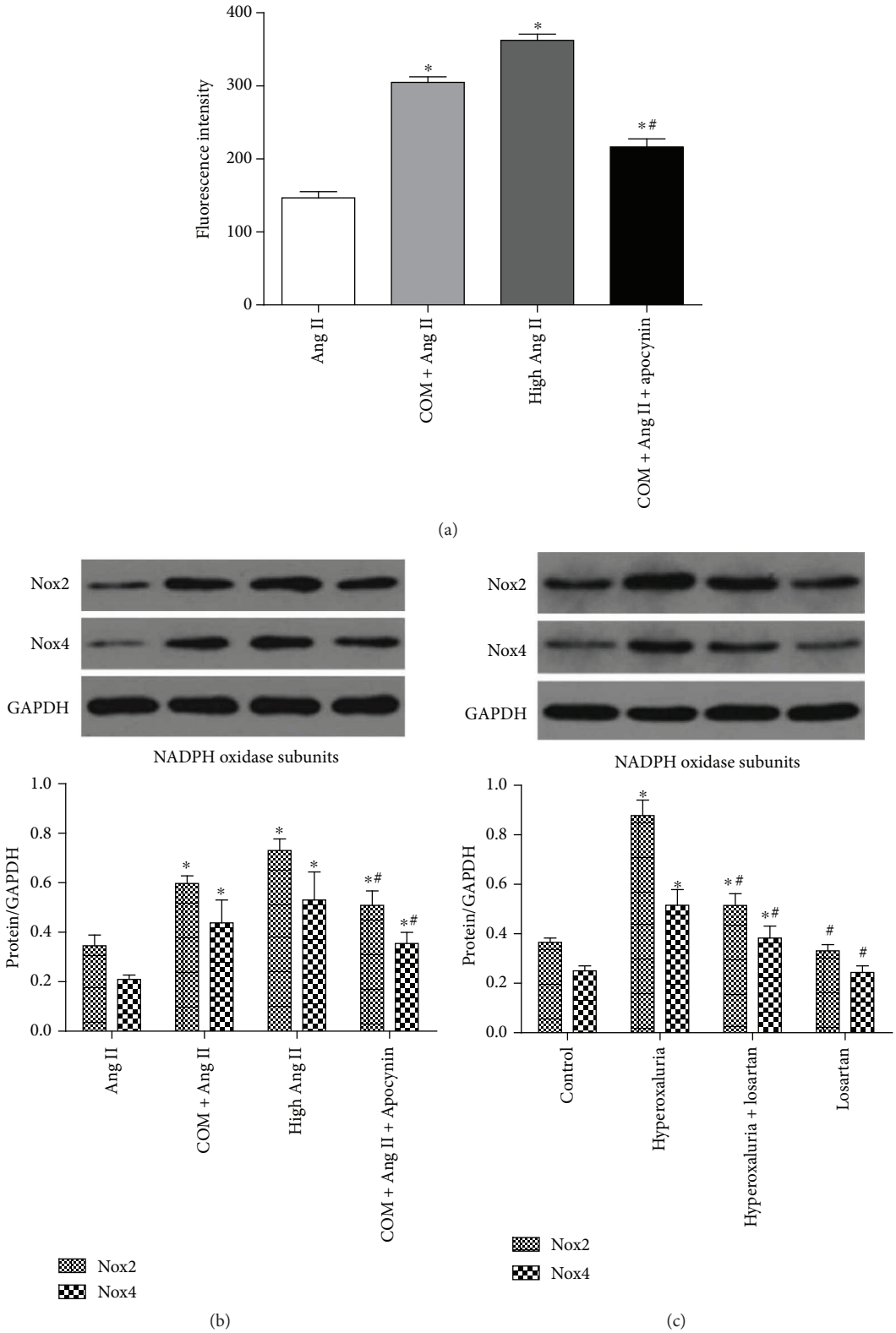

Figure 3: Continued.

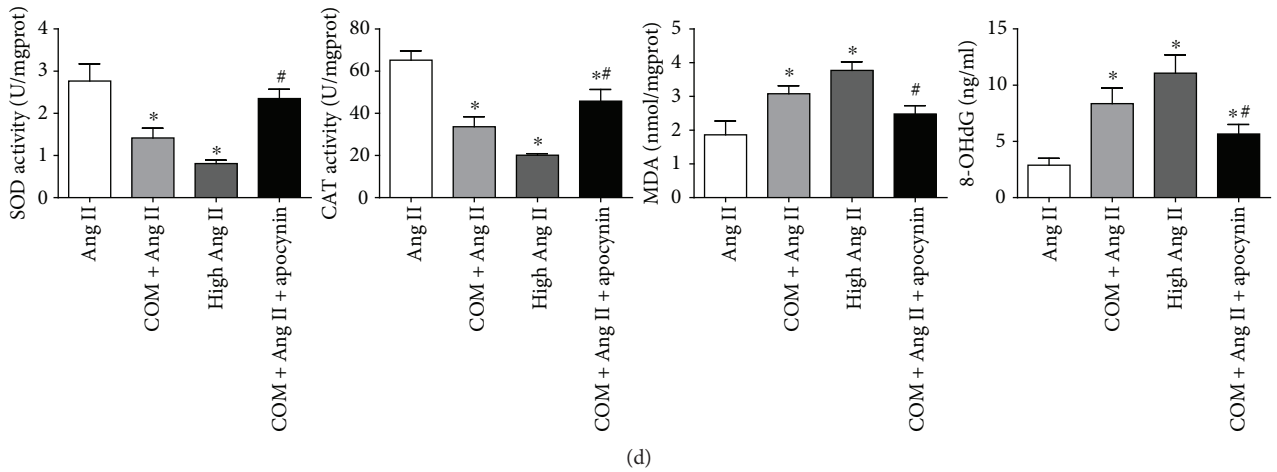

Figure 3: ROS and NADPH oxidase were upregulated under stimulation of CaOx crystals. (a) NRK-52E cells were induced by COM (1 mM) for 6 h with or without apocynin preincubation, and then intracellular ROS was detected by flow cytometry. Expression of Nox2 and Nox4 was upregulated in CaOx-induced NRK-52E cells (b) and rat kidneys in the hyperoxaluria group (c), as determined by Western blotting analysis, and the alteration could be reversed by apocynin or losartan administration. (d) COM (1 mM) reduced cellular SOD and CAT activities and increased MDA and 8-OHdG expression in NRK-52E cells which was reversed by apocynin administration. The data are expressed as mean ± SEM. $^{*}P < 0.05$ compared with the Ang II group or control group and $^{\#}P < 0.05$ compared with the COM + Ang II group or hyperoxaluria group.

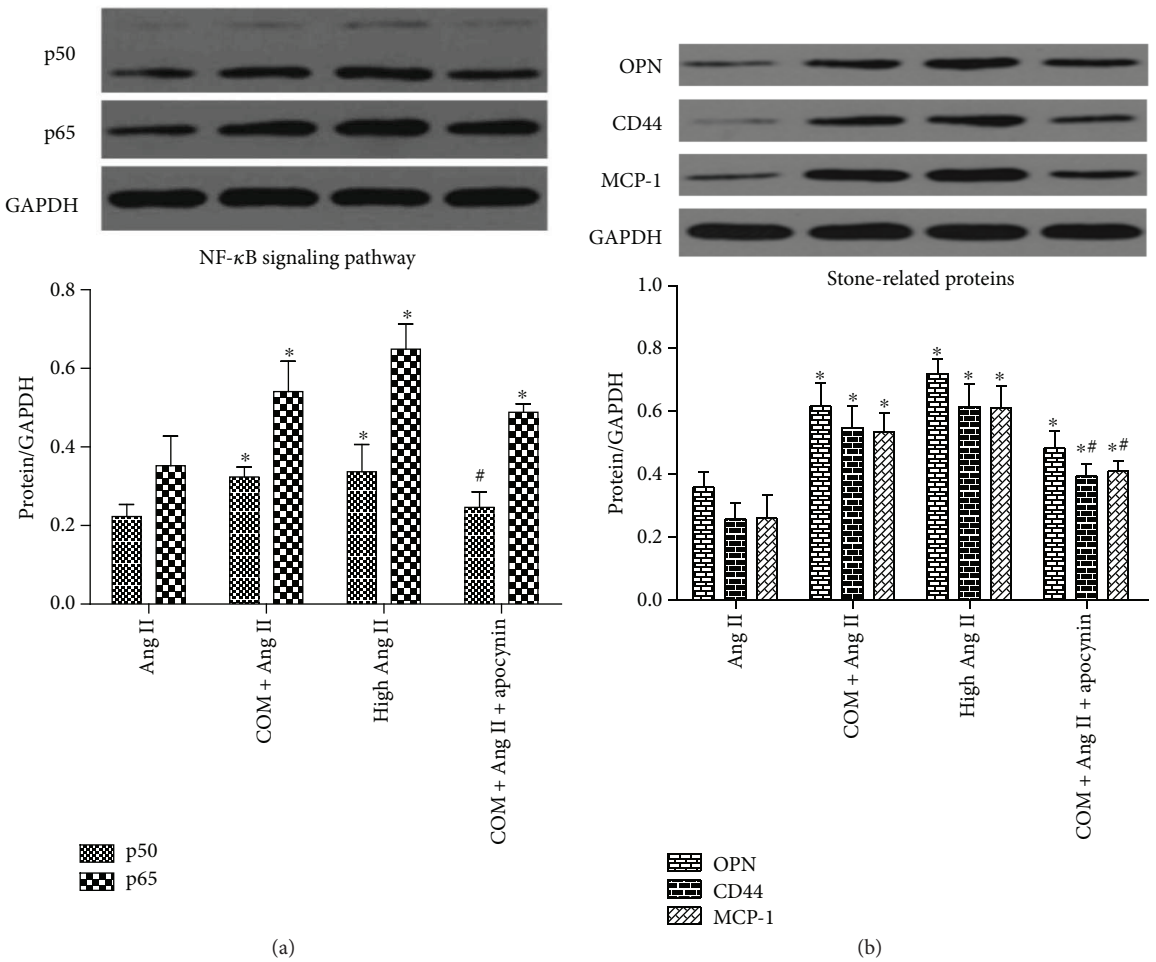

Figure 4: CaOx activated the ROS-mediated NF-κB pathway and expression of stone-related proteins. NRK-52E cells were induced by COM (1 mM) for 6 h with or without apocynin preincubation, and then NF-κB subunits (p50 and p65) (a) and expression of stone-related proteins (OPN, CD44, and MCP-1) (b) were detected by Western blotting. The data are expressed as mean ± SEM. $^{*}P < 0.05$ compared with the Ang II group and $^{\#}P < 0.05$ compared with the COM + Ang II group. $^{*\#}P < 0.05$ compared with the Ang II group and the COM + Ang II group.

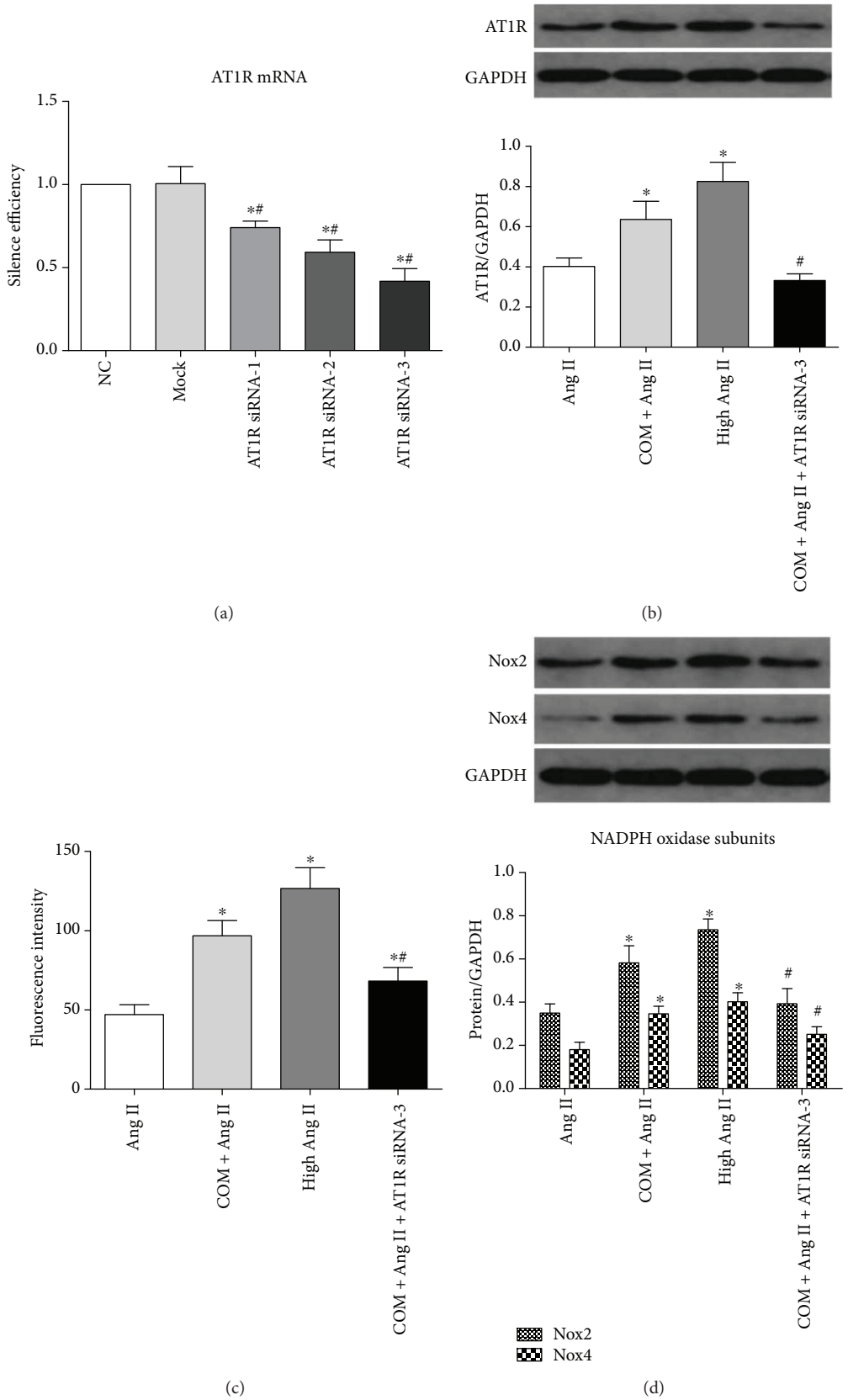

Figure 5: Continued.

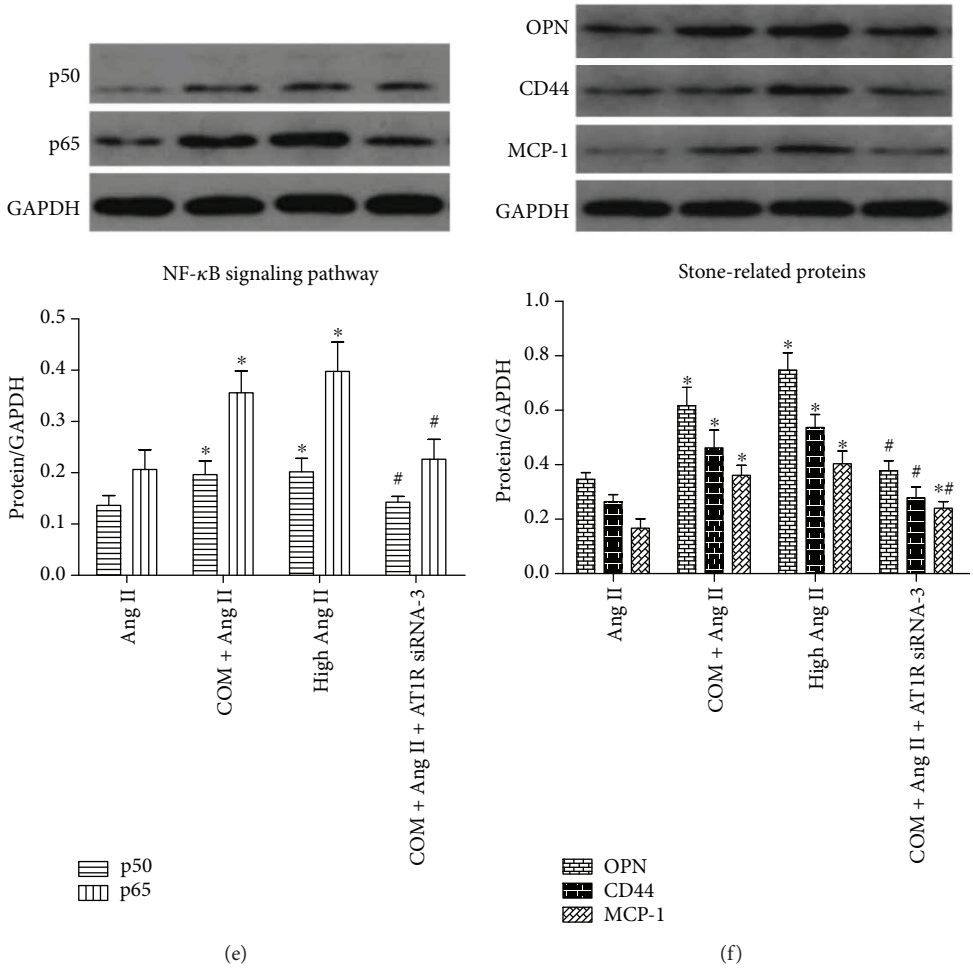

Figure 5: CaOx induced ROS generation and overproduction of stone-related proteins was activated via Ang II/AT1R. (a) The mRNA level of AT1R in NRK-52E cells transfected with AT1R siRNA-1, siRNA-2, or siRNA-3 compared with the negative control group (NC group) (scrambled siRNA transfected) and the mock group (transfection reagent treated only). $^{*}P < 0.05$ compared with the NC group and $^{\#}P < 0.05$ compared with the mock group. (b) The protein level of AT1R was downregulated in the COM + Ang II + AT1R siRNA-3 group compared with the COM + Ang II group. (c) The ROS generation was decreased in the COM + Ang II + AT1R siRNA-3 group compared with the COM + Ang II group. The expression of NADPH oxidase subunits (Nox2 and Nox4) (d), NF-κB subunits (p50 and p65) (e), and stone-related proteins (OPN, CD44, and MCP-1) (f) in the COM + Ang II and COM + Ang II + AT1R siRNA-3 groups was detected by Western blotting in NRK-52E cells. The data are expressed as mean ± SEM. $^{*}P < 0.05$ compared with the Ang II group and $^{\#}P < 0.05$ compared with the COM + Ang II group. $^{*\#}P < 0.05$ compared with the Ang II group and the COM + Ang II group.

inhibitor, reverses renal injury and significantly decreases kidney deposition of CaOx crystals in a rat model of hydroxyproline-induced hyperoxaluria [21].

The RAS regulates homeostasis of electrolytes, body fluids, and blood pressure under physiological conditions. It has been recognized as a key regulator of many cardiovascular diseases such as hypertension, myocardial ischemia, and congestive heart failure [22–24]. High levels of Ang II were reported to increase ROS production in cardiomyocytes [25]. Recent studies showed activation of the RAS in a hyperoxaluric rat model, which might be associated with ROS production and CaOx crystallization [16, 26]. Decreasing angiotensin production or blocking angiotensin receptors may reduce OPN expression and ameliorate crystal deposition [8]. These previous studies implied that Ang II might have a regulating effect on ROS production and CaOx stone formation.

In our study, we explored the physiological concentration of Ang II, which had little impact on ROS generation. The results showed that 1 nM Ang II was able to simulate the physiological state and was adopted as a physiological concentration in subsequent experiments. Ang II at 1 μM significantly increased ROS generation and was used as a positive control. Next, we detected the expression of Ang II/AT1R in COM-treated NRK-52E cells and in hyperoxaluric rats. The results showed that the serum Ang II concentration was increased in hyperoxaluric rats and AT1R expression was increased in kidney tissues and the cell line. We also examined ROS production and OS status after treatment with CaOx *in vivo* and *in vitro*. The results confirmed that intracellular ROS production and lipid peroxidation levels were increased by CaOx treatment. The activity of NADPH oxidase was enhanced by upregulation of Nox2 and Nox4 under CaOx exposure, and apocynin reversed this increased

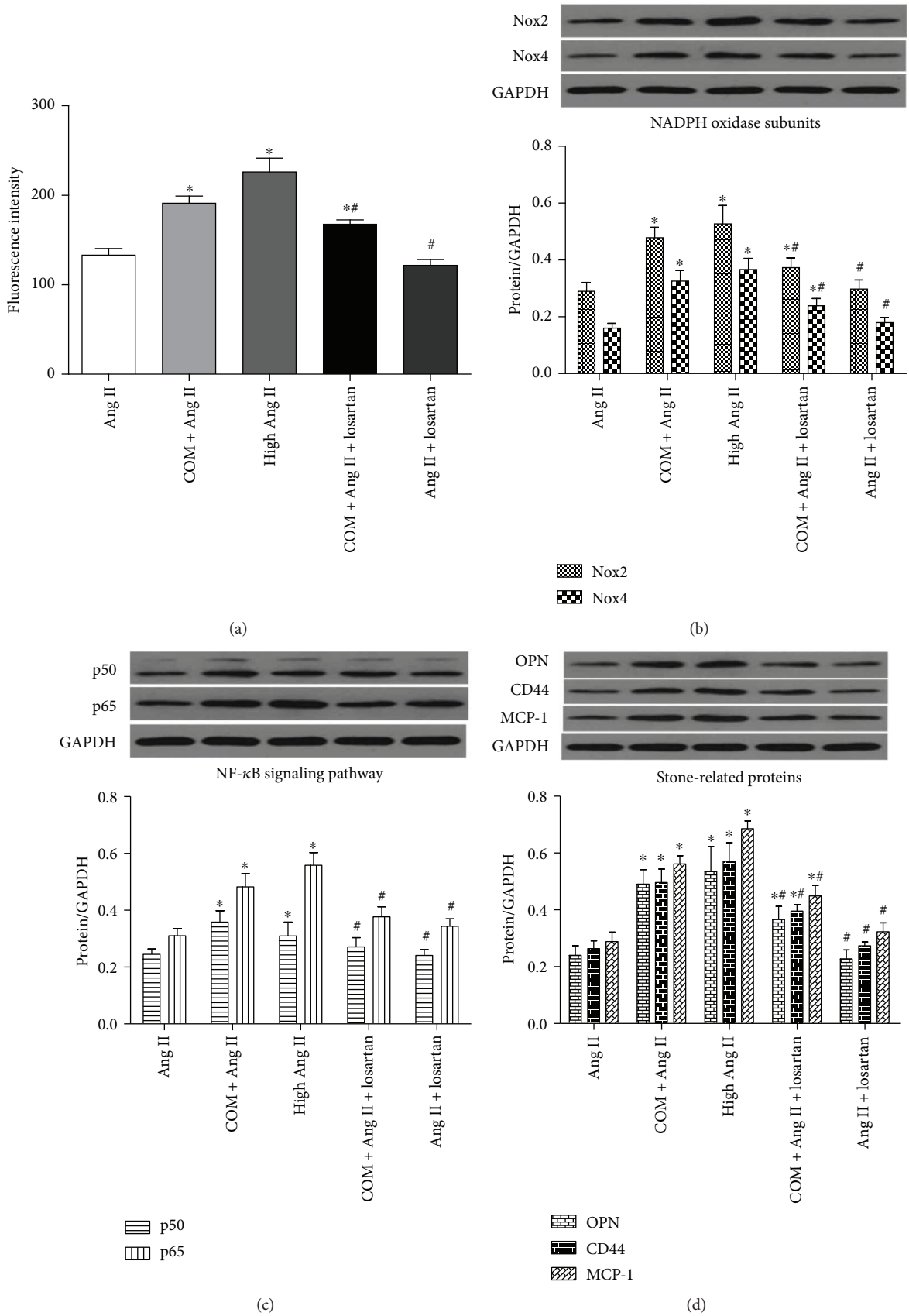

Figure 6: Continued.

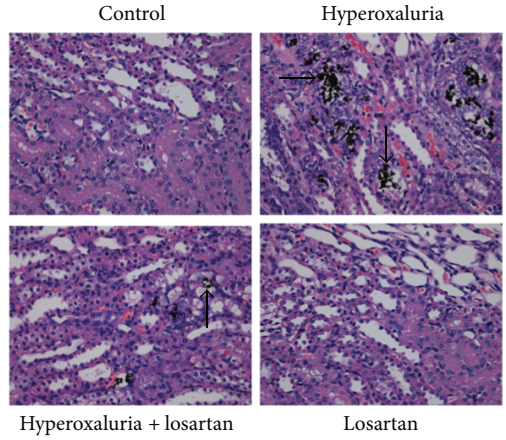

(e)

Figure 6: Losartan downregulated NF-κB pathway activity and stone-related protein expression by attenuation of renal tubular cell oxidative stress. (a) NRK-52E cells were induced by COM (1 mM) for 6 h with or without losartan preincubation, and then intracellular ROS was detected by flow cytometry. The expression of NADPH oxidase subunits (Nox2 and Nox4) (b), NF-κB subunits (p50 and p65) (c), and stone-related proteins (OPN, CD44, and MCP-1) (d) was decreased in the COM + Ang II + losartan group compared with the COM + Ang II group in NRK-52E cells. (e) Losartan administration ameliorated the CaOx depositions (black arrow) compared with the rat kidneys of the hyperoxaluria group (Von Kossa staining, magnification: ×400). The data are expressed as mean ± SEM. $^{*}P < 0.05$ compared with the Ang II group and $^{\#}P < 0.05$ compared with the COM + Ang II group. $^{*\#}P < 0.05$ compared with the Ang II group and the COM + Ang II group.

effect. We also found that the activity of NF-κB and expression of stone-related proteins (OPN, CD44, and MCP-1) were increased by CaOx treatment and similarly reversed by apocynin.

Furthermore, we examined the relationship between Ang II/AT1R and ROS production. Our *in vivo* results demonstrated that CaOx-induced ROS upregulation was mediated by Ang II/AT1R. Moreover, inhibition of AT1R by losartan or AT1R siRNA attenuated ROS production and oxidative stress levels in renal tubular cells by inhibiting NADPH oxidase. The NF-κB pathway activity and expression of stone-related proteins were downregulated simultaneously.

There are some limitations in our study. First, we merely investigated total ROS production and expression of NADPH oxidase subunits, but did not refer to ROS generated by mitochondria. Second, the role of AT2R under stimulation by CaOx was not involved in this study. Moreover, the detailed mechanism of Ang II/AT1R-mediated expression of NADPH oxidase and production of ROS is yet to be studied.

5. Conclusion

In summary, the present study provided evidence of upregulated Ang II/AT1R in NRK-52E cells treated with CaOx and in hyperoxaluric rat kidneys. We preliminarily demonstrated that CaOx-induced ROS and stone-related protein upregulation were mediated by Ang II/AT1R via activation of NADPH oxidase. Losartan reduced renal tubular cell expression of stone-related proteins and renal crystallization via inhibiting NADPH oxidase and oxidative stress. These findings indicate that AT1R inhibitor losartan might be a promising preventive and therapeutic candidate for hyperoxaluria nephrolithiasis.

Disclosure

The funders had no role in study design, data collection and analysis, decision to publish, or preparation of the manuscript.

Conflicts of Interest

The authors have declared that no competing interests exist.

Acknowledgments

This study was supported by grants from the National Natural Science Foundation of China (no. 81570631 and no. 81770704).

References

[1] A. Neisius and G. M. Preminger, "Stones in 2012: epidemiology, prevention and redefining therapeutic standards," *Nature Reviews Urology*, vol. 10, no. 2, pp. 75–77, 2013.

[2] J. Zhang, Q. Wang, C. Xu et al., "MitoTEMPO prevents oxalate induced injury in NRK-52E cells via inhibiting mitochondrial dysfunction and modulating oxidative stress," *Oxidative Medicine and Cellular Longevity*, vol. 2017, Article ID 7528090, 9 pages, 2017.

[3] S. R. Khan, "Reactive oxygen species as the molecular modulators of calcium oxalate kidney stone formation: evidence from clinical and experimental investigations," *The Journal of Urology*, vol. 189, no. 3, pp. 803–811, 2013.

[4] M. Sedeek, R. Nasrallah, R. M. Touyz, and R. L. Hébert, "NADPH oxidases, reactive oxygen species, and the kidney: friend and foe," *Journal of the American Society of Nephrology*, vol. 24, no. 10, pp. 1512–1518, 2013.

[5] S. Joshi, A. B. Peck, and S. R. Khan, "NADPH oxidase as a therapeutic target for oxalate induced injury in kidneys," *Oxidative*

Medicine and Cellular Longevity, vol. 2013, Article ID 462361, 18 pages, 2013.

[6] S. Joshi, B. T. Saylor, W. Wang, A. B. Peck, and S. R. Khan, "Apocynin-treatment reverses hyperoxaluria induced changes in NADPH oxidase system expression in rat kidneys: a transcriptional study," *PLoS One*, vol. 7, no. 10, article e47738, 2012.

[7] H. Tsuji, W. Wang, J. Sunil et al., "Involvement of renin–angiotensin–aldosterone system in calcium oxalate crystal induced activation of NADPH oxidase and renal cell injury," *World Journal of Urology*, vol. 34, no. 1, pp. 89–95, 2016.

[8] T. Umekawa, Y. Hatanaka, T. Kurita, and S. R. Khan, "Effect of angiotensin II receptor blockage on osteopontin expression and calcium oxalate crystal deposition in rat kidneys," *Journal of the American Society of Nephrology*, vol. 15, no. 3, pp. 635–644, 2004.

[9] C. Cabello-Verrugio, M. J. Acuña, M. G. Morales, A. Becerra, F. Simon, and E. Brandan, "Fibrotic response induced by angiotensin-II requires NAD(P)H oxidase-induced reactive oxygen species (ROS) in skeletal muscle cells," *Biochemical and Biophysical Research Communications*, vol. 410, no. 3, pp. 665–670, 2011.

[10] Q. Su, C.-J. Huo, H.-B. Li et al., "Renin-angiotensin system acting on reactive oxygen species in paraventricular nucleus induces sympathetic activation *via* AT1R/PKCγ/Rac1 pathway in salt-induced hypertension," *Scientific Reports*, vol. 7, article 43107, 2017.

[11] K. Tozawa, T. Yasui, A. Okada et al., "NF–κB activation in renal tubular epithelial cells by oxalate stimulation," *International Journal of Urology*, vol. 15, no. 10, pp. 924–928, 2008.

[12] Y. Lu, B. Qin, H. Hu et al., "Integrative microRNA-gene expression network analysis in genetic hypercalciuric stone-forming rat kidney," *PeerJ*, vol. 4, article e1884, 2016.

[13] S. R. Khan and B. K. Canales, "Unified theory on the pathogenesis of Randall's plaques and plugs," *Urolithiasis*, vol. 43, no. S1, Supplement 1, pp. 109–123, 2015.

[14] S. R. Khan, "Reactive oxygen species, inflammation and calcium oxalate nephrolithiasis," *Translational Andrology and Urology*, vol. 3, no. 3, pp. 256–276, 2014.

[15] K. P. Aggarwal, S. Narula, M. Kakkar, and C. Tandon, "Nephrolithiasis: molecular mechanism of renal stone formation and the critical role played by modulators," *BioMed Research International*, vol. 2013, Article ID 292953, 21 pages, 2013.

[16] J. E. Toblli, G. Cao, G. Casas, I. Stella, F. Inserra, and M. Angerosa, "NF-κB and chemokine-cytokine expression in renal tubulointerstitium in experimental hyperoxaluria. Role of the renin-angiotensin system," *Urological Research*, vol. 33, no. 5, pp. 358–367, 2005.

[17] H. K. Koul, M. Menon, L. S. Chaturvedi et al., "COM crystals activate the p38 mitogen-activated protein kinase signal transduction pathway in renal epithelial cells," *Journal of Biological Chemistry*, vol. 277, no. 39, pp. 36845–36852, 2002.

[18] L. S. Chaturvedi, S. Koul, A. Sekhon, A. Bhandari, M. Menon, and H. K. Koul, "Oxalate selectively activates p38 mitogen-activated protein kinase and c-Jun N-terminal kinase signal transduction pathways in renal epithelial cells," *Journal of Biological Chemistry*, vol. 277, no. 15, pp. 13321–13330, 2002.

[19] C. E. Holterman, N. C. Read, and C. R. J. Kennedy, "Nox and renal disease," *Clinical Science*, vol. 128, no. 8, pp. 465–481, 2015.

[20] V. Thallas-Bonke, K. A. M. Jandeleit-Dahm, and M. E. Cooper, "Nox-4 and progressive kidney disease," *Current Opinion in Nephrology and Hypertension*, vol. 24, no. 1, pp. 74–80, 2015.

[21] J. Zuo, A. Khan, P. A. Glenton, and S. R. Khan, "Effect of NADPH oxidase inhibition on the expression of kidney injury molecule and calcium oxalate crystal deposition in hydroxy-L-proline-induced hyperoxaluria in the male Sprague–Dawley rats," *Nephrology Dialysis Transplantation*, vol. 26, no. 6, pp. 1785–1796, 2011.

[22] L. Te Riet, J. H. M. van Esch, A. J. M. Roks, A. H. van den Meiracker, and A. H. J. Danser, "Hypertension: renin–angiotensin–aldosterone system alterations," *Circulation Research*, vol. 116, no. 6, pp. 960–975, 2015.

[23] R. E. Schmieder, K. F. Hilgers, M. P. Schlaich, and B. M. W. Schmidt, "Renin-angiotensin system and cardiovascular risk," *The Lancet*, vol. 369, no. 9568, pp. 1208–1219, 2007.

[24] A. J. Ferreira, R. A. S. Santos, C. N. Bradford et al., "Therapeutic implications of the vasoprotective axis of the renin-angiotensin system in cardiovascular diseases," *Hypertension*, vol. 55, no. 2, pp. 207–213, 2010.

[25] C.-Z. Chiu, B.-W. Wang, and K.-G. Shyu, "Angiotensin II and the JNK pathway mediate urotensin II expression in response to hypoxia in rat cardiomyocytes," *Journal of Endocrinology*, vol. 220, no. 3, pp. 233–246, 2014.

[26] I. Yoshioka, M. Tsujihata, W. Akanae, N. Nonomura, and A. Okuyama, "Angiotensin type-1 receptor blocker candesartan inhibits calcium oxalate crystal deposition in ethylene glycol-treated rat kidneys," *Urology*, vol. 77, no. 4, pp. 1007.e9–1007.e14, 2011.

Hindawi
Oxidative Medicine and Cellular Longevity
Volume 2018, Article ID 2835787, 14 pages
https://doi.org/10.1155/2018/2835787

Review Article

Biological Activities and Potential Oral Applications of N-Acetylcysteine: Progress and Prospects

Yanping Pei,[1] Huan Liu,[2] Yi Yang,[3] Yanwei Yang,[4] Yang Jiao,[5] Franklin R. Tay,[6] and Jihua Chen[2]

[1]*Stomatology Department of Navy General Hospital, Beijing 100048, China*
[2]*State Key Laboratory of Military Stomatology & National Clinical Research Center for Oral Diseases & Shaanxi Key Laboratory of Oral Diseases, Department of Prosthodontics, School of Stomatology, The Fourth Military Medical University, Xi'an 710032, China*
[3]*Department of Neurosurgery, PLA Army General Hospital, Beijing 100700, China*
[4]*Department of Stomatology, Lanzhou General Hospital, Lanzhou Military Area Command of Chinese PLA, Lanzhou, Gansu 730050, China*
[5]*Department of Stomatology, PLA Army General Hospital, Beijing 100700, China*
[6]*Department of Endodontics, The Dental College of Georgia, Augusta University, Augusta, GA 30912, USA*

Correspondence should be addressed to Yang Jiao; jiaoyang1989731@163.com, Franklin R. Tay; ftay@augusta.edu, and Jihua Chen; jhchen@fmmu.edu.cn

Received 6 December 2017; Revised 22 January 2018; Accepted 30 January 2018; Published 22 April 2018

Academic Editor: Jolanta Czuczejko

N-Acetylcysteine (NAC), a cysteine prodrug and glutathione (GSH) precursor, has been used for several decades in clinical therapeutic practices as a mucolytic agent and for the treatment of disorders associated with GSH deficiency. Other therapeutic activities of NAC include inhibition of inflammation/NF-κB signaling and expression of proinflammatory cytokines. N-Acetylcysteine is also a nonantibiotic compound possessing antimicrobial property and exerts anticarcinogenic and antimutagenic effects against certain types of cancer. Recently, studies describing potentially important biological and pharmacological activities of NAC have stimulated interests in using NAC-based therapeutics for oral health care. The present review focused on the biological activities of NAC and its potential oral applications. The potential side effects of NAC and formulations for drug delivery were also discussed, with the intent of advancing NAC-associated treatment modalities in oral medicine.

1. Introduction

N-acetylcysteine (NAC) possesses therapeutic effects over a wide range of disorders. These disorders include cystic fibrosis, acetaminophen poisoning, chronic obstructive pulmonary disease, chronic bronchitis, doxorubicin-induced cardiotoxicity, human immunodeficiency virus infection, heavy metal toxicity, and psychiatric/neurological disorders [1]. Being a N-acetyl derivative of the amino acid L-cysteine, NAC is a cysteine prodrug and glutathione (GSH) precursor that helps scavenge free radicals and bind metal ions into complexes [1] (Figure 1). Because NAC possesses anti-inflammatory activity via inhibition of nuclear factor kappa-light-chain-enhancer of activated B cells (NF-κB) and modulation of proinflammatory cytokine synthesis [2], it has been used for modulating oxidative stress- and inflammation-related diseases [3]. Although NAC is not an antibiotic, it possesses antimicrobial properties and breaks down bacterial biofilms of medically relevant pathogens [4]. These characteristics render NAC a potential candidate for managing oral diseases.

The oral cavity is the first point of entry for different forms of environmental insults, including toxic chemicals, microbial infections, and mechanical injury. These insults

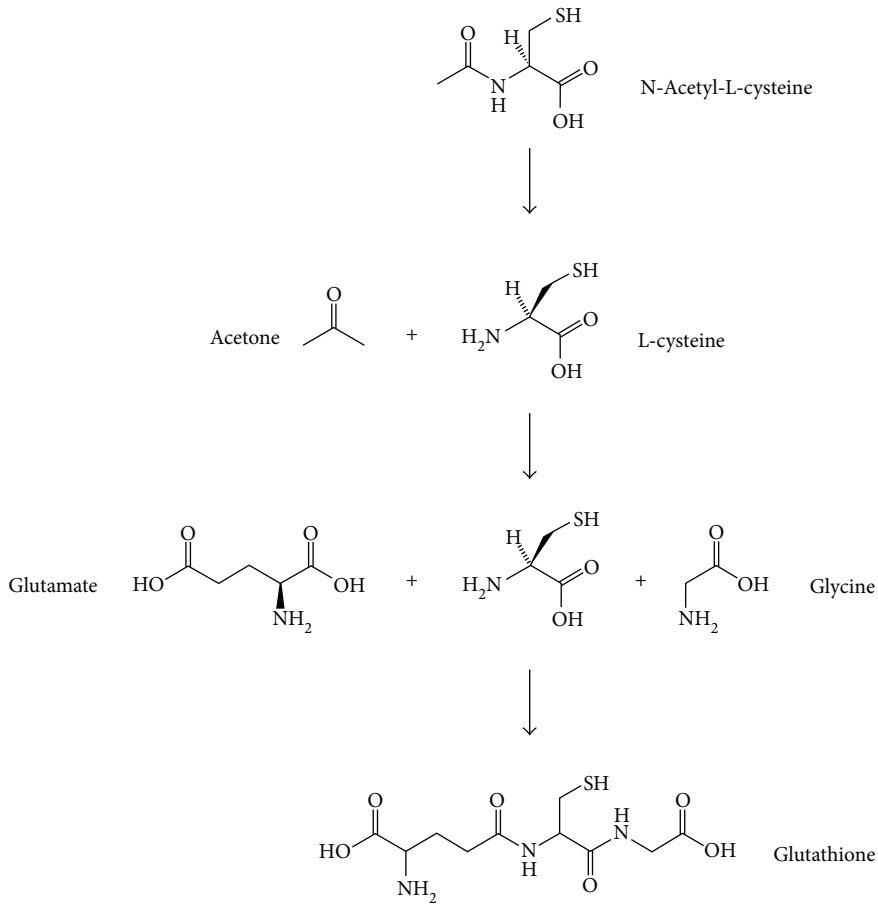

Figure 1: Chemical formula of N-acetyl cysteine and its conversion to glutathione.

generate oxidative stress, induce inflammation, and may even initiate cancer (Figure 2). Some dental materials such as resins, metals, and ceramics are cytotoxic and have the potential to induce oxidative stress, DNA damage, inflammatory reactions, and cell death via apoptosis [5–7]. Disturbances in the regulation of the host inflammatory responses to bacterial infection in the dental pulp and periodontal tissues result in pulpitis and periodontitis [8]. Cigarette smoking, alcohol consumption, and betel nut chewing increase the risk of oral cancer [9]. Mechanical stresses produced during physiological masticatory activities, orthodontic tooth movement, or occlusal trauma, as well as heat stresses caused by tooth cavity preparation, light-initiated resin polymerization, or laser irradiation, may create oxidative stresses and inflammatory reactions in the dental pulp, resulting in pulpal necrosis [10, 11]. Hence, there is a need for oral cells and tissues to efficiently detoxify xenobiotic toxicity, neutralize oxidative stress, kill invading pathogens, and eliminate inflammatory responses. In light of its potentially important biological and pharmacological activities, NAC has been advocated as a therapeutic agent in oral health care [12]. The present review focuses on the biological activities of NAC and its potential oral applications. The review also explores the potential side effects of NAC and its medical formulations. Understanding the actions of NAC and its biological effects on oral pathological processes is helpful in the design of future clinical trials and expedites clinical translation of the use of this drug in oral medicine.

2. Antioxidation Activity

Intracellular oxidative stress occurs when reactive oxygen species (ROS)/reactive nitrogen species (RNS) are produced beyond the cell's antioxidation capacity. Excessive oxidative stress results in oxidative modification of proteins, lipids, DNA, and subsequent cell death [13]. This process contributes to numerous pathological conditions including oral diseases [14]. Antioxidants, either natural or synthetic, are effective in diminishing the cumulative effects of oxidative stress and NAC is of particular interest. N-Acetylcysteine is a direct antioxidant that interacts with the electrophilic groups of free radicals through its free thiol side-chain. The rate constants of the reactions of NAC with various substrates under experimental conditions are summarized in Table 1. Because NAC reacts rapidly with hydroxyl radical ($^{\cdot}OH$), nitrogen dioxide ($^{\cdot}NO_2$), and carbon trioxide ion ($CO_3^{\cdot -}$), it detoxifies ROS produced by leukocytes [15]. Although NAC does not react directly with nitric oxide (NO), it reacts with its reduced and protonated form, nitroxyl (HNO) [16]. In addition, NAC chelates transition metal ions such as Cu^{2+} and Fe^{3+}, as well as heavy metal ions such as Cd^{2+}, Hg^{2+}, and Pb^{2+}, through

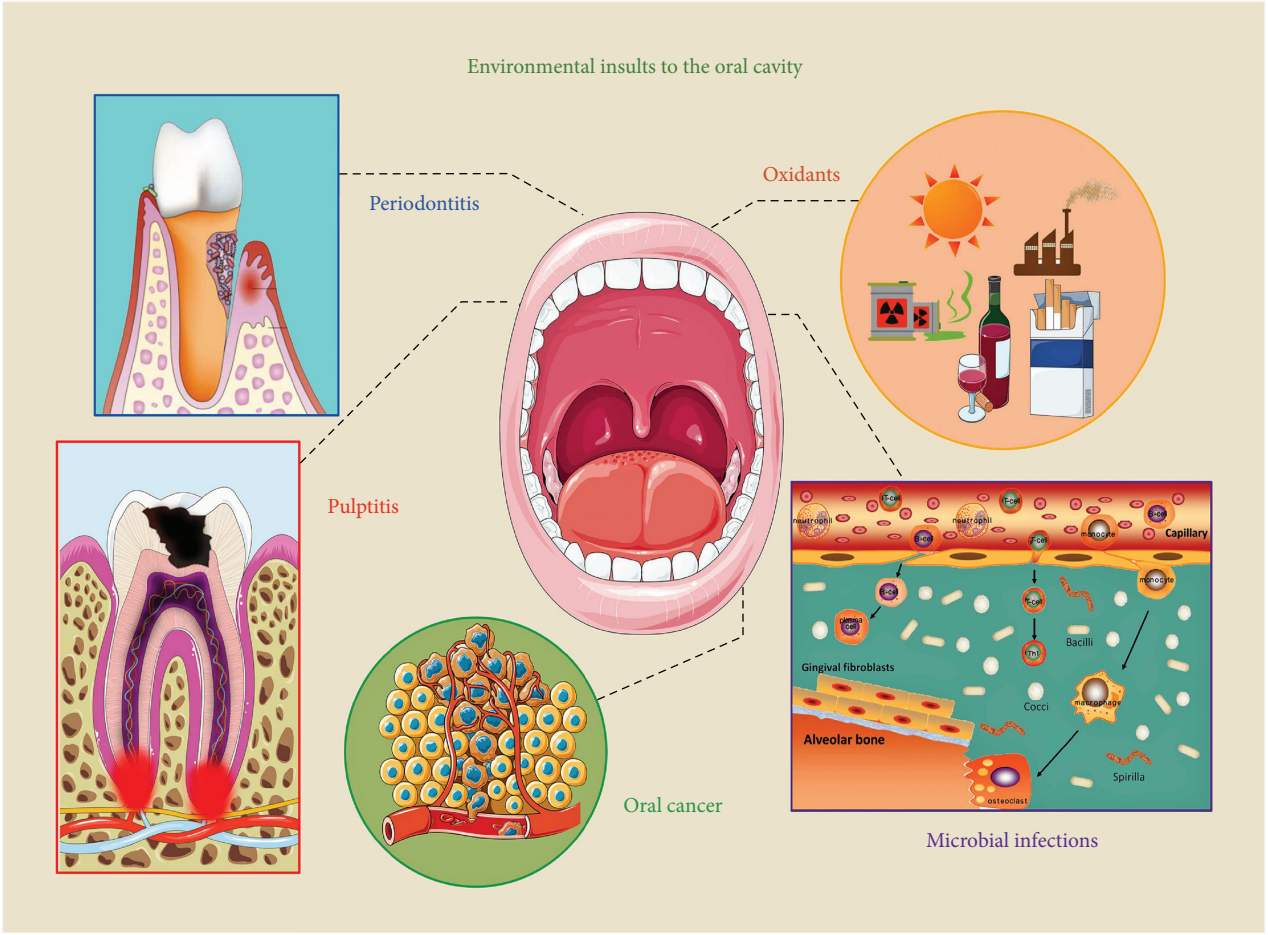

Figure 2: The oral cavity is exposed to different forms of environmental insults, including toxic chemicals, microbial infections, and mechanical injury. These insults generate oxidative stress, induce inflammation, and may even instigate cancer.

Table 1: Rate constants of N-acetylcysteine reactions with representative compounds (adapted from [12]).

Compounds	Rate constant (M^{-1} s^{-1})	Experimental conditions	Reference
$CO_3^{\cdot-}$	$\approx 1.0 \times 10^7$ 1.8×10^8	pH = 7; RT pH = 12; RT	[90]
HNO	5.0×10^5	pH = 7.4; 37°C	[91]
HOCl	$>10^7$	pH ≈ 7.4; 21–24°C	[92]
HOSCN	7.7×10^3	pH = 7.4; 22°C	[93]
H_2O_2	0.16 ± 0.01 0.85 ± 0.09	pH = 7.4; 25°C pH = 7.4; 37°C	[94] [95]
$^{\cdot}NO_2$	$\approx 2.4 \times 10^8$ $\approx 1.0 \times 10^7$	pH > pK_a; RT pH = 7.4; RT	[96]
$O_2^{\cdot-}$	68 ± 6 $<10^3$	pH = 7; RT pH = 7.4; 25°C	[97] [95]
$^{\cdot}OH$	1.36×10^{10}	pH = 7; RT	[95]
$ONOO^-$	415 ± 10	pH = 7.4; 37°C	[98]

RT: room temperature.

its thiol side-chain to produce complexes. This chelation process facilitates removal of these metal ions from the body [17].

Apart from its role as a direct antioxidant, NAC also functions as an indirect antioxidant. The rate constants of the reactions of NAC with superoxide ($O_2^{\cdot-}$), hydrogen peroxide (H_2O_2), and peroxynitrite ($ONOO^-$) are relatively low under physiological conditions. The indirect antioxidation action of NAC relies on replenishment of intracellular GSH, the body's major antioxidant with versatile cellular functions (see [18] for review). Considering the overwhelming antioxidation potential of GSH and the very low concentrations of NAC inside cells, it is likely that the predominant antioxidation effects of NAC are associated with maintaining GSH levels in the intracellular environment [19].

A plethora of *in vitro* and *in vivo* studies have demonstrated the protective effectiveness of NAC against various oxidative insults in the oral cavity. These insults include blue light irradiation [20], exposure to fluoride [21], H_2O_2 [22] and NO [23], and lipopolysaccharides [24], as well as dental and implantable materials [25] (Table 2). Residual monomers released from resin restorations due to incomplete polymerization could cause adverse biological reactions in oral tissues [26]. Based on *in vitro* studies of multiple target cells, resin monomers were detected to induce cytotoxic and genotoxic effects and specifically interfere with

Table 2: Representative studies on the protective effects of N-acetylcysteine against various oxidative insults in the oral cavity.

Insult	Cell model	Mode of action	NAC dose	NAC function	Reference
Co-Cr dental alloys	Human gingival fibroblasts, human osteoblasts	ROS ↑, TNF-α ↑, IL-1β ↑, IL-6 ↑, IL-8 ↑, iNOS ↑, NO ↑, COX-2 ↑, PGE2 ↑, Nrf2 ↑, NQO ↑, HO-1 ↑, GST ↑, GR ↑, GCL ↑, p-JAK2 ↑, p-STAT3 ↑, p-p38 MAPK ↑, p-ERK ↑, p-JNK ↑, NF-κB p65 ↑	20 mM	NAC pretreatment inhibited Co-Cr alloy-induced proinflammatory cytokine production and NF-κB activation	[99]
Dental resin monomers (e.g., HEMA, TEGDMA, MMA)	Human dental pulp cells	ROS ↑, GSH ↓, MDA ↑, SOD ↓, CAT ↑, GPx ↓, mitochondria dysfunction, intrinsic mitochondrial apoptosis	10 mM	NAC remarkably relieved dental resin monomer-induced oxidative stress and subsequently protected the cells against apoptosis	[25]
Dental quaternary ammonium monomer (e.g., DMAE-CB)	Human dental pulp cells, mouse fibroblasts	ROS ↑, cell cycle arrest, mitochondria dysfunction, intrinsic mitochondrial apoptosis	10 mM	NAC could reduce the cytotoxicity of quaternary ammonium monomers	[29, 100]
Dentin bonding agents	Human dental pulp cells	ALP ↓, DSPP ↓, OCN ↓, matrix, mineralization ↓	5 mM	NAC was useful for reversing cytotoxicity and antidifferentiation effects of dentin bonding agents on human dental pulp cells	[101]
Mineral trioxide aggregate (MTA)	Rat dental pulp cells	ROS ↑, GSH ↓	5 mM	The addition of NAC improved the number and spreading behavior, reduced ROS production, and increased the cellular antioxidant resources of rat dental pulp cells cultured on MTA	[102]
Root canal sealers	Mouse osteoblastic cell line	GSH ↓	10 mM	NAC prevented cytotoxicity and intracellular GSH depletion of root canal sealers	[103]
Photoinitiators (e.g., CQ)	Human dental pulp cells	ROS ↑, collagen I ↓, p21 ↑, HO-1 ↑, COX-2 ↑, p-ATM ↑, p-Chk2 ↑, p-p53 ↑, GADD45α ↑, 8-isoprostane ↑, PGE2 ↑, cell cycle arrest, apoptosis	2.5 mM, 5 mM	NAC prevented CQ-induced cytotoxicity, cell cycle arrest, apoptosis and PGE_2 production of pulp cells	[104]
Fluoride exposure	Rat hepatocytes	MDA ↑, SOD ↓, GPx ↓, GR ↑, GSH ↓, TAS ↓	1 mM	NAC pretreatment provided protection against fluoride-induced oxidative stress	[105]
Heat stress	Human dental pulp cells	ROS ↑, IL- 8↑, IL-8R ↑, HO-1 ↑, nuclear Nrf2 ↑, cytosolic Nrf2 ↓, SOD ↑, HO-1 ↑, GST ↑, GCL ↑, GR ↑	20 mM	The addition of NAC to cells blocked heat stress-activated proinflammatory chemokines and Nrf2-mediated antioxidant responses	[10]
Hydrogen peroxide (H_2O_2)	Rat palatal mucosal cells			NAC substantially reduced H_2O_2-induced elevation of cellular	[22]

Table 2: Continued.

Insult	Cell model	Mode of action	NAC dose	NAC function	Reference
		Apoptosis, collagen I ↓, collagen III ↓, P4H ↓, GSH ↓, GSSG ↑	2.5 mM, 5 mM, 10 mM	proliferation and collagen production associated with an increase in intracellular GSH reserves and decrease in GSSG	
Lipopolysaccharide (LPS)	Human gingival fibroblasts	ROS ↑, GSH/GSSG ↓, IL-1β ↑, IL-6 ↑, IL-8 ↑, TNF-α ↑, MMP2 ↑	10 mM, 20 mM	NAC prevented LPS-induced proinflammatory cytokines and MMP2 production	[41]
Mechanical stress	Human dental pulp cells	ROS ↑, IL-1β ↑, IL-6 ↑, IL-8 ↑, TNF-α ↑, HO-1 ↑, NQO-1 ↑, GPx ↑, SOD ↑, Nrf2 ↑	20 mM	NAC prevented the production of proinflammatory cytokines and ROS, as well as the activation of subsequent Nrf2-mediated gene transcription in response to mechanical strain	[11]
Nitric oxide (NO)	Human dental pulp cells	ROS ↑, intrinsic mitochondrial apoptosis	5 mM	NAC rescued the cell viability decreased by NO and downregulated NO-induced activation of proapoptotic mitochondria-dependent pathways	[23]

ALP: alkaline phosphatase; ATM: ataxia-telangiectasia mutated; CAT: catalase; Chk2: checkpoint kinase 2; Co: cobalt; COX-2: cyclooxygenase-2; CQ; camphorquinone; Cr: chromium; DSPP: dentin sialophosphoprotein; DMAE-CB: methacryloxylethyl cetyl ammonium chloride; ERK: extracellular signal-regulated kinase; GADD45α: growth arrest and DNA damage-inducible protein GADD45 alpha; GCL: γ-glutamylcysteine lygase; (GPx: glutathione peroxidase; GR: glutathione reductase; GSH: reduced glutathione; GSSG: oxidized form of glutathione; GST: glutathione S-transferase; HEMA: 2-hydroxyethyl methacrylate; HO-1: heme oxygenase 1; H_2O_2: hydrogen peroxide; IL-1β: interleukin-1beta; iNOS: inducible nitric oxide synthetase; JNK: c-Jun N-terminal kinase; LDH: lactate dehydrogenase; LPS: lipopolysaccharide; MDA: malondialdehyde; MMA: methyl methacrylate; MMP: matrix metalloproteinase; MTA: mineral trioxide aggregate; NAC: N-acetylcysteine; NF-κB: nuclear factor kappa-light-chain-enhancer of activated B cells; NO: nitric oxide; NQO: nitroquinoline 1-oxide; Nrf2: NF-E2-related factor 2; OCN: osteocalcin; PGE2: prostaglandin E2; p21: cyclin-dependent kinase inhibitor 1; p38 MAPK: p38 mitogen-activated protein kinase; P4H: prolyl-4 hydroxylase; p-JAK2: phosphorylation of janus kinase 2; ROS: reactive oxygen species; SOD: superoxide dismutase; STAT3: signal transducer and activator of transcription 3; TAS: total antioxidant status; TEGDMA: triethylenglycol dimethacrylate; TNF-α: tumor necrosis factor-alpha.

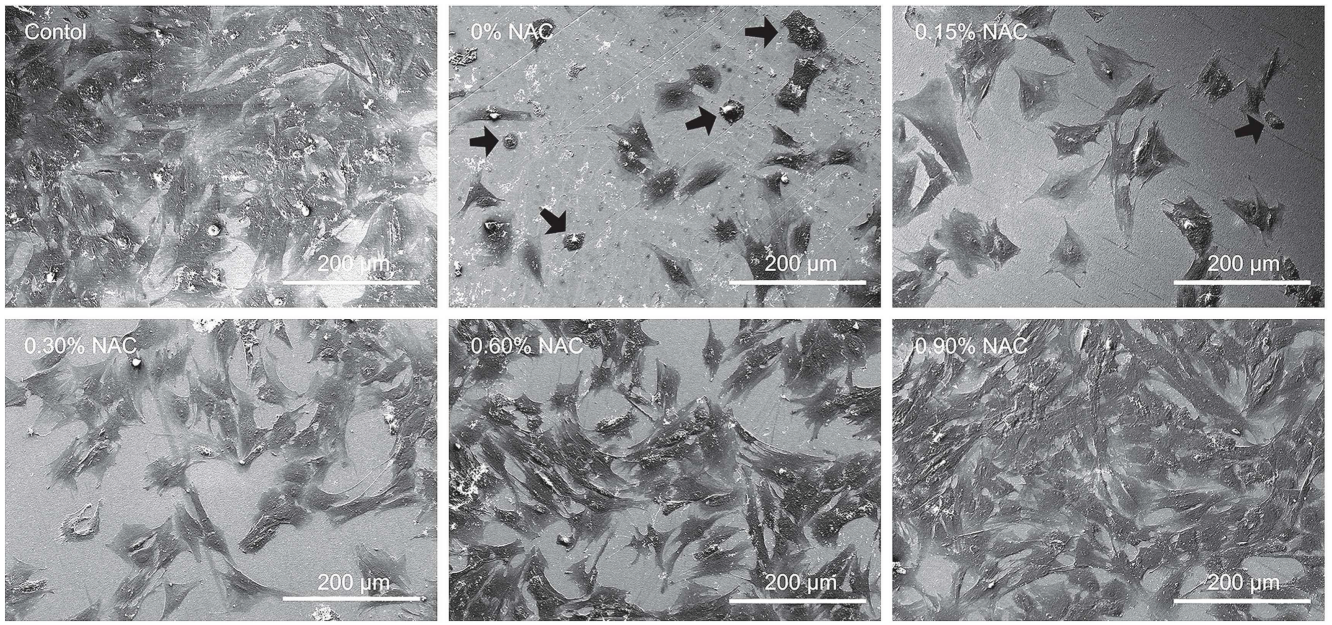

Figure 3: Representative scanning electron microscopy images showing attachment and morphology of human dental pulp cells on the surface of poly(methyl methacrylate) resin in the presence or absence of N-acetylcysteine (NAC). After culturing for 24 hours, human dental pulp cells grew poorly with round or collapsed appearances in subgroup 0 wt.% NAC and subgroup 0.15 wt.% NAC (arrows). In contrast, the cells attached and spread well with spindle or polygonal shapes in subgroups 0.3 wt.%, 0.6 wt.%, and 0.9 wt.% NAC. The number of adhering cells increased as the concentration of NAC increased in the experimental poly(methyl methacrylate) resin. Similar to the control, the resin surface of subgroup 0.9 wt.% NAC was almost fully covered by cells. Reprinted with permission [31].

various vital cellular functions [27]. Although the exact mechanism is still largely unknown, many prior reports suggest that these adverse effects are associated with monomer-induced oxidative stress as a consequence of the formation of ROS and concomitant with depletion of GSH [6]. Based on the findings that disturbance of intracellular redox balance is involved in the cytotoxic effects of resin monomers, NAC has been used and identified as an effective molecule to reduce such cytotoxicity [28]. At first, it was believed that NAC exerts protective effects against monomer-related cytotoxicity mainly through its antioxidative properties by directly scavenging overproduced ROS, meanwhile replenishing the exhausted intracellular GSH. However, very recently, some researchers have suggested a further relevant protective mechanism by providing evidence showing that NAC can directly react with the methacrylic group of resin monomers through Michael-type addition reaction thus reducing the availability of free dental resin monomers [29, 30]. Accordingly, NAC has been incorporated into poly(methyl methacrylate) (PMMA) dental resin. Addition of 0.15 weight percent (wt.%) NAC remarkably improves the biocompatibility of PMMA resin without exerting significant adverse influence on its mechanical properties [31] (Figure 3). NAC has also been shown to enhance differentiation of osteoblastic cells *in vitro* and accelerate bone healing when added to a collagenous sponge implanted in rat femoral critical size defects [32, 33]. These data highlight the potential of NAC for clinical application as an osteogenic enhancer in bone regeneration therapies. Significantly higher salivary ROS, lipid peroxidation, and NO and nitrite levels are present in oral lichen planus patients [34], suggesting antioxidants such as NAC have therapeutic potential in managing this disease.

3. Anti-Inflammatory Activity

Another potential therapeutic application of NAC stems from its anti-inflammatory activity (Figure 4). The transcription factor NF-κB plays a critical role in many aspects of the inflammation cascade and immune response by regulating the expression of related genes [35]. The anti-inflammatory effect of NAC is associated with the decrease of NF-κB activity; NAC suppresses ubiquitination and degradation of I-κB (an inhibitor of NF-κB) and thereby blocks NF-κB nuclear translocation and activation [36, 37]. As a direct antioxidant and GSH precursor, NAC scavenges free radicals and inhibits upstream NF-κB-activating events [38]. N-Acetylcysteine also modulates transcription activities through several pathways involving c-Fos/c-Jun, STAT, and cyclin inhibitors [39]. In oral inflammation, NAC prevents expression of lipopolysaccharide-induced proinflammatory cytokines such as interleukin-1β (IL-1β), IL-6 and IL-8, tumor necrosis factor-alpha (TNF-α), and transforming growth factor β (TGF- β) in macrophages [40] and gingival fibroblasts [41]. Restorative resin materials may cause inflammatory responses by monocyte activation and changes in the levels of released cytokines. This is demonstrated by augmented proinflammatory cytokine levels in the gingival crevicular fluid [42]. N-Acetylcysteine has been used to prevent inflammation in cytotoxicity studies of resinous

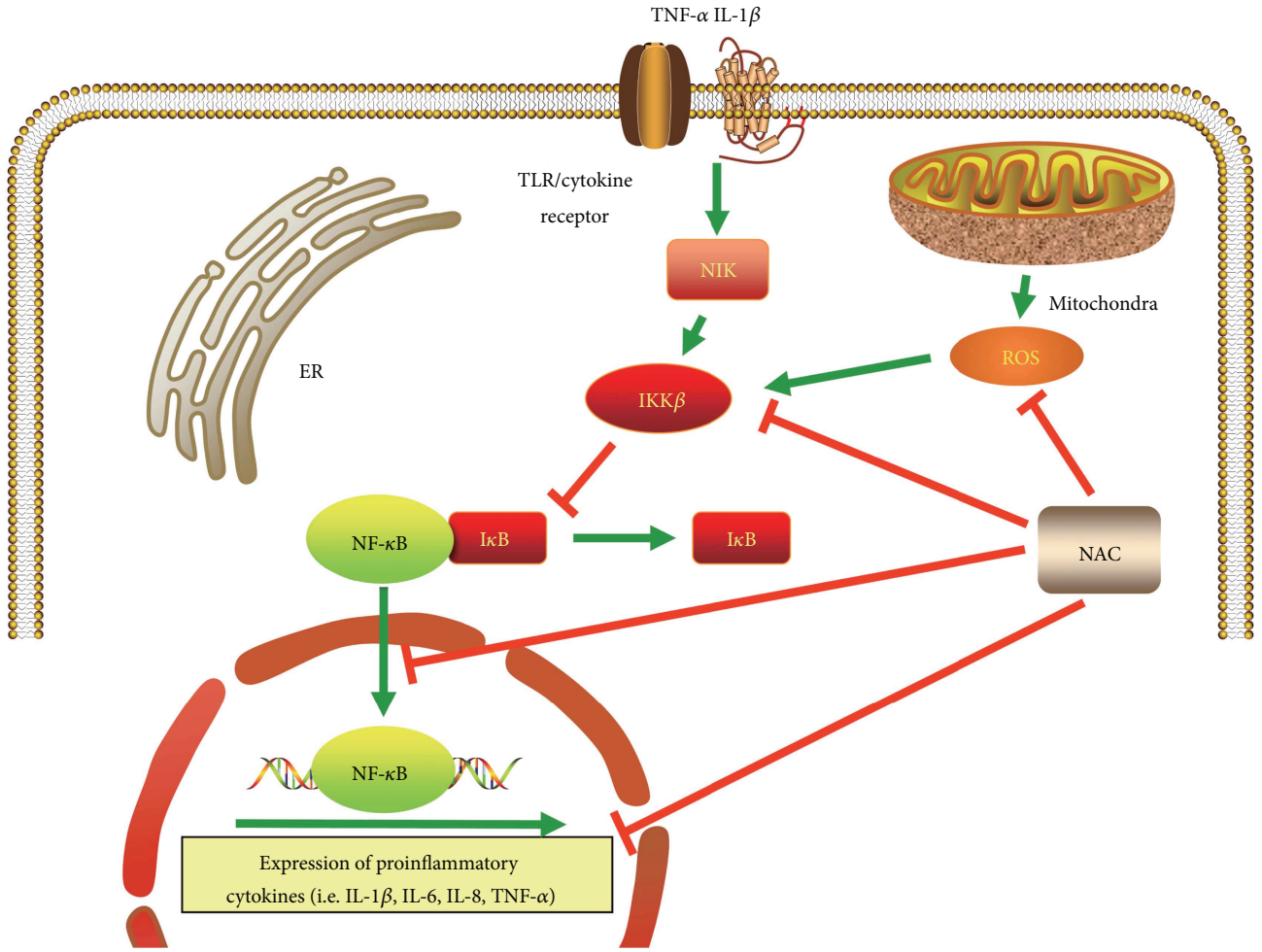

Figure 4: Model of the anti-inflammatory activity of N-acetylcysteine. NF-κB is naturally bound to IκB that prevents its nuclear translocation. Phosphorylation of IκB by IKKβ results in dissociation of IκB from NF-κB. This process facilitates nuclear translocation of NF-κB as well as transcription of genes involved in the inflammation cascade and immune response. N-Acetylcysteine prevents activation of NF-κB by removal of ROS, inhibition of IKKβ, and nuclear translocation of NF-κB. N-Acetylcysteine also inhibited the synthesis of proinflammatory cytokines such as IL-1β, IL-6, IL-8, and TNFα. ER: endoplasmic reticulum; IκB: inhibitor of NF-κB; IKKβ: inhibitor of κB kinase; IL: interleukin; NF-κB: nuclear factor kappa-light-chain-enhancer of activated B cells; NIK: NF-κB-inducing kinase; ROS: reactive oxygen species; TLR: toll-like receptor; TNF-α: tumor necrosis factor-α.

materials [43]. Oral administration of NAC decreases alveolar bone loss in a dose-dependent manner in a rat model of experimental periodontitis [44]. Considering that NAC acts as an osteogenesis-enhancing molecule [12], NAC-loaded nanotube titanium dental implants have been developed that are capable of enhancing bone regeneration and osseointegration through sustained release of NAC [45]. The loaded NAC increased the hydrophilicity of the implant surface, thereby facilitating osteoblast adhesion and proliferation. The NAC released from the loaded nanotubes also inhibits lipopolysaccharide-induced oxidative stress and inflammatory cytokines, as well as reduces expression of receptor activator of nuclear factor kappa B ligand (RANKL). These findings support the use of NAC-loaded nanotube titanium dental implants in clinical applications, although their immunomodulatory activities require further substantiation. Nevertheless, it has been reported that long-term, low-dose NAC application increases the expression of proinflammatory cytokines in lipopolysaccharide-stimulated macrophages through enhancement of kinase phosphorylation [46].

4. Antimicrobial Activity

Although NAC is not an antibiotic, it possesses antimicrobial properties. Since the initial demonstration of inactivation of *Staphylococcus epidermidis* biofilm formation by NAC in 1997 [47], many studies have demonstrated the efficacy of NAC in reducing biofilm formation induced by a broad array of medically important microorganisms (Table 3). One of those studies evaluated the antibacterial and biofilm eradication potential of NAC on *Enterococcus faecalis* [48], one of the most important opportunistic pathogens responsible for persistent root canal infections [49]. In that study, the authors demonstrated that NAC was effective against both the planktonic and biofilm forms of *E. faecalis*; antimicrobial efficacy was not reduced by the presence of dentin powder for

Table 3: Representative studies on antimicrobial and antibiofilm activities of N-acetylcysteine against various oral pathogenic microorganisms.

Pathogens examined	NAC concentrations (mg/mL)	Related niche	Reference
Gram-positive bacteria			
Actinomyces naeslundii	1.56–25	C/E	[50]
Enterococcus faecalis	1.56–50	E	[48]
	1.56–25	E	[50]
	2.5–20	E	[57]
Lactobacillus salivarius	1.56–25	C	[50]
Staphylococcus aureus	20	C	[106]
	6–24	C	[107]
	80	C	[108]
	2–4	C	[109]
	80	C	[110]
Staphylococcus epidermidis	4–40	C	[111]
	0.03–2	C	[112]
	4–40	C	[113]
	80	C	[108]
	2–4	C	[109]
	0.5–32	C	[114]
	80	C	[110]
	0.003–8	C	[47]
Streptococcus mutans	0.78–6.25	C/E	[50]
Gram-negative bacteria			
Acinetobacter baumannii	0.25–2	C/E	[62]
Enterobacter cloacae	80	E	[108]
	0.25–2	E	[62]
Escherichia coli	2–4	C/E/P	[109]
	0.007-8	C/E/P	[115]
Klebsiella pneumoniae		E	[106]
		E	[108]
		E	[109]
		E	[110]
		E	[62]
Prevotella intermedia	0.375–3	E/P	[58]
Proteus spp.	2.5	C/E/P	[106]
	2–4	C/E/P	[109]
Pseudomonas aeruginosa	2.5	C/E/P	[106]
	12.5	C/E/P	[116]
	3–24	C/E/P	[107]
	80	C/E/P	[108]
	0.5–10	C/E/P	[117]
Yeasts			
Candida albicans	0.5–32	C/E/P	[114]
	0.312–40	C/E/P	[118]

C: caries; E: endodontic infections; P: periodontitis.

up to 14 days. A more recent study reported that NAC has potent antibacterial effects against planktonic endodontic pathogens (*Actinomyces naeslundii*, *Lactobacillus salivarius*, *Streptococcus mutans*, and *E. faecalis*) and effectively inhibits biofilm formation by all the monospecies and multispecies bacteria [50]. Eradication of mature multispecies biofilms was also observed by scanning electron microscopy after a 10 min treatment with NAC at concentrations of 25 mg/mL or higher. The biofilm disrupting activity of NAC is significantly higher than that of saturated calcium hydroxide or 2% chlorhexidine.

During root canal treatment, it is essential to eradicate residual bacterial infections from the root canal system with intracanal medicaments such as chlorhexidine or calcium hydroxide. Although chlorhexidine exhibits substantivity, it is inactivated by dentin and has a limited ability to penetrate the deep layer of biofilms [51]. Calcium hydroxide, on the other hand, decreases the bond strength of resin-based endodontic sealer to dentin [52] and is less effective against *E. faecalis* and *Candida albicans* [53]. Because NAC possesses anti-inflammatory effect on lipopolysaccharide-induced inflammatory responses [40] and analgesic property for relieving postendodontic pain that is comparable to the effect of ibuprofen [54], it has immense potential to be used as an alternate intracanal medicament in root canal treatment. Some research groups have combined additional components with NAC to achieve augmented or broad-spectrum antimicrobial applications. These additional components include alexidine [55], chlorhexidine [56], taurolidine [57], and other antibiotics [58]. Despite the potent antimicrobial efficacy of NAC, when used alone or in association with antibiotics in oral cavity infections, few studies to date have evaluated the antimicrobial activity of NAC using animal models. In a murine experimental periodontitis model, a dose-dependent reduction was observed in the invasion of *Fusobacterium nucleatum* in immortalized human gingival epithelial cells by NAC [59]. This is achieved by inhibition of *F. nucleatum*-induced activation of Rac1, an important regulator of actin cytoskeleton dynamics responsible for the bacterial invasion of host cells [60]. Furthermore, NAC completely eliminates experimental periodontitis induced in mice by the periodontal pathogens *Prevotella gingivalis* and *Treponema denticola* [59]. Although extensive efforts have been made in

this field, the exact mechanisms responsible for the antimicrobial and antibiofilm activities of NAC are still speculative. These speculations include (1) inhibition of cysteine utilization in bacteria, (2) reaction between the thiol group of NAC and bacterial cell proteins, (3) reduction of bacterial extracellular polymeric substances that are responsible for bacterial adhesion and pathogenicity, and (4) disturbance of intracellular redox equilibrium with potential indirect effects on cell metabolism and intracellular signal transduction pathways [61, 62].

NAC also shows its therapeutic potential for wound healing and tissue regeneration. It was shown that NAC exerted the bacteriostatic effects on wound pathogens such as *Staphylococcus aureus* and *Streptococcus pyogenes* both in brain heart infusion (BHI) broth and on agar *in vitro* [63]. Addition of NAC to the collagen scaffold was shown to protect gingival fibroblasts and bone marrow-derived osteoblasts from bacterial infection by coincubation with *S. aureus* or *S. pyogenes* and preserve bacteria-induced impairment of fibroblastic viability, attachment, adhesion behavior, and osteoblastic differentiation. In addition, NAC assists the cells' ability to diminish the damaging effects of ROS and reduce inflammation during wound healing [64]. NAC was beneficial for treating grave burn injuries in a rat comb burn model when administered via the oral or intraperitoneal route [65]. The effects on wound healing of nasal mucosa were also confirmed, when NAC was intraperitoneally administered to rats with nasal trauma [66]. Experimental rat skin wounds were effectively treated with topical NAC, and the efficacy of NAC in wound healing was comparable to dexpanthenol, a molecule widely used to improve wound healing [67]. NAC has also been functionalized as a scaffold with anti-infective capabilities, thus assisting healing of soft and hard tissues. Recently, a topically administered eye drop (Lacrimera®) based on chitosan-N-acetylcysteine (C-NAC) has been recently introduced and received CE marking in Europe. This eye drop has been shown to effectively improve corneal wound healing in a rabbit model of corneal epithelial debridement [68].

5. Anticarcinogenic Activity

Since the first report on the anticarcinogenic function of NAC in 1984 [69], modulation of genotoxicity, oncogenicity, and tumor progression processes by NAC has been extensively studied in cellular experiments, animal models, and human clinical trials by independent researchers. It has become apparent that NAC exerts its anticarcinogenic actions by a broad array of mechanisms including the attenuation of genotoxic ROS, modulation of metabolism and mitochondrial pathways, induction of DNA repair, inhibition of genotoxicity and cell transformation, modulation of signal transduction pathways, regulation of cell survival and apoptosis, anti-inflammatory activity, immunological effects, influence on cell cycle progression, antiangiogenetic activity, and inhibition of invasion and metastasis [70].

Oral cancer is one of the most frequently diagnosed cancers worldwide. This type of cancer constitutes 90% of head and neck cancers and involves squamous cell carcinomas of several anatomical sites such as the lip and oral cavity, pharynx, and larynx. According to the American Cancer Society, approximately 30,000 new cases of oral cancer are diagnosed in the United States alone in 2015, of which 5990 cases are fatal [71]. Despite technical advances in treatment modalities such as surgery, radiotherapy, and chemotherapy, the prognosis of oral cancer remains inauspicious; the estimated 5-year overall survival is only 56% [72]. Major risk factors associated with the development of oral cancer include smoking, tobacco chewing, alcohol consumption, and betel nut chewing. Focusing on the potential positive effects of NAC on smoke-related carcinogenesis, a phase II trial (EUROSCAN) was conducted on 2592 patients suffering from head and neck cancer or lung cancer, most of whom were former or current smokers. No statistically significant improvement in terms of survival, event-free survival, or tumor remission was observed in those patients after a 2-year supplement of NAC (600 mg/day) [73]. By contrast, several studies reported the ability of NAC to exert protective effects against preneoplastic lesions, benign tumors, and/or malignant tumors in animal tumorigenesis models induced by individual cigarette smoke components [74]. A randomized double-blind phase II chemoprevention trial was conducted on 41 healthy smoking volunteers. After 6 months of oral NAC (2×600 mg/day), significant decrease in the investigated biomarkers was observed, including the levels of bulky DNA adducts and 8-hydroxy-2′-deoxyguanosine in bronchoalveolar lavage cells, as well as the frequency of micronuclei in mouth floor and soft palate cells [75]. The unfavorable clinical outcome of oral cancer is often associated with aberrant activation of epidermal growth factor receptor (EGFR) signaling [76]. Encouraged by the observation that NAC suppressed EGFR-induced phosphorylation in an earlier study [77], the effects of NAC in EGFR-overexpressing invasive oral cancer was conducted on cancer cell growth in a murine xenograft model [78]. The authors found that NAC suppresses growth of cancer cells by mediating the EGFR/Akt/HMG box-containing protein 1 signaling pathway in oral cancer cells, as well as tumor growth. N-Acetylcysteine has also been investigated as a potential agent to attenuate the side effects of platinum-based chemotherapy. By suppressing oxidative stress and oxidation-associated signals, NAC was found to reduce cisplatin-induced acute renal failure in rats [79]. A pilot randomized study with 13 head and neck cancer patients reported that transtympanic injections with NAC prior to cisplatin exposure appears to prevent cisplatin-induced ototoxicity, although better delivery is required to improve the efficacy of this treatment modality [80]. The protective effect of NAC is believed to be achieved by binding directly to cisplatin molecules and acting as free radical scavengers.

6. Potential Side Effects of NAC and Its Formulations

Although NAC-based therapeutics has been advocated for oral health care, proactive approximations are required to

establish safety conditions and appropriate delivery formulations. N-Acetylcysteine has a long-established safety record in adults and children; the drug has been approved by the US Food and Drug Administration since 1963. The adverse effects experienced with the use of NAC are somewhat dependent on the route of administration. The pharmacokinetics and pharmacodynamics of NAC have been investigated in a phase I clinical study of 26 volunteers with a 6-month oral administration of NAC. The major reported side effects were gastrointestinal symptoms including intestinal gas, diarrhea, nausea, and fatigue with the highest nontoxic dose being 800 mg/m^2/day [81]. In another clinical trial, oral administration of NAC at doses up to 8000 mg/day was reported to cause no significant adverse reactions in patients infected with the human immunodeficiency virus [82]. In contrast, severe anaphylactoid symptoms such as flushing, pruritus, angioedema, bronchospasm, and hypotension have been reported after intravenous administration of NAC. These symptoms are likely to be attributed to the transient high plasma concentrations of NAC and are most prevalent immediately after the initial loading infusion; the symptoms subside rapidly after administration is discontinued [1]. Nevertheless, severe systemic reactions are uncommon. Considering the poor oral absorption of dietary GSH, orally administered NAC has been found to be more efficient than direct GSH administration and is as effective as intravenously administered NAC [83]. Compared with cysteine, the acetyl moiety of NAC reduces the reactivity of the thiol functionality, rendering NAC less toxic and less susceptible to oxidation to disulfide and easier for absorption and distribution [84]. N-Acetylcysteine is rapidly and almost completely absorbed after oral administration in both animals and humans; only 3% of radioactive-labeled NAC is excreted in the feces [85]. Thus, NAC is a better source of cysteine compared with parenteral administration of cysteine. Several *in vitro* studies demonstrated that extremely high NAC concentrations (typically 10 mM and sometimes as high as 100 mM) alter protein structure and function, such as modulation of angiotensin II receptor binding [86] and TNF-α blocking by reducing the affinity of its receptor [87]. Collectively, the toxicity associated with NAC therapy does not appear to be a negligible issue. Oral administration is preferred despite some clinical situations where other drug delivery routes are required. A number of orally administered NAC formulations are commercially available, including Mucomyst™ (Brisol-Myers Squibb Co., Princeton, NJ, USA) as an antidote for acetaminophen overdose, PharmaNAC® (BioAdvantex Pharma Inc., Mississauga, ON, Canada), and several formulations packaged in pill and tablet forms in Europe. Several companies also manufacture and sell NAC in combination with other daily nutritional supplements such as multivitamins and antioxidants (e.g., Swanson Health Products, Fargo, ND, USA). It is important to note that the manufacture of NAC requires prevention of NAC oxidation to the disulfide dimer *N,N′*-diacetylcystine. Unlike NAC, the latter is pharmacologically active and causes immunologic effects at very low concentrations [88]. According to the European Good Manufacturing Practice standards, *N,N′*-diacetylcystine should constitute less than 0.1% of commercialized NAC formulations [89].

7. Conclusions and Prospects

The past decade has witnessed an explosion of data regarding the multifaceted biological activities of NAC, including antioxidant, anti-inflammatory, antimicrobial, and anticarcinogenic activities. The oral cavity has continuously challenged various environmental insults that are likely to generate oxidative stress, induce inflammation, and even initiate cancer. The biological and pharmacological activities of NAC and its ability to circumvent the mechanisms of disease progression make it a potential therapeutic agent for intervention in dental and oral disorders. Still, its clinical effectiveness needs further investigations, since most of the results in this area of research are derived from *in vitro* and *in vivo* studies. The focus of future research should be the following: (i) to develop novel dental and implantable materials with improved biocompatibility by incorporating NAC, (ii) to investigate whether NAC could be used alone or with other drugs to treat oral lichen planus, (iii) to examine NAC clinically to be used as an alternate intracanal medicament in root canal treatment, (iv) to examine the clinical effectiveness of NAC for the treatment of wound healing, and (v) to evaluate the clinical application of NAC as an anticancer adjuvant for oral cancer treatment.

Conflicts of Interest

The authors declare that they have no conflicts of interest.

Authors' Contributions

Yanping Pei, Huan Liu, and Yi Yang contributed equally to this work and should be considered co-first authors.

Acknowledgments

This work was supported by Grant nos. 81600919 (principal investigator Yi Yang) and 81720108011 (principal investigator Jihua Chen) from the National Nature Science Foundation of China, Beijing Nova Program (Grant no. xx2018097) (principal investigator Yi Yang), and Program no. IRT13051 from the Program for Changjiang Scholars and Innovative Research Team in University (PCSIRT).

References

[1] K. R. Atkuri, J. J. Mantovani, L. A. Herzenberg, and L. A. Herzenberg, "N-Acetylcysteine–a safe antidote for cysteine/glutathione deficiency," *Current Opinion in Pharmacology*, vol. 7, no. 4, pp. 355–359, 2007.

[2] M. Berk, G. S. Malhi, L. J. Gray, and O. M. Dean, "The promise of N-acetylcysteine in neuropsychiatry," *Trends in Pharmacological Sciences*, vol. 34, no. 3, pp. 167–177, 2013.

[3] G. F. Rushworth and I. L. Megson, "Existing and potential therapeutic uses for N-acetylcysteine: the need for conversion to intracellular glutathione for antioxidant benefits," *Pharmacology & Therapeutics*, vol. 141, no. 2, pp. 150–159, 2014.

[4] S. Dinicola, S. De Grazia, G. Carlomagno, and J. P. Pintucci, "N-acetylcysteine as powerful molecule to destroy bacterial biofilms: a systematic review," *European Review for Medical*

and Pharmacological Sciences, vol. 18, no. 19, pp. 2942–2948, 2014.

[5] Y. Jiao, L. Niu, S. Ma, J. Li, F. R. Tay, and J. Chen, "Quaternary ammonium-based biomedical materials: state-of-the-art, toxicological aspects and antimicrobial resistance," *Progress in Polymer Science*, vol. 71, pp. 53–90, 2017.

[6] S. Krifka, G. Spagnuolo, G. Schmalz, and H. Schweikl, "A review of adaptive mechanisms in cell responses towards oxidative stress caused by dental resin monomers," *Biomaterials*, vol. 34, no. 19, pp. 4555–4563, 2013.

[7] P. A. Mouthuy, S. J. B. Snelling, S. G. Dakin et al., "Biocompatibility of implantable materials: an oxidative stress viewpoint," *Biomaterials*, vol. 109, pp. 55–68, 2016.

[8] C. L. Hahn and F. R. Liewehr, "Innate immune responses of the dental pulp to caries," *Journal of Endodontics*, vol. 33, no. 6, pp. 643–651, 2007.

[9] Y. C. Ko, Y. L. Huang, C. H. Lee, M. J. Chen, L. M. Lin, and C. C. Tsai, "Betel quid chewing, cigarette smoking and alcohol consumption related to oral cancer in Taiwan," *Journal of Oral Pathology & Medicine*, vol. 24, no. 10, pp. 450–453, 1995.

[10] S. W. Chang, S. I. Lee, W. J. Bae et al., "Heat stress activates interleukin-8 and the antioxidant system via Nrf2 pathways in human dental pulp cells," *Journal of Endodontics*, vol. 35, no. 9, pp. 1222–1228, 2009.

[11] S. K. Lee, K. S. Min, Y. Kim et al., "Mechanical stress activates proinflammatory cytokines and antioxidant defense enzymes in human dental pulp cells," *Journal of Endodontics*, vol. 34, no. 11, pp. 1364–1369, 2008.

[12] Y. F. Feng, L. Wang, Y. Zhang et al., "Effect of reactive oxygen species overproduction on osteogenesis of porous titanium implant in the present of diabetes mellitus," *Biomaterials*, vol. 34, no. 9, pp. 2234–2243, 2013.

[13] B. M. Hybertson, B. Gao, S. K. Bose, and J. M. McCord, "Oxidative stress in health and disease: the therapeutic potential of Nrf2 activation," *Molecular Aspects of Medicine*, vol. 32, no. 4–6, pp. 234–246, 2011.

[14] A. H. Kesarwala, M. C. Krishna, and J. B. Mitchell, "Oxidative stress in oral diseases," *Oral Diseases*, vol. 22, no. 1, pp. 9–18, 2016.

[15] T. Akca, H. Canbaz, C. Tataroglu et al., "The effect of N-acetylcysteine on pulmonary lipid peroxidation and tissue damage," *The Journal of Surgical Research*, vol. 129, no. 1, pp. 38–45, 2005.

[16] N. Paolocci, M. I. Jackson, B. E. Lopez et al., "The pharmacology of nitroxyl (HNO) and its therapeutic potential: not just the janus face of NO," *Pharmacology & Therapeutics*, vol. 113, no. 2, pp. 442–458, 2007.

[17] A. S. Koh, T. A. Simmons-Willis, J. B. Pritchard, S. M. Grassl, and N. Ballatori, "Identification of a mechanism by which the methylmercury antidotes N-acetylcysteine and dimercaptopropanesulfonate enhance urinary metal excretion: transport by the renal organic anion transporter-1," *Molecular Pharmacology*, vol. 62, no. 4, pp. 921–926, 2002.

[18] H. Sies, "Glutathione and its role in cellular functions," *Free Radical Biology & Medicine*, vol. 27, no. 9-10, pp. 916–921, 1999.

[19] K. R. Gibson, I. L. Neilson, F. Barrett et al., "Evaluation of the antioxidant properties of N-acetylcysteine in human platelets: prerequisite for bioconversion to glutathione for antioxidant and antiplatelet activity," *Journal of Cardiovascular Pharmacology*, vol. 54, no. 4, pp. 319–326, 2009.

[20] A. Yoshida, Y. Shiotsu-Ogura, S. Wada-Takahashi, S. S. Takahashi, T. Toyama, and F. Yoshino, "Blue light irradiation-induced oxidative stress in vivo via ROS generation in rat gingival tissue," *Journal of Photochemistry and Photobiology B*, vol. 151, no. 3, pp. 48–53, 2015.

[21] M. Suzuki, C. Bandoski, and J. D. Bartlett, "Fluoride induces oxidative damage and SIRT1/autophagy through ROS-mediated JNK signaling," *Free Radical Biology & Medicine*, vol. 89, pp. 369–378, 2015.

[22] N. Sato, T. Ueno, K. Kubo et al., "N-Acetyl cysteine (NAC) inhibits proliferation, collagen gene transcription, and redox stress in rat palatal mucosal cells," *Dental Materials*, vol. 25, no. 12, pp. 1532–1540, 2009.

[23] M. Y. Park, Y. J. Jeong, G. C. Kang et al., "Nitric oxide-induced apoptosis of human dental pulp cells is mediated by the mitochondria-dependent pathway," *The Korean Journal of Physiology & Pharmacology*, vol. 18, no. 1, pp. 25–32, 2014.

[24] H. Schweikl, M. Widbiller, S. Krifka et al., "Interaction between LPS and a dental resin monomer on cell viability in mouse macrophages," *Dental Materials*, vol. 32, no. 12, pp. 1492–1503, 2016.

[25] Y. Jiao, S. Ma, Y. Wang et al., "N-Acetyl cysteine depletes reactive oxygen species and prevents dental monomer-induced intrinsic mitochondrial apoptosis in vitro in human dental pulp cells," *PLoS One*, vol. 11, no. 1, article e0147858, 2016.

[26] H. Schweikl, G. Spagnuolo, and G. Schmalz, "Genetic and cellular toxicology of dental resin monomers," *Journal of Dental Research*, vol. 85, no. 10, pp. 870–877, 2016.

[27] Y. Jiao, S. Ma, Y. Wang, J. Li, L. Shan, and J. Chen, "Epigallocatechin-3-gallate reduces cytotoxic effects caused by dental monomers: a hypothesis," *Medical Science Monitor*, vol. 21, pp. 3197–3202, 2015.

[28] G. Spagnuolo, V. D'Antò, C. Cosentino, G. Schmalz, H. Schweikl, and S. Rengo, "Effect of N-acetyl-L-cysteine on ROS production and cell death caused by HEMA in human primary gingival fibroblasts," *Biomaterials*, vol. 27, no. 9, pp. 1803–9, 2006.

[29] Y. Jiao, S. Ma, J. Li et al., "N-Acetyl cysteine (NAC)-directed detoxification of methacryloxylethyl cetyl ammonium chloride (DMAE-CB)," *PLoS One*, vol. 10, no. 8, article e0135815, 2015.

[30] G. Nocca, V. D'Antò, C. Desiderio et al., "N-Acetyl cysteine directed detoxification of 2-hydroxyethyl methacrylate by adduct formation," *Biomaterials*, vol. 31, no. 9, pp. 2508–2516, 2010.

[31] Y. Jiao, S. Ma, J. Li et al., "The influences of N-acetyl cysteine (NAC) on the cytotoxicity and mechanical properties of poly-methylmethacrylate (PMMA)-based dental resin," *PeerJ*, vol. 3, article e868, 2015.

[32] M. Yamada, N. Tsukimura, T. Ikeda et al., "N-Acetyl cysteine as an osteogenesis-enhancing molecule for bone regeneration," *Biomaterials*, vol. 34, no. 26, pp. 6147–6156, 2013.

[33] J. H. Jun, S. H. Lee, H. B. Kwak et al., "N-Acetylcysteine stimulates osteoblastic differentiation of mouse calvarial cells," *Journal of Cellular Biochemistry*, vol. 103, no. 4, pp. 1246–1255, 2008.

[34] S. Batu, D. Ofluoglu, S. Ergun et al., "Evaluation of prolidase activity and oxidative stress in patients with oral lichen planus and oral lichenoid contact reactions," *Journal of Oral Pathology & Medicine*, vol. 45, no. 4, pp. 281–288, 2016.

[35] Y. Yamamoto and R. B. Gaynor, "Therapeutic potential of inhibition of the NF-κB pathway in the treatment of inflammation and cancer," *The Journal of Clinical Investigation*, vol. 107, no. 2, pp. 135–142, 2001.

[36] S. Oka, H. Kamata, K. Kamata, H. Yagisawa, and H. Hirata, "N-Acetylcysteine suppresses TNF-induced NF-κB activation through inhibition of IκB kinases," *FEBS Letters*, vol. 472, no. 2-3, pp. 196–202, 2000.

[37] F. Pajonk, K. Riess, A. Sommer, and W. H. McBride, "N-Acetyl-L-cysteine inhibits 26S proteasome function: implications for effects on NF-κB activation," *Free Radical Biology & Medicine*, vol. 32, no. 6, pp. 536–543, 2002.

[38] H. Kim, J. Y. Seo, K. H. Roh, J. W. Lim, and K. H. Kim, "Suppression of NF-κB activation and cytokine production by N-acetylcysteine in pancreatic acinar cells," *Free Radical Biology & Medicine*, vol. 29, no. 7, pp. 674–683, 2000.

[39] M. Zafarullah, W. Q. Li, J. Sylvester, and M. Ahmad, "Molecular mechanisms of N-acetylcysteine actions," *Cellular and Molecular Life Sciences*, vol. 60, no. 1, pp. 6–20, 2003.

[40] S. P. Karapinar, Y. Z. A. Ulum, B. Ozcelik et al., "The effect of N-acetylcysteine and calcium hydroxide on TNF-α and TGF-β1 in lipopolysaccharide-activated macrophages," *Archives of Oral Biology*, vol. 68, pp. 48–54, 2016.

[41] D. Y. Kim, J. H. Jun, H. L. Lee et al., "N-Acetylcysteine prevents LPS-induced pro-inflammatory cytokines and MMP2 production in gingival fibroblasts," *Archives of Pharmacal Research*, vol. 30, no. 10, pp. 1283–1292, 2007.

[42] N. Celik, S. Askın, M. A. Gul, and N. Seven, "The effect of restorative materials on cytokines in gingival crevicular fluid," *Archives of Oral Biology*, vol. 84, pp. 139–144, 2017.

[43] C. Di Nisio, S. Zara, A. Cataldi, and V. di Giacomo, "2-Hydroxyethyl methacrylate inflammatory effects in human gingival fibroblasts," *International Endodontic Journal*, vol. 46, no. 5, pp. 466–476, 2013.

[44] H. Toker, H. Ozdemir, K. Eren, H. Ozer, and G. Sahin, "N-Acetylcysteine, a thiol antioxidant, decreases alveolar bone loss in experimental periodontitis in rats," *Journal of Periodontology*, vol. 80, no. 4, pp. 672–678, 2009.

[45] Y. H. Lee, G. Bhattarai, I. S. Park et al., "Bone regeneration around N-acetyl cysteine-loaded nanotube titanium dental implant in rat mandible," *Biomaterials*, vol. 34, no. 38, pp. 10199–10208, 2013.

[46] T. Ohnishi, K. Bandow, K. Kakimoto, J. Kusuyama, and T. Matsuguchi, "Long-time treatment by low-dose N-acetyl-L-cysteine enhances proinflammatory cytokine expressions in LPS-stimulated macrophages," *PLoS One*, vol. 9, no. 2, article e87229, 2014.

[47] C. Pérez-Giraldo, A. Rodríguez-Benito, F. J. Morán, C. Hurtado, M. T. Blanco, and A. C. Gómez-García, "Influence of N-acetylcysteine on the formation of biofilm by Staphylococcus epidermidis," *The Journal of Antimicrobial Chemotherapy*, vol. 39, no. 5, pp. 643–646, 1997.

[48] S. Y. Quah, S. Wu, J. N. Lui, C. P. Sum, and K. S. Tan, "N-Acetylcysteine inhibits growth and eradicates biofilm of Enterococcus faecalis," *Journal of Endodontics*, vol. 38, no. 1, pp. 81–85, 2012.

[49] C. Stuart, S. Schwartz, T. Beeson, and C. Owatz, "Enterococcus faecalis: its role in root canal treatment failure and current concepts in retreatment," *Journal of Endodontics*, vol. 32, no. 2, pp. 93–98, 2006.

[50] J. H. Moon, Y. S. Choi, H. W. Lee, J. S. Heo, S. W. Chang, and J. Y. Lee, "Antibacterial effects of N-acetylcysteine against endodontic pathogens," *Journal of Microbiology*, vol. 54, no. 4, pp. 322–329, 2016.

[51] I. Portenier, H. Haapasalo, D. Orstavik, M. Yamauchi, and M. Haapasalo, "Inactivation of the antibacterial activity of iodine potassium iodide and chlorhexidine digluconate against Enterococcus faecalis by dentin, dentin matrix, type-I collagen, and heat-killed microbial whole cells," *Journal of Endodontics*, vol. 28, no. 9, pp. 634–637, 2002.

[52] J. V. B. Barbizam, M. Trope, É. C. N. Teixeira, M. Tanomaru-Filho, and F. B. Teixeira, "Effect of calcium hydroxide intracanal dressing on the bond strength of a resin-based endodontic sealer," *Brazilian Dental Journal*, vol. 19, no. 3, pp. 224–227, 2008.

[53] Z. Mohammadi and P. M. H. Dummer, "Properties and applications of calcium hydroxide in endodontics and dental traumatology," *International Endodontic Journal*, vol. 44, no. 8, pp. 697–730, 2011.

[54] M. Ehsani, A.-A. Moghadamnia, S. Zahedpasha et al., "The role of prophylactic ibuprofen and N-acetylcysteine on the level of cytokines in periapical exudates and the post-treatment pain," *Daru*, vol. 20, no. 1, p. 30, 2012.

[55] L. F. M. Silveira, P. Baca, M. T. Arias-Moliz, A. Rodríguez-Archilla, and C. M. Ferrer-Luque, "Antimicrobial activity of alexidine alone and associated with N-acetylcysteine against Enterococcus faecalis biofilm," *International Journal of Oral Science*, vol. 5, no. 3, pp. 146–149, 2013.

[56] U. Palaniswamy, S. R. Lakkam, S. Arya, and S. Aravelli, "Effectiveness of N-acetyl cysteine, 2% chlorhexidine, and their combination as intracanal medicaments on Enterococcus faecalis biofilm," *Journal of Conservative Dentistry*, vol. 19, no. 1, pp. 17–20, 2016.

[57] A. T. Ulusoy, E. Kalyoncuoglu, A. Reis, and Z. C. Cehreli, "Antibacterial effect of N-acetylcysteine and taurolidine on planktonic and biofilm forms of Enterococcus faecalis," *Dental Traumatology*, vol. 32, no. 3, pp. 212–218, 2016.

[58] J. H. Moon, E. Y. Jang, K. S. Shim, and J. Y. Lee, "In vitro effects of N-acetyl cysteine alone and in combination with antibiotics on Prevotella intermedia," *Journal of Microbiology*, vol. 53, no. 5, pp. 321–329, 2015.

[59] J. Alam, K. J. Baek, Y. S. Choi, Y. C. Kim, and Y. Choi, "N-acetylcysteine and the human serum components that inhibit bacterial invasion of gingival epithelial cells prevent experimental periodontitis in mice," *Journal of Periodontal & Implant Science*, vol. 44, no. 6, pp. 266–273, 2014.

[60] L. Van Aelst and C. D'Souza-Schorey, "Rho GTPases and signaling networks," *Genes & Development*, vol. 11, no. 18, pp. 2295–2322, 1997.

[61] F. Blasi, C. Page, G. M. Rossolini et al., "The effect of N-acetylcysteine on biofilms: implications for the treatment of respiratory tract infections," *Respiratory Medicine*, vol. 117, pp. 190–197, 2016.

[62] A. C. Olofsson, M. Hermansson, and H. Elwing, "N-Acetyl-L-cysteine affects growth, extracellular polysaccharide production, and bacterial biofilm formation on solid surfaces," *Applied and Environmental Microbiology*, vol. 69, no. 8, pp. 4814–4822, 2003.

[63] M. Yamada, K. Ishihara, T. Ogawa, and K. Sakurai, "The inhibition of infection by wound pathogens on scaffold in tissue-forming process using N-acetyl cysteine," *Biomaterials*, vol. 32, no. 33, pp. 8474–8485, 2011.

[64] M. AlMatar, T. Batool, and E. A. Makky, "Therapeutic potential of N-acetylcysteine for wound healing, acute bronchiolitis, and congenital heart defects," *Current Drug Metabolism*, vol. 17, no. 2, pp. 156–167, 2016.

[65] M. Deniz, H. Borman, T. Seyhan, and M. Haberal, "An effective antioxidant drug on prevention of the necrosis of zone of stasis: N-acetylcysteine," *Burns*, vol. 39, no. 2, pp. 320–325, 2013.

[66] B. Yilmaz, G. Turkcu, E. Sengul, A. Gul, F. E. Ozkurt, and M. Akdag, "Efficacy of N-acetylcysteine on wound healing of nasal mucosa," *The Journal of Craniofacial Surgery*, vol. 26, no. 5, pp. e422–e426, 2015.

[67] A. Oguz, O. Uslukaya, U. Alabalik, A. Turkoglu, M. Kapan, and Z. Bozdag, "Topical N-acetylcysteine improves wound healing comparable to dexpanthenol: an experimental study," *International Surgery*, vol. 100, no. 4, pp. 656–661, 2015.

[68] C. Fischak, R. Klaus, R. M. Werkmeister et al., "Effect of topically administered chitosan-N-acetylcysteine on corneal wound healing in a rabbit model," *Journal of Ophthalmology*, vol. 2017, Article ID 5192924, 6 pages, 2017.

[69] S. De Flora, C. Bennicelli, P. Zanacchi, A. Camoirano, A. Morelli, and A. De Flora, "In vitro effects of N-acetylcysteine on the mutagenicity of direct-acting compounds and procarcinogens," *Carcinogenesis*, vol. 5, no. 4, pp. 505–510, 1984.

[70] S. De Flora, A. Izzotti, F. D'Agostini, and R. M. Balansky, "Mechanisms of N-acetylcysteine in the prevention of DNA damage and cancer, with special reference to smoking-related end-points," *Carcinogenesis*, vol. 22, no. 7, pp. 999–1013, 2001.

[71] R. L. Siegel, K. D. Miller, and A. Jemal, "Cancer statistics, 2015," *CA: a Cancer Journal for Clinicians*, vol. 65, no. 1, pp. 5–29, 2015.

[72] H. Schliephake, "Prognostic relevance of molecular markers of oral cancer–a review," *International Journal of Oral and Maxillofacial Surgery*, vol. 32, no. 3, pp. 233–245, 2003.

[73] N. van Zandwijk, O. Dalesio, U. Pastorino, N. de Vries, and H. van Tinteren, "EUROSCAN, a randomized trial of vitamin A and N-acetylcysteine in patients with head and neck cancer or lung cancer. For the EUropean Organization for Research and Treatment of Cancer Head and Neck and Lung Cancer Cooperative Groups," *Journal of the National Cancer Institute*, vol. 92, no. 12, pp. 977–986, 2000.

[74] S. De Flora, G. Ganchev, M. Iltcheva et al., "Pharmacological modulation of lung carcinogenesis in smokers: preclinical and clinical evidence," *Trends in Pharmacological Sciences*, vol. 37, no. 2, pp. 120–142, 2016.

[75] F. J. Van Schooten, A. Besaratinia, S. De Flora et al., "Effects of oral administration of N-acetyl-L-cysteine: a multi-biomarker study in smokers," *Cancer Epidemiology and Prevention Biomarkers*, vol. 11, no. 2, pp. 167–175, 2002.

[76] S. Temam, H. Kawaguchi, A. K. El-Naggar et al., "Epidermal growth factor receptor copy number alterations correlate with poor clinical outcome in patients with head and neck squamous cancer," *Journal of Clinical Oncology*, vol. 25, no. 16, pp. 2164–2170, 2007.

[77] H. Kamata, Y. Shibukawa, S. I. Oka, and H. Hirata, "Epidermal growth factor receptor is modulated by redox through multiple mechanisms. Effects of reductants and H2O2," *European Journal of Biochemistry*, vol. 267, no. 7, pp. 1933–1944, 2000.

[78] M. F. Lee, C. Y. Chan, H. C. Hung, I. T. Chou, A. S. Yee, and C. Y. Huang, "N-Acetylcysteine (NAC) inhibits cell growth by mediating the EGFR/Akt/HMG box-containing protein 1 (HBP1) signaling pathway in invasive oral cancer," *Oral Oncology*, vol. 49, no. 2, pp. 129–135, 2013.

[79] J. Luo, T. Tsuji, H. Yasuda, Y. Sun, Y. Fujigaki, and A. Hishida, "The molecular mechanisms of the attenuation of cisplatin-induced acute renal failure by N-acetylcysteine in rats," *Nephrology, Dialysis, Transplantation*, vol. 23, no. 7, pp. 2198–2205, 2008.

[80] J. Yoo, S. J. Hamilton, D. Angel et al., "Cisplatin otoprotection using transtympanic L-N-acetylcysteine: a pilot randomized study in head and neck cancer patients," *The Laryngoscope*, vol. 124, no. 3, pp. E87–E94, 2014.

[81] L. Pendyala and P. J. Creaven, "Pharmacokinetic and pharmacodynamic studies of N-acetylcysteine, a potential chemopreventive agent during a phase I trial," *Cancer Epidemiology, Biomarkers & Prevention*, vol. 4, no. 3, pp. 245–251, 1995.

[82] S. C. De Rosa, M. D. Zaretsky, J. G. Dubs et al., "N-Acetylcysteine replenishes glutathione in HIV infection," *European Journal of Clinical Investigation*, vol. 30, no. 10, pp. 915–929, 2000.

[83] A. Witschi, S. Reddy, B. Stofer, and B. H. Lauterburg, "The systemic availability of oral glutathione," *European Journal of Clinical Pharmacology*, vol. 43, no. 6, pp. 667–669, 1992.

[84] L. Bonanomi and A. Gazzaniga, "Toxicological, pharmacokinetic and metabolic studies on acetylcysteine," *European Journal of Respiratory Diseases Supplement*, vol. 111, pp. 45–51, 1980.

[85] L. Borgstrom, B. Kagedal, and O. Paulsen, "Pharmacokinetics of N-acetylcysteine in man," *European Journal of Clinical Pharmacology*, vol. 31, no. 2, pp. 217–222, 1986.

[86] M. E. Ullian, A. K. Gelasco, W. R. Fitzgibbon, C. N. Beck, and T. A. Morinelli, "N-Acetylcysteine decreases angiotensin II receptor binding in vascular smooth muscle cells," *Journal of the American Society of Nephrology*, vol. 16, no. 8, pp. 2346–2353, 2005.

[87] M. Hayakawa, H. Miyashita, I. Sakamoto et al., "Evidence that reactive oxygen species do not mediate NF-κB activation," *The EMBO Journal*, vol. 22, no. 13, pp. 3356–3366, 2003.

[88] B. Sarnstrand, A. H. Jansson, G. Matuseviciene, A. Scheynius, S. Pierrou, and H. Bergstrand, "N,N'-Diacetyl-L-cystine-the disulfide dimer of N-acetylcysteine-is a potent modulator of contact sensitivity/delayed type hypersensitivity reactions in rodents," *The Journal of Pharmacology and Experimental Therapeutics*, vol. 288, no. 3, pp. 1174–1184, 1999.

[89] E. M. Grandjean, P. H. Berthet, R. Ruffmann, and P. H. Leuenberger, "Cost-effectiveness analysis of oral N-acetylcysteine as a preventive treatment in chronic bronchitis," *Pharmacological Research*, vol. 42, no. 1, pp. 39–50, 2000.

[90] S. N. Chen and M. Z. Hoffman, "Effect of pH on the reactivity of the carbonate radical in aqueous solution," *Radiation Research*, vol. 62, no. 1, pp. 18–27, 1975.

[91] K. M. Miranda, N. Paolocci, T. Katori et al., "A biochemical rationale for the discrete behavior of nitroxyl and nitric oxide in the cardiovascular system," *Proceedings of the National Academy of Sciences of the United States of America*, vol. 100, no. 16, pp. 9196–9201, 2011.

[92] A. V. Peskin and C. C. Winterbourn, "Kinetics of the reactions of hypochlorous acid and amino acid chloramines with

thiols, methionine, and ascorbate," *Free Radical Biology & Medicine*, vol. 30, no. 5, pp. 572–579, 2001.

[93] O. Skaff, D. I. Pattison, and M. J. Davies, "Hypothiocyanous acid reactivity with low-molecular-mass and protein thiols: absolute rate constants and assessment of biological relevance," *The Biochemical Journal*, vol. 422, no. 1, pp. 111–117, 2009.

[94] C. C. Winterbourn and D. Metodiewa, "Reactivity of biologically important thiol compounds with superoxide and hydrogen peroxide," *Free Radical Biology & Medicine*, vol. 27, no. 3-4, pp. 322–328, 1999.

[95] O. I. Aruoma, B. Halliwell, B. M. Hoey, and J. Butler, "The antioxidant action of N-acetylcysteine: its reaction with hydrogen peroxide, hydroxyl radical, superoxide, and hypochlorous acid," *Free Radical Biology & Medicine*, vol. 6, no. 6, pp. 593–597, 1989.

[96] W. A. Prutz, H. Monig, J. Butler, and E. J. Land, "Reactions of nitrogen dioxide in aqueous model systems: oxidation of tyrosine units in peptides and proteins," *Archives of Biochemistry and Biophysics*, vol. 243, no. 1, pp. 125–134, 1985.

[97] M. Benrahmoune, P. Therond, and Z. Abedinzadeh, "The reaction of superoxide radical with N-acetylcysteine," *Free Radical Biology & Medicine*, vol. 29, no. 8, pp. 775–782, 2000.

[98] M. Trujillo and R. Radi, "Peroxynitrite reaction with the reduced and the oxidized forms of lipoic acid: new insights into the reaction of peroxynitrite with thiols," *Archives of Biochemistry and Biophysics*, vol. 397, no. 1, pp. 91–98, 2002.

[99] E. C. Kim, M. K. Kim, R. Leesungbok, S. W. Lee, and S. J. Ahn, "Co-Cr dental alloys induces cytotoxicity and inflammatory responses via activation of Nrf2/antioxidant signaling pathways in human gingival fibroblasts and osteoblasts," *Dental Materials*, vol. 32, no. 11, pp. 1394–1405, 2016.

[100] S. Ma, L. Shan, Y. H. Xiao et al., "The cytotoxicity of methacryloxylethyl cetyl ammonium chloride, a cationic antibacterial monomer, is related to oxidative stress and the intrinsic mitochondrial apoptotic pathway," *Brazilian Journal of Medical and Biological Research*, vol. 44, no. 11, pp. 1125–1133, 2011.

[101] N. R. Kim, H. C. Park, I. Kim, B. S. Lim, and H. C. Yang, "In vitro cytocompatibility of N-acetylcysteine-supplemented dentin bonding agents," *Journal of Endodontics*, vol. 36, no. 11, pp. 1844–1850, 2010.

[102] H. Minamikawa, M. Yamada, Y. Deyama et al., "Effect of N-acetylcysteine on rat dental pulp cells cultured on mineral trioxide aggregate," *Journal of Endodontics*, vol. 37, no. 5, pp. 637–641, 2011.

[103] D. H. Lee, B. S. Lim, Y. K. Lee, and H. C. Yang, "Mechanisms of root canal sealers cytotoxicity on osteoblastic cell line MC3T3-E1," *Oral Surgery, Oral Medicine, Oral Pathology, Oral Radiology, and Endodontics*, vol. 104, no. 5, pp. 717–721, 2007.

[104] M. C. Chang, L. D. Lin, M. T. Wu et al., "Effects of camphorquinone on cytotoxicity, cell cycle regulation and prostaglandin E2 production of dental pulp cells: role of ROS, ATM/Chk2, MEK/ERK and hemeoxygenase-1," *PLoS One*, vol. 10, no. 12, article e0143663, 2015.

[105] K. Pawlowska-Goral, E. Kurzeja, and M. Stec, "N-Acetylcysteine protects against fluoride-induced oxidative damage in primary rat hepatocytes," *Toxicology In Vitro*, vol. 27, no. 8, pp. 2279–2282, 2013.

[106] A. Mohsen, A. Gomaa, F. Mohamed et al., "Antibacterial, antibiofilm activity of some non-steroidal anti-inflammatory drugs and N-acetyl cysteine against some biofilm producing uropathogens," *American Journal of Epidemiology and Infectious Disease*, vol. 3, no. 1, pp. 1–9, 2015.

[107] L. Drago, E. De Vecchi, R. Mattina, and C. L. Romano, "Activity of N-acetyl-L-cysteine against biofilm of Staphylococcus aureus and Pseudomonas aeruginosa on orthopedic prosthetic materials," *The International Journal of Artificial Organs*, vol. 36, no. 1, pp. 39–46, 2018.

[108] S. Aslam and R. O. Darouiche, "Role of antibiofilm-antimicrobial agents in controlling device-related infections," *The International Journal of Artificial Organs*, vol. 34, no. 9, pp. 752–758, 2011.

[109] M. A. El-Feky, M. S. El-Rehewy, M. A. Hassan, H. A. Abolella, R. M. Abd El-Baky, and G. F. Gad, "Effect of ciprofloxacin and N-acetylcysteine on bacterial adherence and biofilm formation on ureteral stent surfaces," *Polish Journal of Microbiology*, vol. 58, no. 3, pp. 261–267, 2009.

[110] S. Aslam, B. W. Trautner, V. Ramanathan, and R. O. Darouiche, "Combination of tigecycline and N-acetylcysteine reduces biofilm-embedded bacteria on vascular catheters," *Antimicrobial Agents and Chemotherapy*, vol. 51, no. 4, pp. 1556–1558, 2007.

[111] B. Leite, F. Gomes, P. Teixeira, C. Souza, E. Pizzolitto, and R. Oliveira, "Combined effect of linezolid and N-acetylcysteine against Staphylococcus epidermidis biofilms," *Enfermedades Infecciosas y Microbiología Clínica*, vol. 31, no. 10, pp. 655–659, 2013.

[112] S. Kirmusaoğlu, S. Yurdugül, and M. Esra Koçoğlu, "The effect of N-acetylcysteine on growth and biofilm formation in Staphylococcus epidermidis strains," *Turkish Journal of Medical Sciences*, vol. 42, no. 4, pp. 689–694, 2012.

[113] F. Gomes, B. Leite, P. Teixeira, J. Azeredo, and R. Oliveira, "Farnesol in combination with N-acetylcysteine against Staphylococcus epidermidis planktonic and biofilm cells," *Brazilian Journal of Microbiology*, vol. 43, no. 1, pp. 235–242, 2012.

[114] M. Venkatesh, L. Rong, I. Raad, and J. Versalovic, "Novel synergistic antibiofilm combinations for salvage of infected catheters," *Journal of Medical Microbiology*, vol. 58, no. 7, pp. 936–944, 2009.

[115] A. Marchese, M. Bozzolasco, L. Gualco, E. A. Debbia, G. C. Schito, and A. M. Schito, "Effect of fosfomycin alone and in combination with N-acetylcysteine on E. coli biofilms," *International Journal of Antimicrobial Agents*, vol. 22, pp. 95–100, 2003.

[116] J. Lea, A. Conlin, I. Sekirov et al., "In vitro efficacy of N-acetylcysteine on bacteria associated with chronic suppurative otitis media," *Journal of Otolaryngology - Head & Neck Surgery*, vol. 43, no. 1, p. 20, 2014.

[117] T. Zhao and Y. Liu, "N-acetylcysteine inhibit biofilms produced by Pseudomonas aeruginosa," *BMC Microbiology*, vol. 10, no. 1, p. 140, 2010.

[118] R. M. A. el-Baky, D. M. M. A. el Ela, and G. F. M. Gad, "N-acetylcysteine inhibits and eradicates candida albicans biofilms," *American Journal of Infectious Diseases and Microbiology*, vol. 2, no. 5, pp. 122–130, 2014.

Hindawi
Oxidative Medicine and Cellular Longevity
Volume 2018, Article ID 7459612, 10 pages
https://doi.org/10.1155/2018/7459612

Research Article

Exercise Training Mitigates Water Pipe Smoke Exposure-Induced Pulmonary Impairment via Inhibiting NF-κB and Activating Nrf2 Signalling Pathways

Abderrahim Nemmar[1], **Suhail Al-Salam**[2], **Priya Yuvaraju**[1], **Sumaya Beegam**[1] and **Badreldin H. Ali**[3]

[1]*Department of Physiology, College of Medicine and Health Sciences, United Arab Emirates University, P.O. Box 17666, Al Ain, UAE*
[2]*Department of Pathology, College of Medicine and Health Sciences, United Arab Emirates University, P.O. Box 17666, Al Ain, UAE*
[3]*Department of Pharmacology and Clinical Pharmacy, College of Medicine & Health Sciences, Sultan Qaboos University, P.O. Box 35, Muscat 123, Al Khoudh, Oman*

Correspondence should be addressed to Abderrahim Nemmar; anemmar@uaeu.ac.ae

Received 15 October 2017; Accepted 16 January 2018; Published 6 March 2018

Academic Editor: Karolina Szewczyk-Golec

Water pipe smoking is a tobacco smoking method commonly used in Eastern countries and is gaining popularity in Europe and North America, in particular among adolescents and young adults. Several clinical and experimental studies have reported that exposure to water pipe smoke (WPS) induces lung inflammation and impairment of pulmonary function. However, the mechanisms of such effects are not understood, as are data on the possible palliative effect of exercise training. The present study evaluated the effects of regular aerobic exercise training (treadmill: 5 days/week, 40 min/day) on subchronic exposure to WPS (30 minutes/day, 5 days/week for 2 months). C57BL/6 mice were exposed to air or WPS with or without exercise training. Airway resistance measured using forced oscillation technique was significantly and dose-dependently increased in the WPS-exposed group when compared with the air-exposed one. Exercise training significantly prevented the effect of WPS on airway resistance. Histologically, the lungs of WPS-exposed mice had focal moderate interstitial inflammatory cell infiltration consisting of neutrophil polymorphs, plasma cells, and lymphocytes. There was a mild increase in intra-alveolar macrophages and a focal damage to alveolar septae in some foci. Exercise training significantly alleviated these effects and also decreased the WPS-induced increase of tumor necrosis factor α and interleukin 6 concentrations and attenuated the increase of 8-isoprostane in lung homogenates. Likewise, the lung DNA damage induced by WPS was significantly inhibited by exercise training. Moreover, exercise training inhibited nuclear factor kappa-B (NF-κB) expression induced by WPS and increased that of nuclear factor erythroid 2-related factor 2 (Nrf2). Our findings suggest that exercise training significantly mitigated WPS-induced increase in airway resistance, inflammation, oxidative stress, and DNA damage via mechanisms that include inhibiting NF-κB and activating Nrf2 signalling pathways.

1. Introduction

Water pipe smoking, known under various synonyms including hubble-bubble, shisha, hookah, or narghile, is a tobacco smoking method widely utilized in the Middle East, Turkey, India, and China and is at present gaining increasing popularity in Europe and North America, in particular among adolescents and young adults. [1–4]. The prevalence of current WPS in adults was found to reach 4 to 12% in Gulf countries, 15% in Lebanon, and 9 to 12% in Syria [5]. In North America, studies reported a prevalence of 8.8% in adults who have ever used WPS and 11.4% reported current WPS use [6, 7]. The popularity of WPS in adolescents and young adults is increasing at disturbing rates. For example, 43 to 61% of college students in the Middle East indicated lifetime WPS and 5 to 43% mentioned previous-month or

present WPS use [8]. Moreover, it has been described that 1 out of 5 American and European college students reported previous-year WPS use while lifetime WPS was found to reach 15–41% and previous-month WPS rates went from 7 to 21% [9].

Studies on the adverse pulmonary effects of WPS are relatively scarce compared with those related to cigarette smoking. Clinical studies have reported that both acute and chronic WPS induce increase in COHb, blood pressure, and heart and respiratory rates and induced lung inflammation and impairment in pulmonary function [10–13]. Likewise, experimental studies have reported that subacute and chronic exposure to WPS induces lung inflammation, oxidative stress, and increase in airway resistance [14–16].

Although numerous antismoking campaigns are in place, many sufferers are left with permanent damage and need ongoing treatment, even after cessation of smoking. In fact, in view of the challenging tobacco-dependence syndrome, management requires various approaches, including compliance to medication and behavioral and other modalities of treatment [17]. Nevertheless, no study has been reported on how to reduce the pulmonary adverse effects of WPS. Exercise training is essential in averting and treating lung disorders. Moderate exercise training has been reported to improve cardiopulmonary capacity and airway immunity and protect the lungs against oxidative stress observed in lung diseases [18, 19]. As it is well recognized that exposure to WPS induces pulmonary inflammation and oxidative stress [14–16], we sought, here, to evaluate whether, and to what extent, can exercise training improve WPS-induced lung inflammation and oxidative stress and increase in airway resistance. Such study has, as far as we are aware, never been reported so far.

Here, the aim of this study was to assess the possible ameliorative effect of aerobic exercise training against WPS-induced pulmonary impairment and the mechanisms underlying these effects.

2. Material and Methods

2.1. Animals and Treatments. This project was evaluated and accepted by the Institutional Review Board of the United Arab Emirates University, College of Medicine and Health Sciences, and experiments were done in agreement with protocols agreed by the Institutional Animal Care and Research Advisory Committee.

2.2. WPS Exposure. C57BL/6 mice (Taconic Farms Inc., Germantown, NY, USA) were housed in a conventional animal house and kept on a 12-hour light-dark cycle (lights on at 6:00 a.m.). The animals were put in cages and provided with pelleted food and H_2O ad libitum. Mice were allowed to adjust to the exposure structure for 1 week prior the beginning of exposure to WPS or air.

Animals were put in soft restraints and connected to the exposure tower [14, 15, 20–22]. The animals were exposed to either air or WPS via their noses by a nose-only exposure system linked to a water pipe (InExpose System, Scireq, Canada). Mice were exposed to a commercially available apple-flavored tobacco (Al Fakher Tobacco Trading, Ajman, United Arab Emirates). Tobacco was lit with an instant light charcoal disk (Star, 3.5 cm diameter and 1 cm width). As seen in human use, the smoke from the water pipe goes initially through the water before it was drawn into the exposure tower. The exposure regime is controlled by a computerized system (InExpose System, Scireq, Canada) [23]. A computer-controlled puff was produced every minute, leading to a 2 s puff period of WPS exposure followed by 58 s of air. The duration of an exposure session was 30 min/day [14, 15, 20, 21, 23]. The latter was chosen from a recent work that has evaluated the cardiorespiratory impact of WPS in human subjects [13]. Mice were exposed for 2 consecutive months (30 minutes/day, 5 days/week).

2.3. Exercise protocol. The exercise protocol used was similar to that reported before by Vieira et al. [24]. Animals were exercised during their active period, that is, 09:00 and 12:00 on an Exer 3/6 treadmill—Columbus motorized treadmill (Columbus Instruments, Columbus, OH, USA)—for 40 min/day at 12 m/min, 12% grade, 5 times/week for the duration of two months. The latter intensity coincides to 65–70% of maximal oxygen uptake [24, 25]. A foam sponge was put at the back of each treadmill lane to avoid the injury of the mice. All mice conformed to this exercise protocol. The interval and intensity were augmented gradually so that the mice were running at the set level by the 8 training session [24]. Control animals were exposed to the same noise and handling as the mice group which went through exercise training.

One hour following the end of the exercise training period, animals were exposed to WPS as described above. In total, 4 groups of mice were studied, that is, air (nonexercisers), WPS (nonexercisers), exercise + air, and exercise + WPS.

2.4. Airway Reactivity to Methacholine. Airway hyperreactivity responses were assessed using a forced oscillation technique (FlexiVent, SCIREQ, Montreal, Canada) as described before [15, 26, 27].

2.5. Histopathology. In separate animals, the heart-lung block was excised and fixed in 10% neutral formalin at a constant hydrostatic pressure of 20–25 cm fluid column for 24 hours [23, 28] which was followed by dehydration in increasing concentrations of ethanol, clearing with xylene and embedding with paraffin. Three μm sections were prepared from paraffin blocks and stained with haematoxylin and eosin [29]. The stained sections were blindly evaluated by the histopathologist who participates in this project using light microscopy.

2.6. Measurement of Tumor Necrosis Factor (TNFα), Interleukin 6 (IL-6), and 8-Isoprostane. At the end of the two-month-exposure period to either WPS or air, with or without exercise training, individual mice were sacrificed by an overdose of sodium pentobarbital, and their lungs were quickly collected and rinsed with ice-cold PBS (pH 7.4) before homogenization, as described before [29, 30]. The homogenates were centrifuged for 10 min at 3000 ×g to

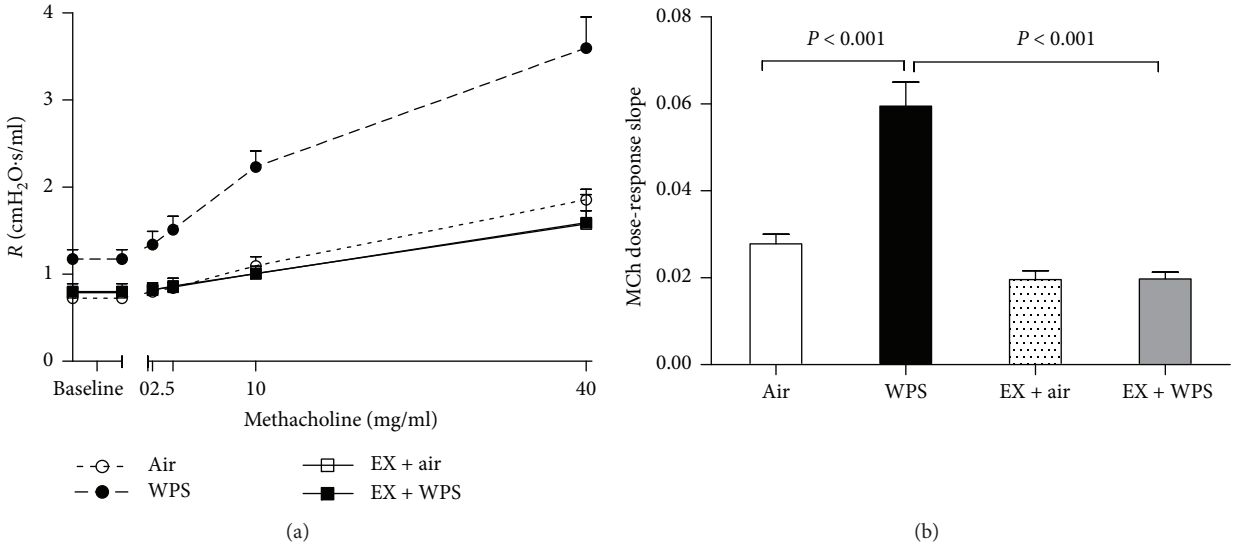

Figure 1: Airway hyperresponsiveness. The airway resistance (R), after increasing concentrations of methacholine (MCh) (0–40 mg/ml), was measured via the forced oscillation technique (FlexiVent), at the end of the 2-month-exposure period to water pipe smoke (WPS) or air with or without exercise training. Dose-response relationship of total respiratory system resistance to increasing doses of MCh (a). From the resistance MCh dose-response curve in (a), an index of airway responsiveness was calculated as the slope of the linear regression using 0–40 mg/ml concentrations (b). Data are mean ± SEM (n = 8–9).

remove cellular debris, and the supernatants were utilized for additional analysis [29]. Protein content was assessed by Bradford's technique. The concentrations of TNFα and IL-6 were measured using ELISA Kits (Duo Set, R & D systems, Minneapolis, MN, USA). 8-Isoprostane concentrations were evaluated using an ELISA Kit (Cayman Chemicals, Michigan, USA) [31].

2.7. DNA Damage Assessment by COMET Assay. In separate mice, the lungs of mice obtained from the various studied groups were used to quantify the DNA damage by COMET assay. The latter was evaluated as previously described [15, 32–35], and the assessment of length of the DNA migration (i.e., diameter of the nucleus plus migrated DNA) was measured using the image analysis AxioVision 3.1 software (Carl Zeiss, Canada) [15, 36].

2.8. Western Blot Analysis. Protein expressions for NF-κB p65 and Nrf2 were assessed using Western blotting techniques [34]. Lung tissues collected from the mice were straightway snap frozen with liquid nitrogen and kept at −80°C. After that, the tissues were weighed, rinsed with saline, and homogenized with lysis buffer (pH 7.4) containing NaCl (140 mM), KCl (300 mM), Trizma base (10 mM), EDTA (1 mM), Triton X-100 0.5% (v/v), sodium deoxycholate 0.5% (w/v), protease, and phosphatase inhibitor [34]. The homogenates were centrifuged for 20 min at 4°C. The supernatants were collected, and protein quantification was performed with a Pierce bicinchoninic acid protein assay kit (Thermo Scientific) [34]. A protein sample (35 μg) was electrophoretically isolated by 10% sodium dodecyl sulfate polyacrylamide gel electrophoresis and then transferred onto polyvinylidene difluoride membranes. The immunoblots were then blocked with 5% nonfat milk and then probed with either the rabbit monoclonal NF-κB p65 antibody (1 : 25,000 dilution, Abcam) or rabbit monoclonal Nrf2 antibody (1 : 2000 dilution, Abcam) at 4°C overnight. The blots were then incubated with goat anti-rabbit IgG horseradish peroxidase conjugated secondary antibody (1 : 5000 dilution, Abcam) for 2 h at room temperature and developed using Pierce enhanced chemiluminescent plus Western blotting substrate Kit (Thermo Scientific). The densitometric analysis of the protein bands was performed for NF-κB p65 and Nrf2 with Typhoon FLA 9500 (GE Healthcare Bio-Sciences AB, Uppsala, Sweden). Blots were then reprobed with mouse monoclonal GAPDH antibody (1 : 5000 dilution, Abcam) and used as a control.

2.9. Statistics. All statistical analyses were executed with GraphPad Prism Software version 5. Comparisons between the various groups were achieved by one-way analysis of variance (ANOVA), followed by Newman-Keuls multiple range tests. The data in figures were reported as mean ± SEM. P values < 0.05 are considered significant.

3. Results

3.1. Airway Hyperreactivity to Methacholine. Figure 1(a) illustrates the airway resistance, following increasing concentrations of methacholine (0–40 mg/ml), after exposure to WPS or air, with or without exercise training. The airway resistance was dose-dependently increased in the WPS group compared with the air-exposed group. No difference in airway resistance was seen between the air group and the exercise + air group. Remarkably, exercise training significantly inhibited the increase in airway resistance induced by WPS. From the resistance methacholine dose-response curve, an index of airway responsiveness was calculated as

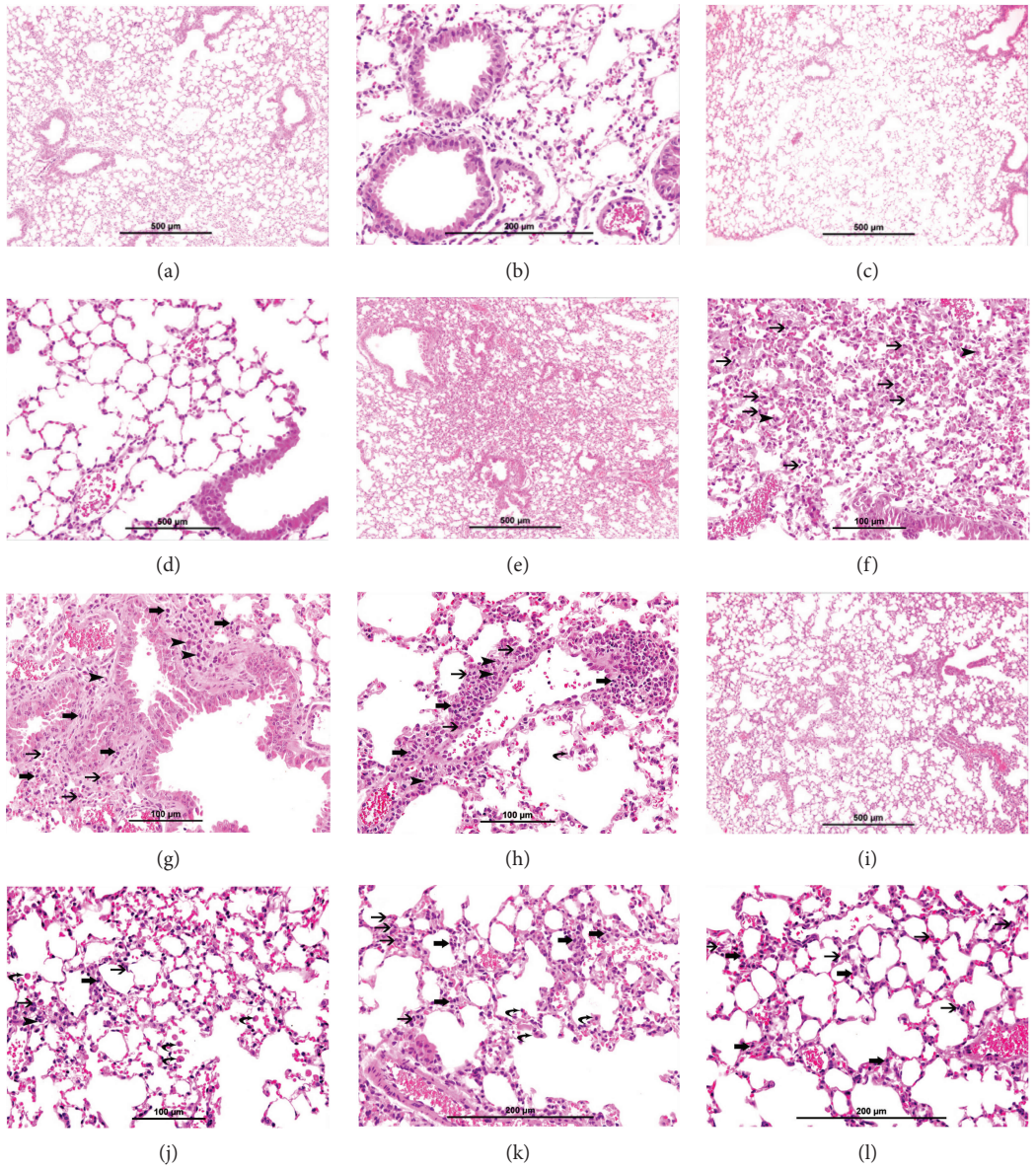

Figure 2: Representative light microscopy sections of lung tissues of mice, at the end of the 2-month-exposure period to water pipe smoke (WPS) or air with or without exercise training. (a, b) The air-exposed group shows normal lung tissue with unremarkable changes. (c, d) The exercise + air group shows normal lung tissue with unremarkable changes. (e–h) The WPS group: (e) low power view showing widening of interstitial space with mixed inflammatory cell infiltration. (f) shows moderate expansion of the alveolar interstitial space with many neutrophil polymorphs (thin arrow) and increased intra-alveolar macrophages (arrow head). (g) shows moderate expansion of the alveolar interstitial space with many neutrophil polymorphs (thin arrow), lymphocytes (thick arrow), and plasma cells (arrow head). (h) shows moderate expansion of the alveolar interstitial space with many neutrophil polymorphs (thin arrow), lymphocytes (thick arrow), and plasma cells (arrow head). There is a focal destruction of interalveolar septae (curved arrow). (i–l) The exercise + WPS group: (i) low power view showing focal mild widening of interstitial space with focal mild mixed inflammatory cell infiltration. (j–l) show focal mild expansion of the alveolar interstitial space with few neutrophil polymorphs (thin arrow) and few lymphocytes (thick arrow). There is a mild increase of alveolar macrophages (curved arrow).

the slope of the linear regression using 0–40 mg/ml concentration (Figure 1(b)). The methacholine dose-response slope was significantly increased in the WPS group compared with the air group ($P < 0.001$), and this effect was significantly inhibited by exercise training ($P < 0.001$).

3.2. Lung Histopathology. The light microscopy analysis of the lung sections from air-exposed mice (Figures 2(a) and 2(b)) and the exercise + air mice (Figures 2(c) and 2(d)) showed normal lung tissue with unremarkable changes. The lung sections of WPS-exposed mice (Figures 2(e)–2(h)) showed focal moderate interstitial inflammatory cell infiltration consisting of neutrophil polymorphs, plasma cells, and lymphocytes. There was a moderate increase in intra-alveolar macrophages and focal damage to alveolar septae in some foci. In the exercise + WPS group

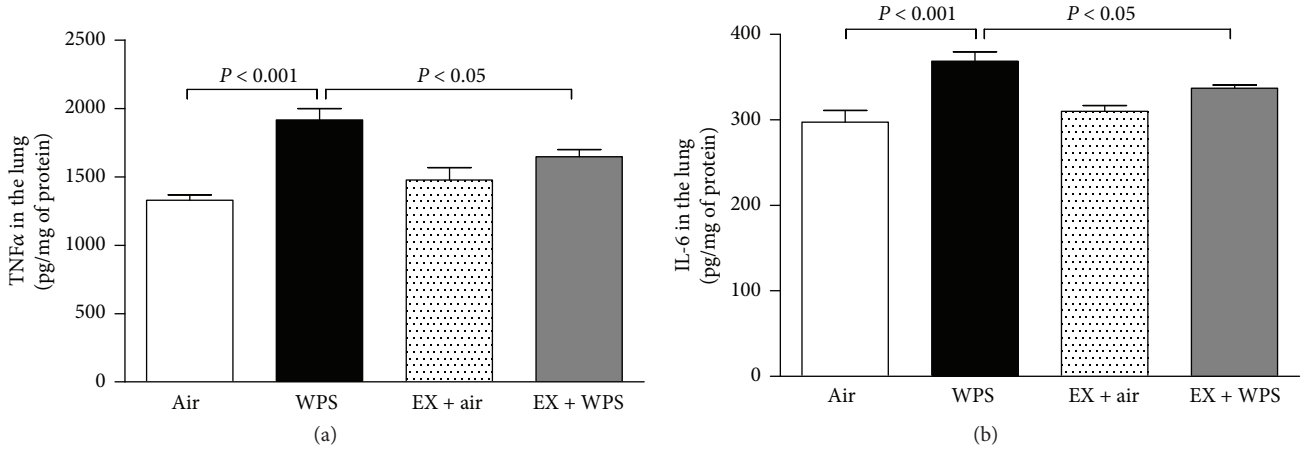

Figure 3: Tumor necrosis factor α (TNFα) (a) and interleukin 6 (IL-6) (b) concentrations in lung homogenate, at the end of the 2-month-exposure period to water pipe smoke (WPS) or air with or without exercise (EX) training. Data are mean ± SEM ($n = 7$–9 in each group).

(Figures 2(i)–2(l)), there was preservation of lung architecture with only few foci of mild interstitial inflammatory cell infiltration consisting of neutrophil polymorphs, lymphocytes, and very few plasma cells and mild increase in intra-alveolar macrophages.

3.3. TNFα and IL-6 in Lung Homogenate. The concentration of TNFα in lung homogenates was significantly increased following WPS exposure compared with the air-exposed group ($P < 0.001$; Figure 3(a)). Exercise training has significantly prevented the increase in TNFα concentration caused by WPS (Figure 3(a)). Likewise, IL-6 concentration was significantly increased by the subchronic exposure to WPS compared with the control group (Figure 3(b)). The latter augmentation of IL-6 was significantly abrogated in the exercise training + WPS group.

3.4. 8-Isoprostane Concentrations in Lung Homogenates. Figure 4 illustrates the concentrations of 8-isoprostane in lung homogenates after the subchronic exposure to WPS or air, with or without exercise training.

Compared with the air-exposed group, WPS exposure induced a significant increase in 8-isoprosatne concentration ($P < 0.05$). The latter effect was completely prevented in the exercise + WPS group compared with the WPS group ($P < 0.01$).

3.5. Lung DNA Damage. Figure 5 illustrates the effect of subchronic WPS exposure on lung DNA damage and the influence of exercise training thereon. Compared with the air-exposed group, WPS exposure caused a significant increase in DNA migration ($P < 0.001$). The latter effect was significantly reversed in the exercise + WPS group compared with the WPS group ($P < 0.01$).

3.6. Western Blot Analysis for the Detection of NF-κB and Nrf2. The subchronic exposure to WPS caused an increase in the expression of NF-κB ($P < 0.05$). Such effect was significantly prevented in the exercise + WPS group compared with the WPS group ($P < 0.05$) (Figure 6).

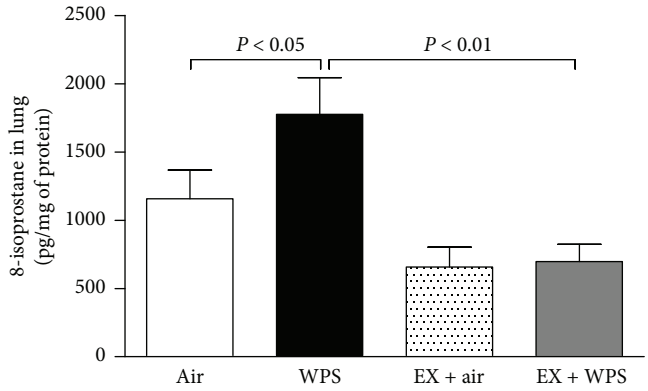

Figure 4: 8-Isoprostane concentrations in lung homogenate, at the end of the 2-month-exposure period to water pipe smoke (WPS) or air with or without exercise (EX) training. Data are mean ± SEM ($n = 5$–6 in each group).

Figure 7 shows that, compared with the control group, the subchronic exposure to WPS induced a statistically insignificant increase of Nrf2 expression. The levels of expression of Nrf2 were significantly increased in the exercise + WPS versus WPS ($P < 0.001$) and the exercise + WPS versus exercise + air groups ($P < 0.01$).

4. Discussion

The current work provided experimental evidence that exercise training significantly mitigated subchronic pulmonary toxicity of WPS. We showed that regular exercise training alleviated WPS-induced airway resistance, inflammation, oxidative stress, and DNA damage via inhibiting NF-κB and activating Nrf2 signalling pathways.

WPS is gaining extensive popularity all over the world in different populations [8]. A study has reported that in the USA, there are around 300 WPS bars situated in 2/3 of the states, regularly located close to colleges and universities [37]. Also, it has been reported that WPS could be a gateway

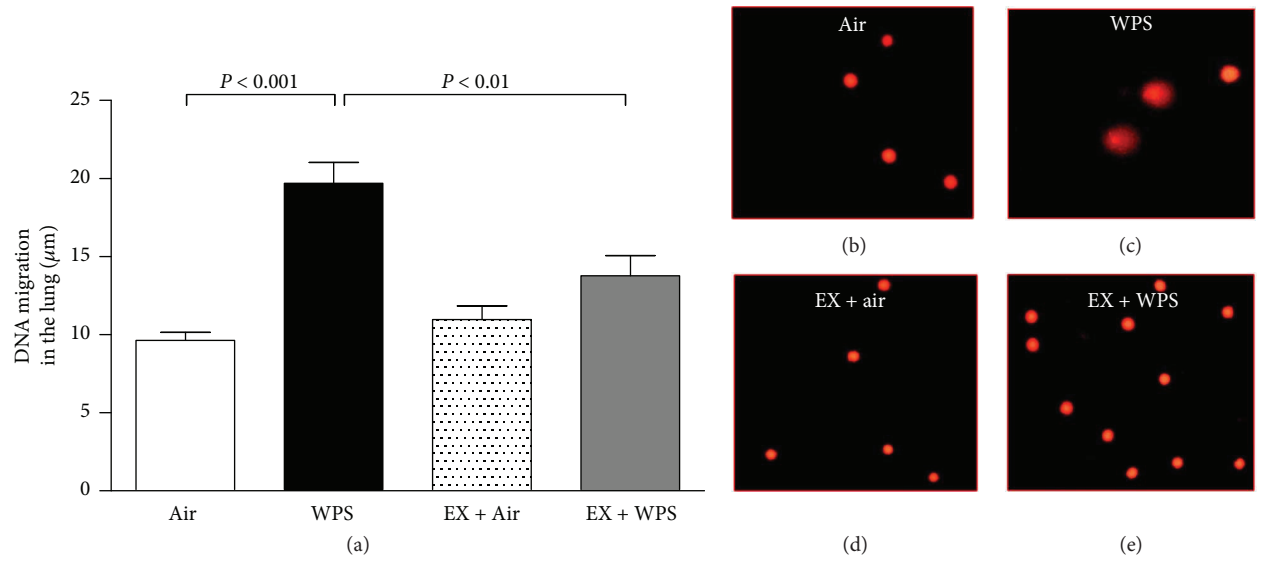

Figure 5: DNA migration (mm) in the lung tissues (a) evaluated by Comet assay, at the end of the 2-month-exposure period to water pipe smoke (WPS) or air with or without exercise (EX) training. Data are mean ± SEM ($n = 5$ in each group). Representative images illustrating the quantification of the DNA migration by the Comet assay under alkaline conditions, in control (b), WPS (c), EX + air (d), and EX + WPS (e).

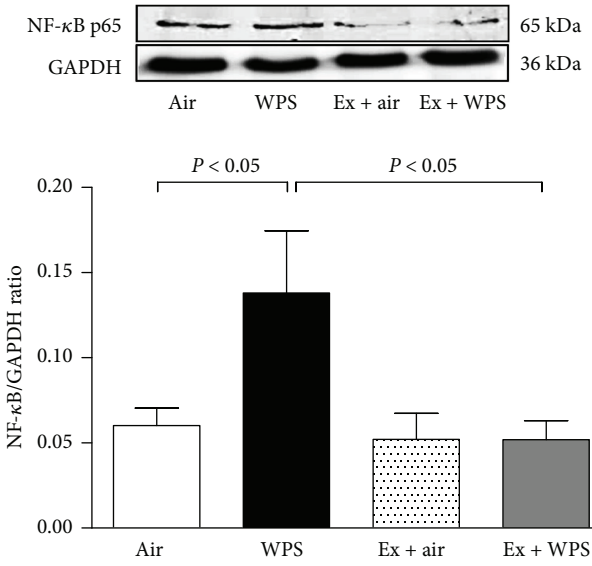

Figure 6: Western blot analysis and graphic representation of nuclear factor kappa-B (NF-κB) protein levels in the lung tissues, at the end of the 2-month-exposure period to water pipe smoke (WPS) or air with or without exercise (EX) training. Data are mean ± SEM ($n = 4$–5 in each group).

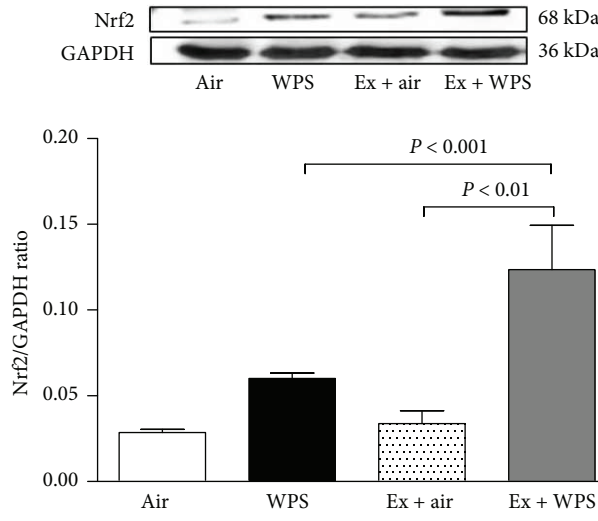

Figure 7: Western blot analysis and graphic representation of nuclear factor erythroid 2-related factor 2 (Nrf2) protein levels in the lung tissues, at the end of the 2-month-exposure period to water pipe smoke (WPS) or air with or without exercise (EX) training. Data are mean ± SEM ($n = 4$–5 in each group).

to other forms of smoking including cigarette smoking, which could decline the progresses in tobacco reduction over the past decades [38]. Owing to the fact that the majority of water pipe smokers are also current or past smokers of cigarettes, clinical investigations on the adverse effects of WPS have described problems in investigating the sole effects of WPS [39]. Consequently, experimental research on this topic is important and necessary to uncover the possible mechanisms underlying the adverse effects of WPS and enable therapeutic or preventative strategies aiming at alleviating the pathophysiological effects of WPS.

Previous experimental studies have reported the positive impact of exercise training on cigarette smoke or particulate air pollution [40, 41]. However, as far as we are aware, no study has investigated the impact of exercise training on WPS-induced pulmonary impairment and the mechanisms underlying these effects.

The nose-only and whole body exposure systems are the two principal techniques currently used to study the

impact of tobacco smoke and water pipe exposure in mice or rats [28, 42]. The shortcoming of using whole body exposure is that the animals may ingest nicotine or tar substances when cleaning their fur [28]. The nose-only exposure system avoids this problematic and most probably best resembles the human exposure circumstances [28, 43]. Moreover, we have recently reported that the levels of carboxyhemoglobin found in mice exposed to nose-only WPS were comparable with those reported in water-pipe smokers [23]. We have previously reported that acute (5 days) exposure to WPS induces lung inflammation but no change in airway resistance [44]. We have also reported that both lung inflammation and airway resistance were significantly increased following subacute (1 month) and chronic (6 months) exposures to WPS [14, 15]. In the present study, we showed that subchronic (2 months) exposure to WPS causes airway hyperresponsiveness to methacholine and that this effect was significantly prevented by regular exercise training. Moreover, we have also found that exercise training preserved the lung architecture and has significantly alleviated the interstitial and intra-alveolar infiltration of inflammatory cells and prevented the focal damage of alveolar septum induced by the subchronic exposure to WPS. It has been reported that aerobic physical training of moderate intensity attenuated the development of pulmonary emphysema and lung elastance induced by chronic (24 weeks) cigarette smoke exposure [40]. It has also been shown that regular aerobic exercise training exerts a protective effect against pulmonary inflammation induced by exposure to diesel exhaust particles (DEP) for 5 weeks [41].

Since several studies have reported that long-term regular aerobic exercise reduces oxidative stress and inflammation in animal models of chronic obstructive pulmonary disease [40] and asthma [45], we, presently, wanted to assess the effect of subchronic exposure to WPS on markers of inflammation and oxidative stress, and the possible protective effect of exercise training thereon. Our data show that subchronic exposure to WPS induced a significant increase of TNFα and IL-6. The latter proinflammatory cytokines were found to increase following 1 month of exposure to WPS. Both cytokines were shown to play an important role in the continuation of cigarette smoke-induced inflammation even following smoking cessation [46, 47]. Interestingly, here, we show that exercise training significantly reduced the increase of TNFα and IL-6 caused by WPS. Our findings are in agreement with a previous report which showed that exercise training prevented DEP-induced increase of TNFα and IL-6 in the lung [41]. Moreover, in this study, we have also measured the pulmonary concentrations of 8-isoprostane, a marker of lipid peroxidation. Our data show that exposure to WPS induced oxidative stress in lung tissue evidenced by a significant increase of 8-isoprostane in the lung tissue and that exercise training significantly reduced these effects. Our data is in line with a previous report which showed that exercise markedly prevented the increase in reactive oxygen species and 8-isoprostane expression in lung tissue caused by chronic exposure to cigarette smoke in mice [40].

It is well established that inflammation and oxidative stress result in cell membrane injury and DNA damage [48]. We have previously demonstrated that chronic exposure to WPS causes lung DNA damage [15]. Here, we show that subchronic exposure to WPS causes DNA damage and, remarkably, regular exercise training significantly averted this effect. This protective effect could be explained by the anti-inflammatory and antioxidant effects of exercise training. It has been previously reported that the use of gum acacia, a natural anti-inflammatory and antioxidant agent, averted the DNA damage in adenine-induced chronic kidney disease in rats [49].

NF-κB, a nuclear transcription factor, plays an important role in several pathophysiological processes comprising inflammation, immune reaction, and apoptosis [50]. The activation of the NF-κB signalling pathway induces the upregulations of proinflammatory cytokines including TNFα, IL-6, and IL-1β [50]. Studies in mouse models have reported that NF-κB is an important mediator of many inflammatory disease states and strategies aiming at blocking this transcription factor may prevent inflammation-associated pulmonary diseases [50]. Also, it has been shown that inhibition of NF-κB by geraniin, a natural compound with anti-inflammatory effect, [51] or penehyclidine hydrochloride, a selective anticholinergic agent, [52] alleviated lipopolysaccharide- (LPS-) induced acute lung injury in mice by blocking the production of proinflammatory cytokine. To investigate the mechanism by which exercise training exerts its beneficial effect against WPS-induced lung toxicity, we have assessed the effect of exercise training on NF-κB activation. Our data show that WPS exposure induced a significant increase in the expression of NF-κB and that exercise training significantly inhibited this effect. These results suggest that the protective effect exerted by exercise training is, at least partly, related to the inhibition of NF-κB expression.

The transcription factor Nrf2 regulates the expression of antioxidant genes which regulate oxidative stress, xenobiotic metabolism and excretion, inflammation, and apoptosis, and several experimental studies showed the key role of Nrf2 activation to decrease oxidative stress and inflammation in animal models of pulmonary fibrosis, emphysema, acute lung injury, and asthma [53]. Our data show that subchronic exposure to WPS induced an insignificant increase in the expression of Nrf2 and the level of expression of this transcription factor was substantially and significantly increased in the exercise + WPS group. These data suggest that exercise training exerts its protective role against WPS-induced pulmonary toxicity by activating the Nrf2 signalling pathway. It has been recently reported in mice that Nrf2 expression is augmented in LPS-induced lung injury and the administration of geraniin caused an upregulation of Nrf2 expression and mitigated LPS-induced acute lung injury [51]. Additionally, another study reported that platycodin D, a natural compound with anti-inflammatory action, given i.p. to mice exerts a protective effect against cigarette smoke-induced pulmonary inflammation by averting inflammatory and oxidative response through activating the Nrf2 signalling pathway [54].

In conclusion, our data showed, for the first time, that aerobic exercise training significantly mitigated subchronic WPS-induced airway resistance, inflammation, oxidative stress, and DNA damage via inhibiting NF-κB and activating Nrf2 signalling pathways. Further studies on the effect of different modalities of exercise on mice exposed to WPS for different durations are warranted. These preclinical findings may encourage further controlled studies in current water pipe smokers and in those who have stopped smoking to assess its clinical usefulness.

Conflicts of Interest

The authors declare that they have no conflicts of interest.

Authors' Contributions

All authors have read and approved the manuscript. Abderrahim Nemmar designed, planned, and supervised all the experiments; analyzed the data; and wrote the manuscript. Suhail Al-Salam preformed, analyzed, interpreted, and wrote the histopathology part of the study. Priya Yuvaraju and Sumaya Beegam performed the experiments. Badreldin H. Ali contributed in the study design and writing of the manuscript.

Acknowledgments

This work was supported by funds of the College of Medicine and Health Sciences grant (31M215) and United Arab Emirates University UPAR (31M189) and center-based interdisciplinary (31R052) grants. The authors would like to thank Professor Gerald Blunden (University of Portsmouth, UK) for critically reading the manuscript.

References

[1] W. Maziak, K. D. Ward, R. A. Afifi Soweid, and T. Eissenberg, "Tobacco smoking using a waterpipe: a re-emerging strain in a global epidemic," *Tobacco Control*, vol. 13, no. 4, pp. 327–333, 2004.

[2] K. Chaouachi, "Hookah (shisha, narghile) smoking and environmental tobacco smoke (ETS). A critical review of the relevant literature and the public health consequences," *International Journal of Environmental Research and Public Health*, vol. 6, no. 2, pp. 798–843, 2009.

[3] B. Knishkowy and Y. Amitai, "Water-pipe (narghile) smoking: an emerging health risk behavior," *Pediatrics*, vol. 116, no. 1, pp. e113–e119, 2005.

[4] A. Mandil, A. BinSaeed, S. Ahmad, R. Al Dabbagh, M. Alsaadi, and M. Khan, "Smoking among university students: a gender analysis," *Journal of Infection and Public Health*, vol. 3, no. 4, pp. 179–187, 2010.

[5] E. A. Akl, S. K. Gunukula, S. Aleem et al., "The prevalence of waterpipe tobacco smoking among the general and specific populations: a systematic review," *BMC Public Health*, vol. 11, no. 1, p. 244, 2011.

[6] R. McMillen, J. Maduka, and J. Winickoff, "Use of emerging tobacco products in the United States," *Journal of Environmental and Public Health*, vol. 2012, Article ID 989474, 8 pages, 2012.

[7] P. Abdullah, C. Costanian, N. Khanlou, and H. Tamim, "Prevalence and characteristics of water-pipe smoking in Canada: results from the Canadian Tobacco Use Monitoring Survey," *Public Health*, vol. 148, pp. 102–108, 2017.

[8] H. M. Bou Fakhreddine, A. N. Kanj, and N. A. Kanj, "The growing epidemic of water pipe smoking: health effects and future needs," *Respiratory Medicine*, vol. 108, no. 9, pp. 1241–1253, 2014.

[9] E. R. Grekin and D. Ayna, "Waterpipe smoking among college students in the United States: a review of the literature," *Journal of American College Health*, vol. 60, no. 3, pp. 244–249, 2012.

[10] M. H. Boskabady, L. Farhang, M. Mahmodinia, M. Boskabady, and G. R. Heydari, "Comparison of pulmonary function and respiratory symptoms in water pipe and cigarette smokers," *Respirology*, vol. 17, no. 6, pp. 950–956, 2012.

[11] D. Raad, S. Gaddam, H. J. Schunemann et al., "Effects of water-pipe smoking on lung function: a systematic review and meta-analysis," *Chest*, vol. 139, no. 4, pp. 764–774, 2011.

[12] L. Bentur, E. Hellou, A. Goldbart et al., "Laboratory and clinical acute effects of active and passive indoor group water-pipe (narghile) smoking," *Chest*, vol. 145, no. 4, pp. 803–809, 2014.

[13] F. Hakim, E. Hellou, A. Goldbart, R. Katz, Y. Bentur, and L. Bentur, "The acute effects of water-pipe smoking on the cardiorespiratory system," *Chest*, vol. 139, no. 4, pp. 775–781, 2011.

[14] A. Nemmar, H. Raza, P. Yuvaraju et al., "Nose-only water-pipe smoking effects on airway resistance, inflammation and oxidative stress in mice," *Journal of Applied Physiology*, vol. 115, no. 9, pp. 1316–1323, 2013.

[15] A. Nemmar, S. Al-Salam, P. Yuvaraju, S. Beegam, J. Yasin, and B. H. Ali, "Chronic exposure to water-pipe smoke induces alveolar enlargement, DNA damage and impairment of lung function," *Cellular Physiology and Biochemistry*, vol. 38, no. 3, pp. 982–992, 2016.

[16] Khabour OF, K. H. Alzoubi, M. Bani-Ahmad, A. Dodin, T. Eissenberg, and A. Shihadeh, "Acute exposure to waterpipe tobacco smoke induces changes in the oxidative and inflammatory markers in mouse lung," *Inhalation Toxicology*, vol. 24, no. 10, pp. 667–675, 2012.

[17] J. W. Klein, "Pharmacotherapy for substance use disorders," *The Medical Clinics of North America*, vol. 100, no. 4, pp. 891–910, 2016.

[18] R. P. Vieira, V. F. de Andrade, A. C. Duarte et al., "Aerobic conditioning and allergic pulmonary inflammation in mice. II. Effects on lung vascular and parenchymal inflammation and remodeling," *American Journal of Physiology. Lung Cellular and Molecular Physiology*, vol. 295, no. 4, pp. L670–L679, 2008.

[19] C. Garvey, "Recent updates in chronic obstructive pulmonary disease," *Postgraduate Medicine*, vol. 128, no. 2, pp. 231–238, 2016.

[20] A. Nemmar, P. Yuvaraju, S. Beegam, A. John, H. Raza, and B. H. Ali, "Cardiovascular effects of nose-only water-pipe smoking exposure in mice," *American Journal of Physiology. Heart and Circulatory Physiology*, vol. 305, no. 5, pp. H740–H746, 2013.

[21] A. Nemmar, P. Yuvaraju, S. Beegam, and B. H. Ali, "Short-term nose-only water-pipe (shisha) smoking exposure accelerates coagulation and causes cardiac inflammation and

oxidative stress in mice," *Cellular Physiology and Biochemistry*, vol. 35, no. 2, pp. 829–840, 2015.

[22] A. Nemmar, S. Al-Salam, S. Beegam, P. Yuvaraju, A. Oulhaj, and B. H. Ali, "Water-pipe smoke exposure-induced circulatory disturbances in mice, and the influence of betaine supplementation thereon," *Cellular Physiology and Biochemistry*, vol. 41, no. 3, pp. 1098–1112, 2017.

[23] A. Nemmar, S. Al-Salam, P. Yuvaraju, S. Beegam, J. Yasin, and B. H. Ali, "Chronic exposure to water-pipe smoke induces cardiovascular dysfunction in mice," *American Journal of Physiology Heart and Circulatory Physiology*, vol. 312, no. 2, pp. H329–H339, 2017.

[24] V. J. Vieira, R. J. Valentine, K. R. Wilund, N. Antao, T. Baynard, and J. A. Woods, "Effects of exercise and low-fat diet on adipose tissue inflammation and metabolic complications in obese mice," *American Journal of Physiology Endocrinology and Metabolism*, vol. 296, no. 5, pp. E1164–E1171, 2009.

[25] V. Schefer and M. I. Talan, "Oxygen consumption in adult and AGED C57BL/6J mice during acute treadmill exercise of different intensity," *Experimental Gerontology*, vol. 31, no. 3, pp. 387–392, 1996.

[26] A. Nemmar, D. Subramaniyan, S. Zia, J. Yasin, and B. H. Ali, "Airway resistance, inflammation and oxidative stress following exposure to diesel exhaust particle in angiotensin II-induced hypertension in mice," *Toxicology*, vol. 292, no. 2-3, pp. 162–168, 2012.

[27] A. Nemmar, S. Al-Salam, D. Subramaniyan et al., "Influence of experimental type 1 diabetes on the pulmonary effects of diesel exhaust particles in mice," *Toxicology Letters*, vol. 217, no. 2, pp. 170–176, 2013.

[28] M. Rinaldi, K. Maes, S. De Vleeschauwer et al., "Long-term nose-only cigarette smoke exposure induces emphysema and mild skeletal muscle dysfunction in mice," *Disease Models & Mechanisms*, vol. 5, no. 3, pp. 333–341, 2012.

[29] A. Nemmar, S. Al-Salam, P. Yuvaraju, S. Beegam, and B. H. Ali, "Emodin mitigates diesel exhaust particles-induced increase in airway resistance, inflammation and oxidative stress in mice," *Respiratory Physiology & Neurobiology*, vol. 215, pp. 51–57, 2015.

[30] S. Hodge, G. Matthews, V. Mukaro et al., "Cigarette smoke-induced changes to alveolar macrophage phenotype and function are improved by treatment with procysteine," *American Journal of Respiratory Cell and Molecular Biology*, vol. 44, no. 5, pp. 673–681, 2011.

[31] A. Nemmar, S. Al-Salam, S. Beegam, P. Yuvaraju, J. Yasin, and B. H. Ali, "Pancreatic effects of diesel exhaust particles in mice with type 1 diabetes mellitus," *Cellular Physiology and Biochemistry*, vol. 33, no. 2, pp. 413–422, 2014.

[32] M. F. de Souza, T. A. Goncales, A. Steinmetz et al., "Cocaine induces DNA damage in distinct brain areas of female rats under different hormonal conditions," *Clinical and Experimental Pharmacology & Physiology*, vol. 41, no. 4, pp. 265–269, 2014.

[33] P. L. Olive, J. P. Banath, and C. D. Fjell, "DNA strand breakage and DNA structure influence staining with propidium iodide using the alkaline comet assay," *Cytometry*, vol. 16, no. 4, pp. 305–312, 1994.

[34] A. Nemmar, T. Karaca, S. Beegam, P. Yuvaraju, J. Yasin, and B. H. Ali, "Lung oxidative stress, DNA damage, apoptosis, and fibrosis in adenine-induced chronic kidney disease in mice," *Frontiers in Physiology*, vol. 8, p. 896, 2017.

[35] A. Nemmar, P. Yuvaraju, S. Beegam, M. A. Fahim, and B. H. Ali, "Cerium oxide nanoparticles in lung acutely induce oxidative stress, inflammation, and DNA damage in various organs of mice," *Oxidative Medicine and Cellular Longevity*, vol. 2017, Article ID 9639035, 12 pages, 2017.

[36] A. Hartmann and G. Speit, "The contribution of cytotoxicity to DNA-effects in the single cell gel test (comet assay)," *Toxicology Letters*, vol. 90, no. 2-3, pp. 183–188, 1997.

[37] A. Chan and S. Murin, "Up in smoke: the fallacy of the harmless hookah," *Chest*, vol. 139, no. 4, pp. 737-738, 2011.

[38] P. D. Jensen, R. Cortes, G. Engholm, S. Kremers, and M. Gislum, "Waterpipe use predicts progression to regular cigarette smoking among Danish youth," *Substance Use & Misuse*, vol. 45, no. 7-8, pp. 1245–1261, 2010.

[39] W. Maziak, "Rise of waterpipe smoking," *BMJ*, vol. 350, article h1991, 2015.

[40] A. C. Toledo, R. M. Magalhaes, D. C. Hizume et al., "Aerobic exercise attenuates pulmonary injury induced by exposure to cigarette smoke," *The European Respiratory Journal*, vol. 39, no. 2, pp. 254–264, 2012.

[41] R. P. Vieira, A. C. Toledo, L. B. Silva et al., "Anti-inflammatory effects of aerobic exercise in mice exposed to air pollution," *Medicine and Science in Sports and Exercise*, vol. 44, no. 7, pp. 1227–1234, 2012.

[42] C. S. Stevenson and M. A. Birrell, "Moving towards a new generation of animal models for asthma and COPD with improved clinical relevance," *Pharmacology & Therapeutics*, vol. 130, no. 2, pp. 93–105, 2011.

[43] R. M. Tuder, T. Yoshida, I. Fijalkowka, S. Biswal, and I. Petrache, "Role of lung maintenance program in the heterogeneity of lung destruction in emphysema," *Proceedings of the American Thoracic Society*, vol. 3, no. 8, pp. 673–679, 2006.

[44] A. Nemmar, H. A. Al, H. N. Al et al., "Early pulmonary events of nose-only water pipe (shisha) smoking exposure in mice," *Physiological Reports*, vol. 3, no. 3, article e12258, 2015.

[45] A. Pastva, K. Estell, T. R. Schoeb, T. P. Atkinson, and L. M. Schwiebert, "Aerobic exercise attenuates airway inflammatory responses in a mouse model of atopic asthma," *Journal of Immunology*, vol. 172, no. 7, pp. 4520–4526, 2004.

[46] A. Churg, R. D. Wang, H. Tai, X. Wang, C. Xie, and J. L. Wright, "Tumor necrosis factor-α drives 70% of cigarette smoke-induced emphysema in the mouse," *American Journal of Respiratory and Critical Care Medicine*, vol. 170, no. 5, pp. 492–498, 2004.

[47] D. Mineo, V. Ambrogi, M. E. Cufari et al., "Variations of inflammatory mediators and α1-antitrypsin levels after lung volume reduction surgery for emphysema," *American Journal of Respiratory and Critical Care Medicine*, vol. 181, no. 8, pp. 806–814, 2010.

[48] P. Moller, P. H. Danielsen, D. G. Karottki et al., "Oxidative stress and inflammation generated DNA damage by exposure to air pollution particles," *Mutation Research, Reviews in Mutation Research*, vol. 762, pp. 133–166, 2014.

[49] B. H. Ali, B. K. Al, I. Al-Husseini et al., "Gum acacia mitigates genetic damage in adenine-induced chronic renal failure in rats," *European Journal of Clinical Investigation*, vol. 45, no. 12, pp. 1221–1227, 2015.

[50] A. Rahman and F. Fazal, "Blocking NF-κB: an inflammatory issue," *Proceedings of the American Thoracic Society*, vol. 8, no. 6, pp. 497–503, 2011.

[51] G. Zhu, X. Xin, Y. Liu, Y. Huang, K. Li, and C. Wu, "Geraniin attenuates LPS-induced acute lung injury via inhibiting NF-κB and activating Nrf2 signaling pathways," *Oncotarget*, vol. 8, no. 14, pp. 22835–22841, 2017.

[52] W. Shen, J. Gan, S. Xu, G. Jiang, and H. Wu, "Penehyclidine hydrochloride attenuates LPS-induced acute lung injury involvement of NF-κB pathway," *Pharmacological Research*, vol. 60, no. 4, pp. 296–302, 2009.

[53] M. R. de la Vega, M. Dodson, C. Gross et al., "Role of Nrf2 and autophagy in acute lung injury," *Current Pharmacology Reports*, vol. 2, no. 2, pp. 91–101, 2016.

[54] W. Gao, Y. Guo, and H. Yang, "Platycodin D protects against cigarette smoke-induced lung inflammation in mice," *International Immunopharmacology*, vol. 47, pp. 53–58, 2017.